NASA TECHNICAL NOTE

NASA TN D-6391

WIND-TUNNEL INVESTIGATION OF AN EXTERNAL-FLOW JET-FLAP TRANSPORT CONFIGURATION HAVING FULL-SPAN TRIPLE-SLOTTED FLAPS

by

Lysle P. Parlett, H. Douglas Greer, Robert L. Henderson,
Langley Research Center

and

C. Robert Carter
Langley Directorate,
U.S. Army Air Mobility R&D Laboratory

NATIONAL AERONAUTICS AND SPACE ADMINISTRATION • WASHINGTON, D. C. • AUGUST 1971

1. Report No.	2. Government Accession No.	3. Recipient's Catalog No.
NASA TN D-6391		

4. Title and Subtitle	5. Report Date
WIND-TUNNEL INVESTIGATION OF AN EXTERNAL-FLOW JET-FLAP TRANSPORT CONFIGURATION HAVING FULL-SPAN TRIPLE-SLOTTED FLAPS	August 1971
	6. Performing Organization Code
7. Author(s) Lysle P. Parlett, H. Douglas Greer, and Robert L. Henderson (Langley Research Center), and C. Robert Carter (Langley Directorate, U.S. Army Air Mobility R&D Laboratory)	8. Performing Organization Report No. L-7730
	10. Work Unit No. 760-72-01-02
9. Performing Organization Name and Address NASA Langley Research Center Hampton, Va. 23365	11. Contract or Grant No.
	13. Type of Report and Period Covered Technical Note
12. Sponsoring Agency Name and Address National Aeronautics and Space Administration Washington, D.C. 20546	14. Sponsoring Agency Code

15. Supplementary Notes

16. Abstract

A wind-tunnel investigation has been conducted to determine the performance and static stability and control characteristics of an external-flow jet-flap transport configuration having inboard pod-mounted engines and full-span triple-slotted flaps. Tests were made with the engines mounted clustered at 22.0 percent and 30.4 percent semispan to represent double (siamese) pods and with engines mounted at 22.0 percent and 41.7 percent semispan to represent a more spread arrangement. Tests were also made to evaluate the effectiveness of wing leading-edge blowing as a means of improving the aerodynamic efficiency of the configuration and of eliminating the large engine-out roll asymmetries that occurred for the configuration when the wing with an engine out stalled first.

17. Key Words (Suggested by Author(s))	18. Distribution Statement
External-flow jet flap High-lift devices STOL configurations	Unclassified – Unlimited

19. Security Classif. (of this report)	20. Security Classif. (of this page)	21. No. of Pages	22. Price*
Unclassified	Unclassified	266	$3.00

*For sale by the National Technical Information Service, Springfield, Virginia 22151

WIND-TUNNEL INVESTIGATION OF AN EXTERNAL-FLOW JET-FLAP TRANSPORT CONFIGURATION HAVING FULL-SPAN TRIPLE-SLOTTED FLAPS

By Lysle P. Parlett, H. Douglas Greer, Robert L. Henderson,
Langley Research Center

and C. Robert Carter
Langley Directorate, U.S. Army Air Mobility R&D Laboratory

SUMMARY

A wind-tunnel investigation has been conducted to determine the performance and static stability and control characteristics of an external-flow jet-flap transport configuration having inboard pod-mounted engines and full-span triple-slotted flaps. Tests were made with the engines mounted clustered at 22.0 percent and 30.4 percent semispan to represent double (siamese) pods and with engines mounted at 22.0 percent and 41.7 percent semispan to represent a more spread arrangement. Tests were also made to evaluate the effectiveness of wing leading-edge blowing as a means of improving the aerodynamic efficiency of the configuration and of eliminating the large engine-out roll asymmetries that occurred for the configuration when the wing with an engine out stalled first.

The results of the investigation indicated that the use of full-span triple-slotted flaps offered little improvement in aerodynamic performance over the more conventional double-slotted partial-span flaps. In either case, however, it is necessary that the flap chords be large enough to achieve good spreading and turning of the jet exhaust. The location of engines close inboard in a clustered arrangement gave smaller engine-out rolling moments than the more spread engine arrangement without appreciably altering the overall aerodynamic performance. Wing leading-edge blowing provided increases in maximum lift coefficient, stall angle of attack, and overall aerodynamic performance and, when used asymmetrically in combination with differential flap deflection, appeared to offer an effective means of trimming the engine-out rolling moments over the normal operational angle-of-attack range, including the stall. For the close-inboard clustered-engine arrangement, the inboard one-third of the flap span was found to be as effective for roll control as the full flap span.

INTRODUCTION

The present investigation was undertaken as part of a general research program to provide some fundamental information on the performance and stability and control of an external-flow jet-flap STOL airplane configuration. Previous studies conducted under this program (refs. 1 and 2) showed that the application of the jet-flap concept to high-thrust-weight-ratio turbofan airplanes was effective for producing the high lift required for STOL operation but brought out certain problems, such as that of engine-out lateral trim. Although the use of either asymmetric aileron blowing or differential flap deflection was found to be effective for trimming the engine-out moment in references 1 and 2, it was found that the engine-out wing, which had the lower thrust, tended to stall first and produce large roll asymmetries near maximum lift. In the present investigation, one of the objectives was to evaluate the use of leading-edge boundary-layer control as a means of controlling the stall angle of attack and thus eliminating the problem of roll asymmetries at the stall. In addition, the use of full-span triple-slotted flaps in combination with leading-edge boundary-layer control was studied as a possible means of improving the aerodynamic efficiency of the configuration. The model used in this investigation was basically the same as that of reference 2 except for the revised flap system.

The present investigation consisted of tests over an angle-of-attack and angle-of-sideslip range for several thrust coefficients and for several flap deflections. In tests made under various engine-out conditions, the effectiveness of asymmetric blowing over drooped ailerons and the effectiveness of differential flap deflection were evaluated in combination with leading-edge blowing as a means of achieving roll trim. Tests were made with the engines mounted clustered at 22.0 percent and 30.4 percent semispan to represent double (siamese) pods and with engines mounted at 22.0 percent and 41.7 percent semispan to represent a more spread arrangement. In addition to the static force tests, flow survey measurements were made in the vicinity of the horizontal tail to determine the downwash variation for a jet-flap configuration operating at very high lift coefficients.

SYMBOLS

The longitudinal data are referred to the stability-axis system and the lateral data are referred to the body-axis system. (See fig. 1.) The origin of the axes was located to correspond to the center-of-gravity position (0.40 mean aerodynamic chord) shown in figure 2.

Measurements and calculations were made in U.S. Customary Units and are presented in both the International System of Units (SI) and U.S. Customary Units. Equivalent dimensions were determined by using the conversion factors given in reference 3.

b	wing span, meters (feet)
C_D	drag coefficient, F_D/qS
C_L	lift coefficient, F_L/qS
C_l	rolling-moment coefficient, M_X/qSb
$C_{l_\beta} = \frac{\partial C_l}{\partial \beta}$, per degree	
C_m	pitching-moment coefficient, $M_Y/qS\bar{c}$
C_n	yawing-moment coefficient, M_Z/qSb
$C_{n_\beta} = \frac{\partial C_n}{\partial \beta}$, per degree	
C_Y	side-force coefficient, F_Y/qS
$C_{Y_\beta} = \frac{\partial C_Y}{\partial \beta}$, per degree	
C_μ	engine gross-thrust coefficient, $\dot{m}V_E/qS$
$C_{\mu,a}$	aileron blowing jet momentum coefficient, R/qS
$C_{\mu,e}$	elevator blowing jet momentum coefficient, R/qS
$C_{\mu,r}$	rudder blowing jet momentum coefficient, R/qS
$C_{\mu,le}$	wing semispan leading-edge blowing jet momentum coefficient, R/qS
$C_{\mu,le,L}$	wing semispan leading-edge blowing jet momentum coefficient, left wing only, R/qS
c	local chord, meters (feet)
$\bar{c}$	mean aerodynamic chord, meters (feet)
F_A	axial force, newtons (pounds)

F_D	drag force, newtons (pounds)
F_L	lift force, newtons (pounds)
F_N	normal force, newtons (pounds)
F_Y	side force, newtons (pounds)
i_t	horizontal-tail incidence angle, degrees
M_X	rolling moment, meter-newtons (foot-pounds)
M_Y	pitching moment, meter-newtons (foot-pounds)
M_Z	yawing moment, meter-newtons (foot-pounds)
$\dot{m}$	engine mass flow rate, kilograms/second (slugs/second)
q	free-stream dynamic pressure, $\rho V^2/2$, newtons/meter^2 (pounds/foot^2)
R	resultant force, newtons (pounds)
S	wing area, meters^2 (feet^2)
T	thrust, newtons (pounds)
V	free-stream velocity, meters/second (feet/second)
V_E	engine exit velocity, meters/second (feet/second)
X,Y,Z	body reference axes
x,y	flap coordinates, meters (feet)
X_S,Y_S,Z_S	stability reference axes
z	tail height (measured from top of fuselage to horizontal tail), meters (feet)
α	angle of attack, degrees

β angle of sideslip, degrees

δ_e elevator deflection, positive when trailing edge is down, degrees

δ_f deflection of rear element of trailing-edge flap (same as δ_{f3} in fig. 2(b)), positive when trailing edge is down, degrees

$\delta_{f,le}$ leading-edge flap deflection, positive when leading edge is down, degrees

δ_j jet deflection, degrees

δ_r rudder deflection, positive when trailing edge is left, degrees

δ_s spoiler deflection, positive when trailing edge is up, degrees

ϵ downwash angle measured with respect to free stream, degrees

η flap static turning efficiency, $\frac{\sqrt{F_A^2 + F_N^2}}{T}$

ρ air density, kilograms/meter^3 (slugs/foot^3)

$1 - \frac{\partial \epsilon}{\partial \alpha}$ downwash factor

Subscripts:

L left wing

R right wing

MODEL AND APPARATUS

The investigation was conducted on the four-engine high-wing jet transport model illustrated by the three-view drawing of figure 2(a). Additional dimensional characteristics of the model are given in table I. The model was basically the same as that used in reference 2 with the exception that the wing was equipped with full-span triple-slotted flaps shown in figure 2(b). The flaps were divided into three spanwise segments on each wing semispan as indicated in figure 2(a). All three segments were deflected as a unit

(a full-semispan flap), except where otherwise specified. Coordinates for each flap element are given in table II in terms of local wing chord. The basic leading-edge flaps are illustrated in figure 2(c). These leading-edge flaps were used in all tests unless otherwise specified. Additional leading-edge high-lift devices, used in specific tests to determine their effectiveness, are shown in figure 2(d). Details of engine jet exhaust deflectors used in some tests are shown in figure 2(e). These exhaust deflectors were used only in tests to determine static exhaust turning effectiveness and were not used in any wind-on tests. The model was equipped with a conventional spoiler located on the wing and also with a small-chord spoiler located on the flap (see figs. 2(a) and 2(b)). Except where specifically noted, the wing and flap spoilers were used simultaneously. In some cases the spoilers covered the full semispan and in others they were only outboard spoilers having the same span as the outer segment of the flap. Photographs of the model mounted for static force tests in the Langley full-scale tunnel are presented as figure 3.

To facilitate model configuration changes and to insure accurate flap deflection angles, the wing of the model was designed with removable trailing edges. To convert the model from the clean configuration to each of the flap-deflected configurations, the clean trailing edges were replaced with trailing-edge flaps constructed with fixed gaps, overlaps, and deflection angles. Figure 2(b) shows the two basic flap systems used: one, designated as the "take-off flap," had deflections of $17^{\circ}/0.5^{\circ}/35^{\circ}$ and the other, designated as the "landing flap," had deflections of $25^{\circ}/10^{\circ}/50^{\circ}$. In addition, the landing flap was constructed so that the rear flap element could be deflected to other angles and locked in position for flap control studies. In the remainder of the discussion and in all the data figures, only the deflection of the rear flap element is used for identification purposes. The leading-edge flaps were designed so that they could be fastened to the wing leading edge at fixed positions.

The model engines represented high-bypass-ratio turbofans and were installed at -3° incidence so that for the basic condition the jet exhaust impinged directly on the trailing-edge flap system. The engine turbines were driven by compressed air and turned fans which produced the desired thrust. The inboard engines were fixed along the wing at 22.0 percent semispan but the outboard engines were tested at two wing spanwise locations: 30.4 percent semispan in a clustered-engine arrangement and 41.7 percent semispan in a spread-engine arrangement.

All the model control surfaces (elevator, aileron, and rudder) were equipped with blowing. The blowing system consisted of a simple tube arrangement located at the rear of the surfaces and just in front of the controls. Compressed air was supplied to the tubes internally and forced over the surface through a series of small holes spaced equally along the tube. The holes were quite small (0.051 cm (0.020 in.) in diameter)

and far apart (0.635 cm (0.250 in.)) so that it was not an efficient boundary-layer control system. This system was used on all surfaces and is illustrated in the horizontal- and vertical-tail cross sections shown in figure 2(a). "Aileron" blowing consisted of blowing over only the outboard segment of the flaps from the fixed part of the wing as illustrated in figure 2(b). The leading-edge blowing system, shown in figure 2(d), was generally similar in construction to the systems used on the control surfaces. A tube was inserted in the wing leading edge and compressed air was supplied through the tube, from which it exhausted through many small holes into the leading-edge plenum chamber and from there through the leading-edge slot.

The tests were made in the 9.1- by 18.3-meter (30- by 60-foot) open-throat test section of the Langley full-scale tunnel with the model mounted about 3.05 m (10 ft) above the ground board. The model was so small in proportion to the tunnel test section that no wind-tunnel wall corrections were needed or applied. Corrections for flow angularity were applied. All the tests were made with an internal strain-gage balance and conventional sting which entered the rear of the fuselage, as can be seen in figure 3.

TESTS AND PROCEDURES

In preparation for the tests, engine calibrations were made to determine gross thrust as a function of engine rotational speed, in rpm, in the static condition – at zero angle of attack with the thrust deflectors off. The tests were then made by setting the engine speed to give the desired thrust and holding these settings constant through the ranges of angles of attack or sideslip.

Tests of the model were made to investigate mainly the following characteristics:

1. Longitudinal
   - (a) Basic lift and drag characteristics of model with tail off
   - (b) Stability and trim characteristics of model with tail on
   - (c) Downwash characteristics at the tail
   - (d) Effect of deflection of wing spoiler and rear flap element on lift and drag for possible use in direct lift and automatic speed controls
2. Lateral
   - (a) Lateral static stability and control characteristics of model with symmetric thrust
   - (b) Asymmetry with one engine out (inoperative) for model with outboard engine out or inboard engine out

(c) Control of engine-out asymmetry by means of differential deflection of the rear flap element (both partial span and full semispan) or spoiler and blowing on the outboard flap segment – with particular study of the effect of asymmetric leading-edge blowing in reducing the roll-off at the stall

An index of the data figures is given in table III for the longitudinal tests and in table IV for the lateral tests.

Jet deflection angles and flap turning efficiency were determined from measurements of normal and axial forces made in the static thrust condition with flaps deflected. The static thrust used in computing turning efficiency was taken directly from the engine calibrations at the appropriate rpm.

During the tests, six-component longitudinal and lateral static-force data were measured at several flap deflections for a range of engine gross-thrust coefficient C_{μ} (total of all engines) from 0 to 3.74 and through an angle-of-attack range from about -5° to 35°. Tests were made at various incidences of the horizontal tail, at various deflections of the spoiler, rudder, and elevator, and for various amounts of blowing over each of the control surfaces and the wing leading edge. The mass flow rates for each of the blown surfaces were evaluated by measuring the force produced by the respective jets in the wind-off condition. Sideslip tests were made over a range of sideslip angles from -20° to 20°. All wind-on tests were made at a free-stream dynamic pressure of approximately 144 N/m^2 (3 lb/ft^2) which corresponds to a velocity of 15.4 m/sec (50 ft/sec) and to a Reynolds number (based on the mean aerodynamic chord) of 0.35×10^6.

In addition to the force tests, a few flow survey measurements were made in the vicinity of the horizontal tail to determine the downwash variation with changes in thrust coefficient. The measurements were made with a simple balsa-wood vane which was free to pivot for alinement with the local flow. The flow angle was recorded through a potentiometer electrical circuit arrangement.

RESULTS AND DISCUSSION

Lift Characteristics

In the investigation reported in reference 2 it was determined that the use of exhaust deflectors on the engines produced little effect on the aerodynamic characteristics of the model when the engines were clustered and mounted in a close-inboard position along the span. In the present investigation, which was conducted on basically the same model as that used in reference 2 except that the original double-slotted

partial-span flap was replaced with a full-span triple-slotted flap, only a very limited number of tests were made with deflectors on. The results of these tests are presented in figure 4 in terms of the ratio of normal force to thrust F_N/T plotted against the ratio of axial force to thrust F_A/T. These results generally confirmed the fact that the turning efficiency was not significantly altered by the addition of the deflectors from that with the deflectors off. On this basis, and on the basis of a few preliminary wind-on tests, the present investigation was conducted with deflectors off. In the latter part of the test program, the engines were tested in the spread position without deflectors. Data from subsequent static tests and from reference 1 both indicate, however, that deflectors improved the wind-on aerodynamic efficiency for the spread-engine arrangement.

Basic longitudinal data for the model with tail surfaces removed are presented for flap deflections of 60°, 50°, and 35° in figures 5 to 8 for the clustered-engine arrangement and for flap deflections of 60°, 40°, 35°, and 0° in figures 9 to 16 for the spread-engine arrangement. The 0.25c leading-edge flaps were extended for all test conditions except where noted, and leading-edge blowing was used in most of the tests. These figures show that the stall angle and the maximum lift coefficient increased with increasing thrust coefficient and that the effects of power on the lift characteristics were more pronounced at the high flap deflections. The effects of leading-edge blowing are summarized in figure 6 for the clustered-engine case and, as expected, the stall angle of attack and maximum lift coefficient increased with increases in leading-edge blowing, particularly for the power-off and low thrust conditions. Maximum lift coefficients of about 9 (untrimmed) could be produced for a gross-thrust coefficient of 3.74. Because of the rearward location of the flap loads, the nose-down pitching moments are large at high lift. If the required trimming moment is to be generated by a downward force on the tail, the net lift available to the airplane would, of course, be less than that indicated by the untrimmed data. Presented in figures 13 to 16 are data obtained with several wing leading-edge devices installed. These tests were conducted mainly to determine whether leading-edge blowing could be used in place of the large-chord leading-edge flap or if some smaller leading-edge device could be used to produce the desired results. The results of these tests showed, in general, that some type of leading-edge high-lift device would be required even with leading-edge blowing, that the leading-edge droop was not adequate, but that the chord of the leading-edge flap (when the flap is used in conjunction with leading-edge blowing) could be reduced considerably from that used in the basic tests.

In order to provide a direct indication of the relative performance of the spread- and clustered-engine arrangements, drag polars of the data are presented in figures 17 and 18. The data of figure 17(a) show that at the lower thrust setting the spread-engine arrangement was more aerodynamically efficient but, at the higher thrust setting, there

was very little difference in the performance for the two engine arrangements. Figures 17(b) and 17(c) show that, as expected, leading-edge blowing was effective for improving the performance of either configuration and also provided increases in maximum lift coefficient. The data of figure 17(d) show that blowing over the ailerons (or outer one-third of the flap) was also effective for increasing the performance. Figure 18 shows a comparison of drag polars for the model as tested in references 1 and 2 and in the present investigation. In reference 1 the model had double-slotted partial-span flaps, and the engines were spread out and equipped with deflectors. In reference 2 the engines were clustered and the ailerons were drooped to extend the flap span to the wing tip. The data for the model of the present investigation are for the spread-engine arrangement and full-span triple-slotted flaps. The data are not exactly comparable because a sheet-metal flap extension used during the tests of references 1 and 2 resulted in the actual flap deflection being considerably higher than the nominal value of 60°. By comparing polars, however, it was hoped that a comparison of relative efficiency might be obtained although the comparison of maximum lift values would be distorted. Although there are such differences in the model details that the direct effect of flap geometry is difficult to evaluate from this figure, it can be seen that there are no large differences in the relative performance of the various arrangements listed. Also, the differences shown for the lower thrust coefficient are not consistent with those shown for the higher thrust coefficient. For example, at a C_{μ} of 1.87 the model of reference 1 showed the better performance whereas, at a C_{μ} of 3.74 the model of the present investigation showed the better performance. The higher maximum lift coefficient for the reference 1 data might be attributed to a larger leading-edge flap used on the model in that study.

Longitudinal Stability and Control, With Symmetric Thrust

Presented in figure 19 is the variation with thrust coefficient of wing-flap center-of-pressure and wing-body aerodynamic-center location determined from the tail-off data; similar data from references 1 and 2 are shown for comparison. This plot shows that the partial-span flap arrangement of reference 1 had a more forward flap center-of-pressure and aerodynamic-center location than the full-span flap arrangements of reference 2 and of the present study. In all cases the center of pressure moved rearward with increases in thrust and the aerodynamic center moved forward with increases in thrust through the low-thrust range and then began to move rearward with further increases in thrust.

The longitudinal stability and trim characteristics of the model with tail on are plotted in figures 20 to 28 for the clustered-engine arrangement and in figures 29 to 31 for the spread-engine arrangement. These data show, in general, that the model with flap down was longitudinally stable up to the stall and could be trimmed in pitch up to the

highest thrust settings by the application of blowing to the horizontal tail used in the tests. The utilization of blowing on the tail was not meant to imply that blowing would be needed in full-scale operation but was intended to give lift on the model tail which would be representative of a full-scale tail with a slotted elevator (a maximum C_L of 2.5 would be expected). The longitudinal instability indicated in figures 22 and 23 is a result of tail stall caused by improper tail geometry for the particular tests involved. For example, for the data in figure 23 the chord of the tail leading-edge flap was reduced to one-half its original length and this change caused the tail to be ineffective at the high thrust settings. The original tail leading-edge flap was used for all the remaining tests.

Figures 24, 25, and 26 show the effect of changing the rear flap element to higher and lower settings for possible use in glide-path control. Similar data are presented in figure 27 in which the flap element was deflected symmetrically for only the outer flap span. The data of figure 28 show the effect of symmetric spoiler deflection for possible use in glide-path control. In the tests of figure 28(e) the projecting slot lip was removed to enlarge the slot of the inboard and center flap segments. A comparison of the data of figure 28 with data of figure 20(a) shows that a symmetric spoiler deflection of 30° produced decremental lift coefficients of about 1.0 at the higher thrust settings.

A comparison of the spread-engine data of figures 29 to 31 with the clustered-engine data of figures 20 to 28 shows no major differences in longitudinal stability and trim characteristics for the two engine arrangements. A summary of the pitching-moment characteristics from these data and the data from references 1 and 2 (see fig. 32) shows that the static stability and trim characteristics for the model of the present investigation were generally similar to those for the models of references 1 and 2, but the trim requirements were greater.

The results of flow surveys to measure the downwash characteristics in the vicinity of the horizontal tail are presented in figures 33 and 34 for the clustered-engine arrangement and in figures 35 and 36 for the spread-engine arrangement. These data are summarized in figure 37 in terms of the downwash factor $\left(1 - \frac{\partial \epsilon}{\partial \alpha}\right)$ plotted against thrust coefficient C_μ for tests with and without leading-edge blowing. Figure 37 shows that the horizontal-tail effectiveness generally decreased with increasing engine thrust. The use of leading-edge blowing resulted in an increase in horizontal-tail effectiveness for the spread-engine arrangement but generally produced adverse effects for the clustered-engine arrangement.

Lateral Stability

A few tests were made to determine the variation of the lateral aerodynamic coefficients with angle of sideslip. These tests were made with power off and power on and

for both symmetric and asymmetric power conditions. The data, which are presented in figure 38, show that the aerodynamic coefficients varied fairly linearly with sideslip; hence, the remainder of the lateral stability studies were made in terms of sideslip derivatives determined from tests at $\pm 5^{\circ}$ sideslip.

Plots of the static lateral stability derivatives against angle of attack are presented in figures 39 to 46 for various model configurations and thrust levels, with and without leading-edge blowing. These plots show that in all tail-on configurations (figs. 40, 42, and 44 to 46) the model has directional stability $\left(+C_{n_\beta}\right)$ and positive effective dihedral $\left(-C_{l_\beta}\right)$ through most of the angle-of-attack range up to the stall. The directional stability is virtually unaffected by change in angle of attack; effective dihedral, however, increases with increasing angle of attack up to the stall. In all tail-on configurations, the application of thrust produced notable increases in directional stability throughout the angle-of-attack range. At angles of attack near the power-off stall angle, thrust also produced large increments in effective dihedral. Leading-edge blowing, which like thrust is effective in delaying stall, markedly increases the effective dihedral near the power-off stall angle of attack.

The spanwise distribution of the thrust appears to have very little effect on directional stability or effective dihedral. Engine-out static stability data, presented in figures 41 (tail off) and 42 (tail on), are very similar to those for the corresponding all-engine cases presented in figures 39(b) and 40(b), respectively. Likewise, leading-edge-blowing data for the clustered-engine arrangement (fig. 40(b), for instance) are similar to those for the spread-engine arrangement (fig. 45(a)). Spanwise discontinuity in flap deflection has no noticeable effect on the stability derivatives, as is shown by a comparison of figure 45(b) with figure 46.

Basic Asymmetric Moments (Engine Inoperative)

Lateral characteristics obtained for the model with one engine inoperative are presented in figures 47 to 50 for the clustered-engine arrangement and in figures 51 to 53 for the spread-engine arrangement. Because in a powered-lift system a loss of an engine results in loss of lift, plots of the lateral characteristics with one engine out are accompanied by plots of the corresponding longitudinal characteristics.

The data of figures 47 to 50 show that large rolling moments accompany an engine-out condition. As the angle of attack increased, the rolling moments generally increased because the engine-out wing tended to stall first. Comparison of the corresponding lift data and the four-engine lift data shows that large losses in lift occur with an engine failure. Lower flap angle produced the expected reduction in engine-out rolling moments but increased the engine-out yawing moments.

Lateral Control, With Asymmetric Thrust

In reference 2 it was shown that the use of either asymmetric blowing over the ailerons or differential flap deflection offered a means of achieving roll trim under engine-out conditions. One of the problems noted in reference 2, however, was that the engine-out wing tended to stall first as angle of attack was increased and thus resulted in large roll asymmetries at the stall. In the present investigation these two methods of roll trim were studied in combination with leading-edge blowing as a possible means of controlling the stall angle of attack and relieving the asymmetric roll problem.

Clustered engines.- Tests were run with either the left outboard or the left inboard engine not operating. Since the left outboard engine was found to be the more critical, most of the engine-out tests were made for this condition. The results of tests for the clustered-engine arragement with an engine out are presented in figures 54 to 69.

Data for the model with differential flap deflection used for roll trim are presented in figures 54 to 58 for several nominal trim flap deflections. Some of the more important results shown by these data are that without leading-edge blowing there were large rolling asymmetries at the stall (see fig. 54) but that the use of leading-edge blowing on the engine-out wing relieved the asymmetric stall condition and therefore relieved the roll asymmetry (see fig. 55). Comparison of the corresponding lift data shows that higher lift coefficients were achieved with leading-edge blowing and that stall was more gradual and occurred at a higher angle of attack. For none of the configurations tested was complete roll trim achieved over the entire angle-of-attack range with the outboard engine out and at the highest value of C_μ $\left(C_\mu = 2.81\right)$. In many tests, however, the model was almost completely trimmed in roll, and a very small amount of additional differential flap deflection, or spoiler deflection, would be expected to give complete trim.

Presented in figures 59 to 62 are results of engine-out tests of the model with only the inboard one-third of the flap deflected differentially. A general inspection of the data gives the impression that the inboard flap segment was just as effective for roll trim as was the full flap span, and the only direct comparison that can be made (figs. 55(c) and 59(c)) indicates that the inboard flap segment was slightly more effective.

Presented in figures 63 to 69 are data for the engine-out condition with symmetric flap deflection and with various combinations of asymmetric leading-edge and aileron blowing and wing-tip spoiler deflection. In these tests complete roll trim was not achieved for the 60° flap deflection for the higher thrust range.

Spread engines.- The results of tests with an engine out and differential flap deflection for roll trim are presented in figures 70 to 75 for the spread-engine arrangement. Figures 70 to 73 show the effect of differential deflection of several different spanwise

segments of the flap; these data indicate that, because of the larger engine-out moments for the spread-engine arragement, the flaps alone were not as effective for providing roll trim as they were for the clustered-engine arrangement. Also, unlike the clustered-engine arrangement, full-semispan flap deflection for the spread-engine arrangement appeared to be more effective for roll trim than individual deflection of any one of the spanwise segments. This result suggests, as might be expected, that the spanwise flap loads for the spread-engine arrangement extended much farther outboard than for the clustered-engine arrangement. The data of figure 74 show that the use of leading-edge and aileron blowing in combination with differential flap deflection more than trimmed the engine-out rolling moment at low angles of attack but, at the higher angles of attack, roll trim was not achieved at the higher thrust levels.

Presented in figures 76 to 78 are the results of tests for the model with an engine out and symmetric flap deflection, with aileron blowing and spoiler deflection used for control. These figures show that for these conditions additional control would be required for roll trim, possibly in the form of differential aileron deflection in combination with increased aileron blowing or spoiler control.

Lateral Control, With Symmetric Thrust

Presented in figures 79 to 83 are the results of tests with the spoiler deflected for roll control. Comparisons of the data of figures 79(a) and 79(c) show that leading-edge blowing increased the spoiler effectiveness and resulted in the spoiler remaining effective to a higher angle of attack. The use of a small-chord flap spoiler in combination with the wing spoiler did not increase the effectiveness of the spoiler system. (Compare figs. 79 and 80.) The use of only the outer one-third of the wing spoiler (fig. 81) produced average rolling-moment coefficients of about 0.05, and increases in engine thrust generally produced much smaller increases in spoiler effectiveness than for the full-span spoiler. Maximum values of rolling-moment coefficient for the full-span spoiler were about 0.23 for the 60° flap angle.

Presented in figures 84 to 86 are the results of rudder tests for several test conditions. The data of figure 86 show that the rudder effectiveness was increased by the use of boundary-layer control on the rudder surface up to values of C_n of about 0.23 for a $C_{\mu,r}$ of about 0.038. This value of C_n is great enough to trim the greatest yawing moments encountered in engine-out conditions, even with corrective roll control applied.

Presented in figure 87 are the results of tests with the inboard trailing-edge flap segments deflected differentially as ailerons for roll control for the cruise condition (trailing-edge flap deflection of 0°). These tests show that the control effectiveness of these flap segments is greatly increased by engine power. At $C_{\mu} = 0$, which most

closely approximates a cruise thrust setting, however, the rolling moment per degree of deflection of the inboard flap segments is only about one-half that provided by the conventional ailerons of a similar jet transport configuration, as reported in reference 4.

SUMMARY OF RESULTS

From a wind-tunnel investigation of an external-flow jet-flap transport configuration having inboard pod-mounted engines and full-span triple-slotted flaps, the following results were obtained:

1. The use of full-span triple-slotted flaps appeared to offer little improvement in aerodynamic performance over the more conventional double-slotted partial-span flaps. In either case, however, it is necessary that the flap chords be large enough to achieve good spreading and turning of the engine exhaust.

2. Wing leading-edge boundary-layer control provided increases in maximum lift coefficient, stall angle of attack, and overall aerodynamic performance at the higher lift associated with external-flow jet-flap operation.

3. The location of pod-mounted engines close inboard in a clustered arrangement resulted in smaller engine-out rolling moments than for the spread-engine arrangement, without appreciably altering the overall aerodynamic performance.

4. The use of asymmetric blowing over the wing leading edge relieved the large roll asymmetries that occurred when the wing with an engine inoperative stalled first.

5. The combination of asymmetric leading-edge blowing with differential flap deflection offered an effective means for trimming the engine-out rolling moments over the normal operational angle-of-attack range, including the stall.

6. For the clustered-engine arrangement, the inboard one-third of the flap span was found to be about as effective for roll trim as the full flap span.

Langley Research Center,
National Aeronautics and Space Administration,
Hampton, Va., July 14, 1971.

REFERENCES

1. Parlett, Lysle P.; Freeman, Delma C., Jr.; and Smith, Charles C., Jr.: Wind-Tunnel Investigation of a Jet Transport Airplane Configuration With High Thrust-Weight Ratio and an External-Flow Jet Flap. NASA TN D-6058, 1970.

2. Freeman, Delma C., Jr.; Parlett, Lysle P.; and Henderson, Robert L.: Wind-Tunnel Investigation of a Jet Transport Airplane Configuration With an External-Flow Jet Flap and Inboard Pod-Mounted Engines. NASA TN D-7004, 1970.

3. Mechtly, E. A.: The International Systems of Units – Physical Constants and Conversion Factors (Revised). NASA SP-7012, 1969.

4. Parlett, Lysle P.; Fink, Marvin P.; and Freeman, Delma C., Jr. (With appendix B by Marion O. McKinney and Joseph L. Johnson, Jr.): Wind-Tunnel Investigation of a Large Jet Transport Model Equipped With an External-Flow Jet Flap. NASA TN D-4928, 1968.

TABLE I.- DIMENSIONS OF MODEL

Wing:		
Area, m^2 (ft^2)	0.783	(8.43)
Span (to theoretical tip), cm (in.)	238.02	(93.71)
Aspect ratio	7.23	
Length of mean aerodynamic chord, cm (in.)	35.79	(14.09)
Location of quarter chord of mean aerodynamic chord, referenced to nose of model, cm (in.)	103.53	(40.76)
Spanwise station of mean aerodynamic chord, cm (in.)	50.32	(19.81)
Root chord, cm (in.)	49.50	(19.49)
Tip chord (theoretical tip), cm (in.)	16.62	(6.54)
Sweep of quarter-chord line, deg	27.50	
Dihedral of quarter-chord line, deg	-3.50	
Incidence of mean aerodynamic chord, deg	4.50	
Incidence of root chord, deg	6.00	
Geometric twist:		
Root, deg	0.0	
Tip, deg	-3.5	
Vertical tail:		
Area, m^2 (ft^2)	0.155	(1.67)
Span, cm (in.)	50.80	(20.00)
Aspect ratio	1.66	
Sweep angles:		
Leading edge, deg	38	
Trailing edge, deg	31	
Root chord, cm (in.)	35.56	(14.00)
Tip chord, cm (in.)	25.78	(10.15)
Horizontal tail:		
Area, m^2 (ft^2)	0.268	(2.88)
Span, cm (in.)	118.77	(46.76)
Length of mean aerodynamic chord, cm (in.)	24.18	(9.52)
Incidence	Variable	
Engines:		
Spanwise location of inboard engines, cm (in.)	26.59	(10.47)
Spanwise locations of outboard engines, cm (in.)	36.75	(14.47)
	50.77	(19.99)
Incidence of all engine center lines relative to X-axis, deg	-3.00	

TABLE I.- DIMENSIONS OF MODEL – Concluded

Moment reference:		
Longitudinal location, referenced to nose of model, cm (in.)	108.81	(42.84)
Vertical location, referenced to top of fuselage at wing, cm (in.)	12.49	(4.92)
Control-surface dimensions:		
Rudder:		
Span, cm (in.)	40.6	(16.0)
Chord, upper end, parallel to X-axis, cm (in.)	10.92	(4.30)
Chord, lower end, perpendicular to hinge line, cm (in.)	15.2	(6.0)
Hinge-line location, percent chord	57	
Sweep of hinge line, deg	34	
Elevator:		
Span, cm (in.)	43.99	(17.31)
Chord, outboard, cm (in.)	4.21	(1.66)
Chord, inboard, cm (in.)	8.40	(3.31)
Hinge-line location, percent chord	73	
Sweep of hinge line, deg	16.5	

TABLE II.- FLAP COORDINATES

[Coordinates are given as percent of local wing chord]

First Element			Second Element			Third Element		
x	y_{upper}	y_{lower}	x	y_{upper}	y_{lower}	x	y_{upper}	y_{lower}
0.00	1.67	1.67	0.00	0.94	0.94	0.00	0.72	0.72
1.39	4.33	.11	.94	2.39	.11	.72	2.50	.11
2.78	5.67	.00	1.78	2.67	.00	1.83	3.17	.06
4.17	6.44	↓	2.78	2.94	.17	2.78	3.44	.00
5.56	6.83	↓	3.72	3.06	.39	3.72	3.50	↓
6.44	6.83	↓	4.61	2.94	.56	4.44	3.50	↓
8.33	6.67	↓	5.56	2.83	.72	5.56	3.50	↓
9.72	6.28	↓	6.50	2.61	.94	7.39	3.33	↓
11.11	5.94	↓	7.06	2.39	.94	9.28	3.06	↓
12.50	5.56	↓	7.39	2.22	.94	11.11	2.78	.06
13.61	5.11	↓	8.33	1.78	.72	12.94	2.39	.11
15.28	4.61	1.50	9.28	1.27	.56	14.83	2.11	.17
16.67	4.06	2.39	10.17	.72	.28	16.67	1.83	.17
18.06	3.61	3.00	11.00	.11	.00	18.50	1.56	.17
19.17	3.22	3.17				20.39	1.22	.17
						22.22	.83	.11
						24.06	.56	.06
						24.94	.28	.00

TABLE III.- INDEX OF DATA FIGURES FROM LONGITUDINAL TESTS

Type of data	Figure
Static turning efficiency and turning angle of jet exhaust	4
Basic tail-off data:	
Clustered engines	5 to 8
Spread engines	9 to 12
Effect of additional leading-edge devices	13 to 16
Lift-drag polars:	
Effect of engine arrangement and leading-edge or aileron blowing	17
Comparison with previous model configurations	18
Effect of configuration on tail-off center of pressure and aerodynamic center	19
Tail-on stability and control (including direct-lift control):	
Clustered engines:	
Effect of i_t, δ_e, and $C_{\mu,e}$	20 to 23
Effect of flap deflection	24 to 27
Effect of spoiler deflection	28
Spread engines:	
Effect of i_t and $C_{\mu,e}$	29
Effect of flap deflection	30 and 31
Summary of effect of configuration on longitudinal stability	32
Downwash at tail:	
Basic data:	
Clustered engines	33 and 34
Spread engines	35 and 36
Summary of downwash flow surveys $\left(1 - \frac{\partial \epsilon}{\partial \alpha}\right)$	37

TABLE IV.- INDEX OF DATA FIGURES FROM LATERAL STABILITY AND TRIM TESTS

Type of data	Figure
Lateral stability:	
Clustered engines:	
Effect of leading-edge blowing, thrust distribution, tail contribution, and flap deflection	38 to 44
Spread engines:	
Effect of flap deflection	45 and 46
Basic trim problems, engine out:	
Clustered engines:	
Effect of flap deflection, tail contribution, and thrust distribution	47 to 50
Spread engines:	
Effect of flap deflection and thrust distribution	51 to 53
Control of asymmetric thrust condition:	
Clustered engines:	
Differential flap deflection, no leading-edge blowing	54
Differential flap deflection, with blowing	55 to 58
Differential flap deflection (partial span), with leading-edge blowing	59 to 62
Symmetric flap deflection, with asymmetric blowing, and spoiler	63 to 69
Spread engines:	
Differential flap deflection, with asymmetric blowing, and spoiler	70 to 75
Symmetric flap deflection, with asymmetric blowing, and spoiler	76 to 78
Lateral control, symmetric thrust, clustered and spread engines:	
Spoiler, with leading-edge blowing	79 to 83
Rudder, basic and with boundary-layer control	84 to 86
Inboard flap segment as cruise aileron	87

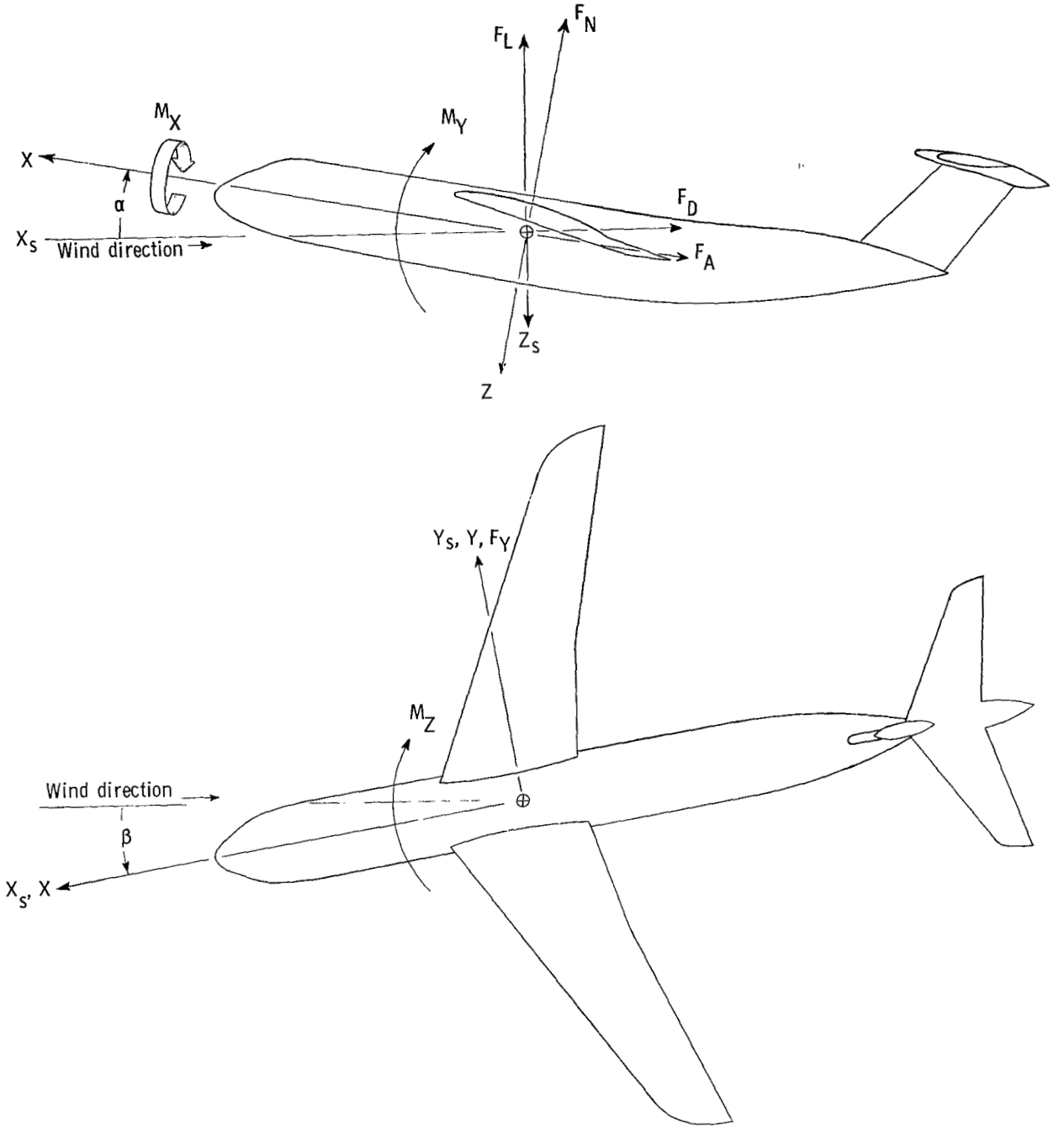

Figure 1.- Axis systems used in presentation of data. Arrows indicate positive direction of forces, moments, axes, and angles.

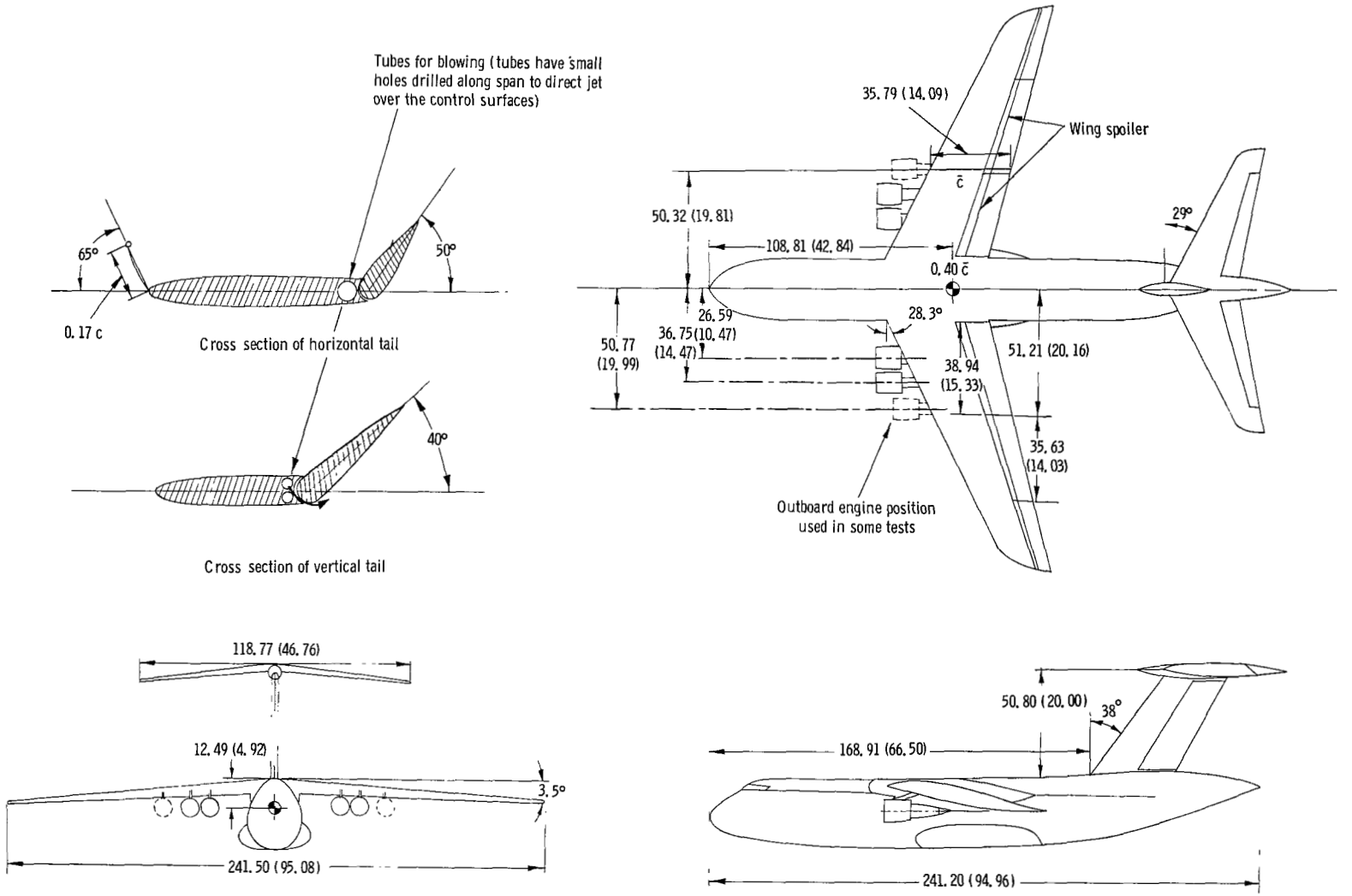

(a) Three-view drawing of complete model.

Figure 2.- Drawings of model used in investigation. All linear dimensions are in centimeters (inches).

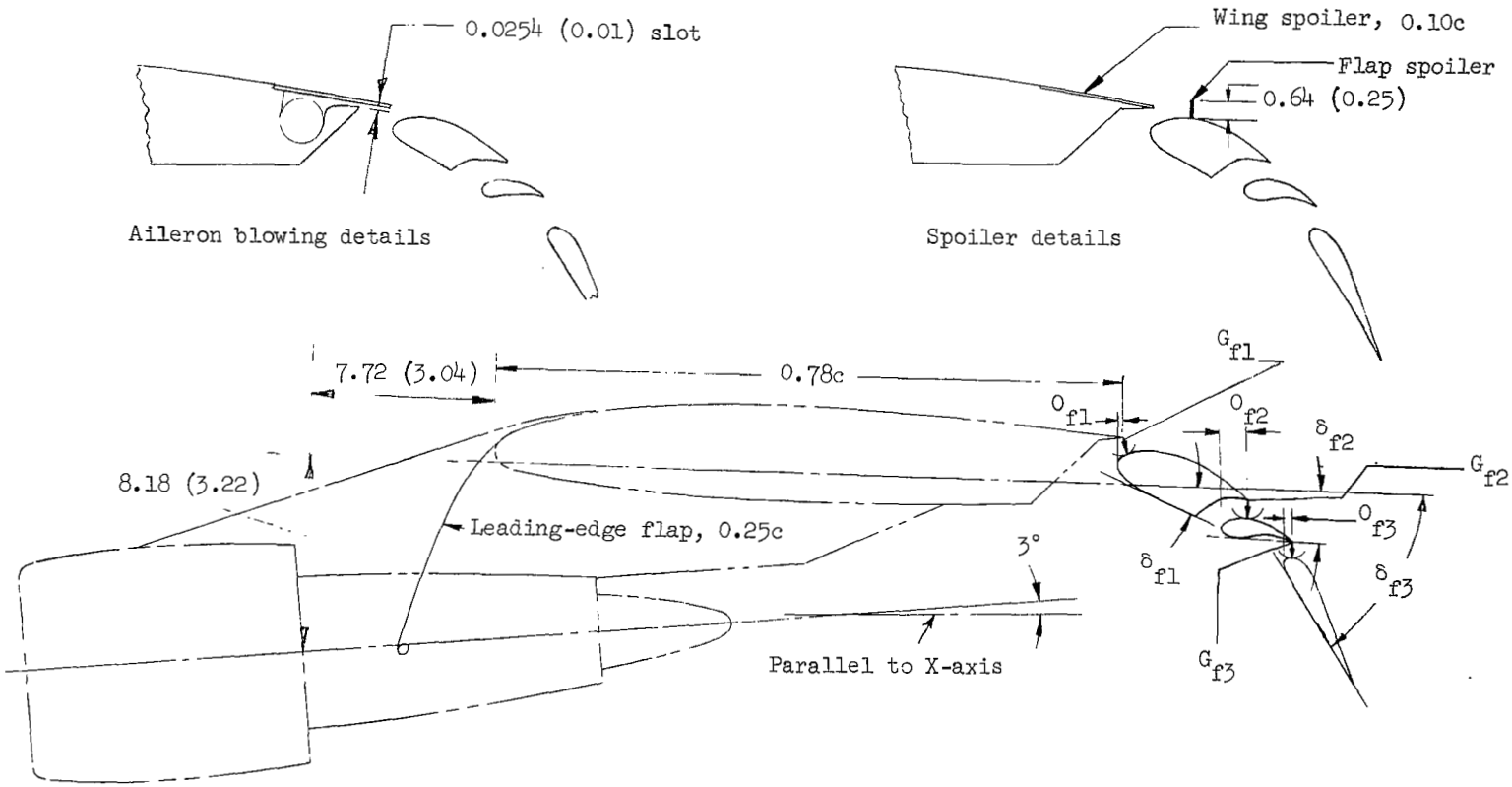

	δ_{f1}, deg	δ_{f2}, deg	δ_{f3}, deg	Overlap 1, O_{f1}, percent c	Gap 1, G_{f1}, percent c	Overlap 2, O_{f2}, percent c	Gap 2, G_{f2}, percent c	Overlap 3, O_{f3}, percent c	Gap 3, G_{f3}, percent c
Take-off	17	0.5	35	1.47	1.61	3.15	1.61	1.52	1.61
Landing	25	10.0	50	1.47	1.61	3.98	1.61	1.39	1.61

(b) Details of flap assembly and engine pylon. See table II for flap coordinates in terms of local wing chord.

Figure 2.- Continued.

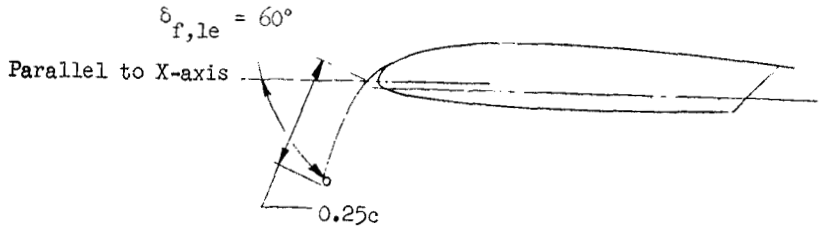

Outboard leading-edge flap

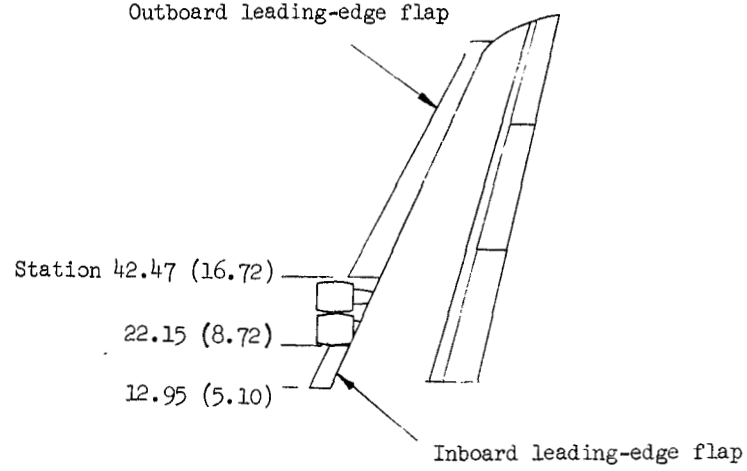

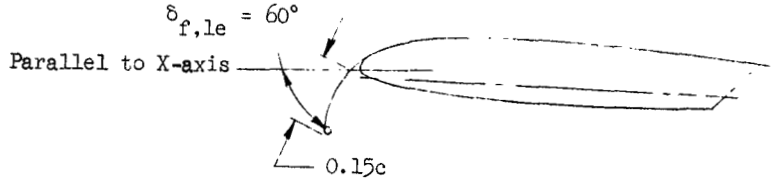

Inboard leading-edge flap

(c) Details of leading-edge flap.

Figure 2.- Continued.

Average slot width = 0.0254 (0.01), full span

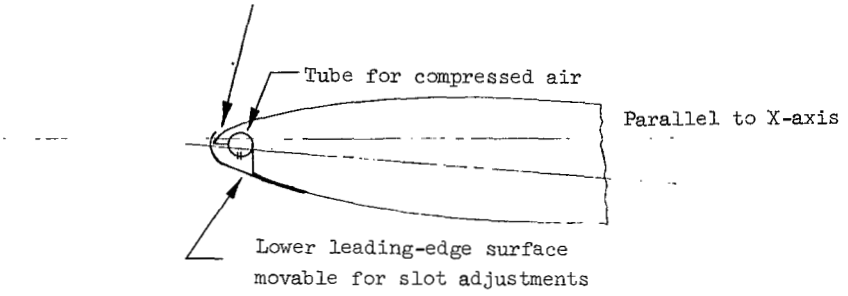

Leading-edge blowing system

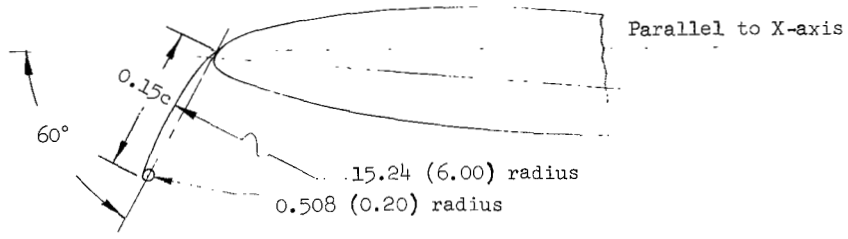

0.15c leading-edge flap

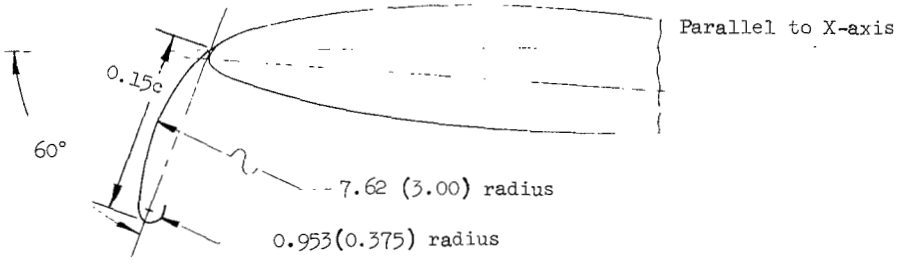

0.15c high-camber leading-edge flap

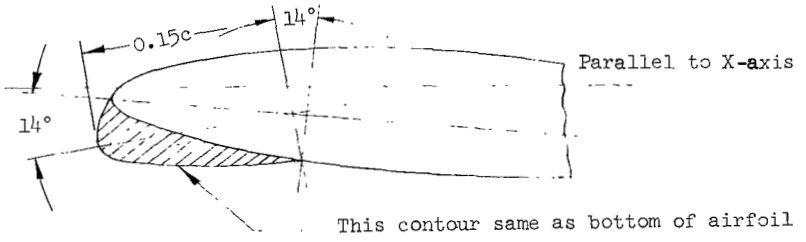

Drooped leading edge

(d) Additional leading-edge devices used in some tests.

Figure 2.- Continued.

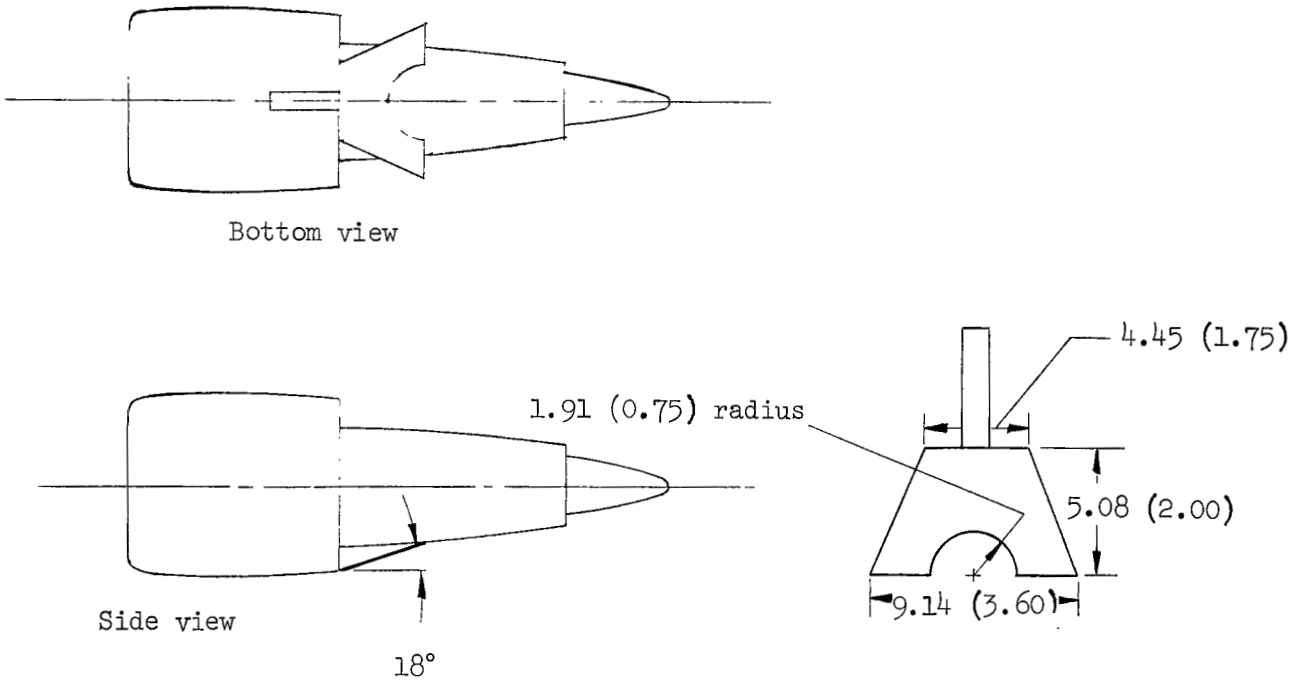

(e) Details of jet exhaust deflector.

Figure 2.- Concluded.

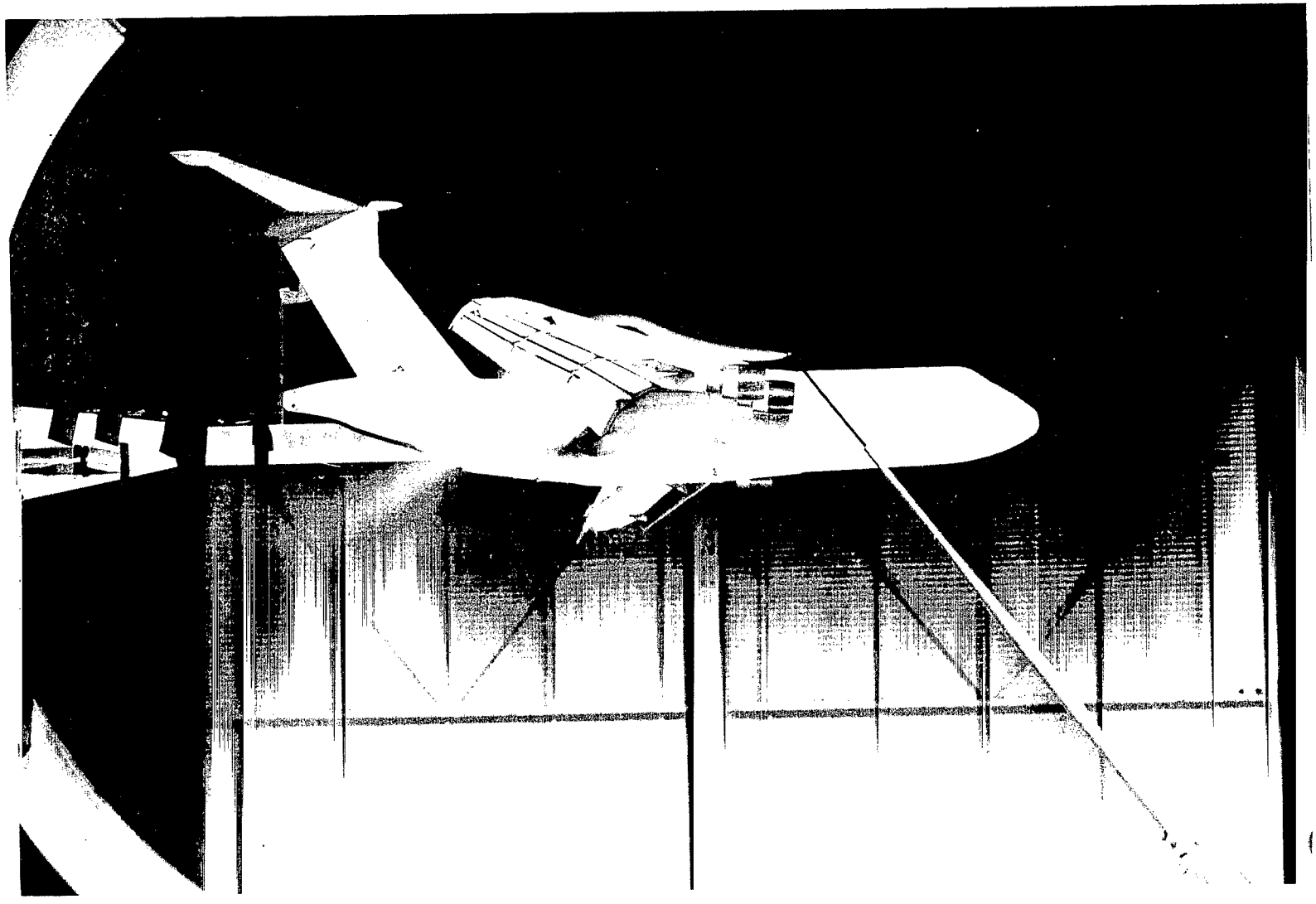

(a) Side view.

L-70-7224

Figure 3.- Photographs of model during smoke-flow studies in Langley full-scale tunnel.

L-70-7223

(b) Three-quarter rear view.

Figure 3.- Concluded.

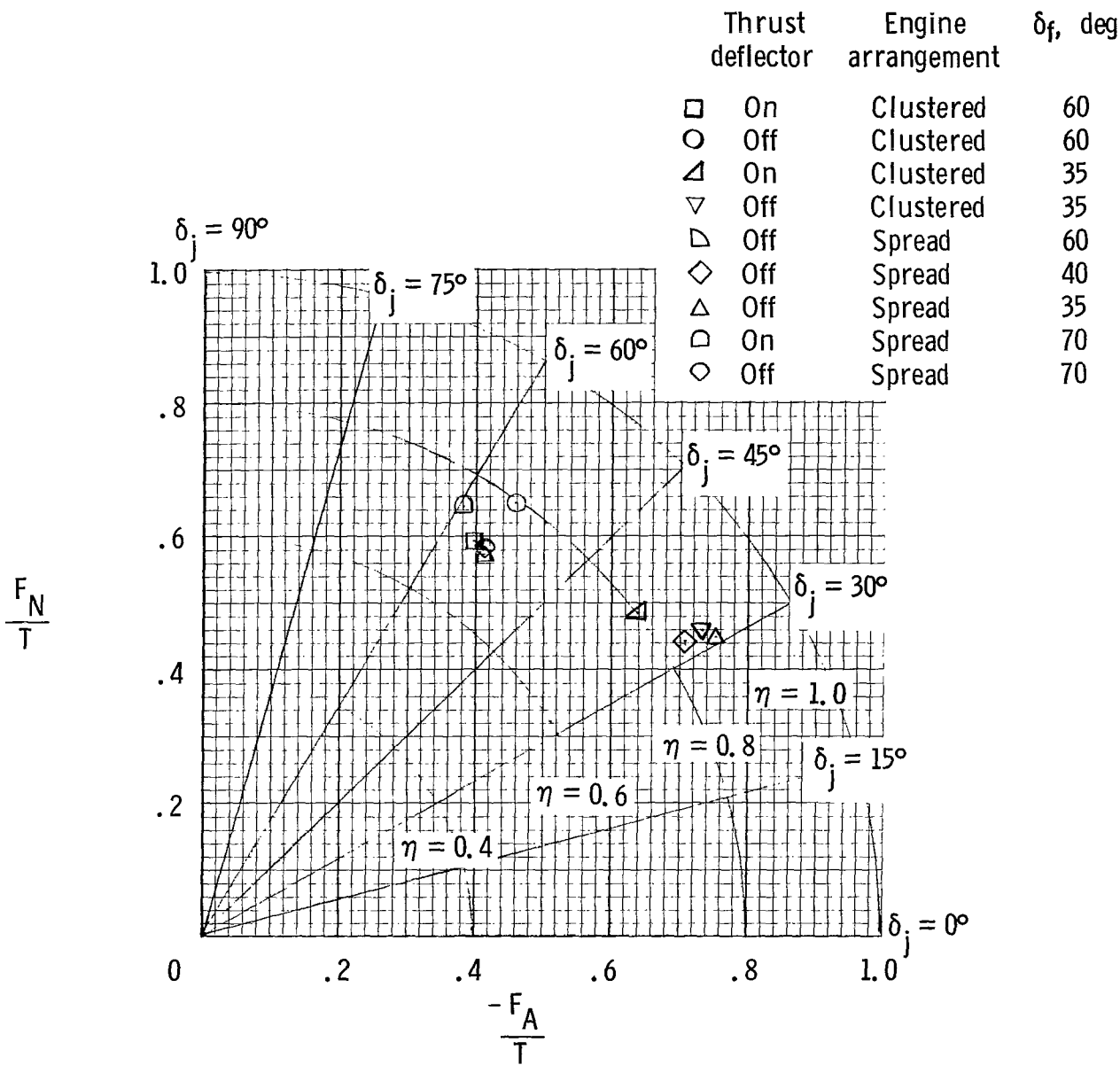

Figure 4.- Summary of static turning efficiency and turning angle of jet exhaust.

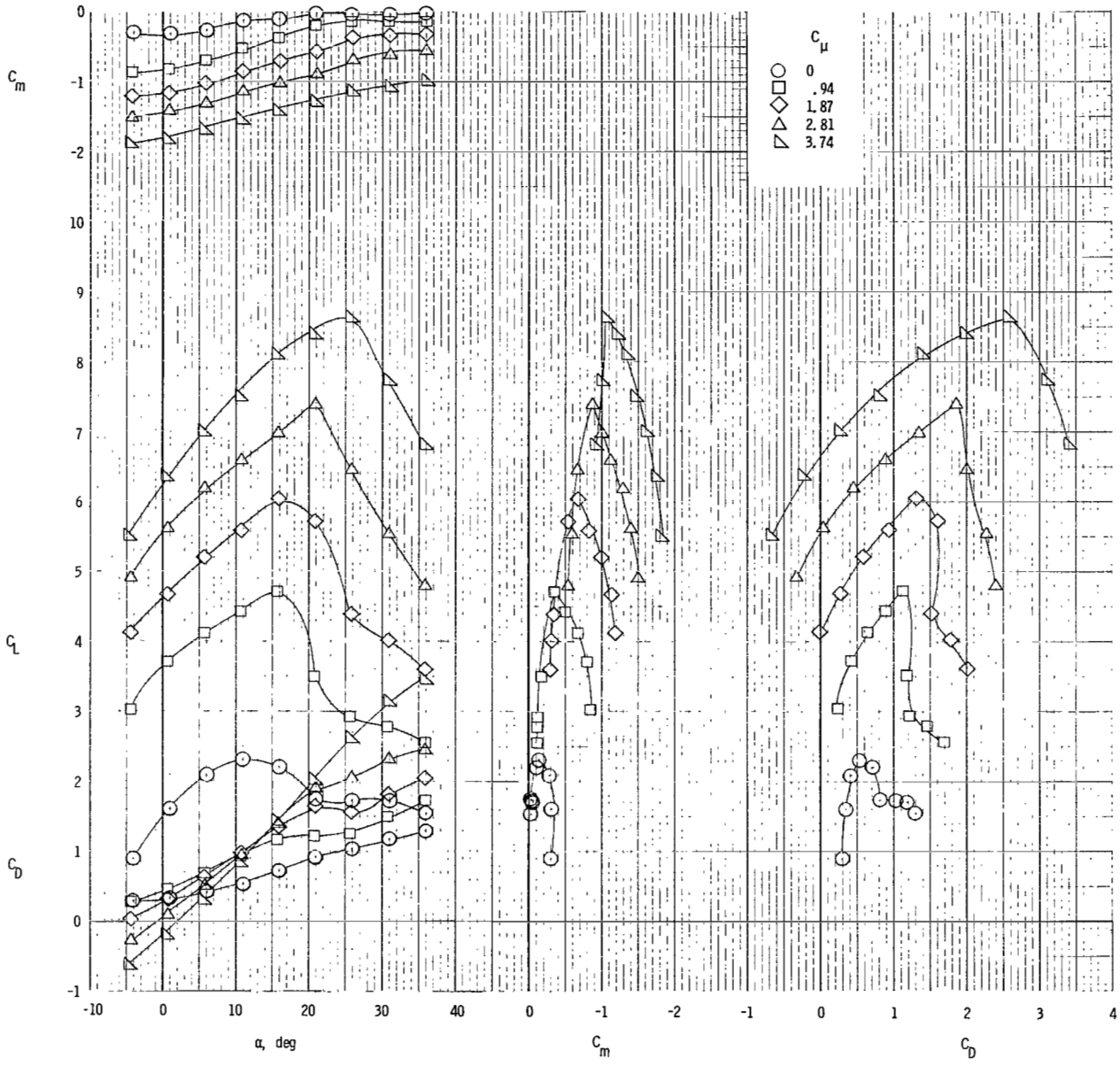

(a) $C_{\mu,le} = 0$.

Figure 5.- Longitudinal characteristics of model with tail off and clustered engines. $\delta_f = 60^o$.

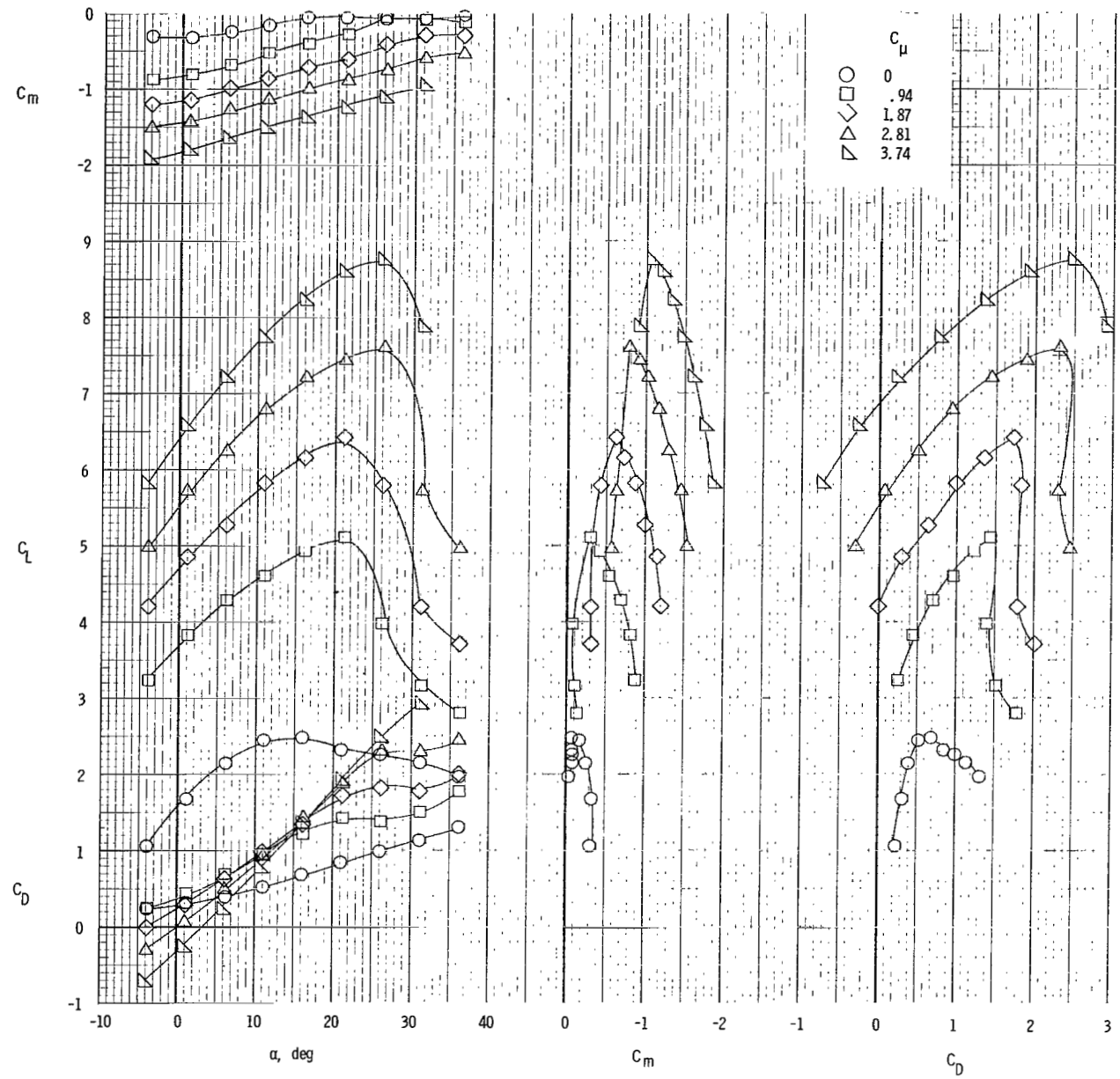

(b) $C_{\mu,le} = 0.010$.

Figure 5.- Continued.

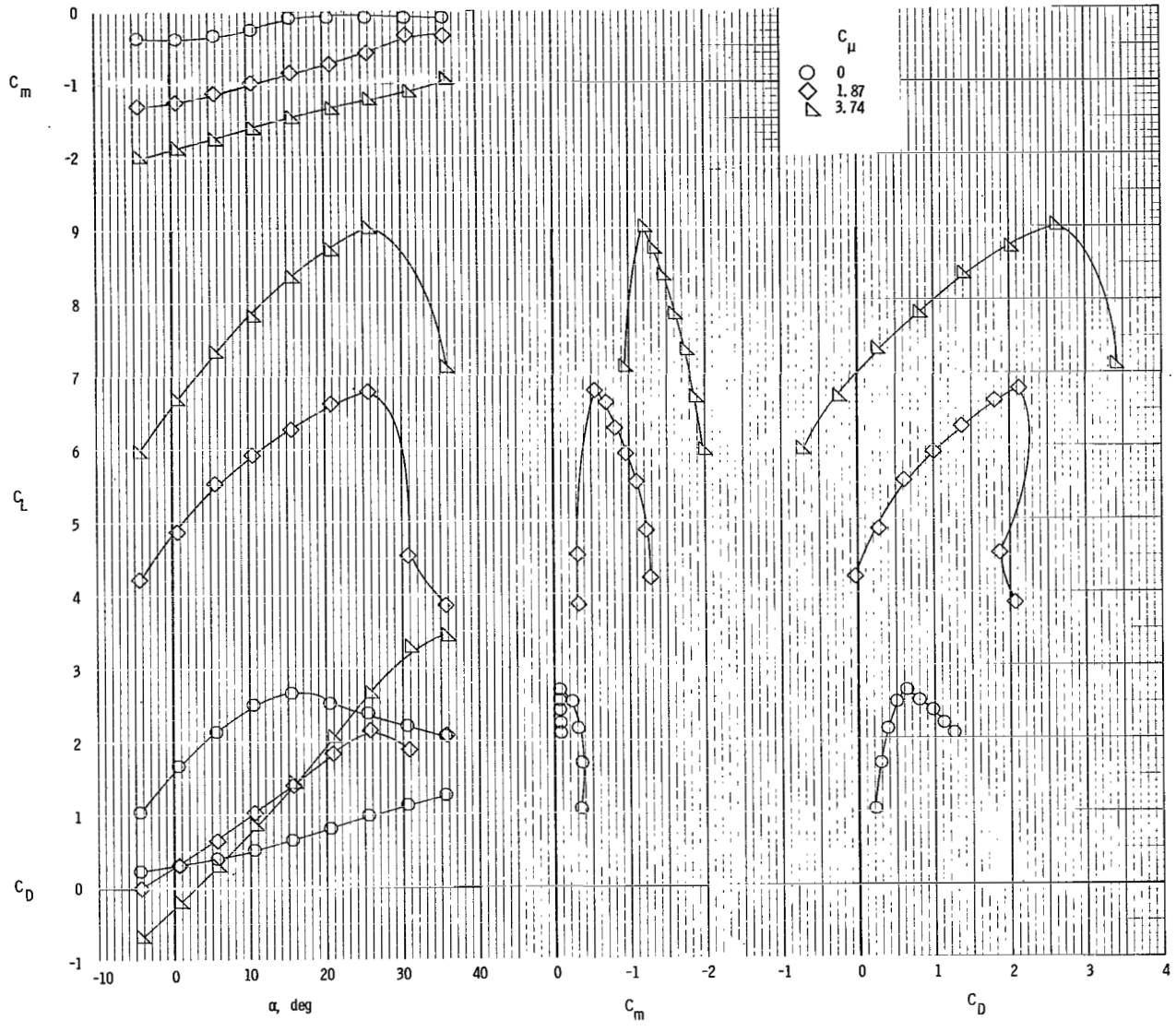

(c) $C_{\mu,le} = 0.024$.

Figure 5.- Continued.

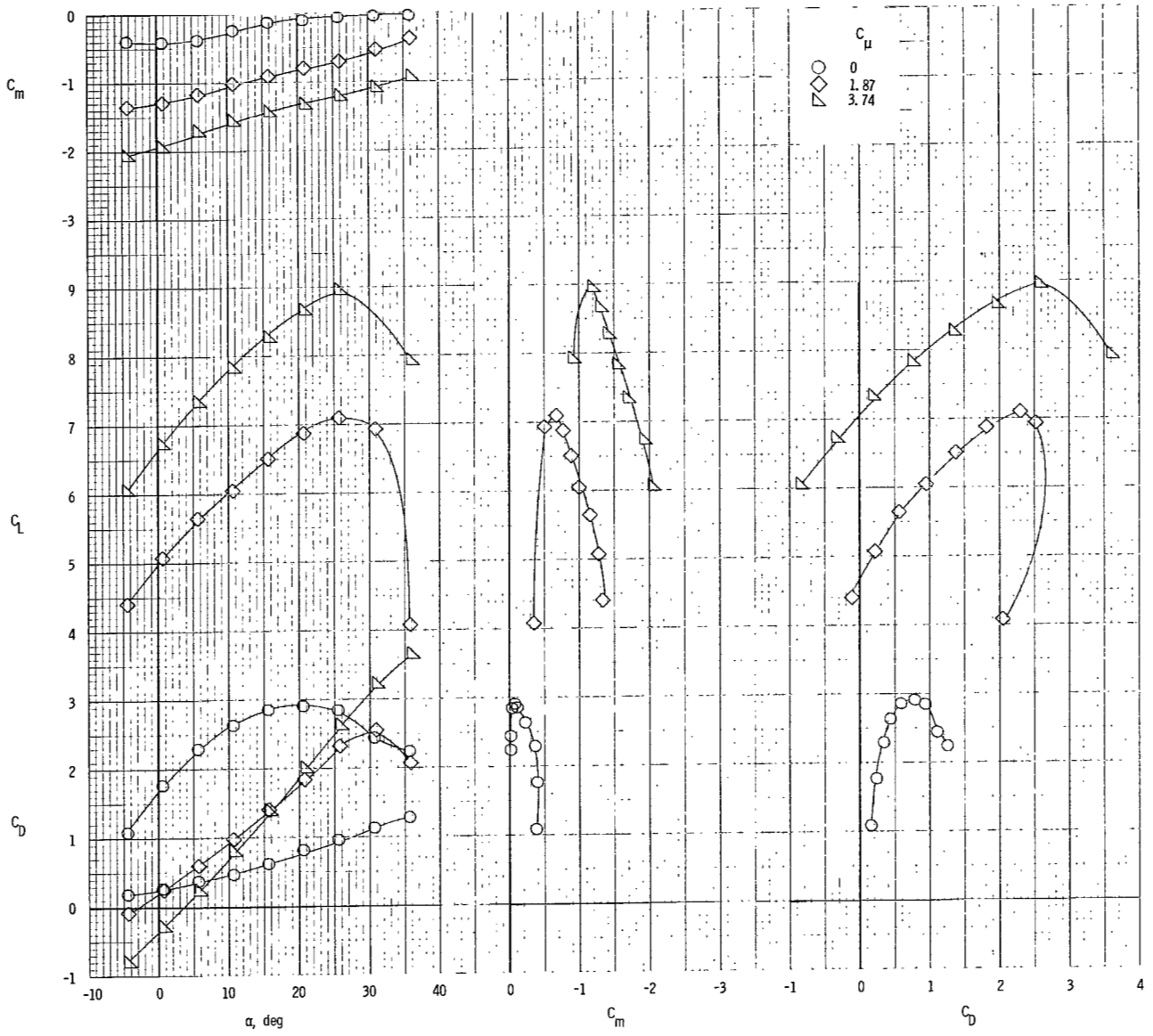

(d) $C_{\mu,le} = 0.065$.

Figure 5.- Continued.

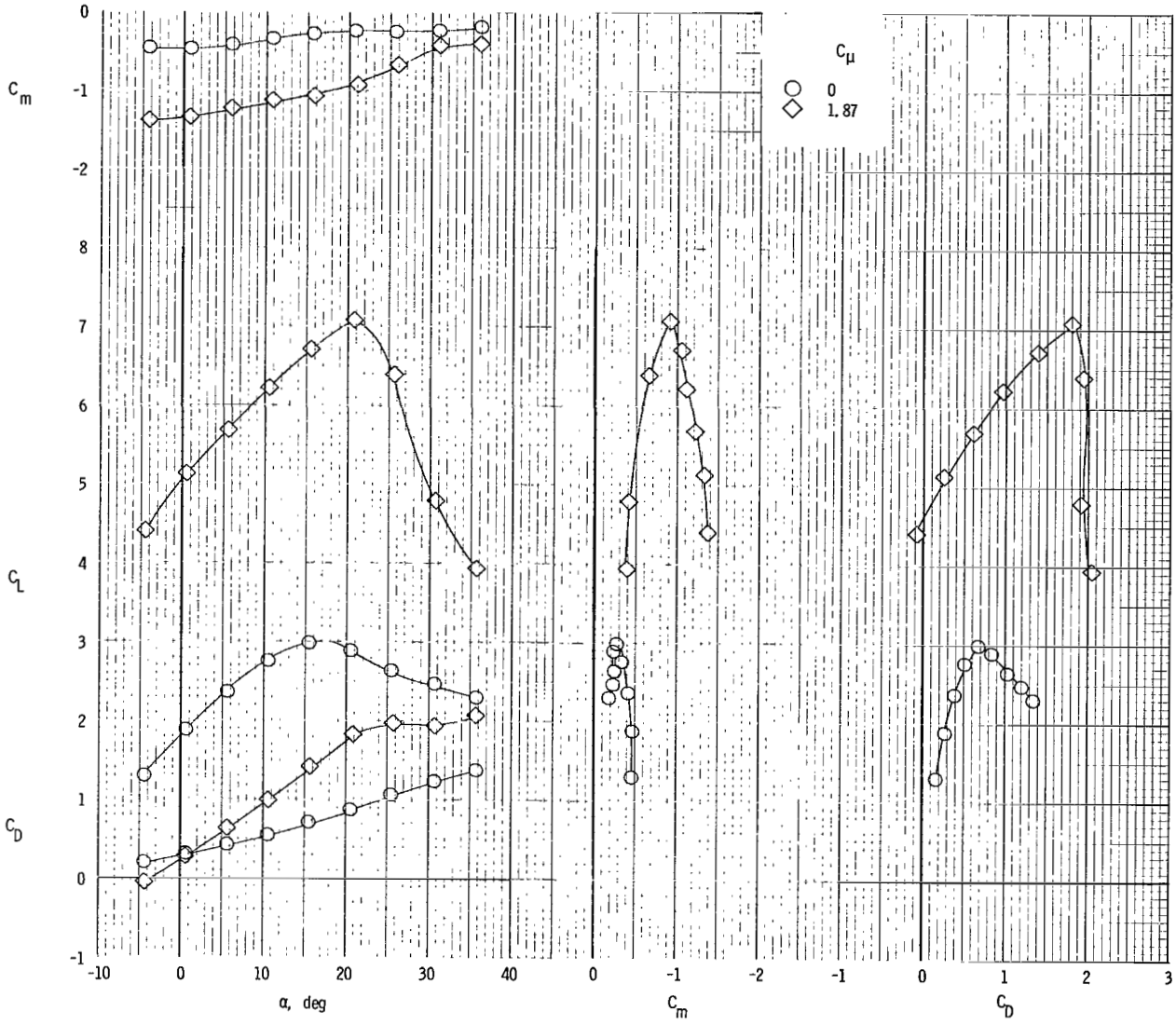

(e) $C_{\mu,le} = 0.024$; $C_{\mu,a} = 0.05$.

Figure 5.- Concluded.

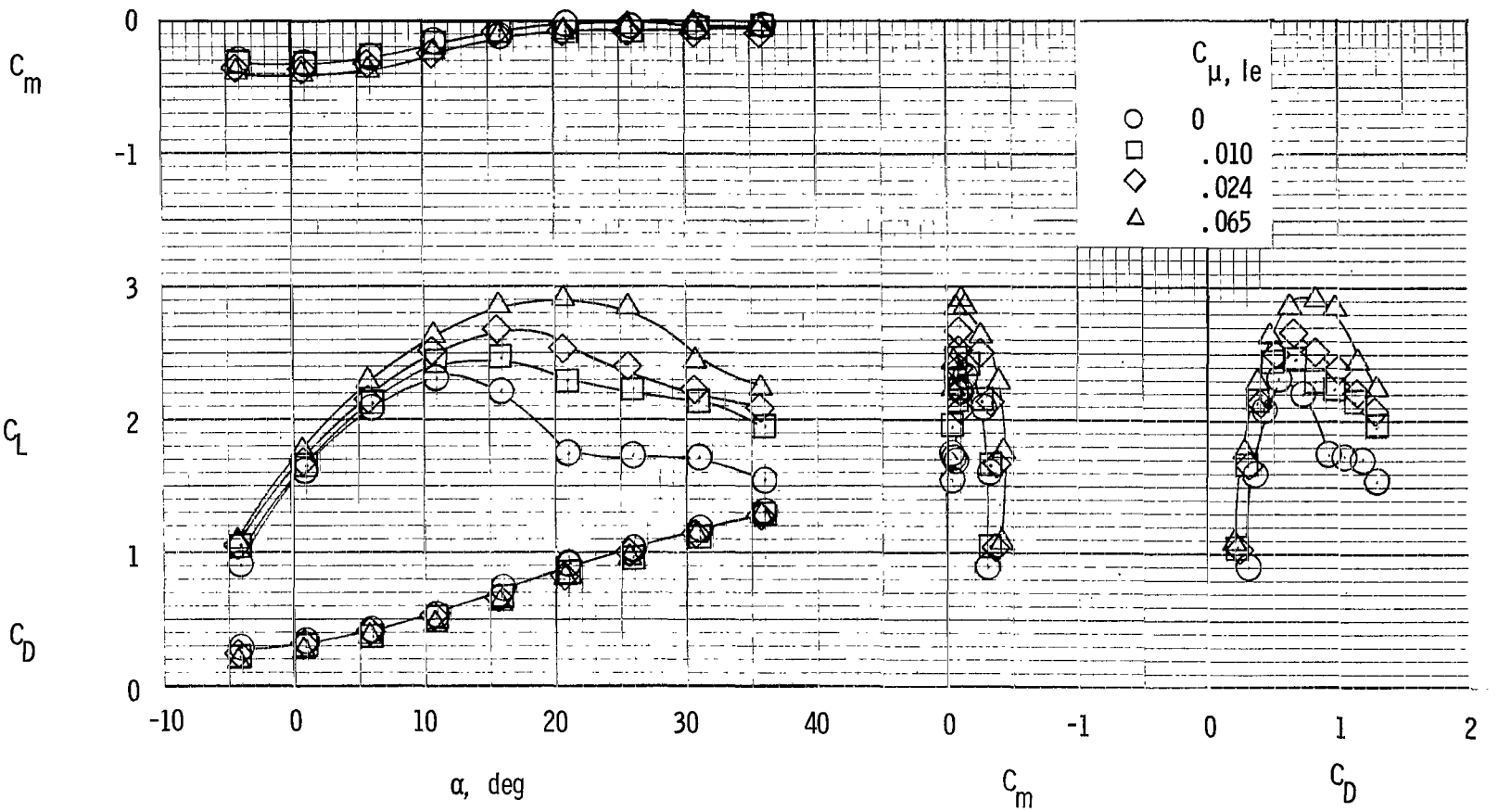

(a) Power off.

Figure 6.- Effect of leading-edge blowing on longitudinal characteristics of model with tail off and clustered engines. $\delta_f = 60^o$.

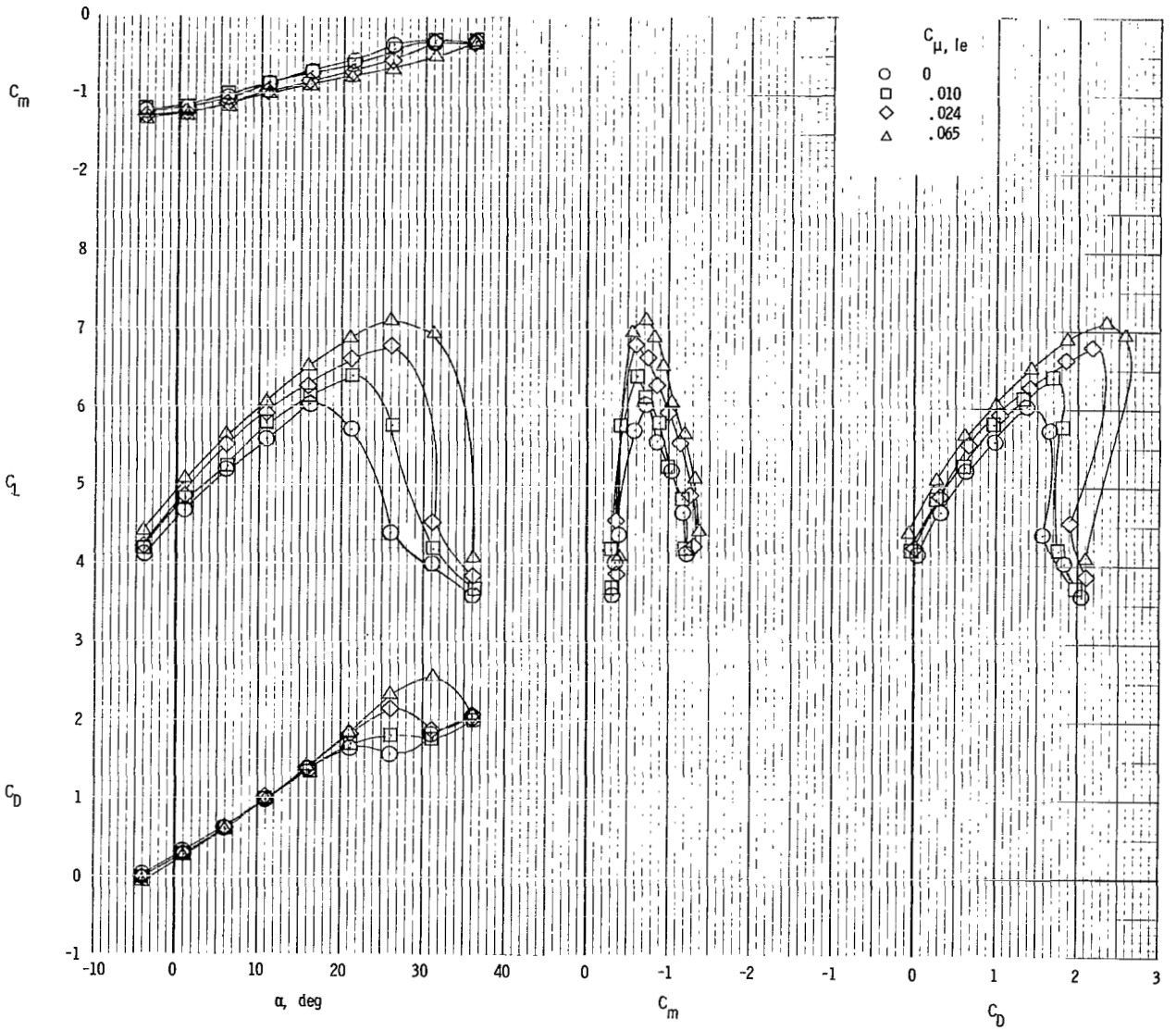

(b) $C_{\mu} = 1.87$.

Figure 6.- Continued.

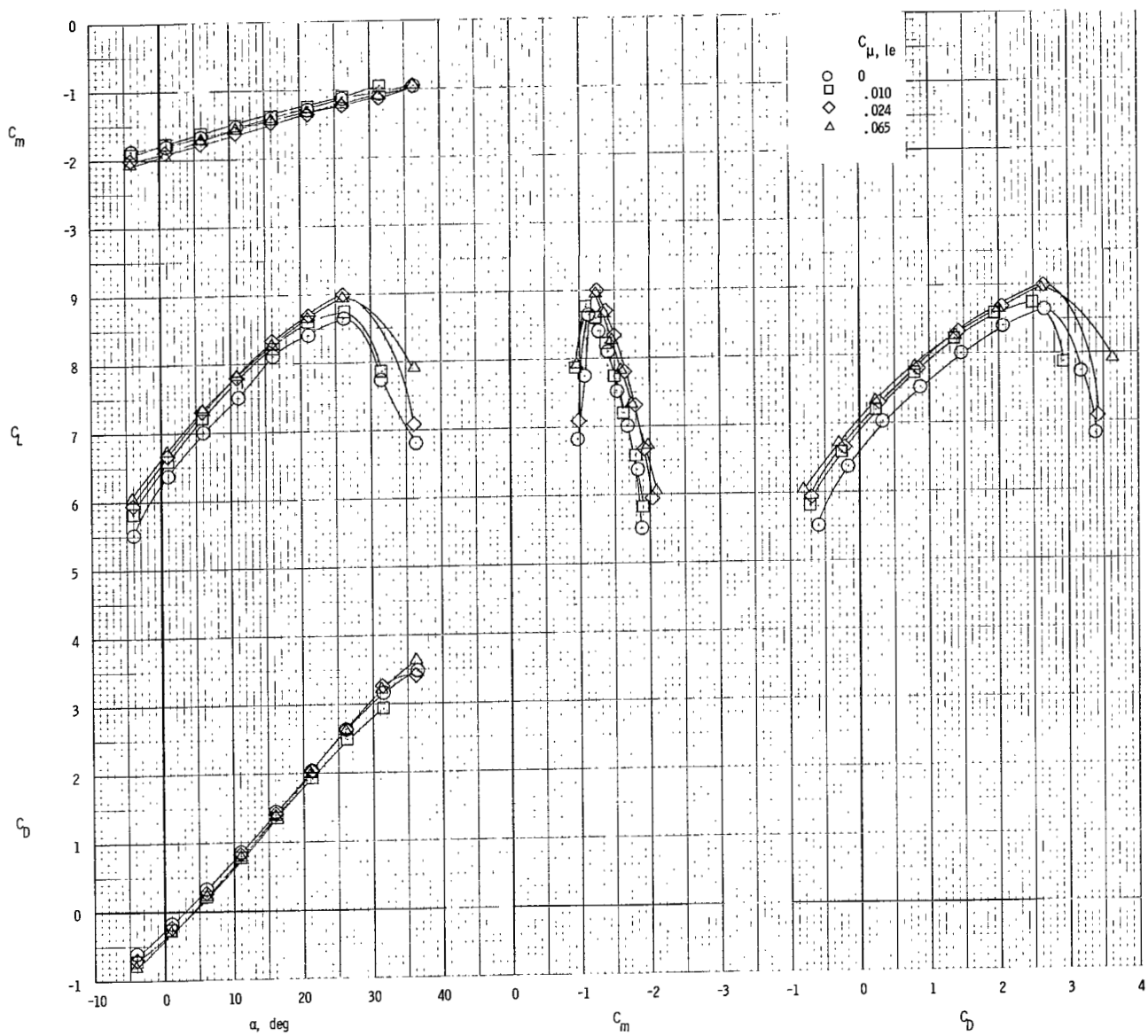

(c) C_μ = 3.74.

Figure 6.- Concluded.

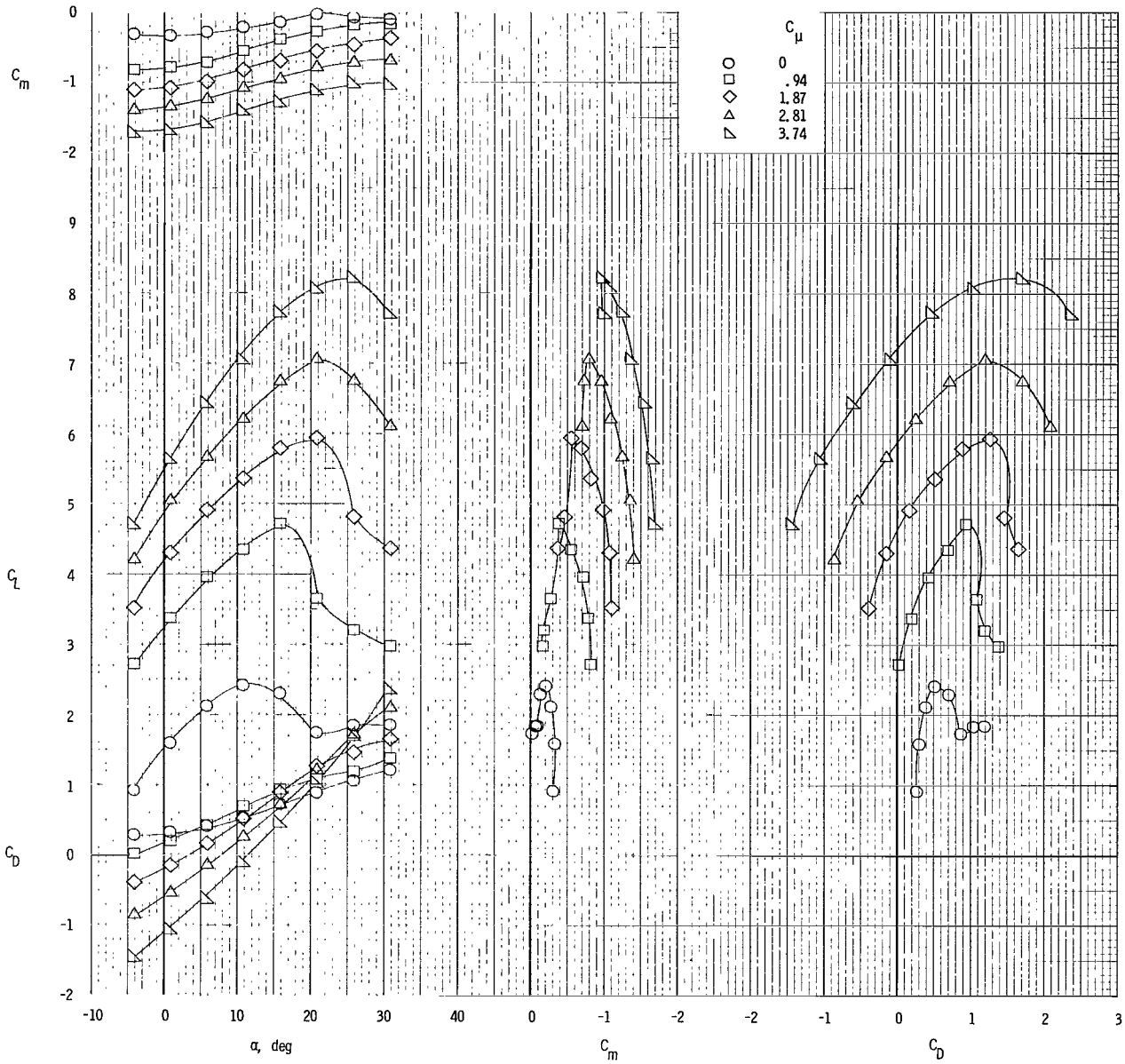

Figure 7.- Longitudinal characteristics of model with tail off and clustered engines. $\delta_f = 50^o$; $C_{\mu,le} = 0$.

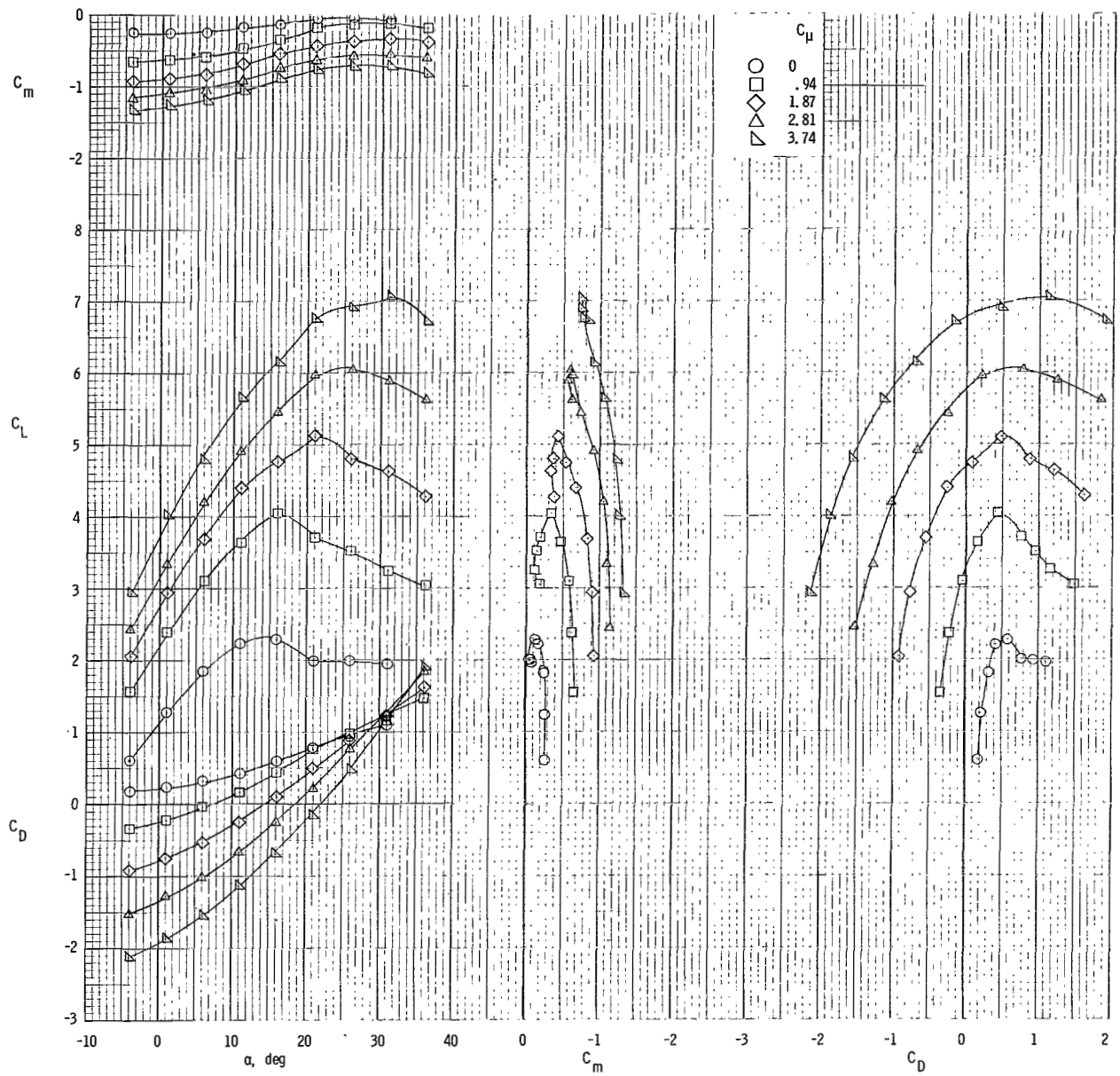

(a) $C_{\mu,le} = 0.$

Figure 8.- Longitudinal characteristics of model with tail off and clustered engines. $\delta_f = 35^0$.

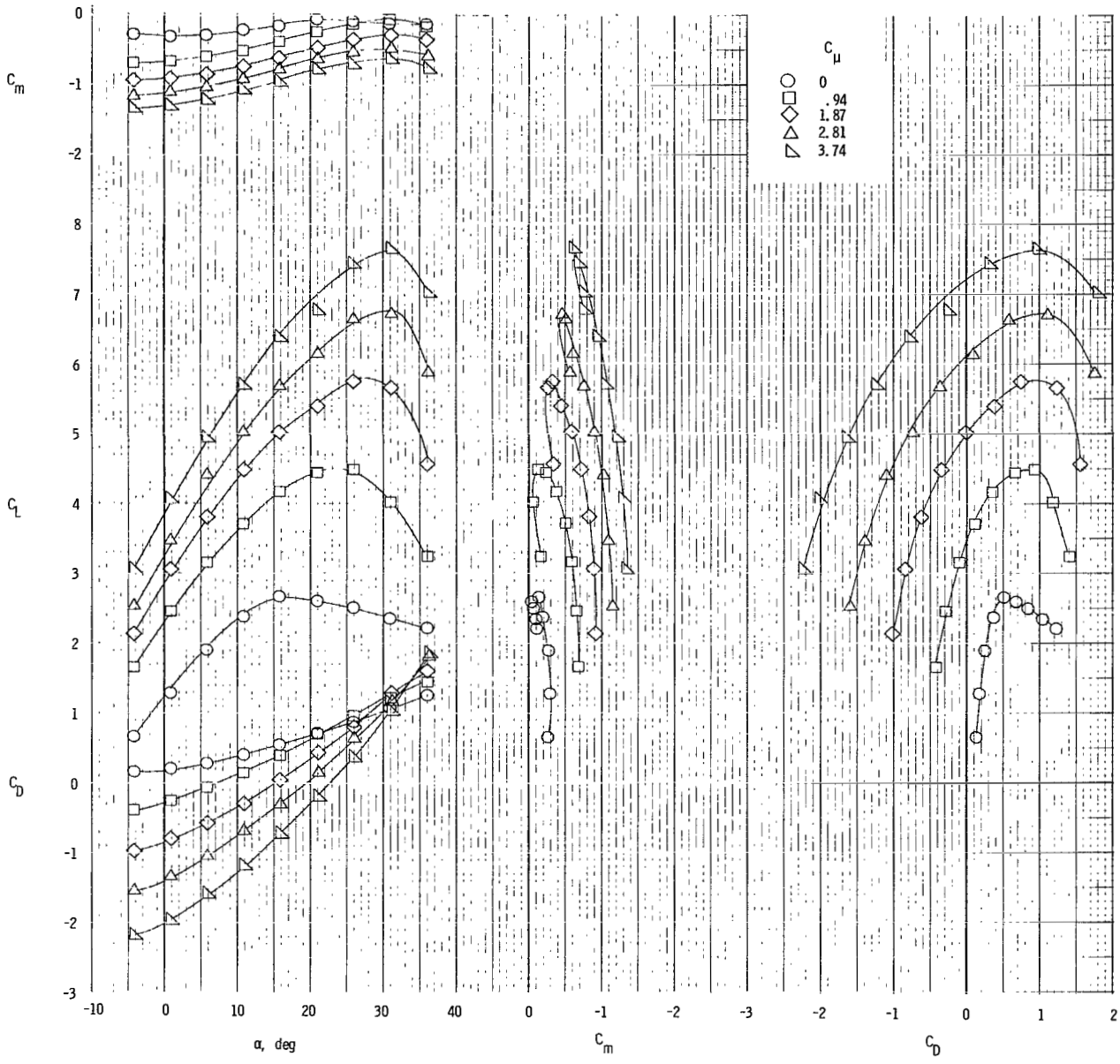

(b) $C_{\mu,le} = 0.010$.

Figure 8.- Continued.

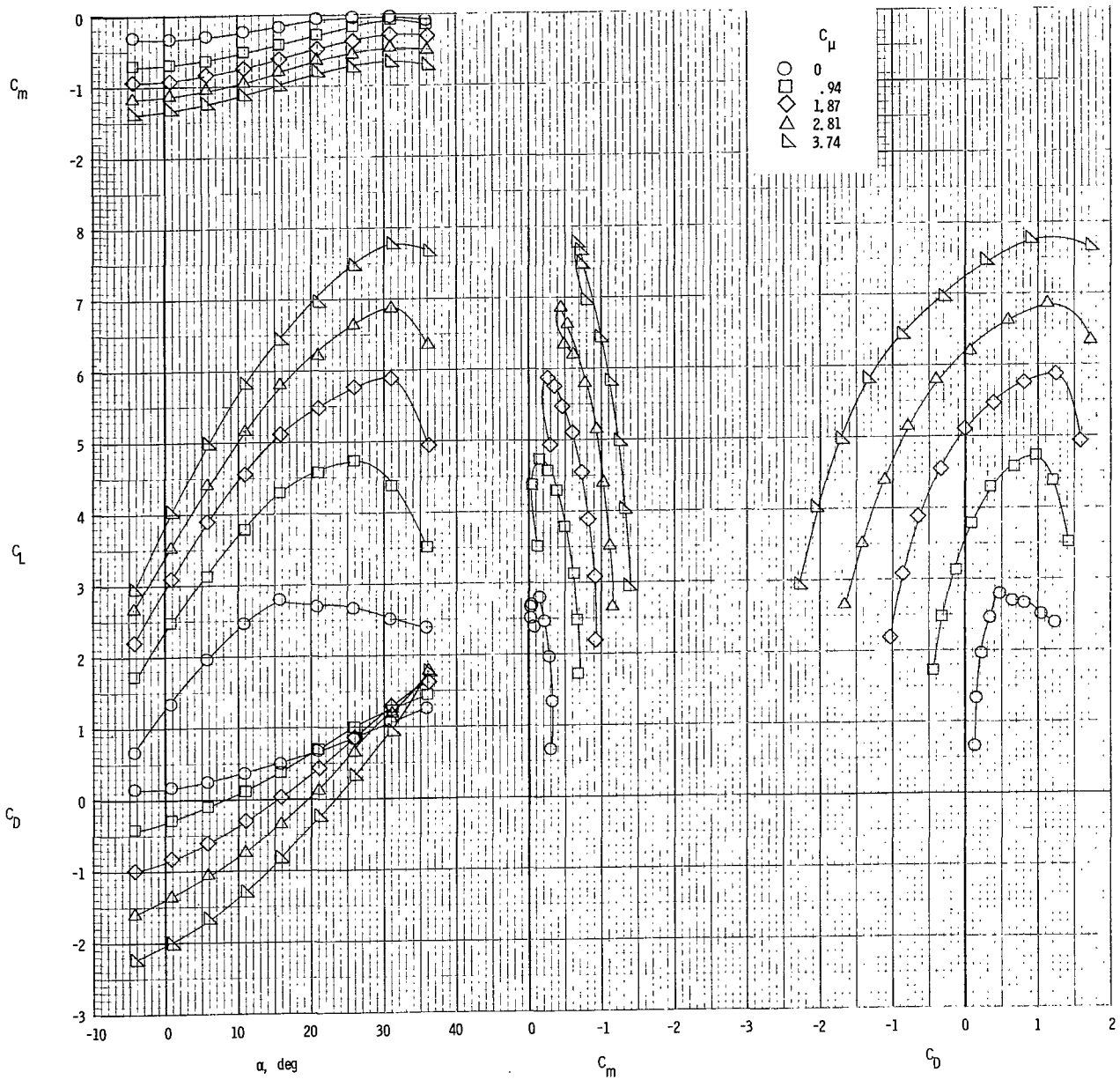

(c) $C_{\mu,le} = 0.024$.

Figure 8.- Concluded.

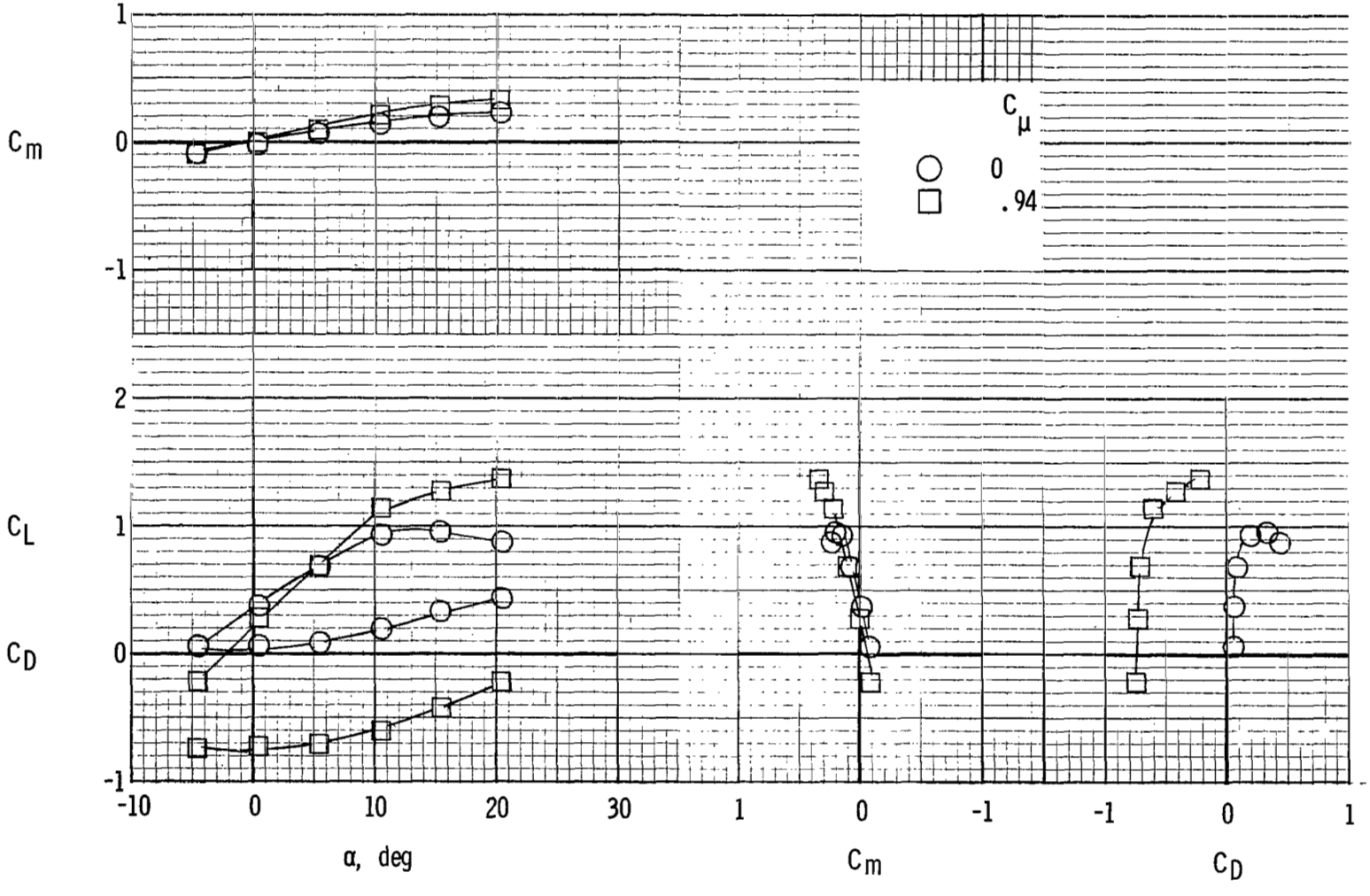

Figure 9.- Longitudinal characteristics of model with tail off and spread engines. Leading-edge flap off; $\delta_f = 0^o$.

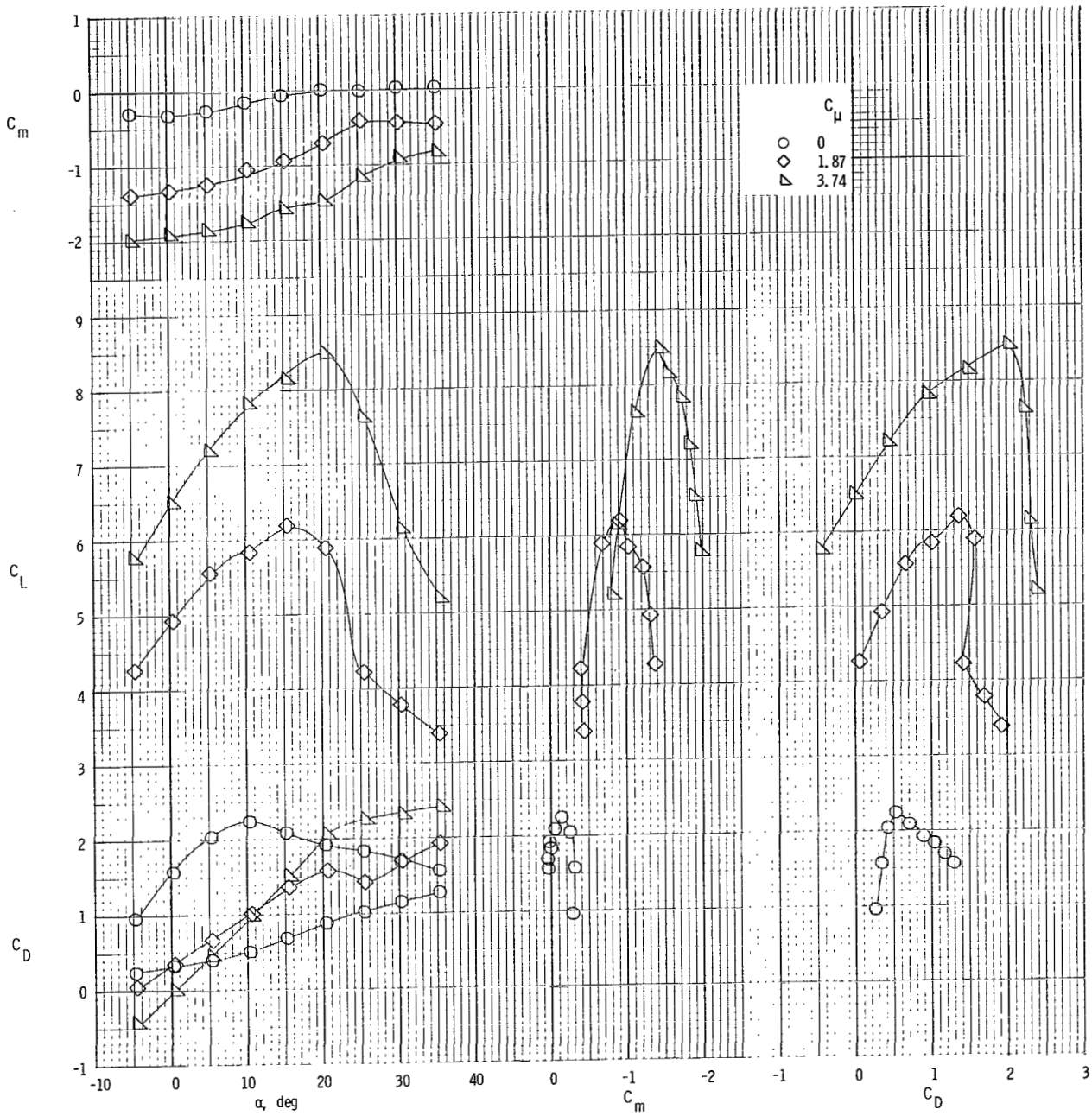

(a) $C_{\mu,le} = 0.$

Figure 10.- Longitudinal characteristics of model with tail off and spread engines. $\delta_f = 60^0$.

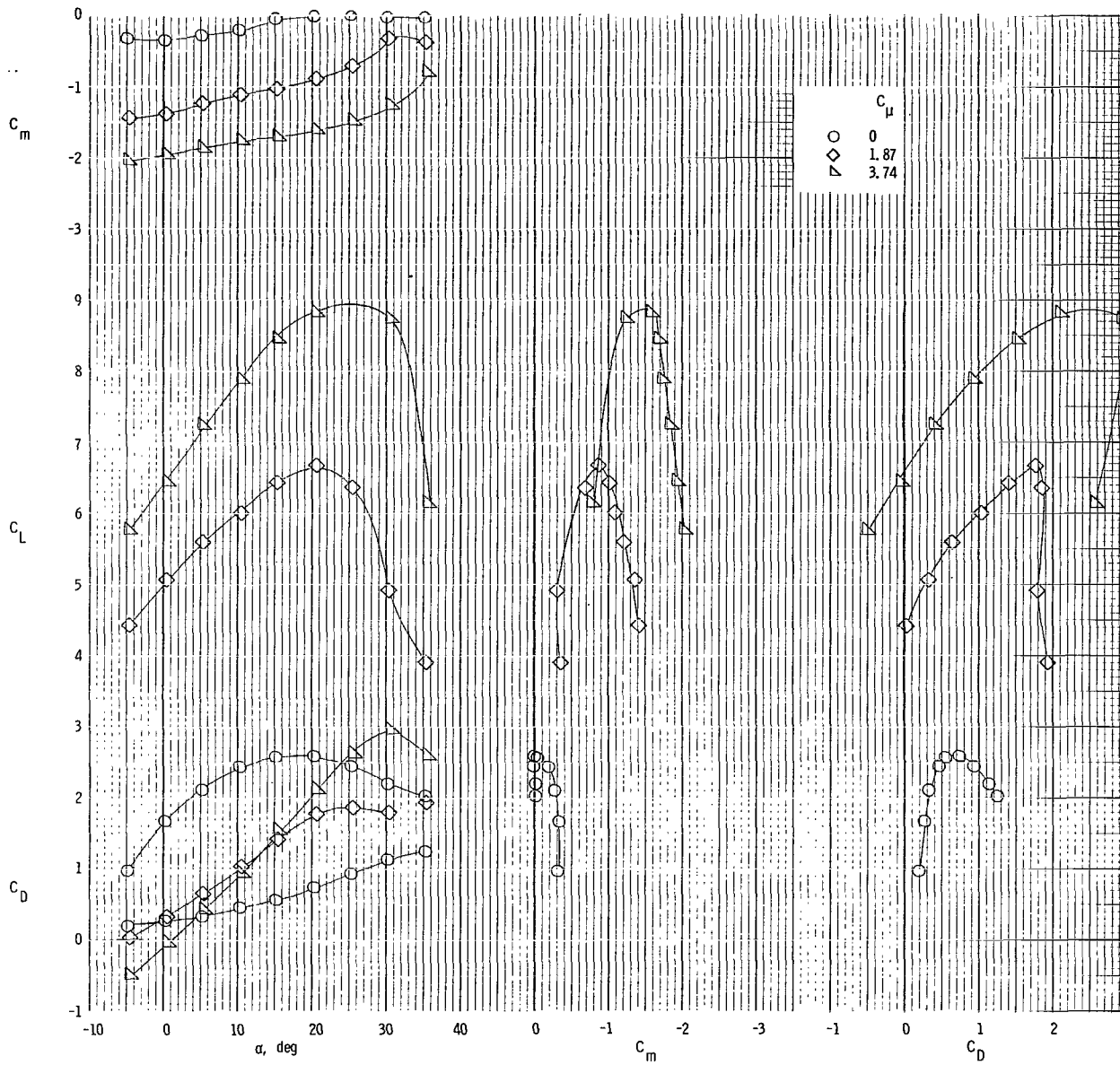

(b) $C_{\mu,le} = 0.024$.

Figure 10.- Concluded.

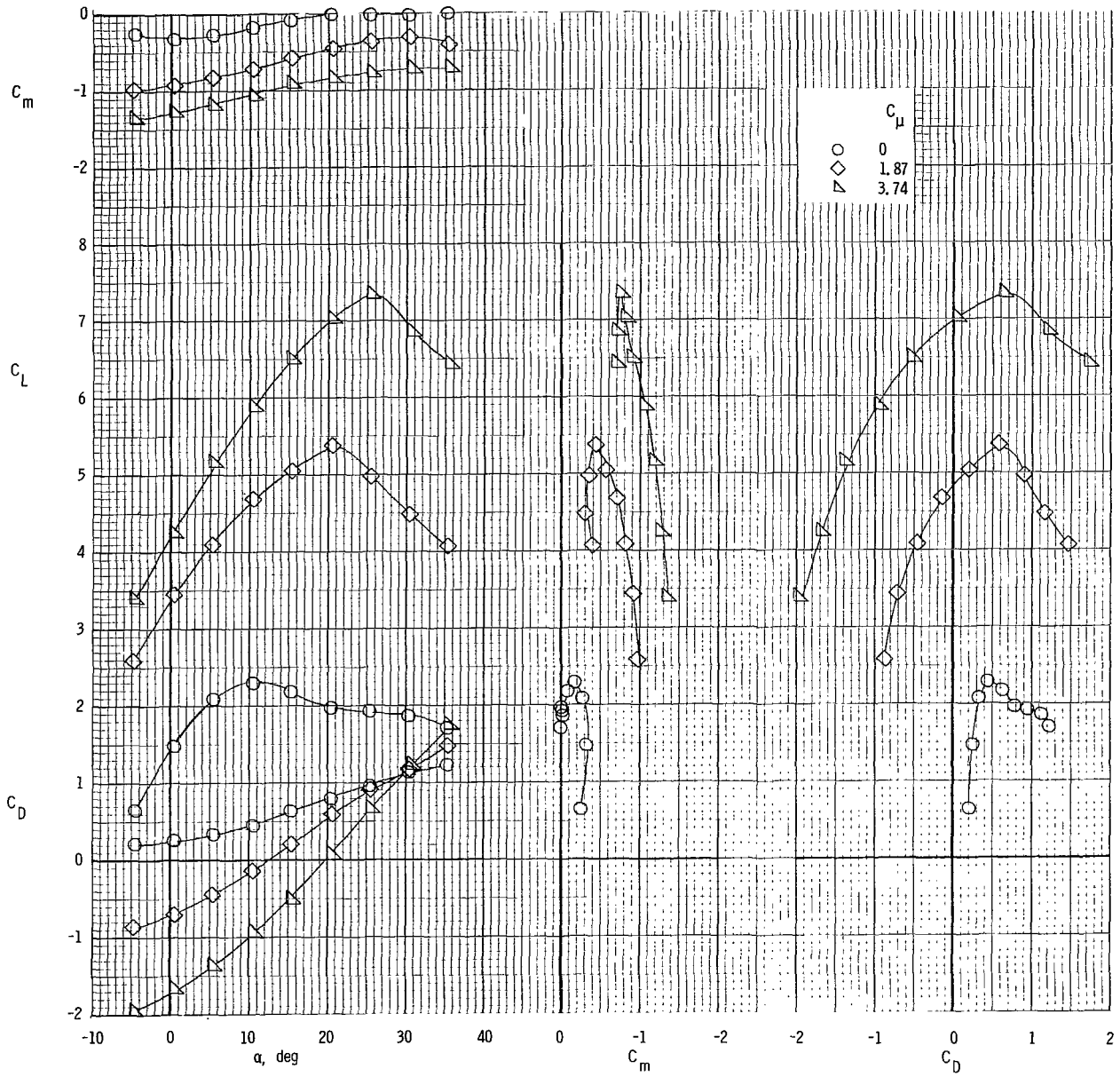

(a) $C_{\mu,le} = 0$.

Figure 11.- Longitudinal characteristics of model with tail off and spread engines. $\delta_f = 40^0$.

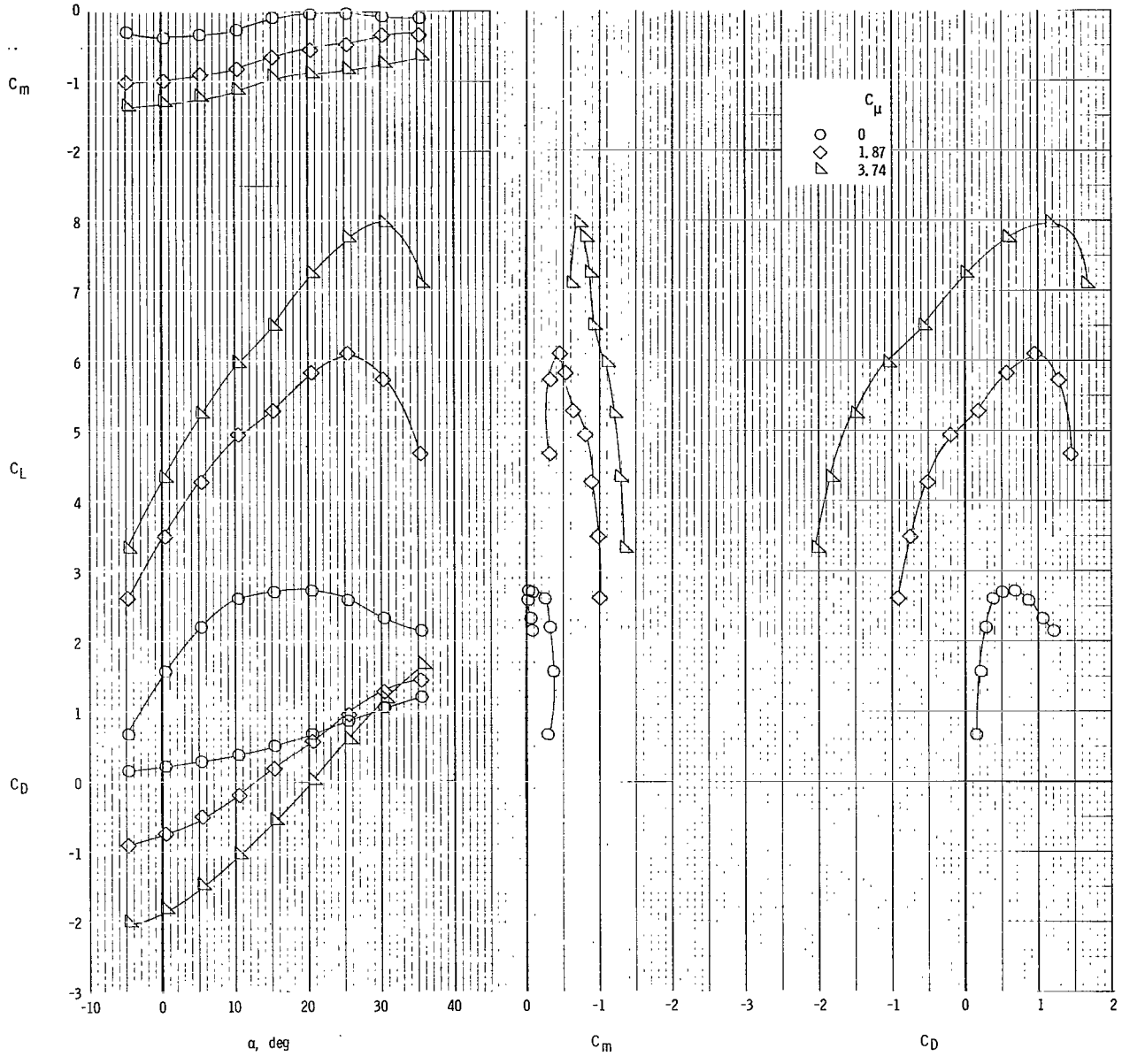

(b) $C_{\mu,le} = 0.024$.

Figure 11.- Concluded.

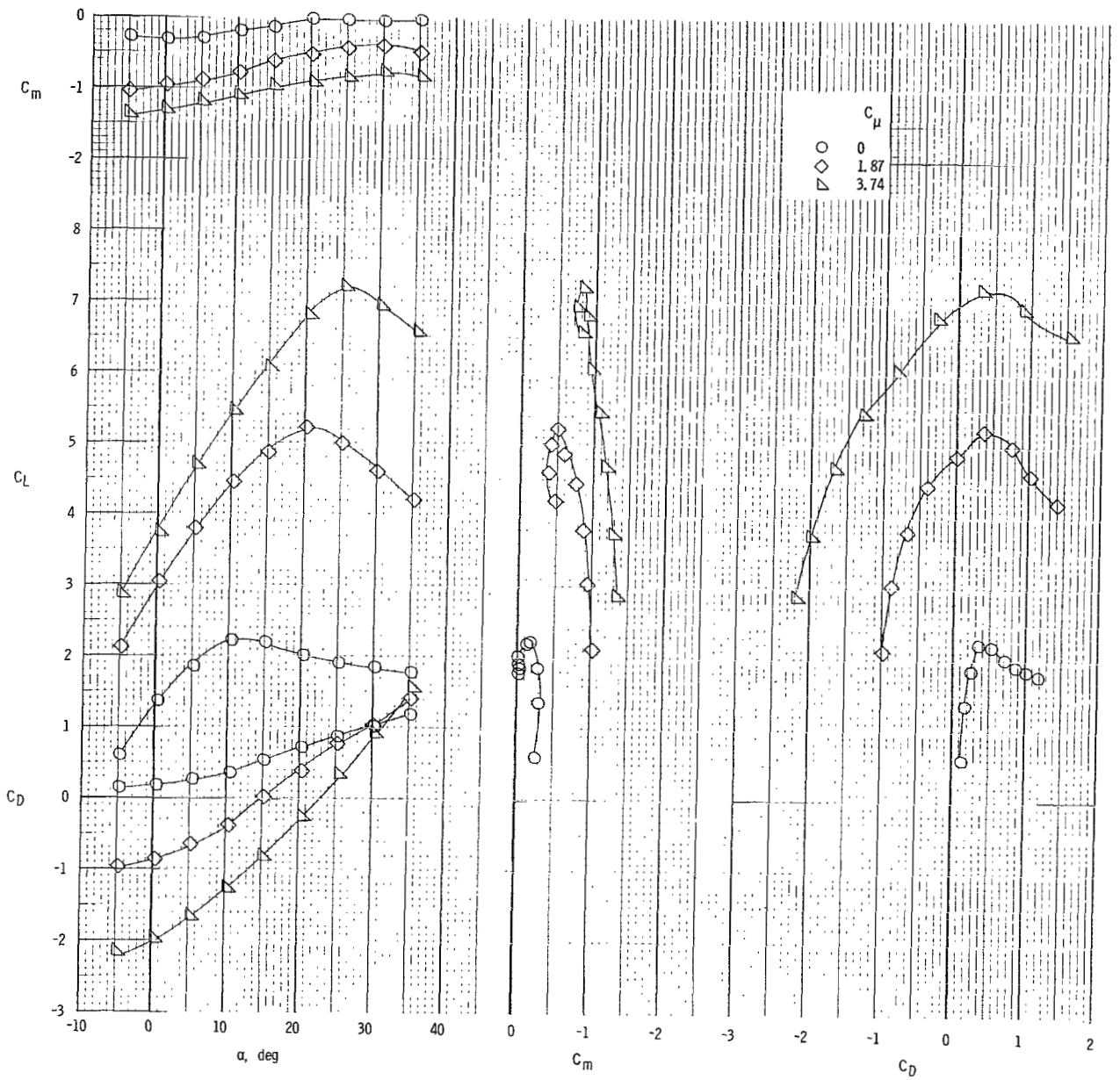

(a) $C_{\mu,le} = 0$.

Figure 12.- Longitudinal characteristics of model with tail off and spread engines. $\delta_f = 35^o$.

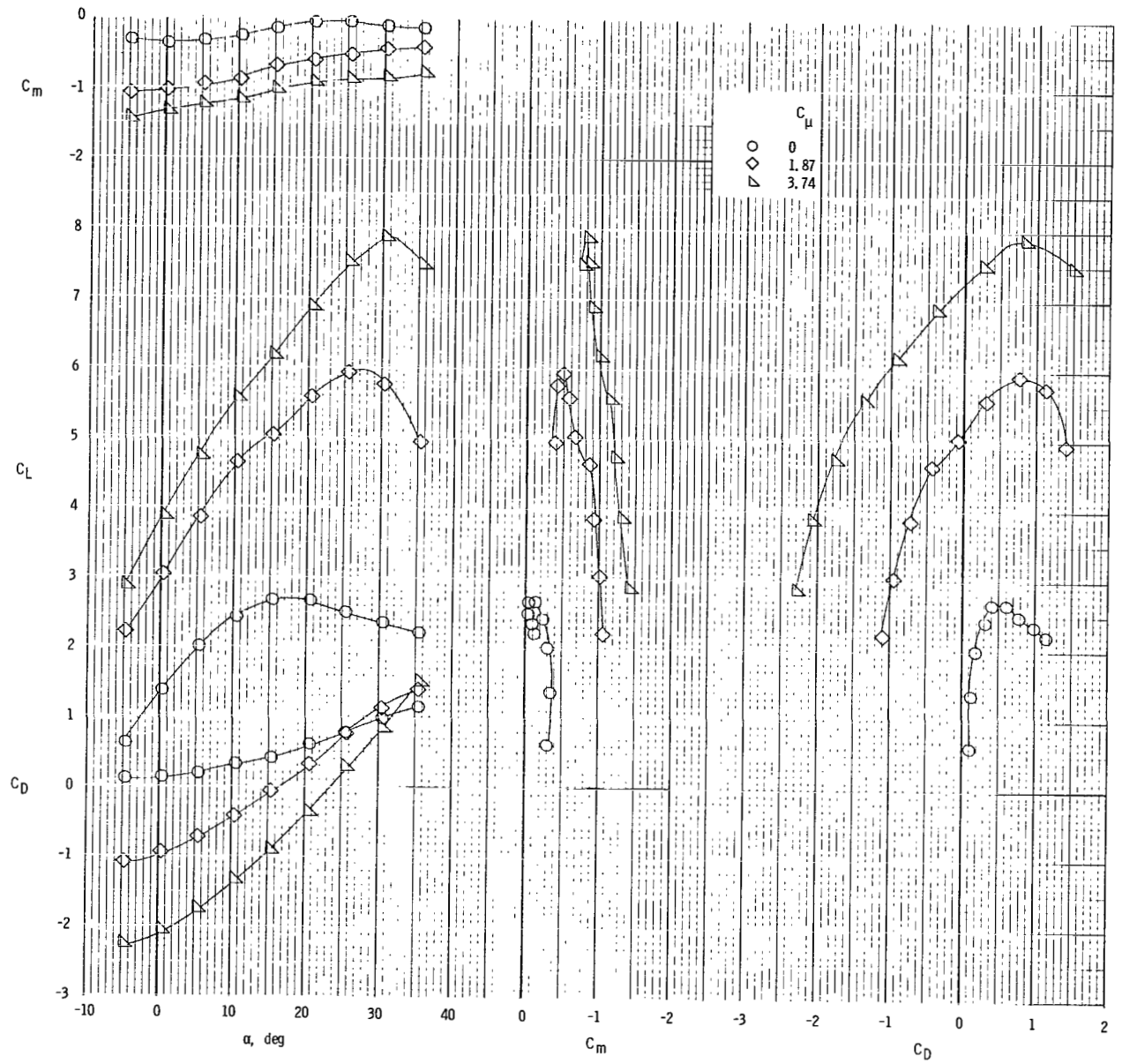

(b) $C_{\mu,le} = 0.024$.

Figure 12.- Concluded.

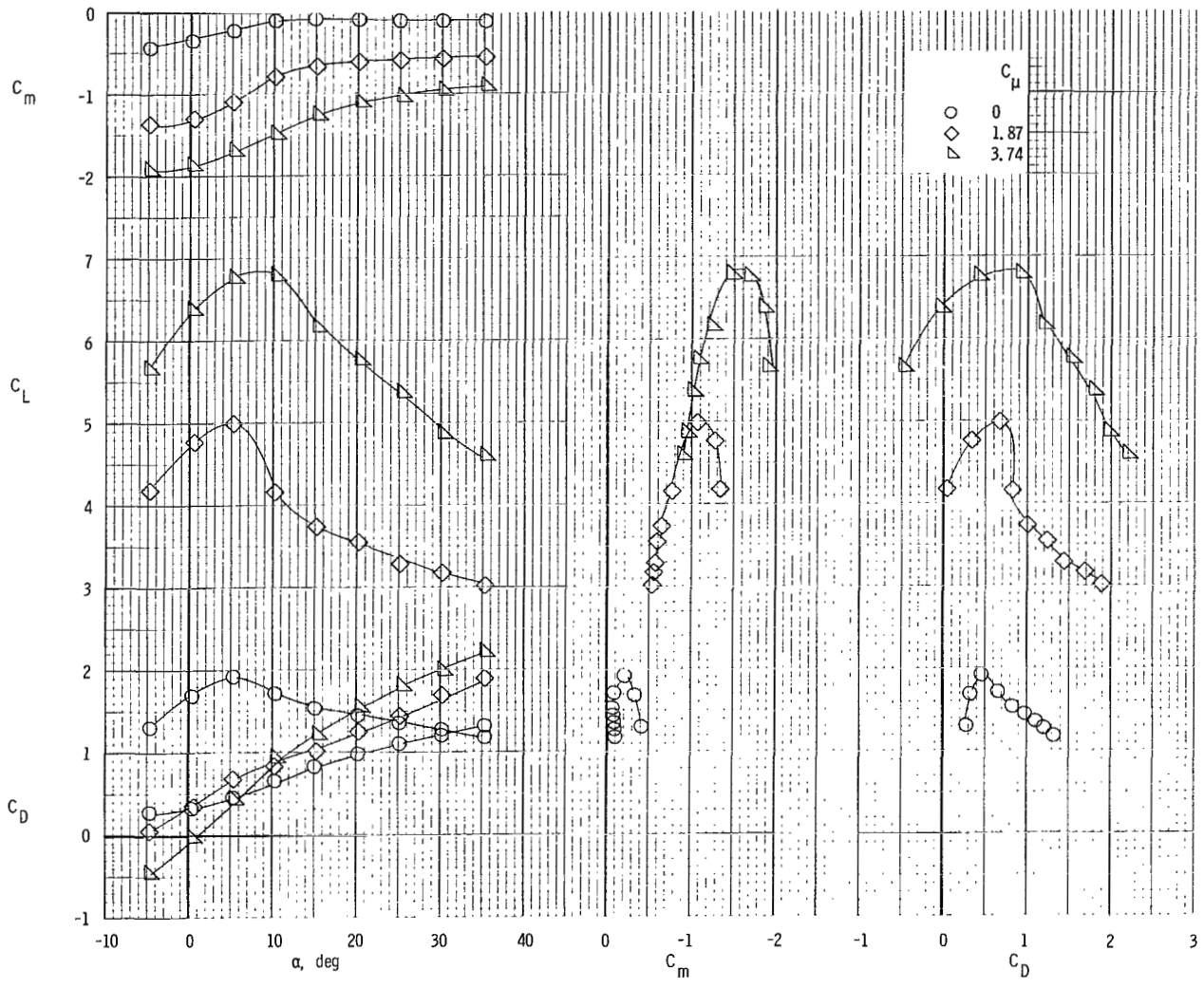

(a) $C_{\mu,le} = 0$.

Figure 13.- Longitudinal characteristics of model with tail off and spread engines. Clean leading edge; $\delta_f = 60^o$.

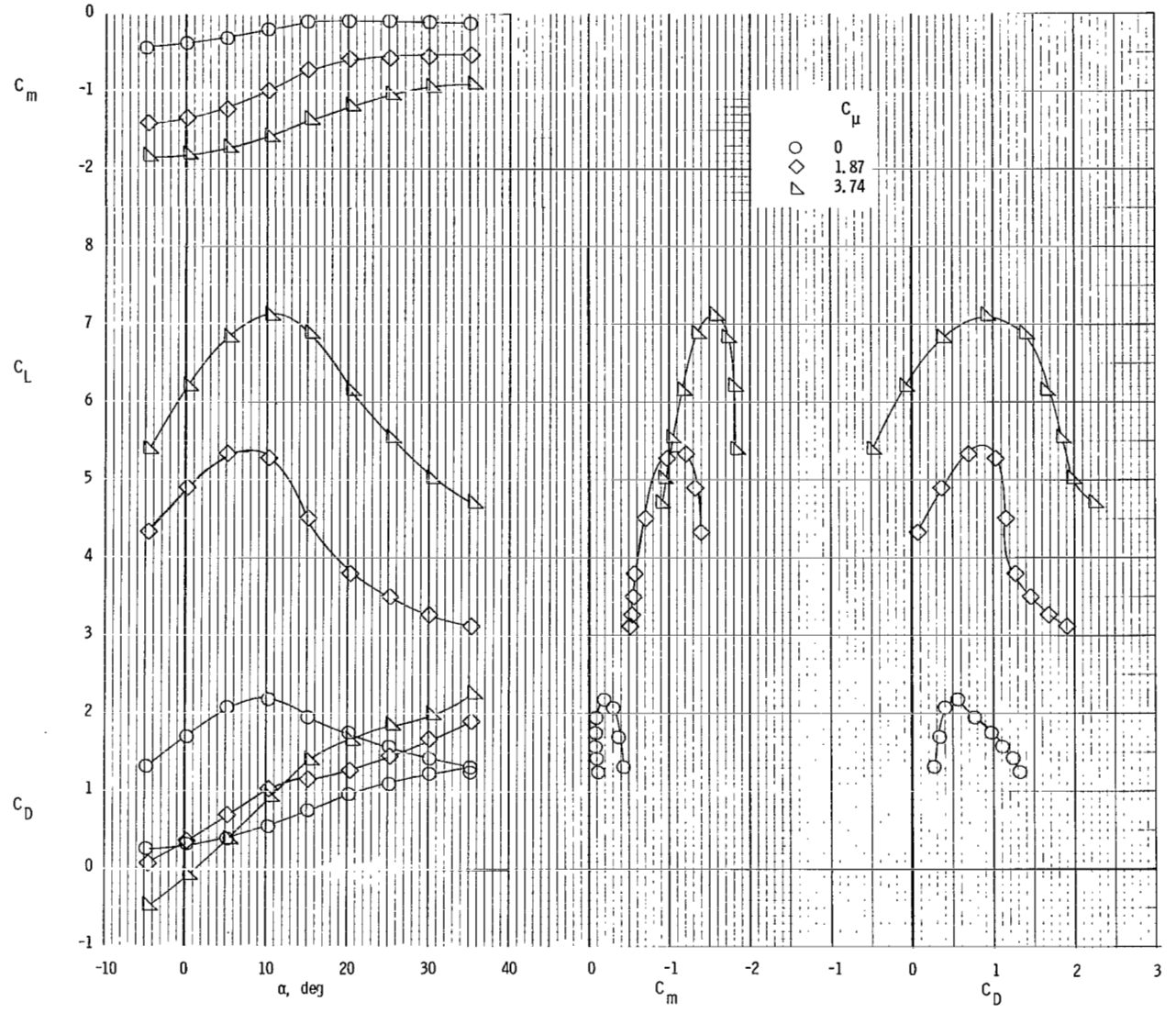

(b) $C_{\mu,le} = 0.010$.

Figure 13.- Continued.

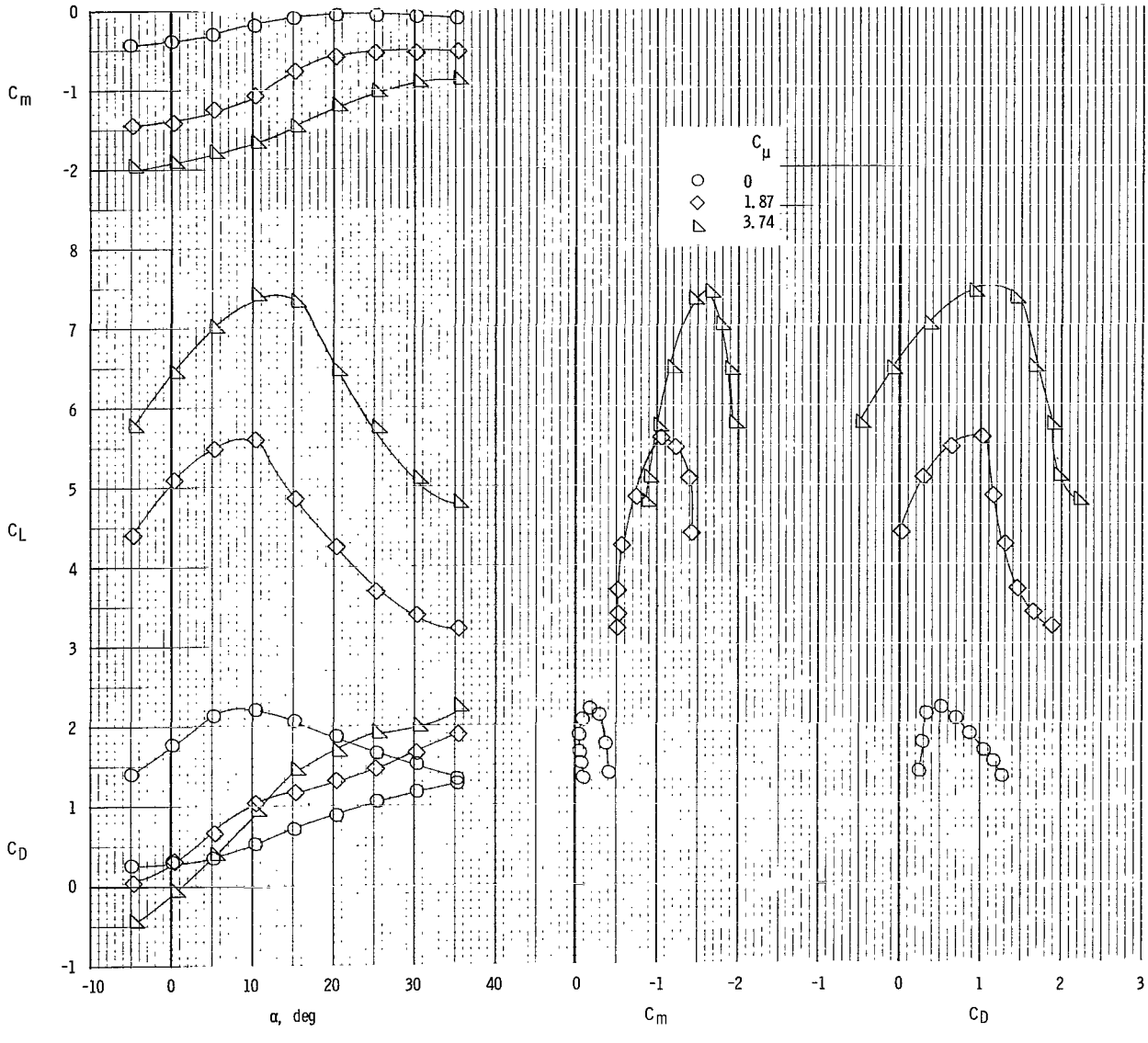

(c) $C_{\mu,le} = 0.024$.

Figure 13.- Continued.

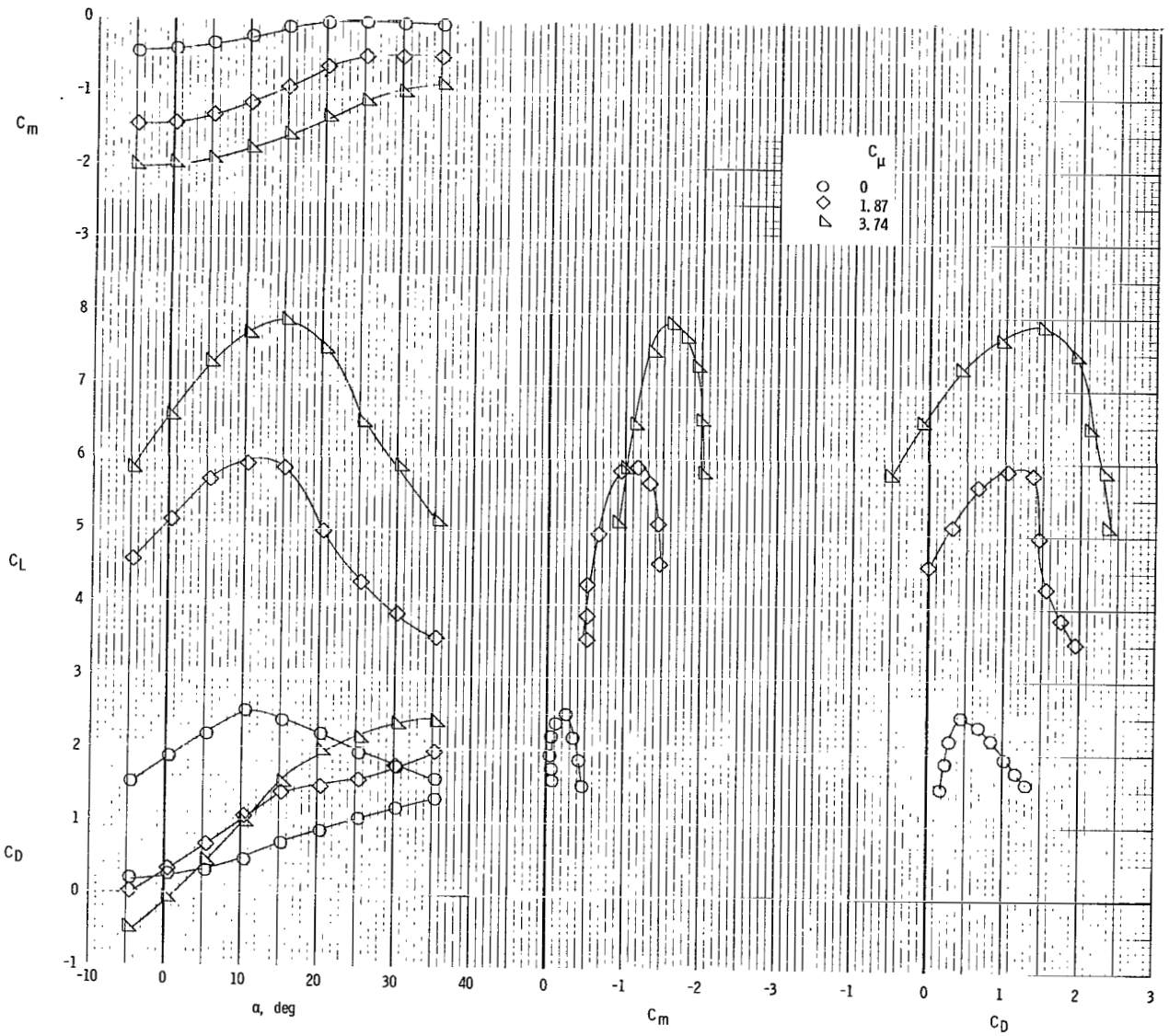

(d) $C_{\mu,le} = 0.065$.

Figure 13.- Concluded.

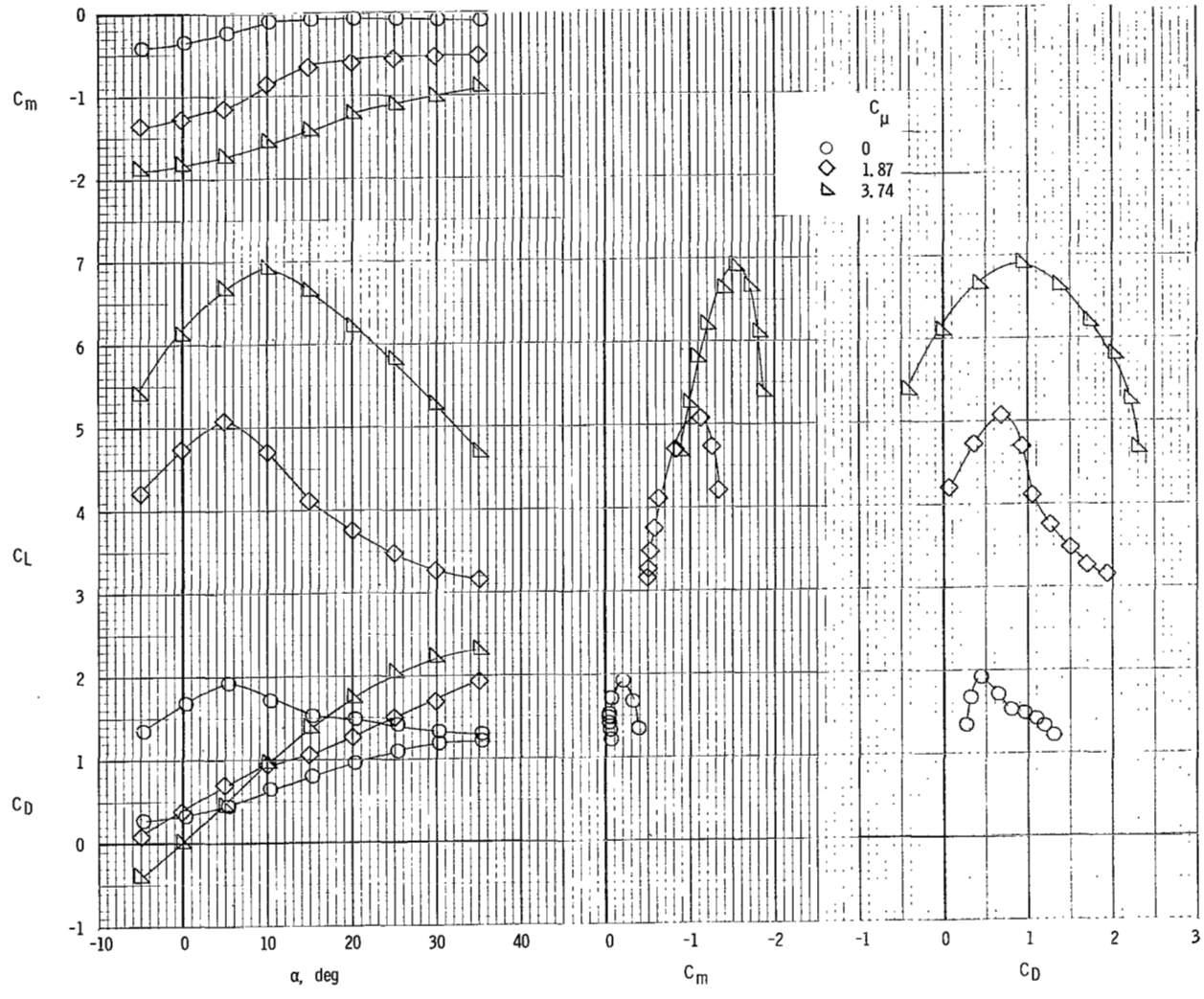

(a) $C_{\mu,le} = 0$.

Figure 14.- Longitudinal characteristics of model with tail off and spread engines. Drooped leading edge; $\delta_f = 60^0$.

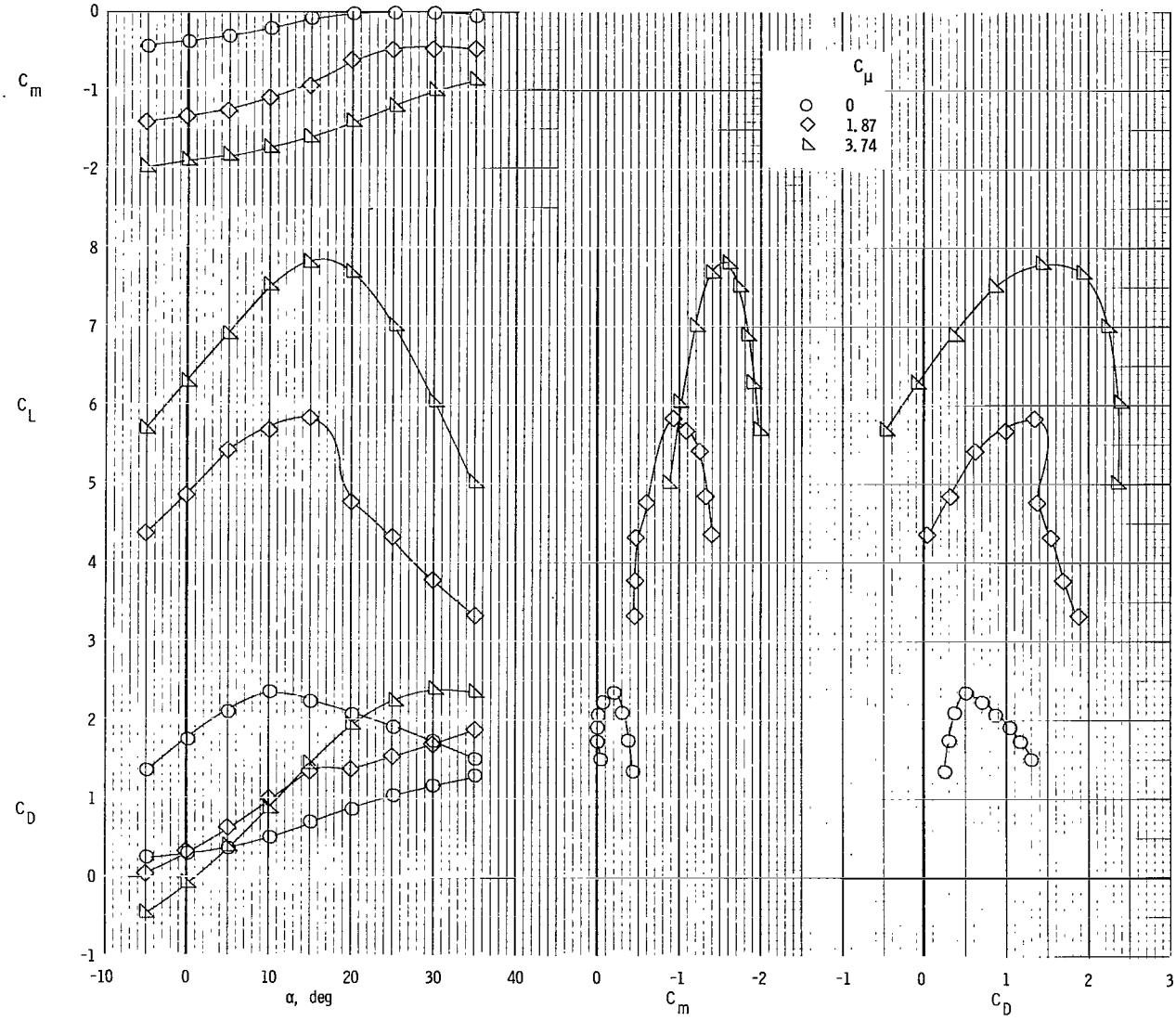

(b) $C_{\mu,le} = 0.024$.

Figure 14.- Continued.

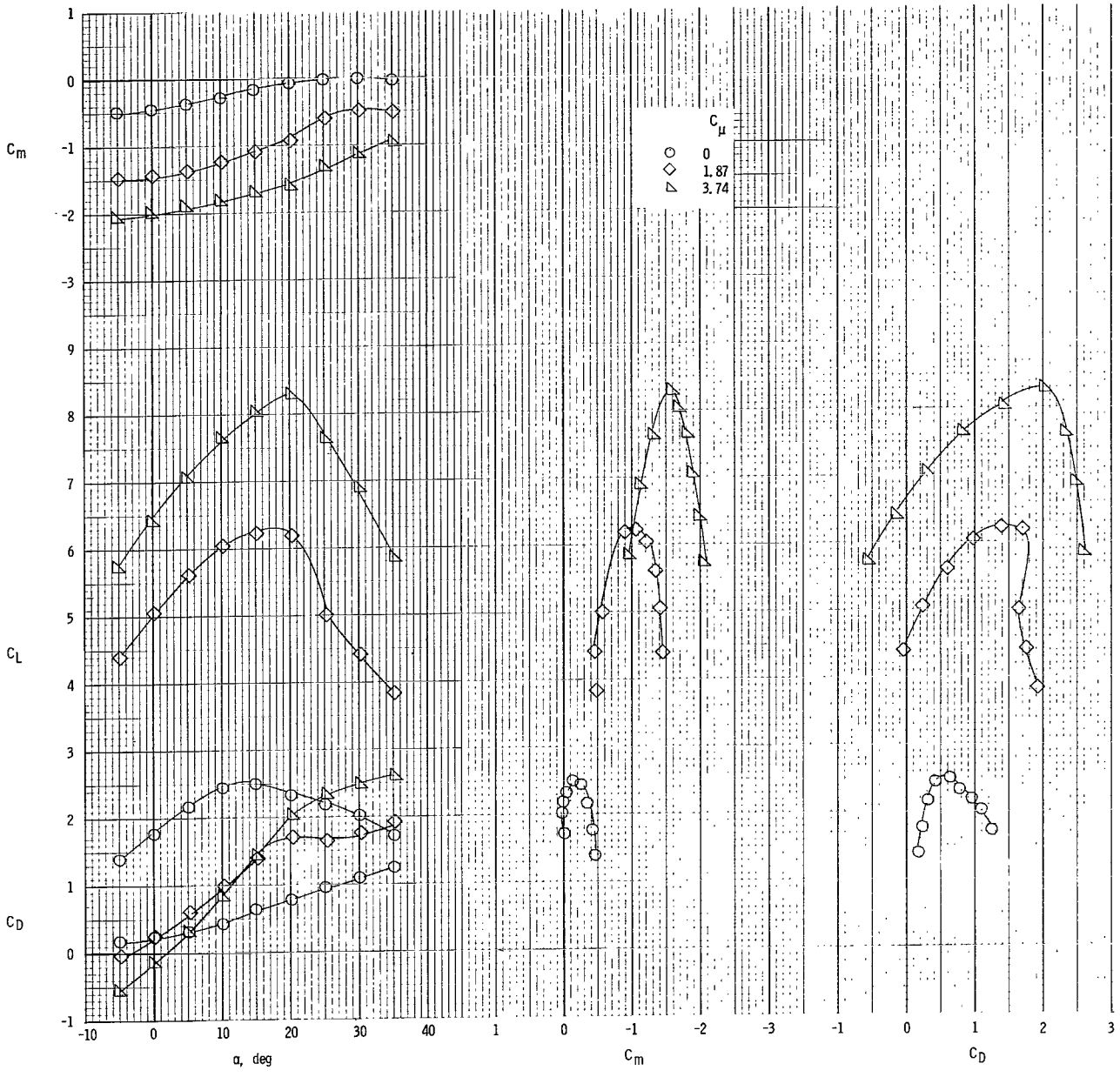

(c) $C_{\mu,le} = 0.065$.

Figure 14.- Concluded.

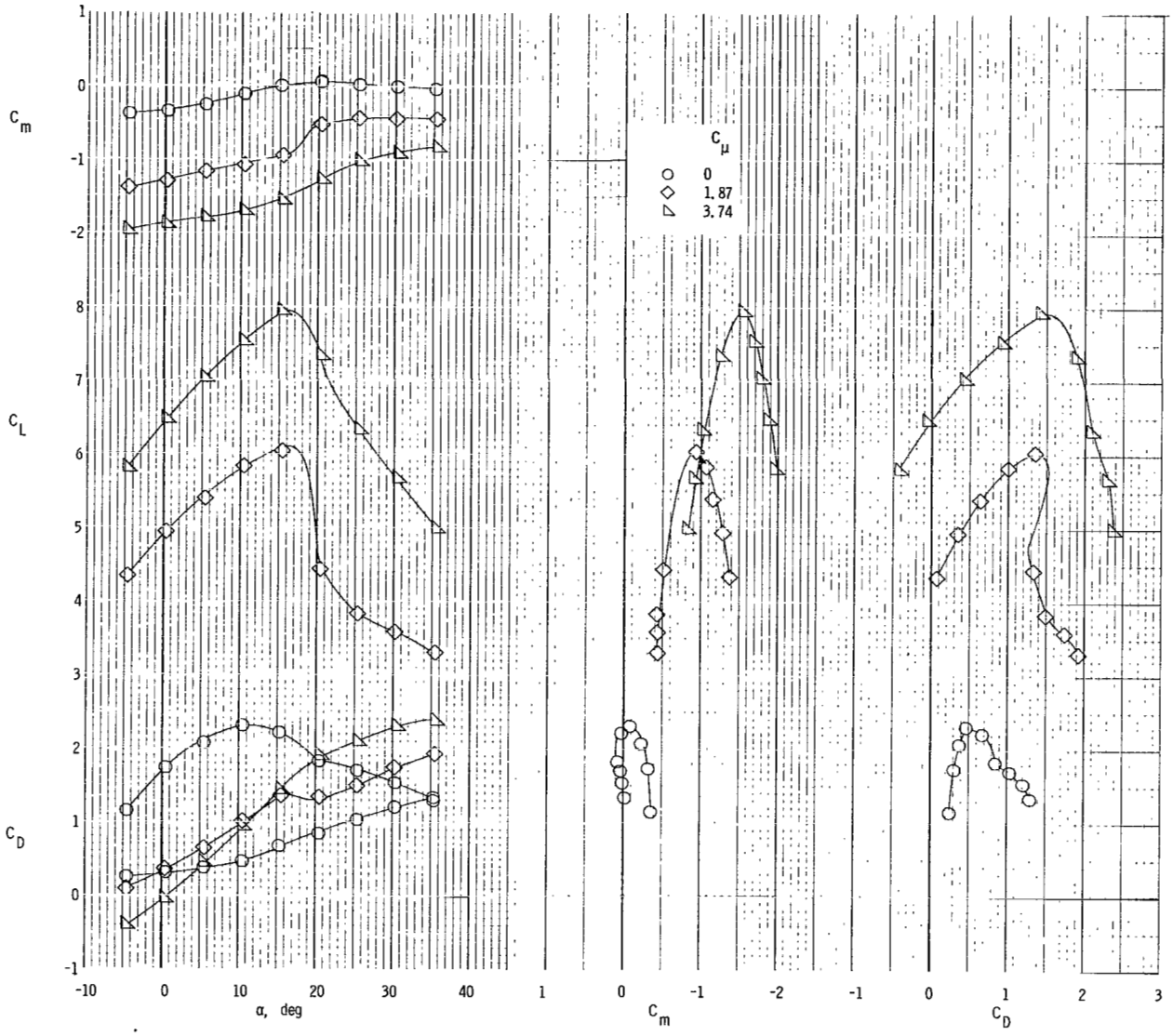

(a) $C_{\mu,le} = 0$.

Figure 15.- Longitudinal characteristics of model with tail off and spread engines. 0.15c leading-edge flap; $\delta_f = 60^o$.

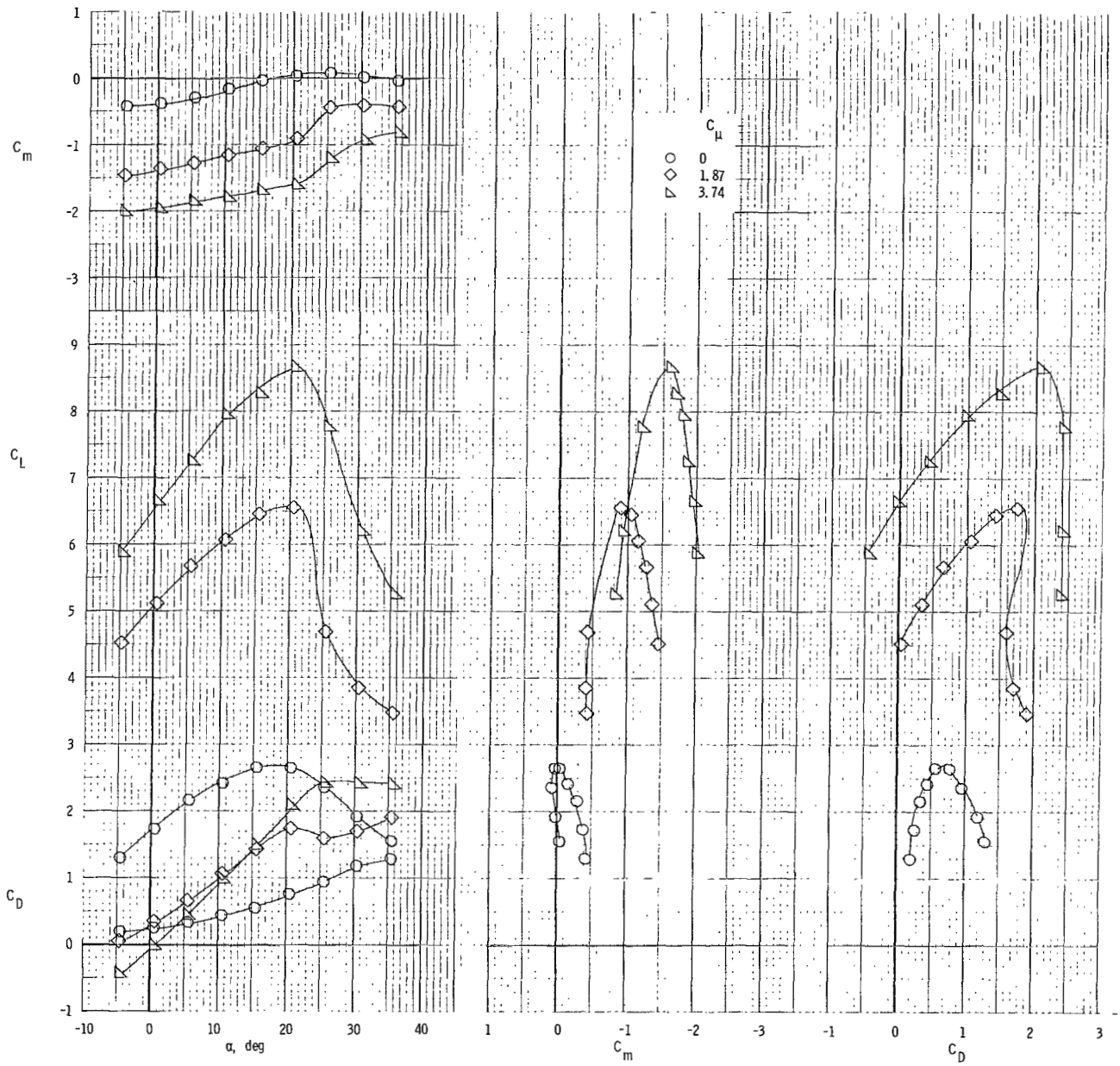

(b) $C_{\mu,le} = 0.024$.

Figure 15.- Concluded.

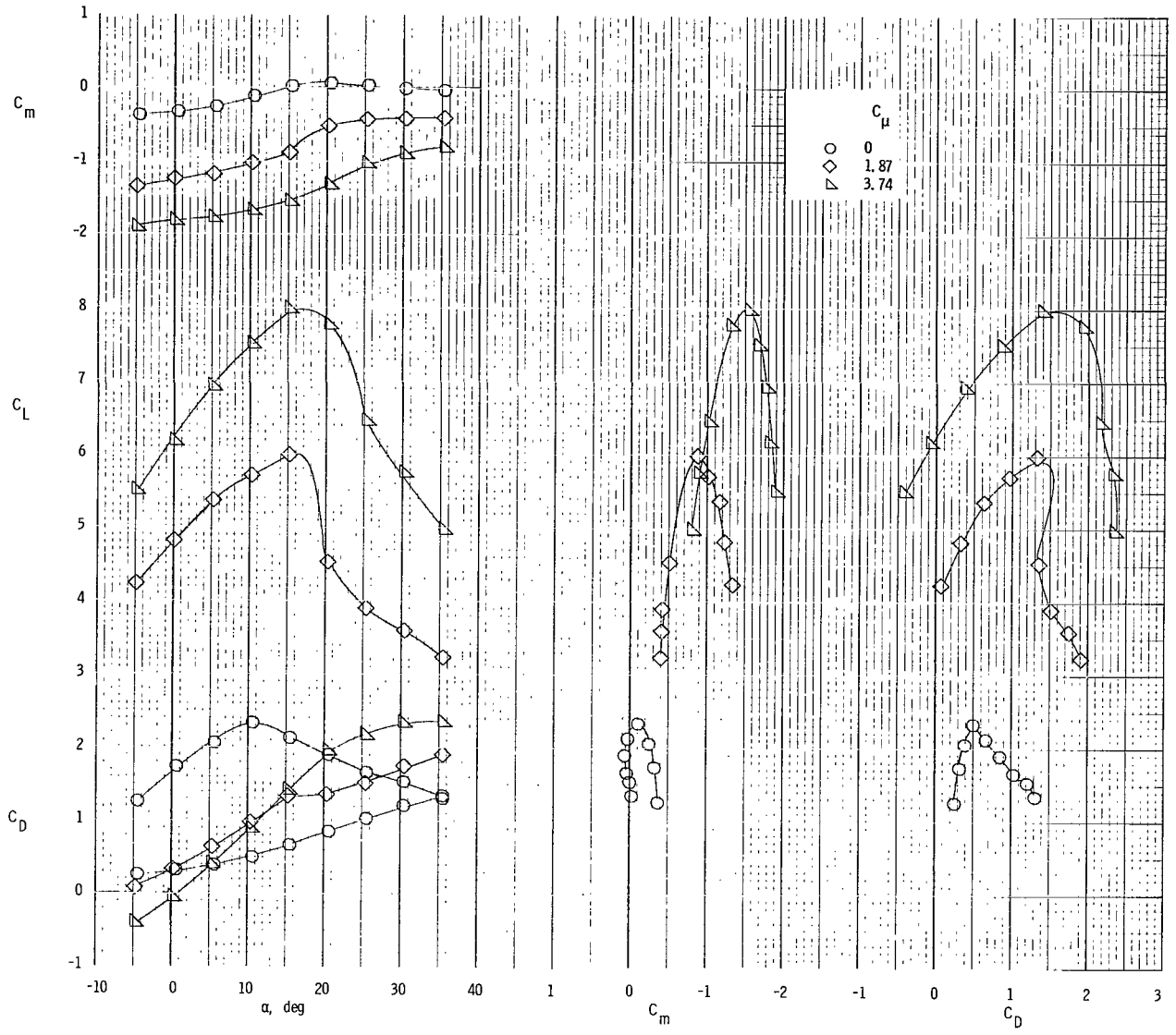

(a) $C_{\mu,le} = 0$.

Figure 16.- Longitudinal characteristics of model with tail off and spread engines. 0.15c high-camber leading-edge flap; $\delta_f = 60^0$.

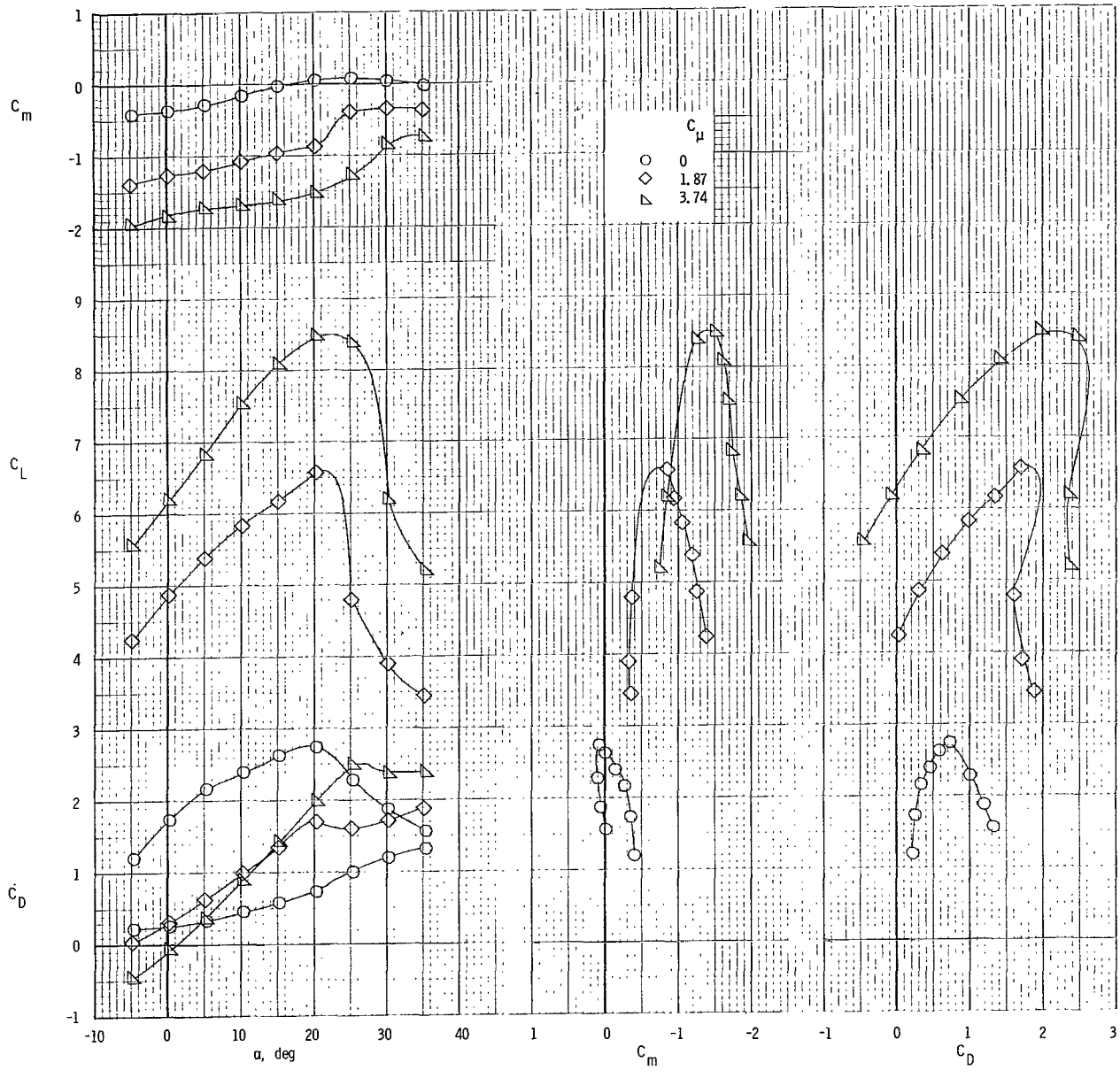

(b) $C_{\mu,le} = 0.024$.

Figure 16.- Concluded.

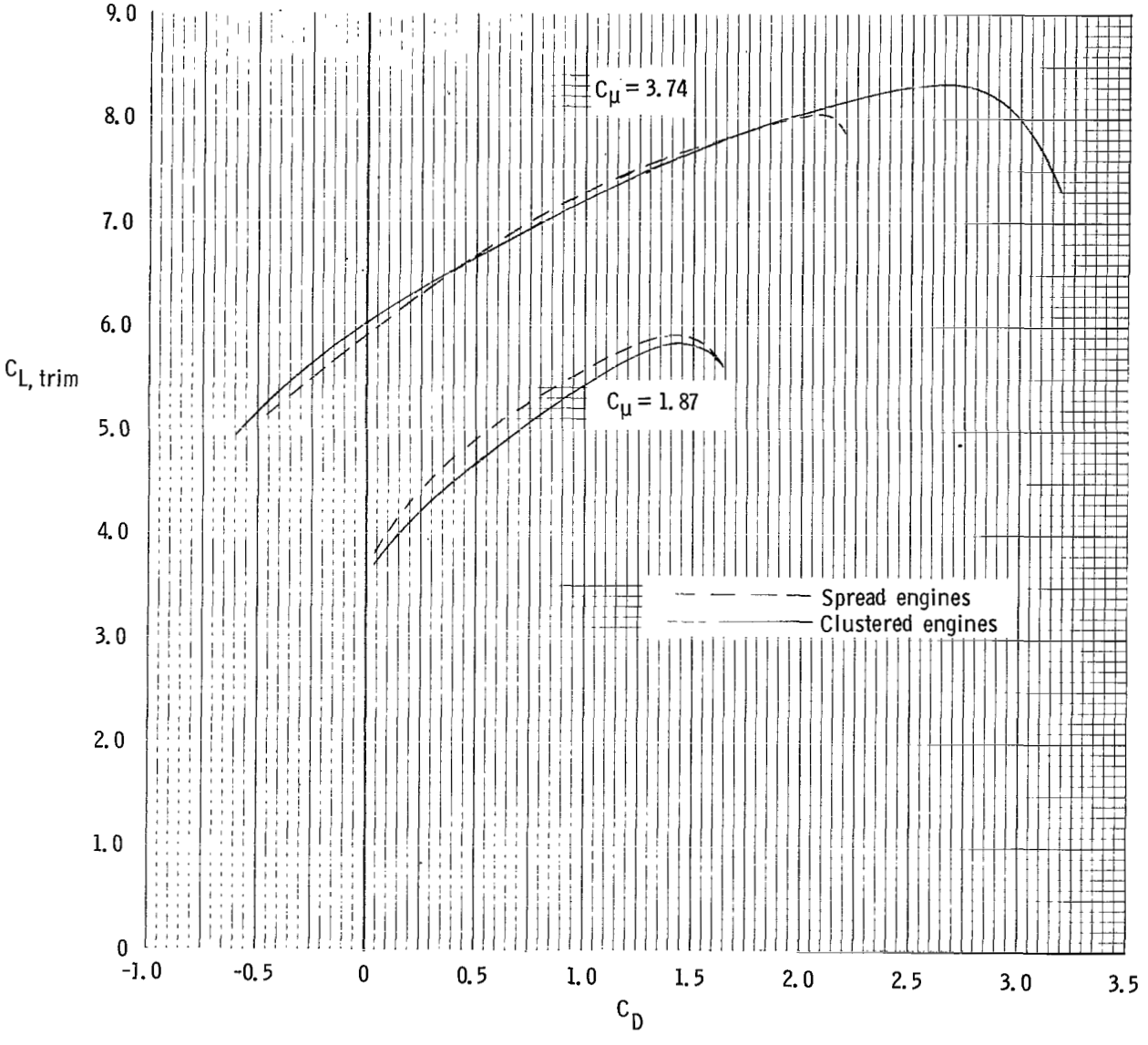

(a) $C_{\mu,le} = 0$. Effect of engine arrangement.

Figure 17.- Lift-drag polars of model. $\delta_f = 60^o$.

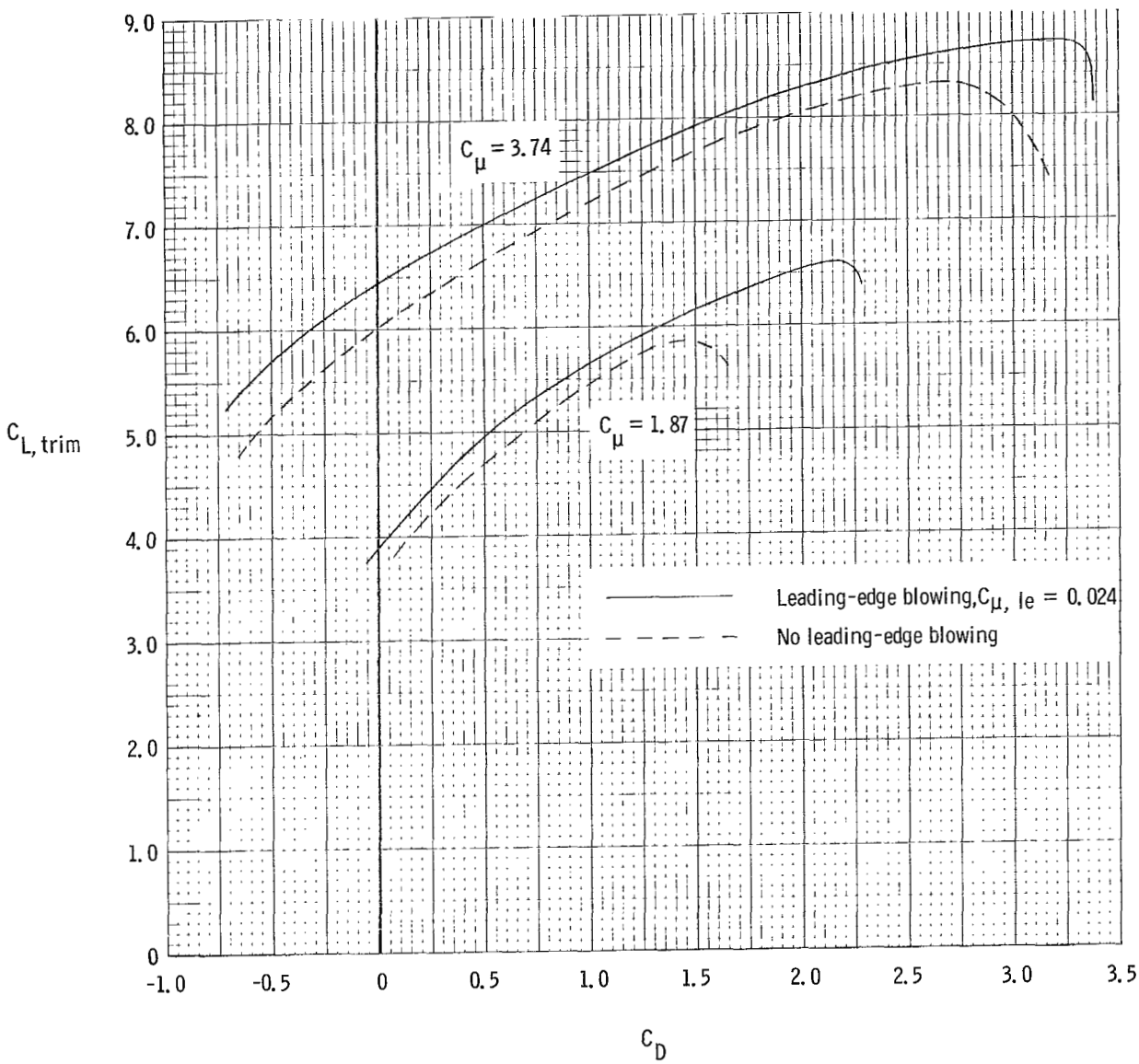

(b) Clustered engines. Effect of leading-edge blowing.

Figure 17.- Continued.

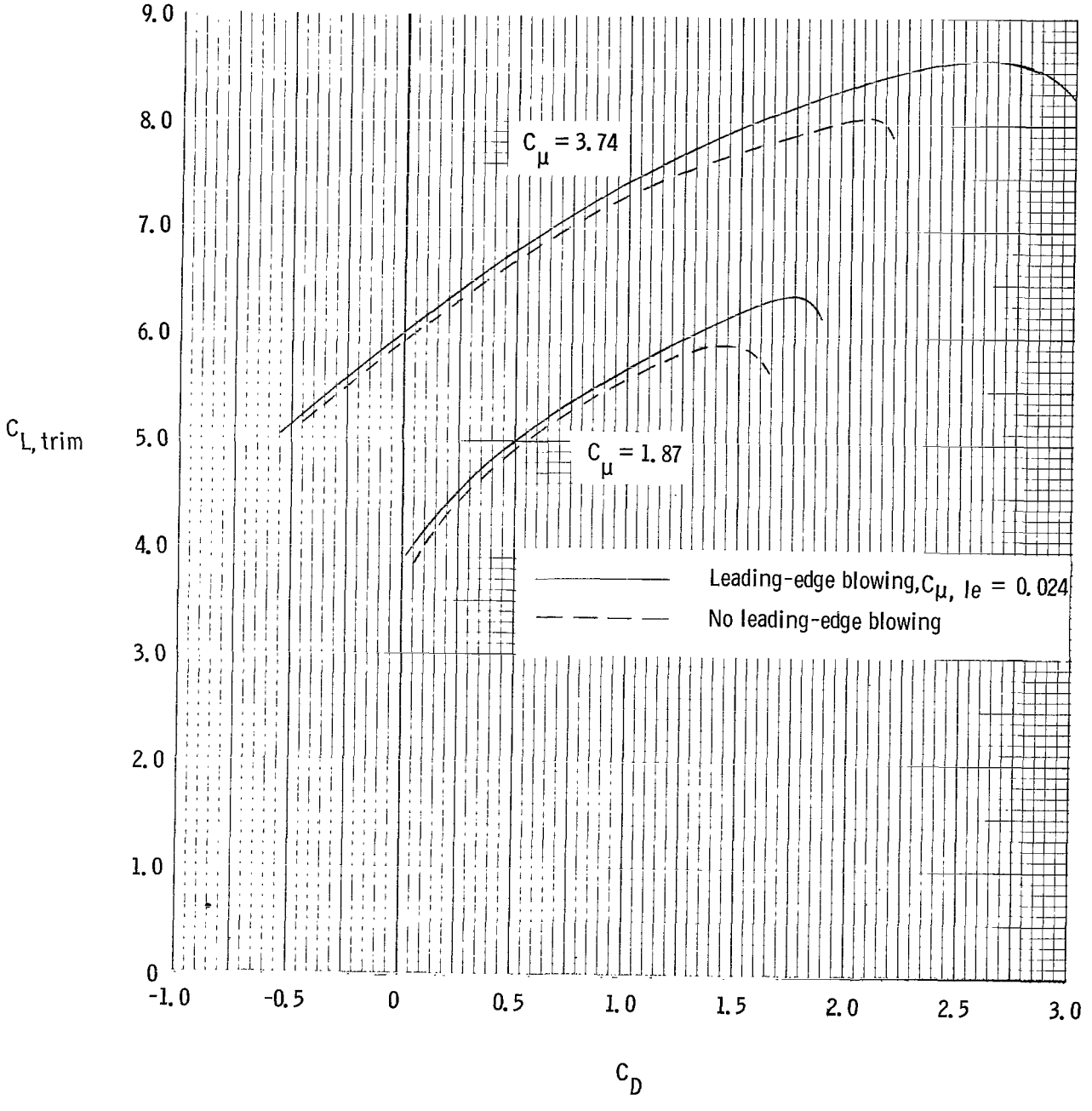

(c) Spread engines. Effect of leading-edge blowing.

Figure 17.- Continued.

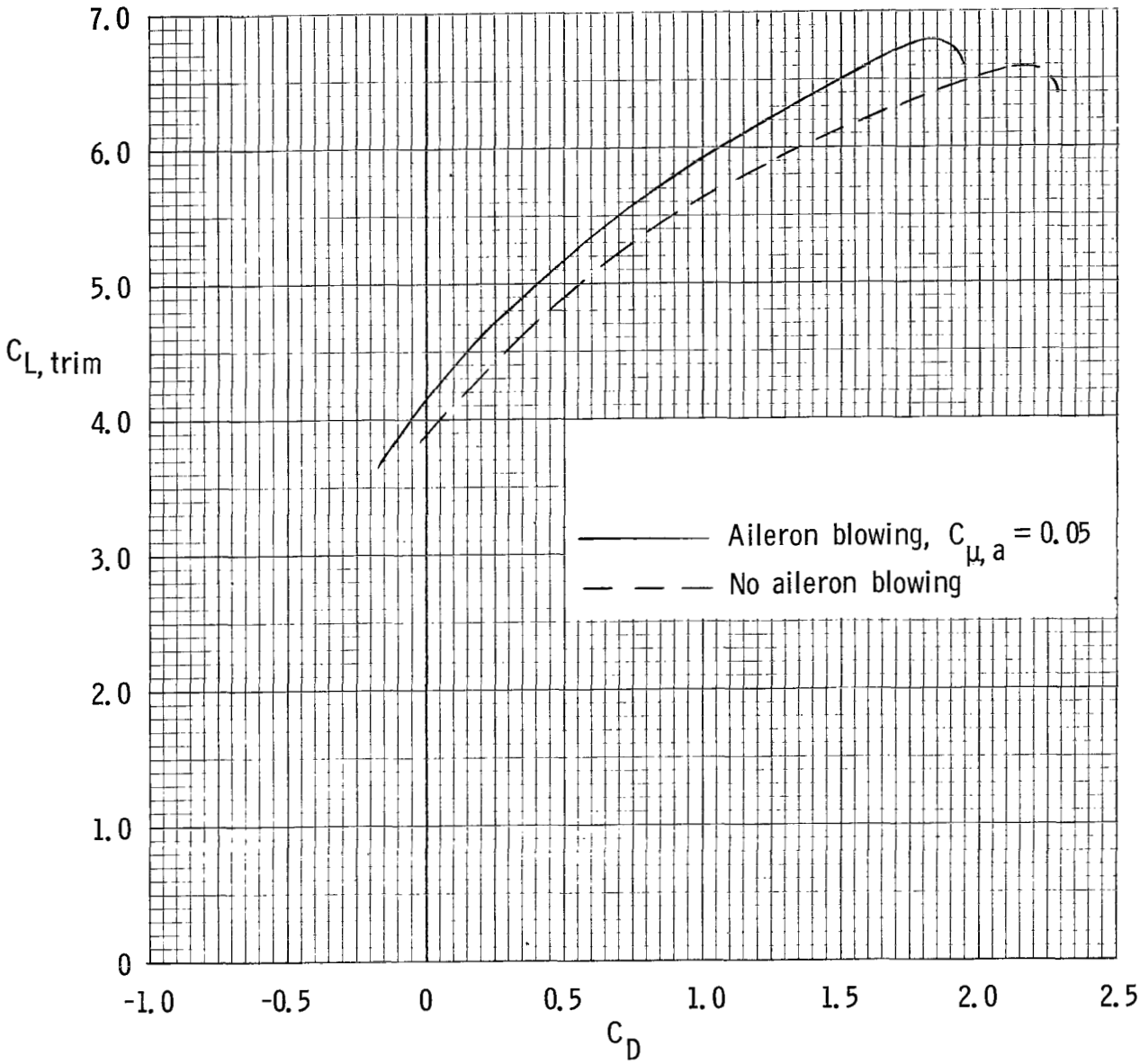

(d) Clustered engines. Effect of aileron blowing.

Figure 17.- Concluded.

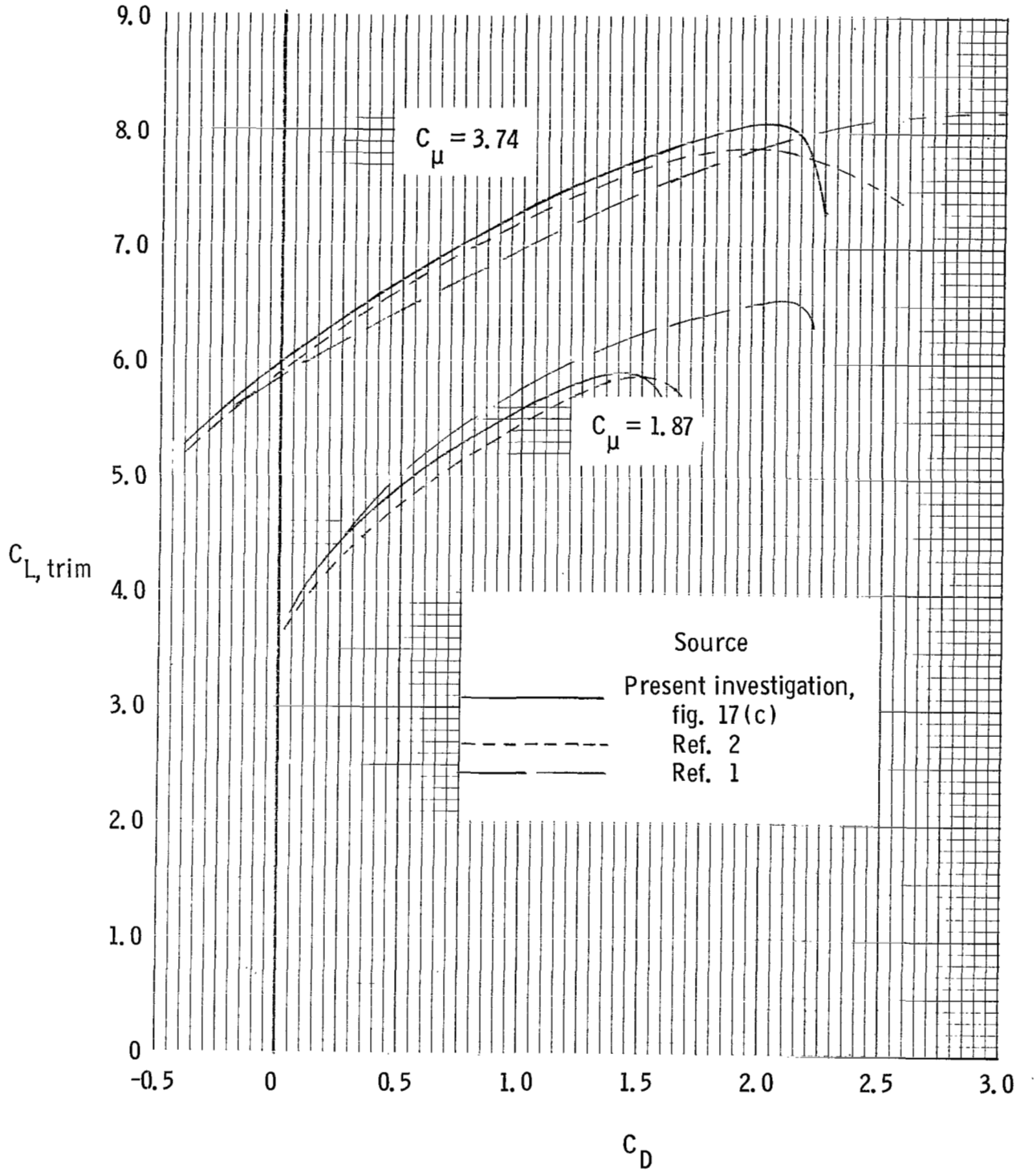

Figure 18.- Comparison of lift-drag polars for several jet-flap configurations. $\delta_f = 60^o$.

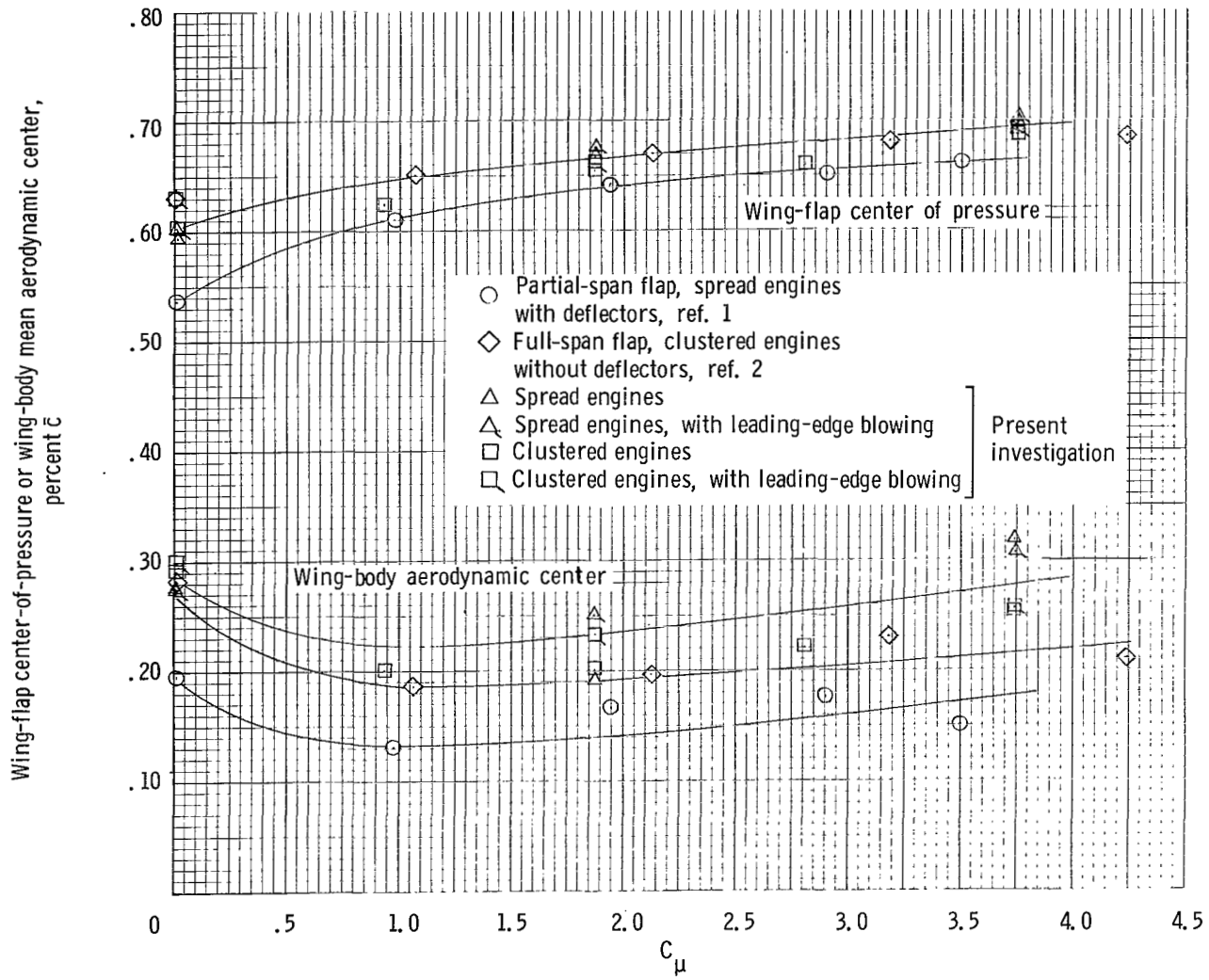

Figure 19.- Variation of wing-flap center of pressure and wing-body aerodynamic center with thrust coefficient. $\delta_f = 60^0$; $\alpha = 5^0$.

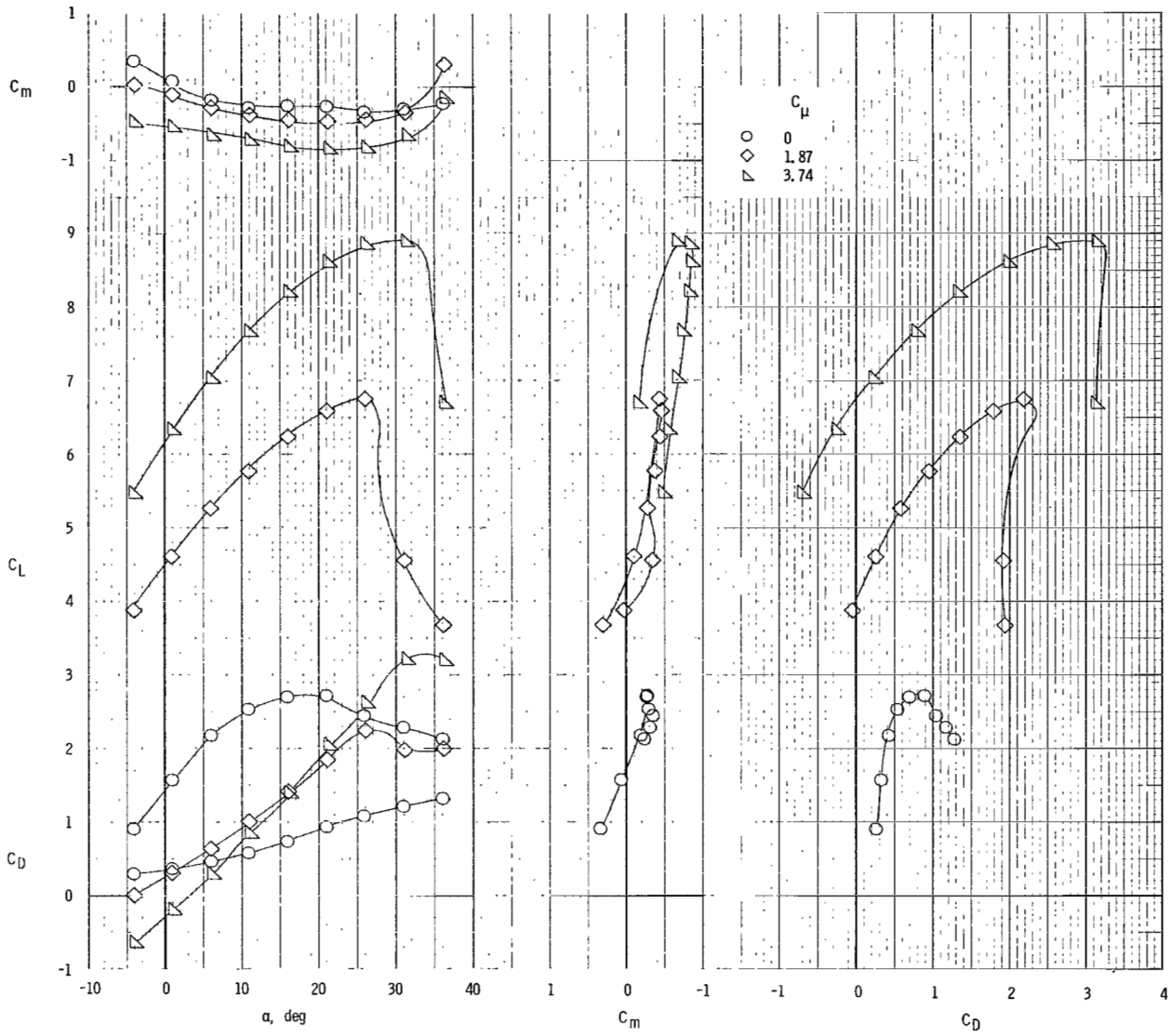

(a) $i_t = 0^0$; $C_{\mu,e} = 0$.

Figure 20.- Longitudinal characteristics of model with tail on and clustered engines. $\delta_f = 60^0$; $\delta_e = -50^0$; $C_{\mu,le} = 0.024$.

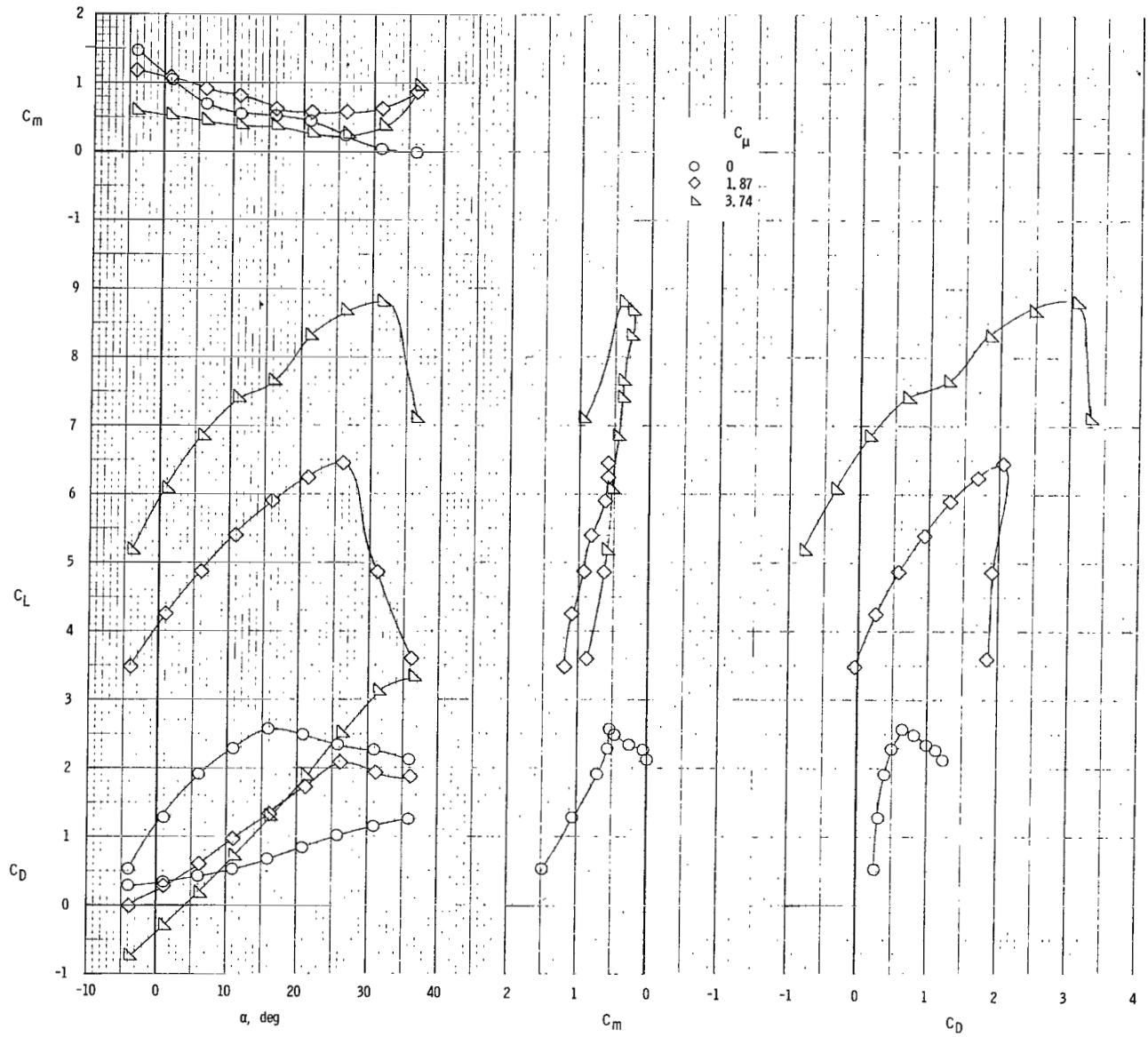

(b) $i_t = 0^0$; $C_{\mu,e} = 0.037$.

Figure 20.- Continued.

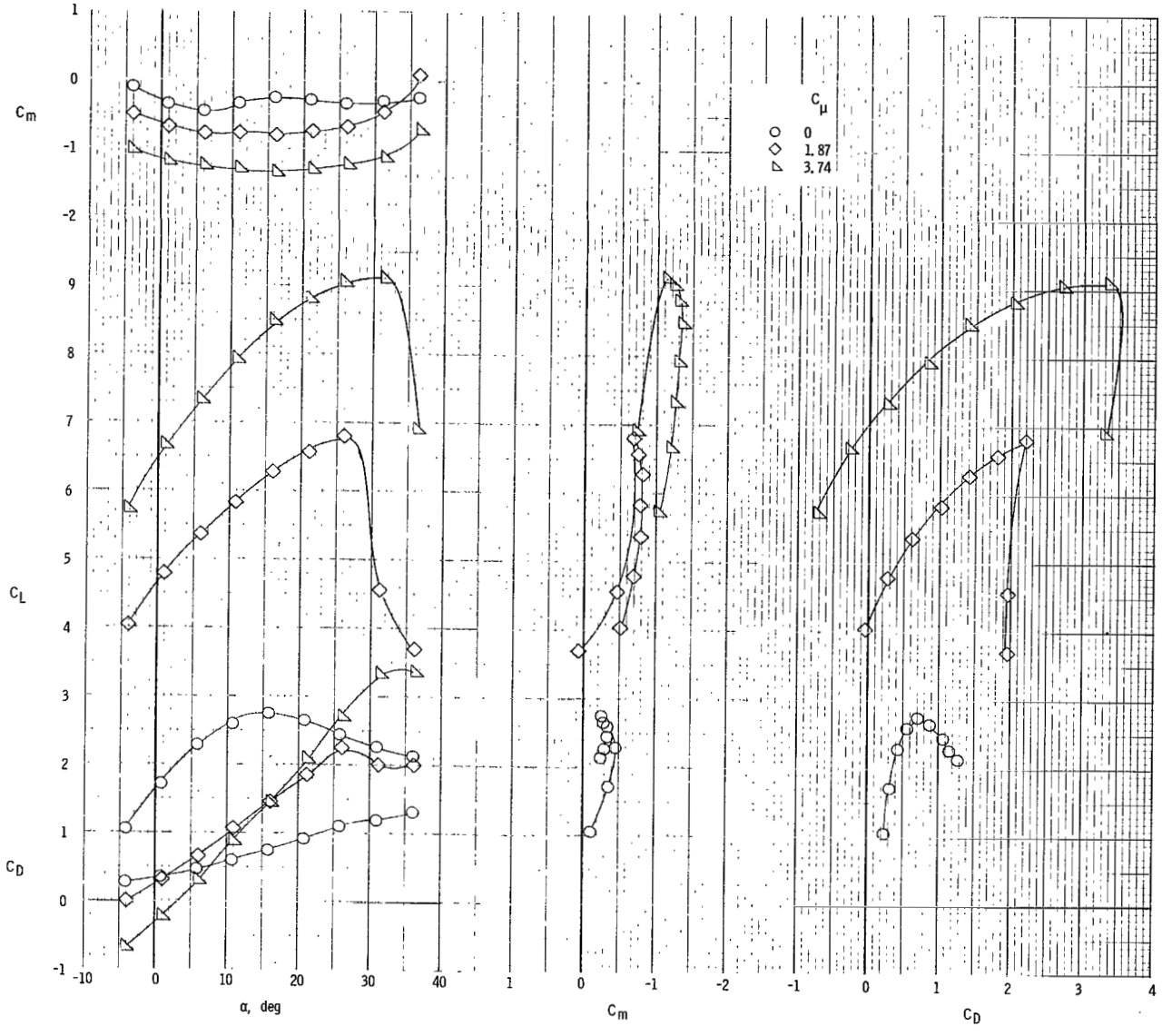

(c) $i_t = 5^0$; $C_{\mu,e} = 0$.

Figure 20.- Continued.

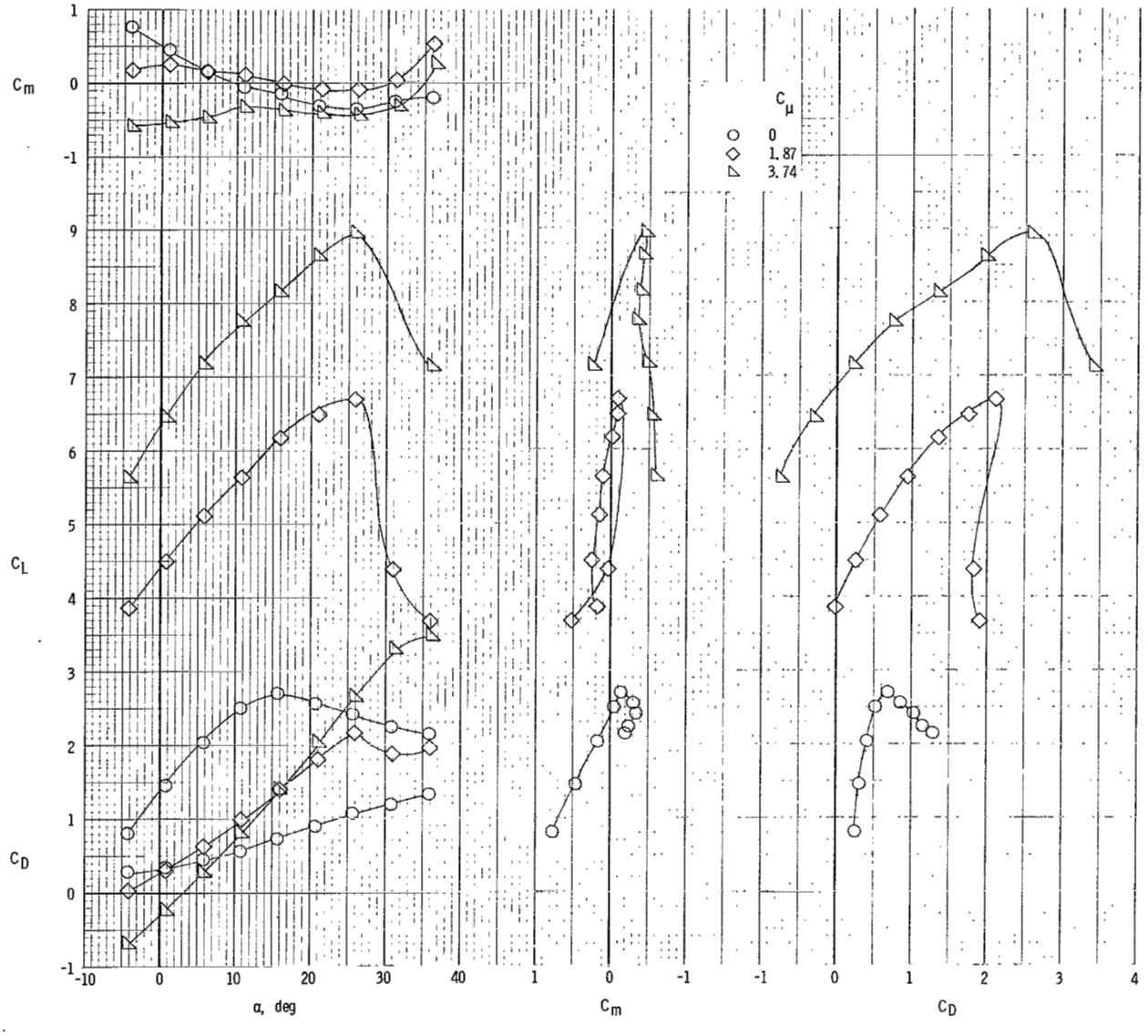

(d) $i_t = -5^0$; $C_{\mu,e} = 0$.

Figure 20.- Continued.

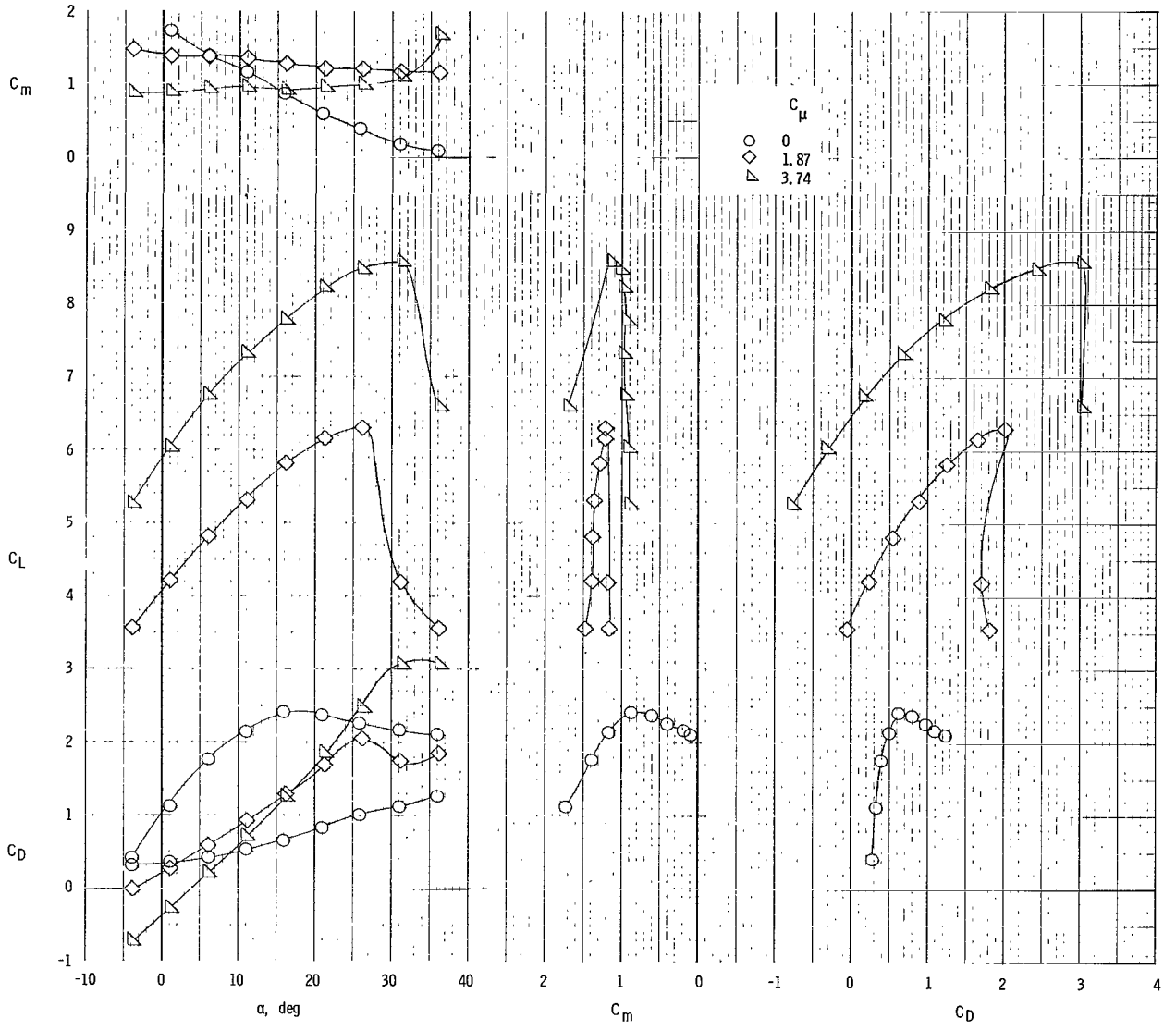

(e) $i_t = -5^0$; $C_{\mu,e} = 0.037$.

Figure 20.- Concluded.

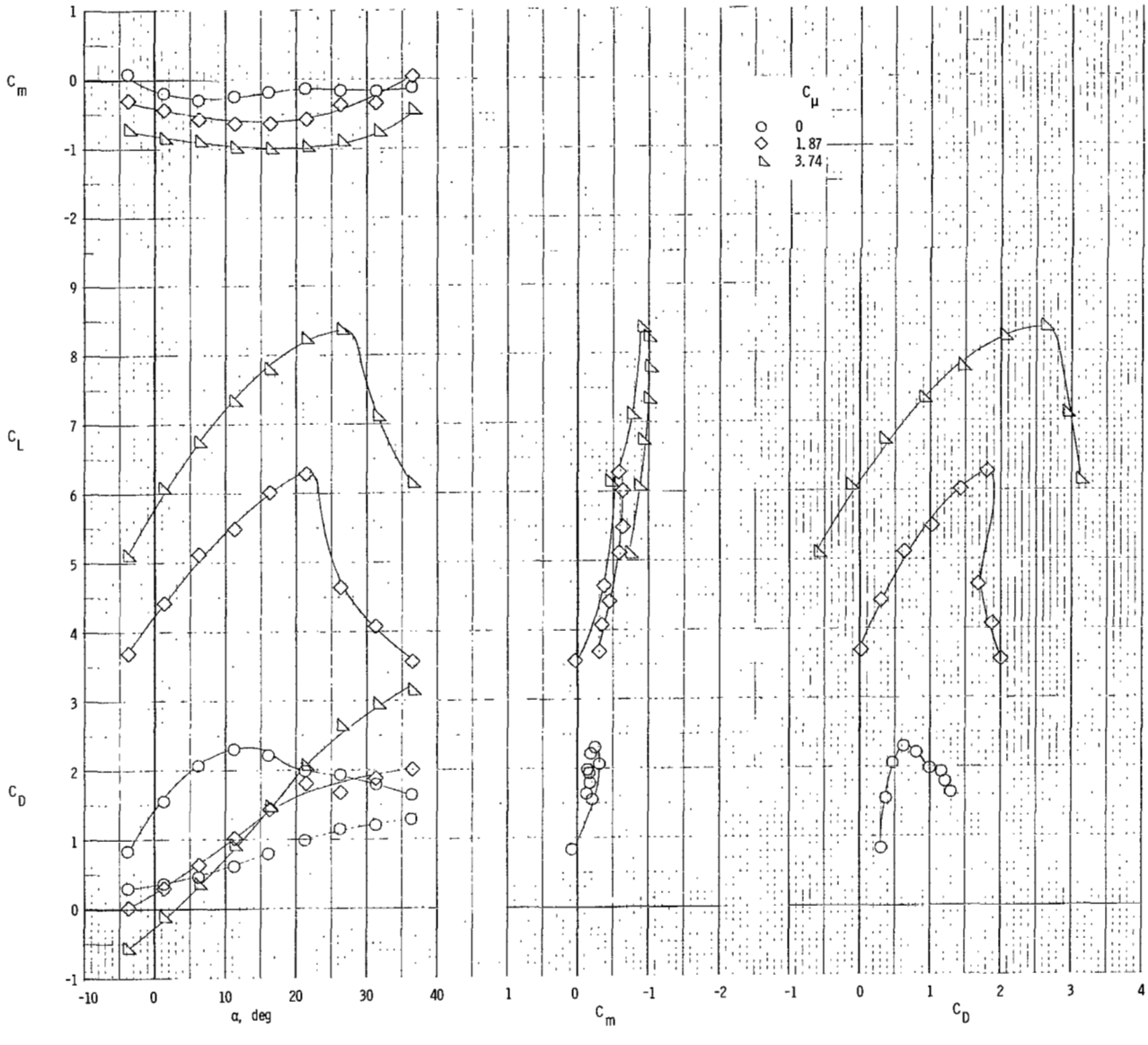

(a) $C_{\mu,e} = 0$.

Figure 21.- Longitudinal characteristics of model with tail on and clustered engines. $\delta_f = 60^0$; $\delta_e = -25^0$; $C_{\mu,le} = 0$; $i_t = 0^0$.

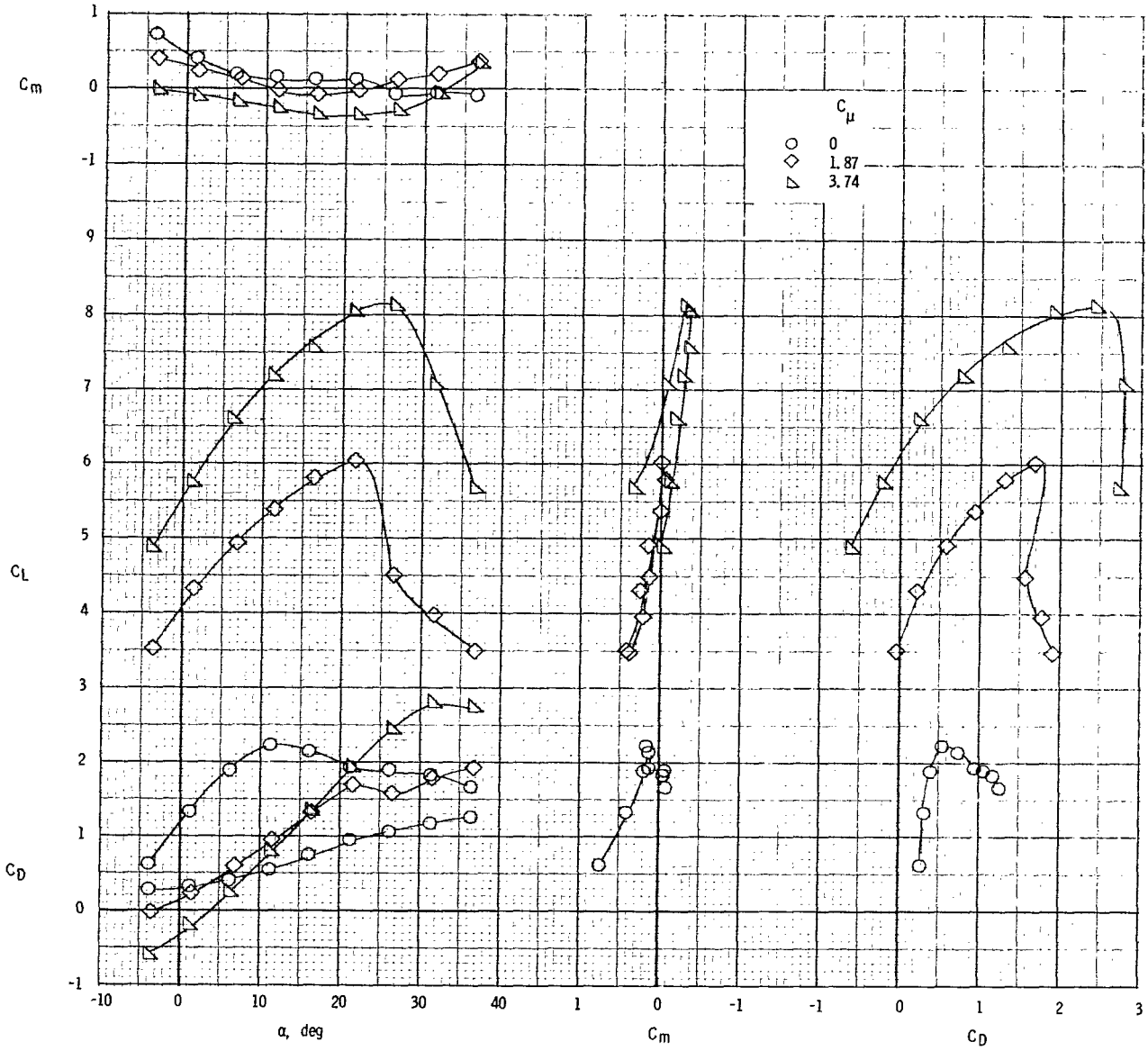

(b) $C_{\mu,e} = 0.037$.

Figure 21.- Concluded.

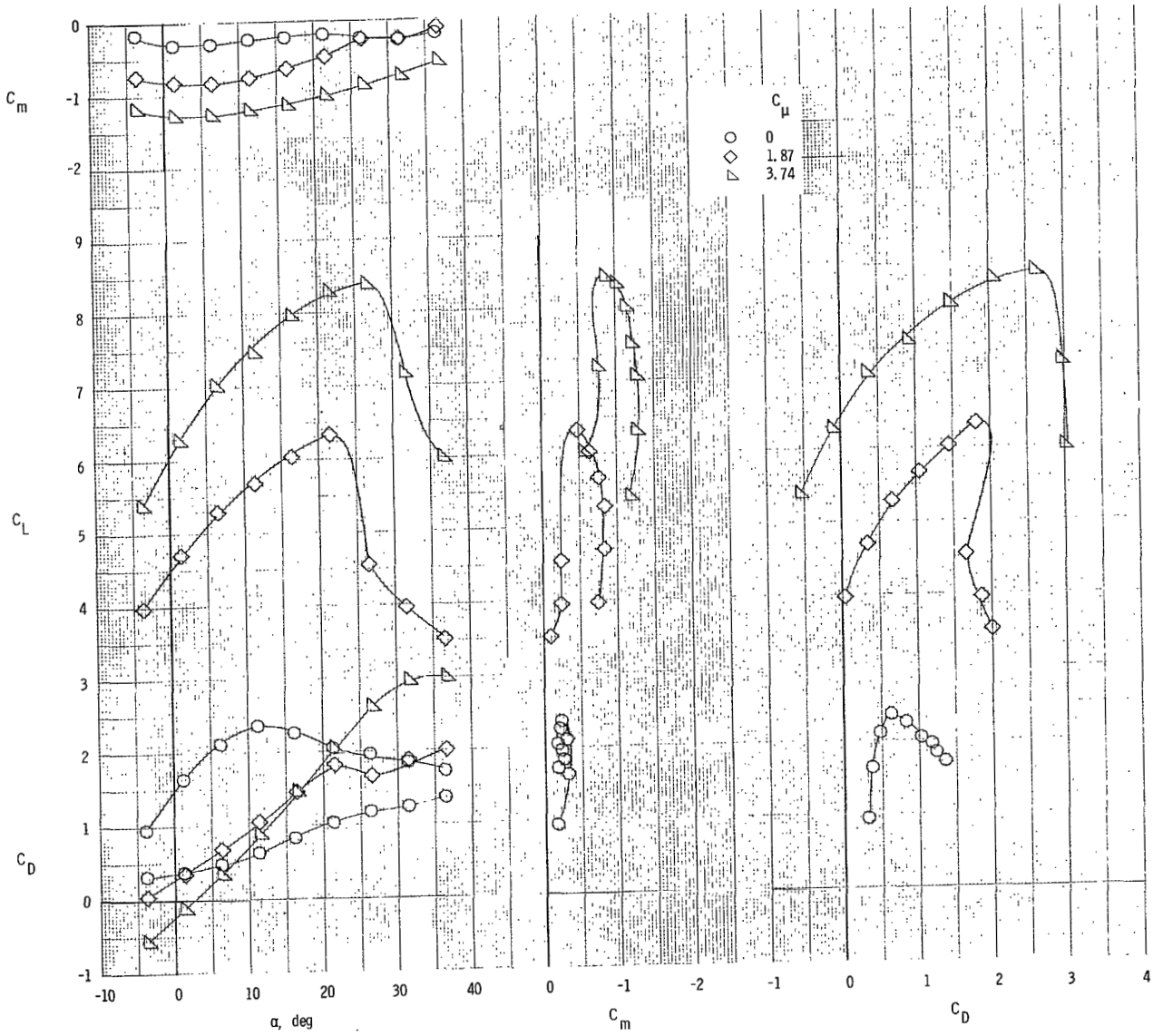

Figure 22.- Longitudinal characteristics of model with tail on and clustered engines. $\delta_f = 60^o$; $\delta_e = 0^o$; $C_{\mu,le} = 0$; $i_t = 0^o$; $C_{\mu,e} = 0$.

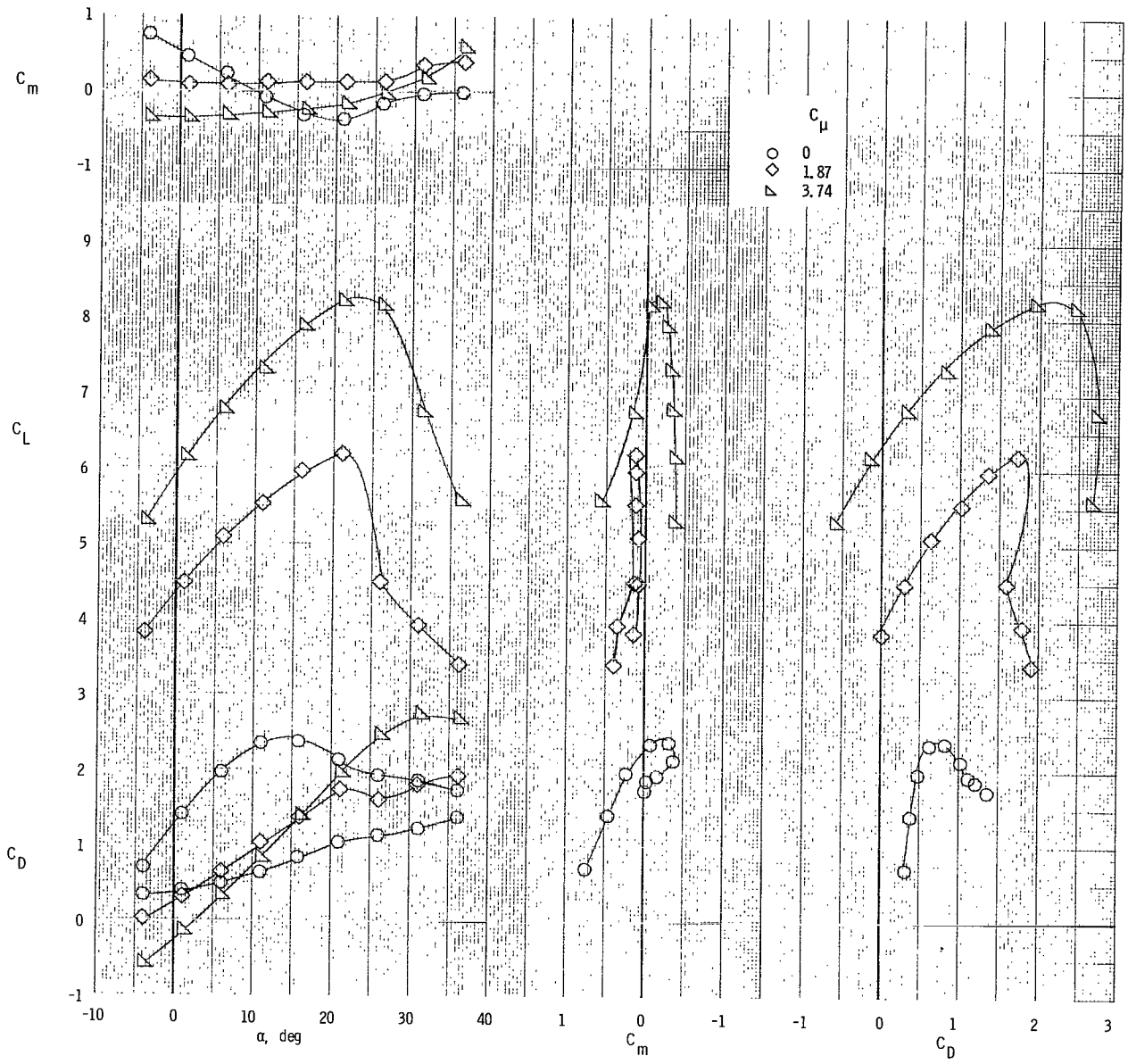

(a) $i_t = 0^0$; $C_{\mu,e} = 0$.

Figure 23.- Longitudinal characteristics of model with tail on and clustered engines. Chord of tail leading-edge flap shortened to 9 percent of tail chord; $\delta_f = 60^0$; $\delta_e = -50^0$; $C_{\mu,le} = 0$.

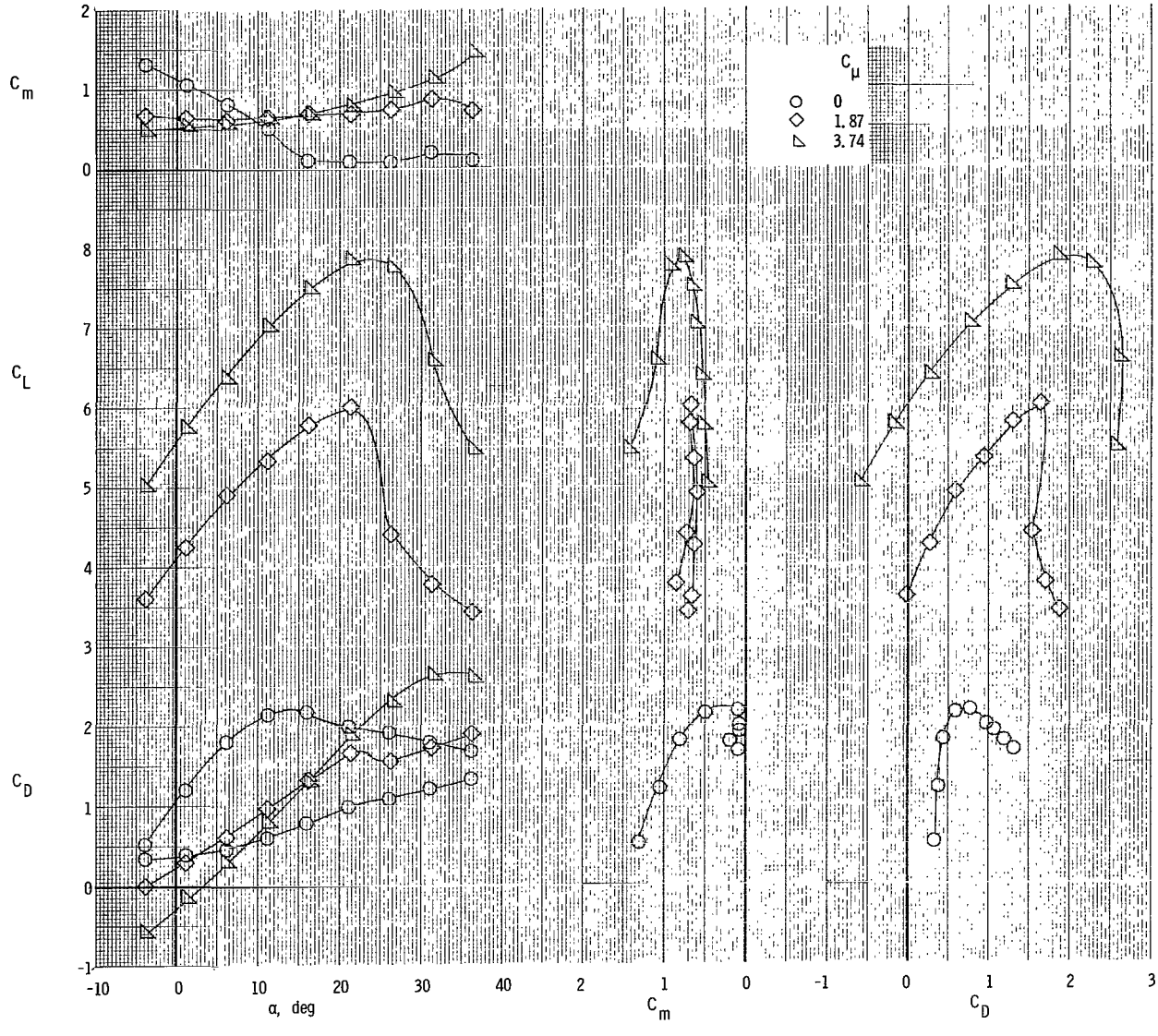

(b) $i_t = 0^o$; $C_{\mu,e} = 0.017$.

Figure 23.- Continued.

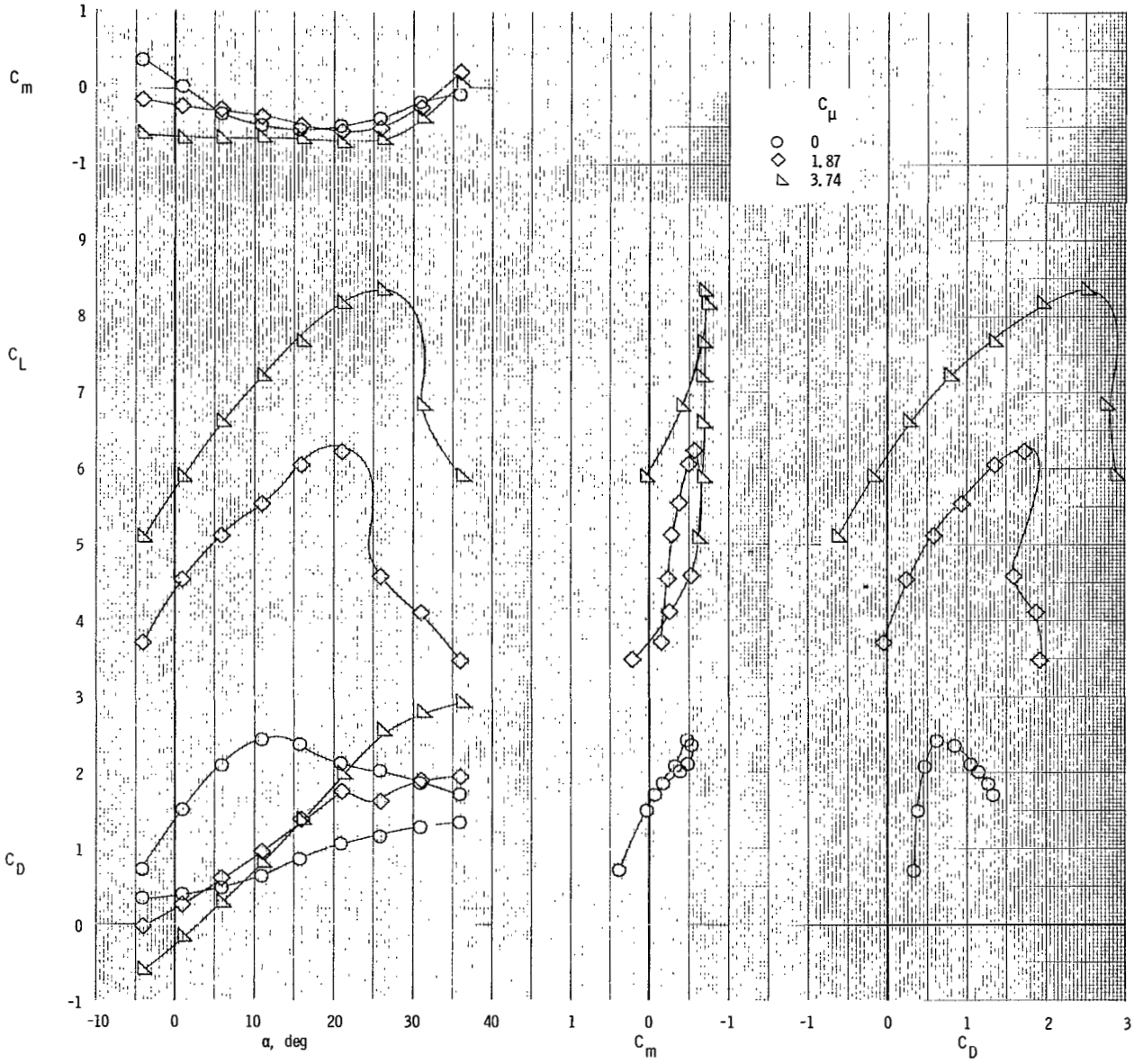

(c) $i_t = 5^0$; $C_{\mu,e} = 0$.

Figure 23.- Continued.

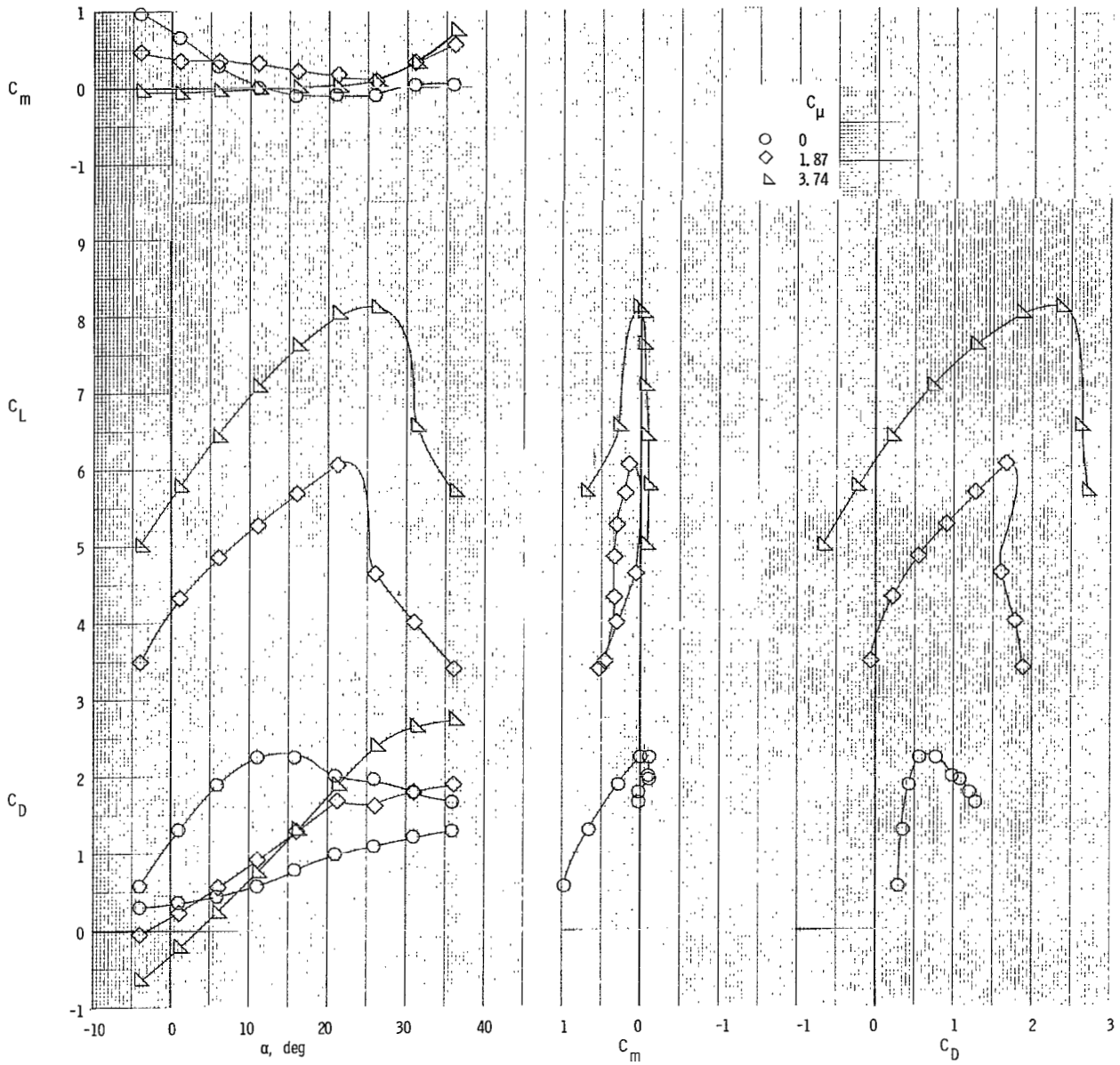

(d) $i_t = 5^0$; $C_{\mu,e} = 0.017$.

Figure 23.- Concluded.

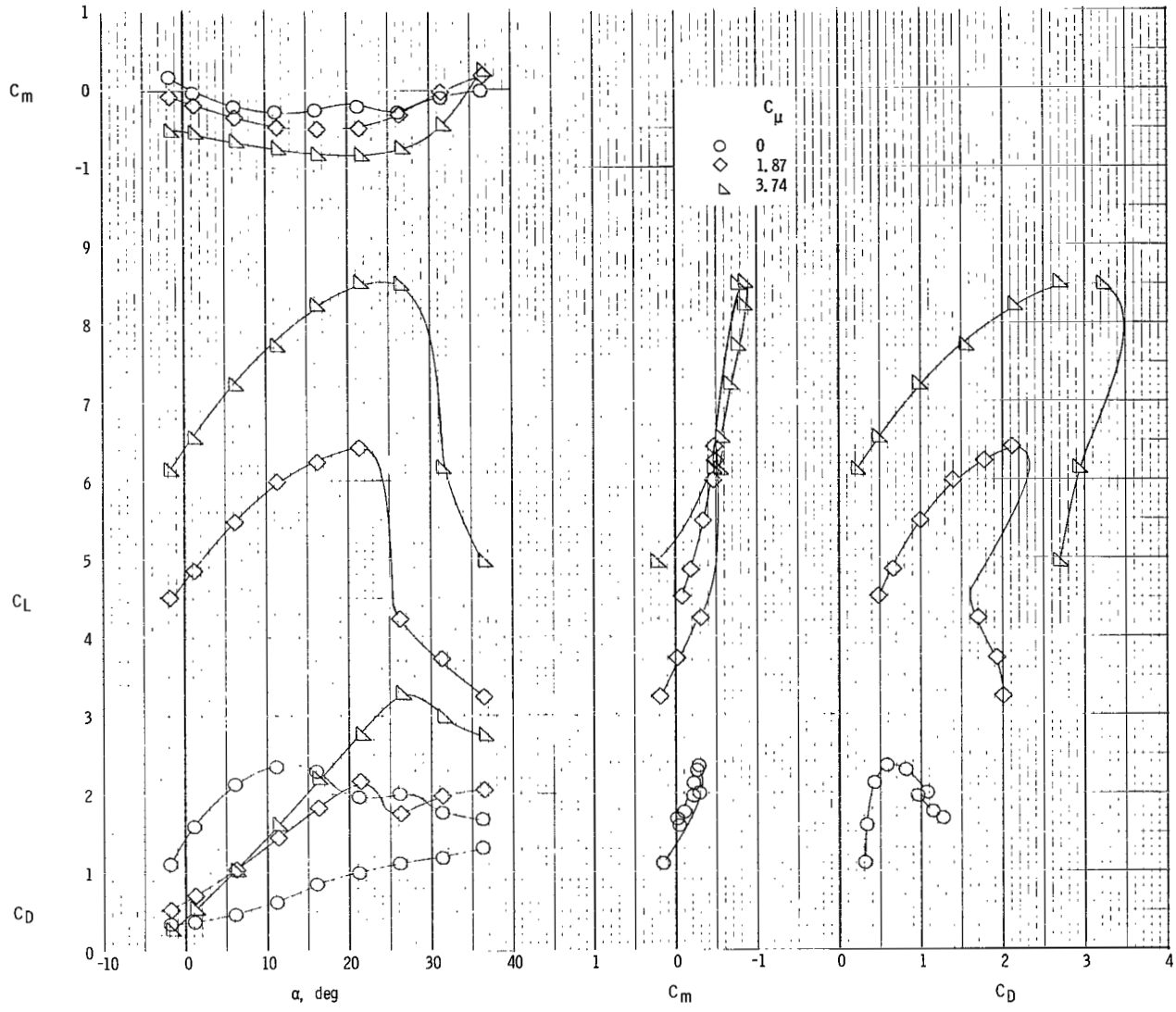

(a) $C_{\mu,le} = 0$.

Figure 24.- Longitudinal characteristics of model with tail on and clustered engines. $\delta_f = 70^0$; $\delta_e = -50^0$; $i_t = 0^0$.

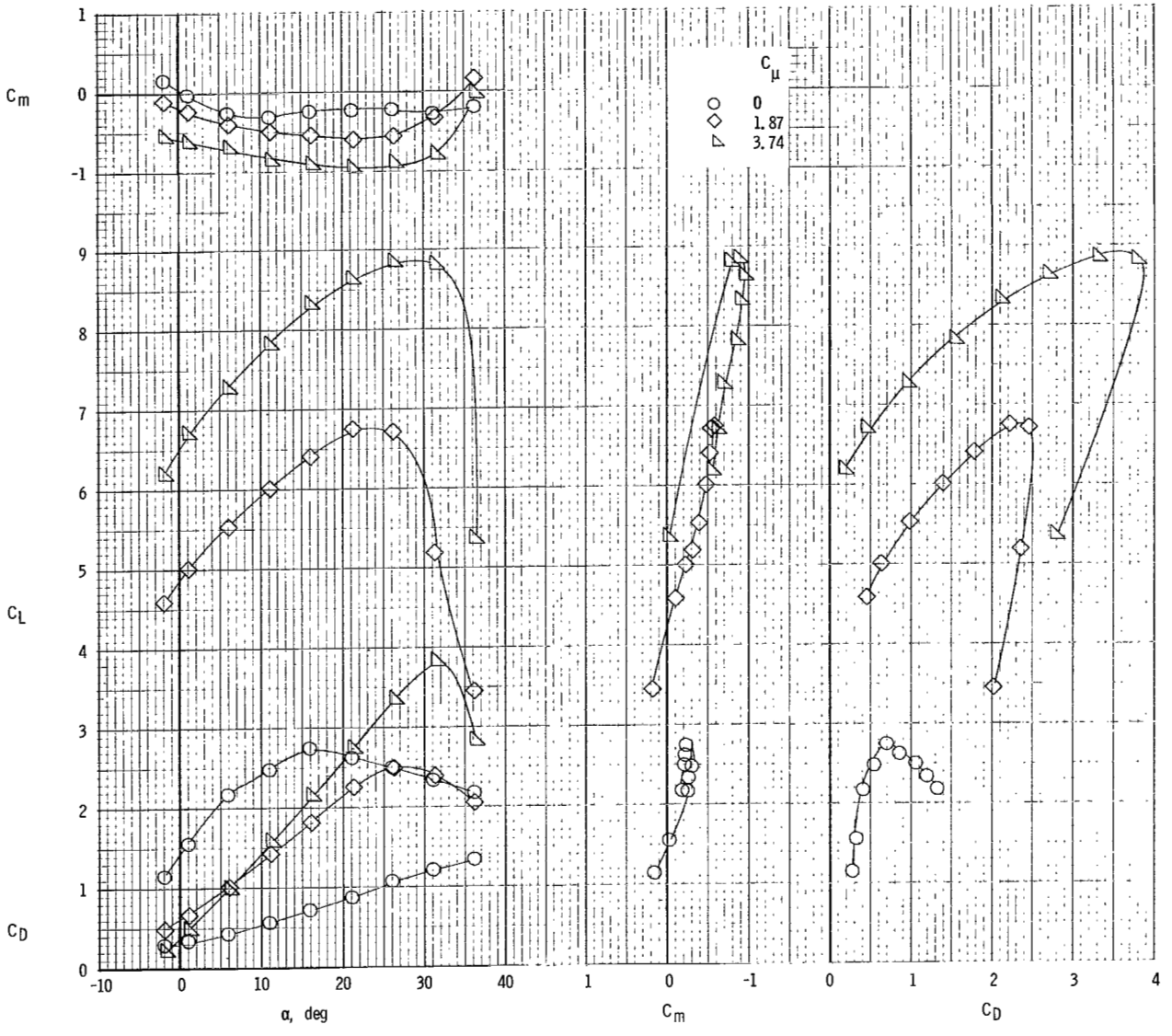

(b) $C_{\mu,le} = 0.024$.

Figure 24.- Concluded.

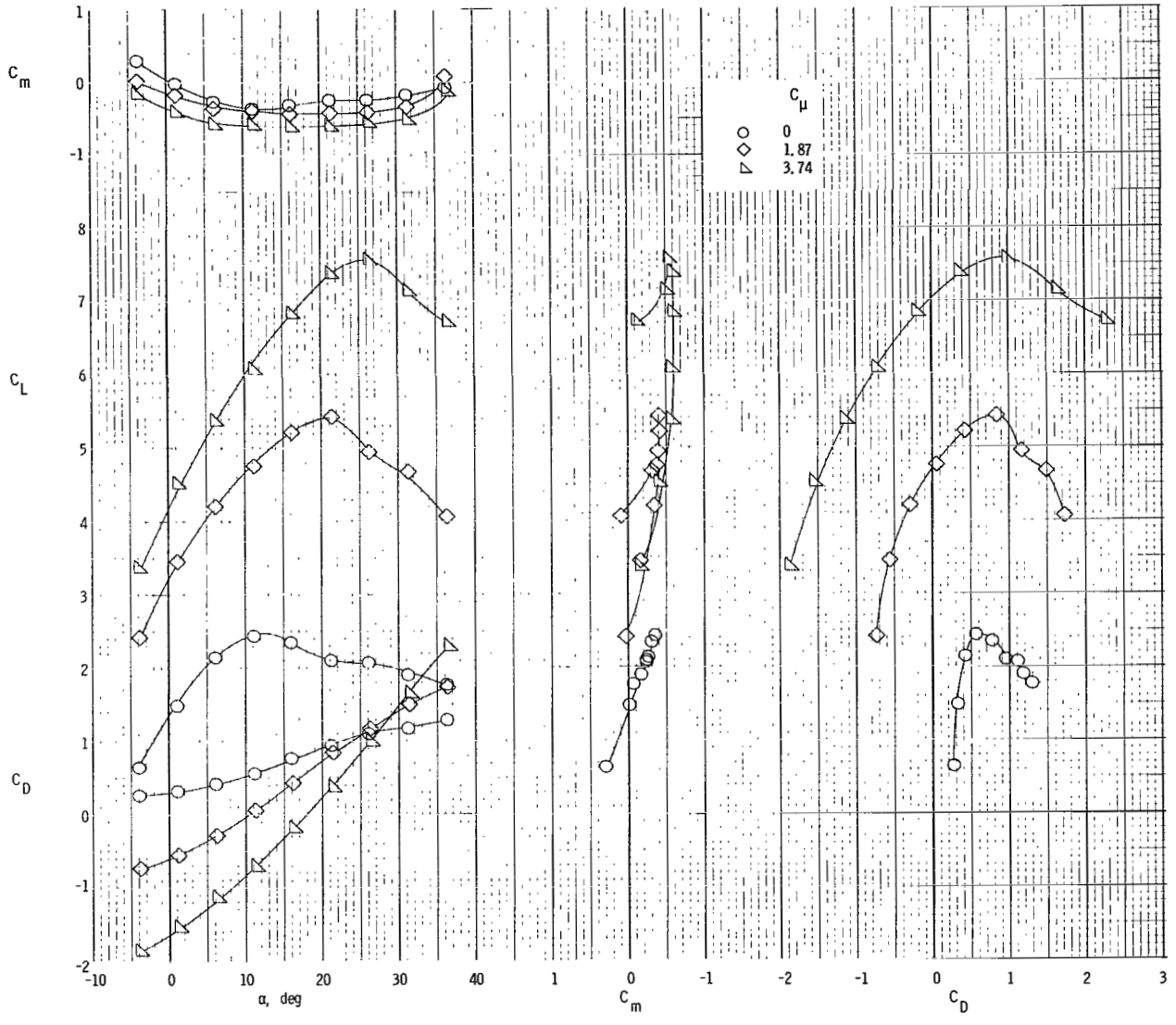

(a) $C_{\mu,le} = 0$.

Figure 25.- Longitudinal characteristics of model with tail on and clustered engines. $\delta_f = 40^0$; $\delta_e = -50^0$; $i_t = 0^0$.

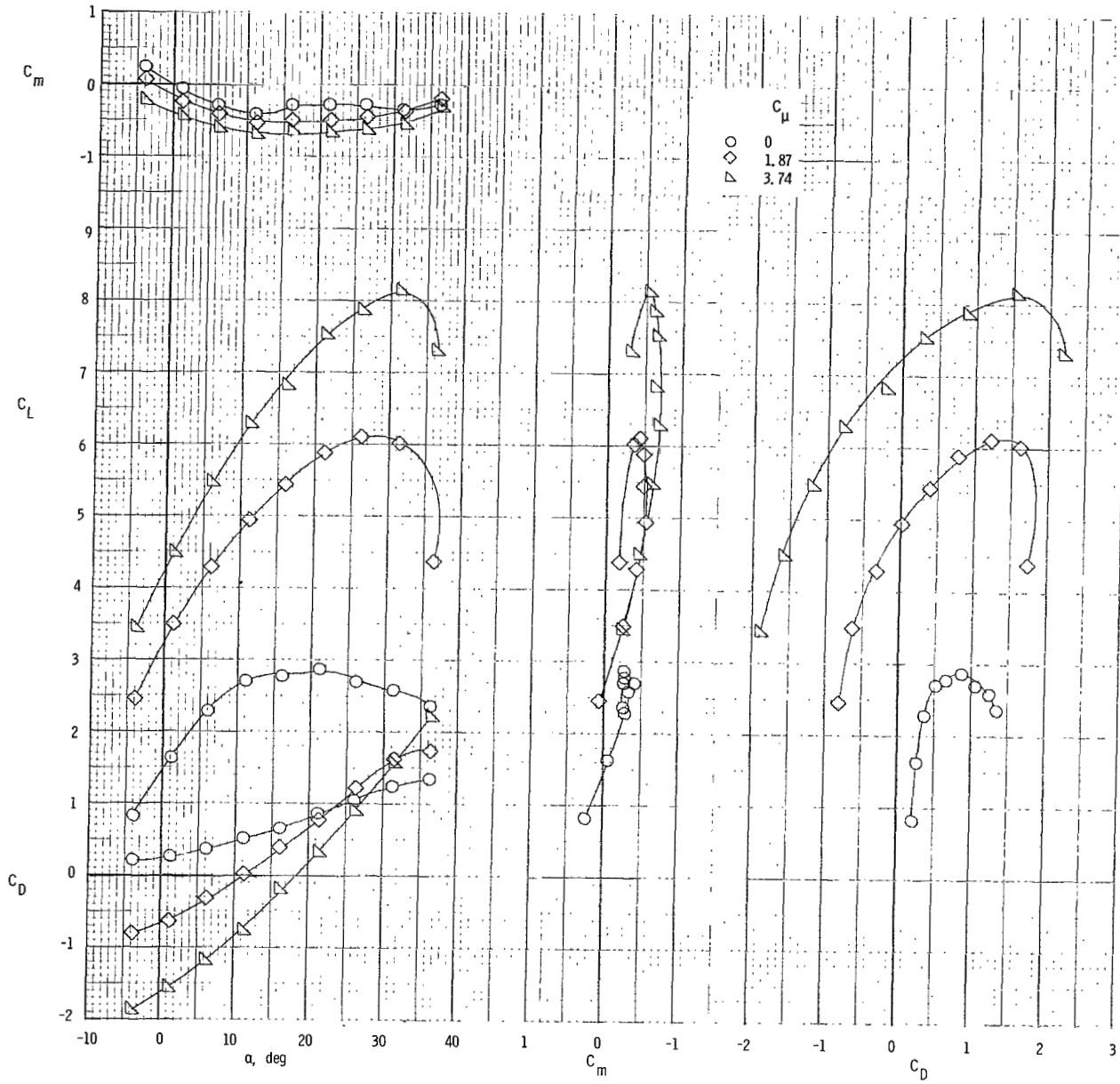

(b) $C_{\mu,le} = 0.024$.

Figure 25.- Concluded.

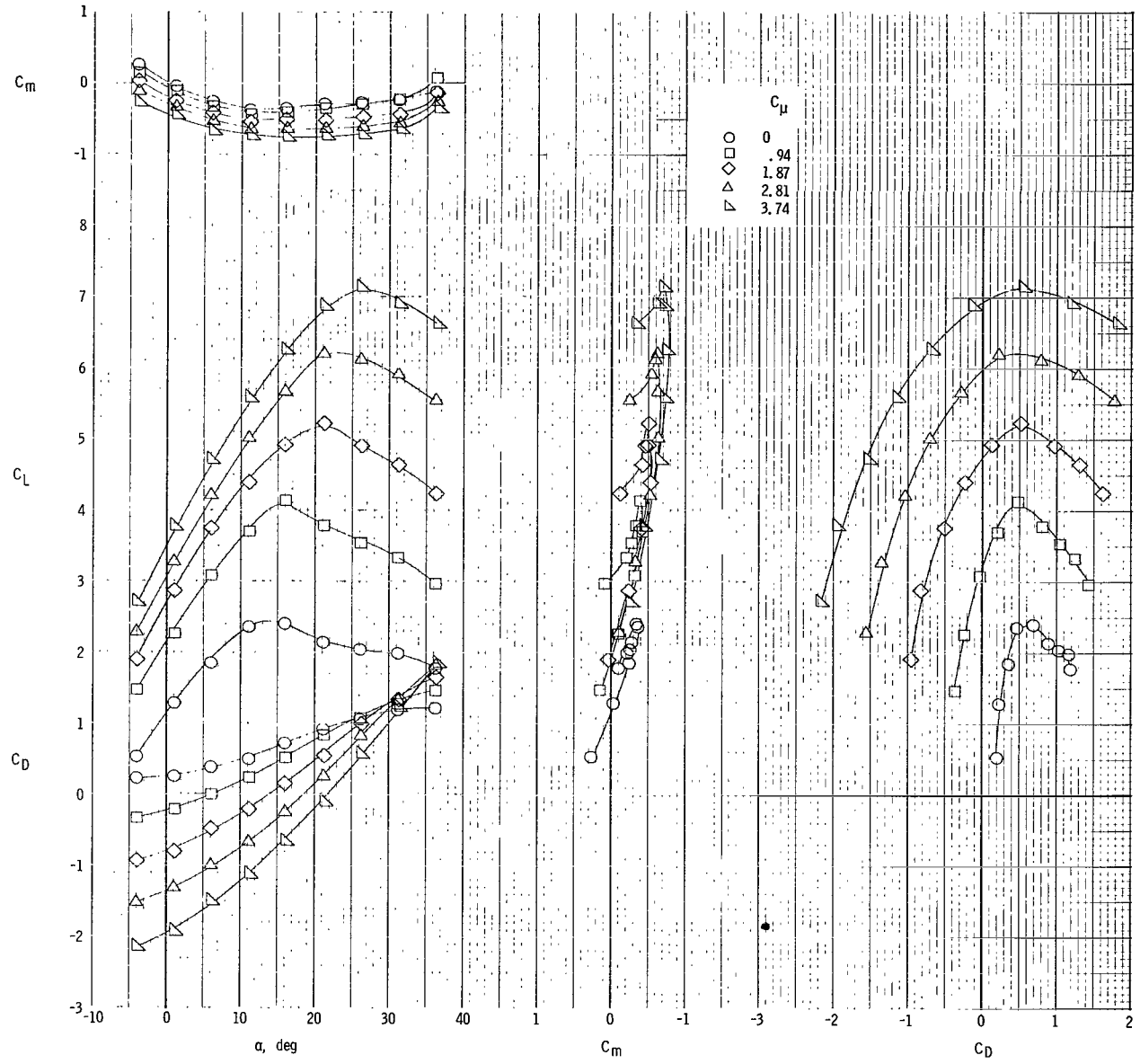

(a) $i_t = 0^o$; $C_{\mu,le} = 0$; $C_{\mu,e} = 0$.

Figure 26.- Longitudinal characteristics of model with tail on and clustered engines. $\delta_f = 35^o$; $\delta_e = -50^o$.

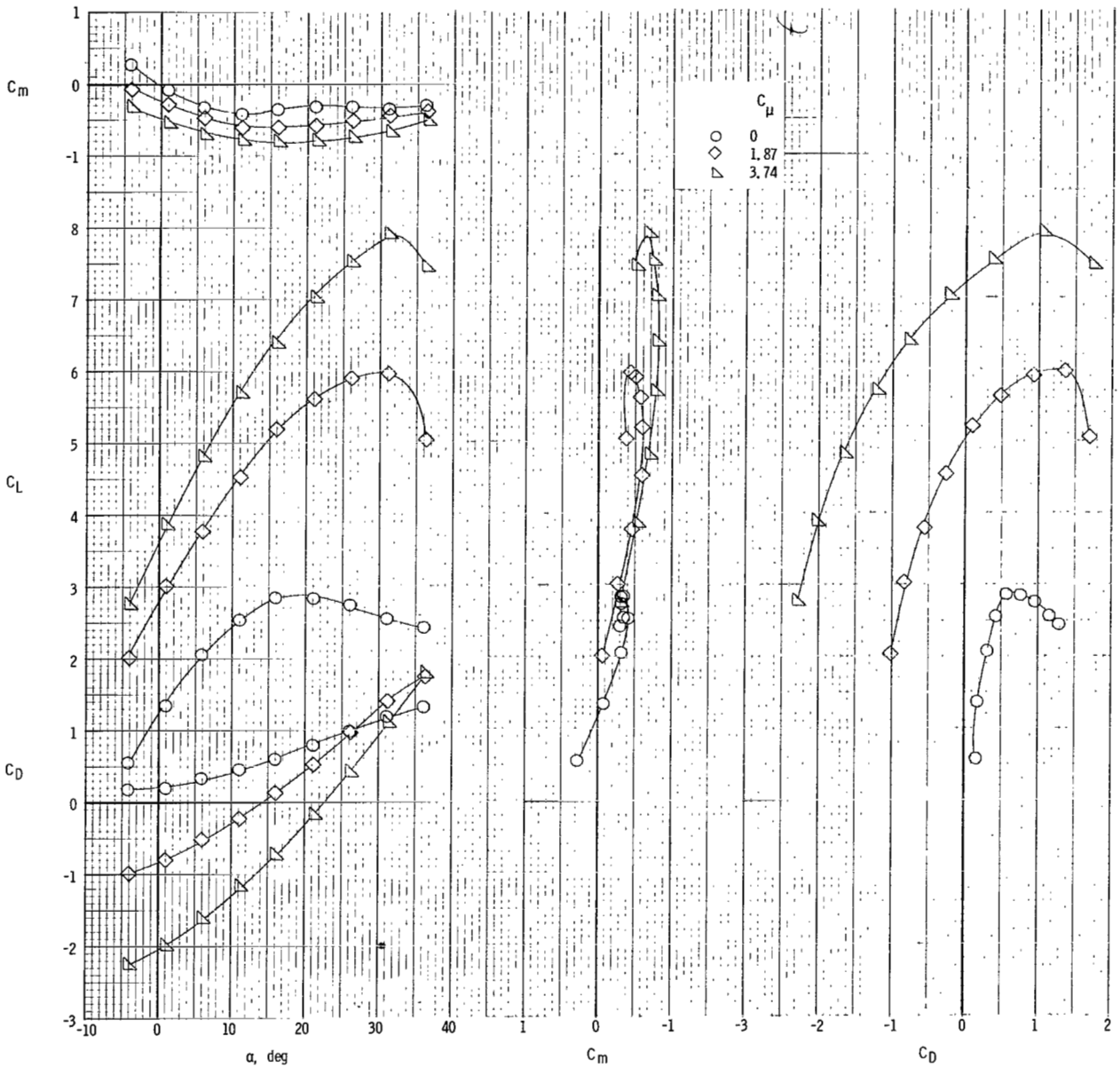

(b) $i_t = 0^0$; $C_{\mu,le} = 0.024$; $C_{\mu,e} = 0$.

Figure 26.- Continued.

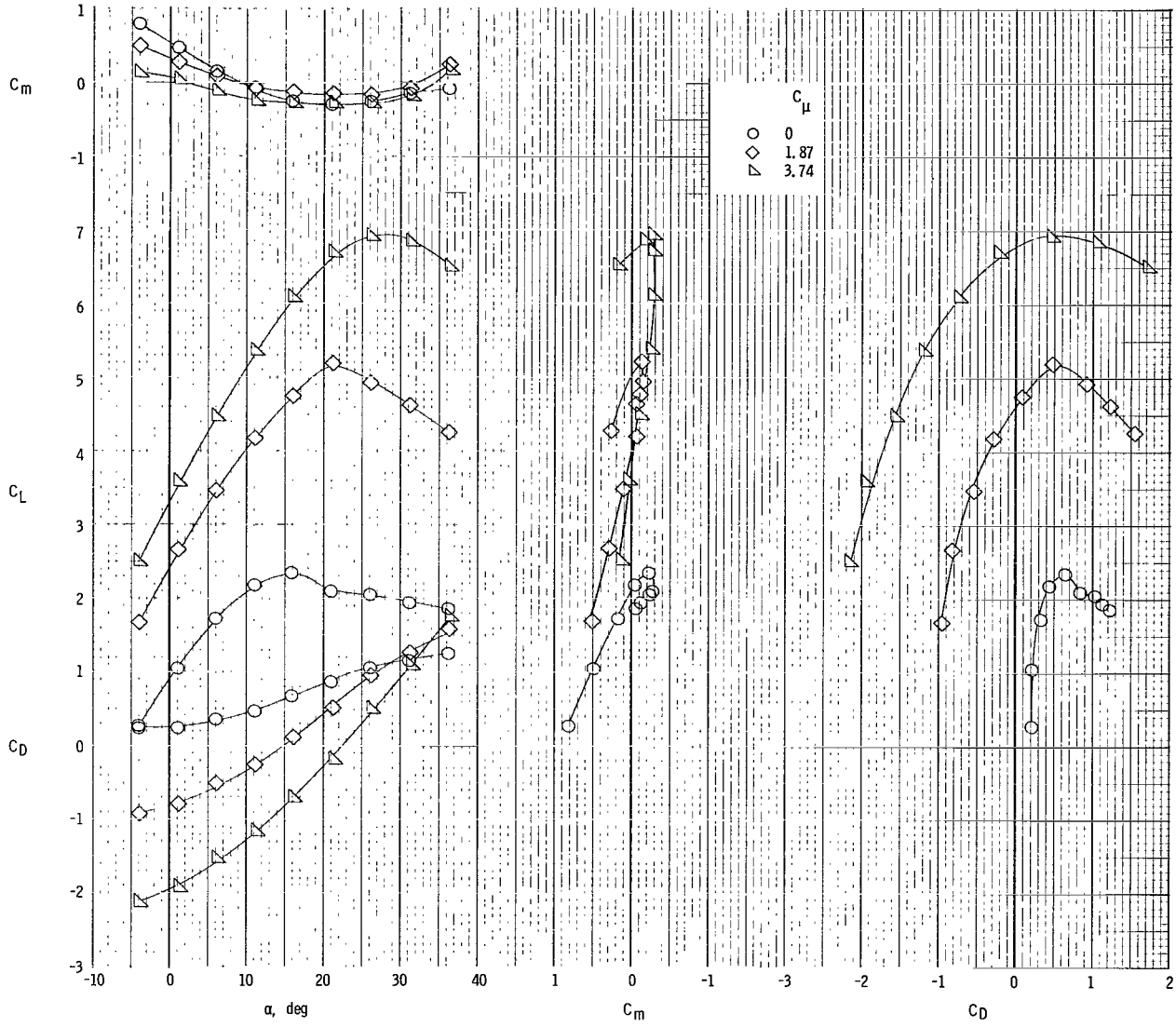

(c) $i_t = -5^0$; $C_{\mu,le} = 0$; $C_{\mu,e} = 0$.

Figure 26.- Continued.

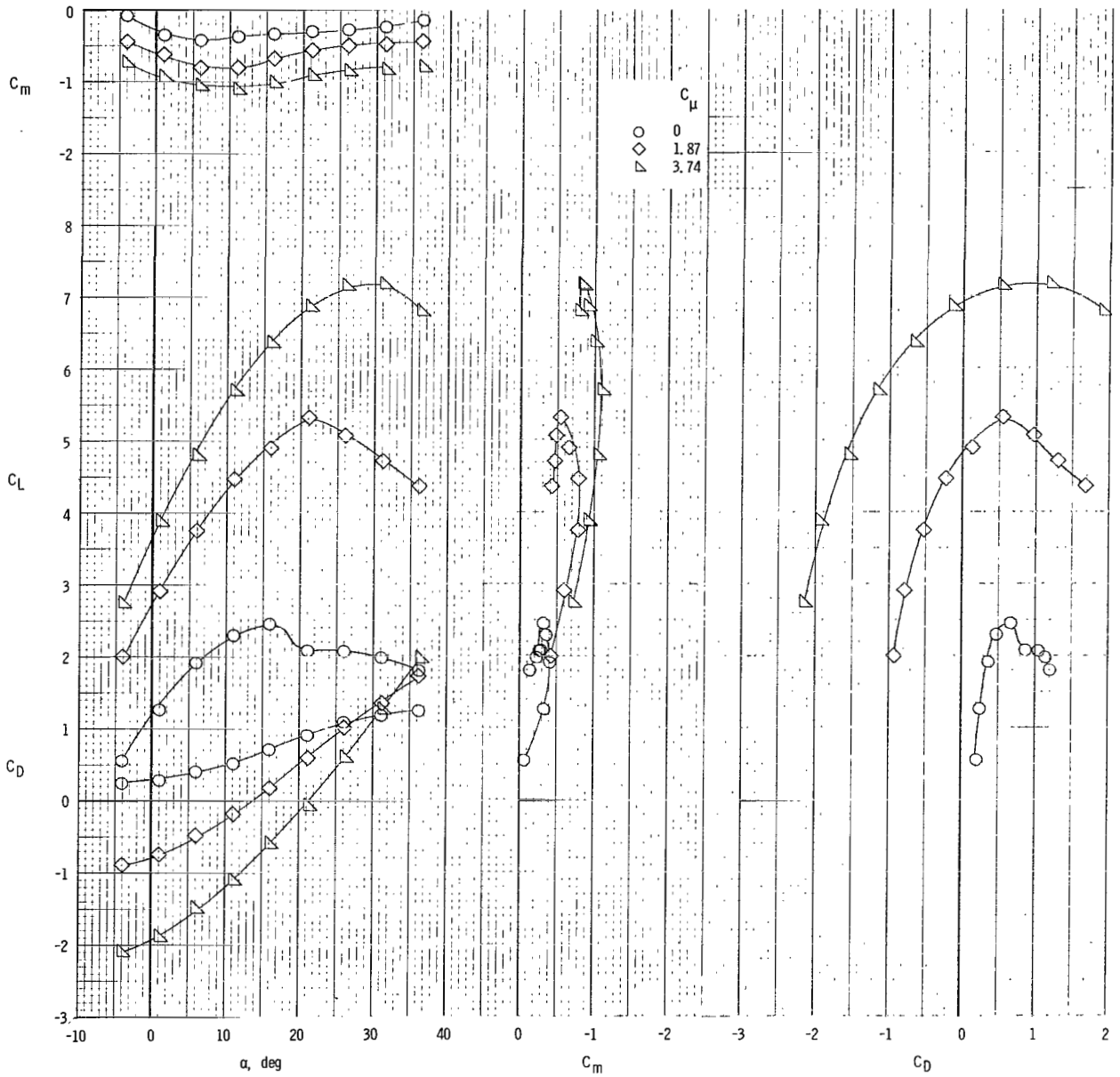

(d) $i_t = 5^0$; $C_{\mu,le} = 0$; $C_{\mu,e} = 0$.

Figure 26.- Continued.

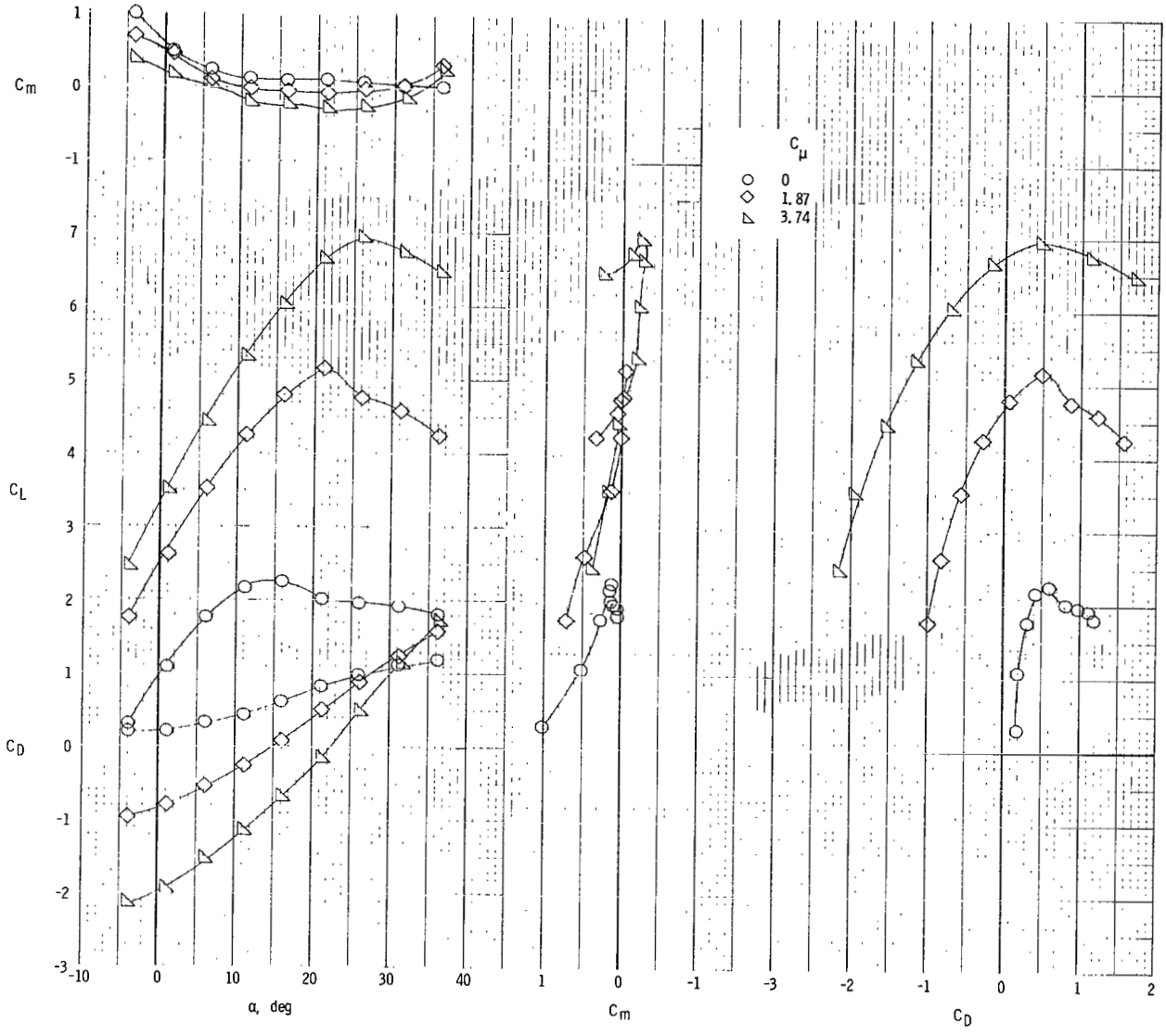

(e) $i_t = 0^0$; $C_{\mu,le} = 0$; $C_{\mu,e} = 0.017$.

Figure 26.- Concluded.

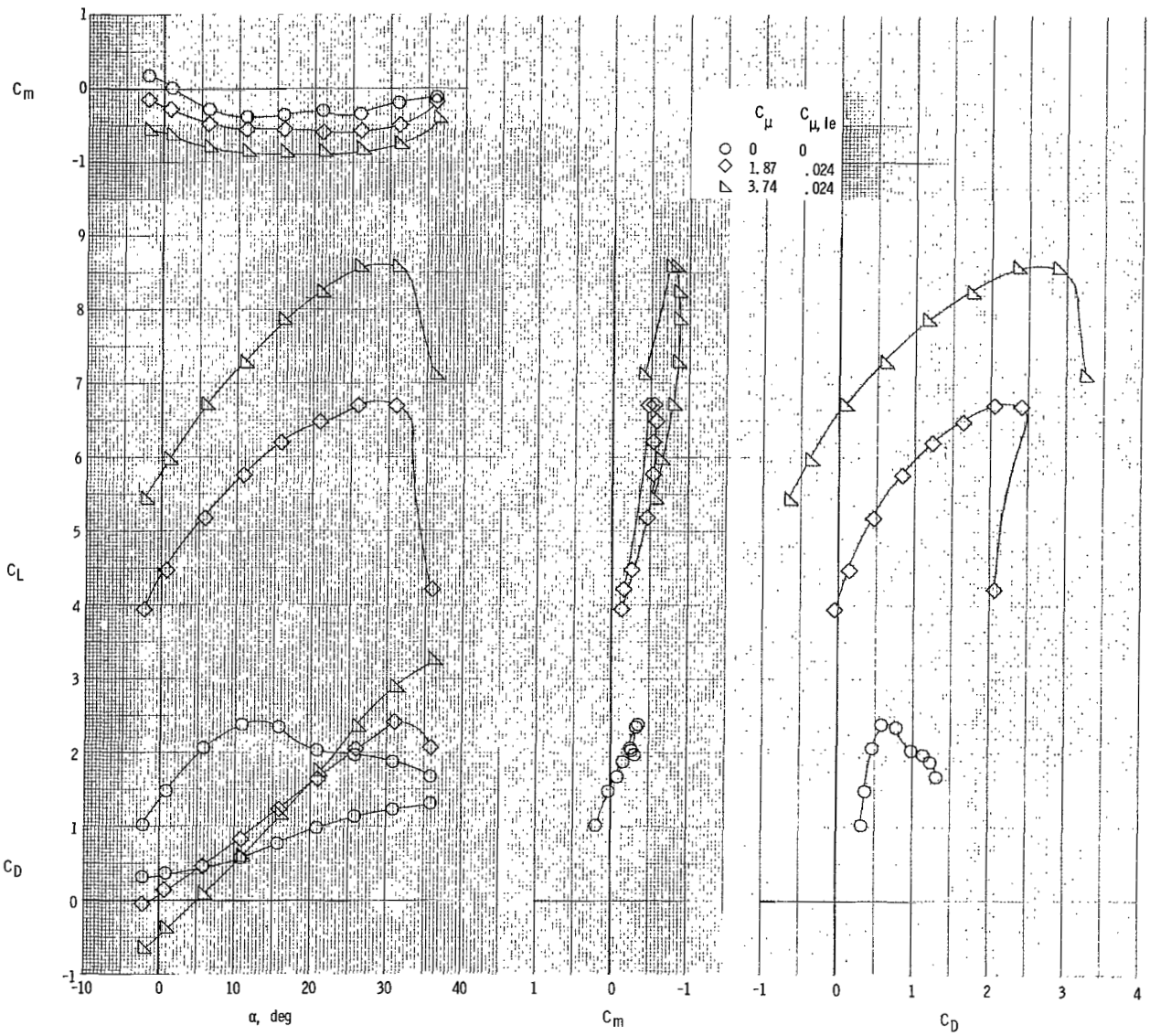

(a) $\delta_f = 40^0$, center and outboard segments.

Figure 27.- Longitudinal characteristics of model with tail on and clustered engines. Spanwise discontinuity in flap deflection; $\delta_f = 60^0$, inboard segments; $\delta_e = -50^0$; $i_t = 0^0$.

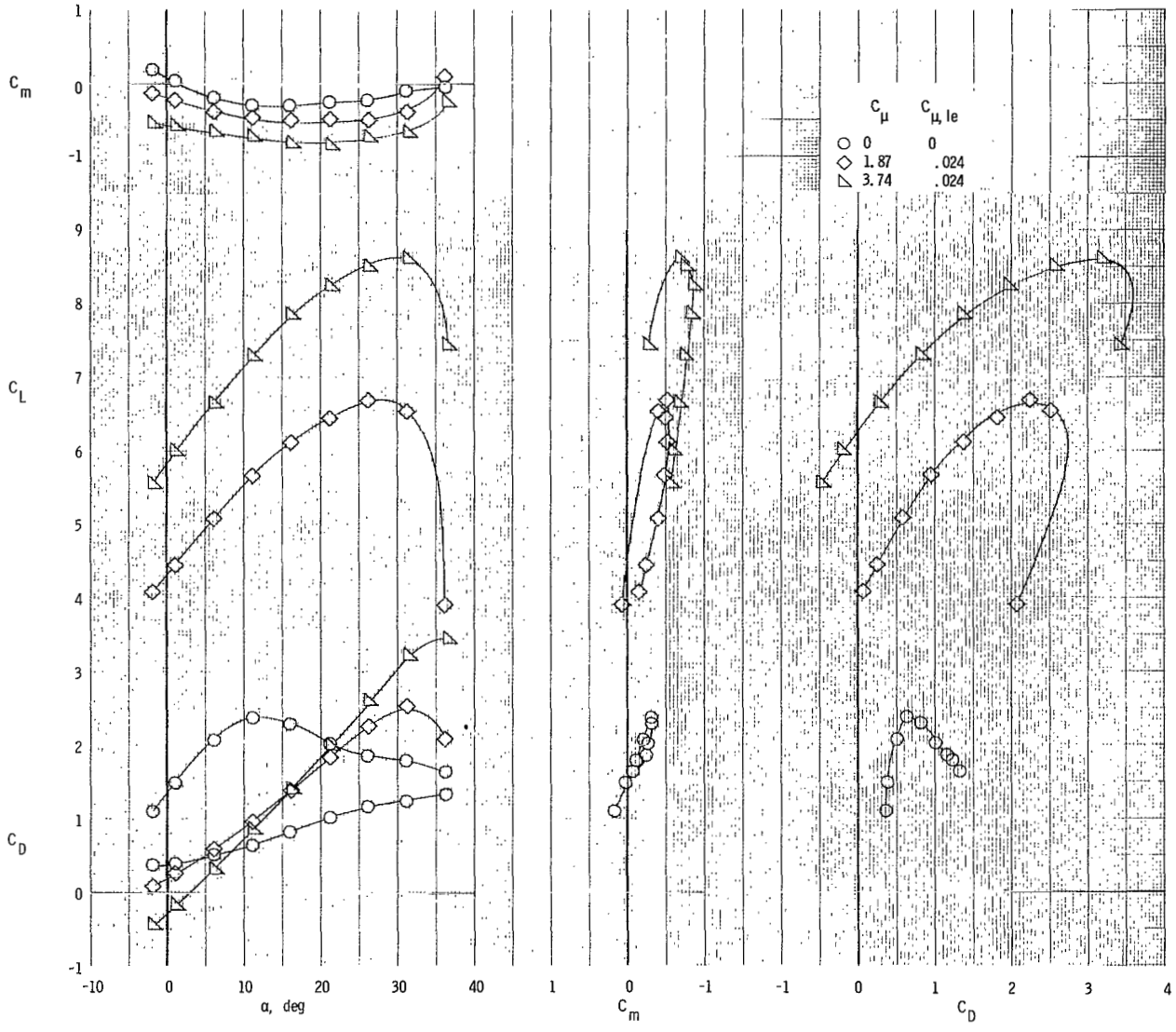

(b) $\delta_f = 80^0$, center and outboard segments.

Figure 27.- Concluded.

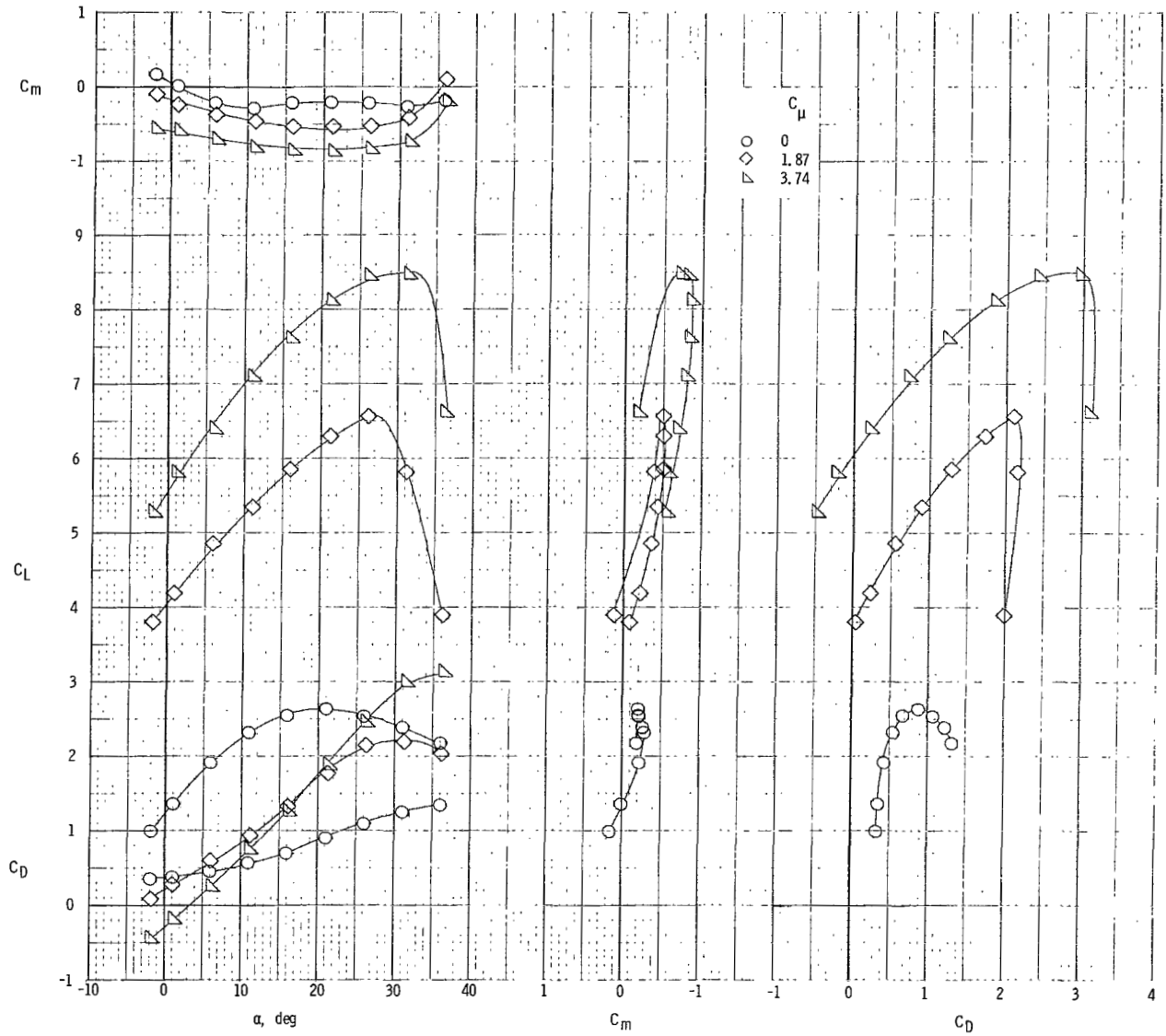

(a) $\delta_s = 10^0$; $C_{\mu,le} = 0.024$.

Figure 28.- Longitudinal characteristics of model with tail on and clustered engines. Symmetric spoiler deflection; $\delta_f = 60^0$; $\delta_e = -50^0$; $i_t = 0^0$.

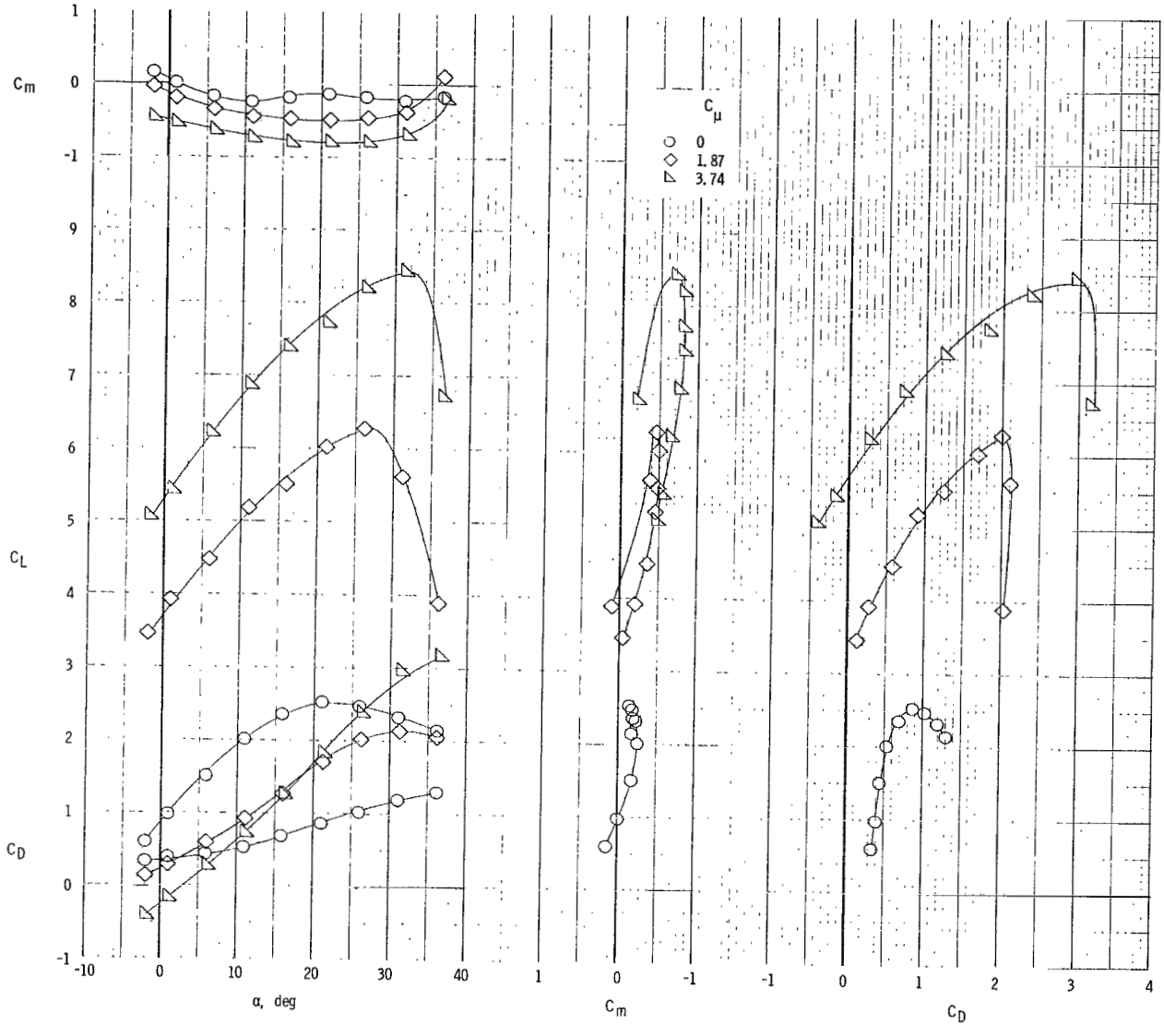

(b) $\delta_s = 20^o$; $C_{\mu,le} = 0.024$.

Figure 28.- Continued.

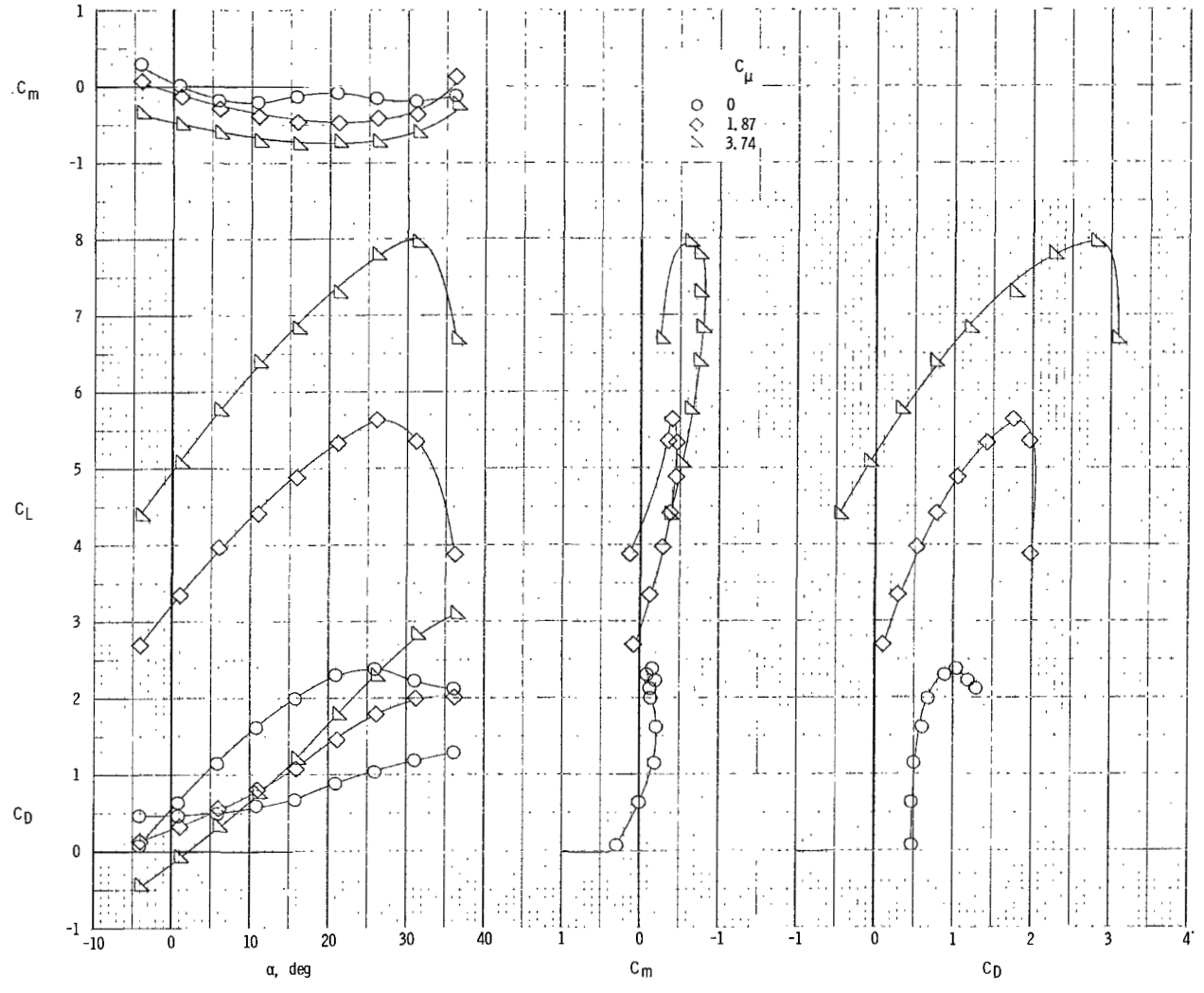

(c) $\delta_s = 30^0$; $C_{\mu,le} = 0.024$.

Figure 28.- Continued.

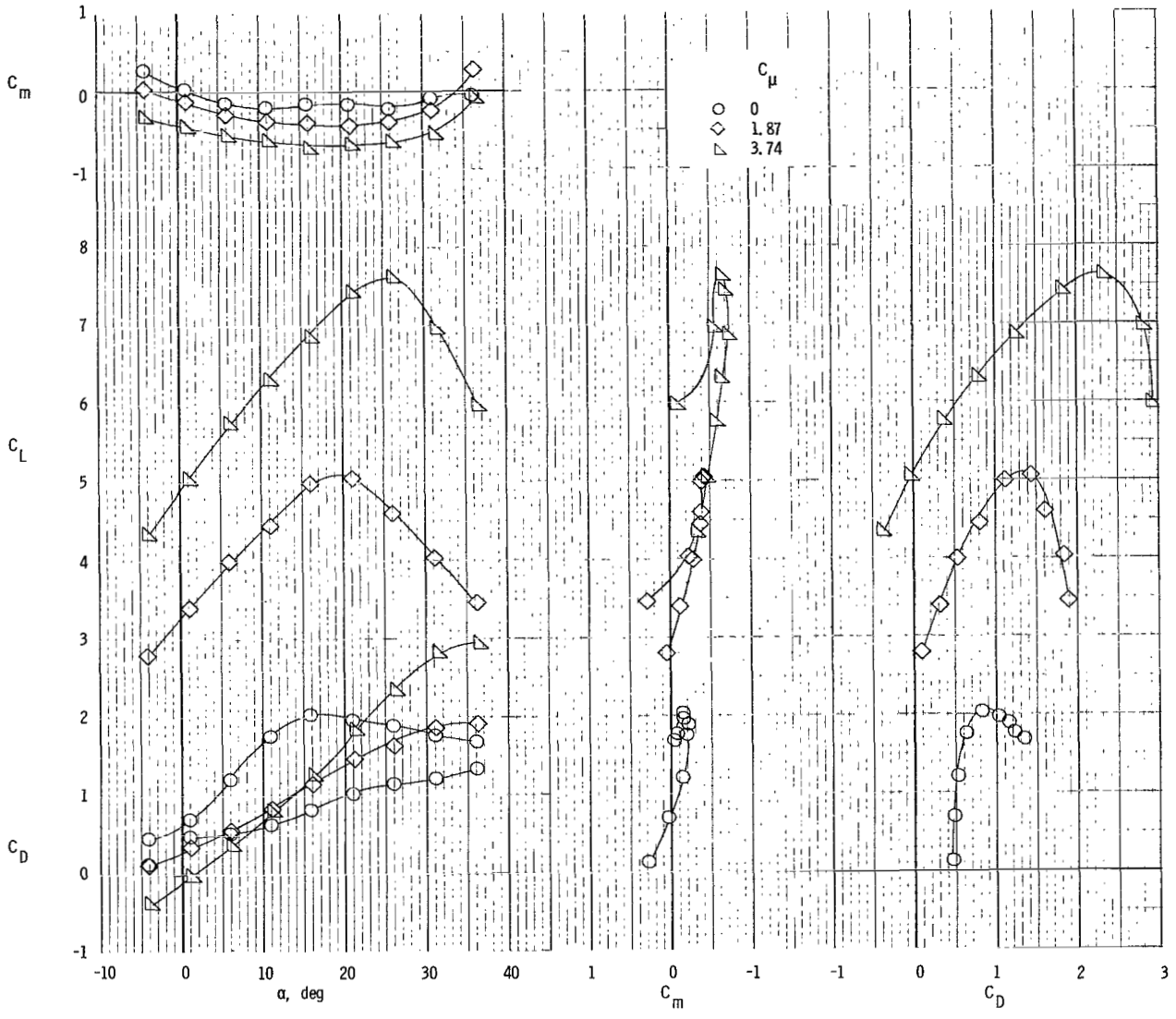

(d) $\delta_s = 30^0$; $C_{\mu,le} = 0.$

Figure 28.- Continued.

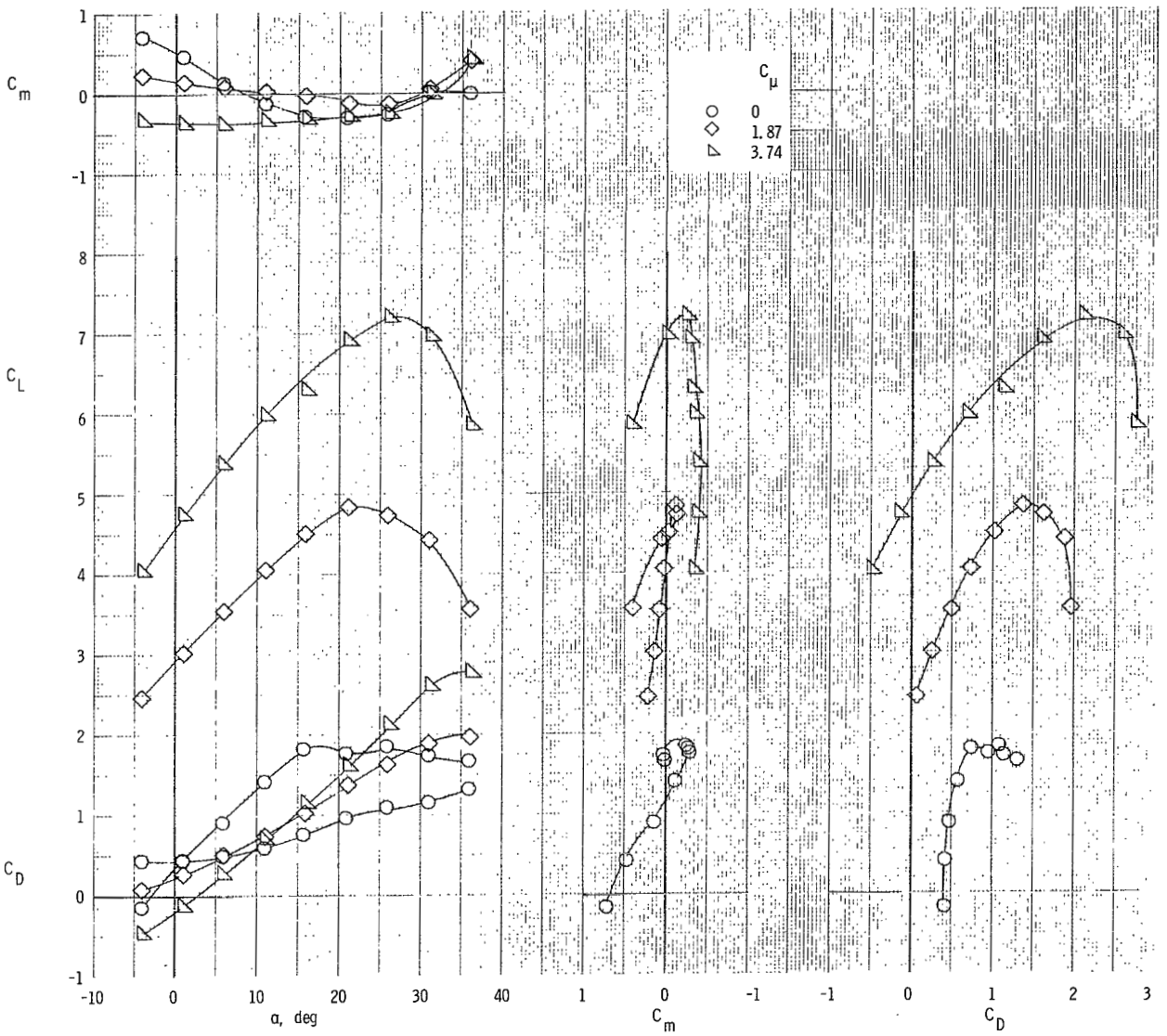

(e) $\delta_s = 30^0$; $C_{\mu,te} = 0$. Slot behind spoiler enlarged.

Figure 28.- Concluded.

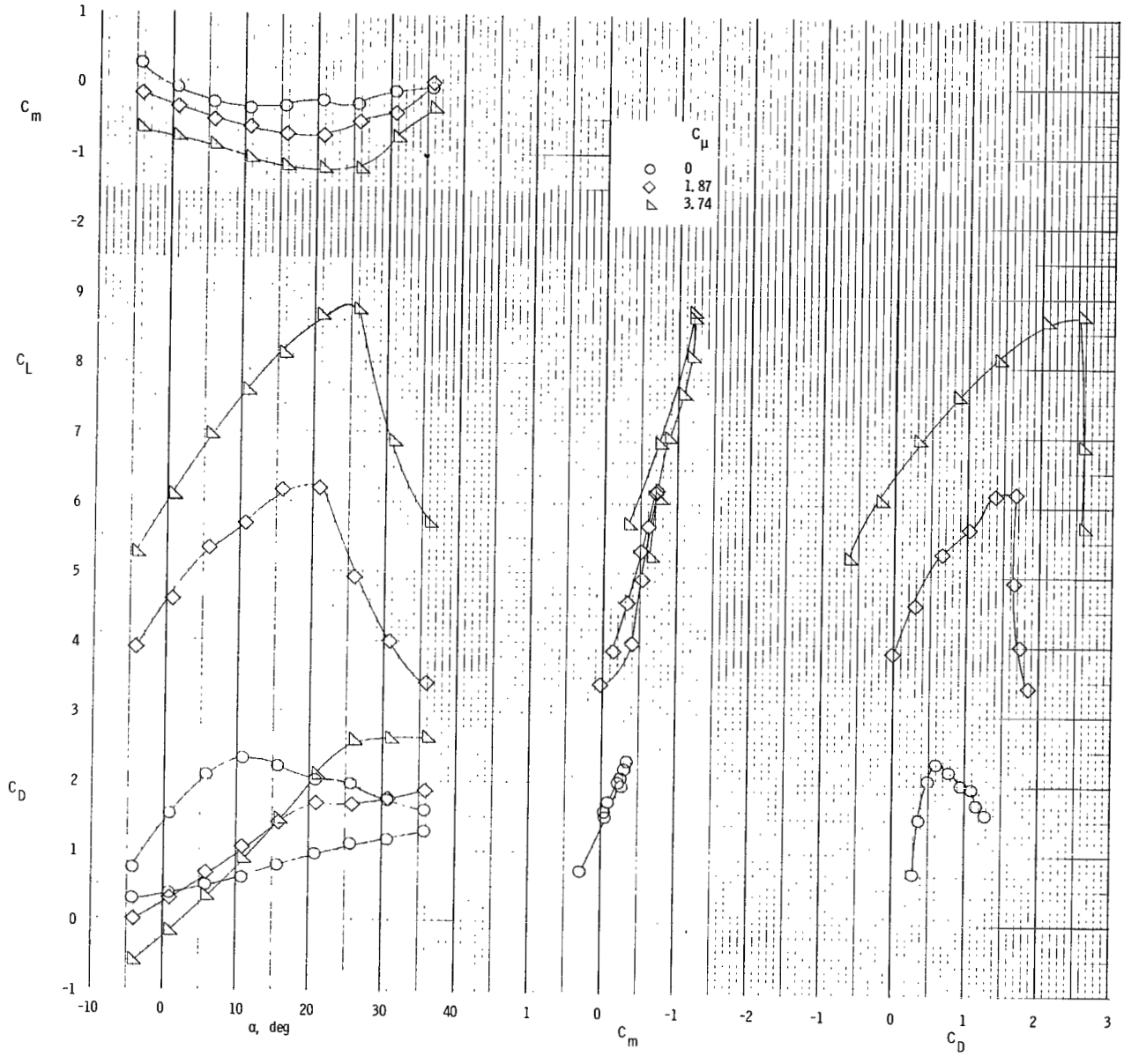

(a) $i_t = 0^o$; $C_{\mu,le} = 0$; $C_{\mu,e} = 0$.

Figure 29.- Longitudinal characteristics of model with tail on and spread engines. $\delta_f = 60^o$; $\delta_e = -50^o$.

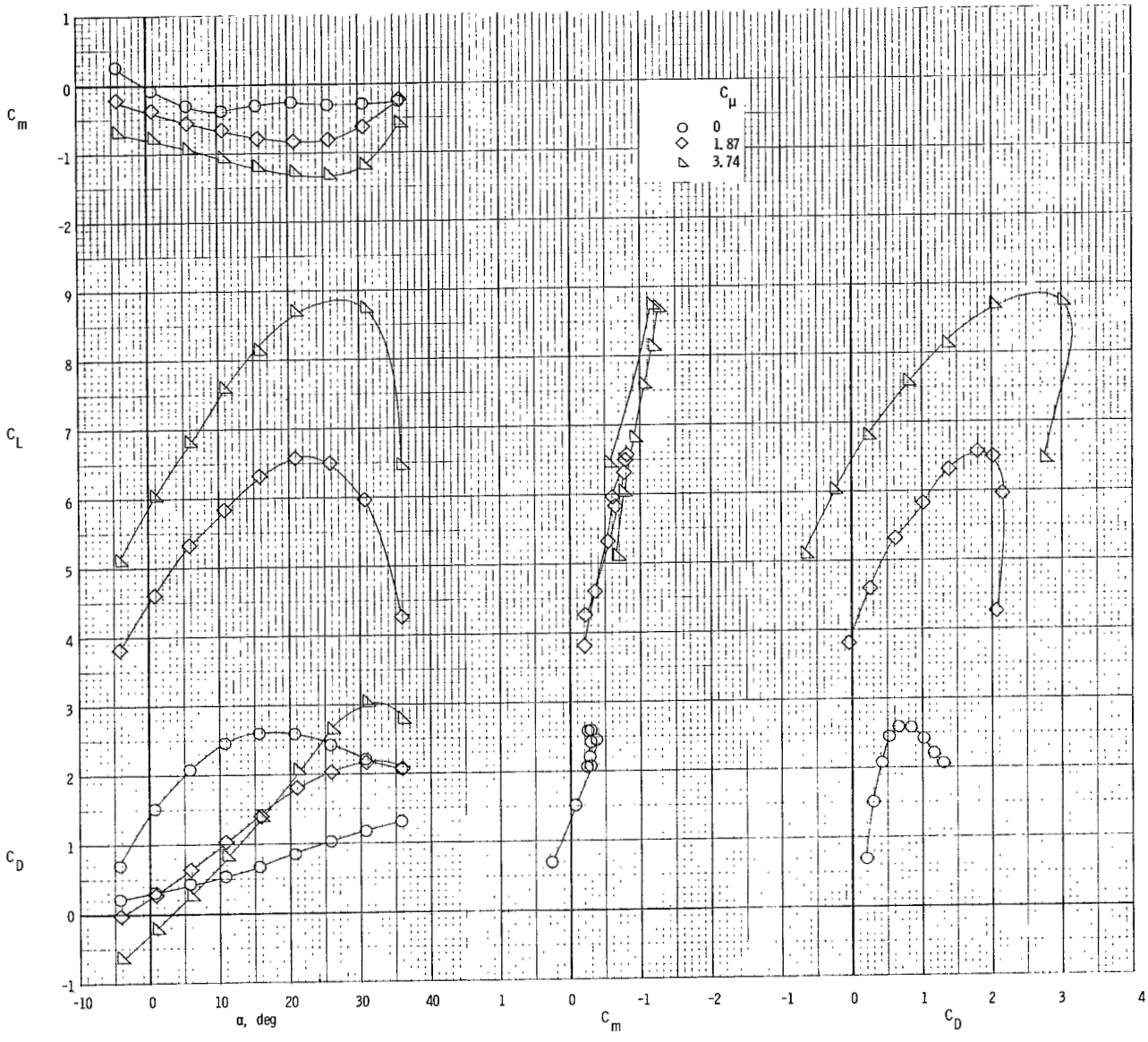

(b) $i_t = 0^o$; $C_{\mu,le} = 0.024$; $C_{\mu,e} = 0$.

Figure 29.- Continued.

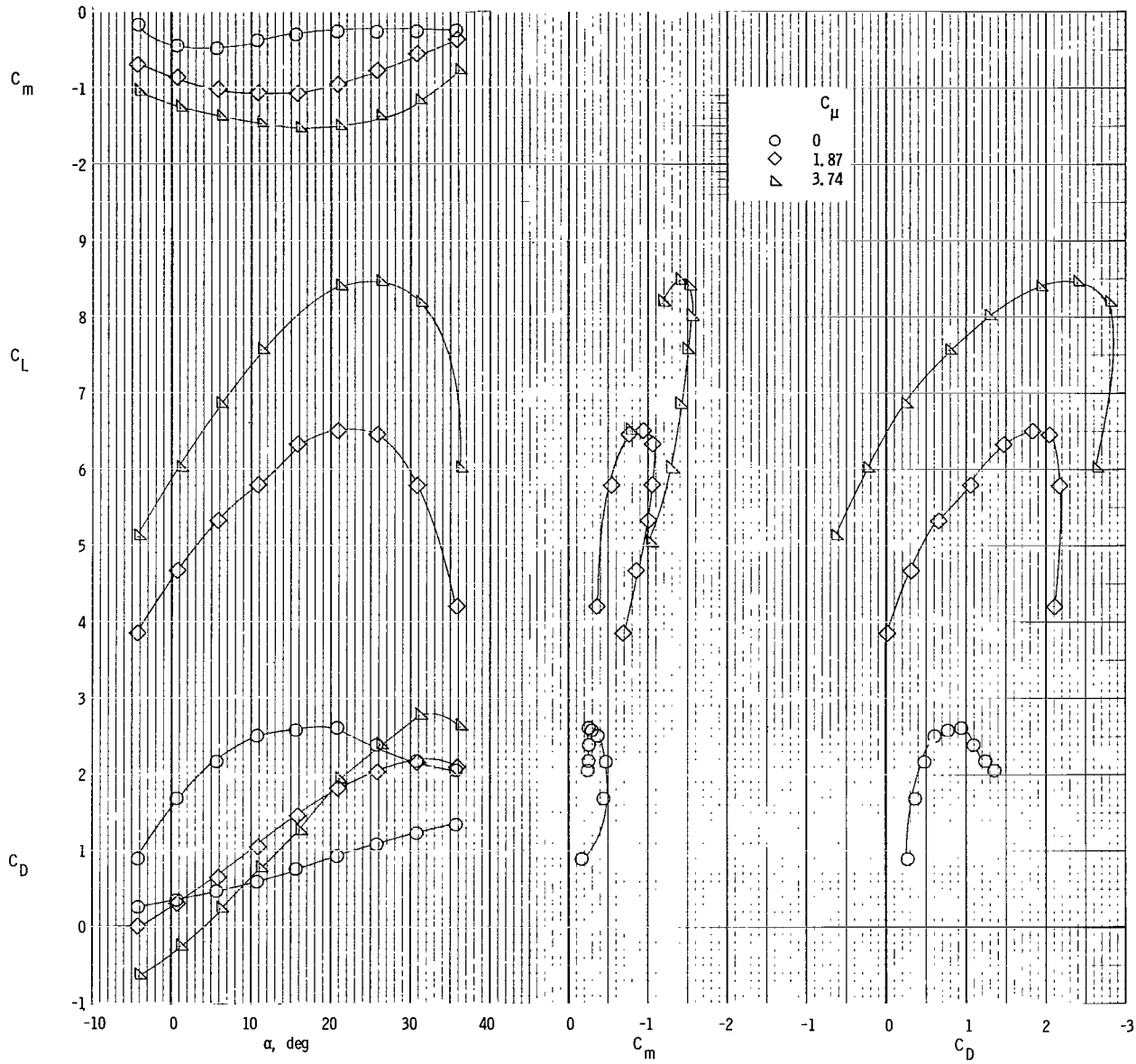

(c) $i_t = 5^0$; $C_{\mu,le} = 0.024$; $C_{\mu,e} = 0$.

Figure 29.- Continued.

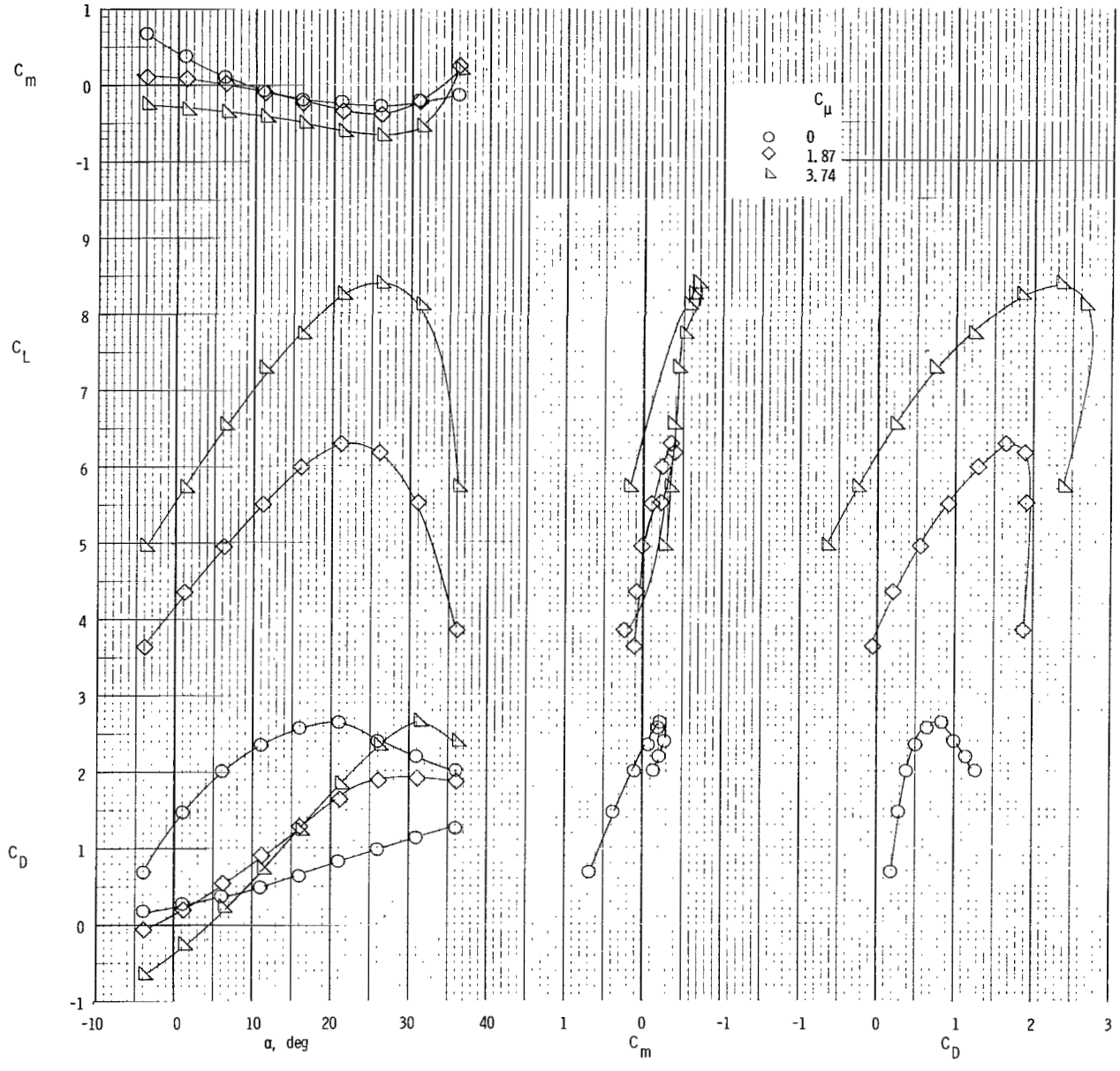

(d) $i_t = -5^0$; $C_{\mu,le} = 0.024$; $C_{\mu,e} = 0$.

Figure 29.- Continued.

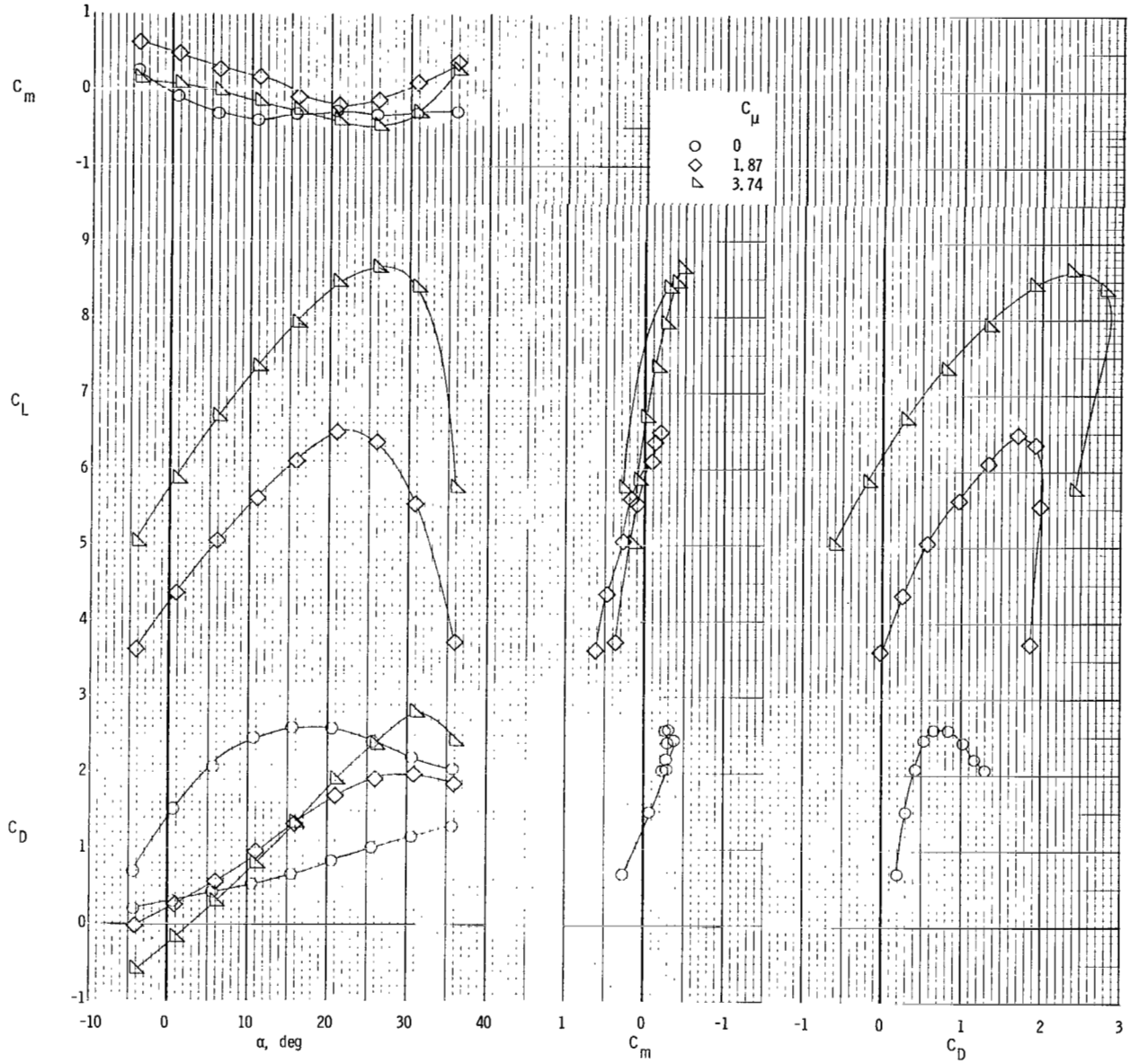

(e) $i_t = 0^o$; $C_{\mu,le} = 0.024$; $C_{\mu,e} = 0.017$.

Figure 29.- Concluded.

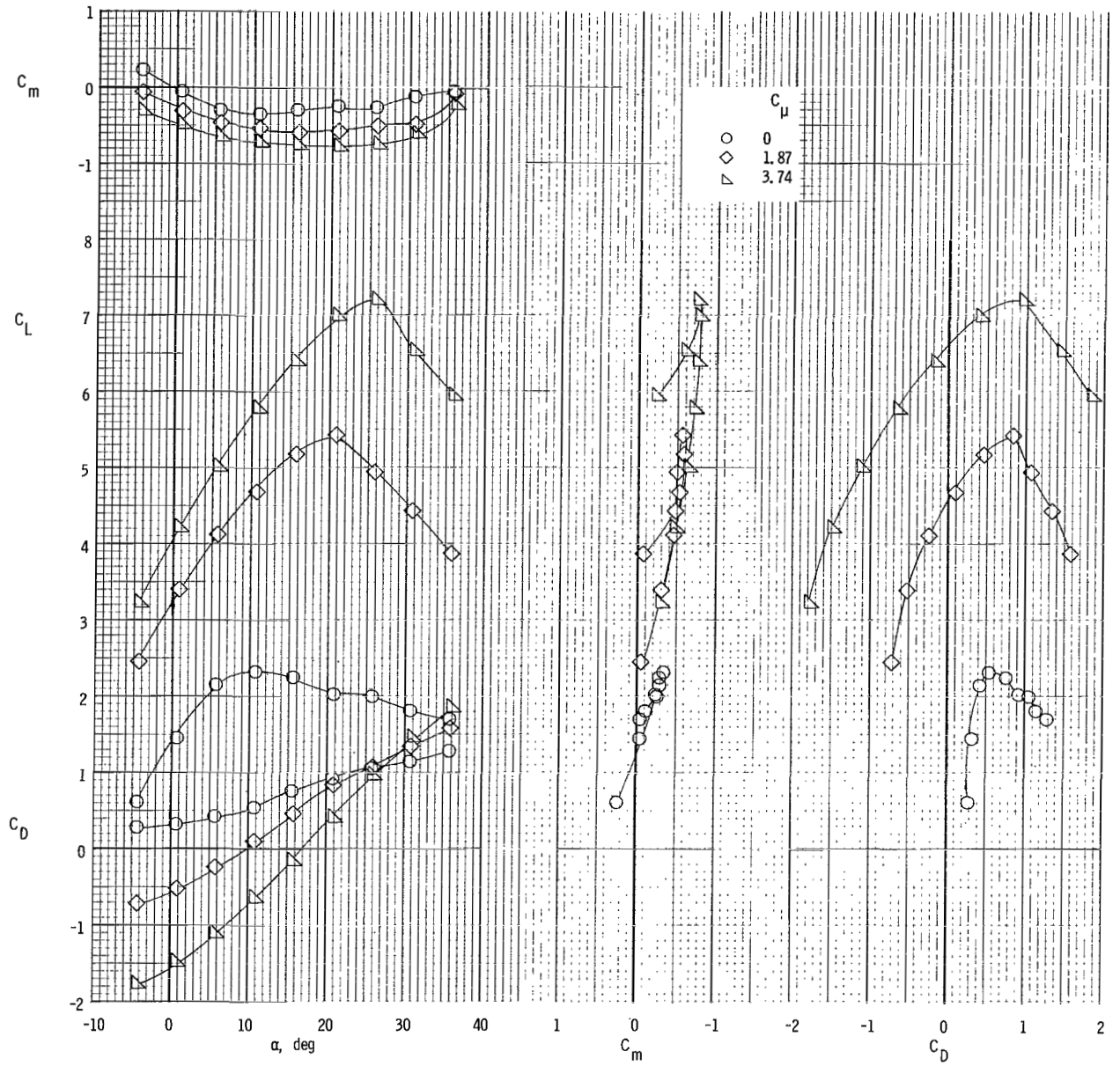

(a) $i_t = 0^o$; $C_{\mu,le} = 0$.

Figure 30.- Longitudinal characteristics of model with tail on and spread engines. $\delta_f = 40^o$; $\delta_e = -50^o$.

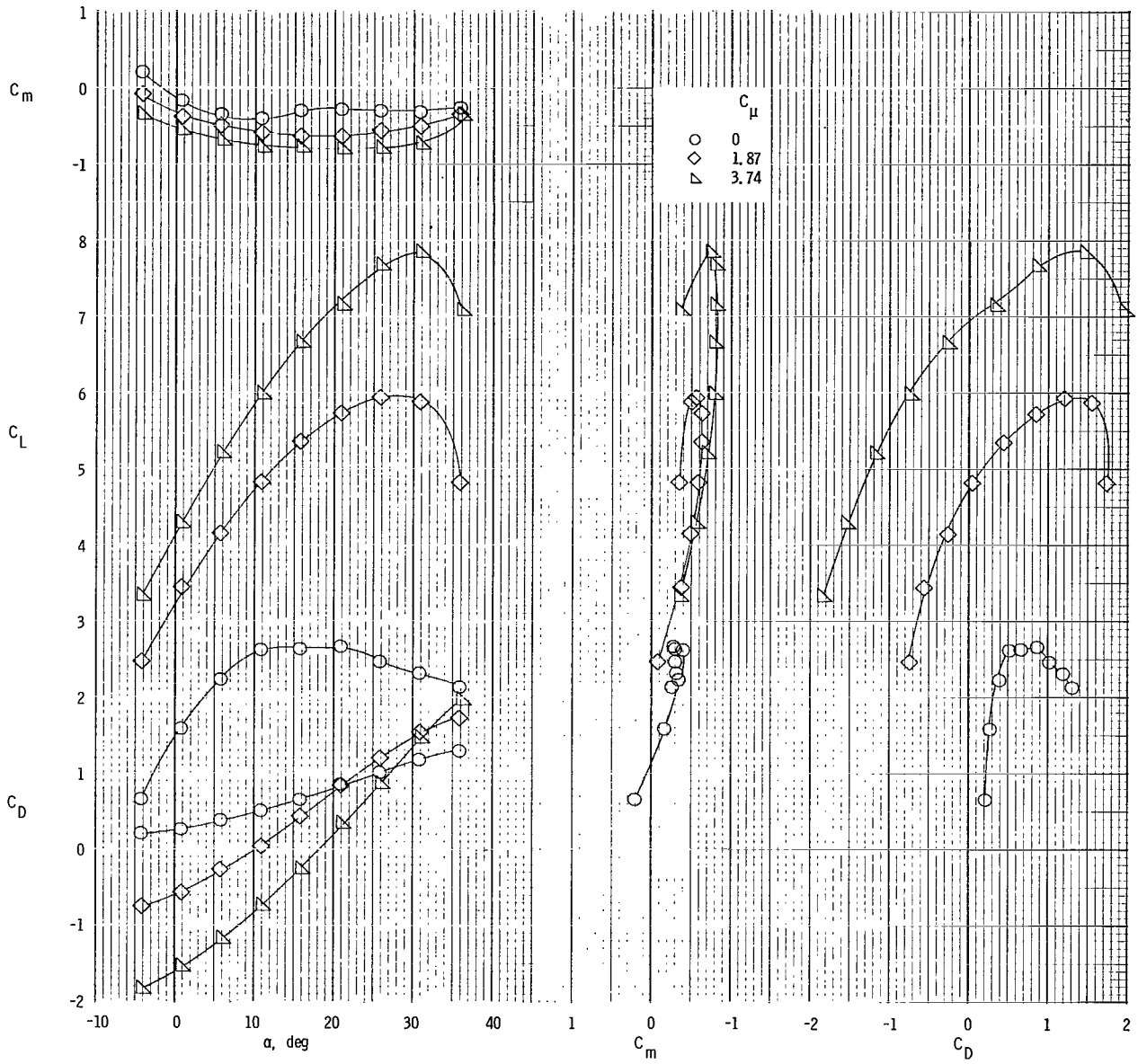

(b) $i_t = 0^o$; $C_{\mu,le} = 0.024$.

Figure 30.- Continued.

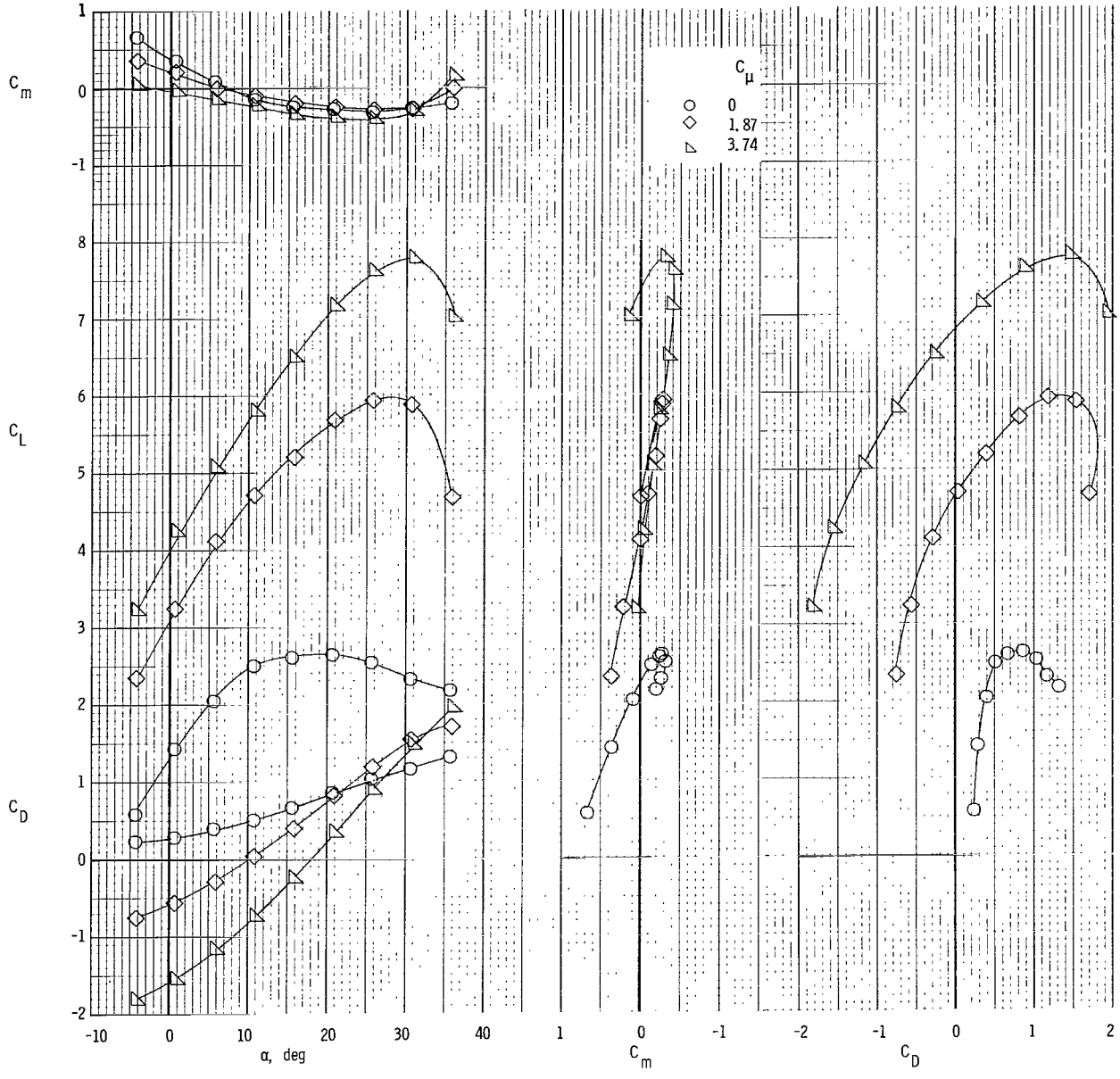

(c) $i_t = -5^o$; $C_{\mu,le} = 0.024$.

Figure 30.- Continued.

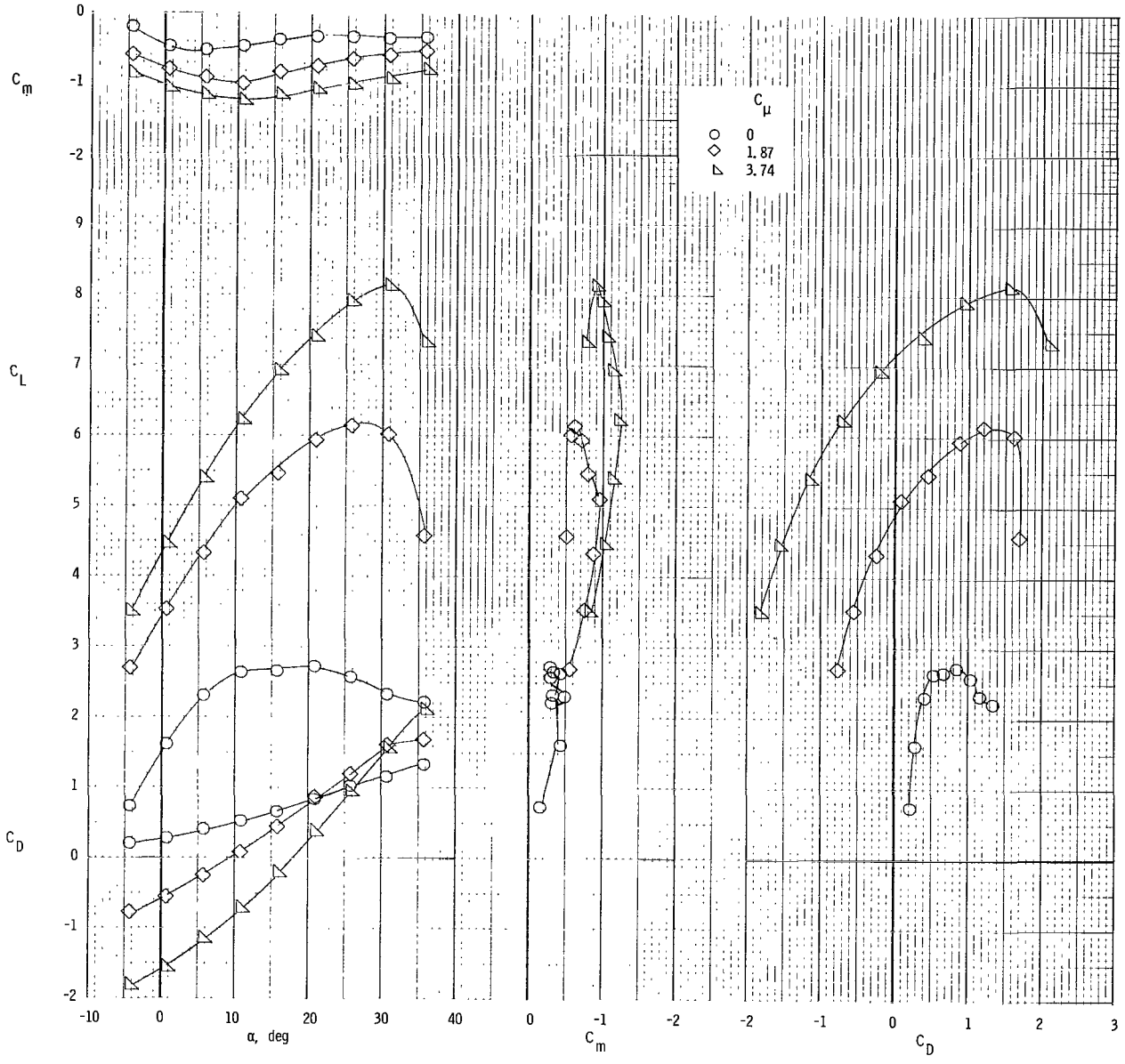

(d) $i_t = 5^o$; $C_{\mu,le} = 0.024$.

Figure 30.- Concluded.

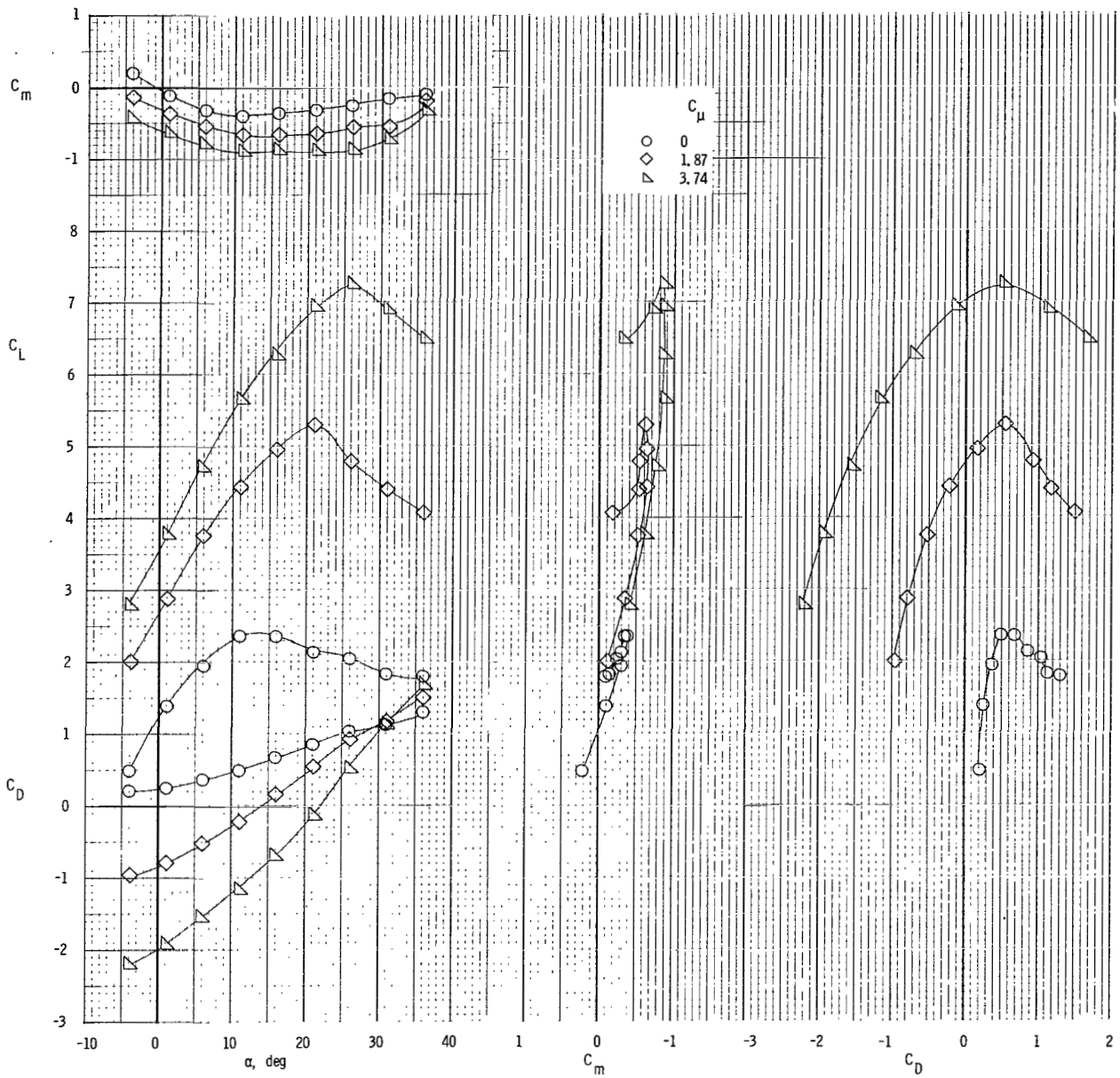

(a) $C_{\mu,ie} = 0$.

Figure 31.- Longitudinal characteristics of model with tail on and spread engines. $\delta_f = 35^0$; $\delta_e = -50^0$; $i_t = 0^0$.

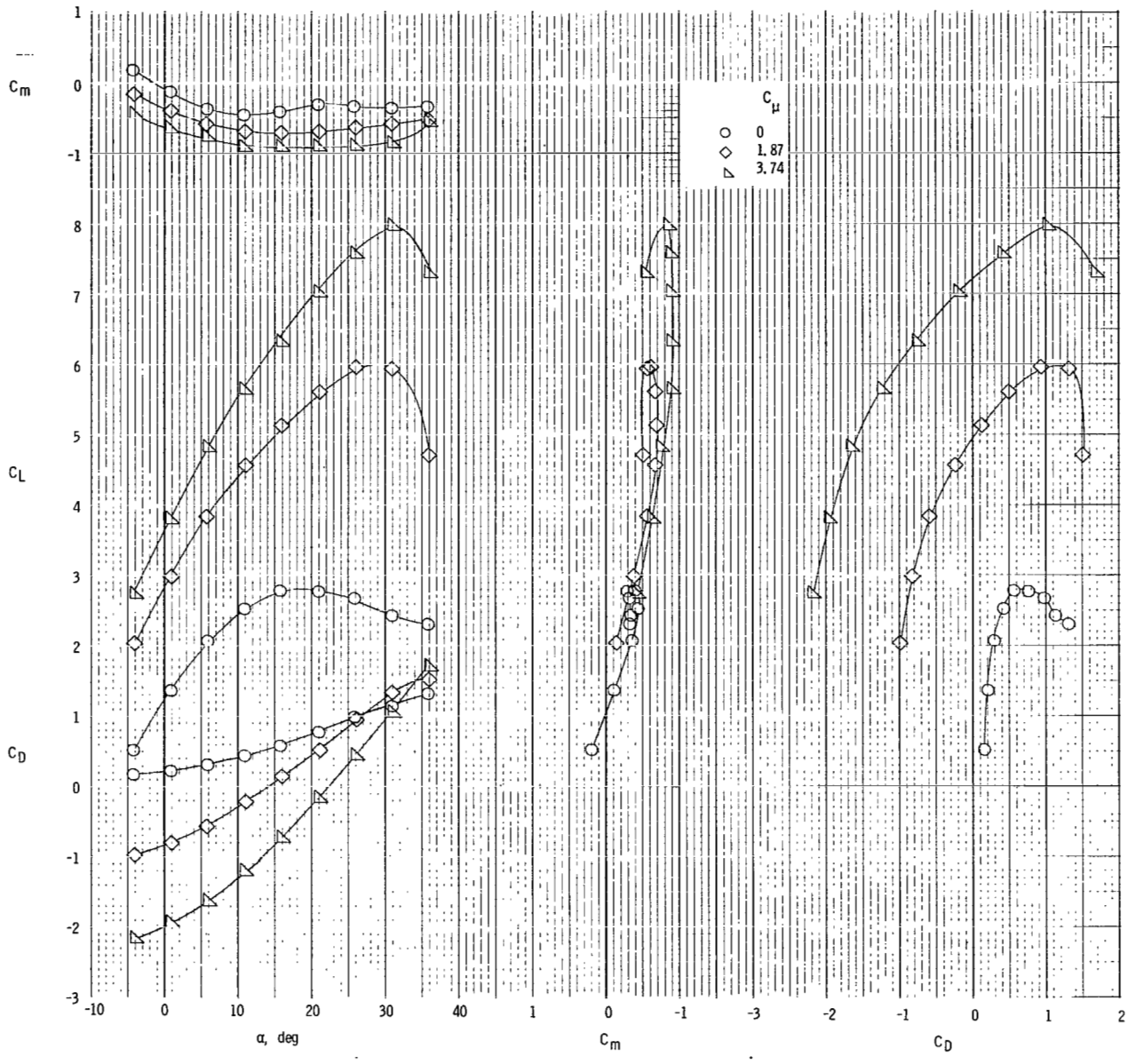

(b) $C_{\mu,le} = 0.024$.

Figure 31.- Concluded.

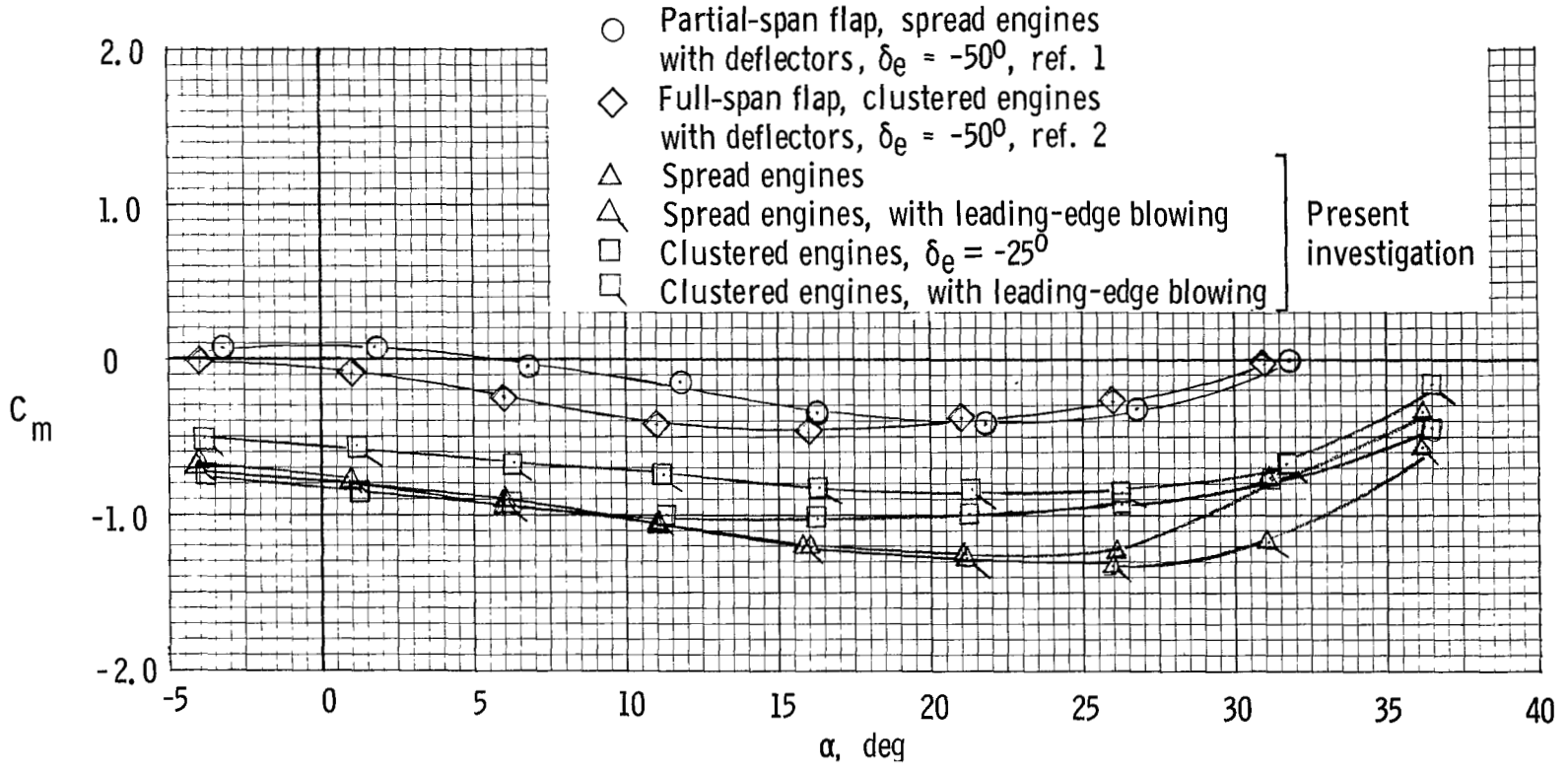

Figure 32.- Summary of tail-on pitching-moment characteristics. $\delta_f = 60^0$; $C_\mu = 3.74$.

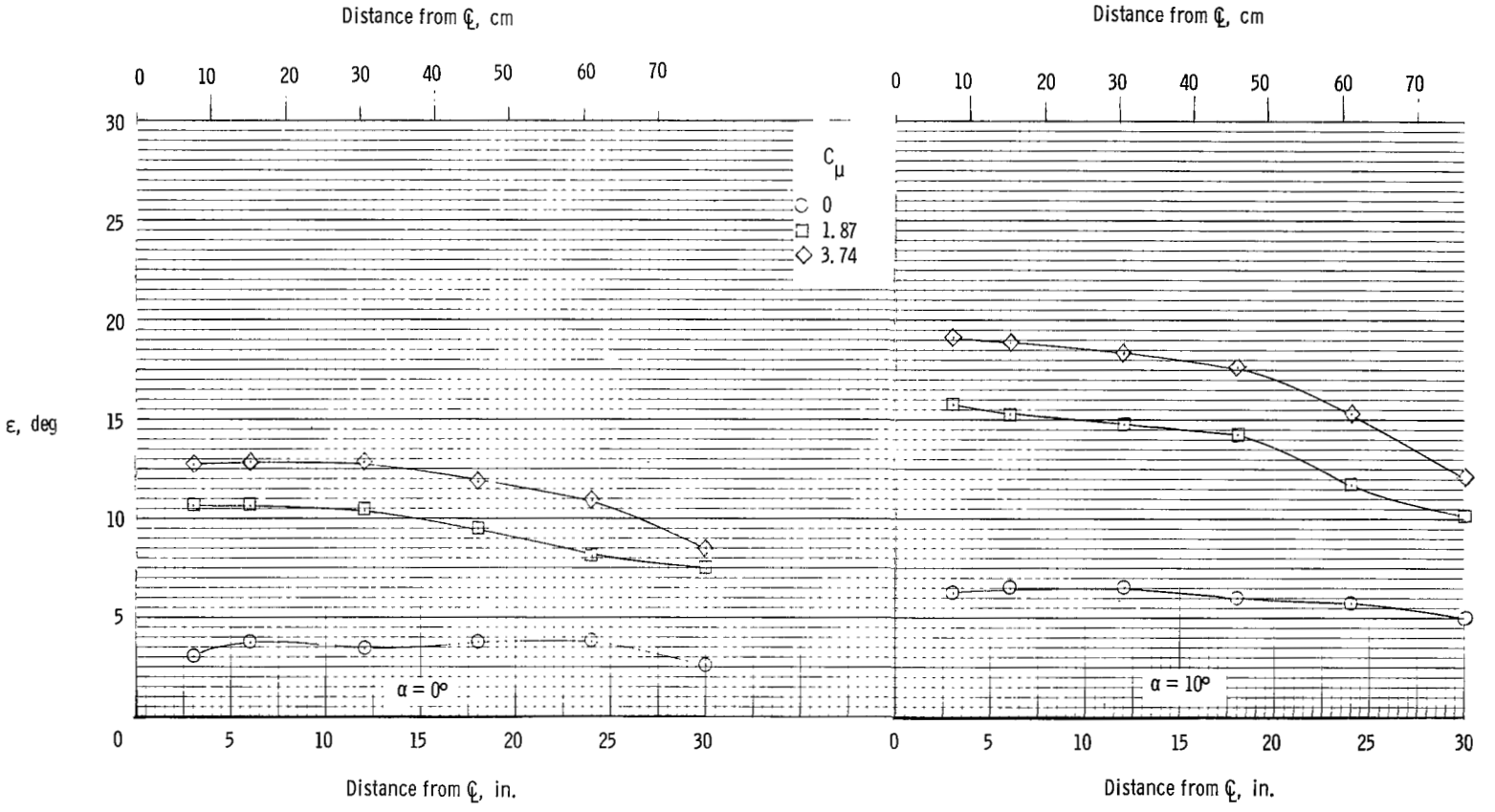

(a) z/c = 1.50.

Figure 33.- Variation of downwash angle with spanwise station for model with clustered engines. $\delta_f = 60^0$; $C_{\mu,le} = 0$.

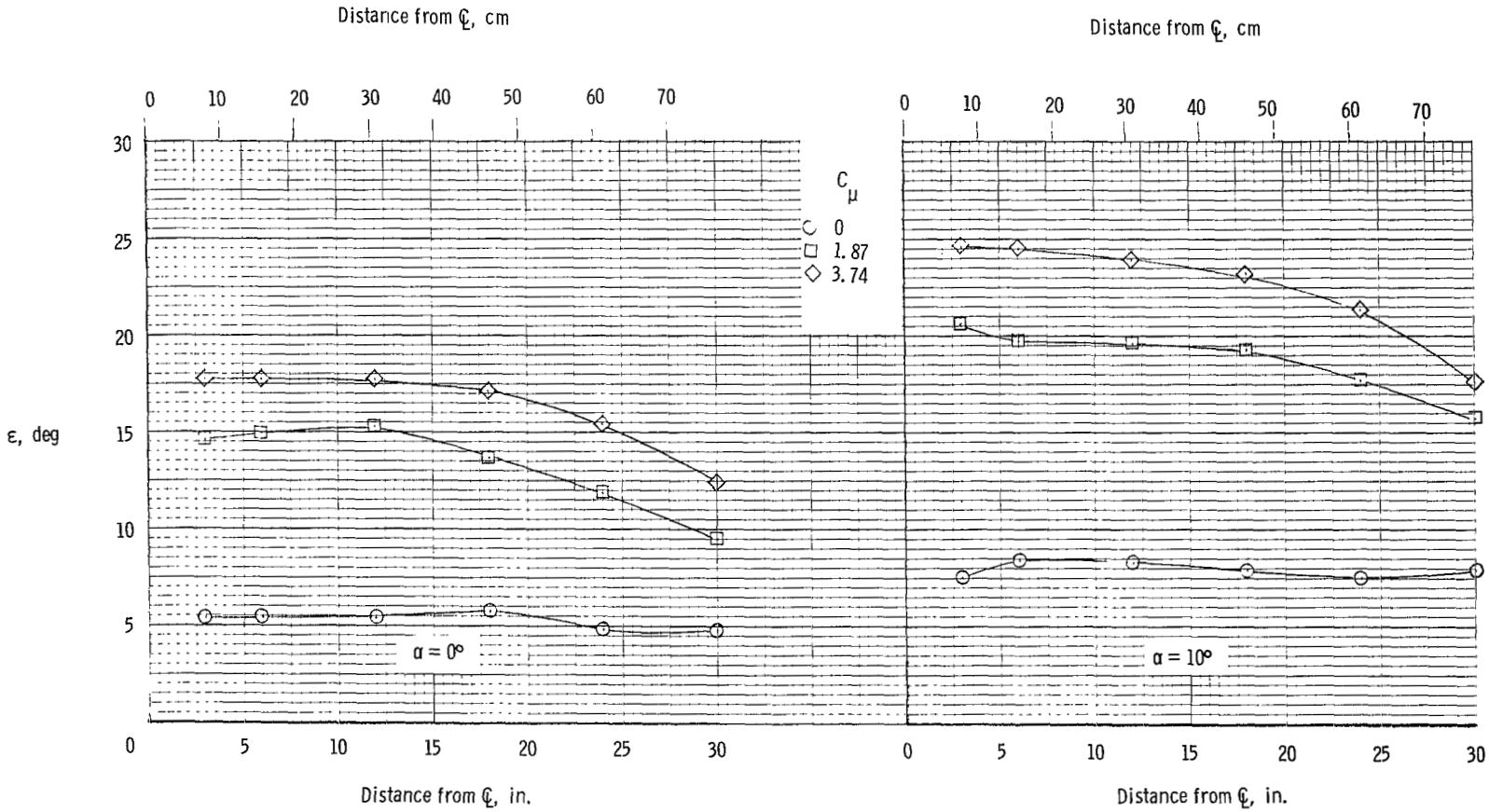

(b) z/c = 0.75.

Figure 33.- Continued.

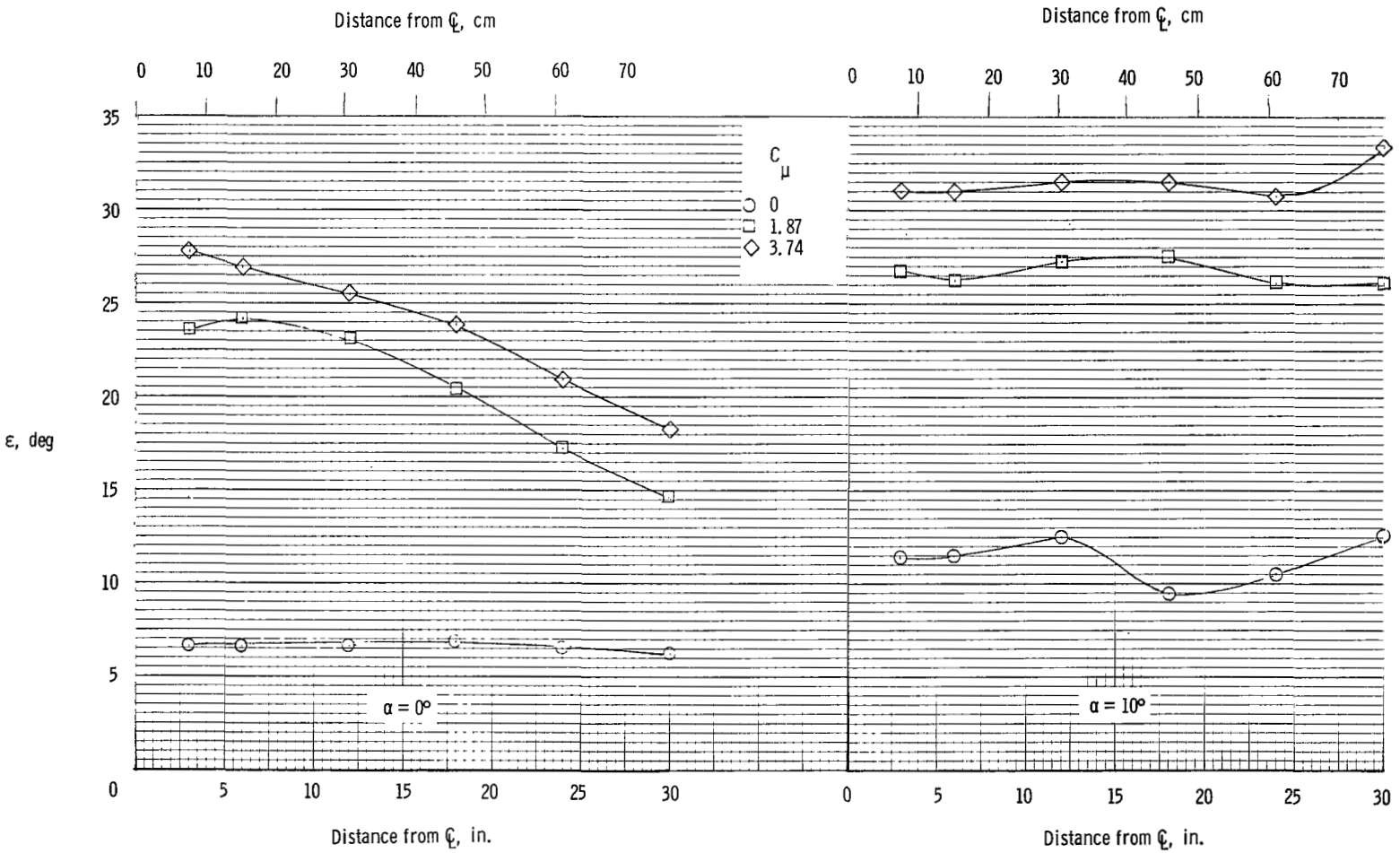

(c) z/c = 0.

Figure 33.- Concluded.

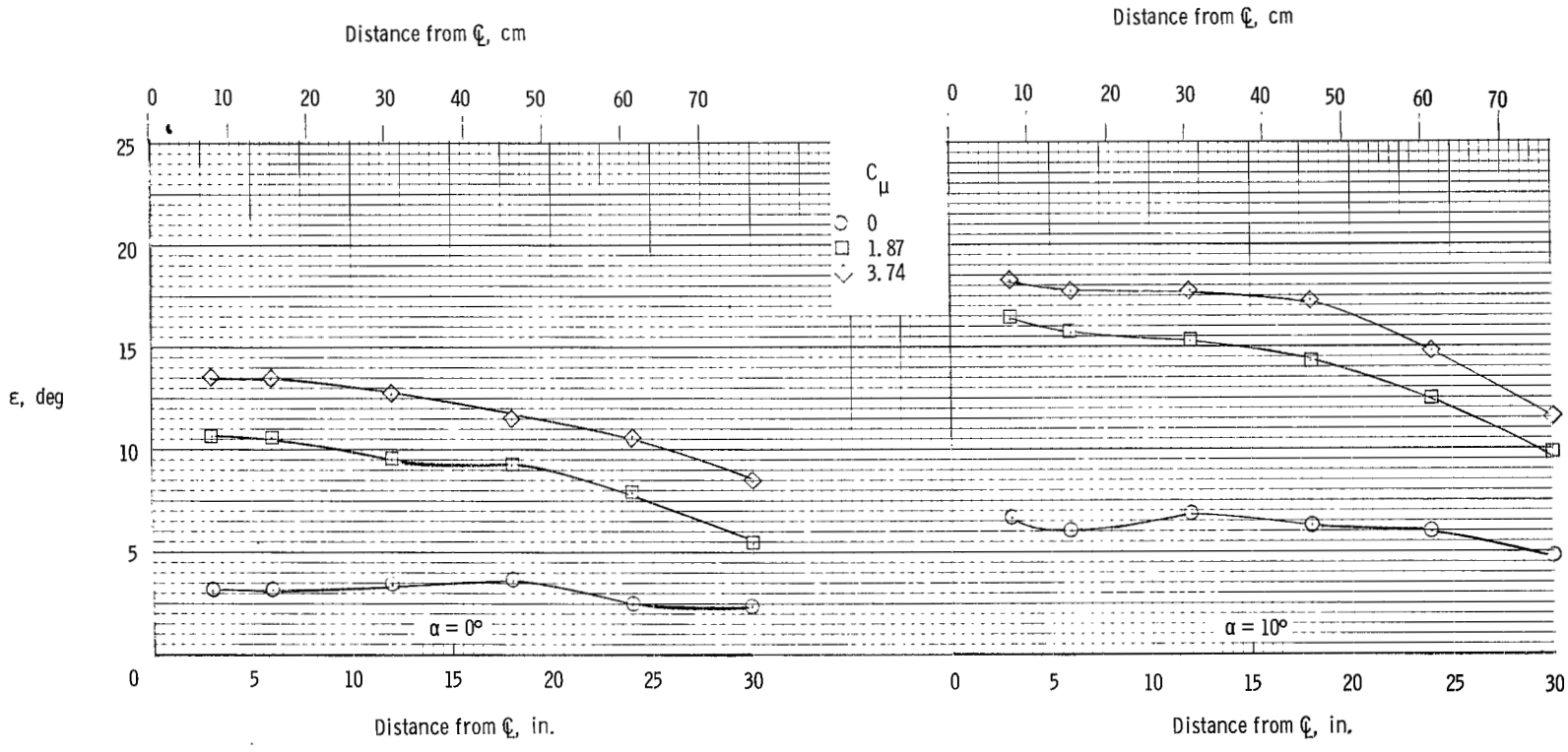

(a) z/c = 1.50.

Figure 34.- Variation of downwash angle with spanwise station for model with clustered engines. $\delta_f = 60^0$; $C_{\mu,le} = 0.024$.

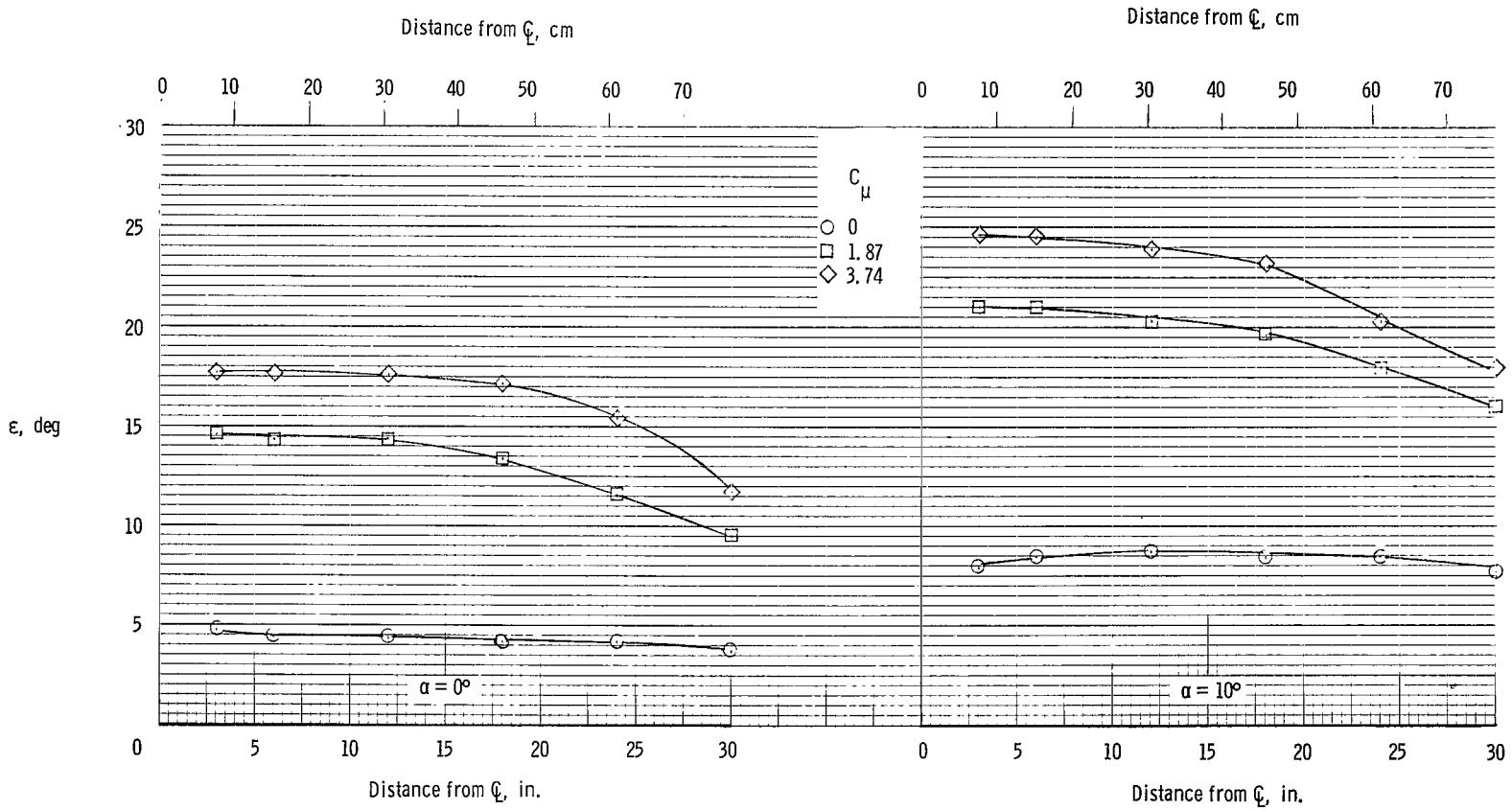

(b) z/c = 0.75.

Figure 34.- Continued.

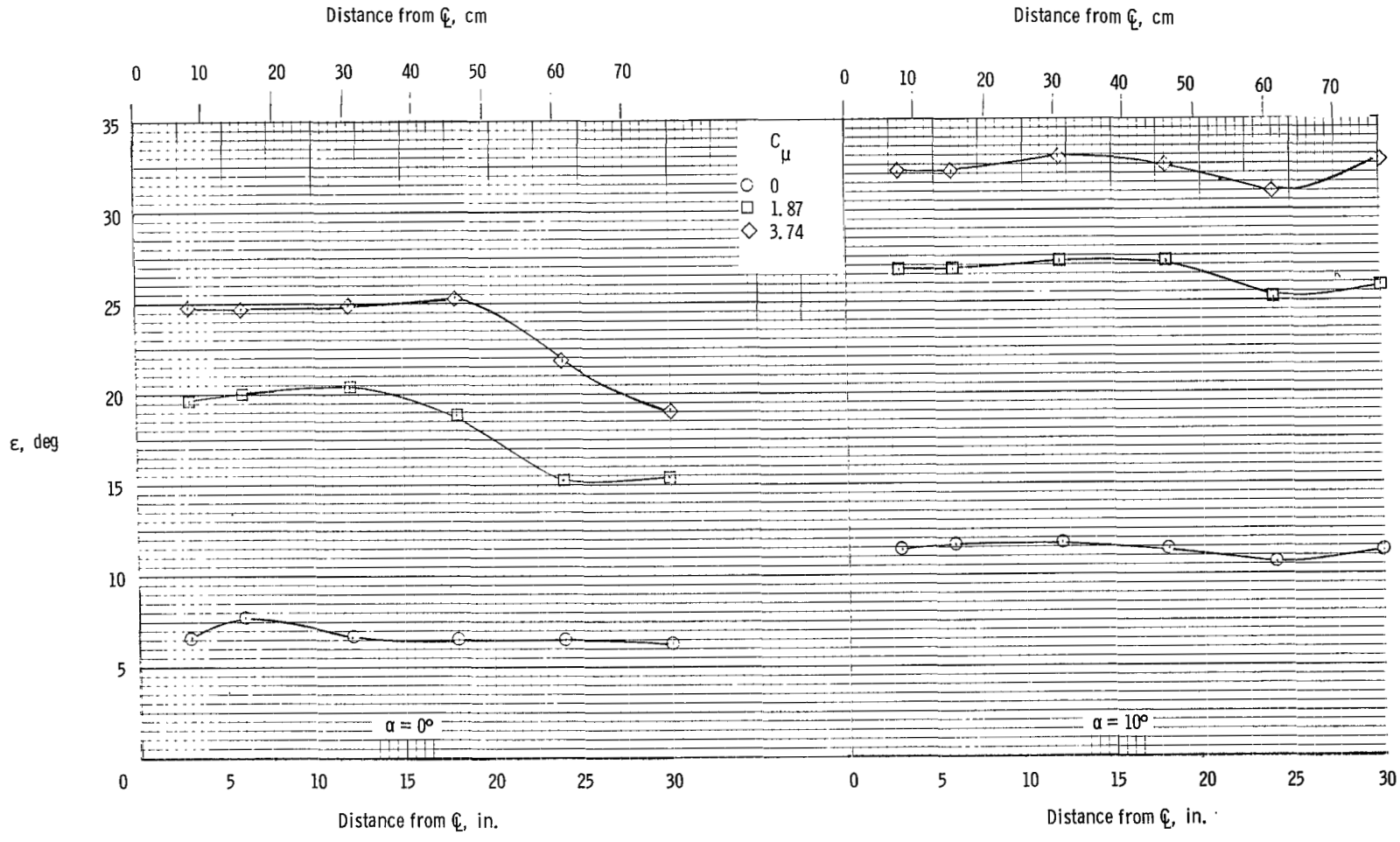

(c) z/c = 0.

Figure 34.- Concluded.

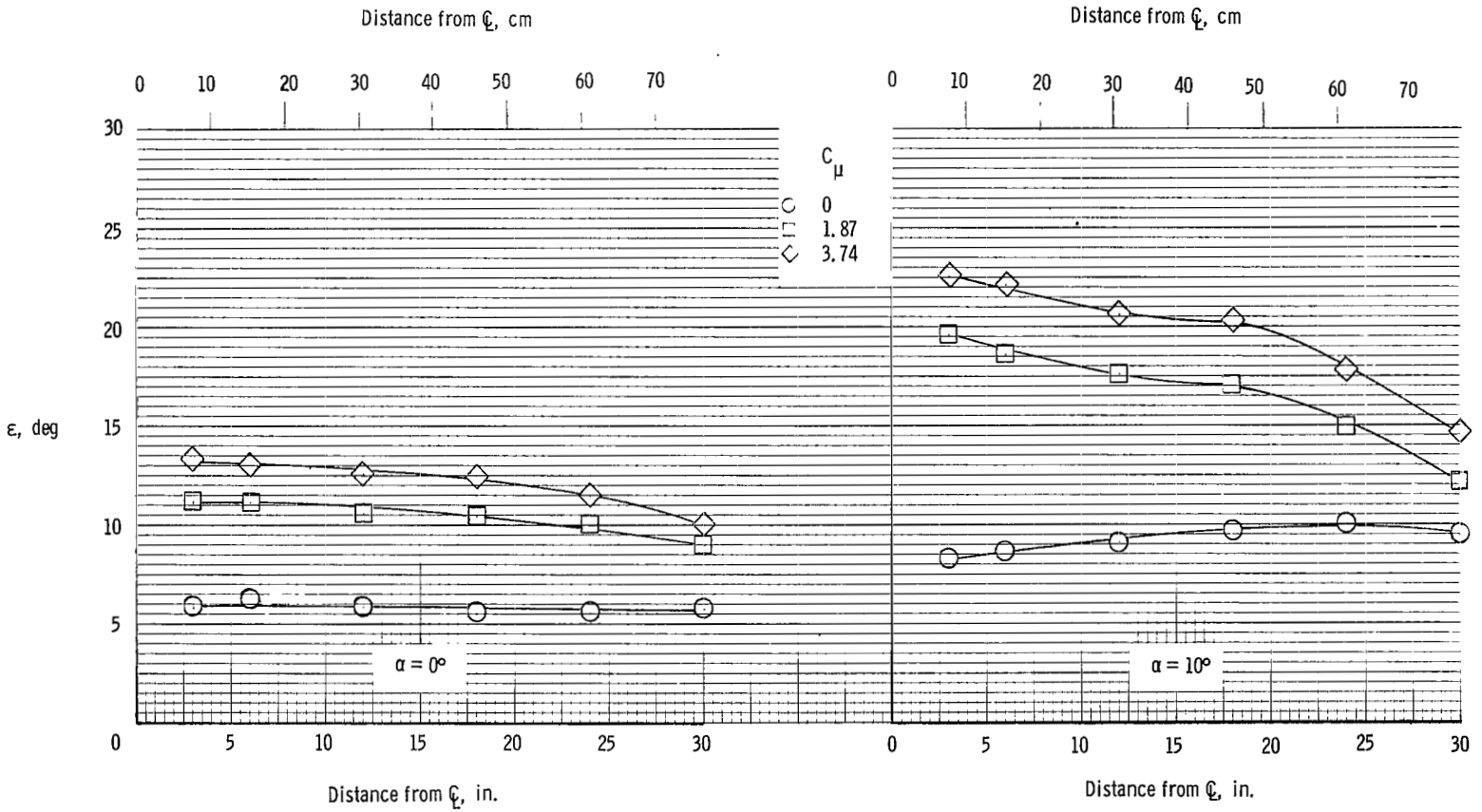

(a) z/c = 1.50.

Figure 35.- Variation of downwash angle with spanwise station for model with spread engines. $\delta_f = 60^o$; $C_{\mu,le} = 0$.

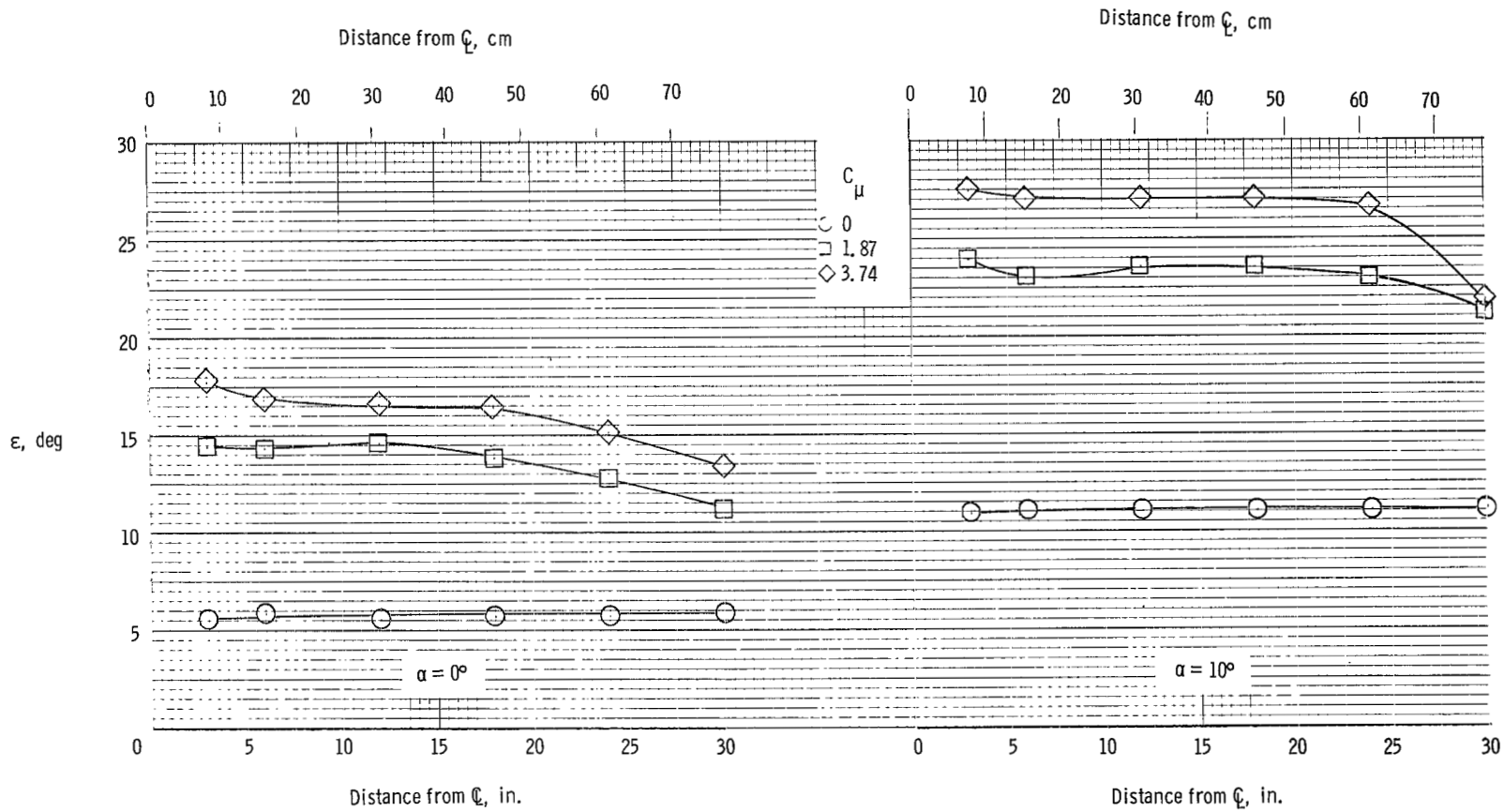

(b) z/c = 0.75.

Figure 35.- Continued.

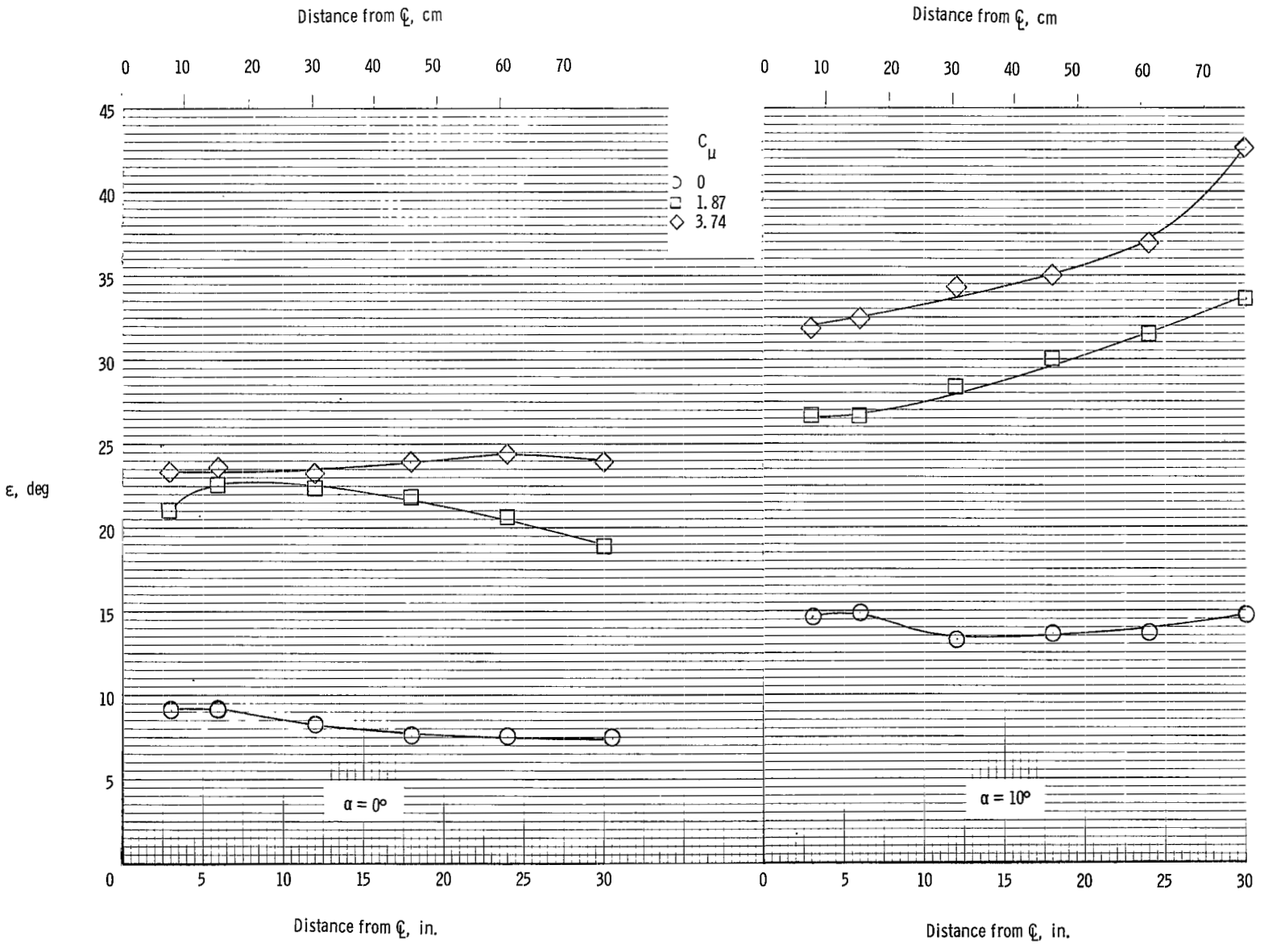

(c) z/c = 0.

Figure 35.- Concluded.

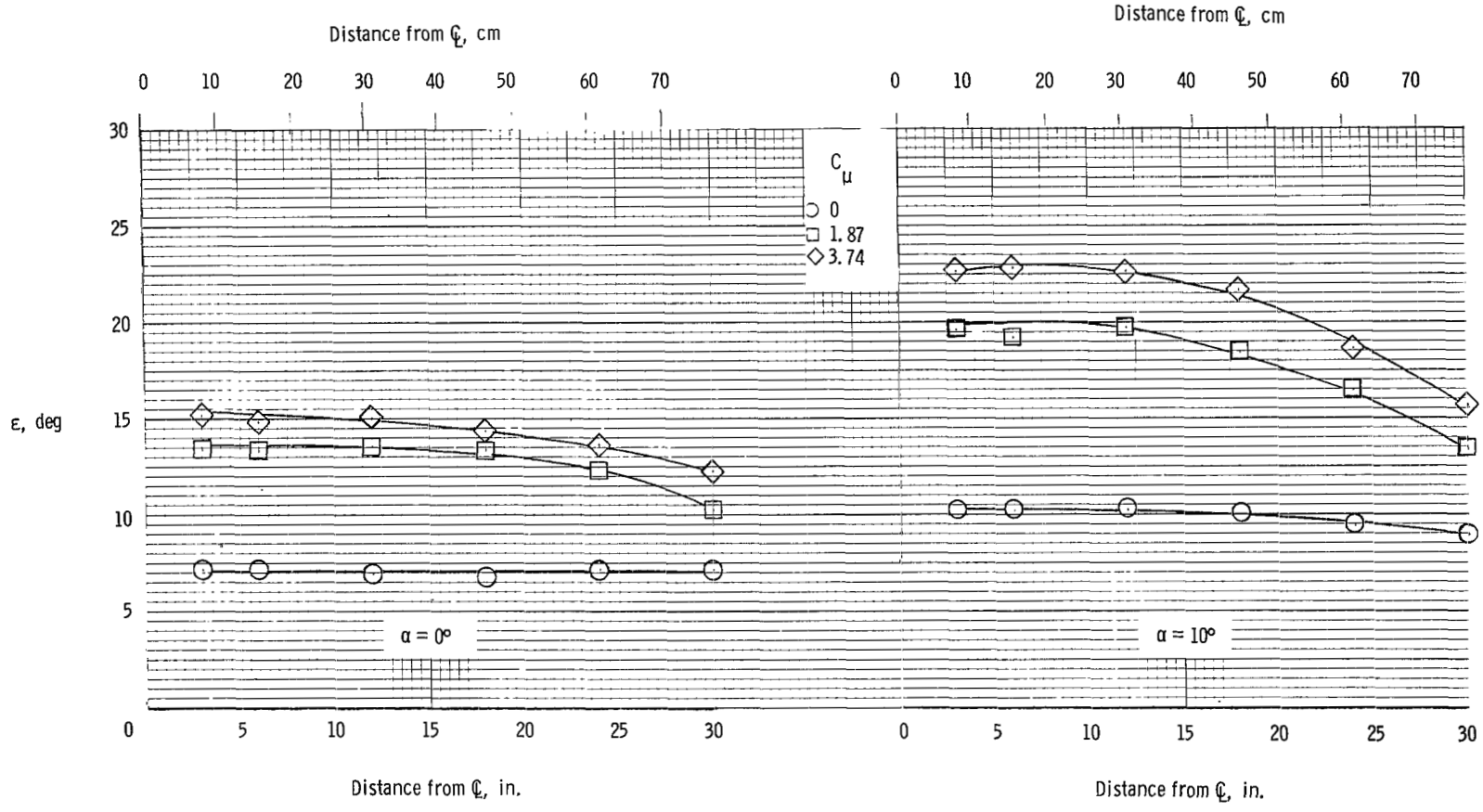

(a) z/c = 1.50.

Figure 36.- Variation of downwash angle with spanwise station for model with spread engines. $\delta_f = 60^o$; $C_{\mu,le} = 0.024$.

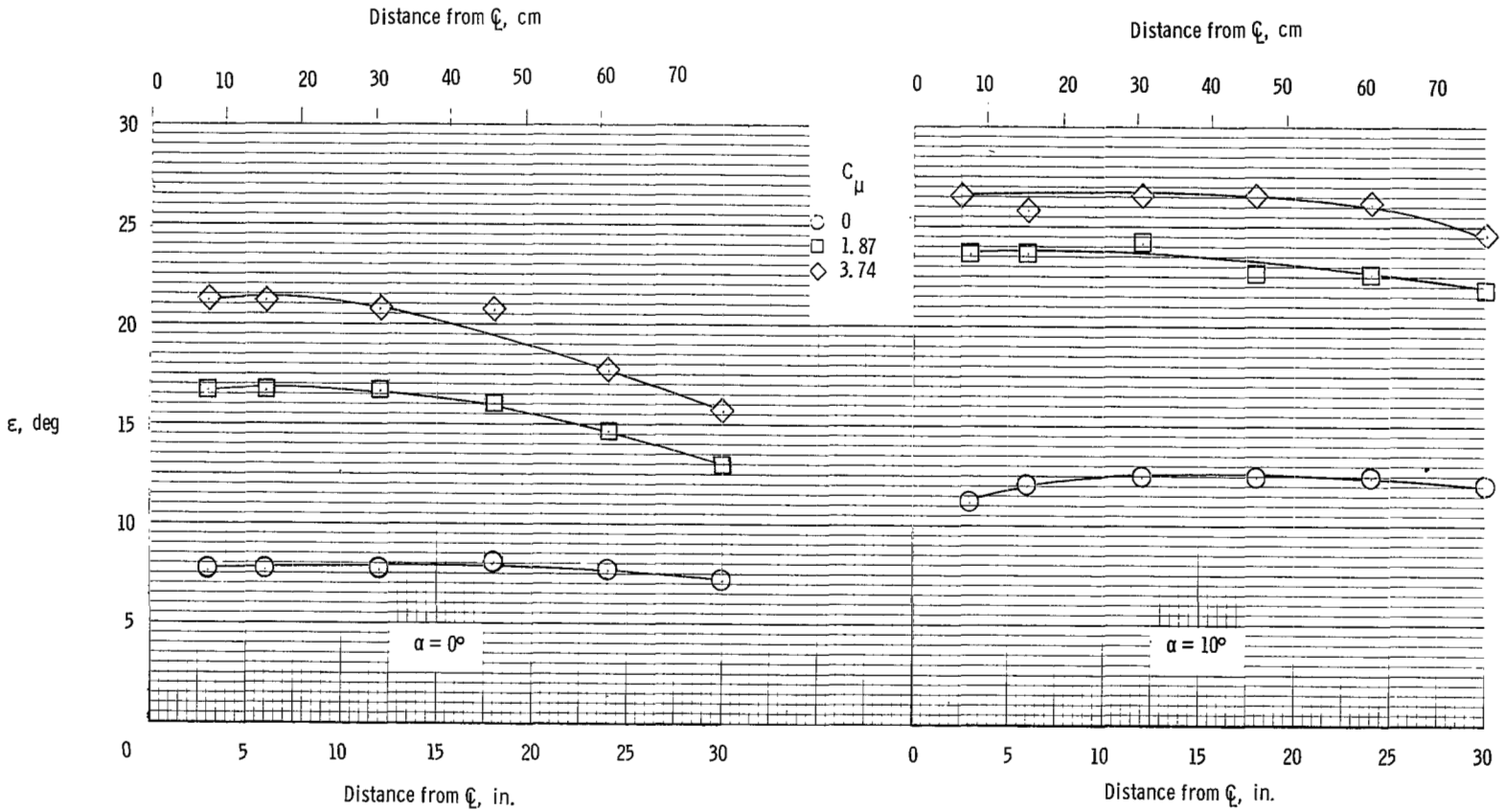

(b) z/c = 0.75.

Figure 36.- Continued.

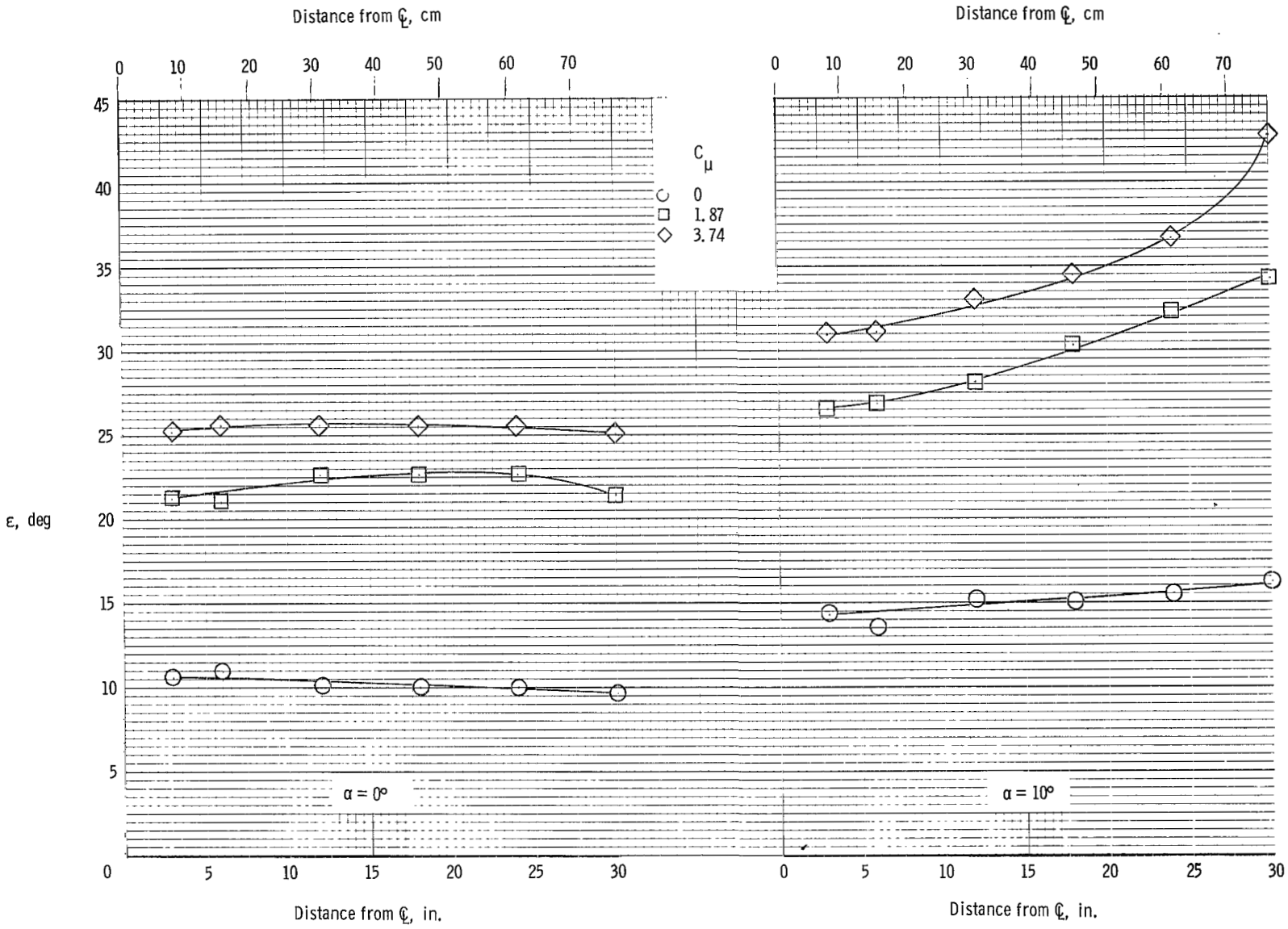

(c) z/c = 0.

Figure 36.- Concluded.

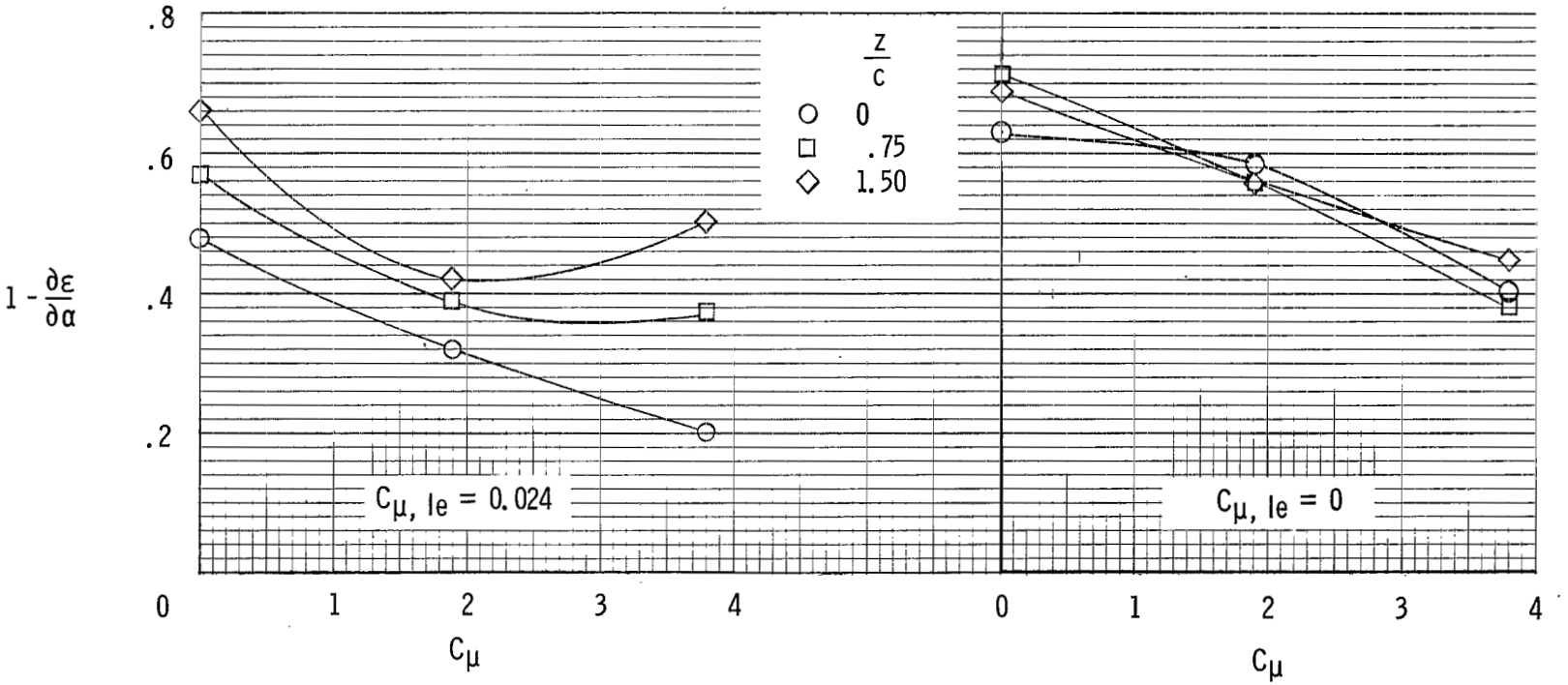

(a) Clustered engines.

Figure 37.- Summary of downwash flow surveys at spanwise station 30.5 cm (12 in.) from model center line.

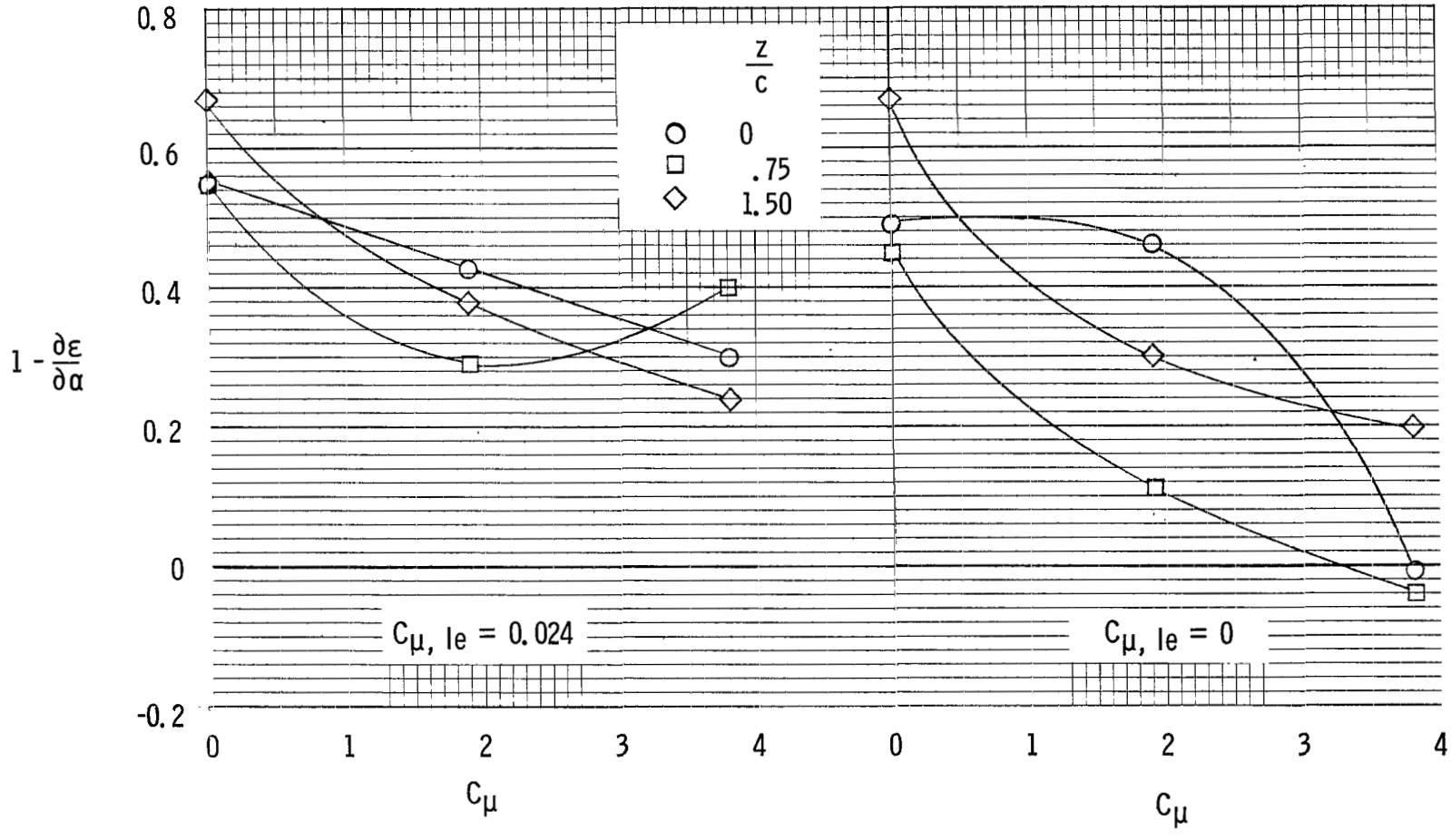

(b) Spread engines.

Figure 37.- Concluded.

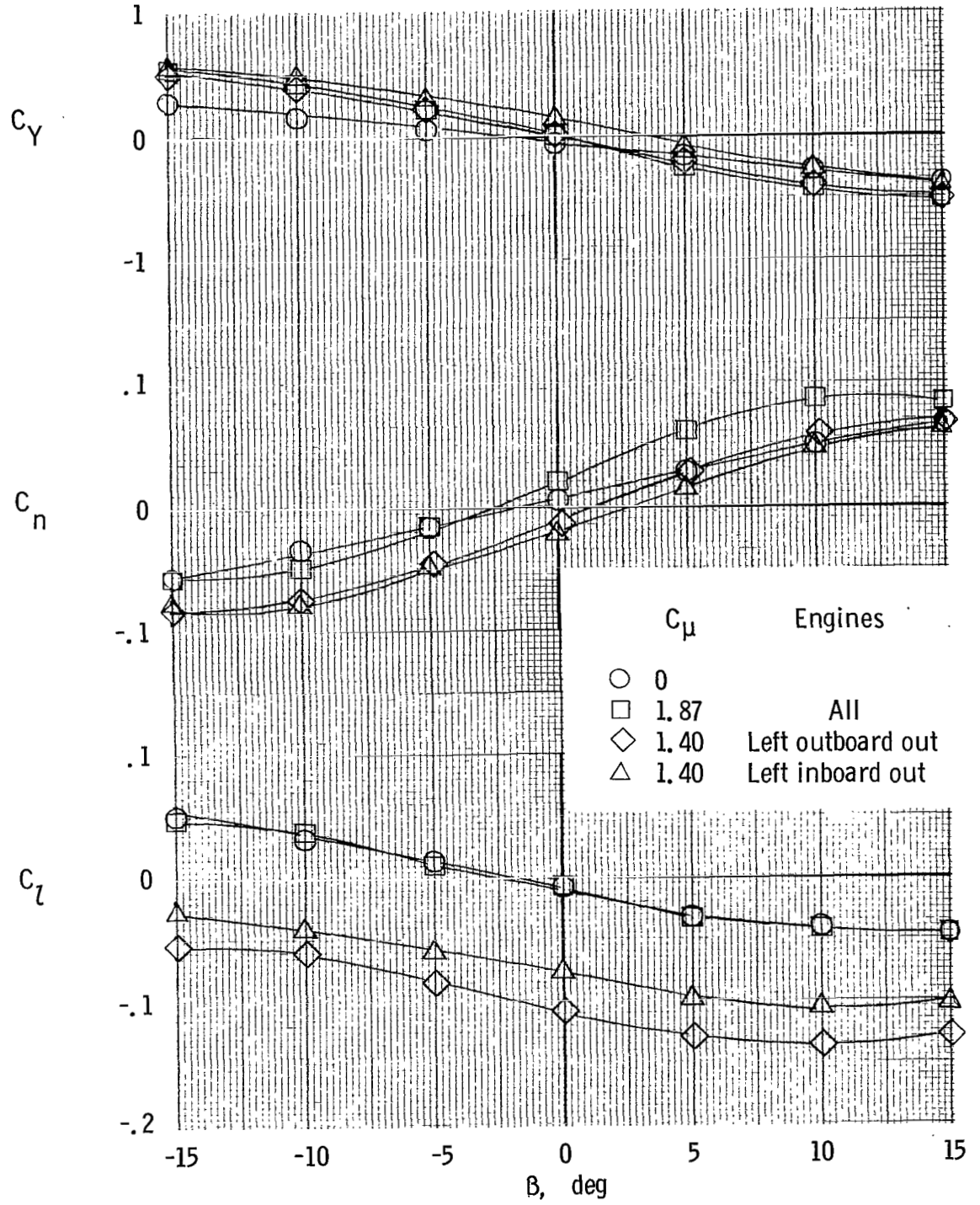

(a) $C_{\mu,le} = 0$.

Figure 38.- Variation of lateral aerodynamic coefficients with angle of sideslip for model with tail on and clustered engines. $\delta_f = 60^0$; $\delta_e = -50^0$; $i_t = 0^0$; $\alpha = 5^0$.

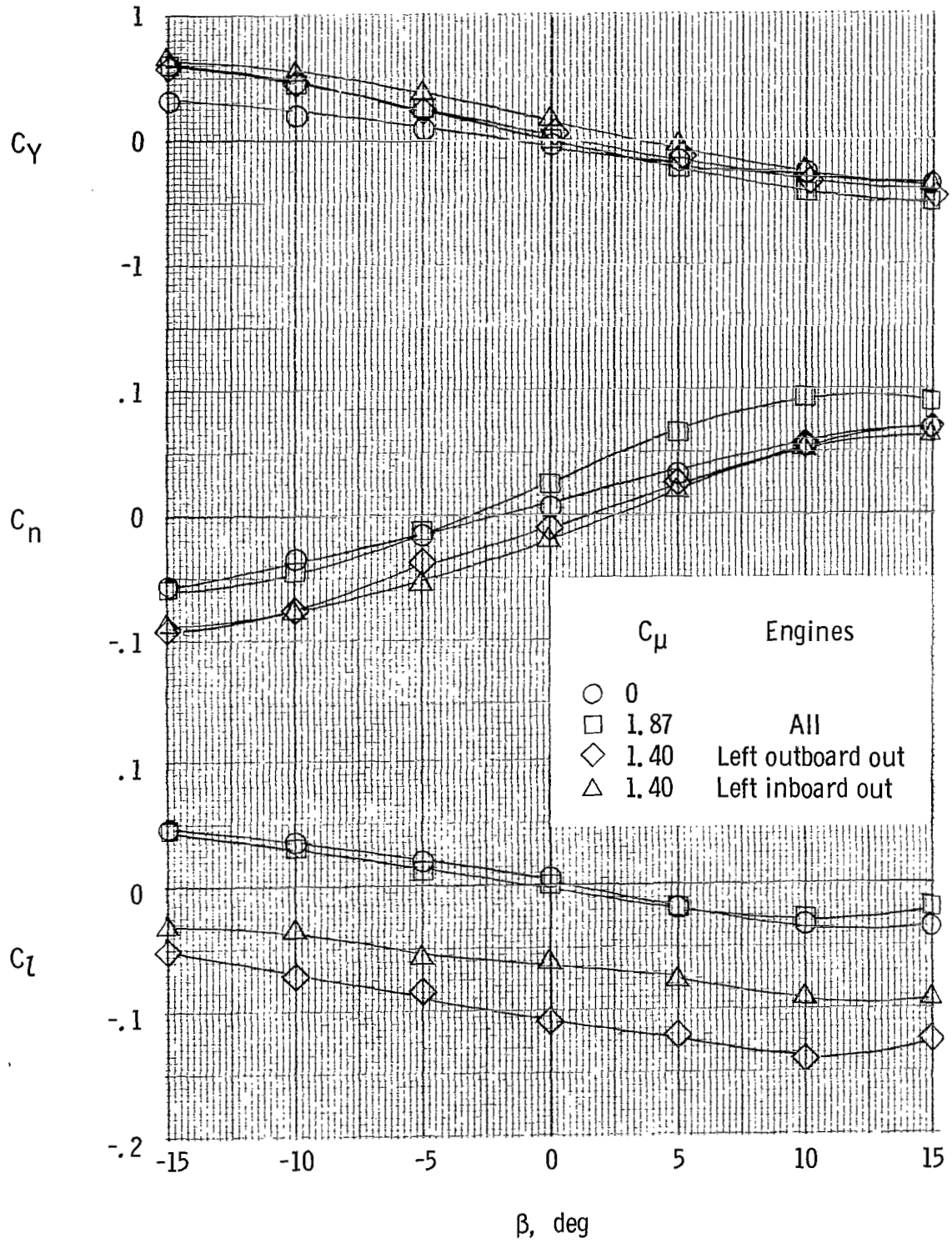

(b) $C_{\mu,le} = 0.024$.

Figure 38.- Concluded.

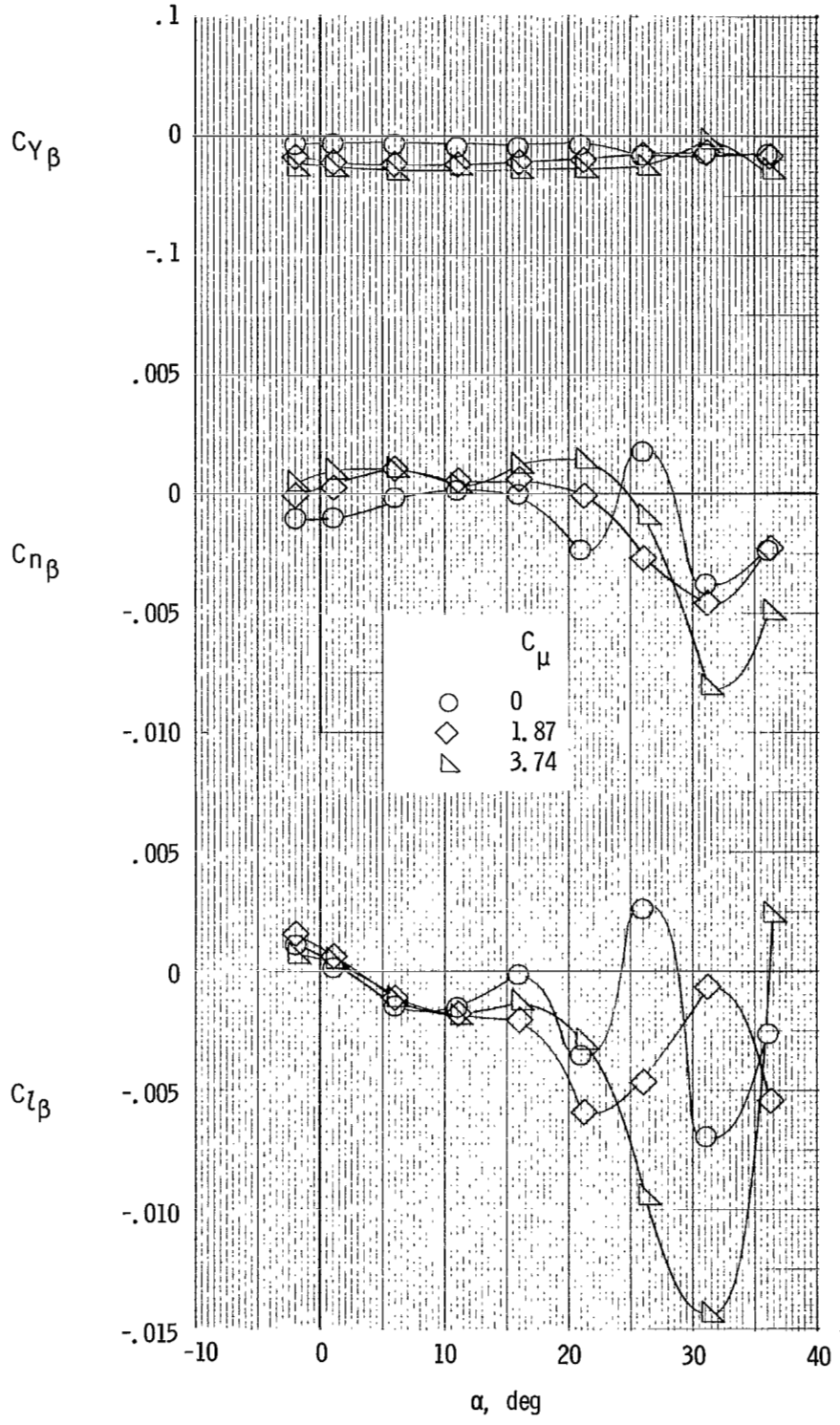

(a) $C_{\mu,te} = 0$.

Figure 39.- Lateral stability characteristics of model with tail off and clustered engines. $\delta_f = 60^0$.

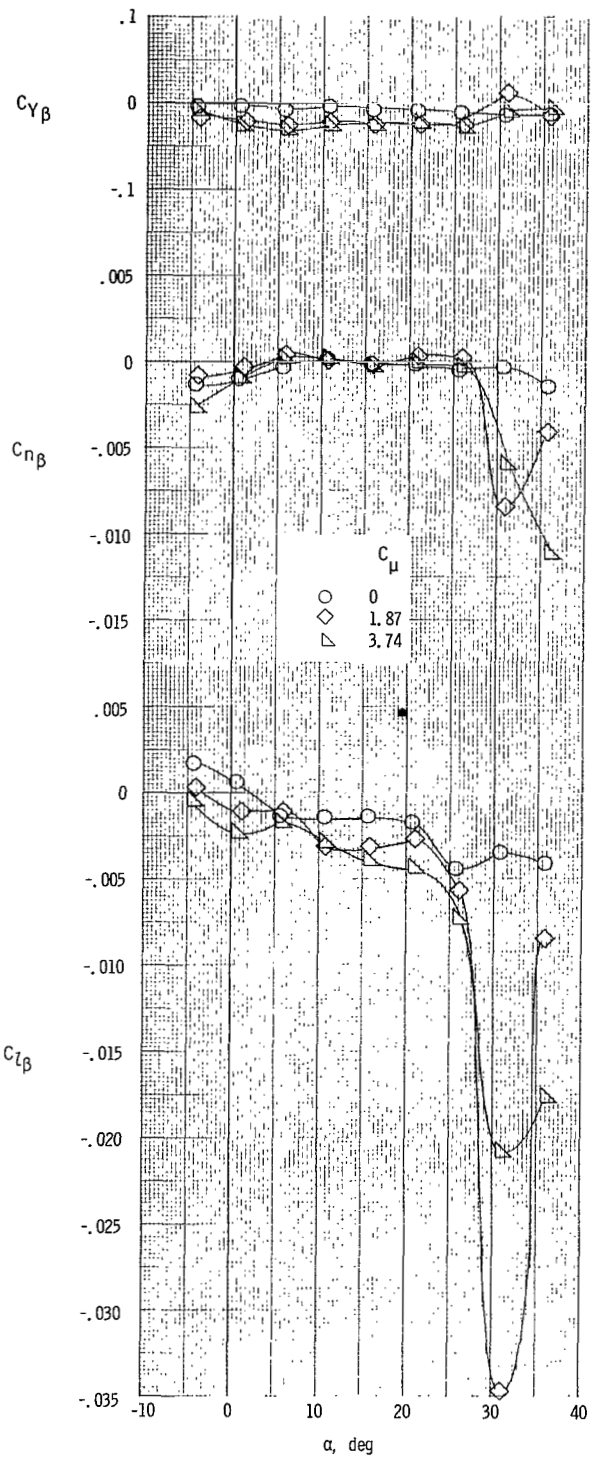

(b) $C_{\mu,le} = 0.024$.

Figure 39.- Concluded.

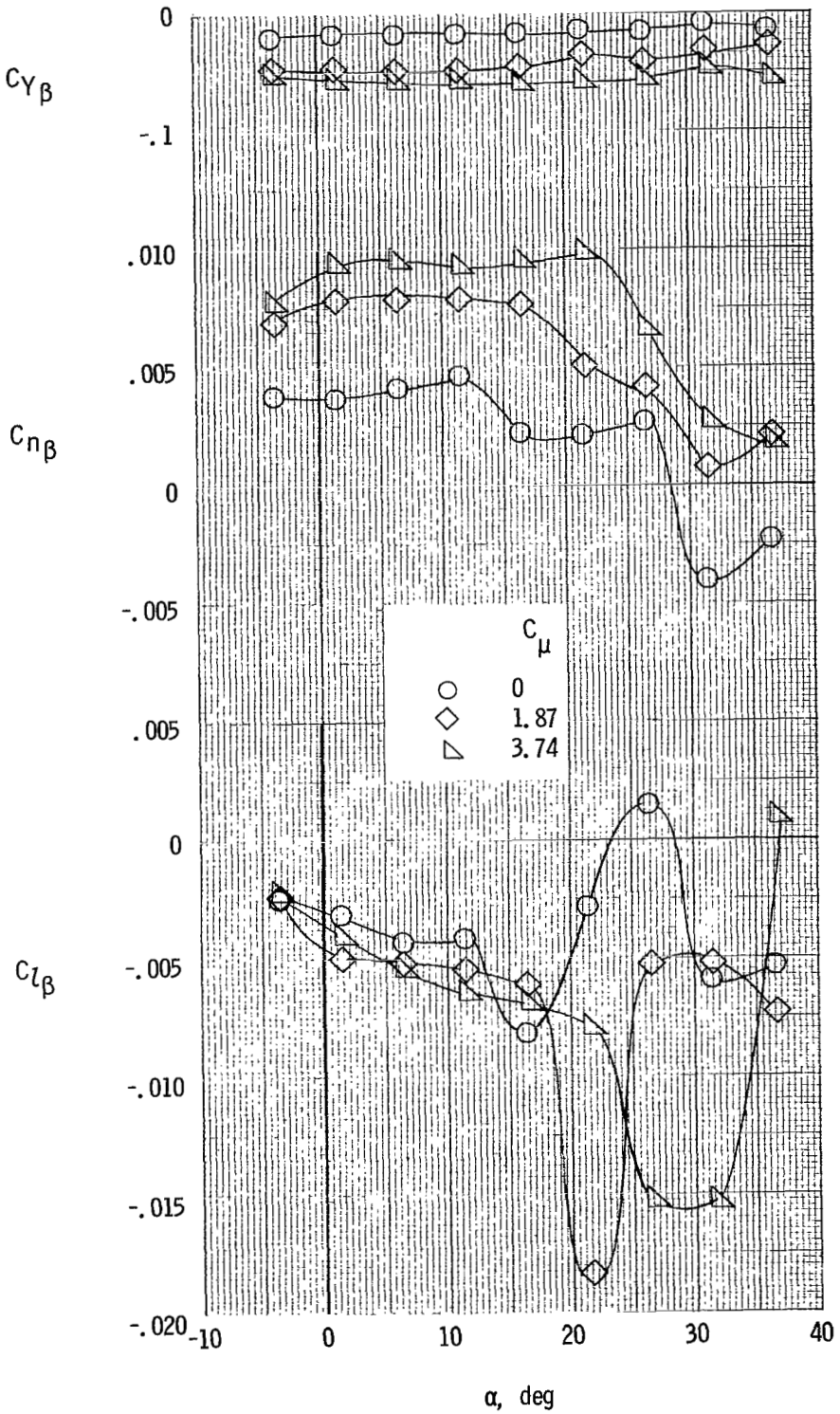

(a) $C_{\mu,le} = 0$.

Figure 40.- Lateral stability characteristics of model with tail on and clustered engines. $\delta_f = 60^0$; $\delta_e = -50^0$; $i_t = 0^0$.

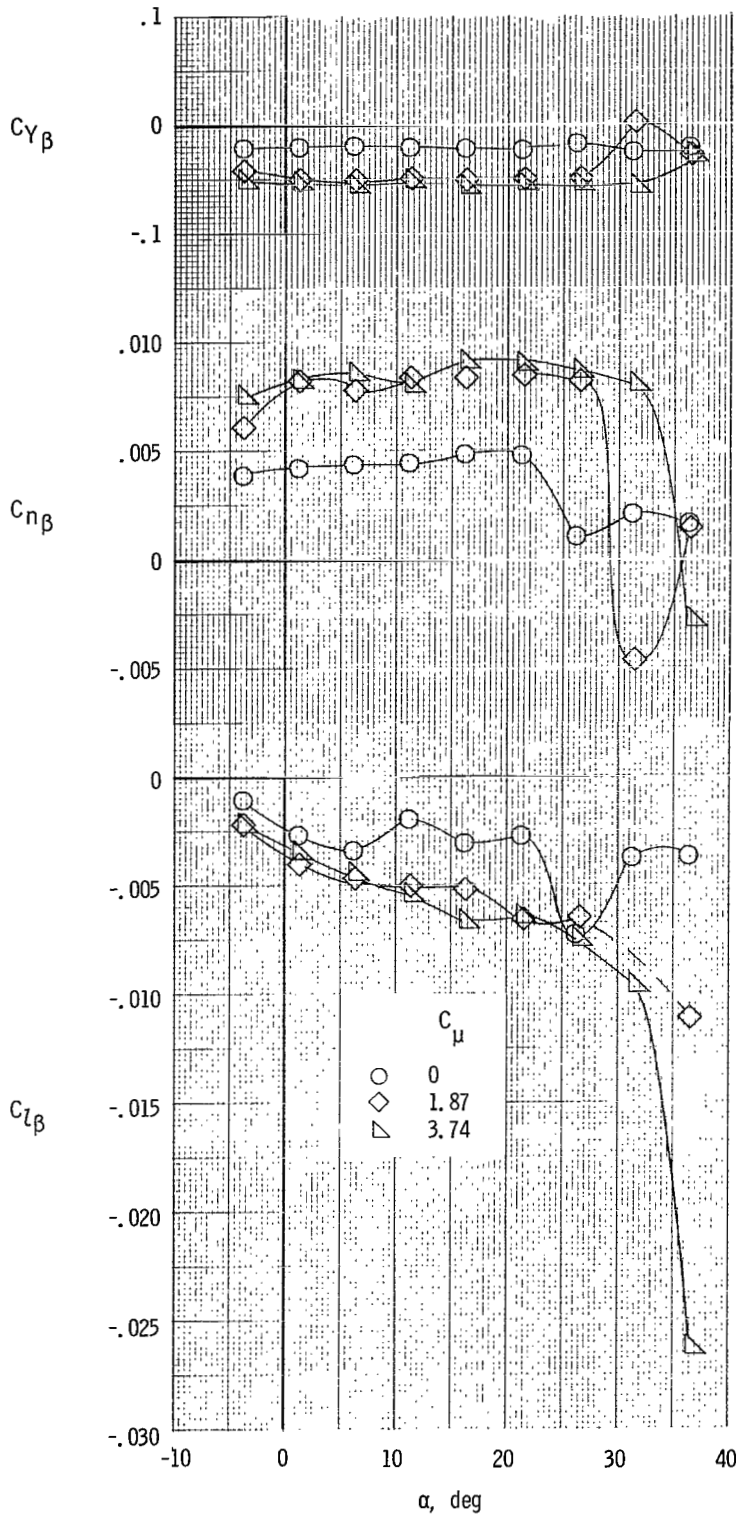

(b) $C_{\mu,le} = 0.024$.

Figure 40.- Concluded.

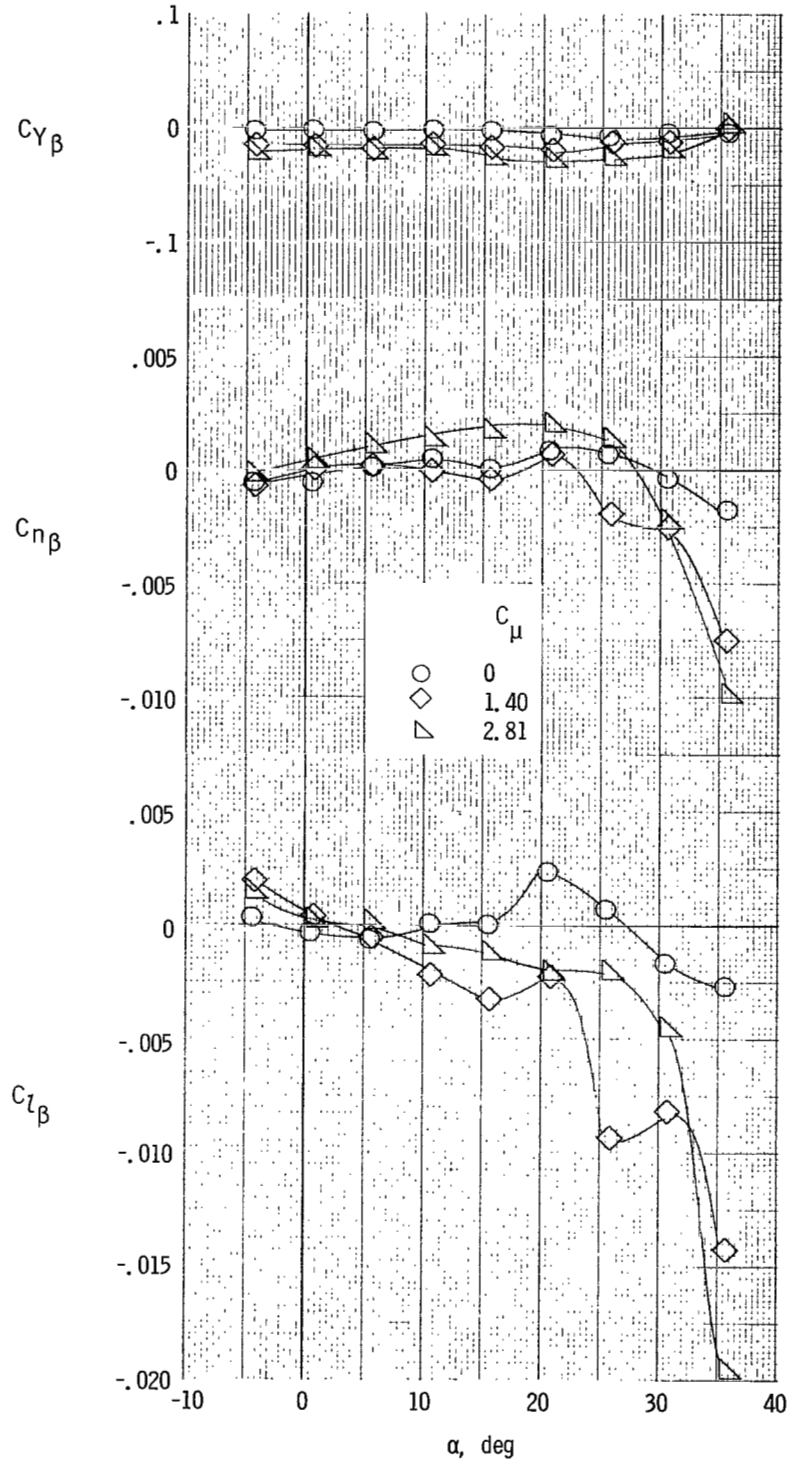

(a) Left outboard engine not operating.

Figure 41.- Effect of asymmetric thrust on lateral stability characteristics of model with tail off and clustered engines. $\delta_f = 60^o$; $C_{\mu,le} = 0.024$.

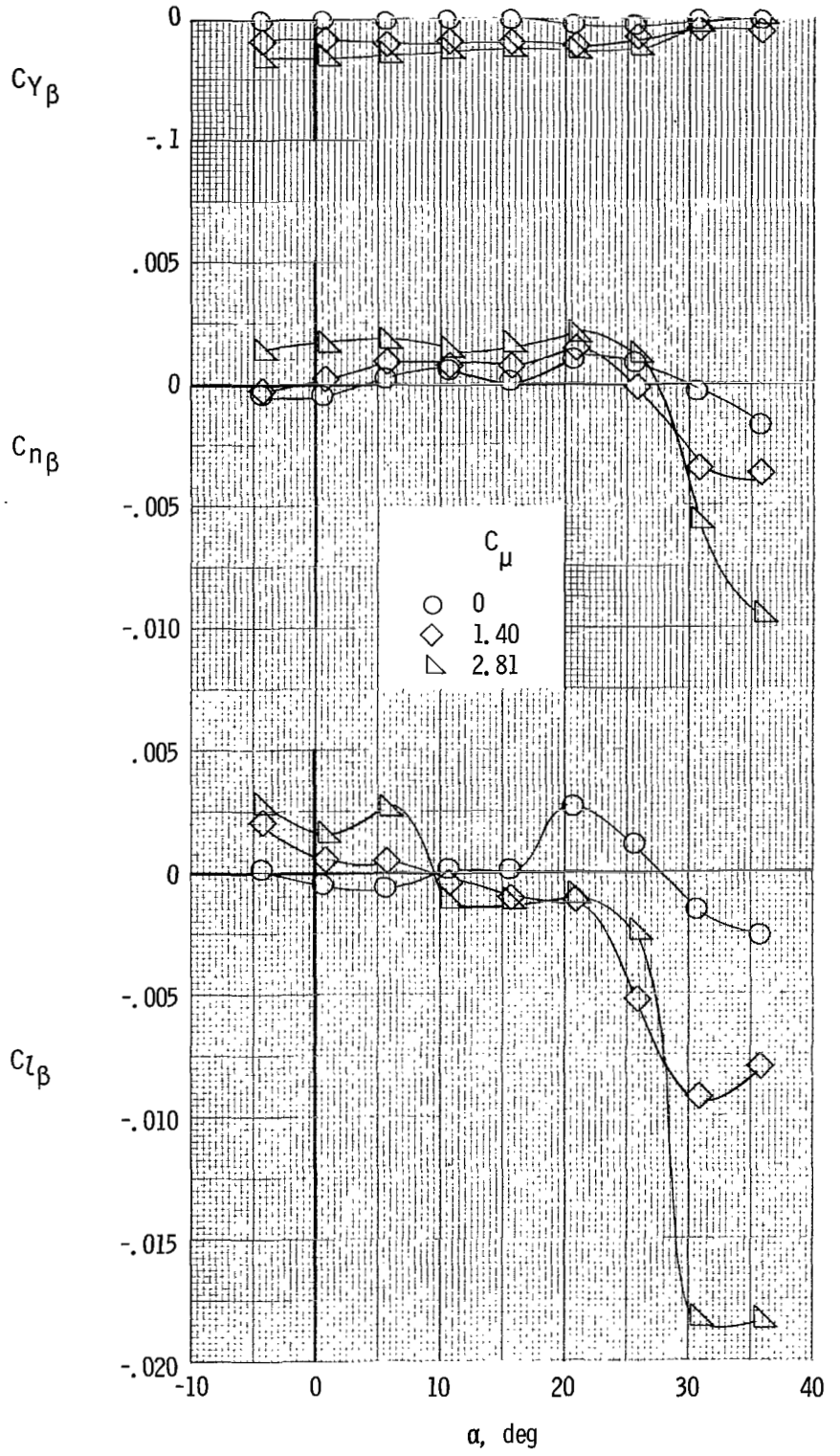

(b) Left inboard engine not operating.

Figure 41.- Concluded.

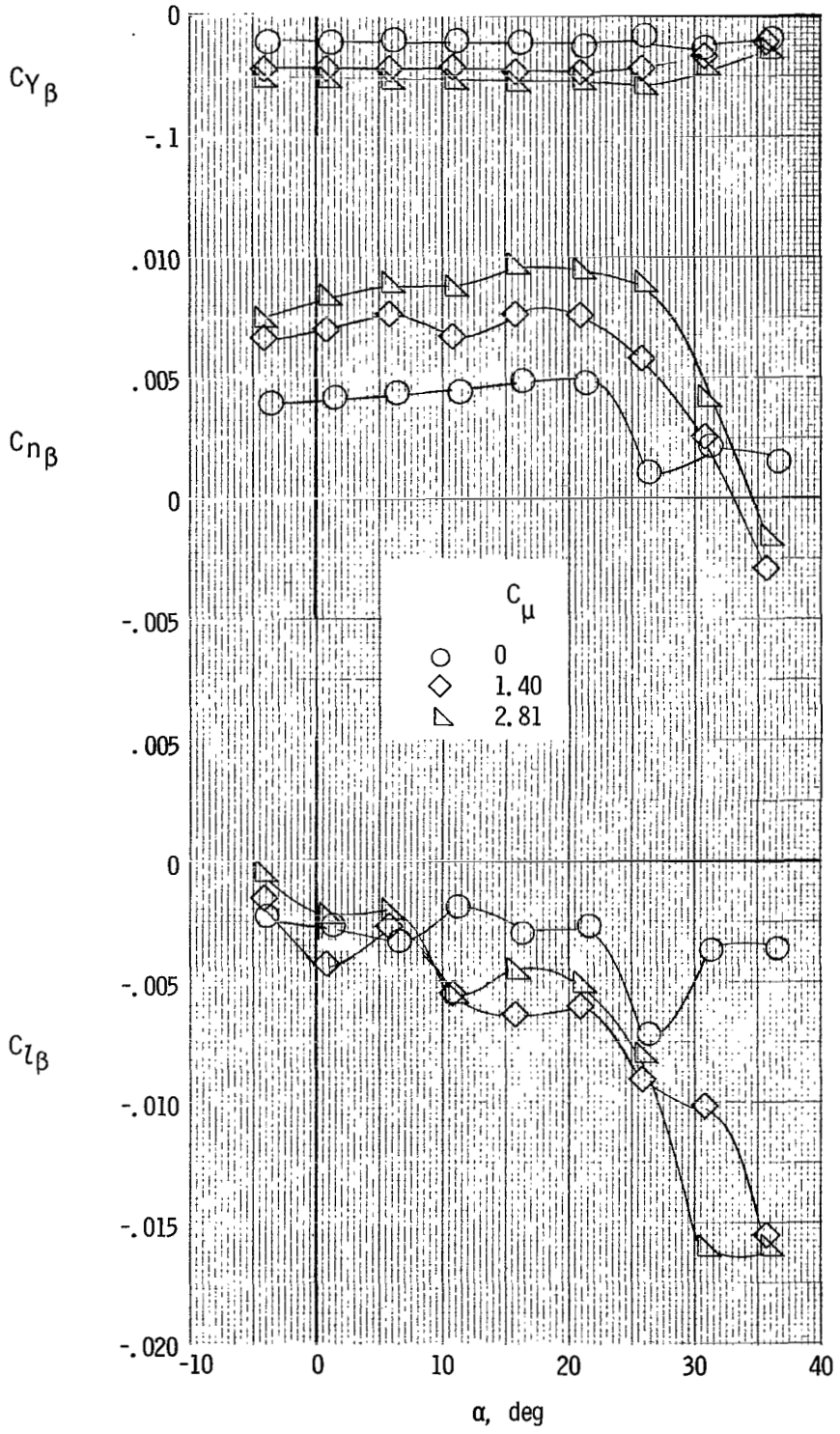

(a) Left outboard engine not operating.

Figure 42.- Effect of asymmetric thrust on lateral stability characteristics of model with tail on and clustered engines. $\delta_f = 60^0$; $\delta_e = -50^0$; $i_t = 0^0$; $C_{\mu,le} = 0.024$.

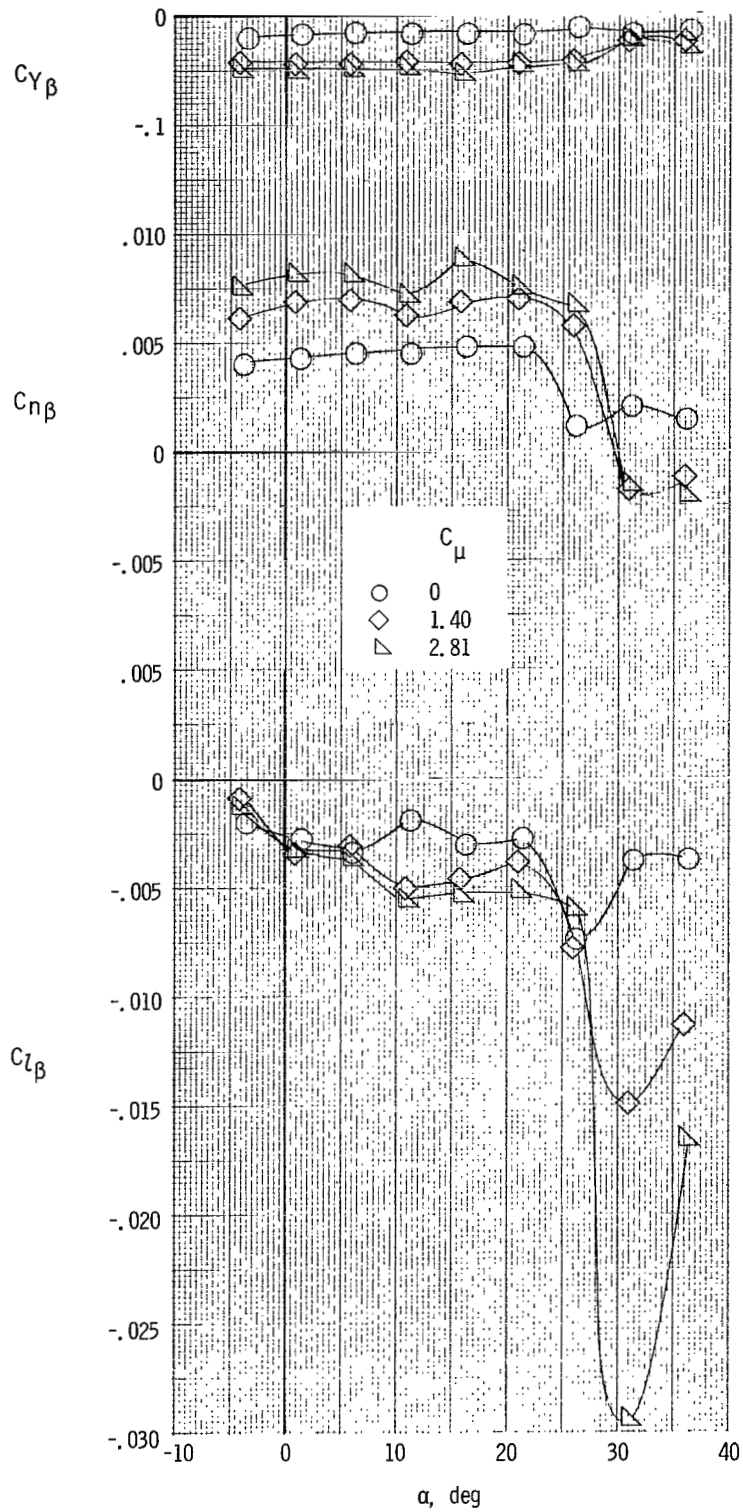

(b) Left inboard engine not operating.

Figure 42.- Concluded.

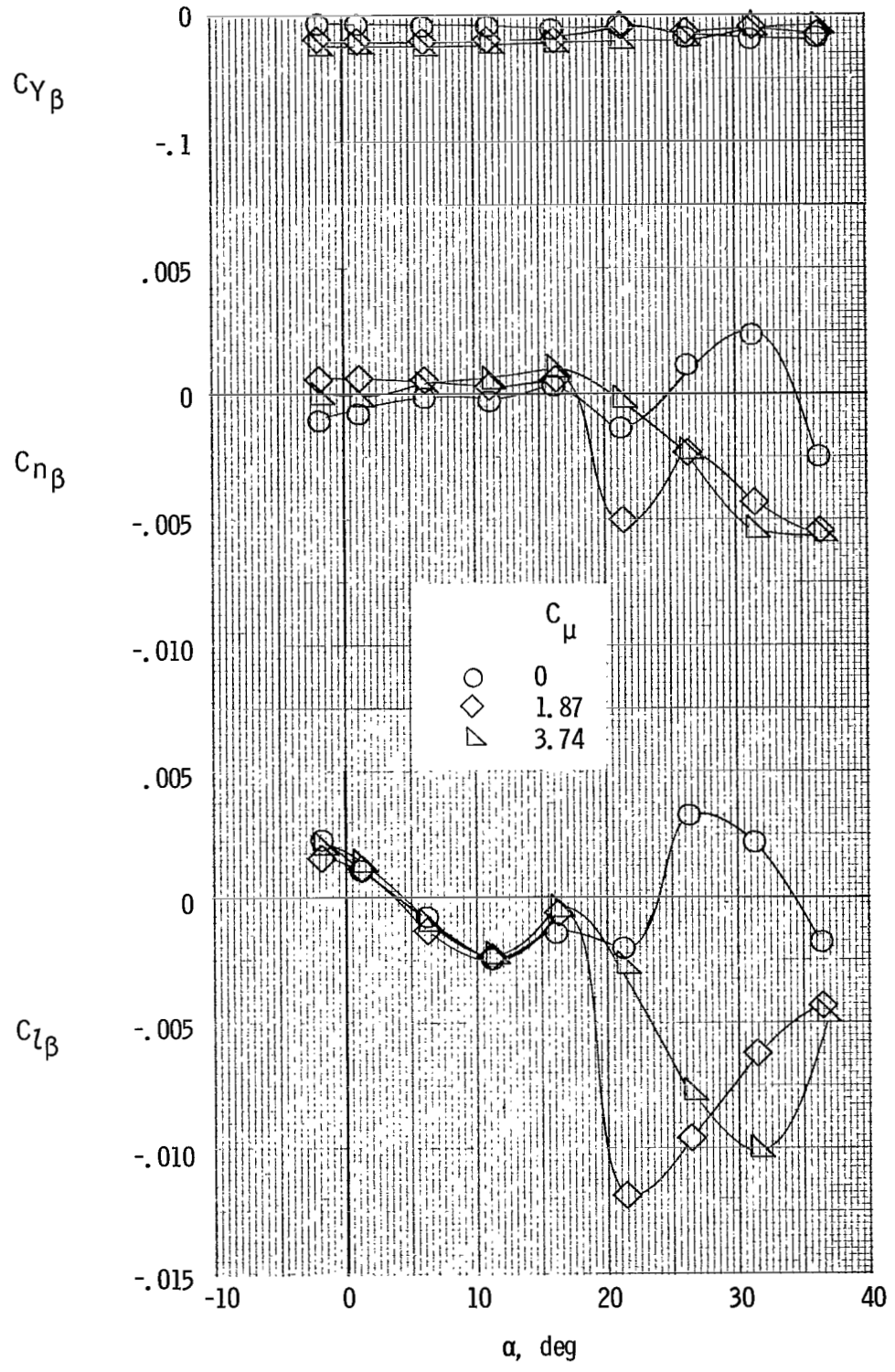

(a) $C_{\mu,le} = 0$.

Figure 43.- Lateral stability characteristics of model with tail off and clustered engines. $\delta_f = 35^o$.

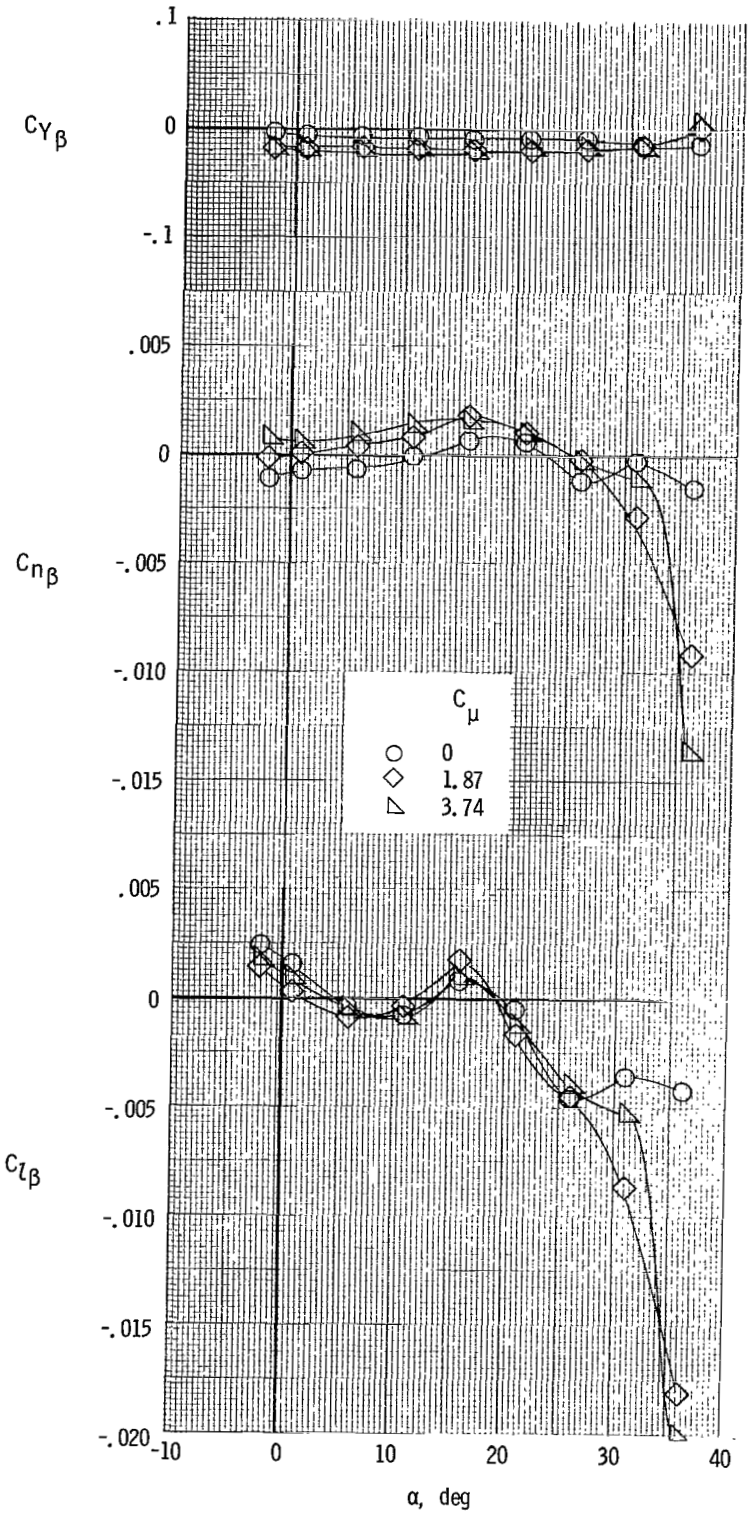

(b) $C_{\mu,le} = 0.024$.

Figure 43.- Concluded.

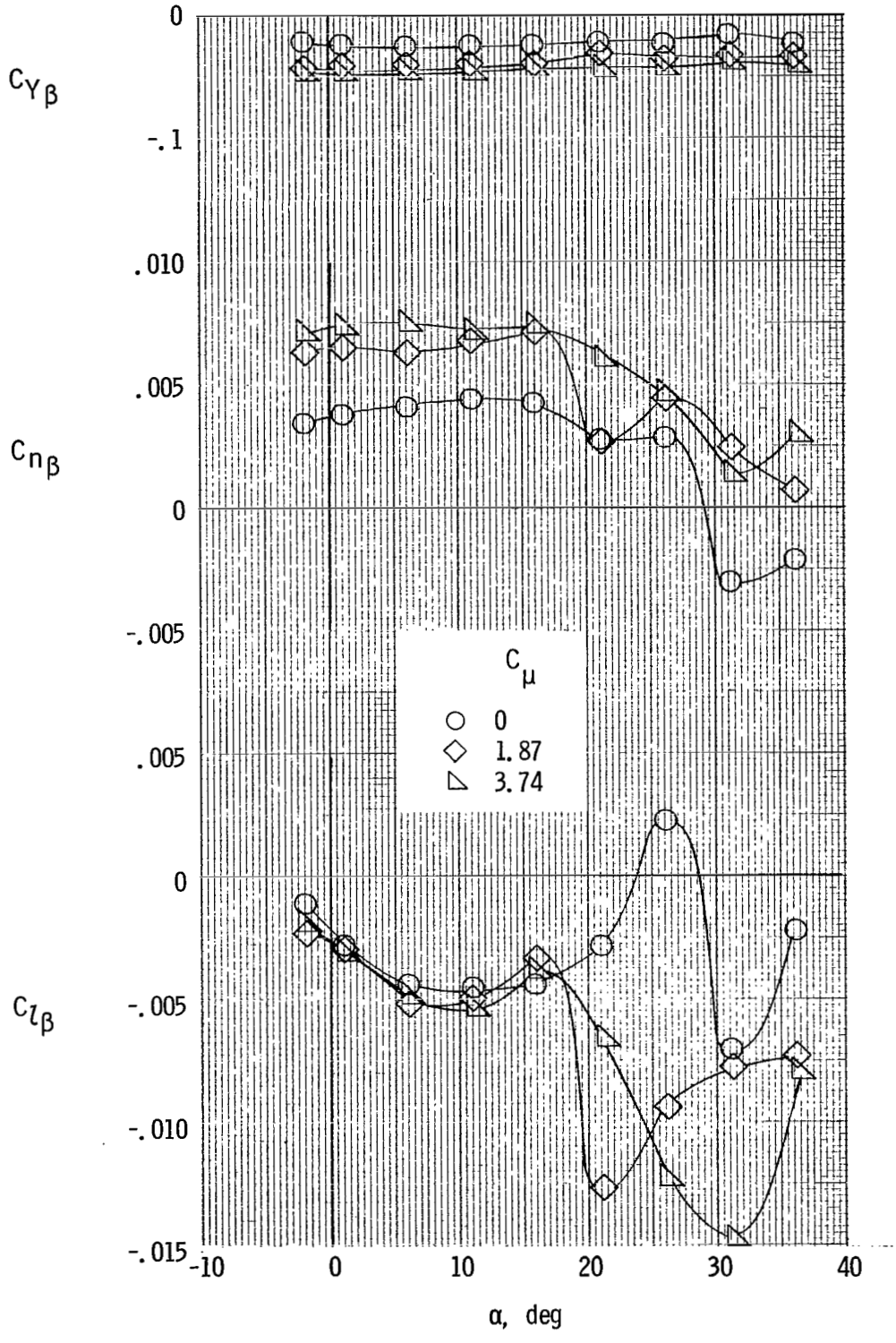

(a) $C_{\mu,le} = 0.$

Figure 44.- Lateral stability characteristics of model with tail on and clustered engines. $\delta_f = 35^0$; $\delta_e = -50^0$; $i_t = 0^0$.

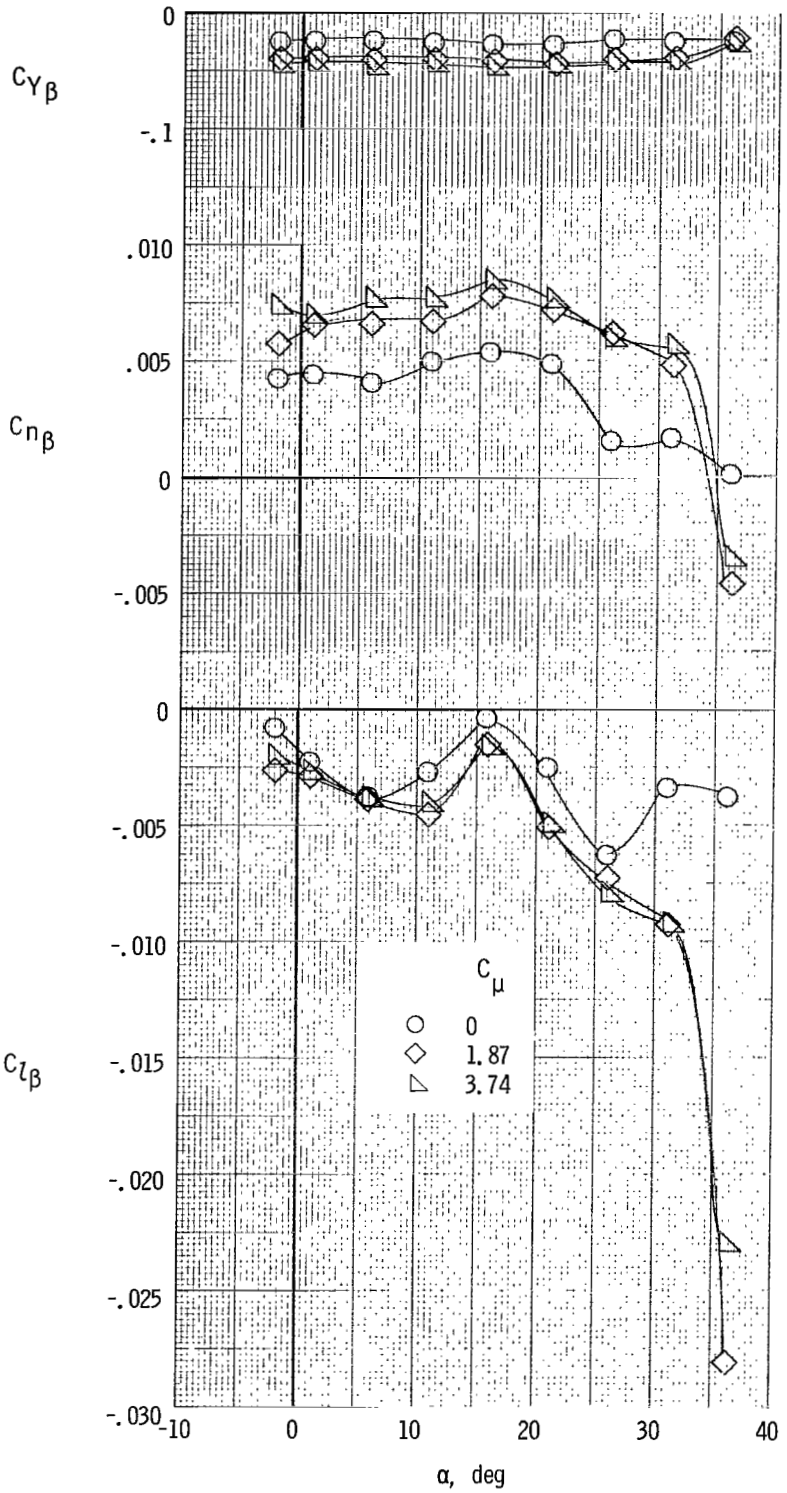

(b) $C_{\mu,le} = 0.024$.

Figure 44.- Concluded.

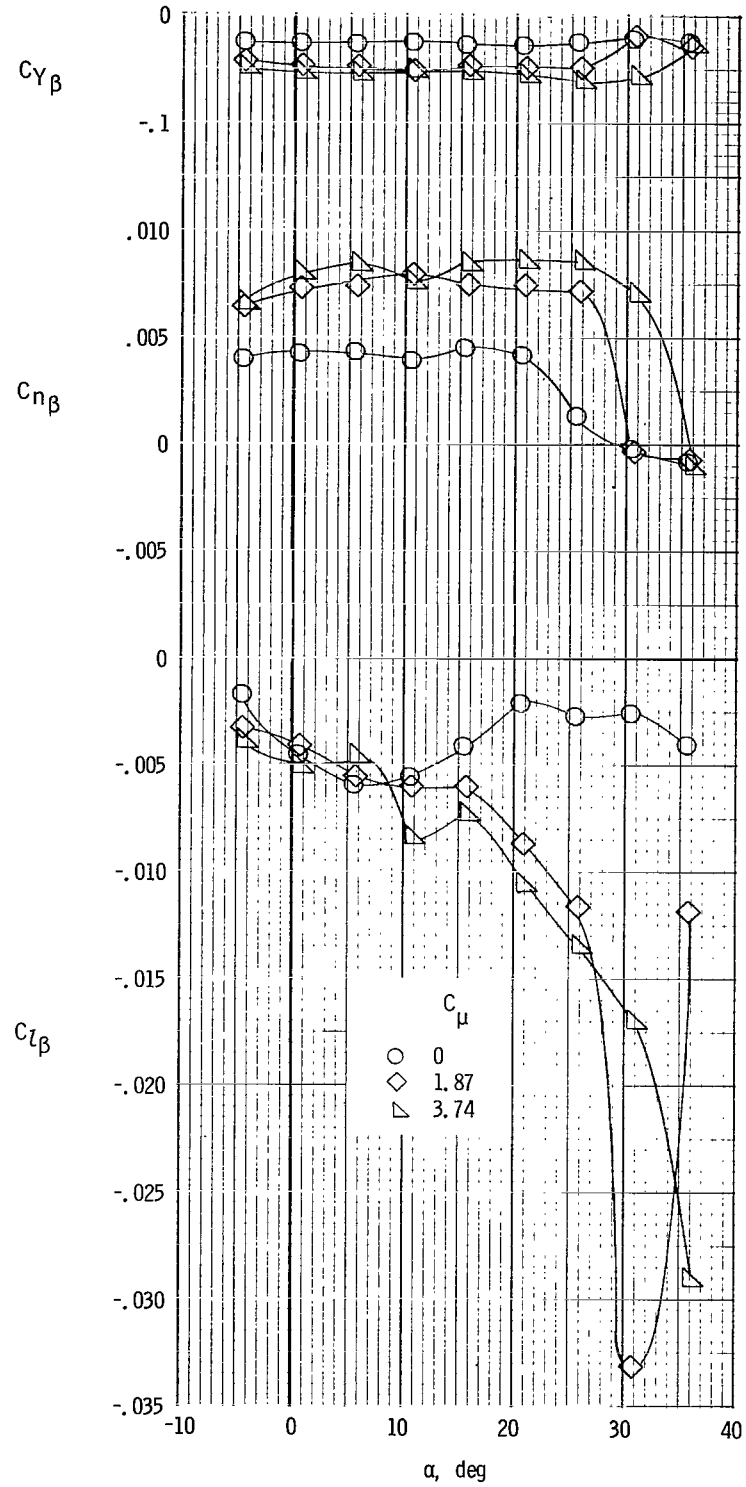

(a) $\delta_f = 60^0$.

Figure 45.- Lateral stability characteristics of model with tail on and spread engines. $\delta_e = -50^0$; $i_t = 0^0$; $C_{\mu,le} = 0.024$.

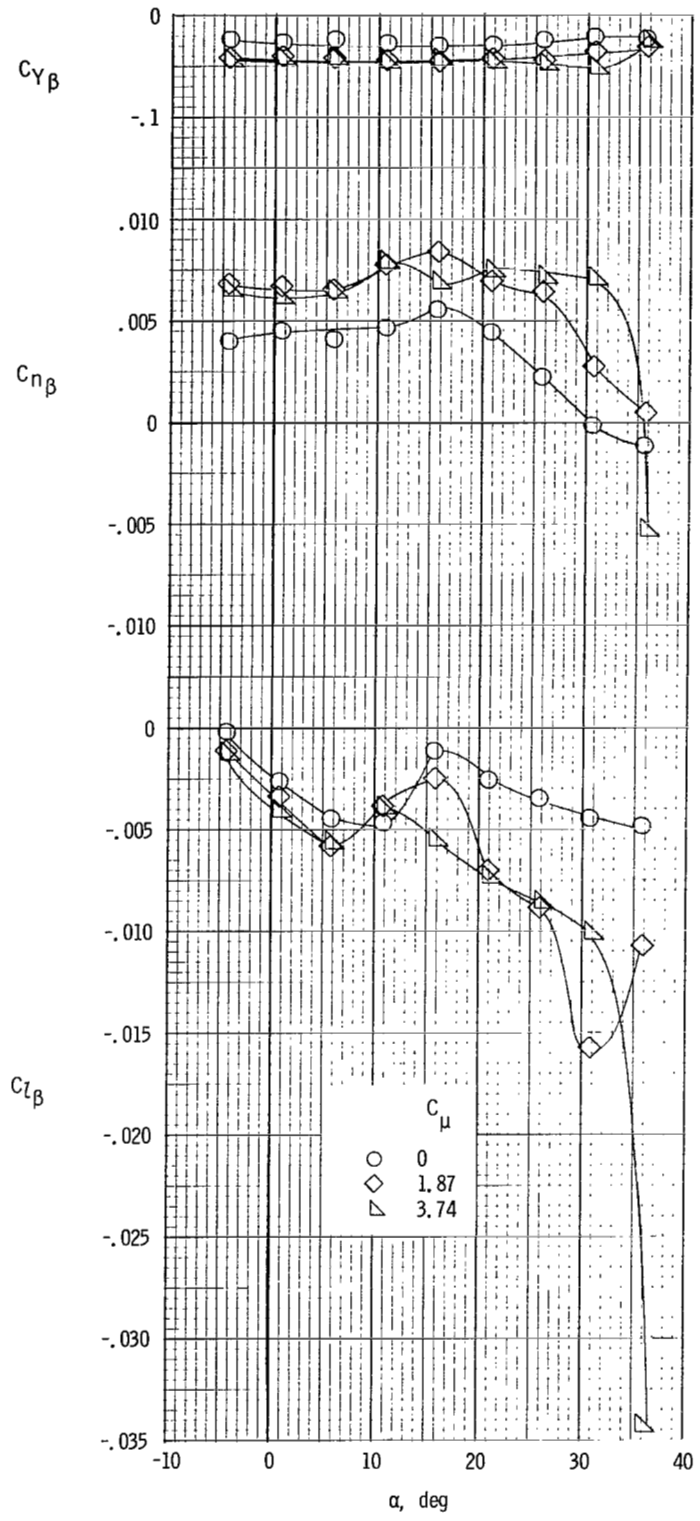

(b) $\delta_f = 40^0$.

Figure 45.- Concluded.

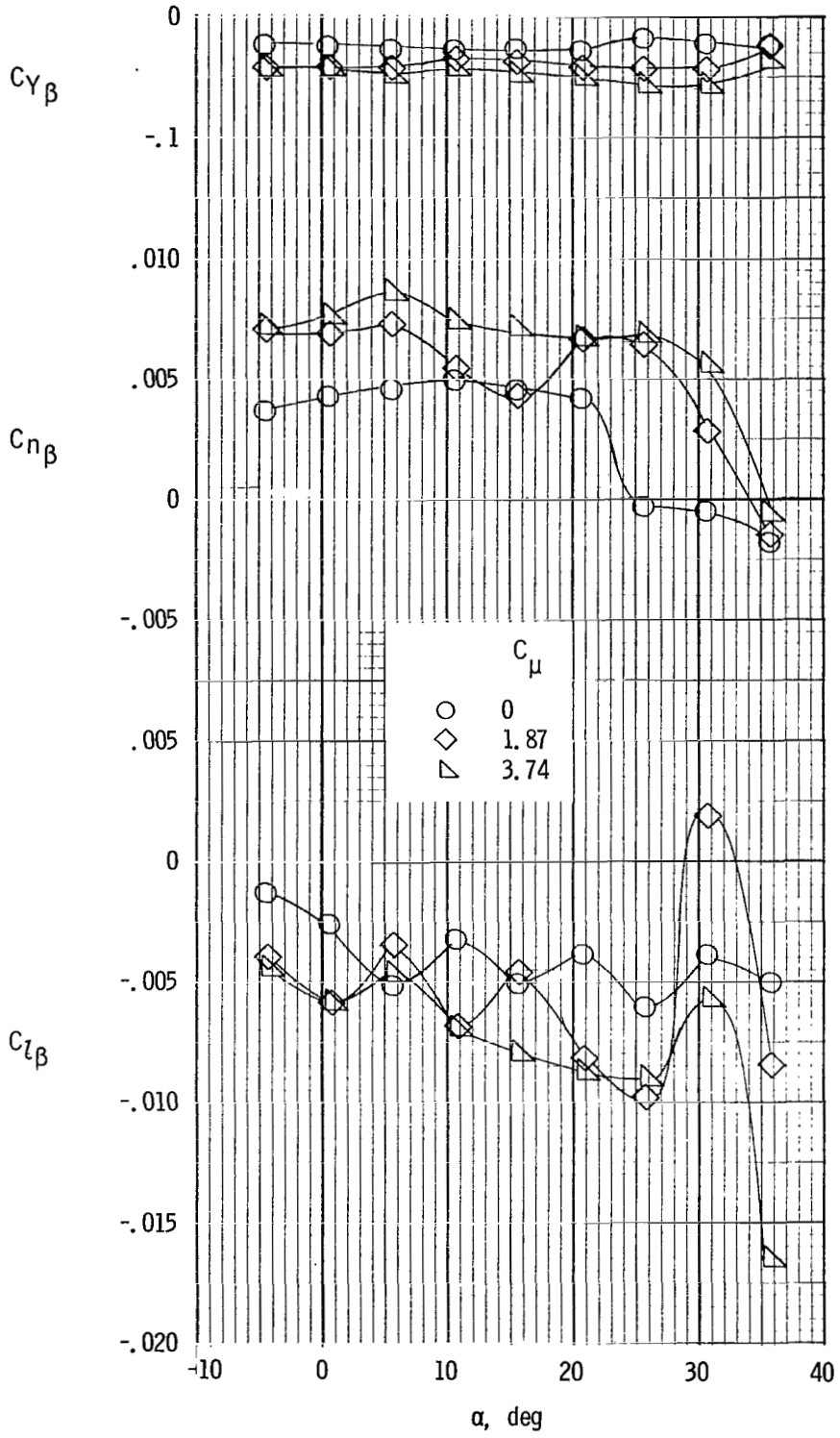

Figure 46.- Lateral stability characteristics of model with tail on and spread engines. $\delta_f = 80^o$, inboard segments; $\delta_f = 60^o$, center and outboard segments; $C_{\mu,le} = 0.024$.

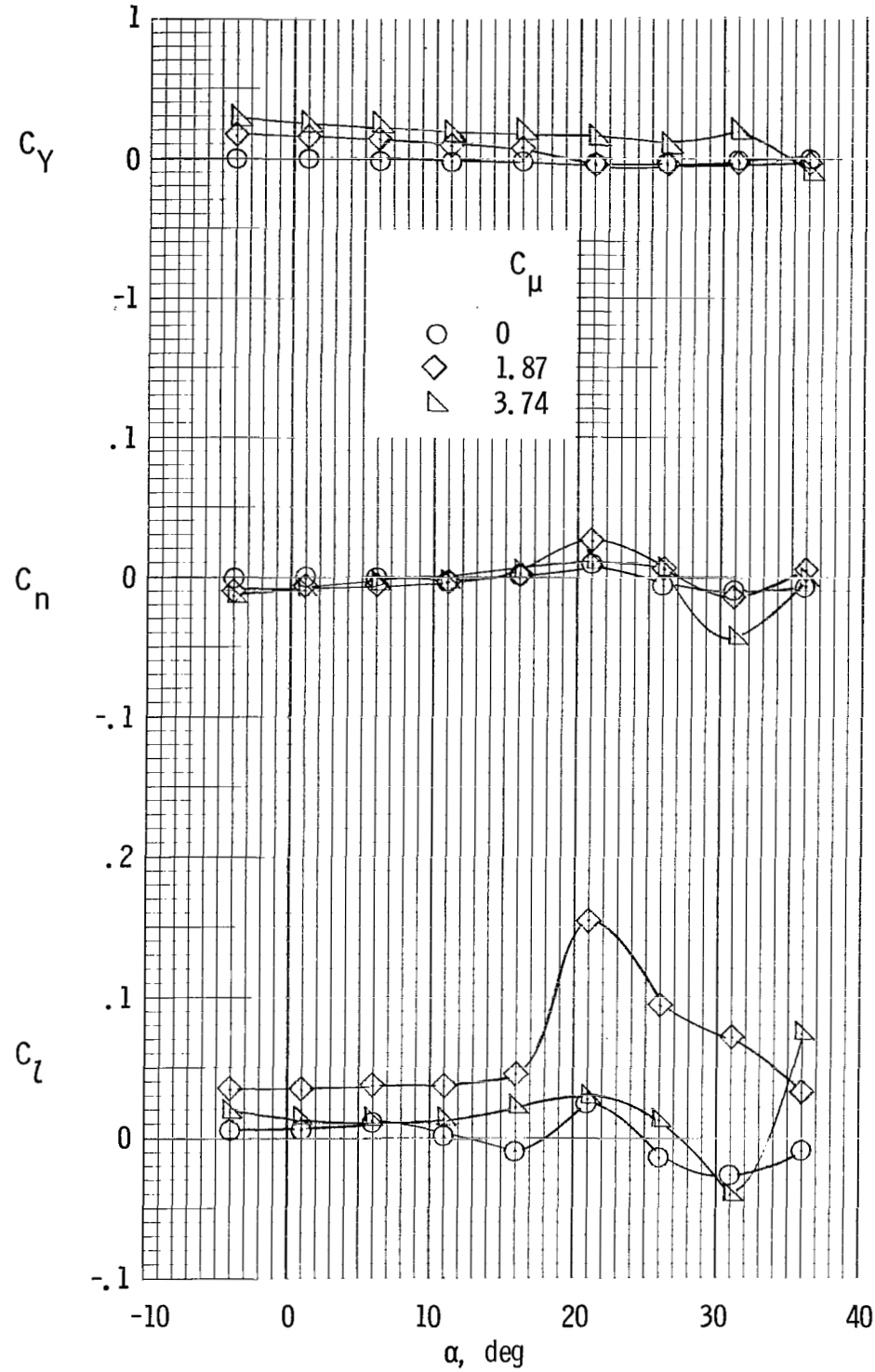

(a) Lateral characteristics. All engines operating.

Figure 47.- Effect on lateral and longitudinal characteristics of left outboard engine not operating for model with tail off and clustered engines. $\delta_f = 60^0$; $C_{\mu,le} = 0$.

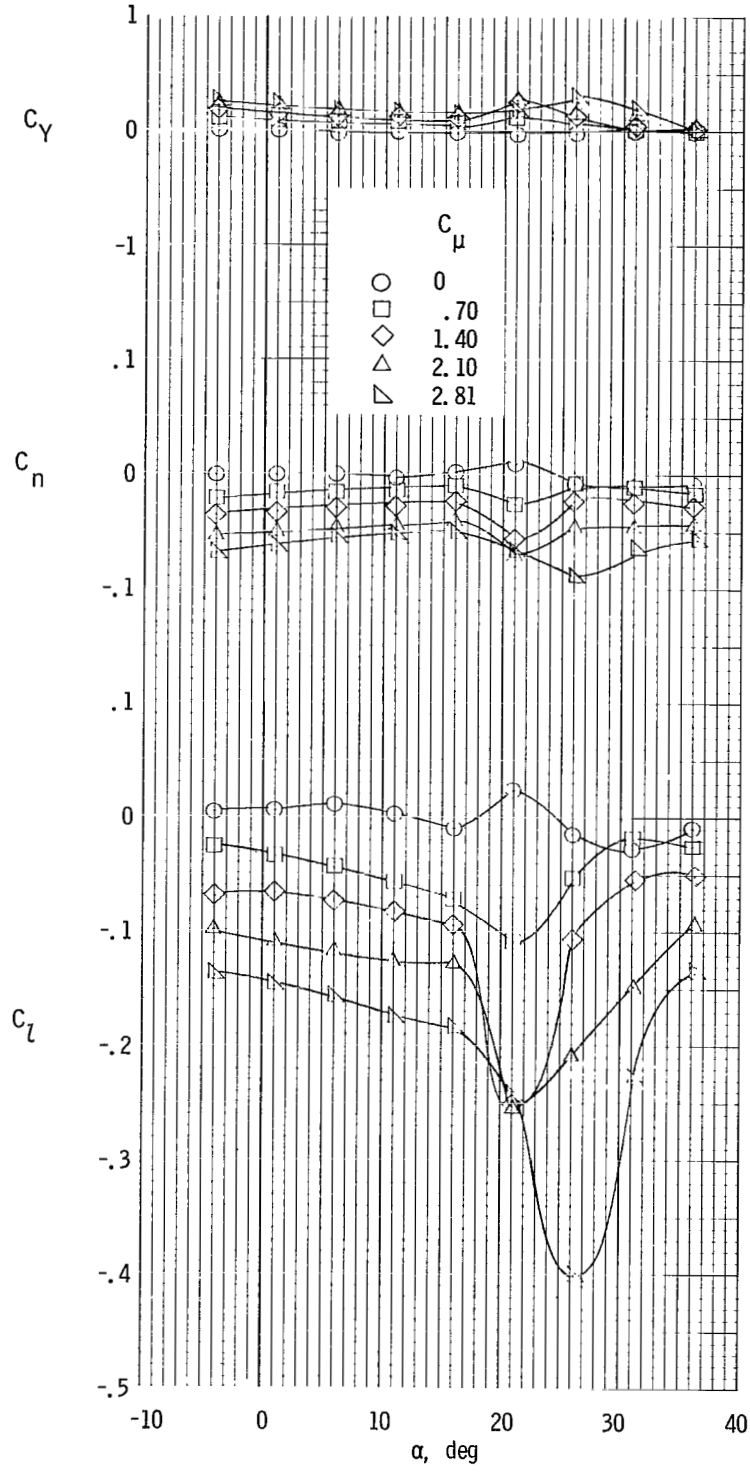

(b) Lateral characteristics. Left outboard engine not operating.

Figure 47.- Continued.

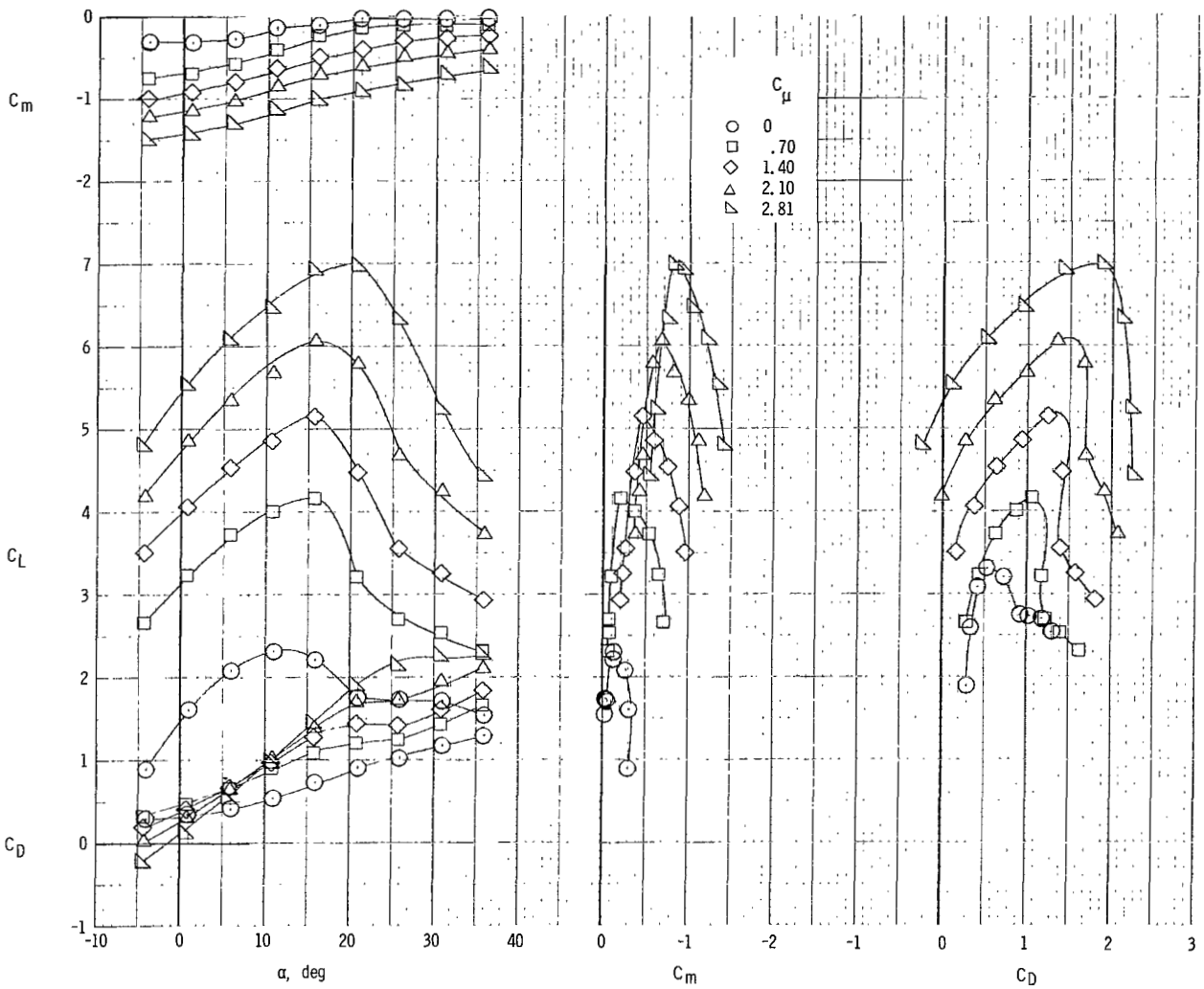

(c) Longitudinal characteristics. Left outboard engine not operating.

Figure 47.- Concluded.

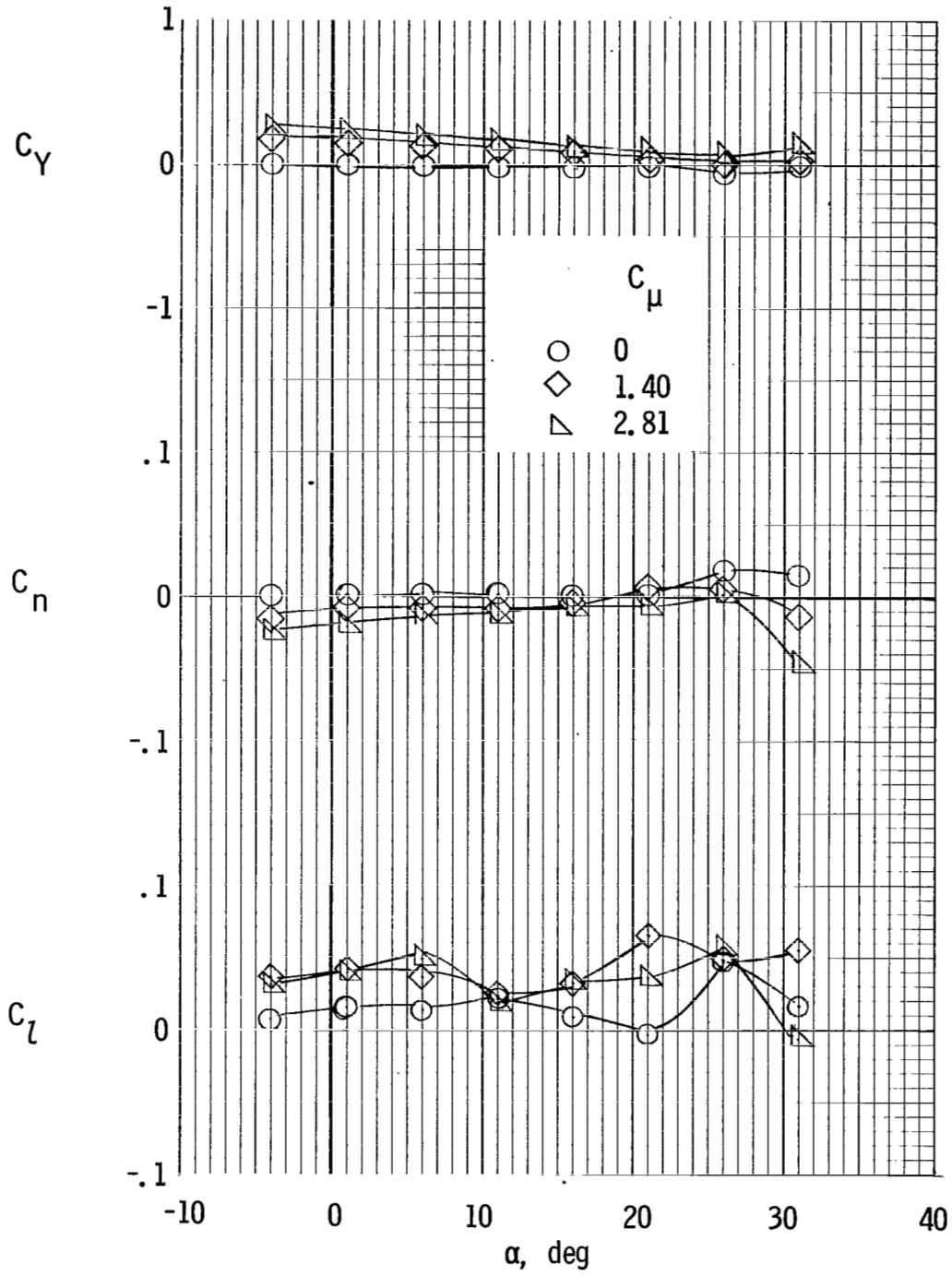

(a) Lateral characteristics. All engines operating.

Figure 48.- Effect on lateral and longitudinal characteristics of left outboard engine not operating for model with tail off and clustered engines. $\delta_f = 50^o$; $C_{\mu,le} = 0$.

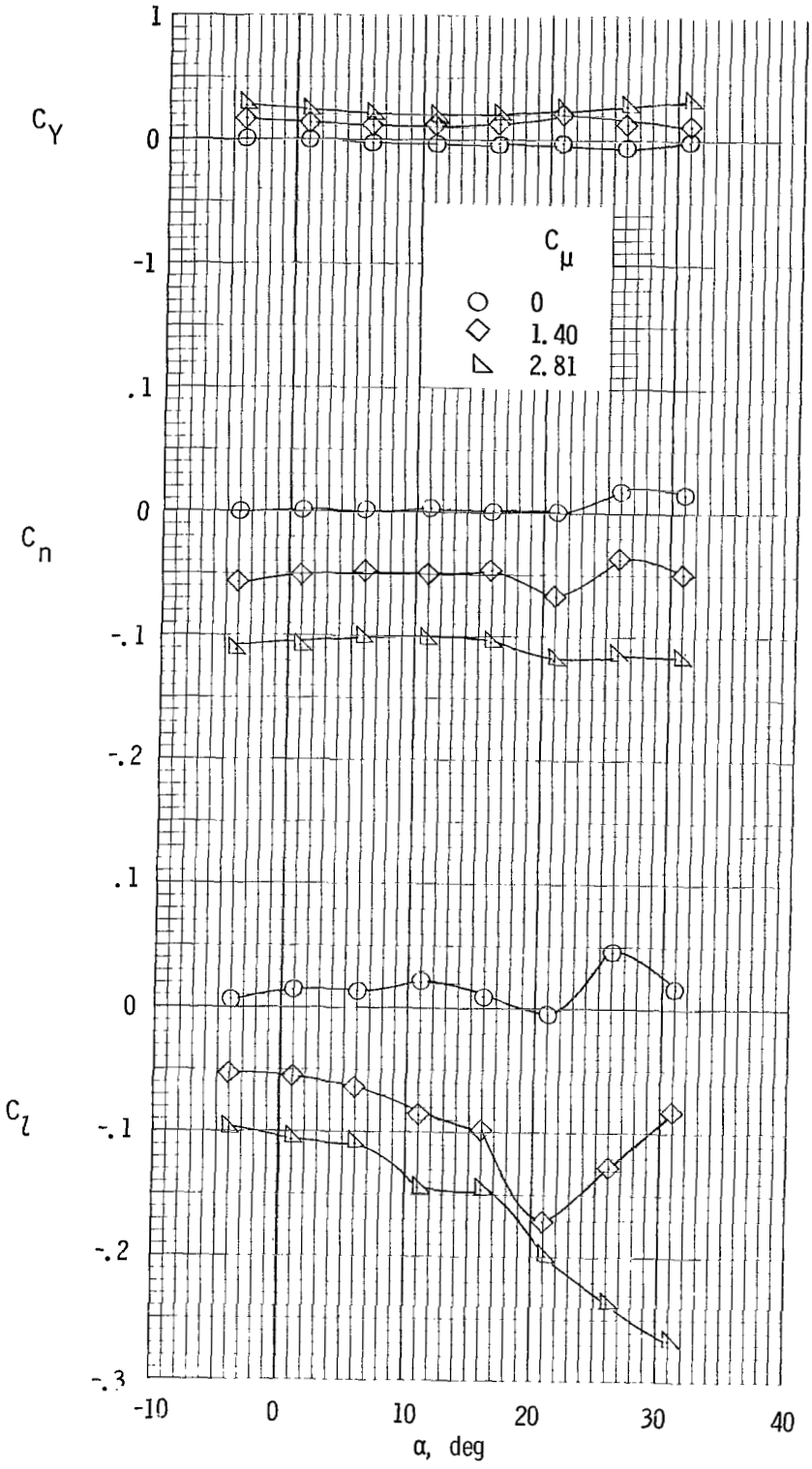

(b) Lateral characteristics. Left outboard engine not operating.

Figure 48.- Continued.

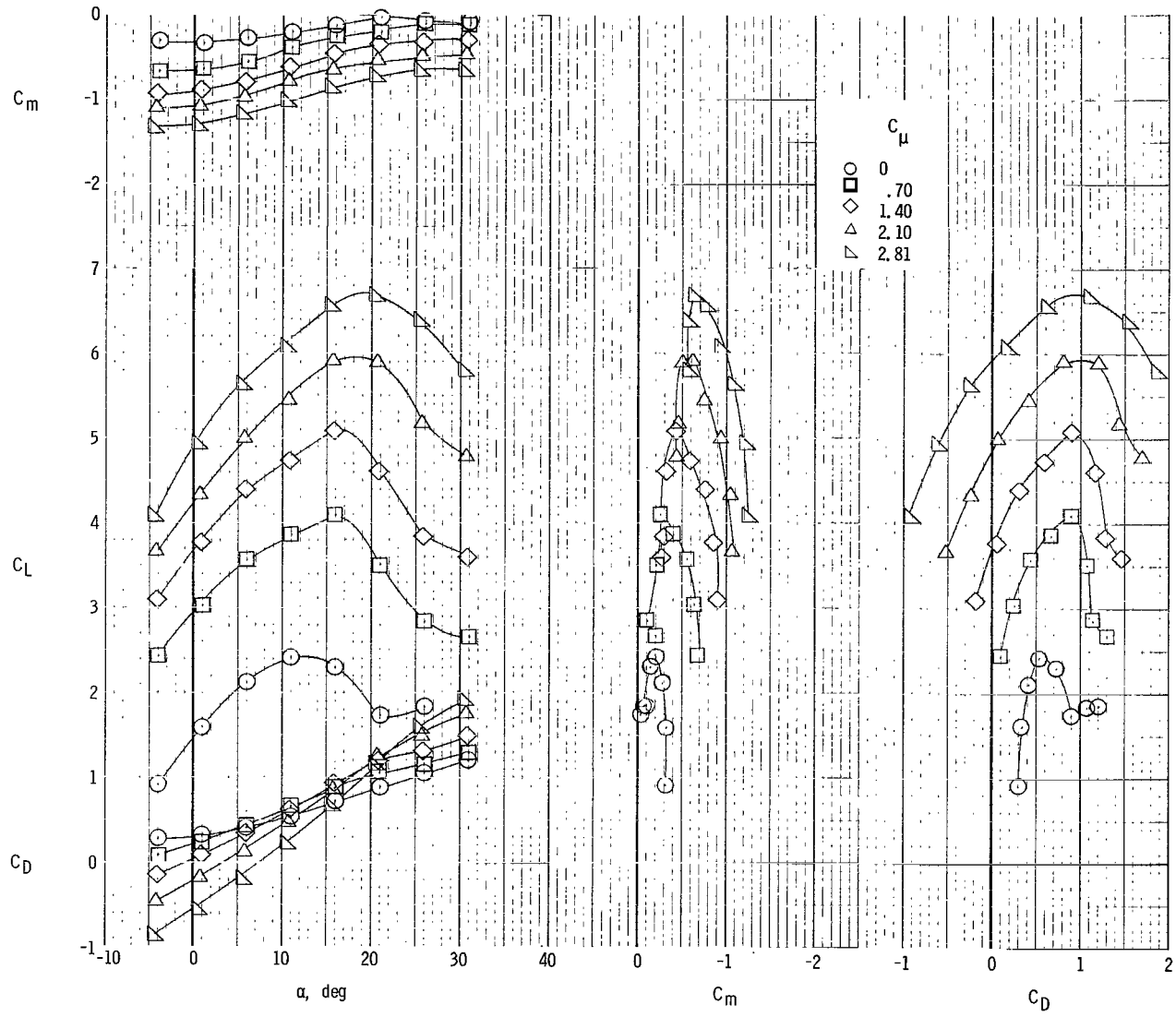

(c) Longitudinal characteristics. Left outboard engine not operating.

Figure 48.- Concluded.

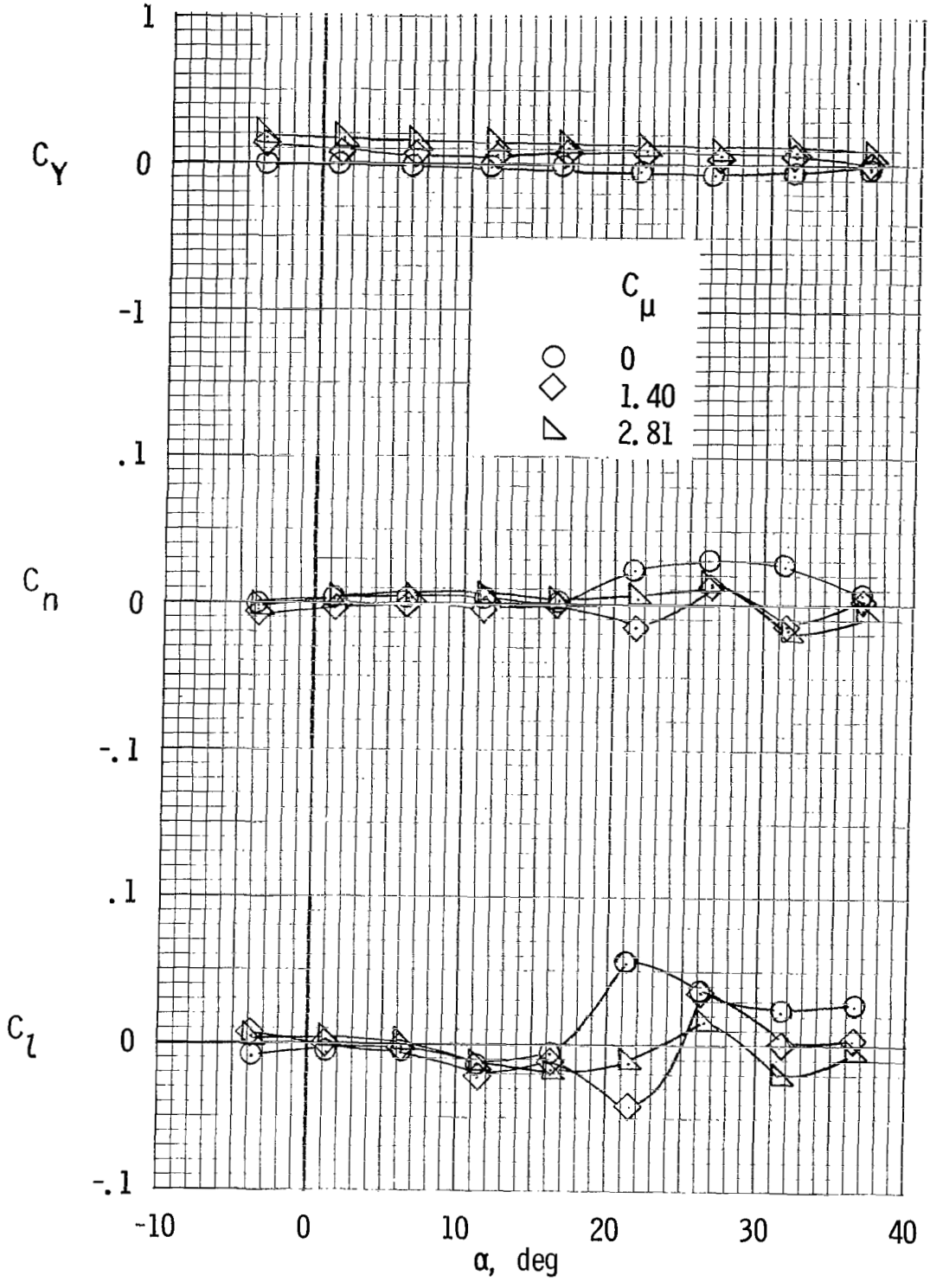

(a) Lateral characteristics. All engines operating.

Figure 49.- Effect on lateral and longitudinal characteristics of left outboard engine not operating for model with tail on and clustered engines. $\delta_f = 40^0$; $C_{\mu,le} = 0$.

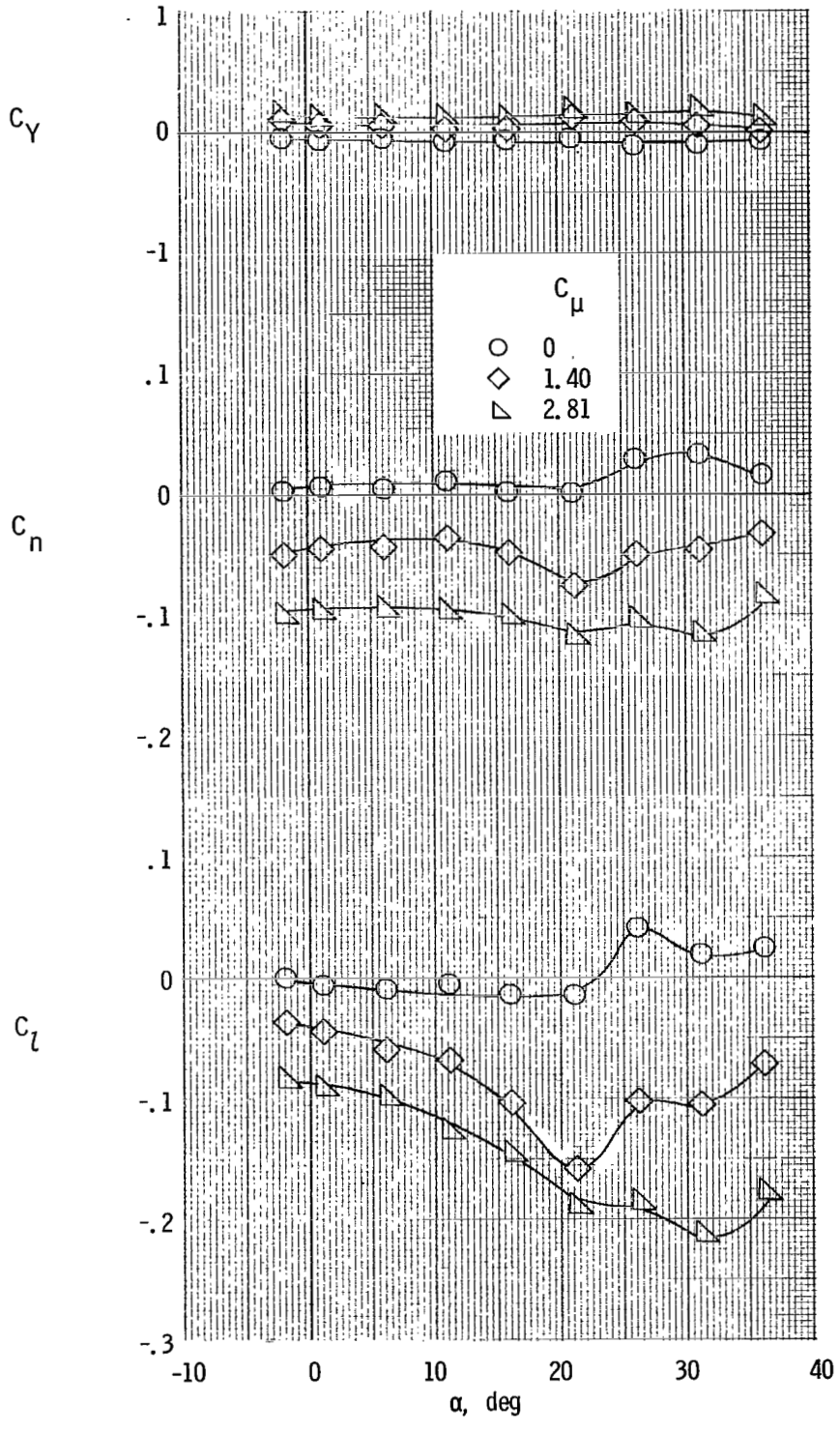

(b) Lateral characteristics. Left outboard engine not operating.

Figure 49.- Continued.

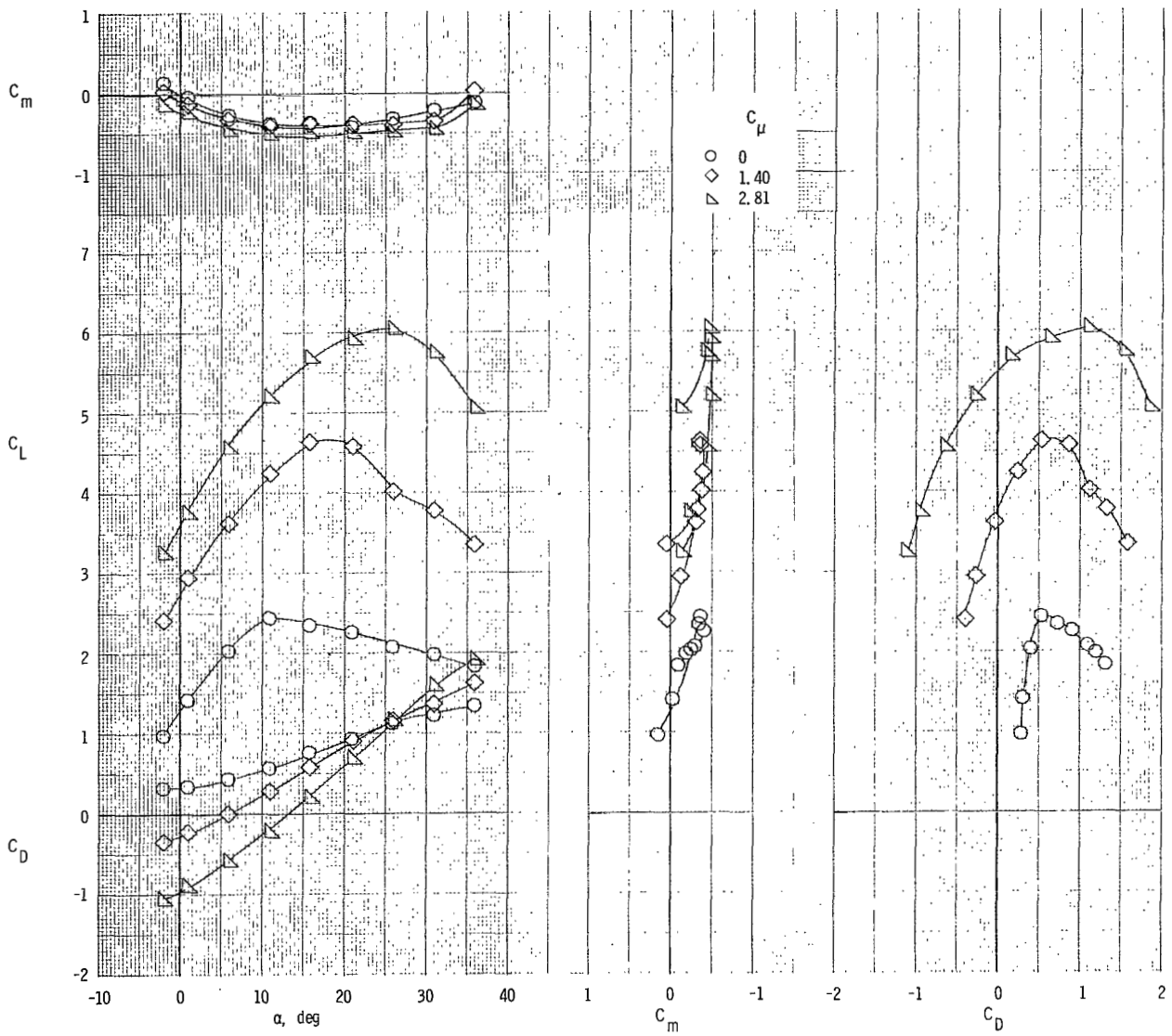

(c) Longitudinal characteristics. Left outboard engine not operating.

Figure 49.- Concluded.

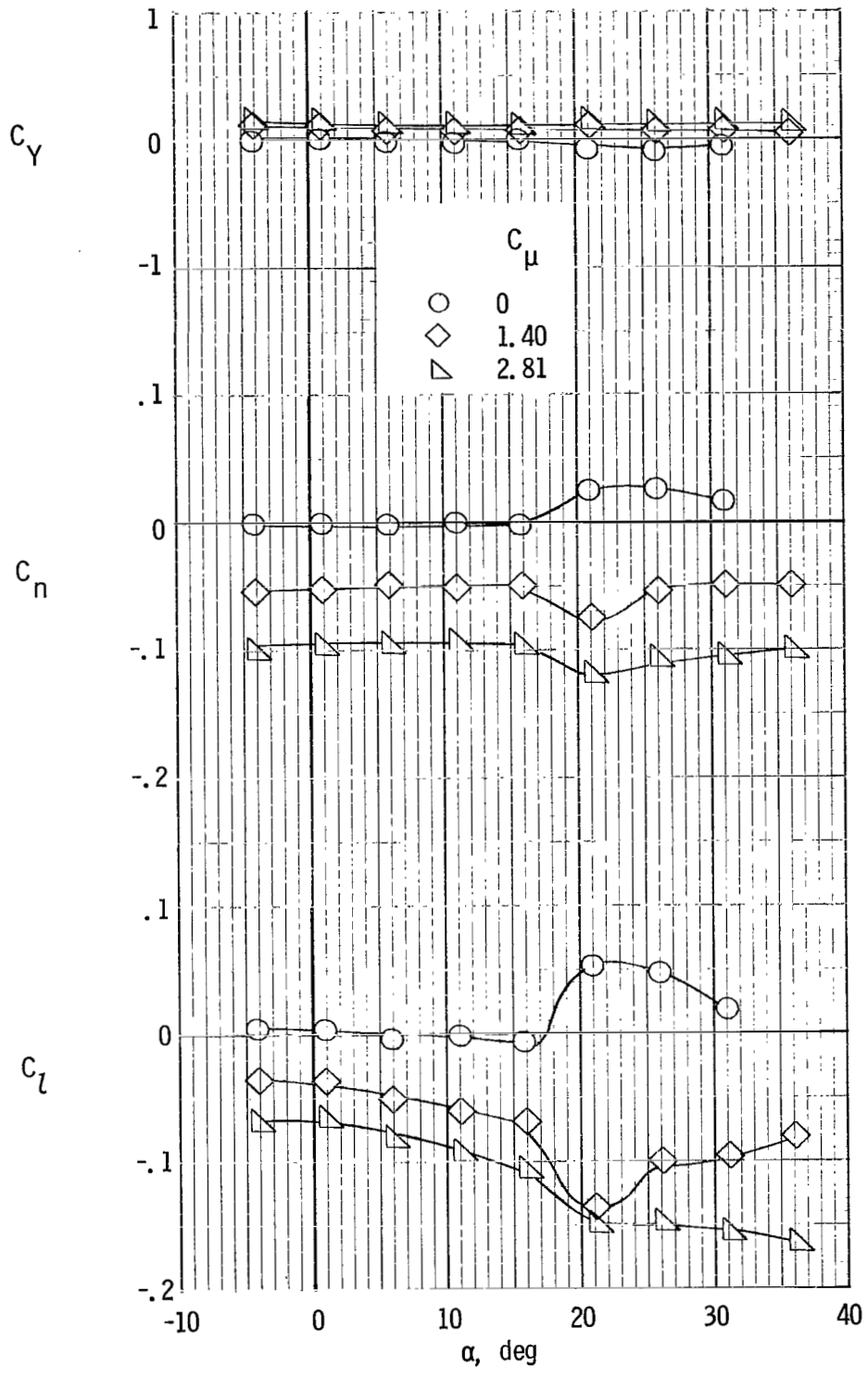

(a) Lateral characteristics. Left outboard engine not operating.

Figure 50.- Lateral and longitudinal characteristics of model with tail off and clustered engines. One left engine not operating; $\delta_f = 35^0$; $C_{\mu,le} = 0$.

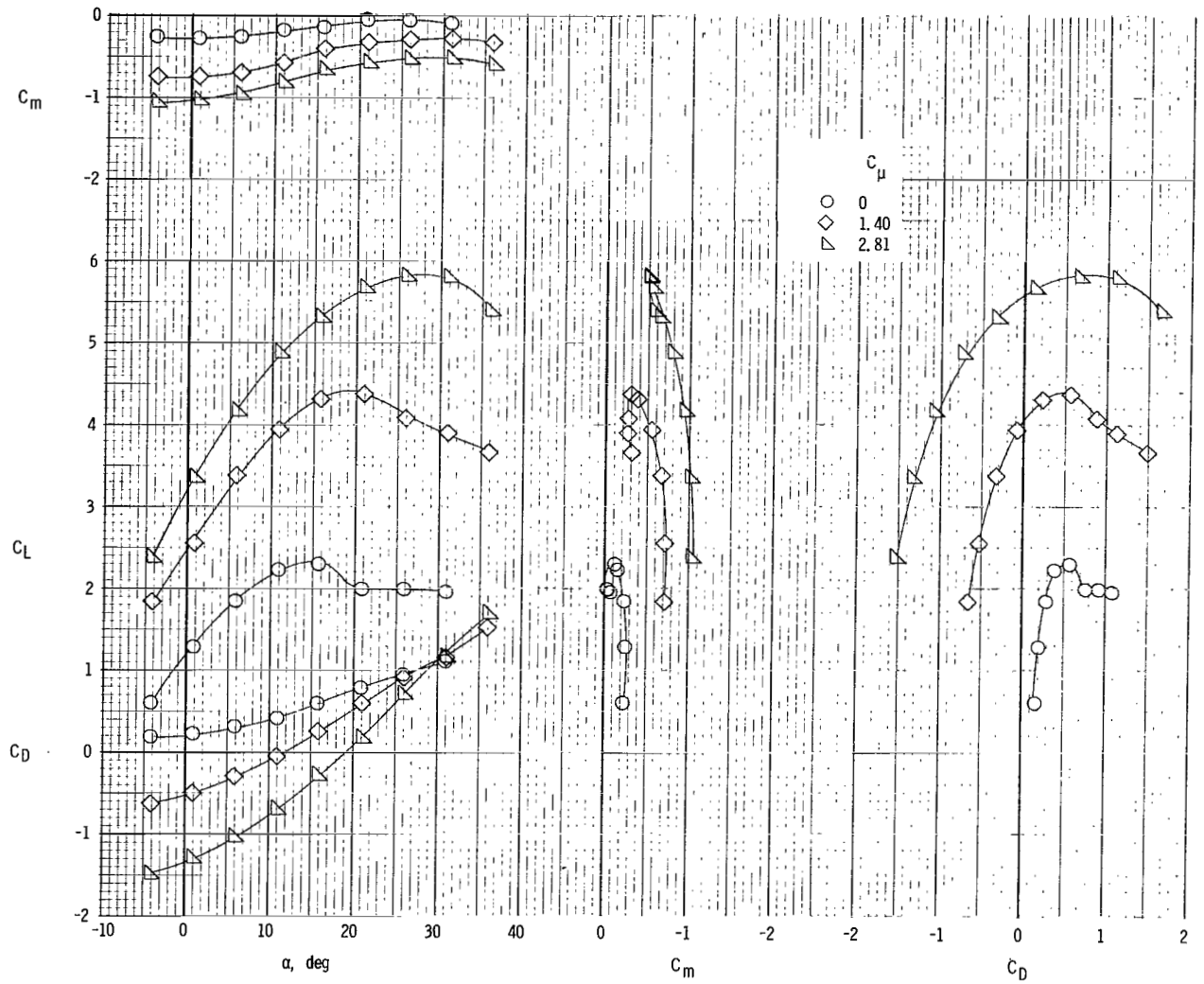

(b) Longitudinal characteristics. Left outboard engine not operating.

Figure 50.- Continued.

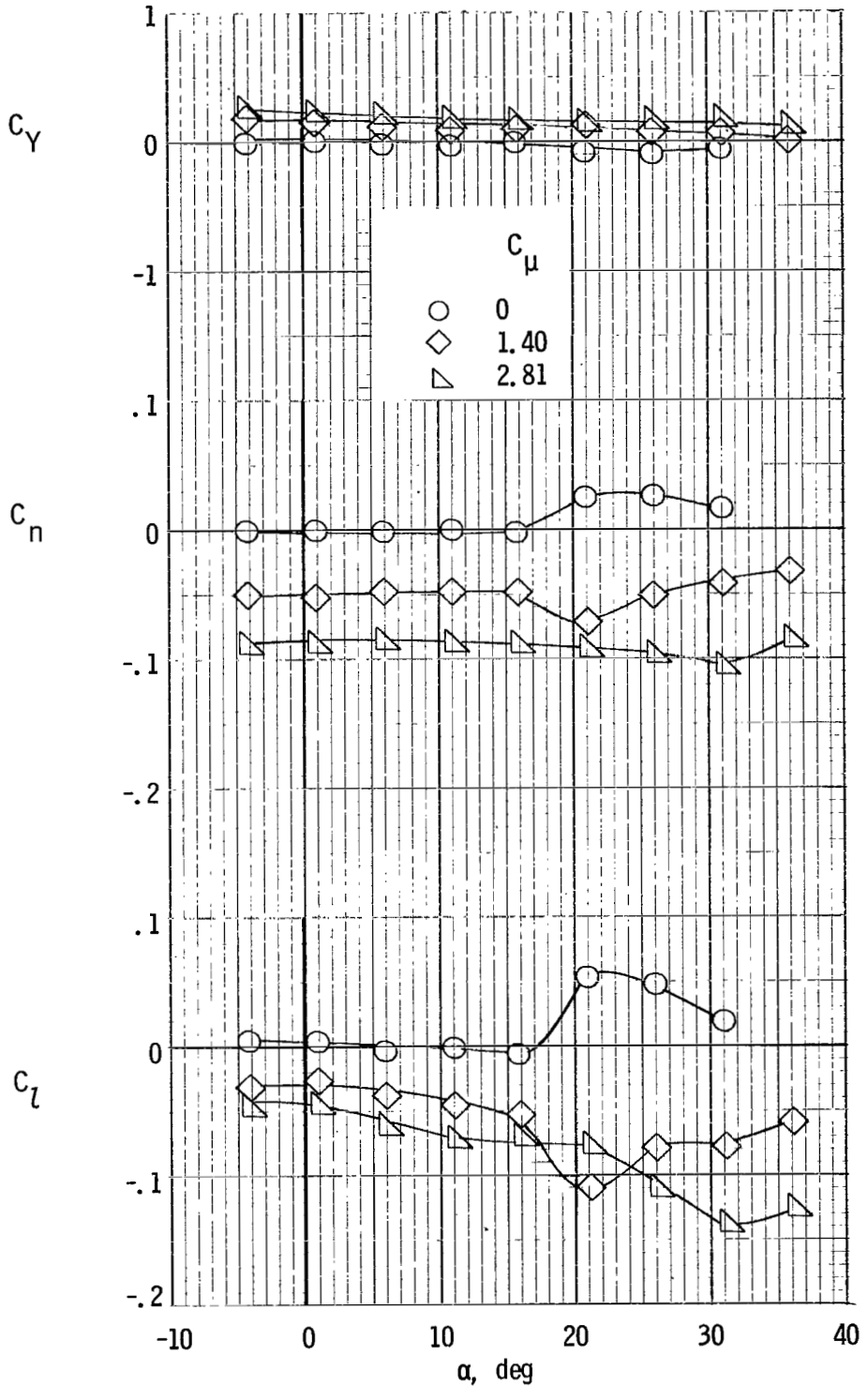

(c) Lateral characteristics. Left inboard engine not operating.

Figure 50.- Continued.

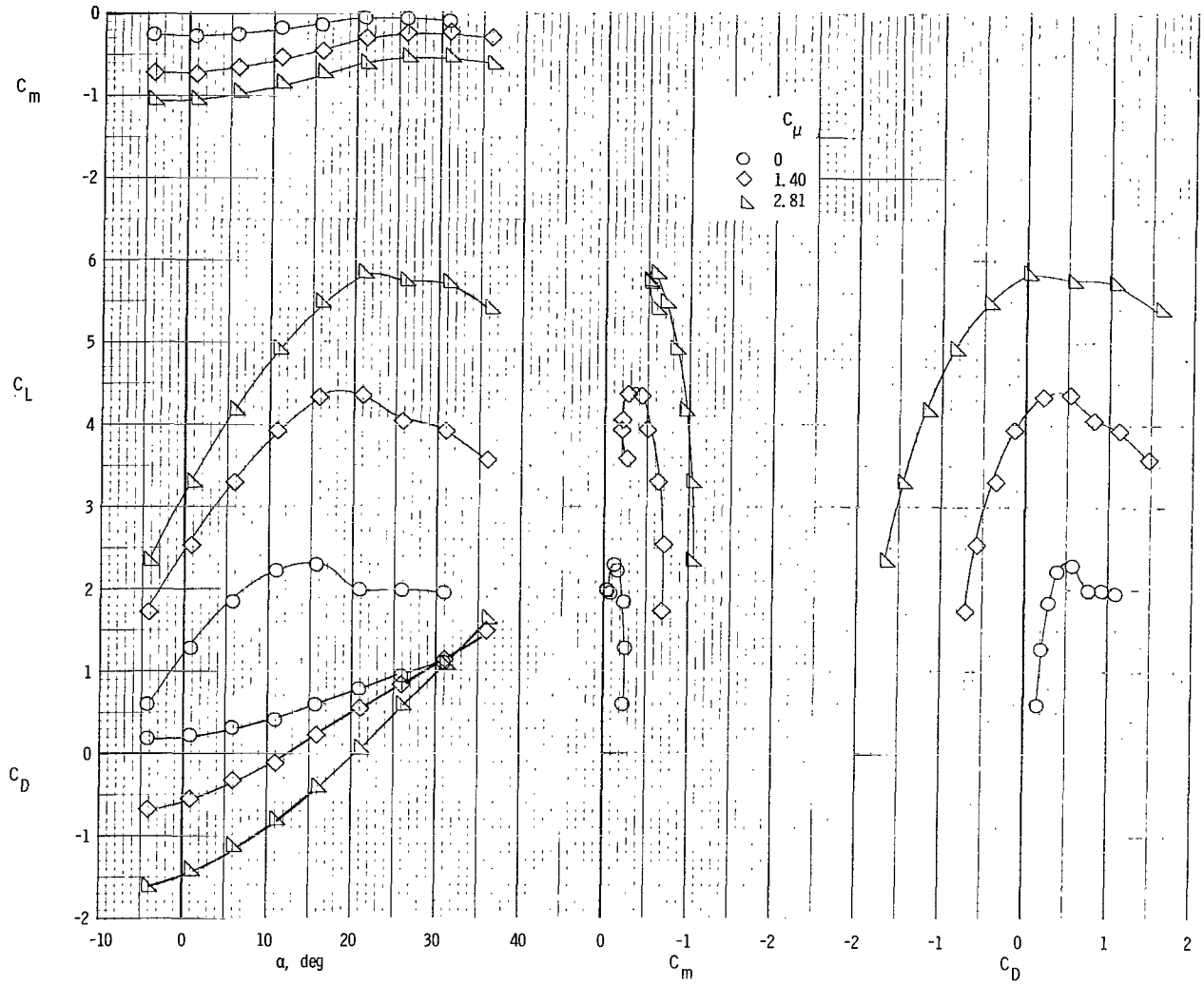

(d) Longitudinal characteristics. Left inboard engine not operating.

Figure 50.- Concluded.

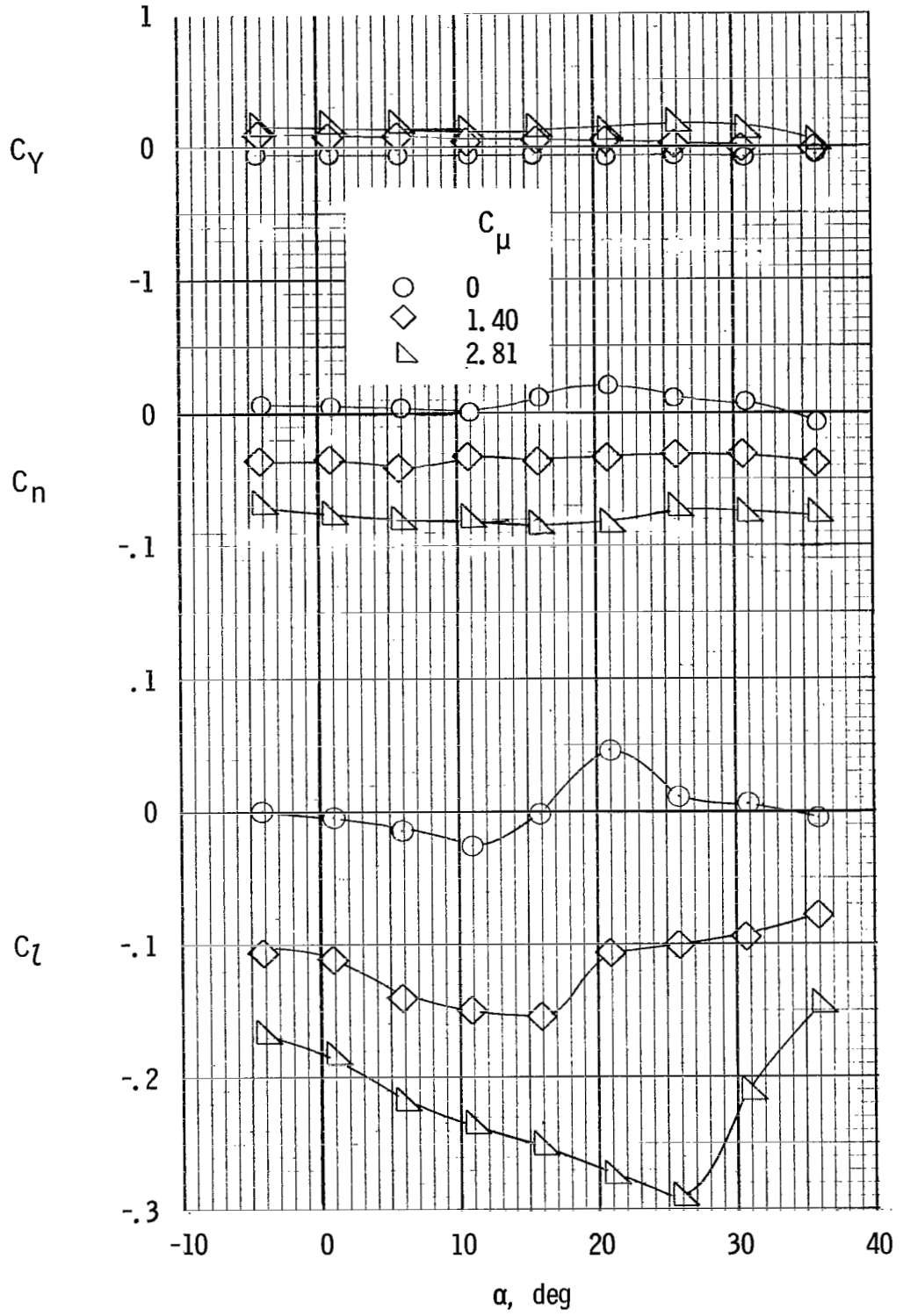

(a) Lateral characteristics. Left outboard engine not operating.

Figure 51.- Lateral and longitudinal characteristics of model with tail on and spread engines. One left engine not operating; $\delta_f = 60^0$; $C_{\mu,le} = 0$.

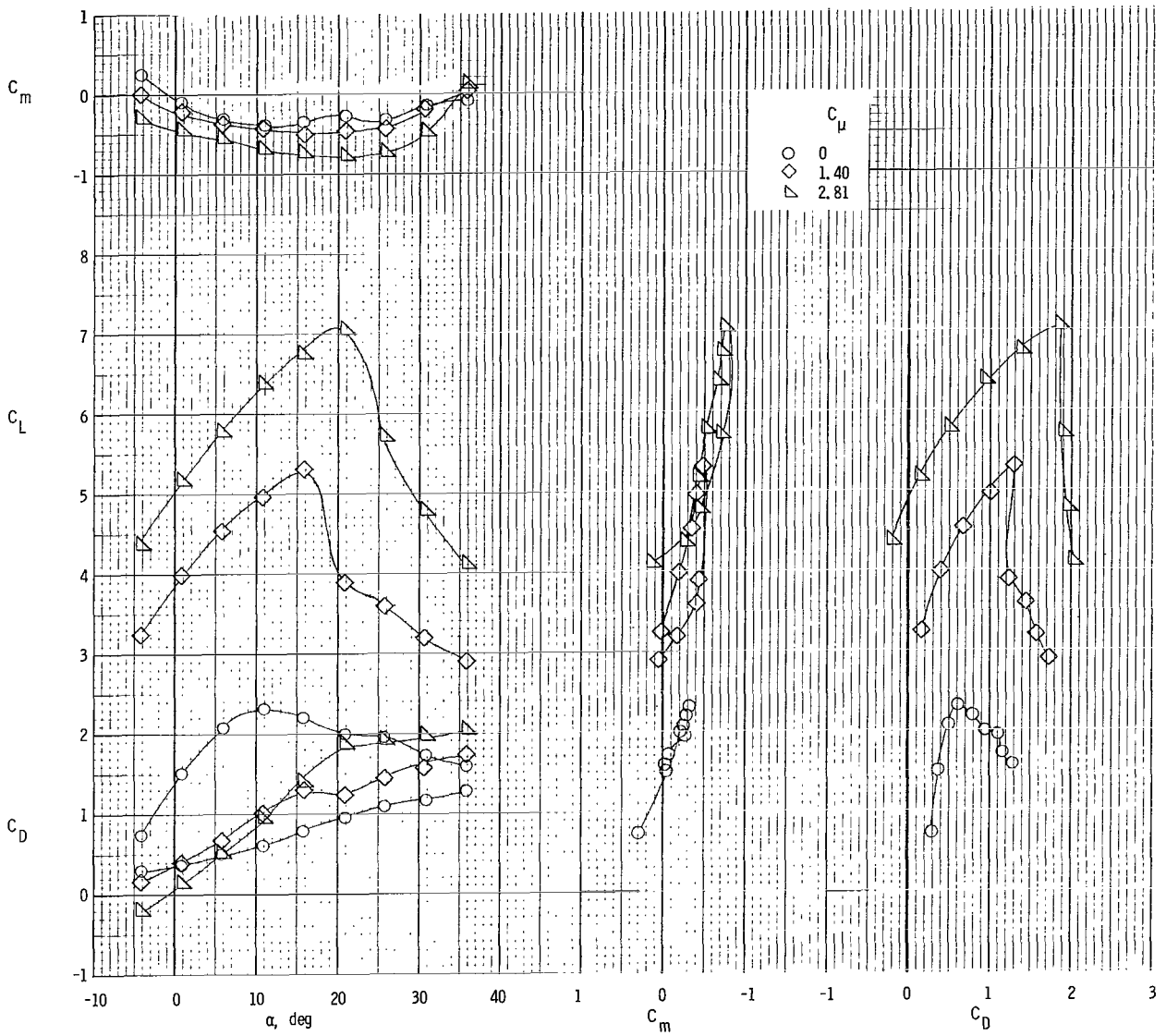

(b) Longitudinal characteristics. Left outboard engine not operating.

Figure 51.- Continued.

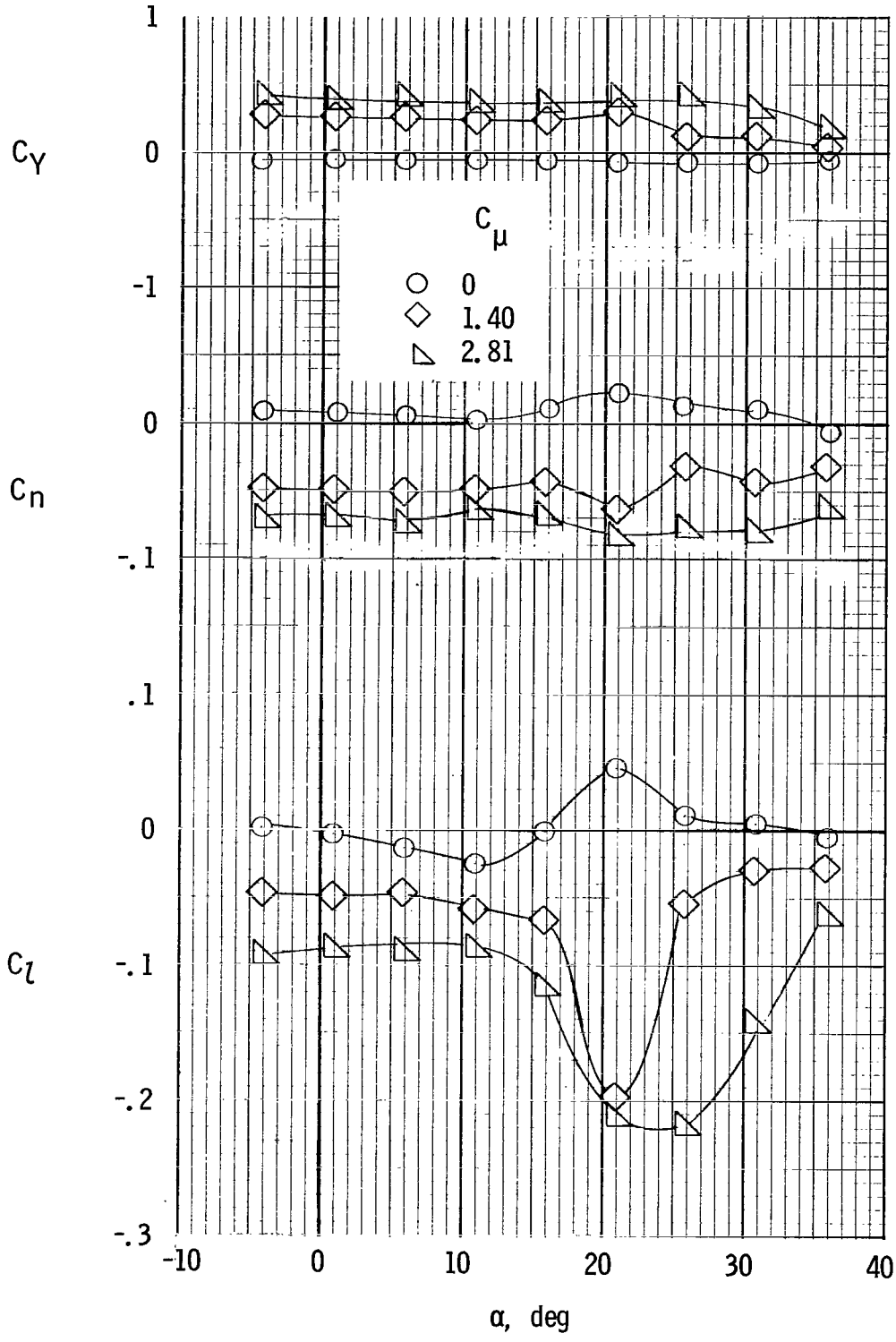

(c) Lateral characteristics. Left inboard engine not operating.

Figure 51.- Continued.

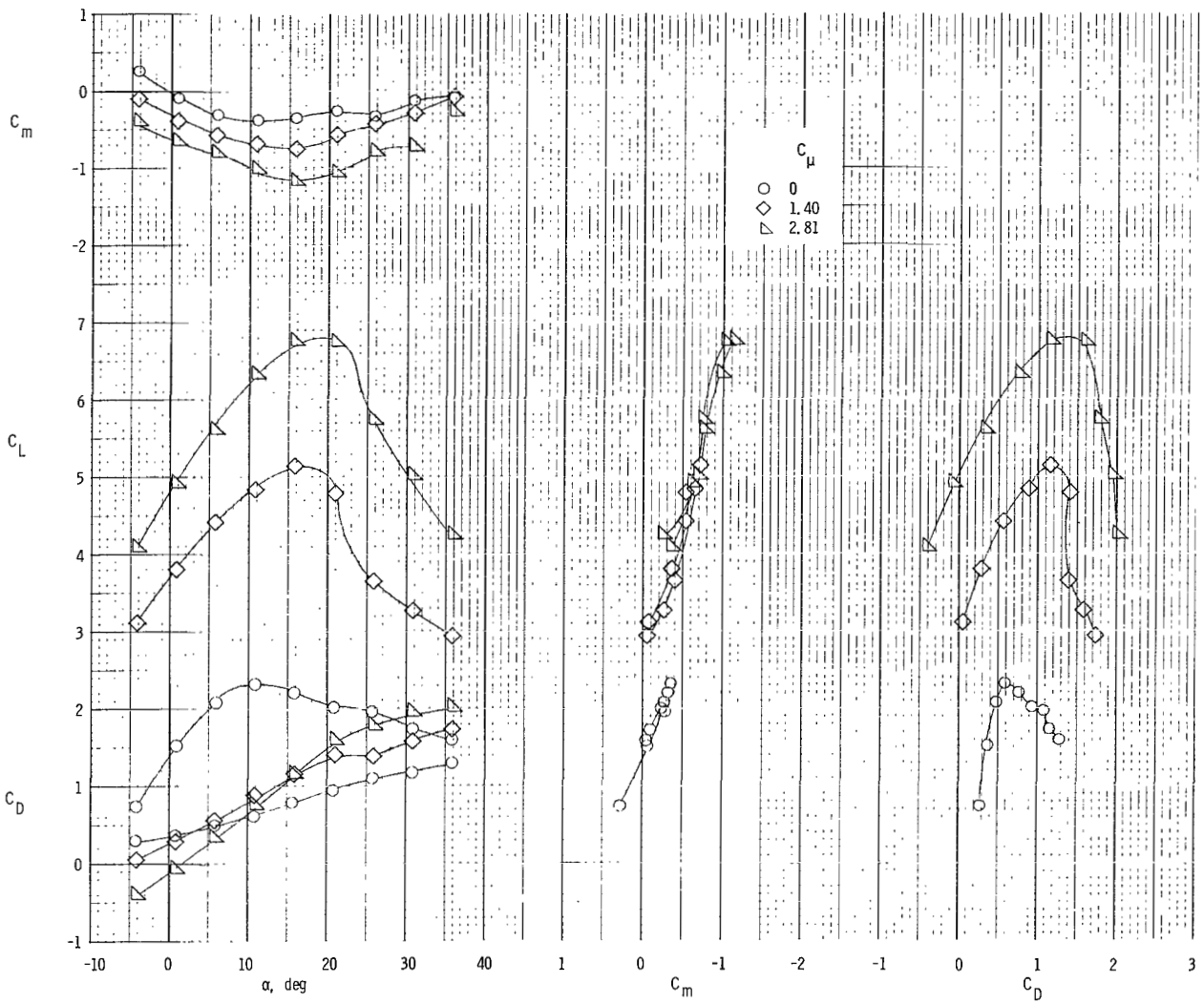

(d) Longitudinal characteristics. Left inboard engine not operating.

Figure 51.- Concluded.

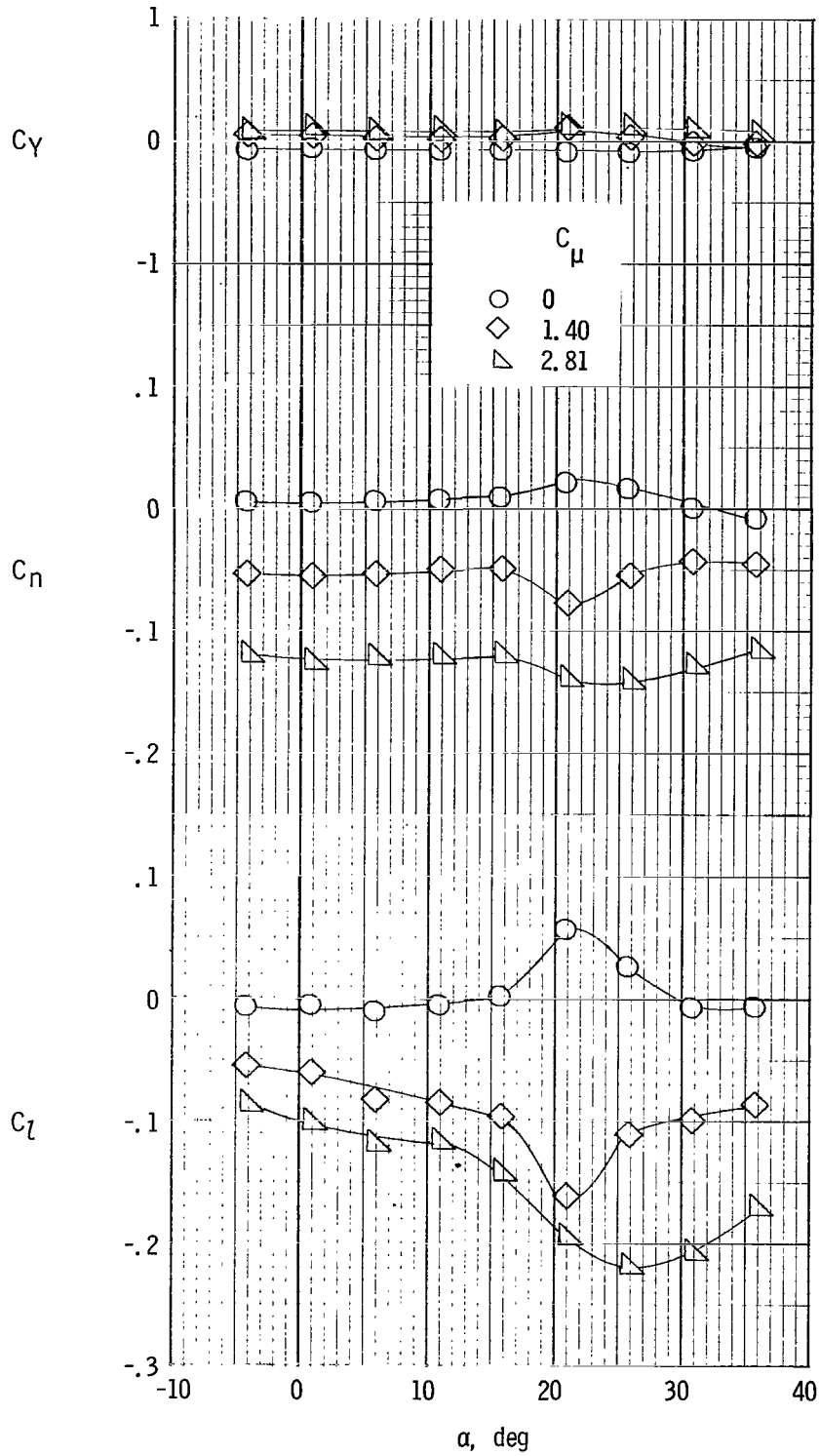

(a) Lateral characteristics. Left outboard engine not operating.

Figure 52.- Lateral and longitudinal characteristics of model with tail on and spread engines. One left engine not operating; $\delta_f = 40^0$; $C_{\mu,le} = 0$.

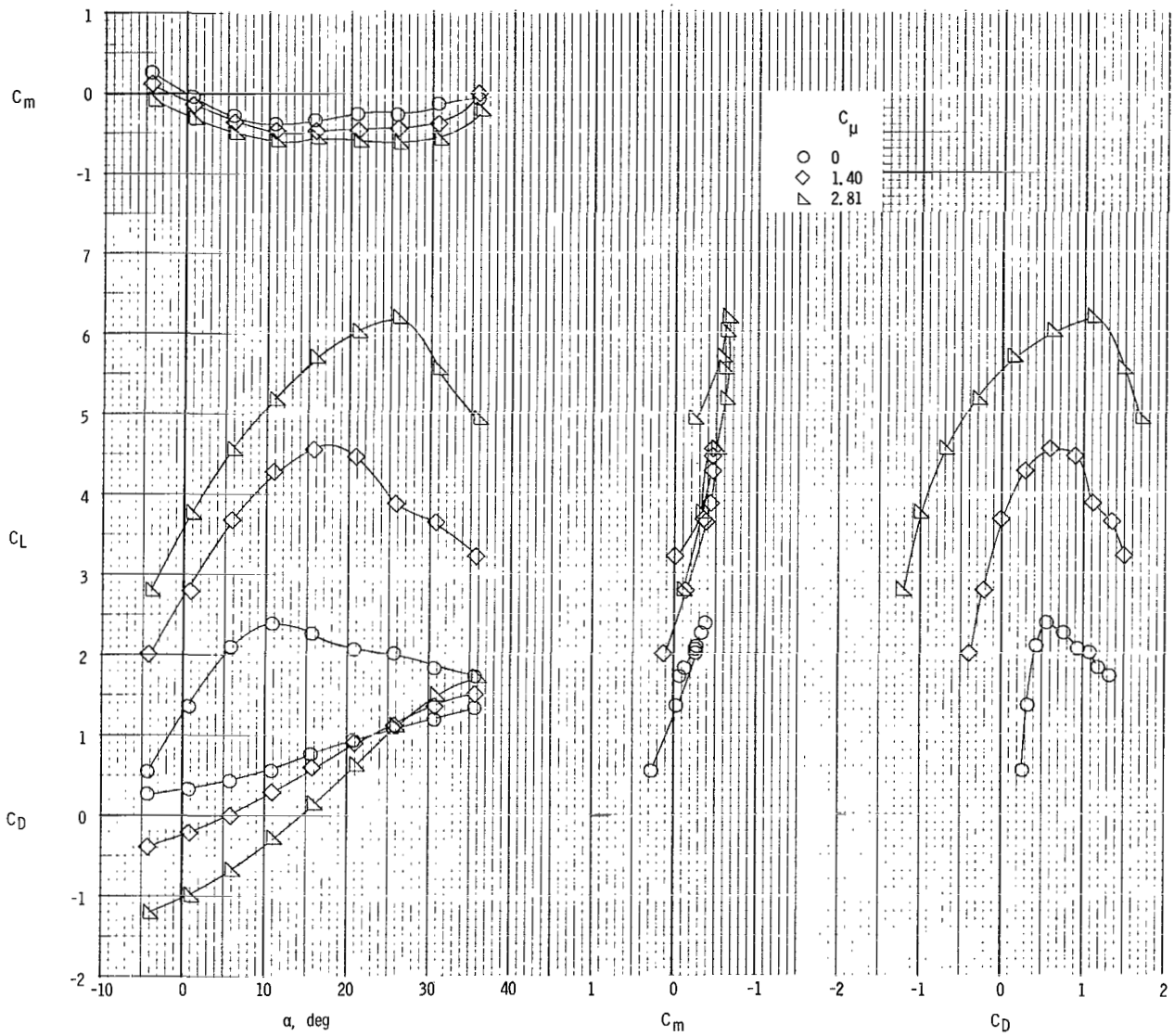

(b) Longitudinal characteristics. Left outboard engine not operating.

Figure 52.- Continued.

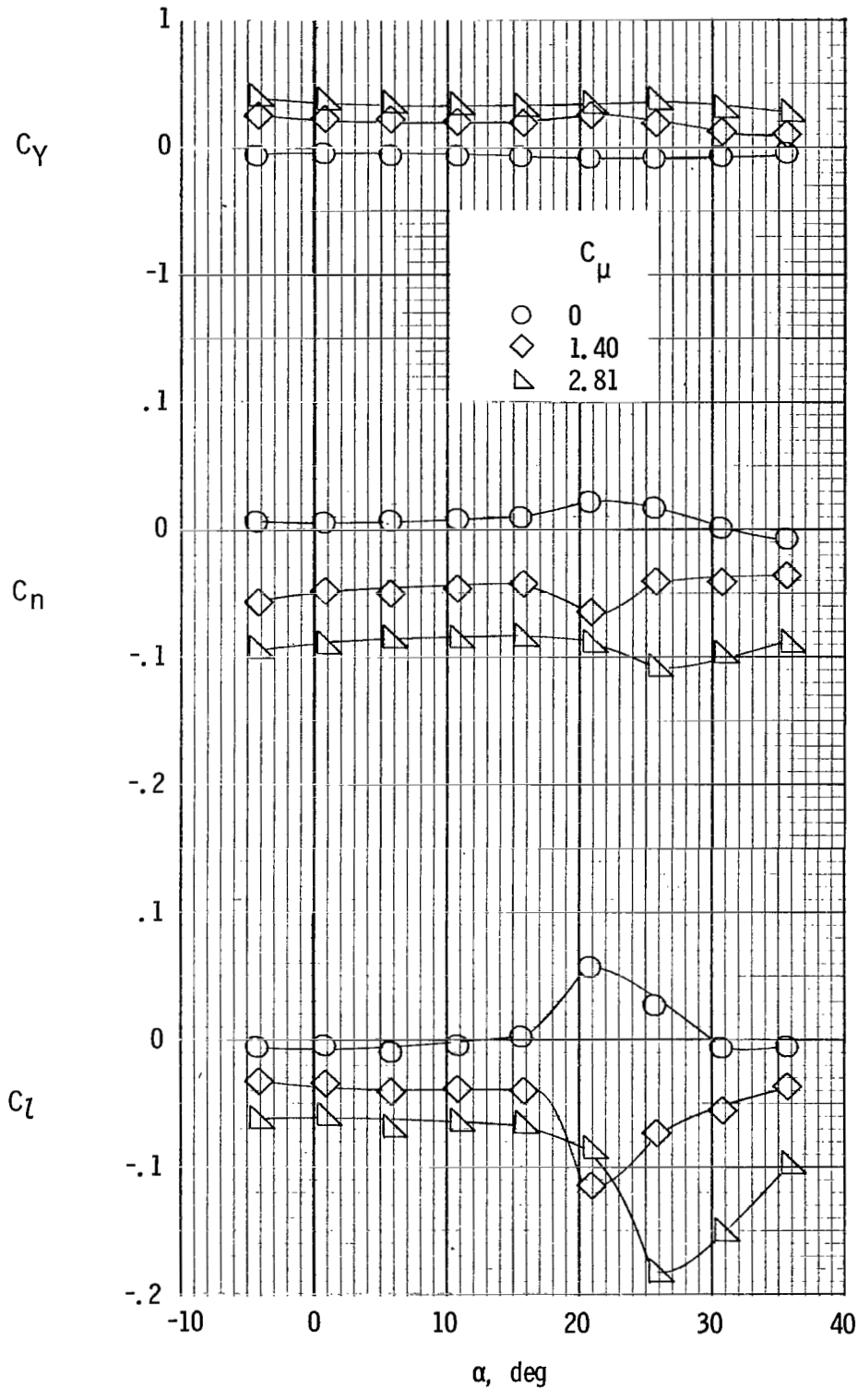

(c) Lateral characteristics. Left inboard engine not operating.

Figure 52.- Continued.

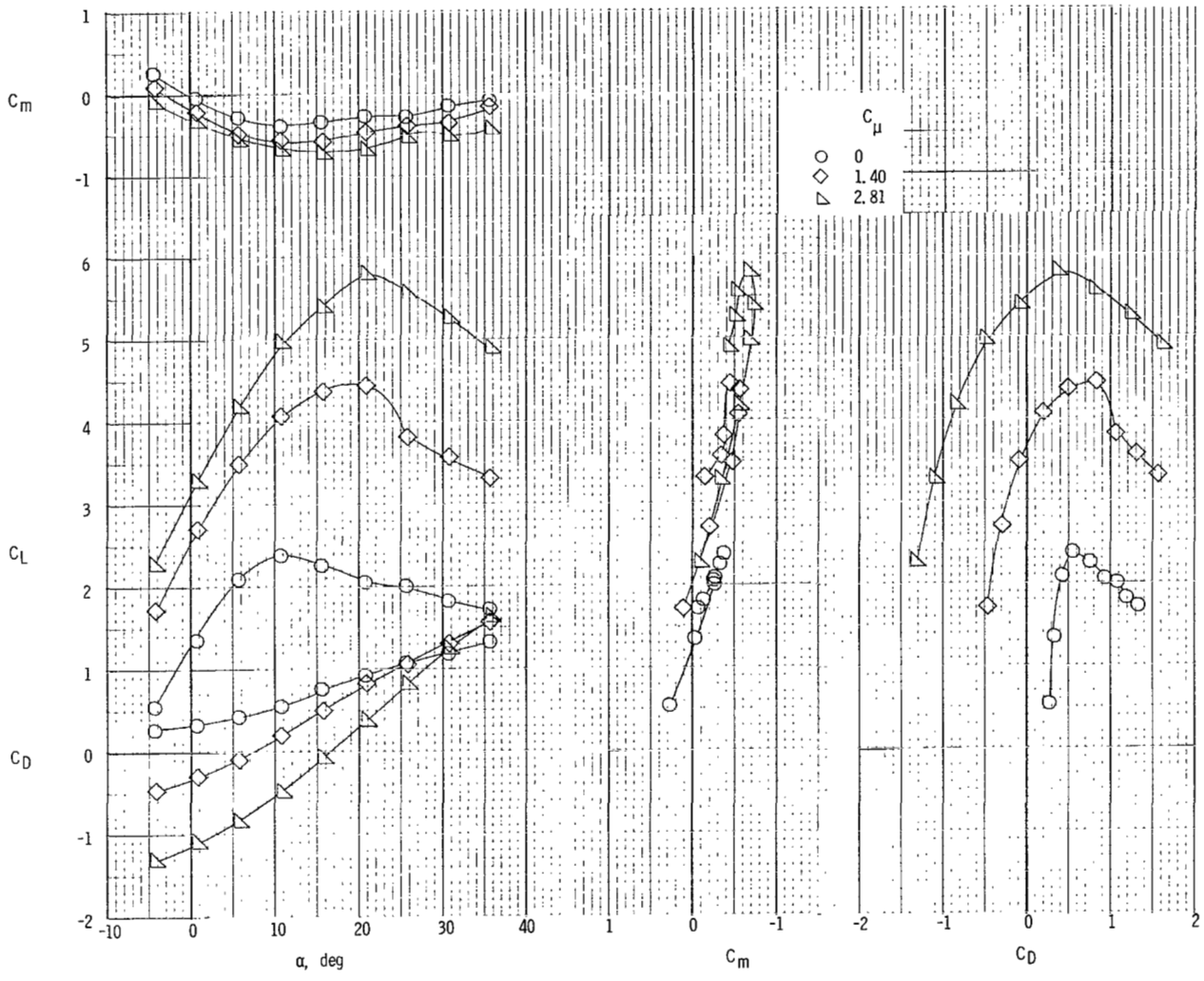

(d) Longitudinal characteristics. Left inboard engine not operating.

Figure 52.- Concluded.

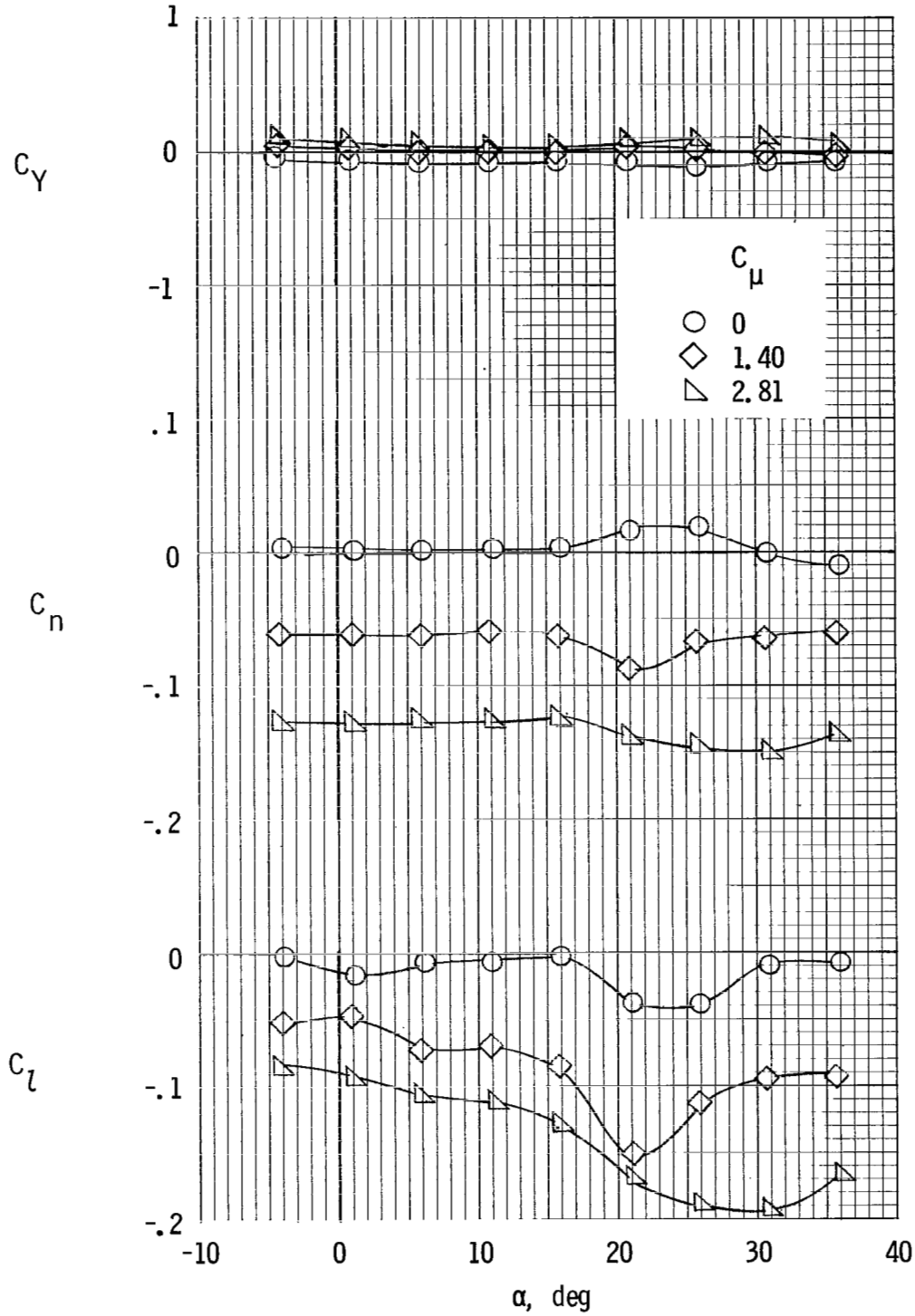

(a) Lateral characteristics.

Figure 53.- Lateral and longitudinal characteristics of model with tail on and spread engines. Left outboard engine not operating; $\delta_f = 35^0$; $C_{\mu,le} = 0$.

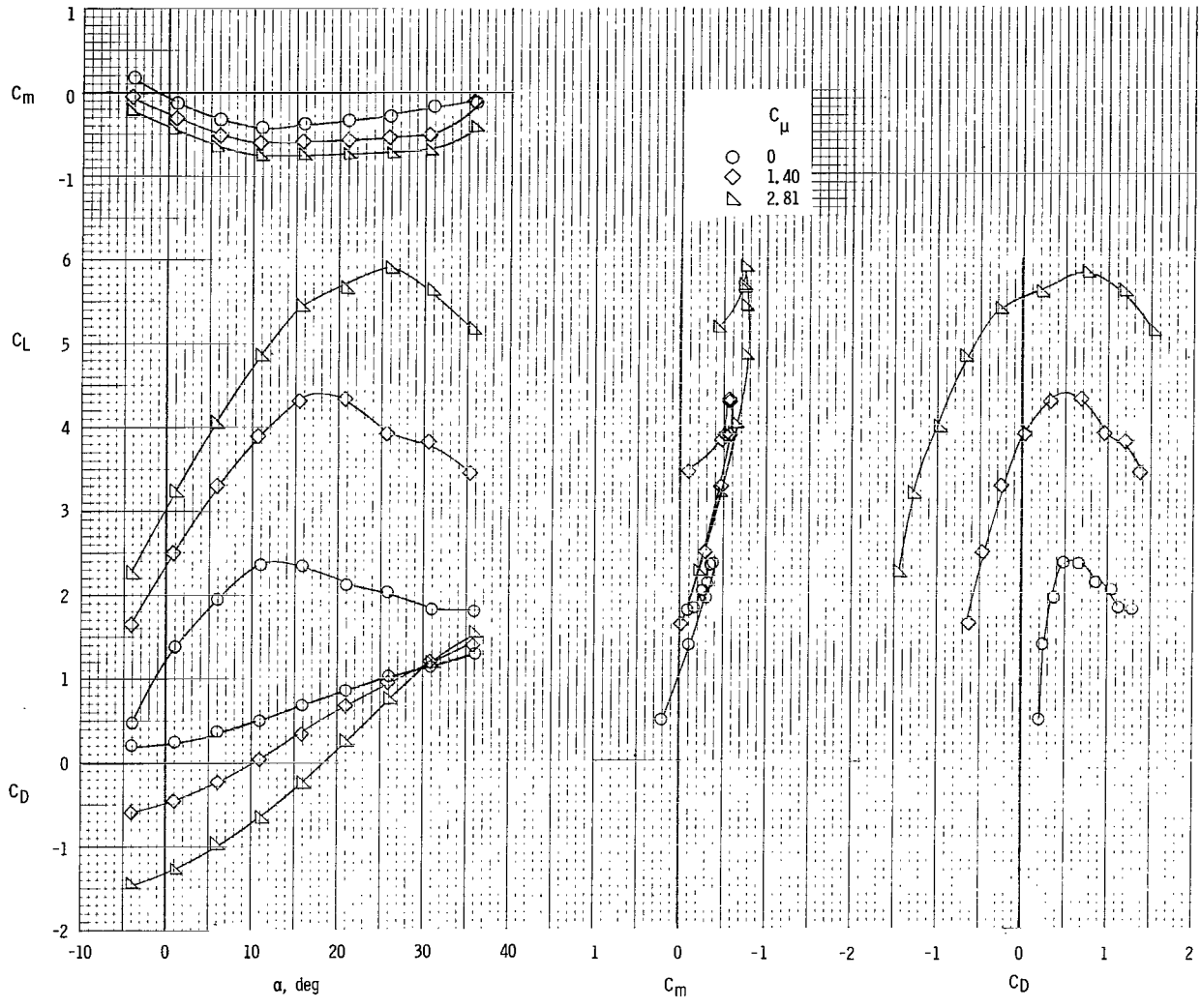

(b) Longitudinal characteristics.

Figure 53.- Concluded.

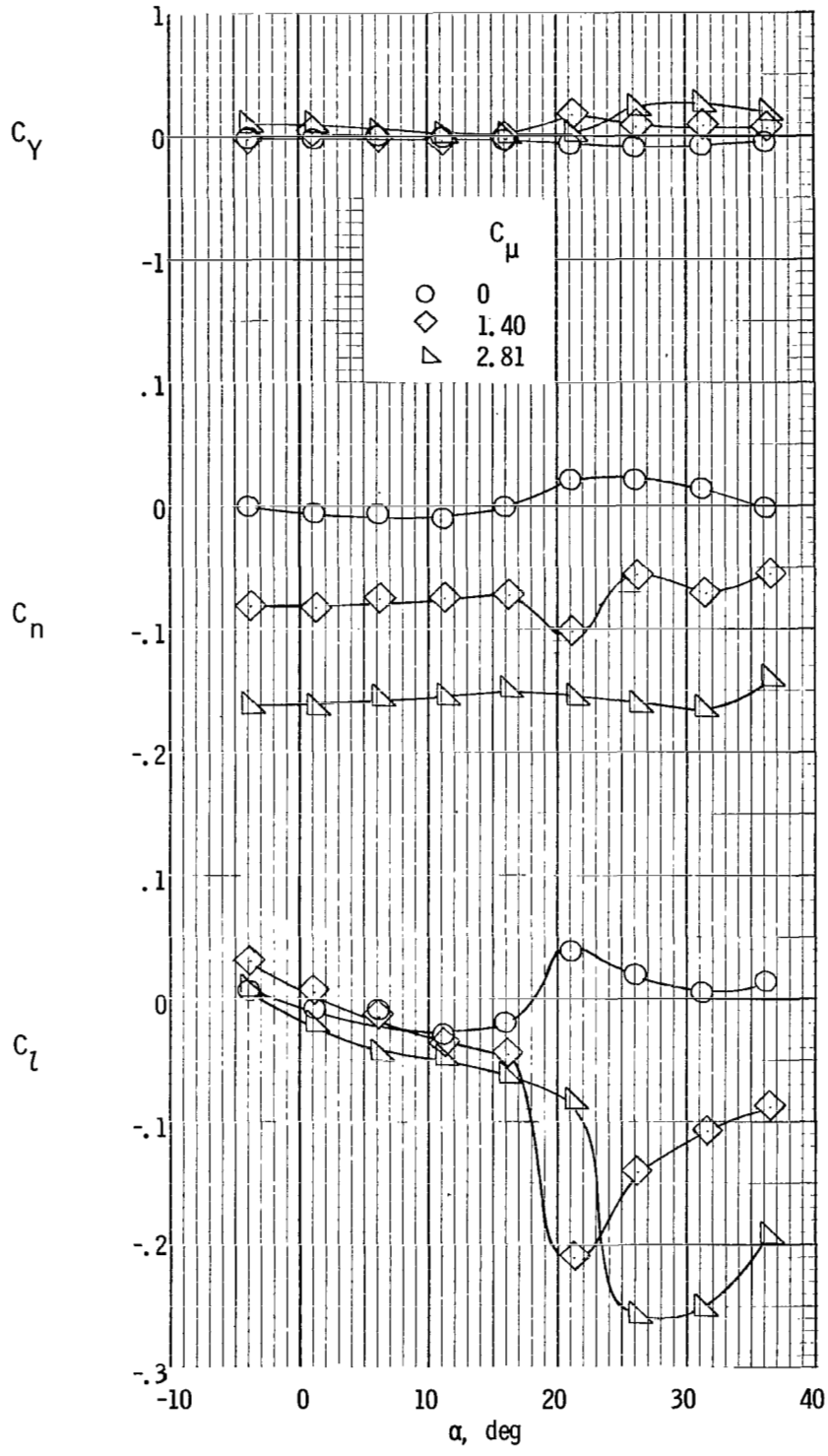

(a) Lateral characteristics. $\delta_{f,L} = 70^0$; $\delta_{f,R} = 40^0$.

Figure 54.- Lateral and longitudinal characteristics for two differential flap deflections for model with tail on and clustered engines. Left outboard engine not operating; $C_{\mu,le} = 0$.

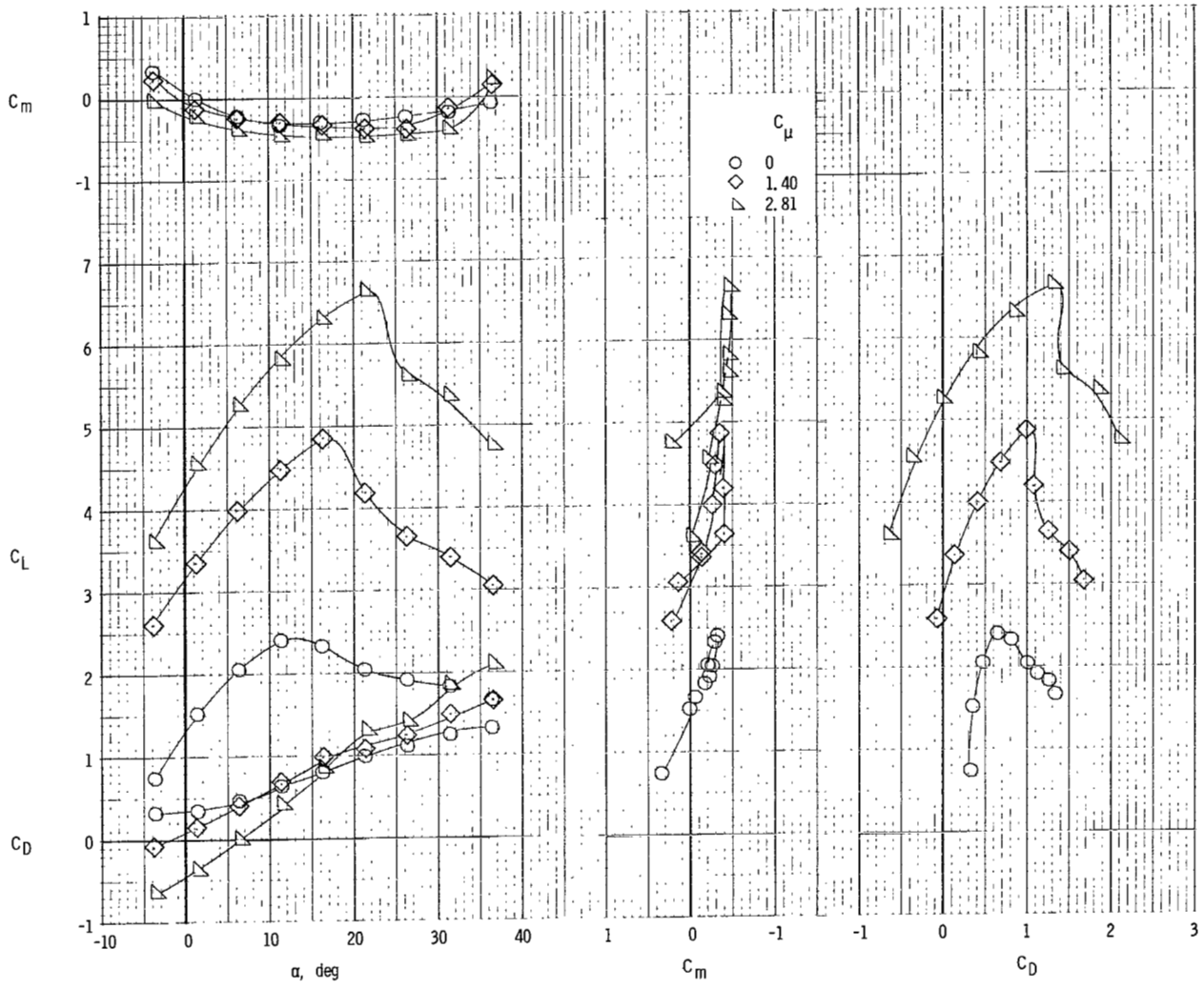

(b) Longitudinal characteristics. $\delta_{f,L} = 70^o$; $\delta_{f,R} = 40^o$.

Figure 54.- Continued.

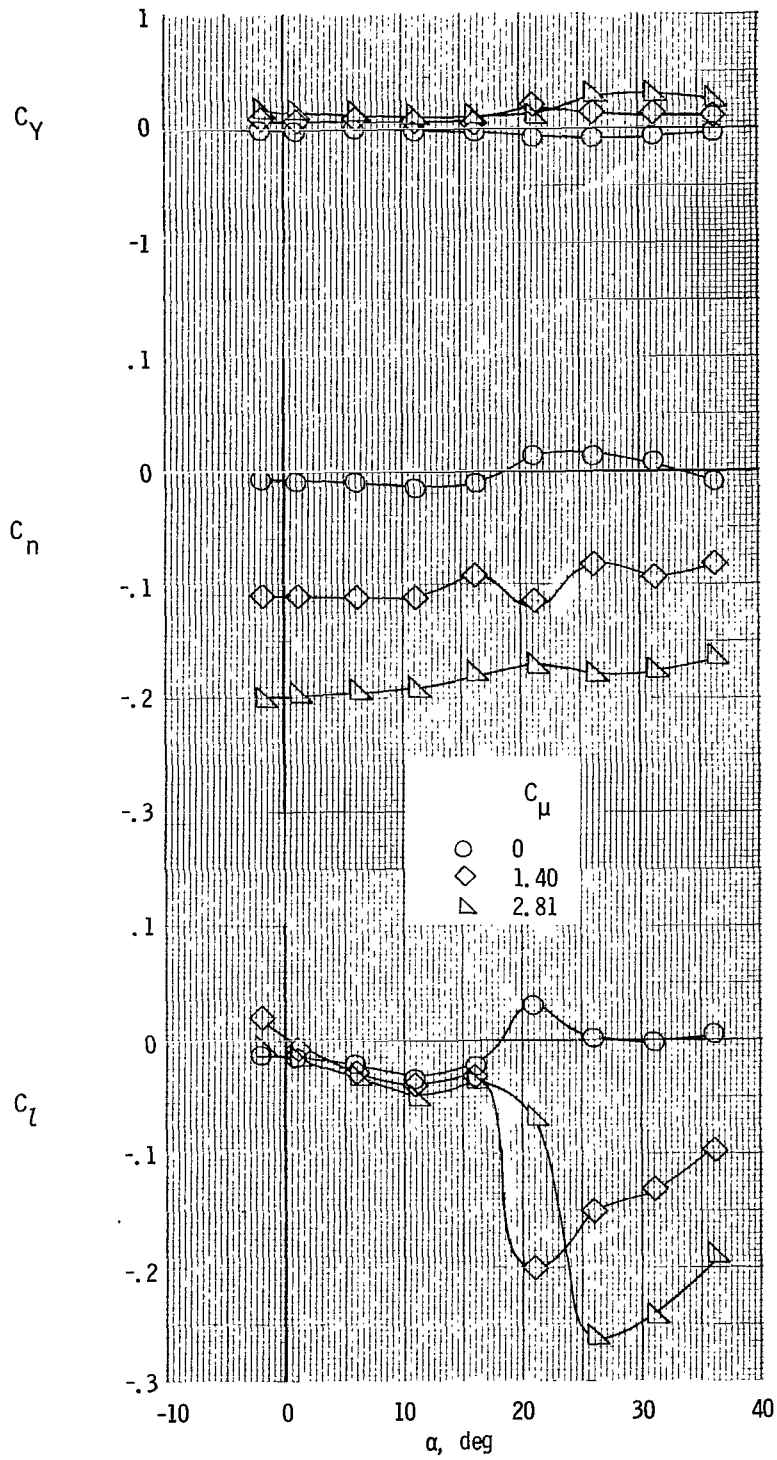

(c) Lateral characteristics. $\delta_{f,L} = 80^o$; $\delta_{f,R} = 40^o$.

Figure 54.- Continued.

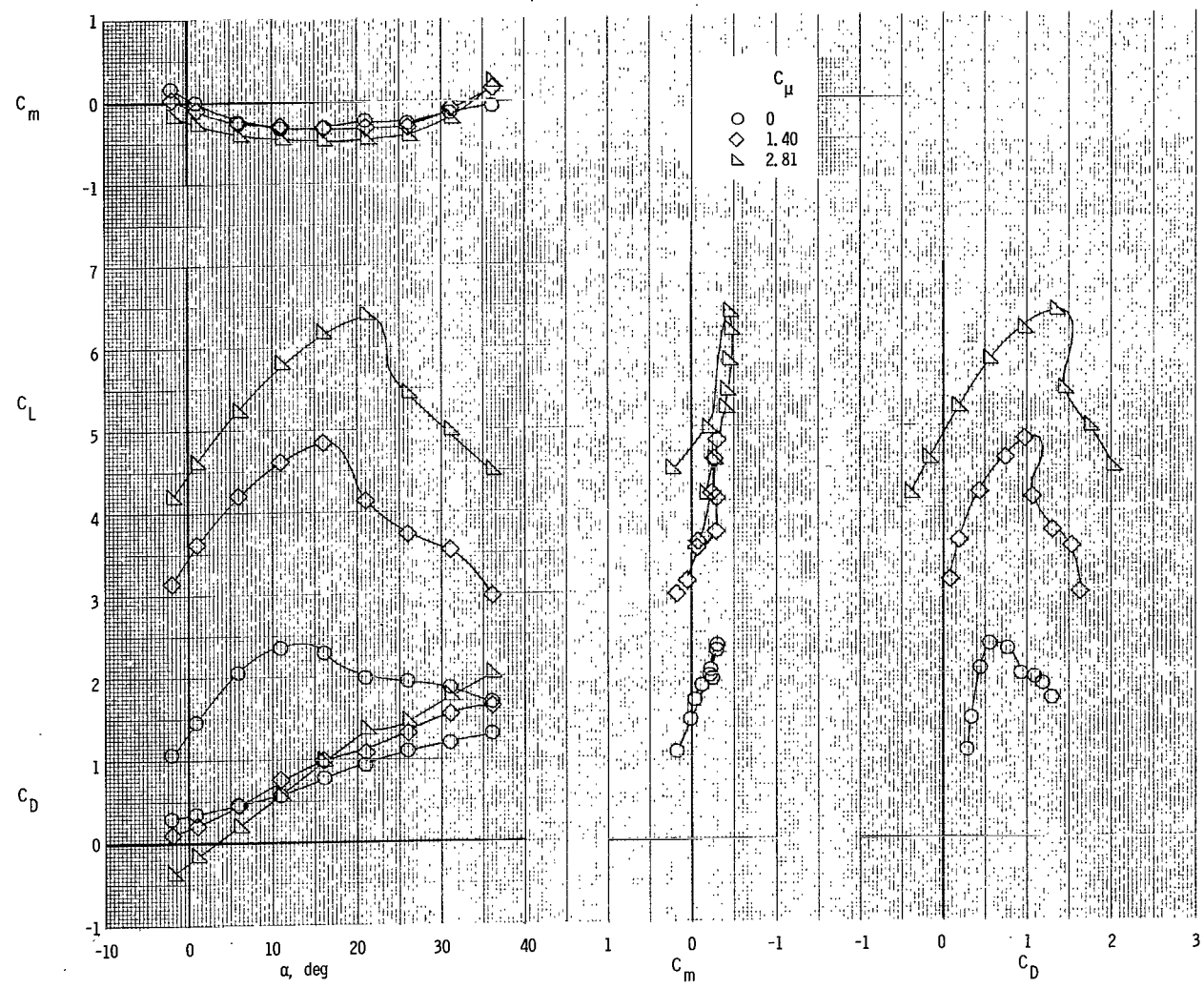

(d) Longitudinal characteristics. $\delta_{f,L} = 80^0$; $\delta_{f,R} = 40^0$.

Figure 54.- Concluded.

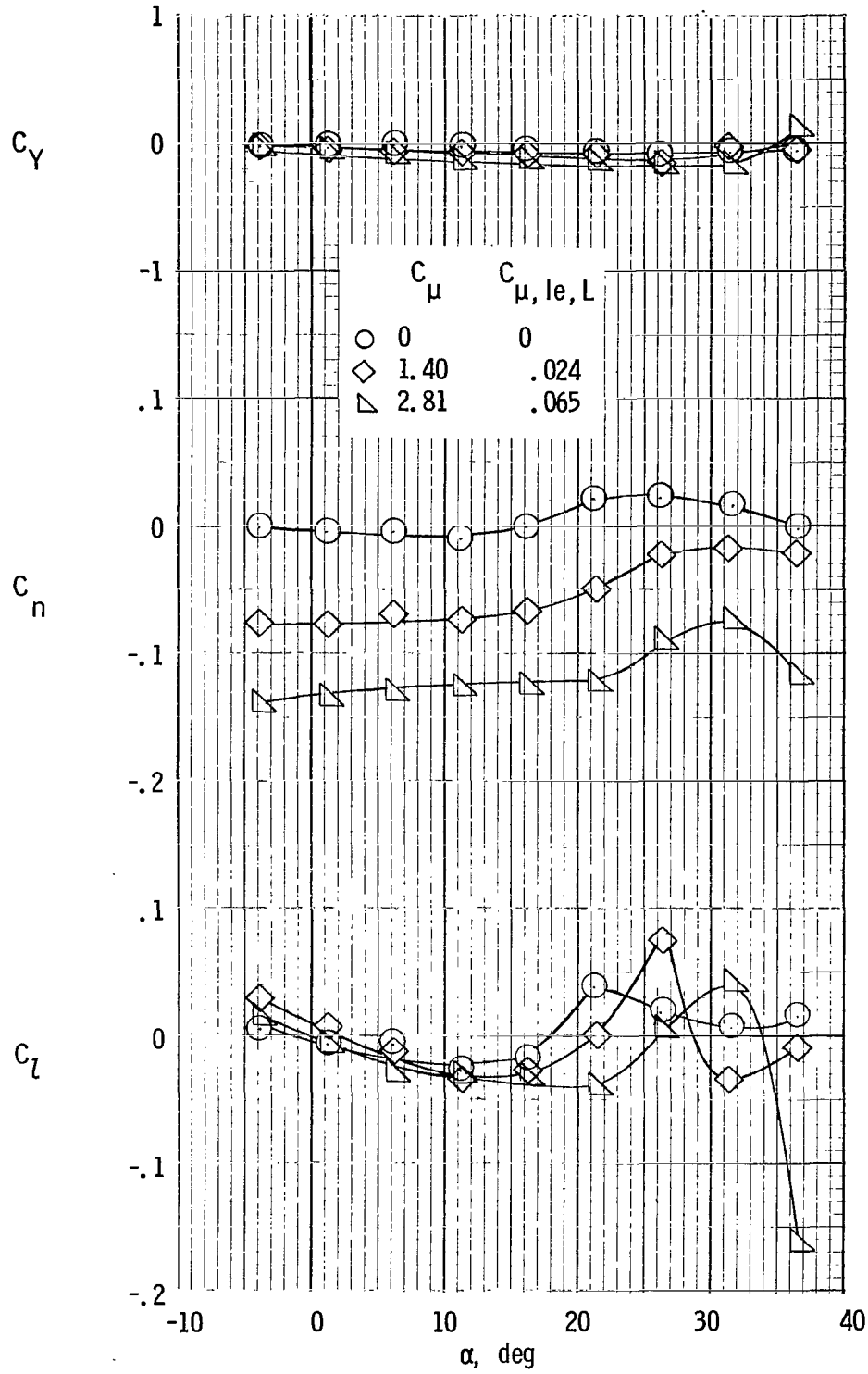

(a) Lateral characteristics. Left outboard engine not operating; $\delta_{f,L} = 70^0$; $\delta_{f,R} = 40^0$.

Figure 55.- Lateral and longitudinal characteristics for two differential flap deflections for model with tail on and clustered engines. Leading-edge blowing; one left engine not operating.

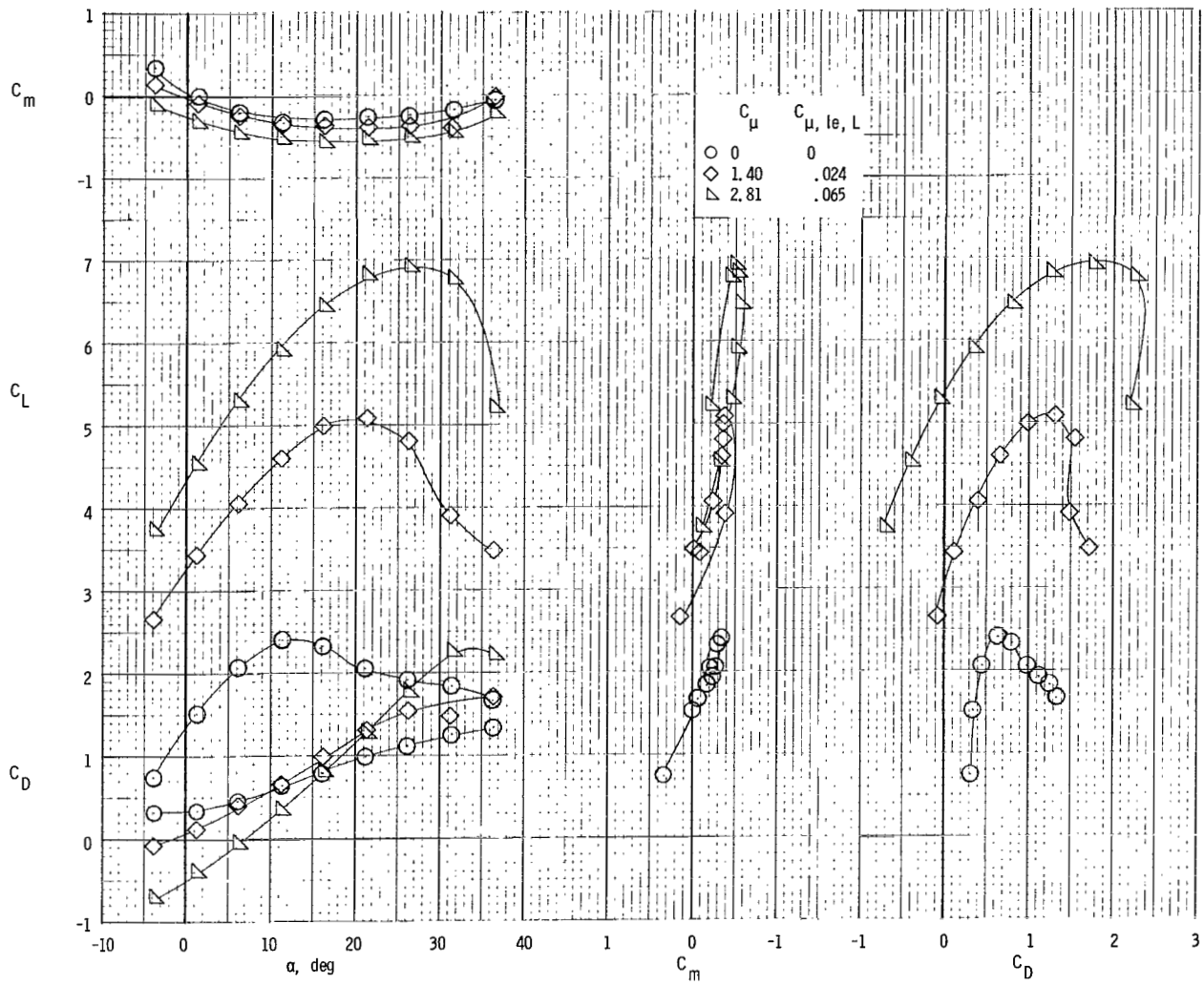

(b) Longitudinal characteristics. Left outboard engine not operating; $\delta_{f,L} = 70^0$; $\delta_{f,R} = 40^0$.

Figure 55.- Continued.

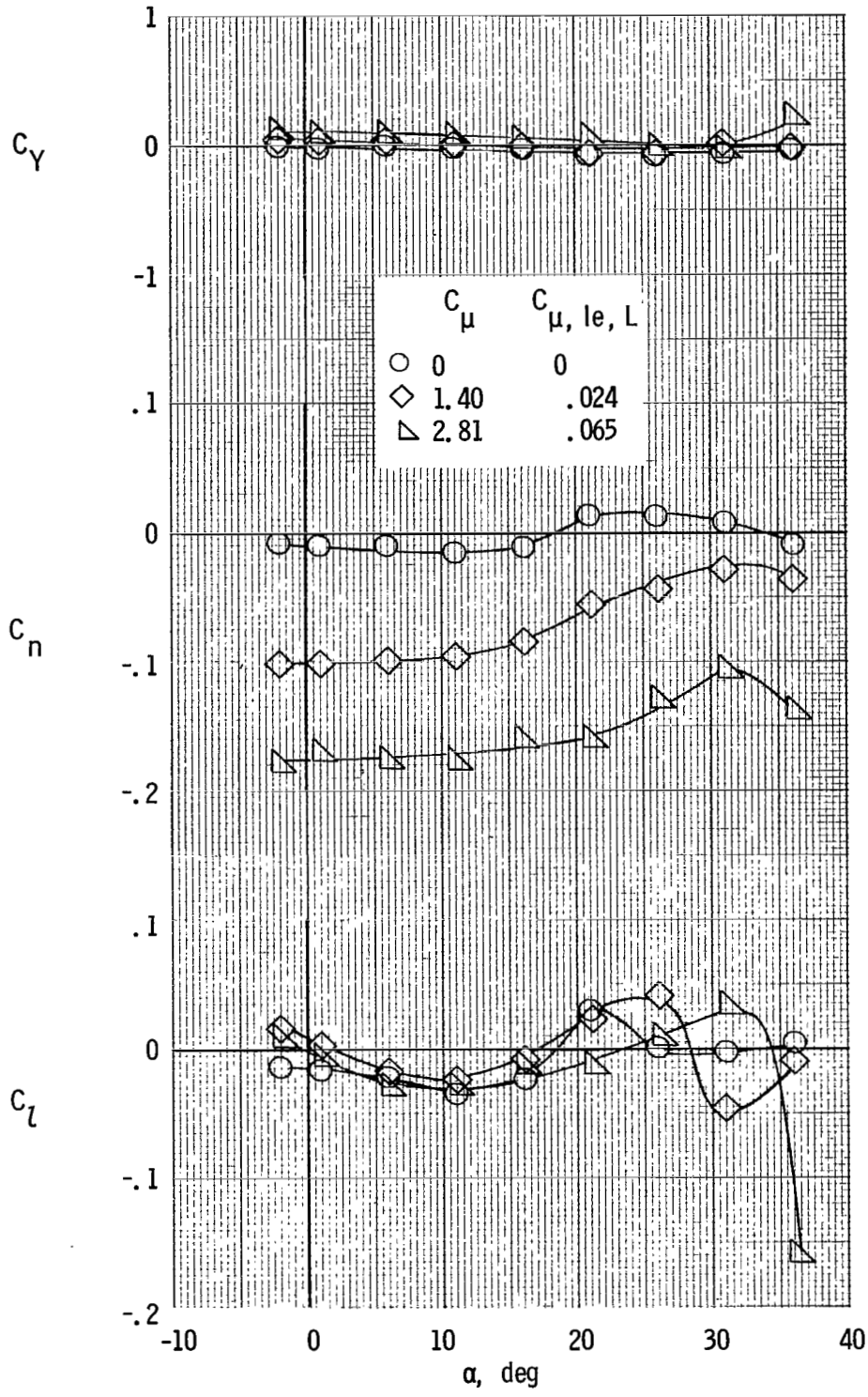

(c) Lateral characteristics. Left outboard engine not operating; $\delta_{f,L} = 80^0$; $\delta_{f,R} = 40^0$.

Figure 55.- Continued.

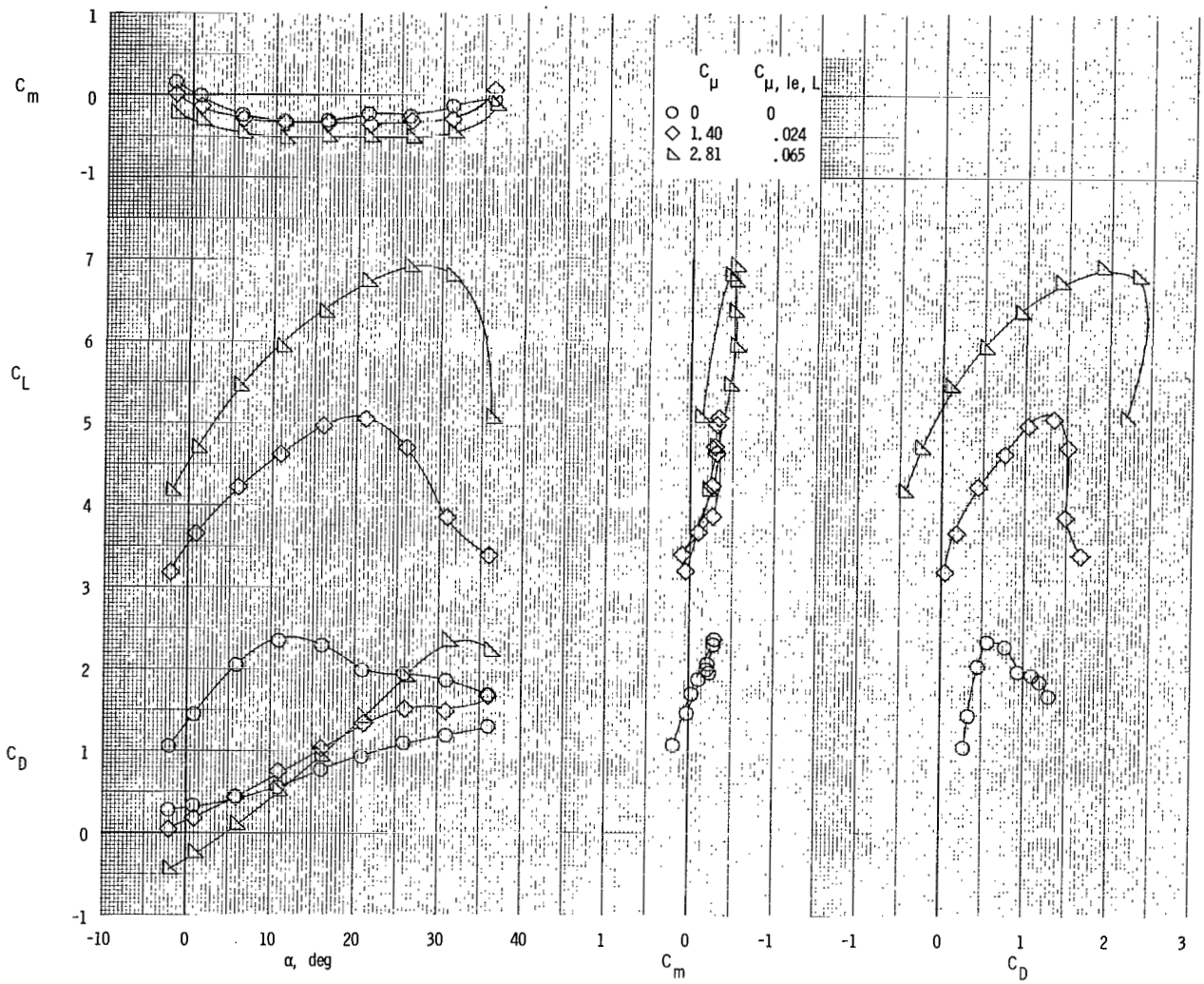

(d) Longitudinal characteristics. Left outboard engine not operating; $\delta_{f,L} = 80^0$; $\delta_{f,R} = 40^0$.

Figure 55.- Continued.

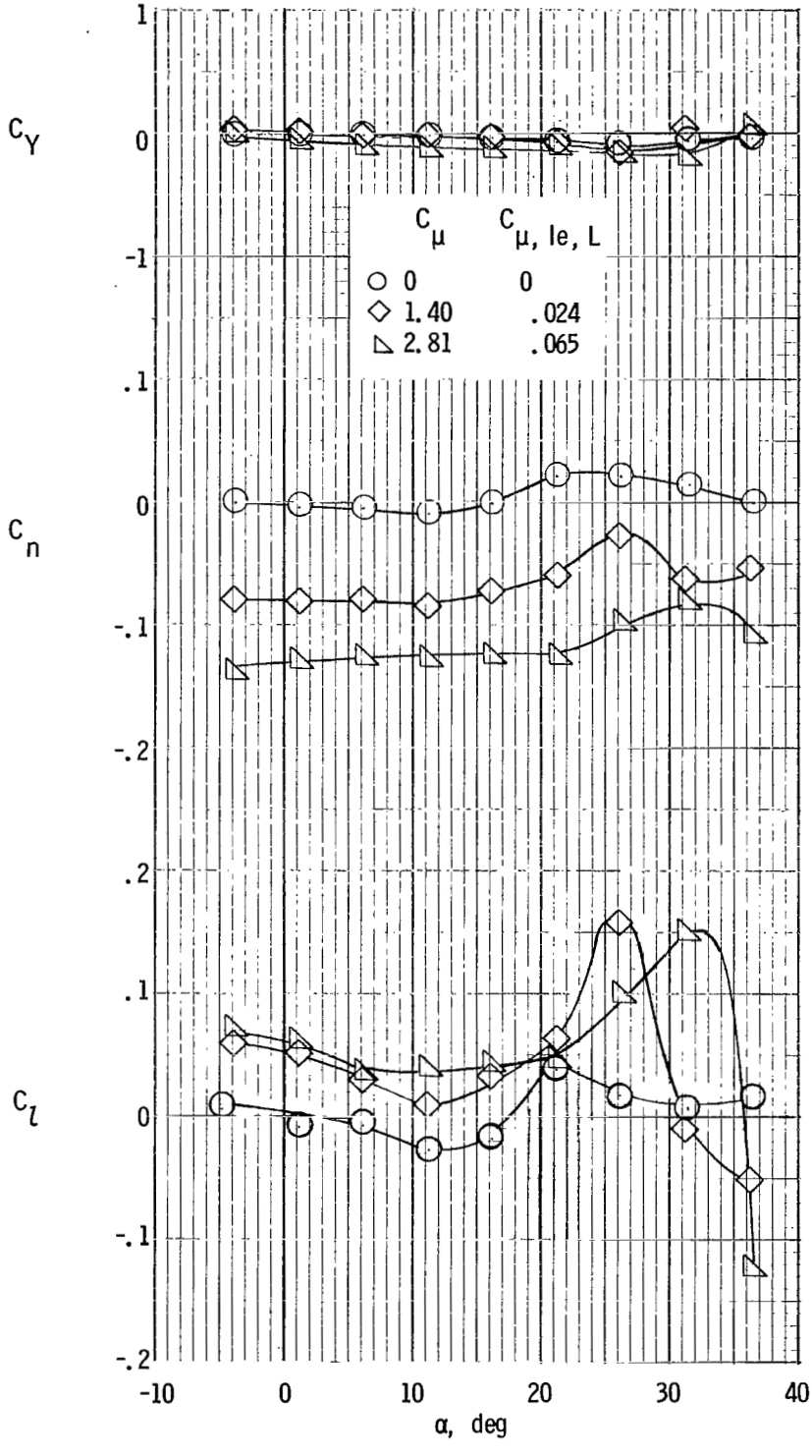

(e) Lateral characteristics. Left inboard engine not operating; $\delta_{f,L} = 70^0$; $\delta_{f,R} = 40^0$.

Figure 55.- Continued.

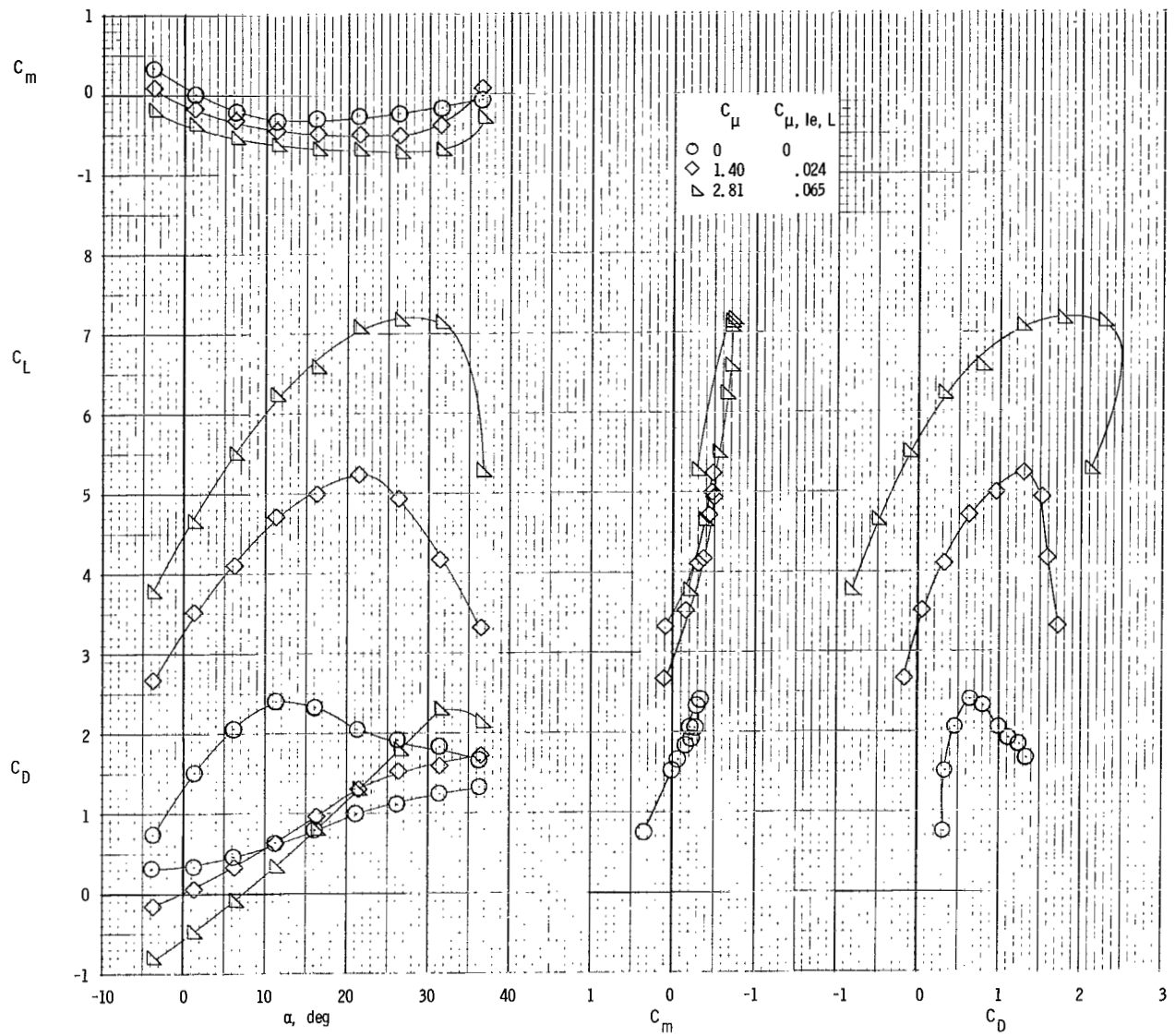

(f) Longitudinal characteristics. Left inboard engine not operating; $\delta_{f,L} = 70^0$; $\delta_{f,R} = 40^0$.

Figure 55.- Concluded.

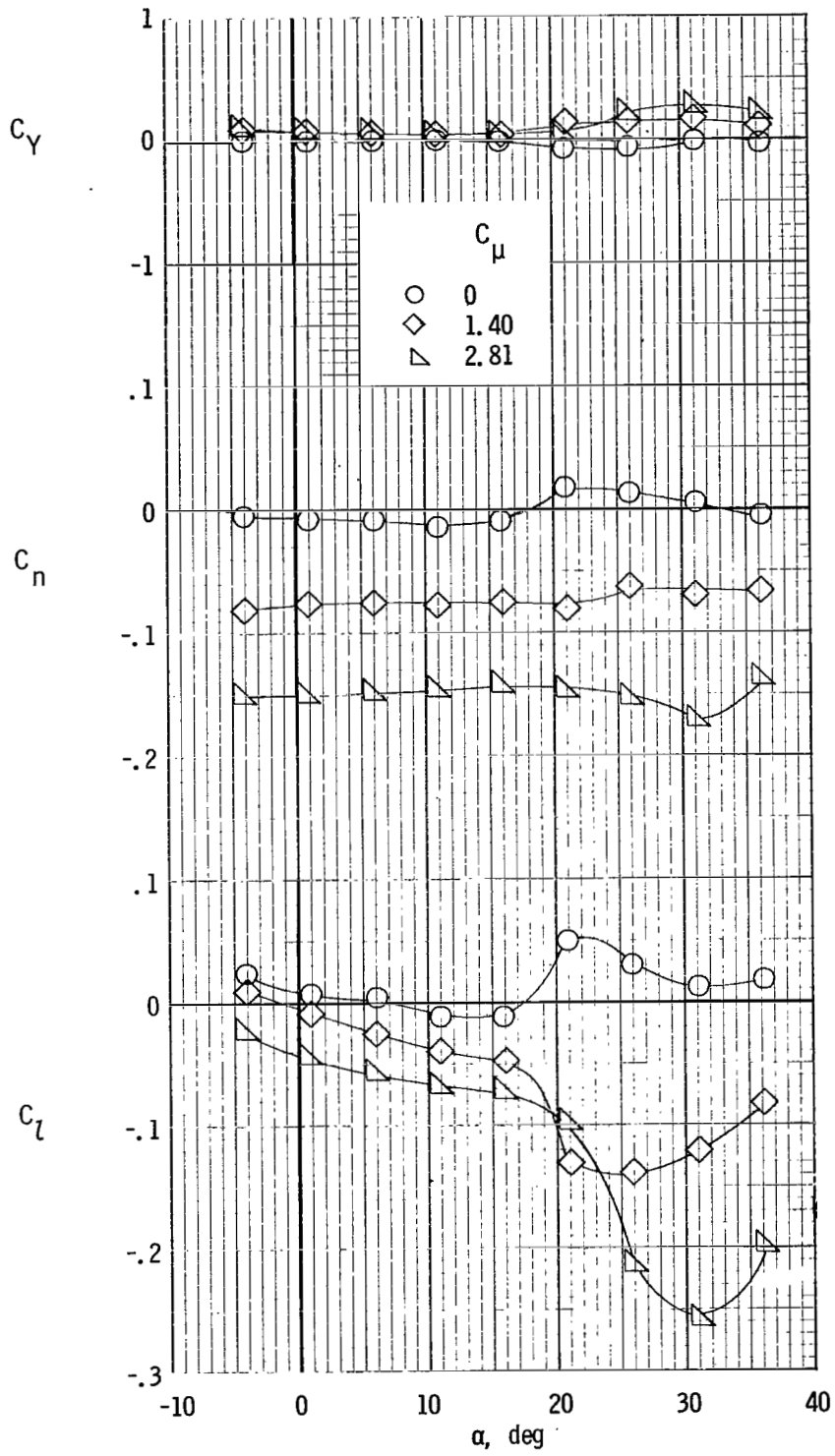

(a) Lateral characteristics.

Figure 56.- Lateral and longitudinal characteristics of model with tail off and clustered engines. Left outboard engine not operating; differential flap deflection; $\delta_{f,L} = 60^0$; $\delta_{f,R} = 40^0$; $C_{\mu,le} = 0$.

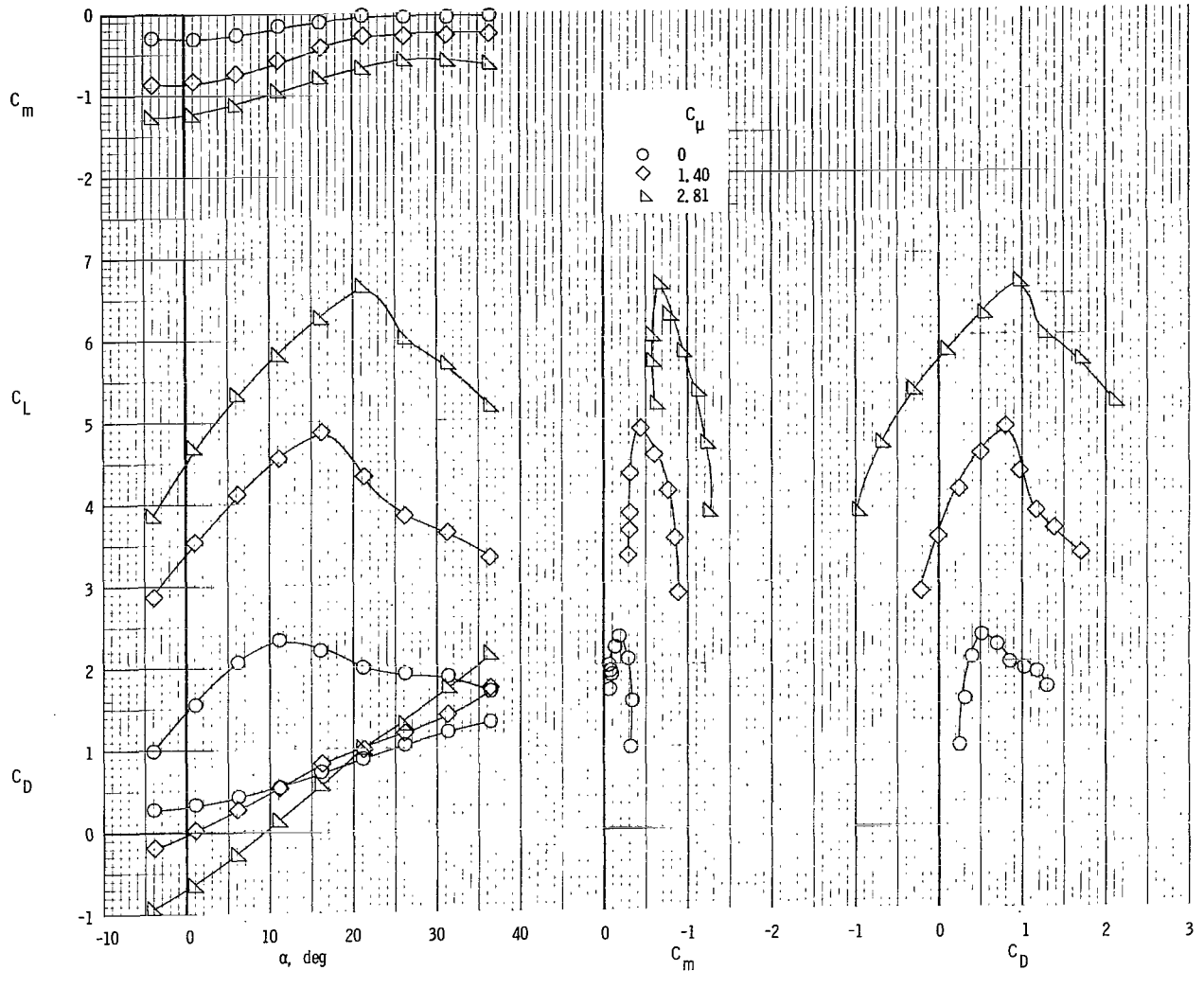

(b) Longitudinal characteristics.

Figure 56.- Concluded.

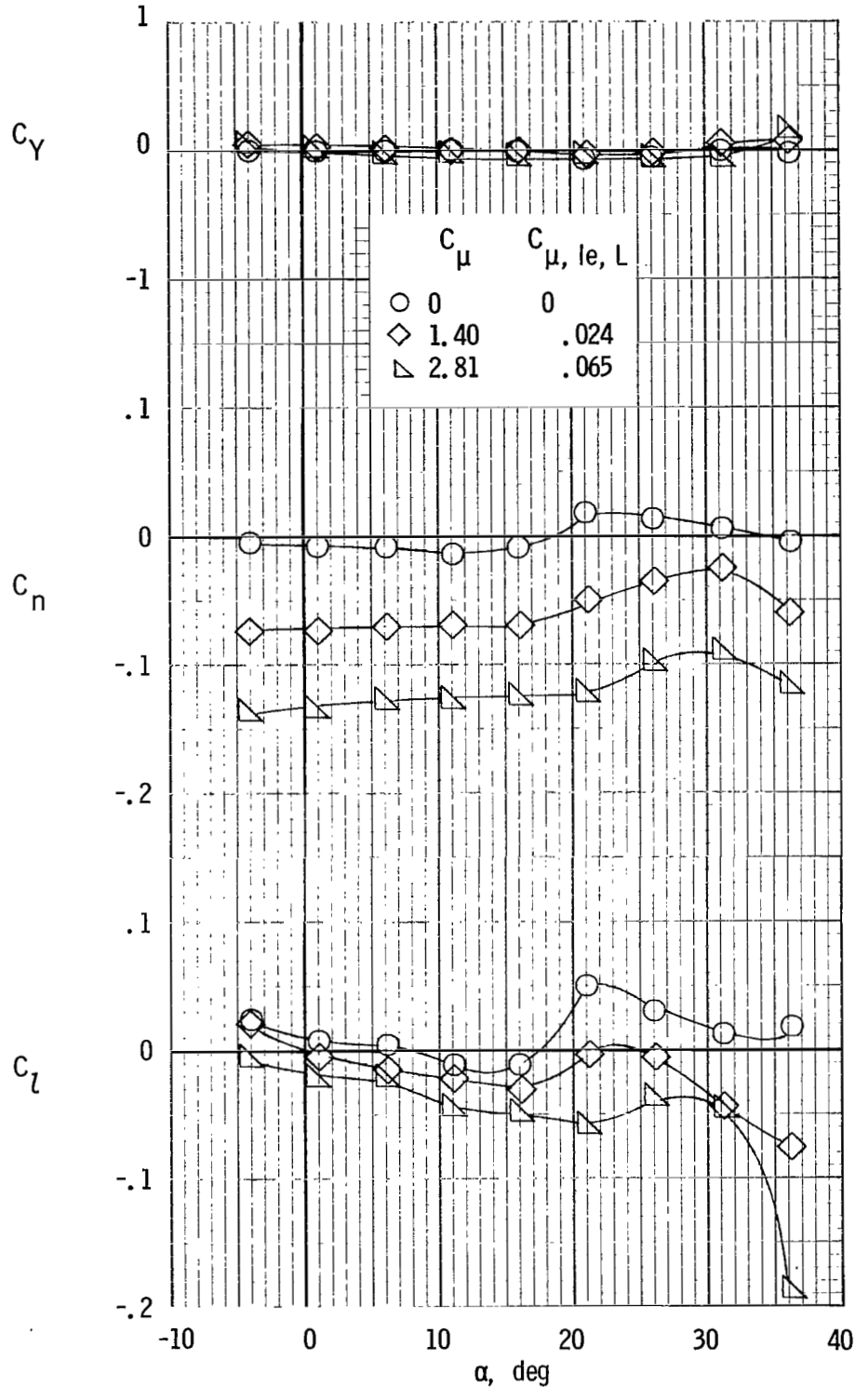

(a) Lateral characteristics.

Figure 57.- Lateral and longitudinal characteristics of model with tail off and clustered engines. Left outboard engine not operating; leading-edge blowing; differential flap deflection; $\delta_{f,L} = 60^0$; $\delta_{f,R} = 40^0$.

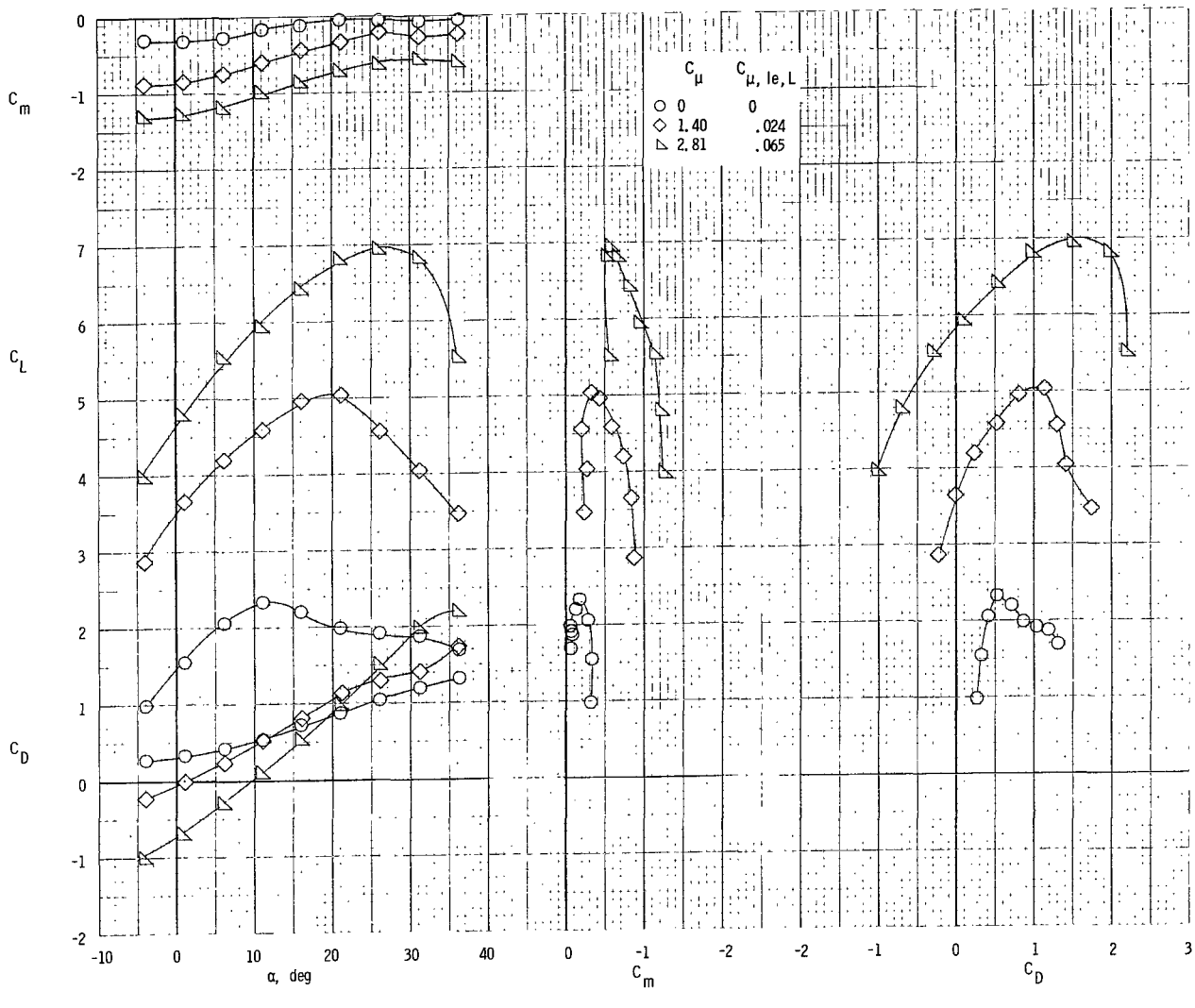

(b) Longitudinal characteristics.

Figure 57.- Concluded.

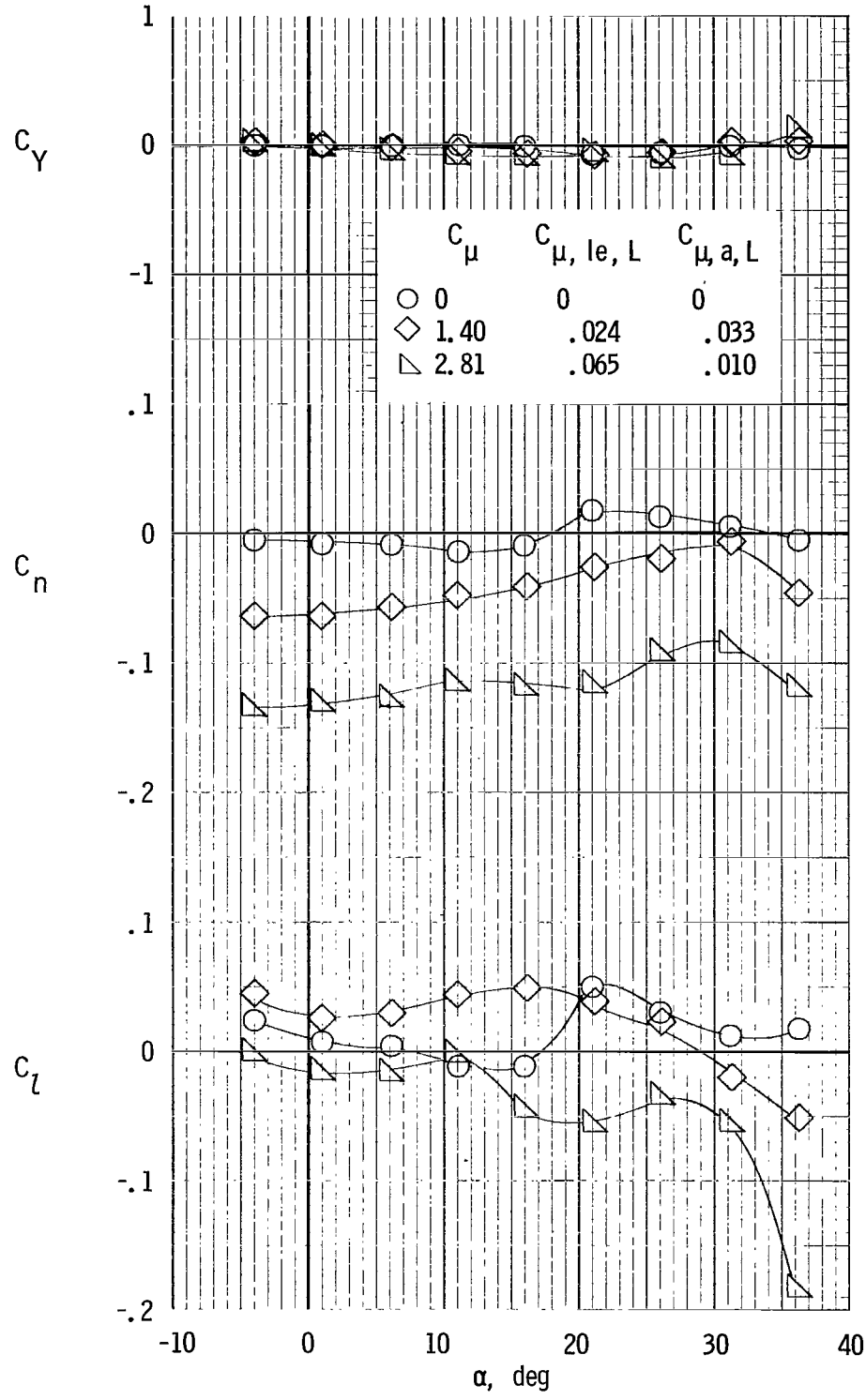

(a) Lateral characteristics.

Figure 58.- Lateral and longitudinal characteristics of model with tail off and clustered engines. Left outboard engine not operating; leading-edge and aileron blowing; differential flap deflection; $\delta_{f,L} = 60^0$; $\delta_{f,R} = 40^0$.

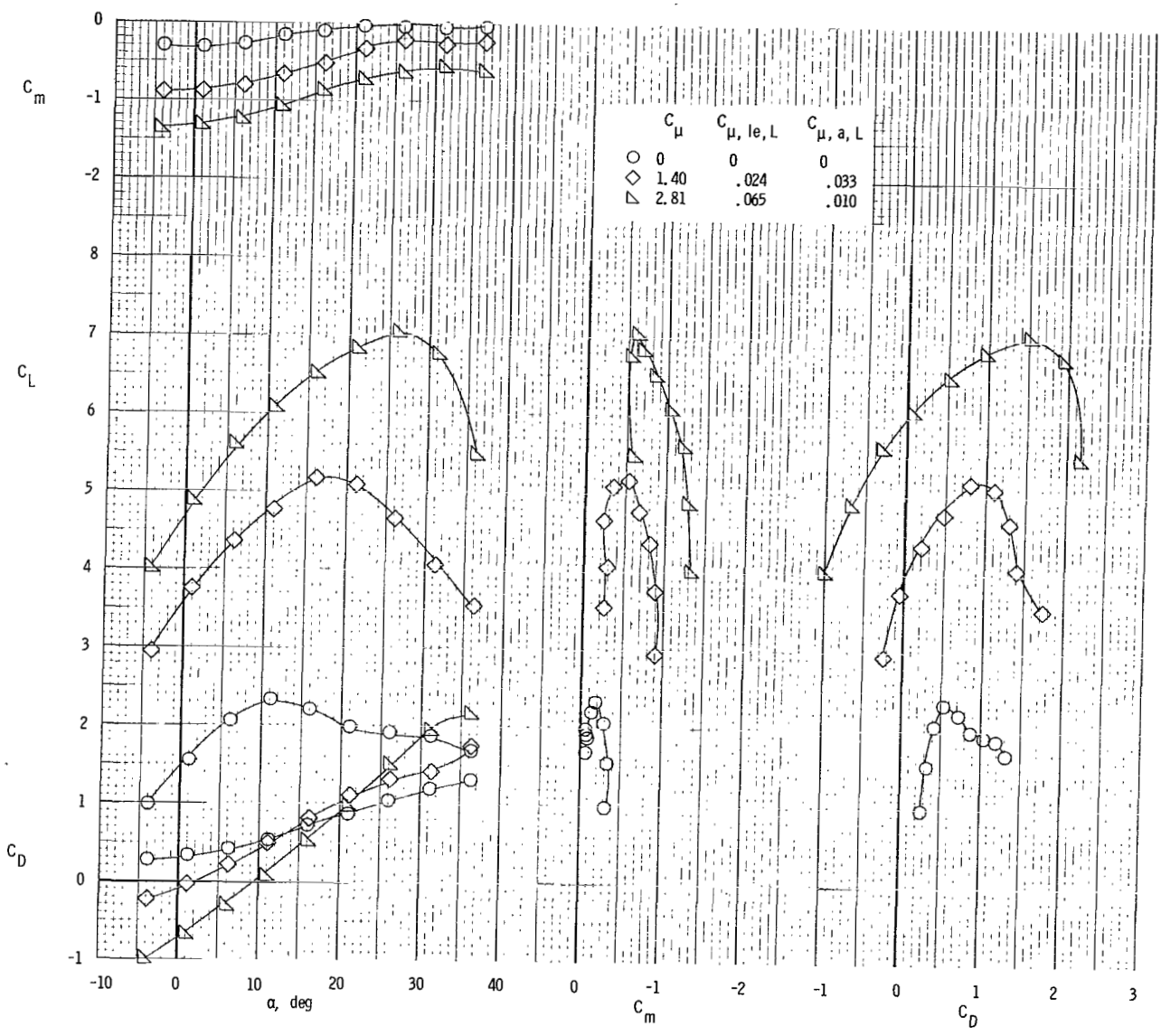

(b) Longitudinal characteristics.

Figure 58.- Concluded.

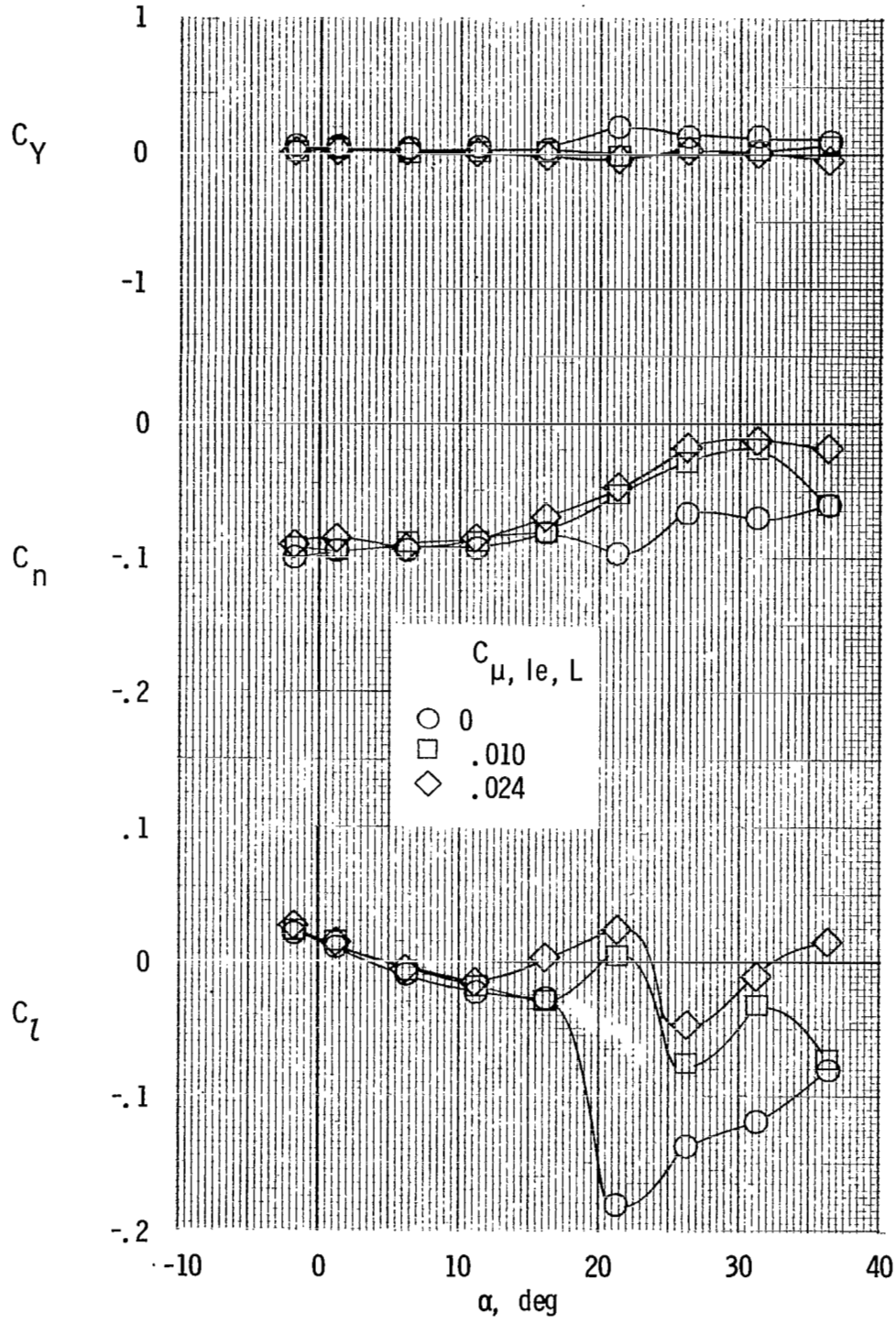

(a) Lateral characteristics. C_μ = 1.40.

Figure 59.- Effect of leading-edge blowing on lateral and longitudinal characteristics of model with tail on and clustered engines. Left outboard engine not operating; $\delta_f = 80^0$, left inboard; $\delta_f = 40^0$, right inboard; $\delta_f = 60^0$, left and right center and outboard.

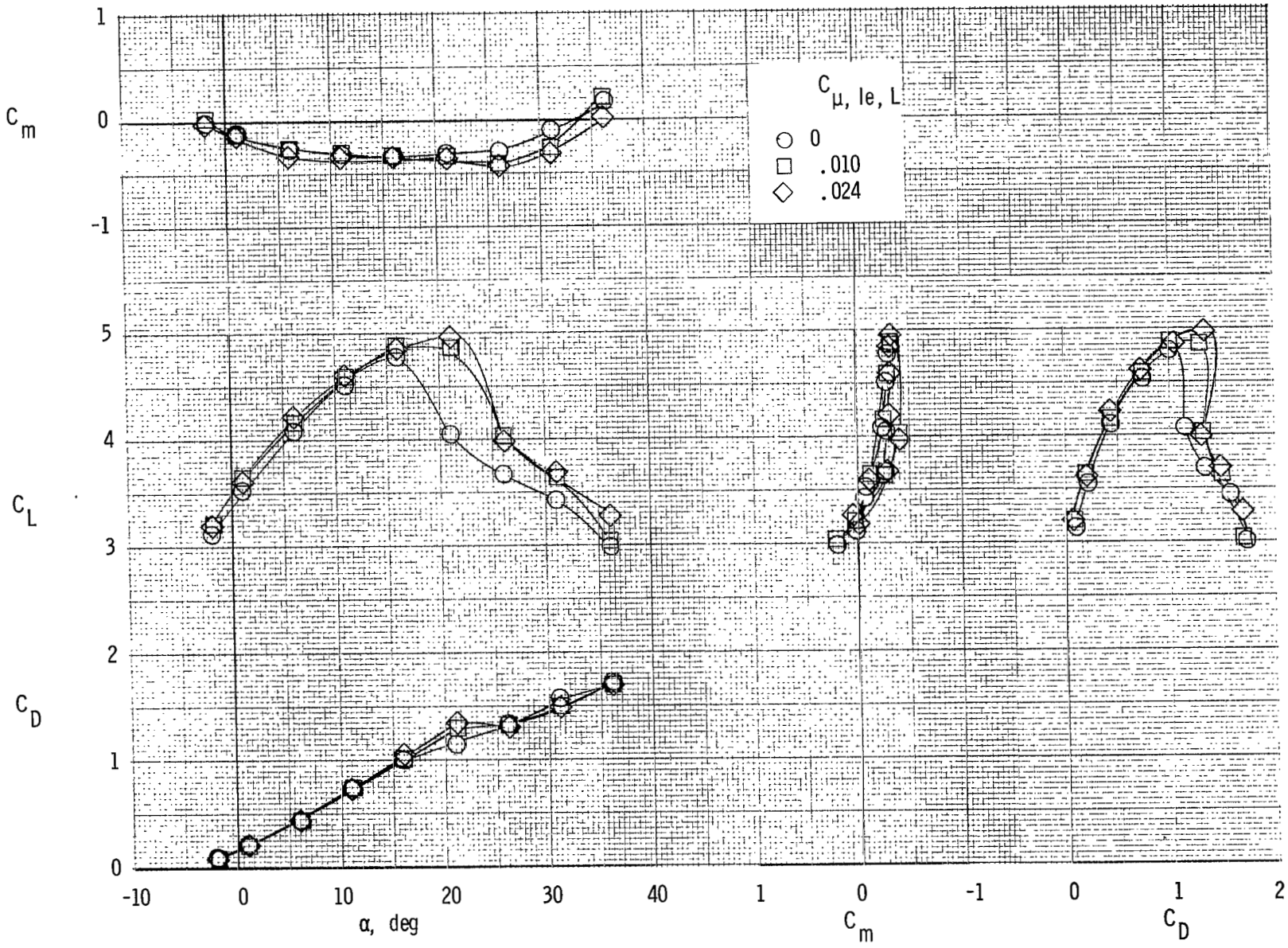

(b) Longitudinal characteristics. $C_{\mu} = 1.40$.

Figure 59.- Continued.

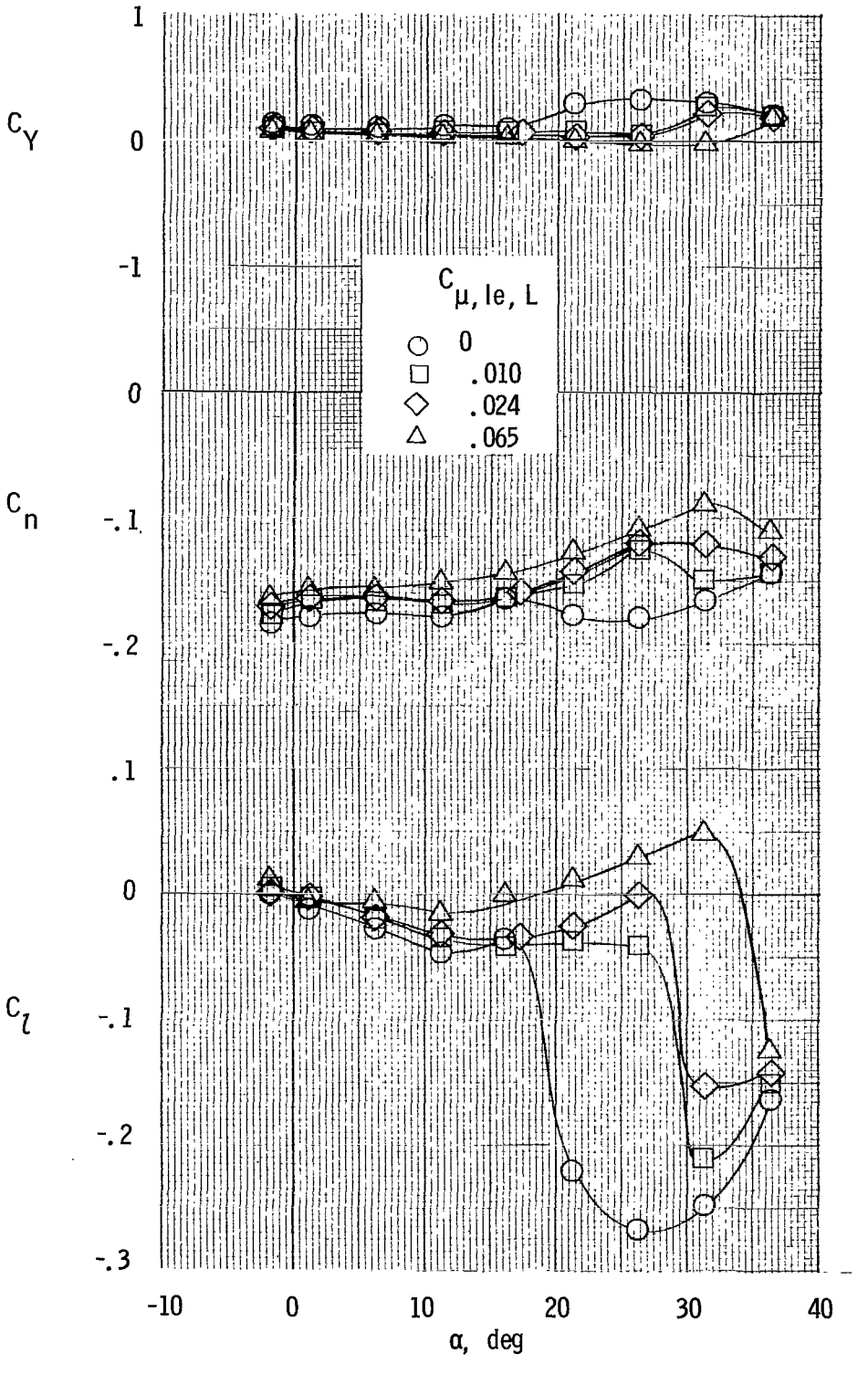

(c) Lateral characteristics. $C_\mu = 2.81$.

Figure 59.- Continued.

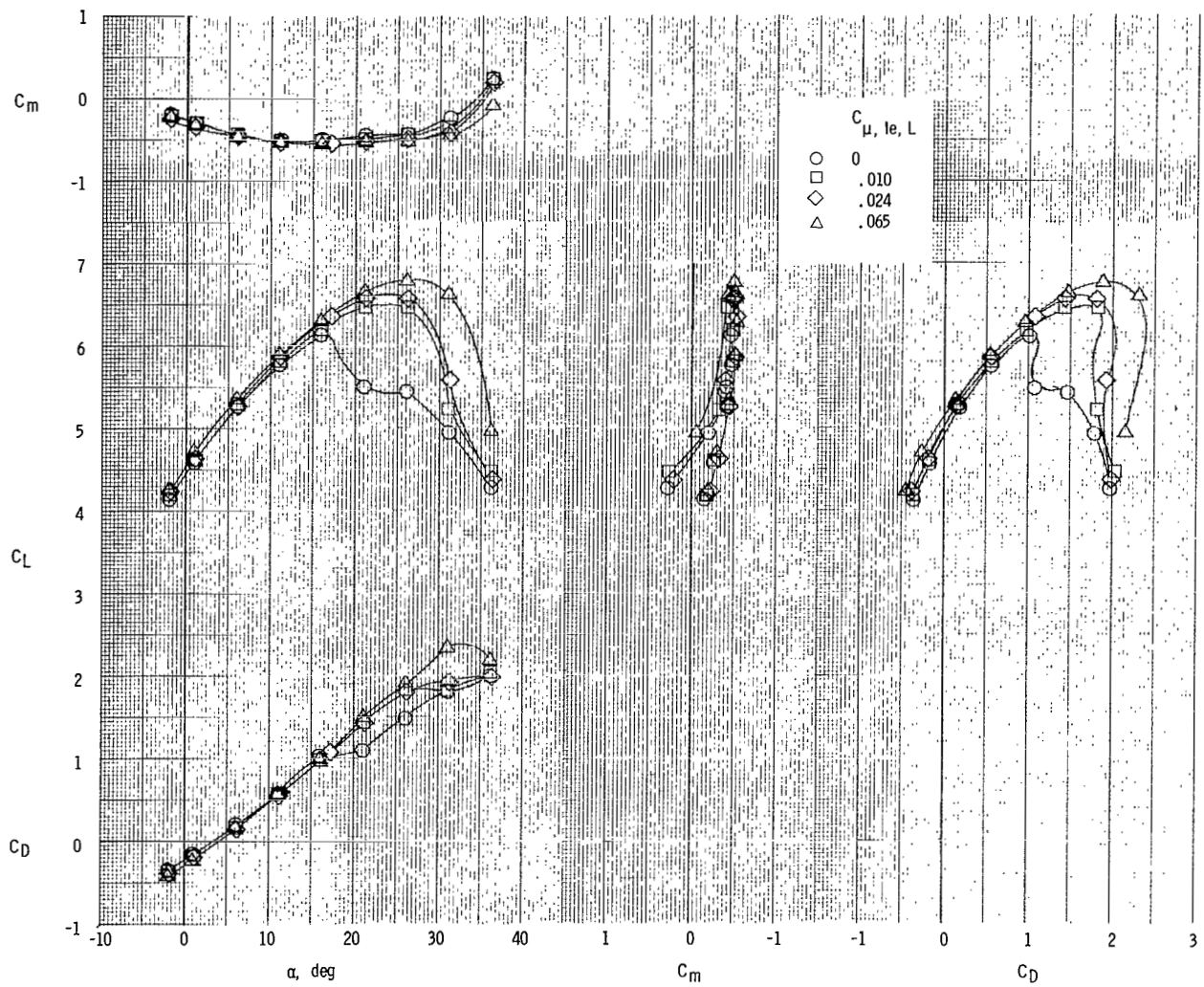

(d) Longitudinal characteristics. $C_{\mu} = 2.81$.

Figure 59.- Concluded.

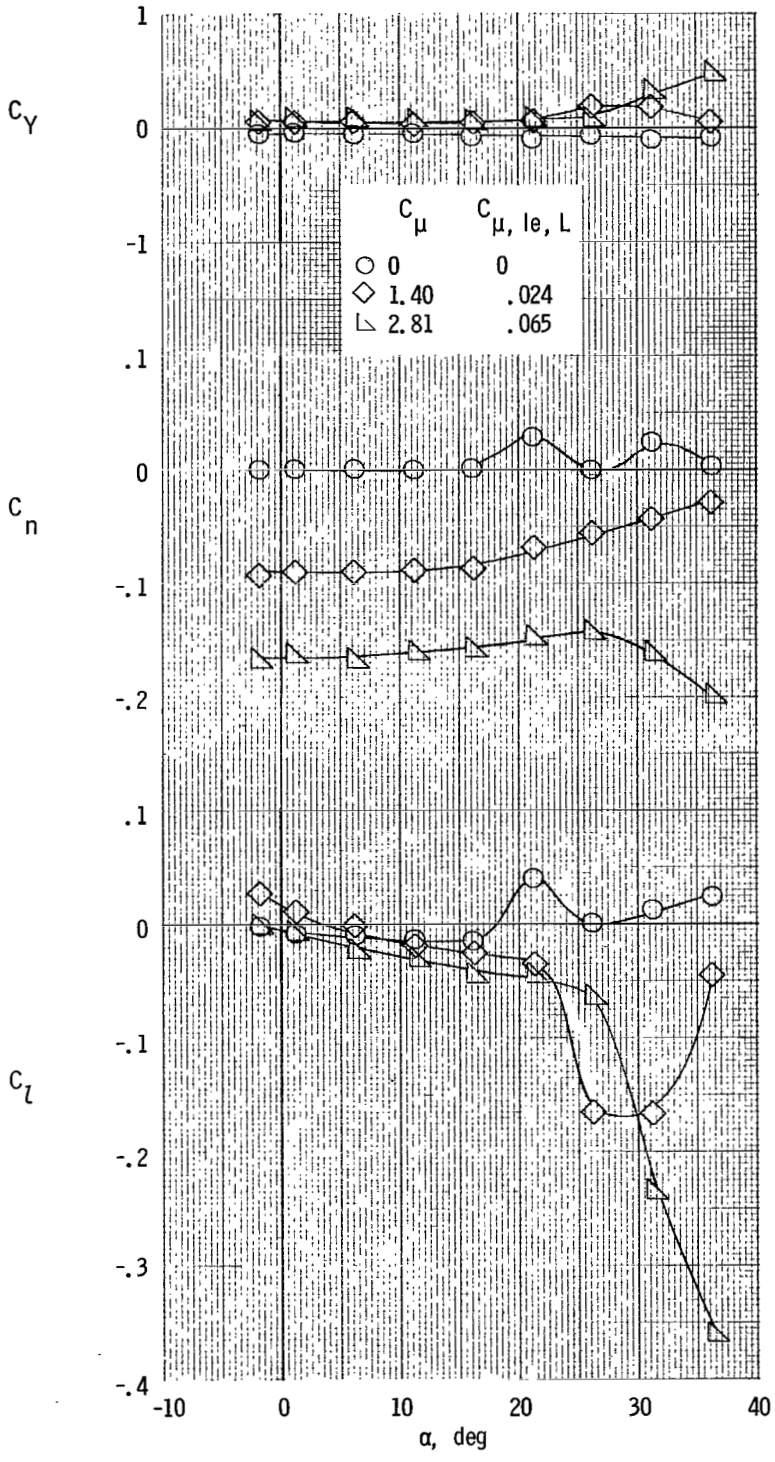

(a) Lateral characteristics.

Figure 60.- Lateral and longitudinal characteristics of model with tail on and clustered engines. Left outboard engine not operating; leading-edge blowing; $\delta_f = 80^0$, left inboard; $\delta_f = 40^0$, right inboard; $\delta_f = 60^0$, left and right center and outboard.

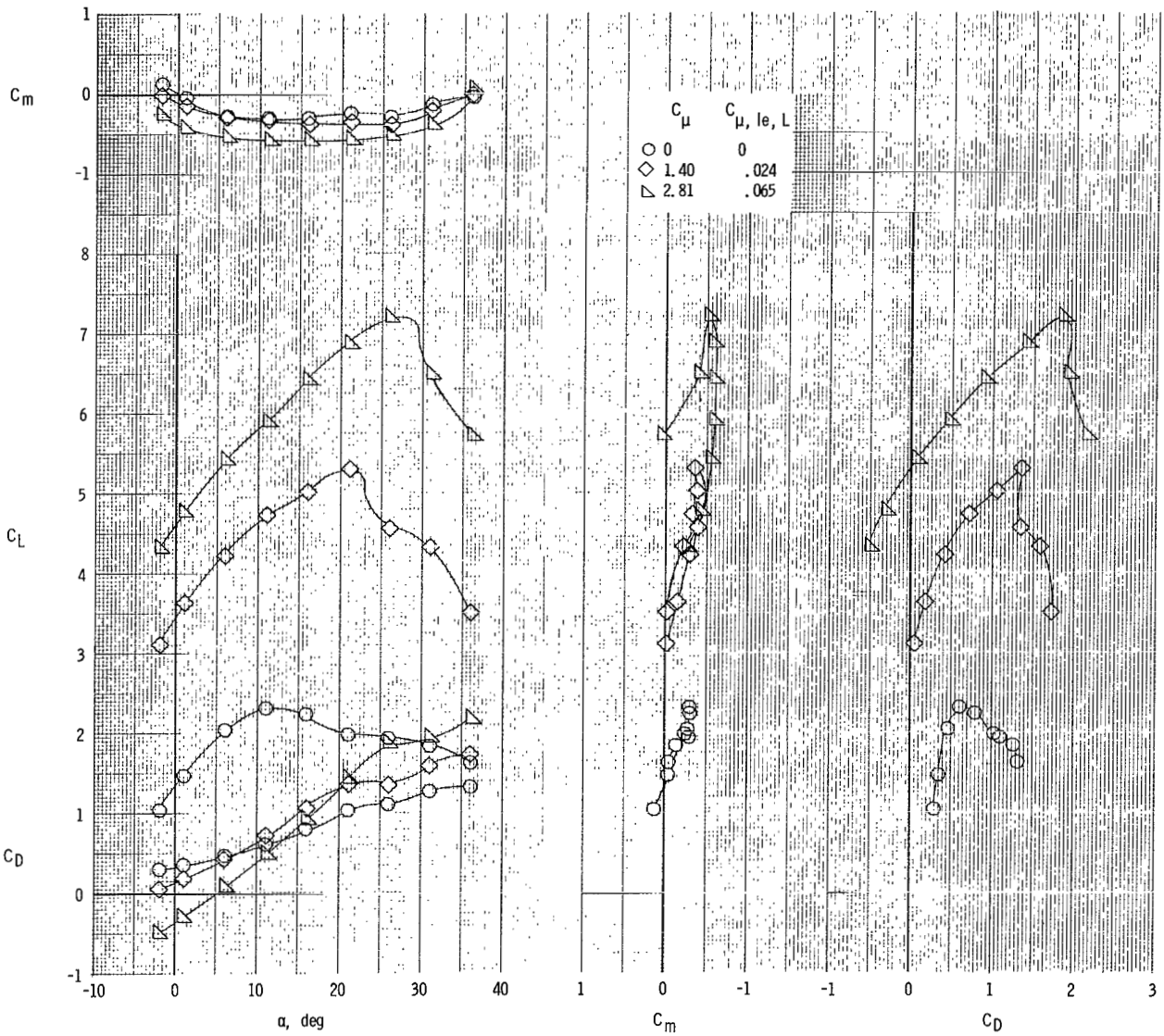

(b) Longitudinal characteristics.

Figure 60.- Concluded.

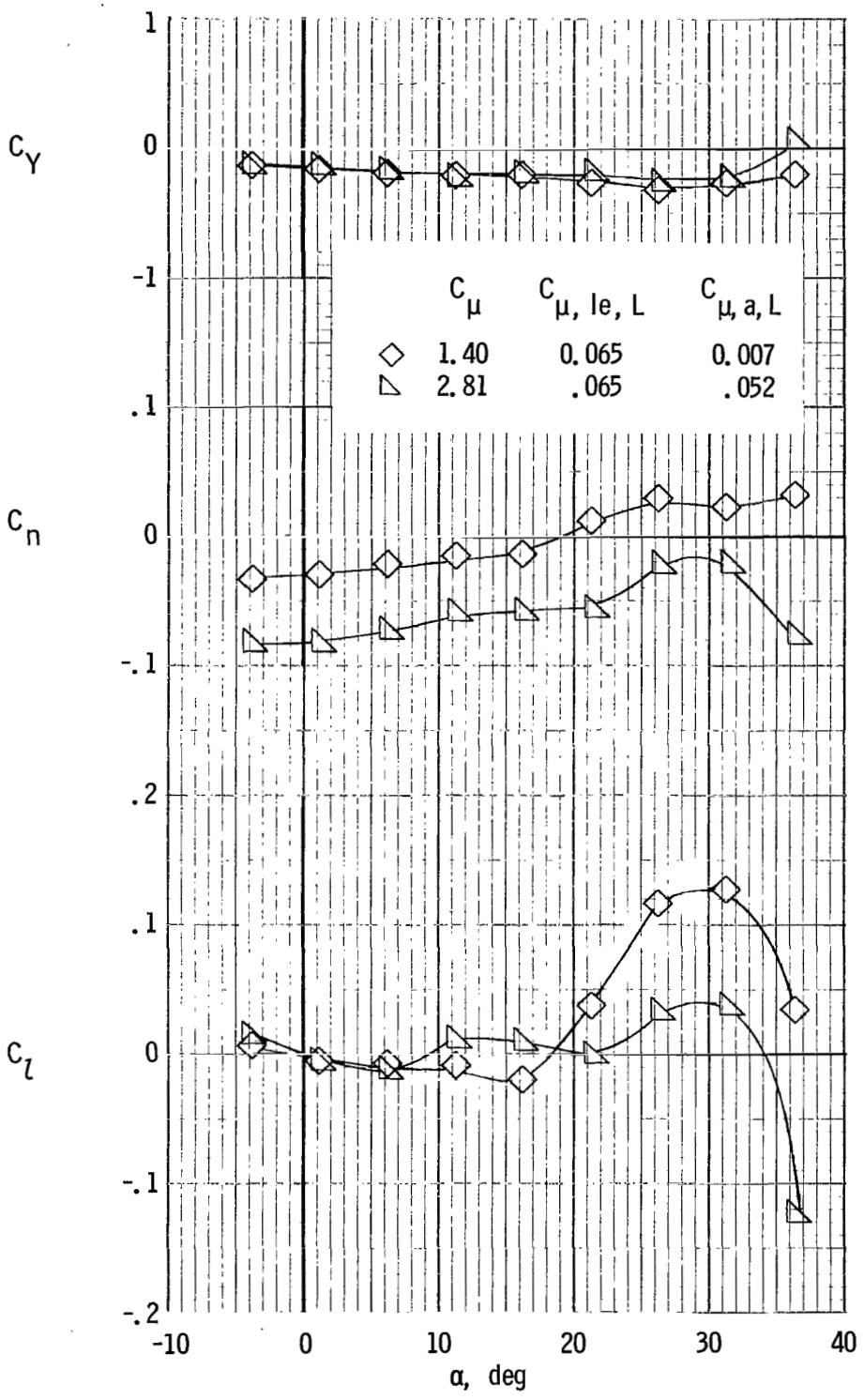

(a) Lateral characteristics. Leading-edge and aileron blowing; $\delta_f = 60^0$, left inboard; $\delta_f = 40^0$, right inboard; $\delta_f = 60^0$, left and right center and outboard.

Figure 61.- Lateral and longitudinal characteristics of model with tail on and clustered engines. Left outboard engine not operating; differential deflection of inboard flap segments.

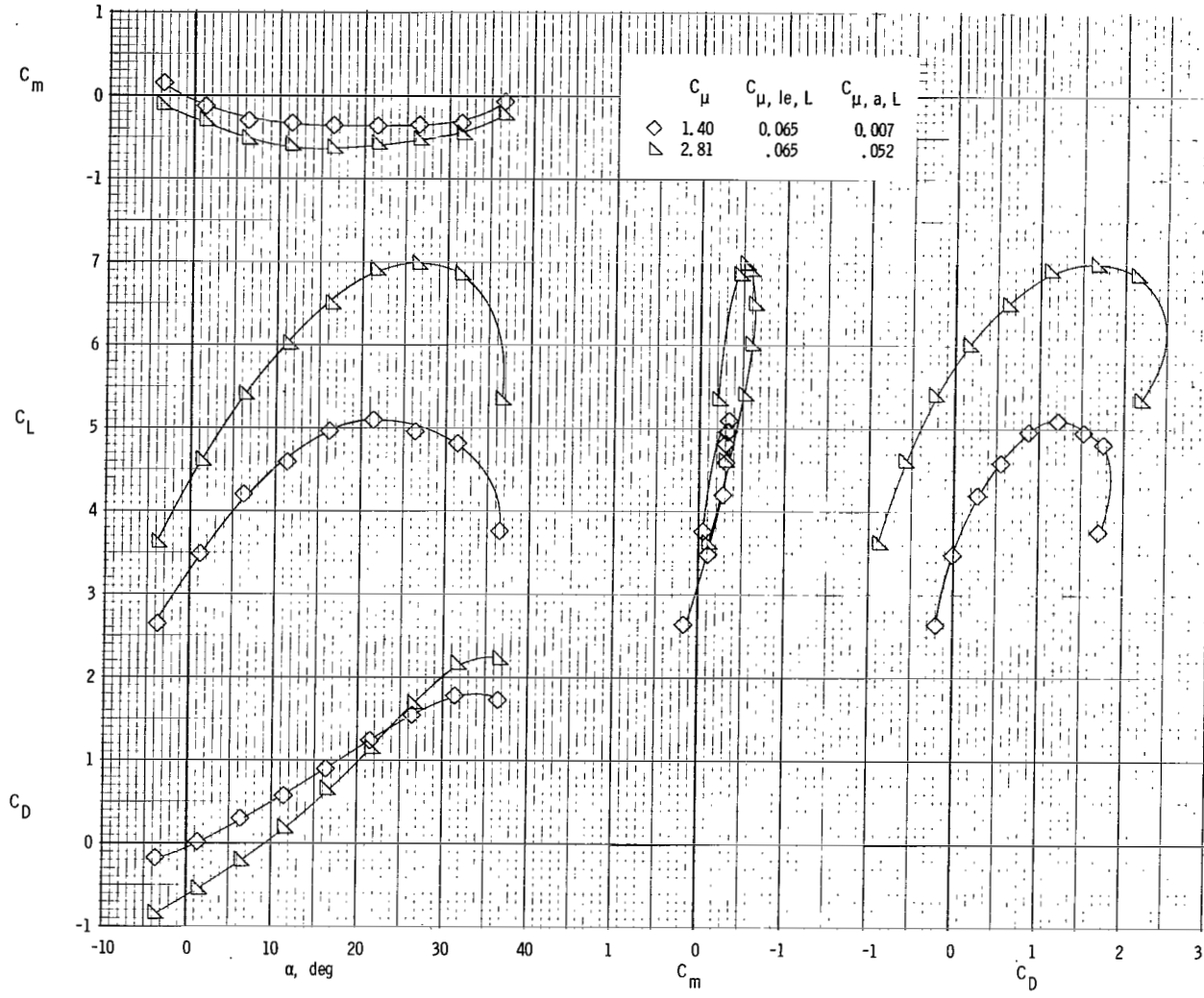

(b) Longitudinal characteristics. Leading-edge and aileron blowing; $\delta_f = 60^o$, left inboard; $\delta_f = 40^o$, right inboard; $\delta_f = 60^o$, left and right center and outboard.

Figure 61.- Continued.

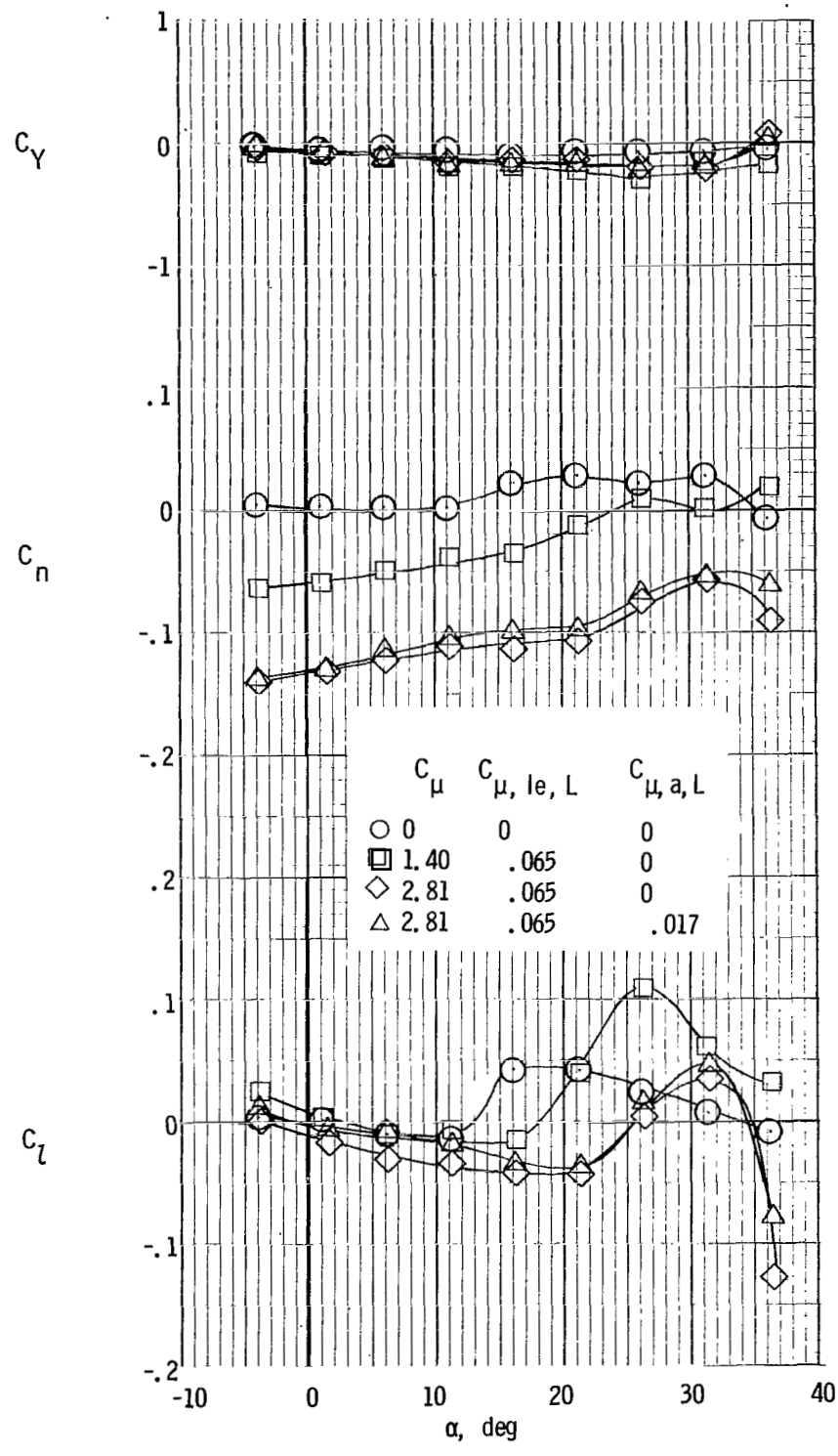

(c) Lateral characteristics. Leading-edge and aileron blowing; $\delta_f = 70^o$, left inboard; $\delta_f = 40^o$, right inboard; $\delta_f = 60^o$, left and right center and outboard.

Figure 61.- Continued.

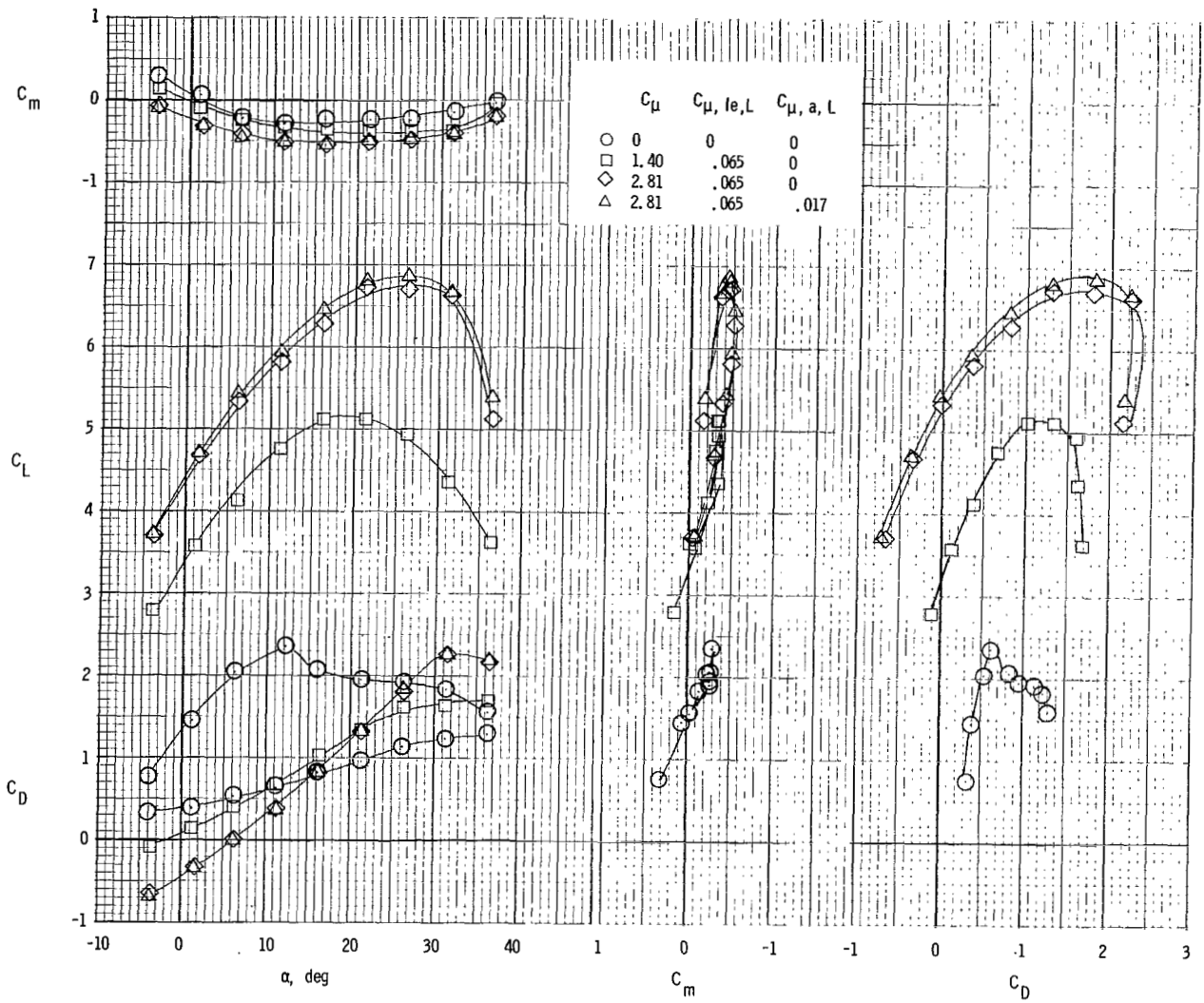

(d) Longitudinal characteristics. Leading-edge and aileron blowing; $\delta_f = 70^0$, left inboard; $\delta_f = 40^0$, right inboard; $\delta_f = 60^0$, left and right center and outboard.

Figure 61.- Continued.

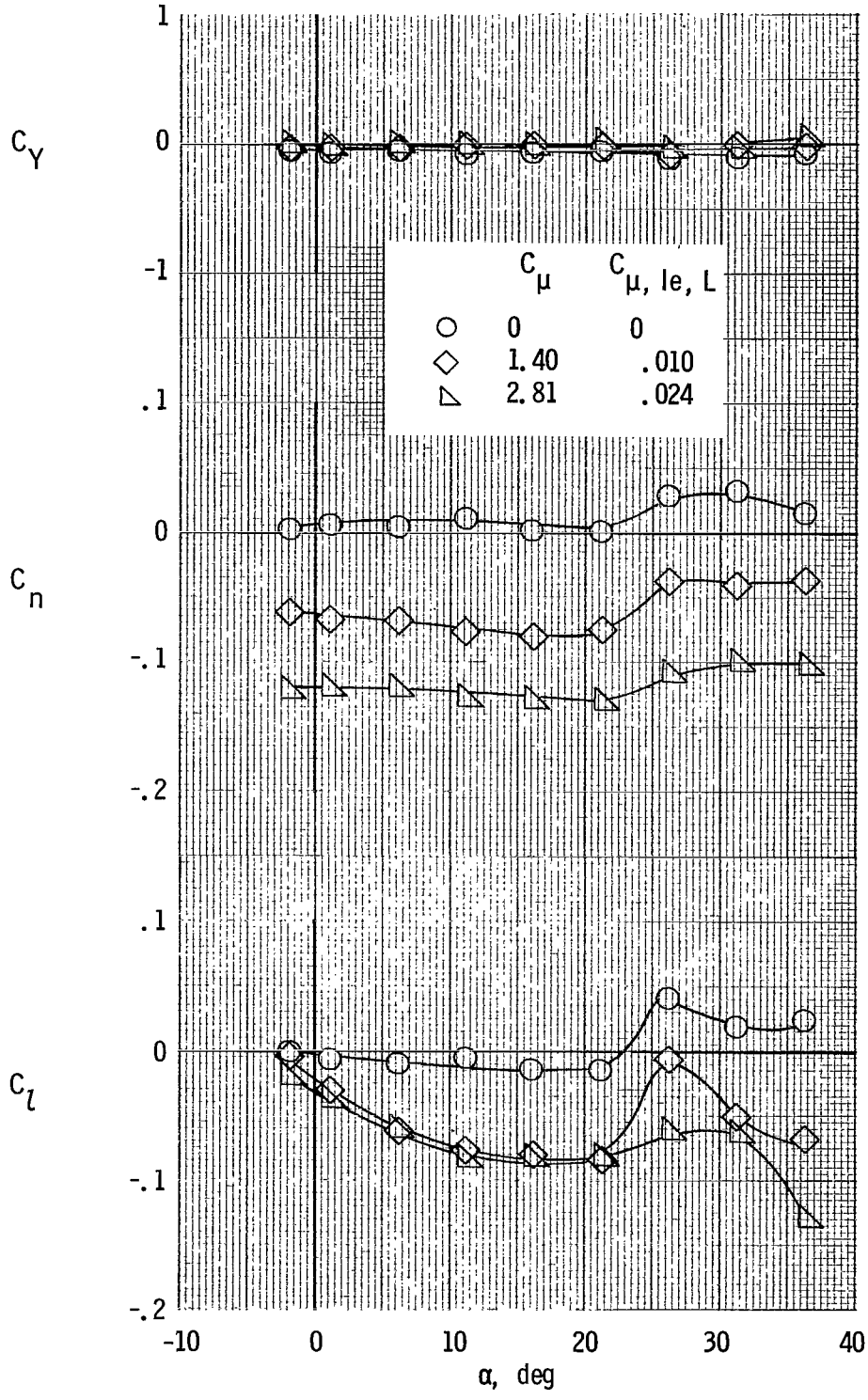

(e) Lateral characteristics. Leading-edge blowing; $\delta_f = 50^o$, left inboard; $\delta_f = 30^o$, right inboard; $\delta_f = 40^o$, left and right center and outboard.

Figure 61.- Continued.

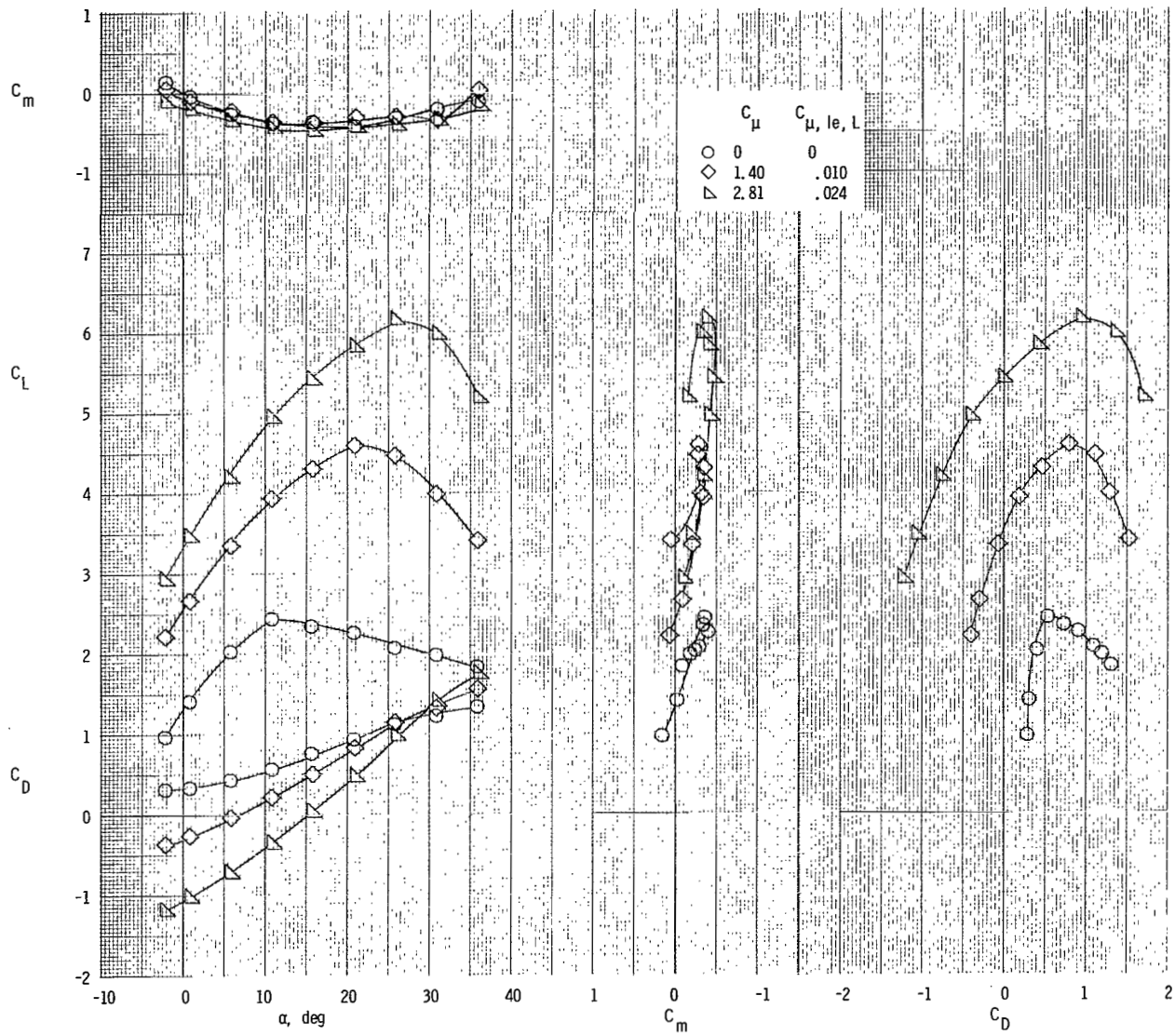

(f) Longitudinal characteristics. Leading-edge blowing; $\delta_f = 50^0$, left inboard; $\delta_f = 30^0$, right inboard; $\delta_f = 40^0$, left and right center and outboard.

Figure 61.- Concluded.

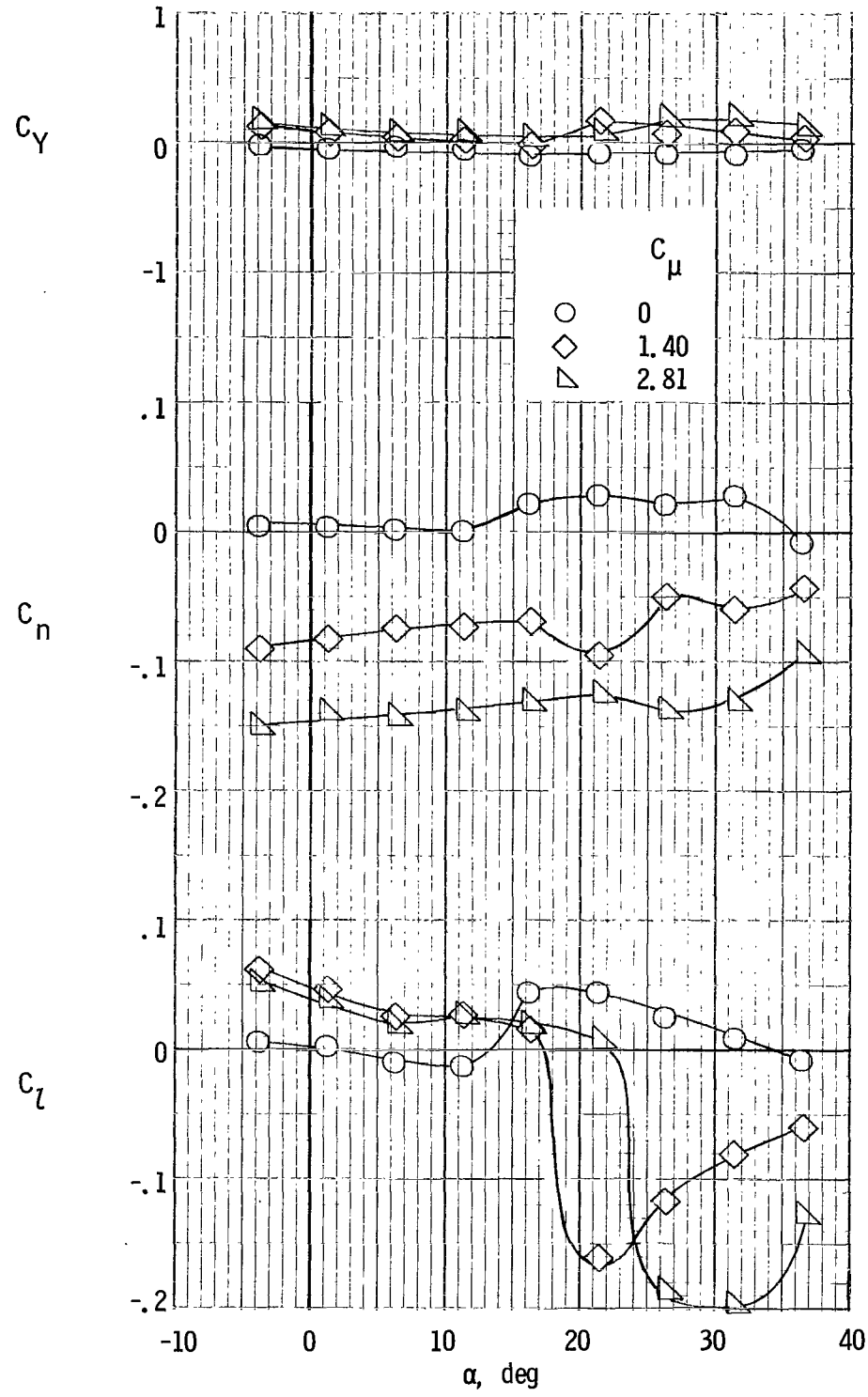

(a) Lateral characteristics. $\delta_f = 70^0$, left inboard; $\delta_f = 40^0$, right inboard; $C_{\mu,le} = 0$.

Figure 62.- Lateral and longitudinal characteristics of model with tail on and clustered engines. Left inboard engine not operating; differential deflection of inboard flap segments; $\delta_f = 60^0$, left and right center and outboard.

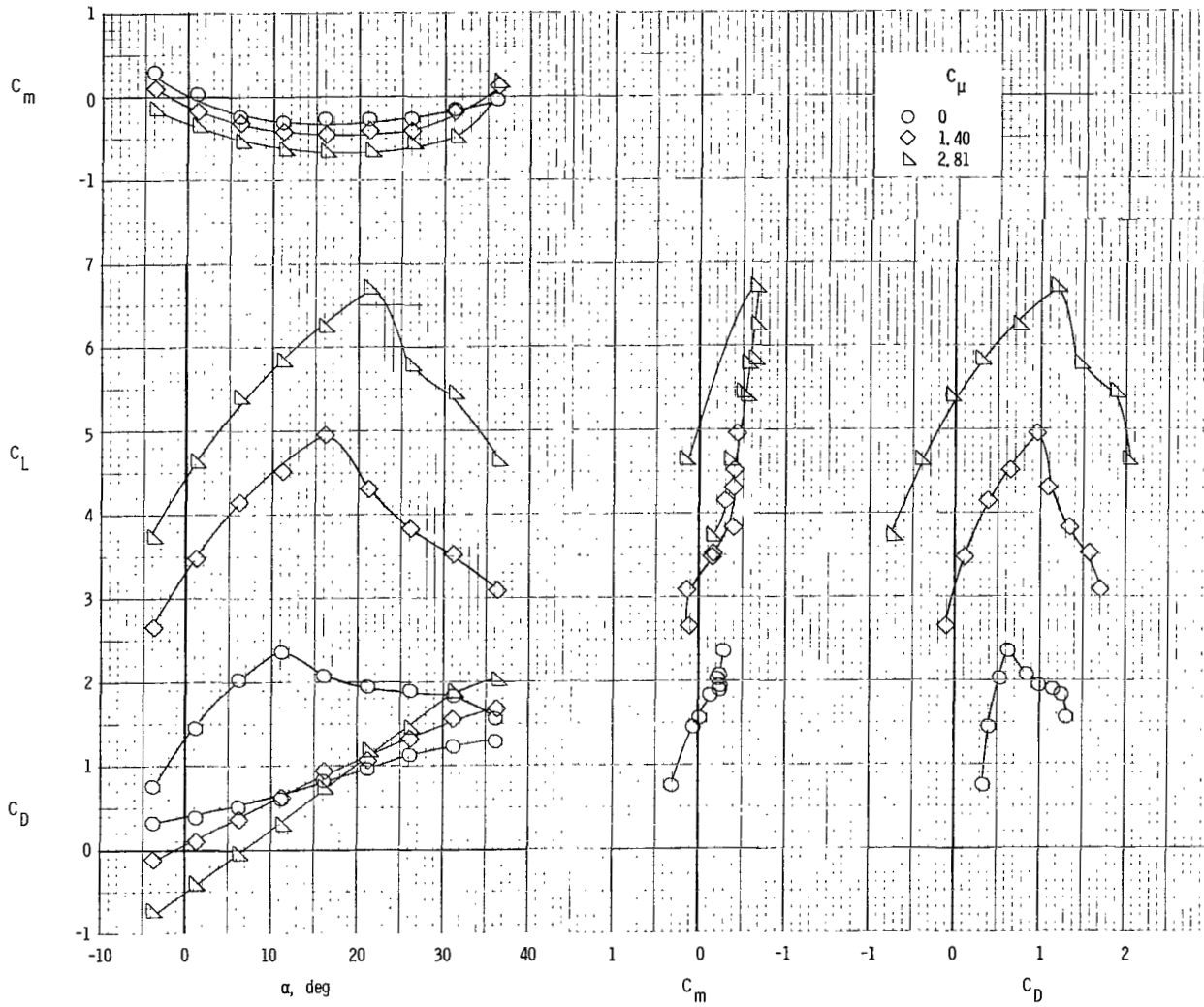

(b) Longitudinal characteristics. $\delta_f = 70^0$, left inboard; $\delta_f = 40^0$, right inboard; $C_{\mu,le} = 0$.

Figure 62.- Continued.

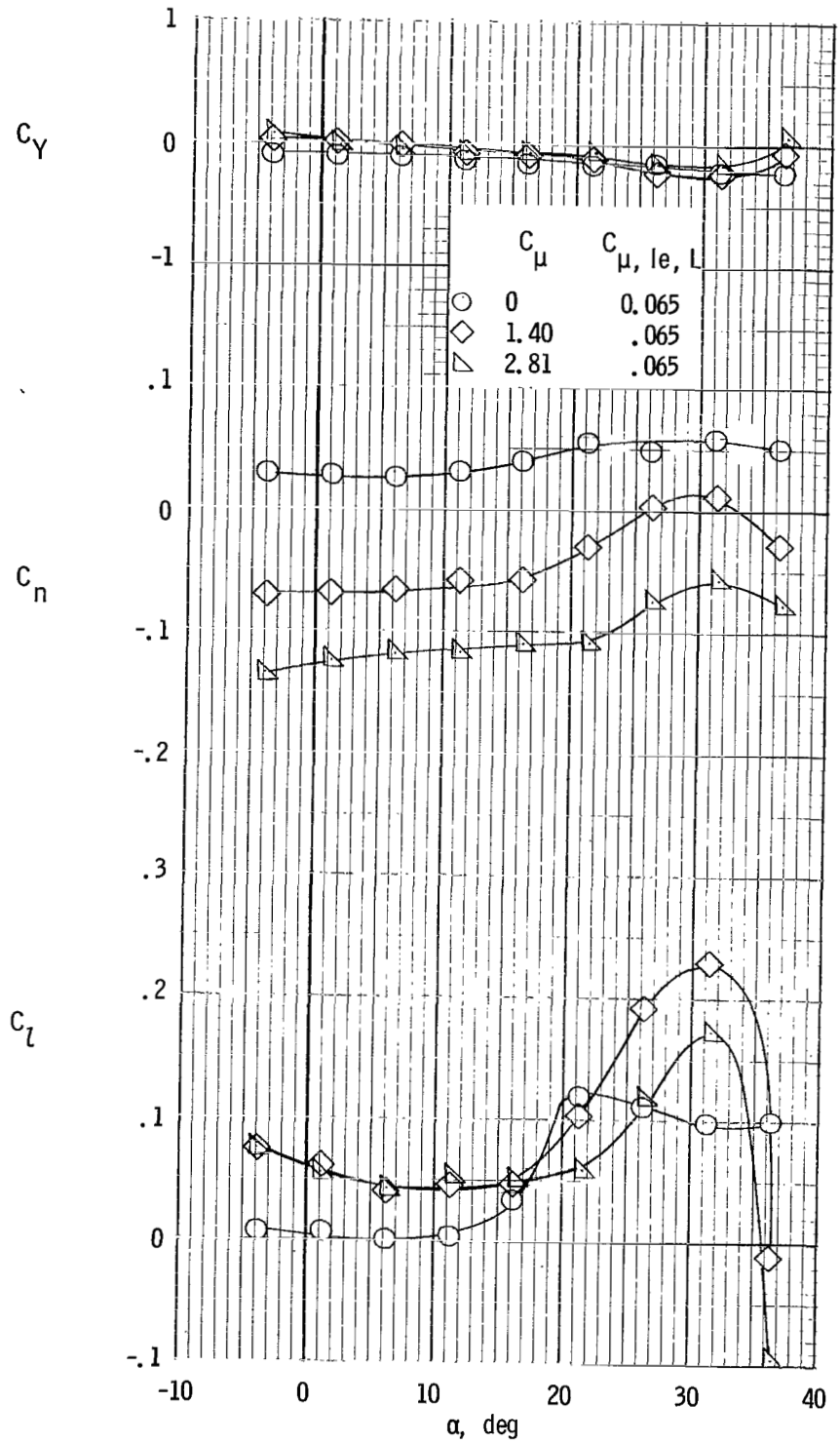

(c) Lateral characteristics. Leading-edge blowing; $\delta_f = 70^0$, left inboard; $\delta_f = 40^0$, right inboard.

Figure 62.- Continued.

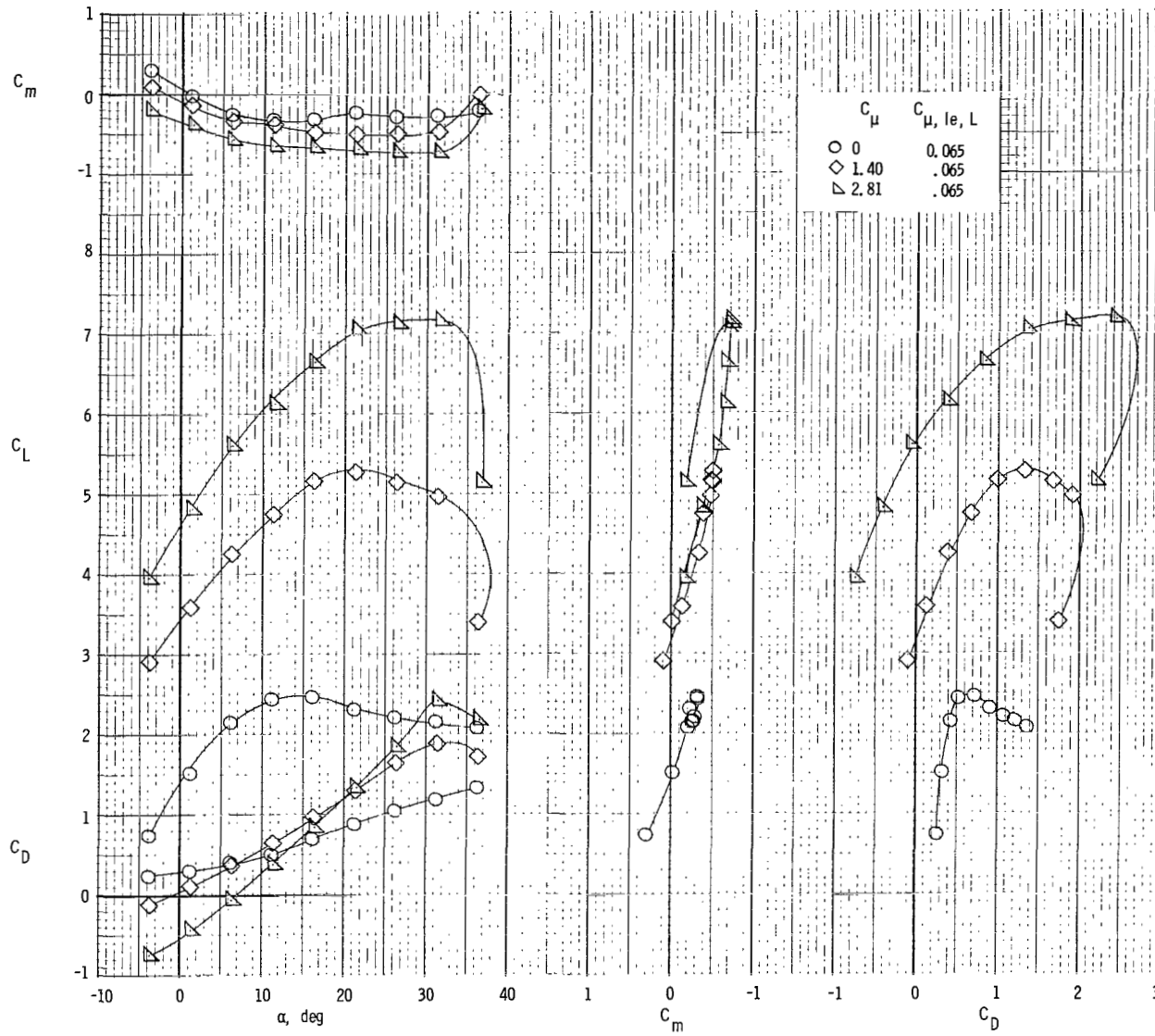

(d) Longitudinal characteristics. Leading-edge blowing; $\delta_f = 70^0$, left inboard; $\delta_f = 40^0$, right inboard.

Figure 62.- Concluded.

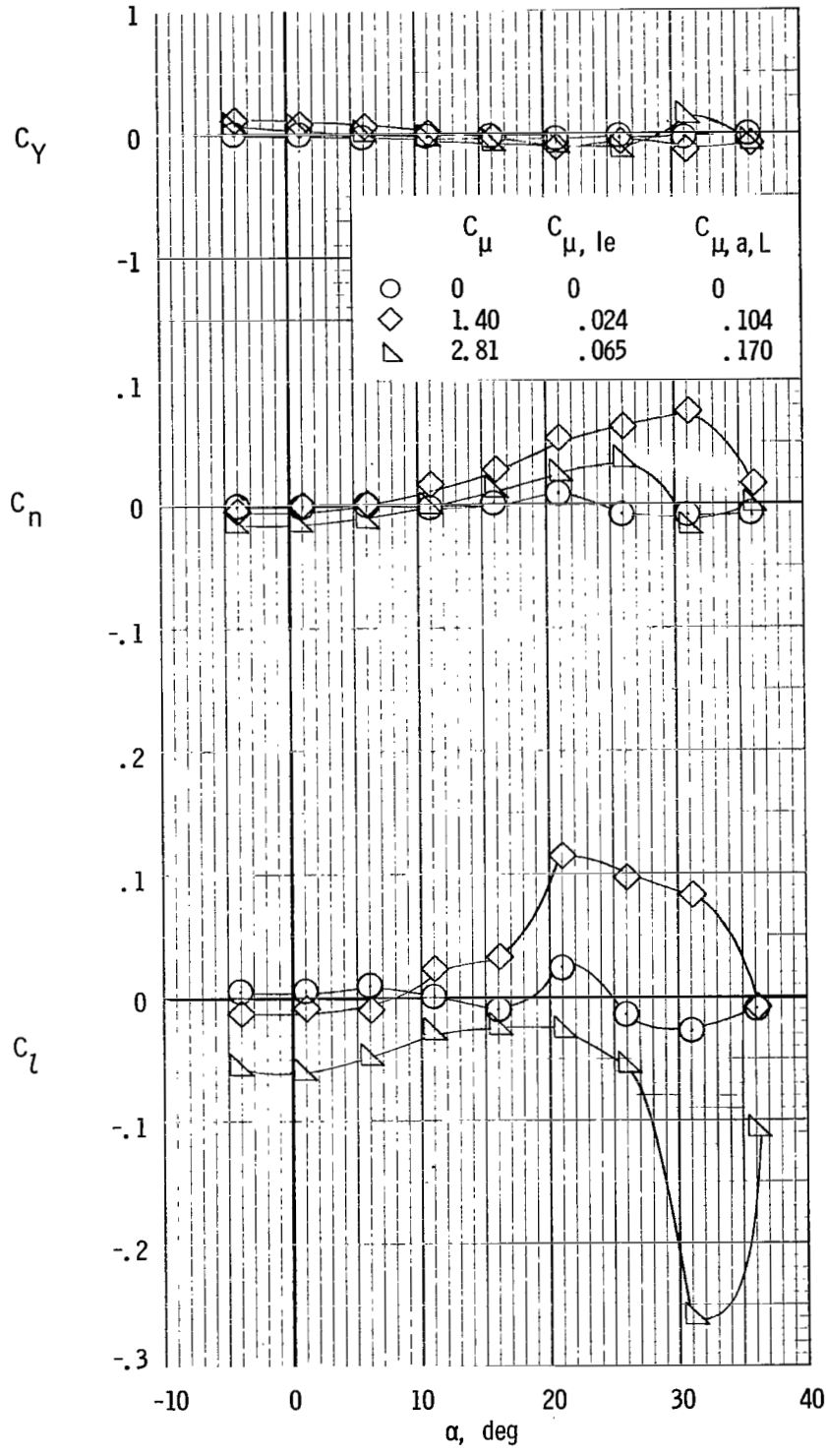

(a) Lateral characteristics.

Figure 63.- Lateral and longitudinal characteristics of model with tail off and clustered engines. Left outboard engine not operating; leading-edge and aileron blowing; $\delta_f = 60^0$.

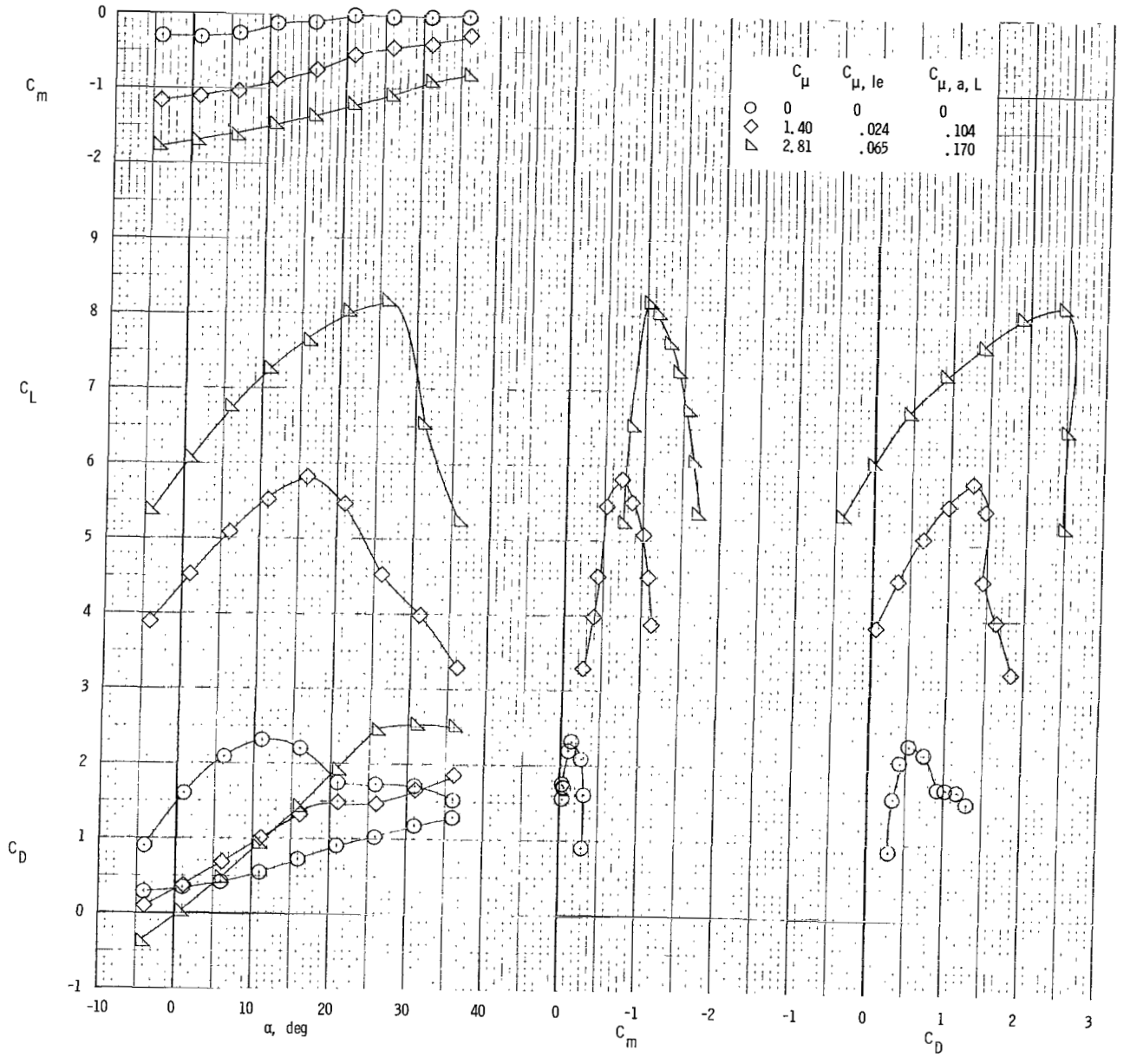

(b) Longitudinal characteristics.

Figure 63.- Concluded.

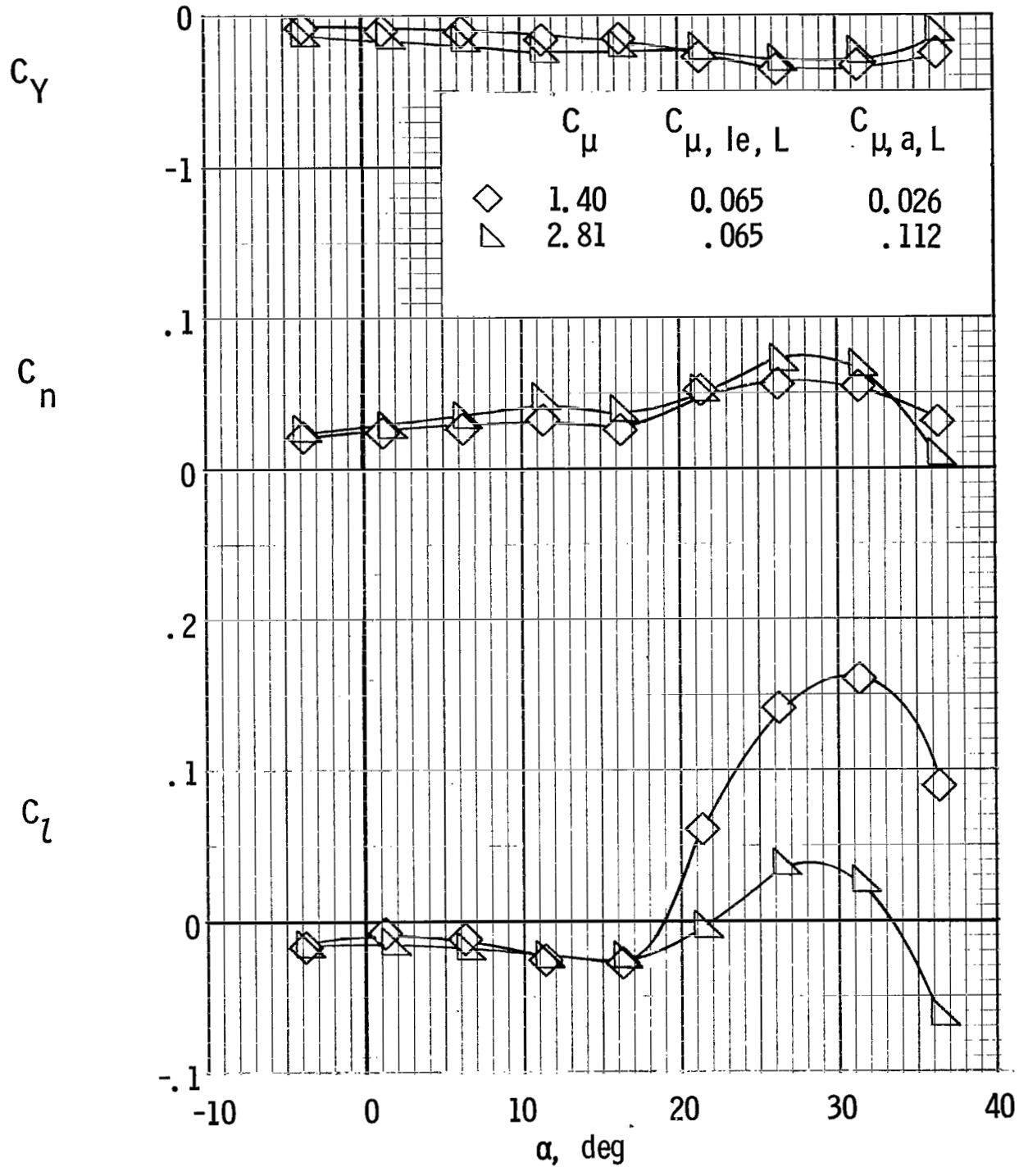

(a) Lateral characteristics.

Figure 64.- Lateral and longitudinal characteristics of model with tail on and clustered engines. Left outboard engine not operating; leading-edge and aileron blowing; $\delta_f = 60^0$; $\delta_s = 40^0$, right wing tip.

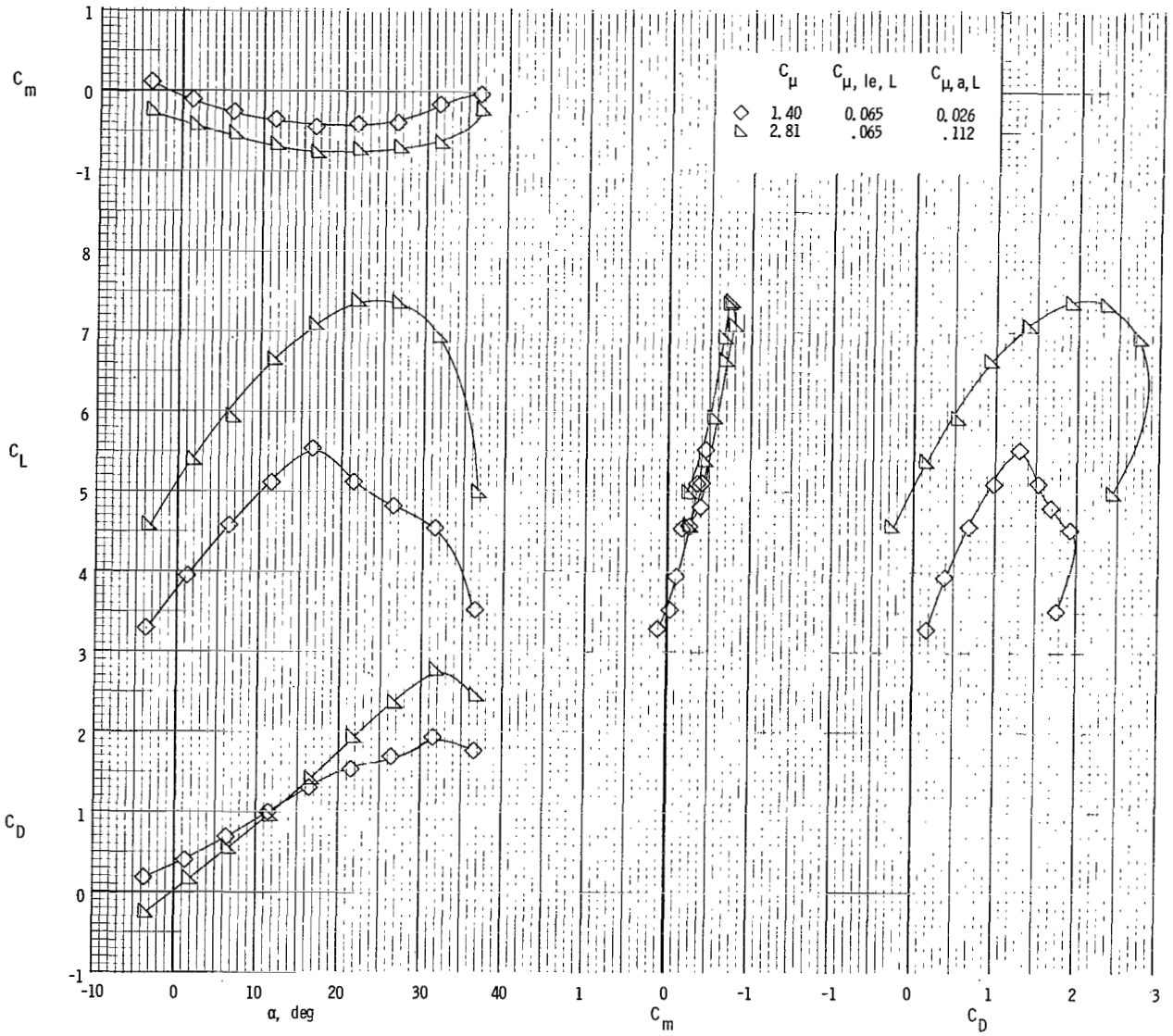

(b) Longitudinal characteristics.

Figure 64.- Concluded.

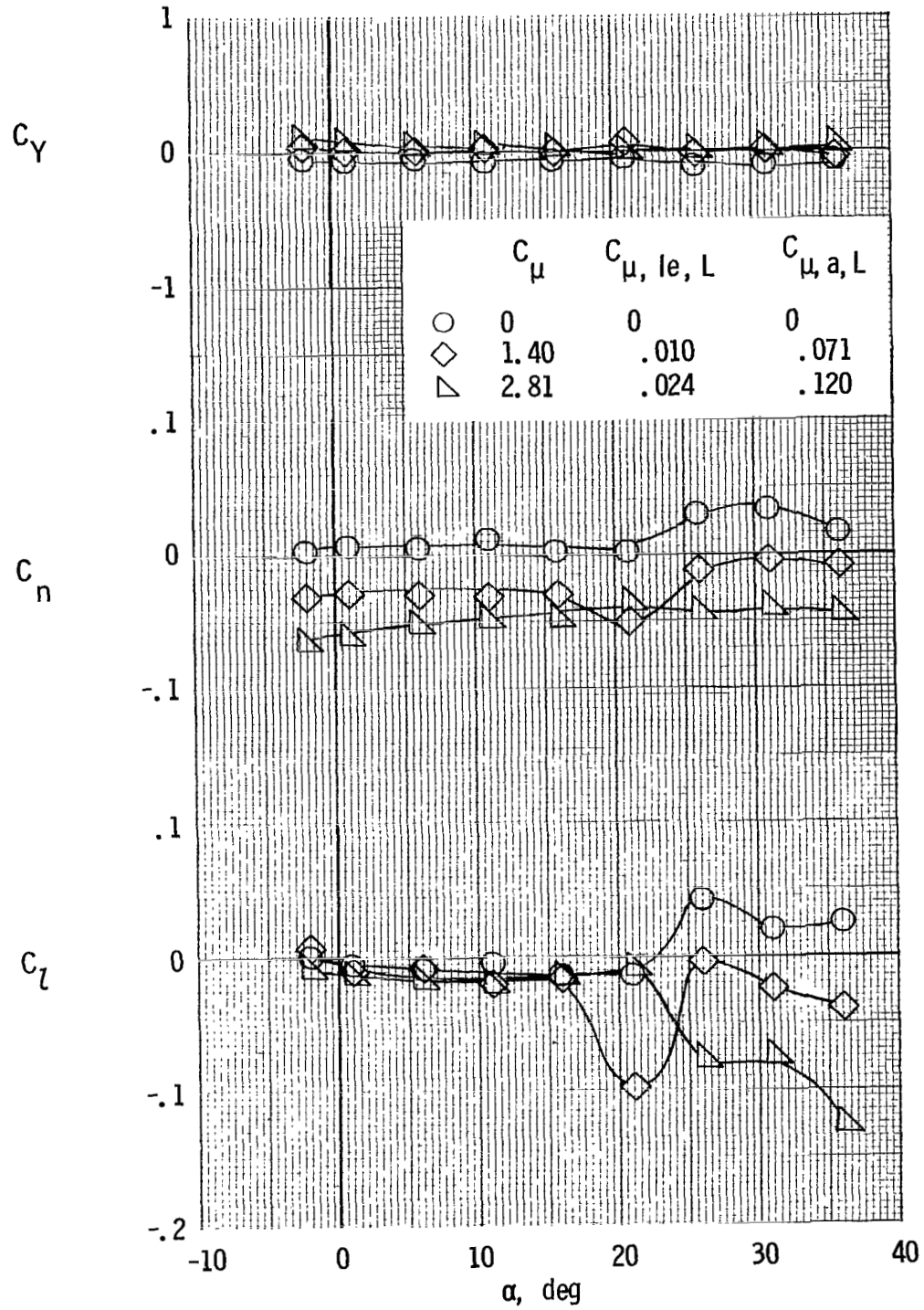

(a) Lateral characteristics.

Figure 65.- Lateral and longitudinal characteristics of model with tail on and clustered engines. Left outboard engine not operating; leading-edge and aileron blowing; $\delta_f = 40^o$.

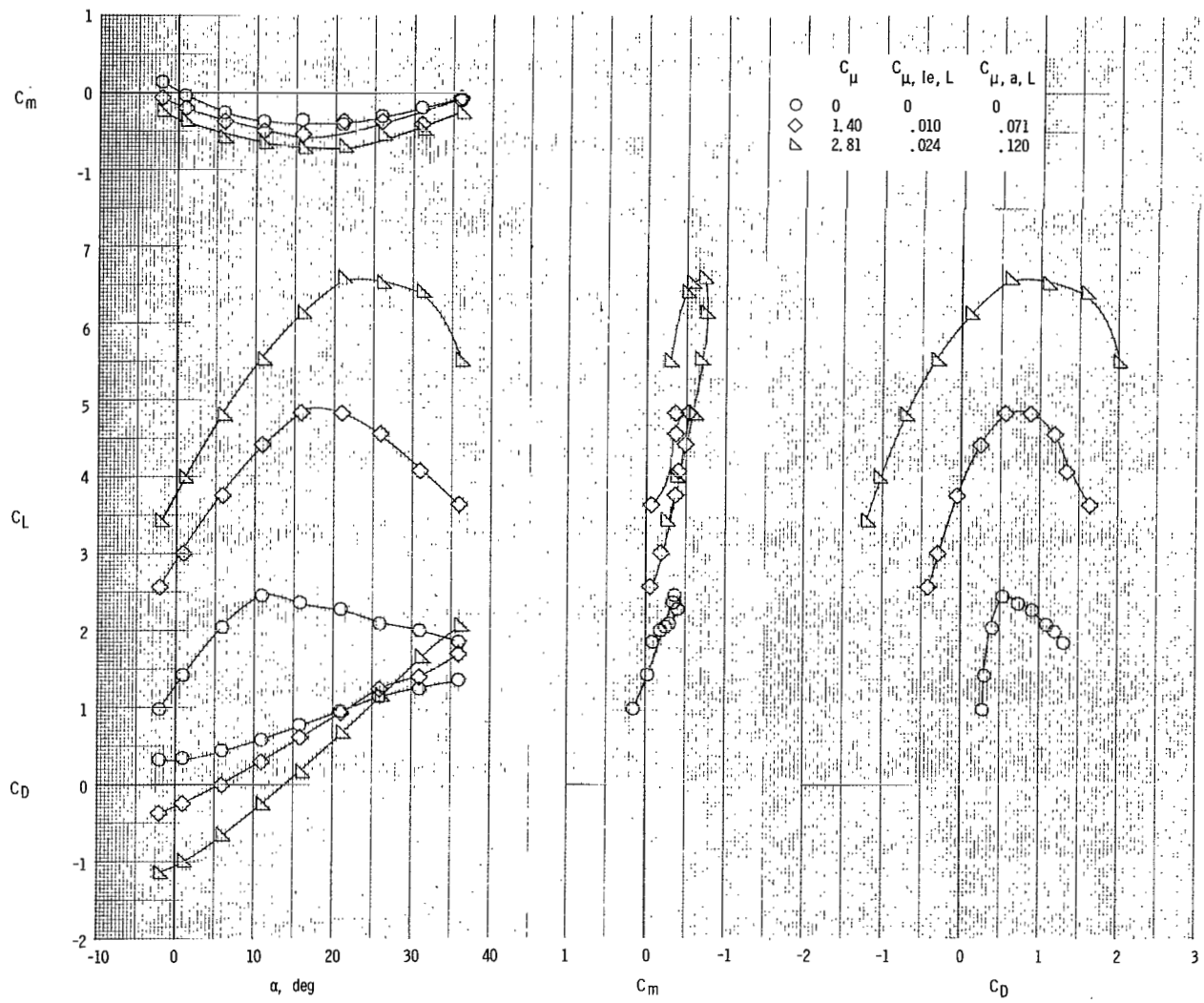

(b) Longitudinal characteristics.

Figure 65.- Concluded.

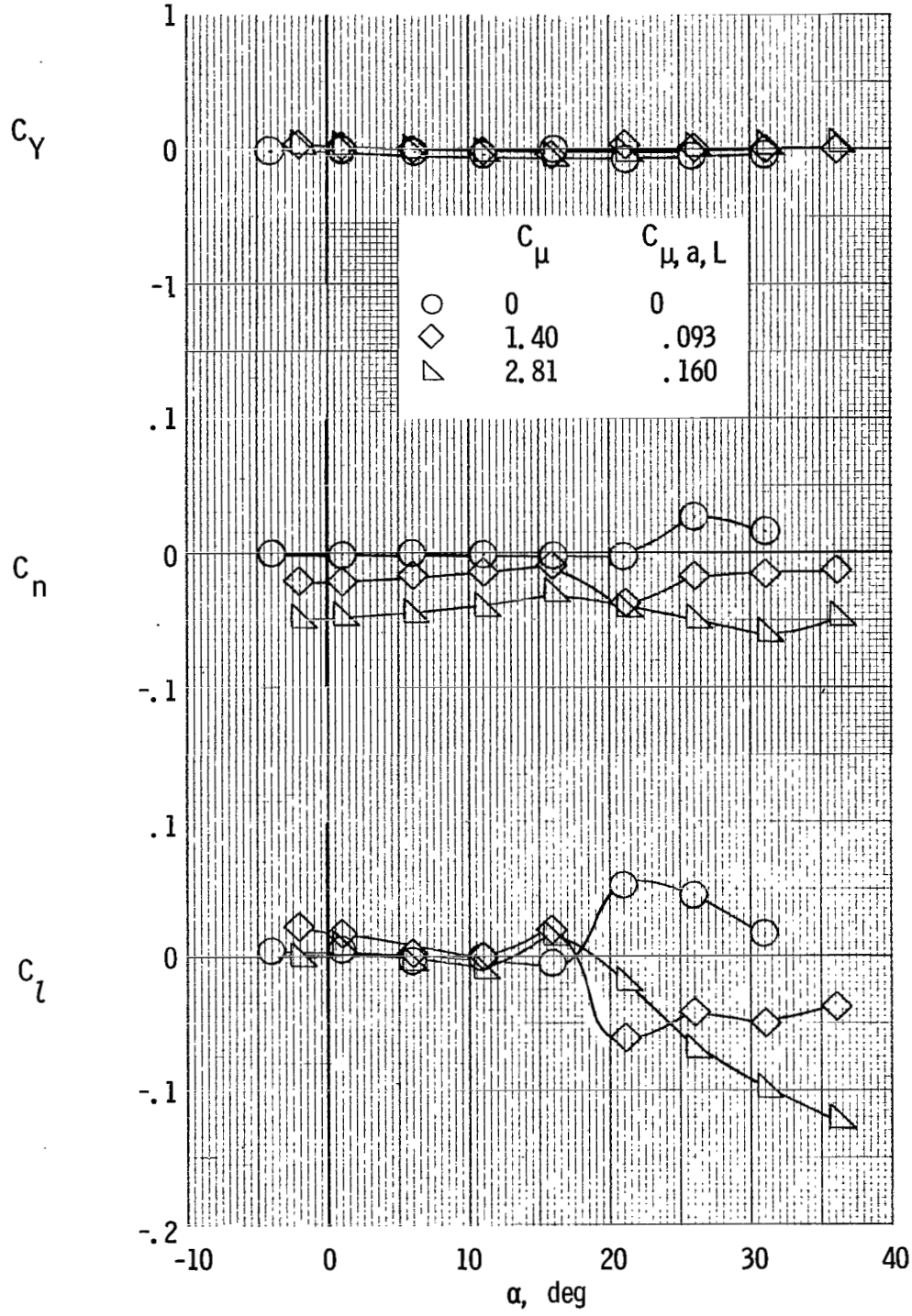

(a) Lateral characteristics.

Figure 66.- Lateral and longitudinal characteristics of model with tail off and clustered engines. Left outboard engine not operating; aileron blowing; $\delta_f = 35^0$; $C_{\mu,le} = 0$.

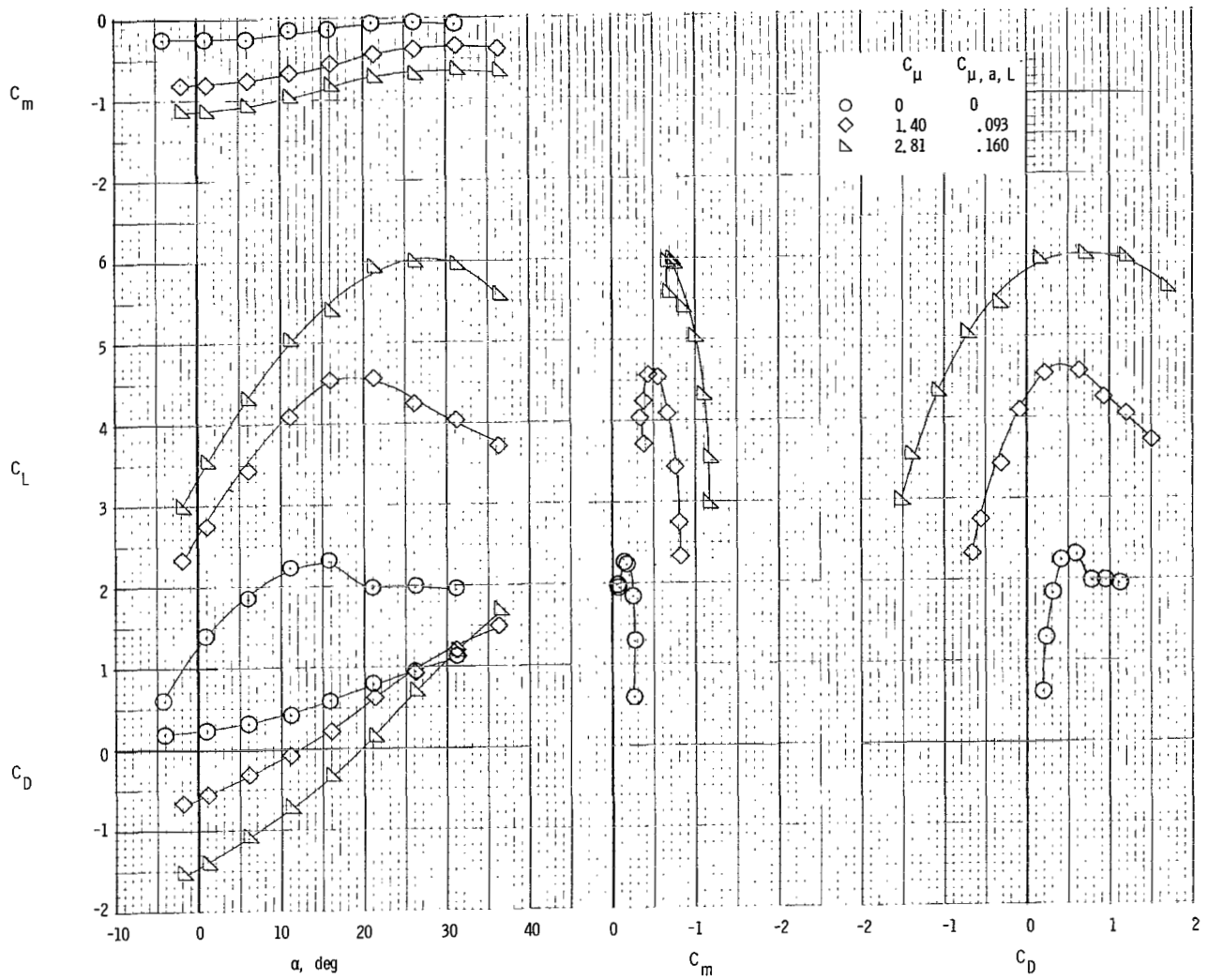

(b) Longitudinal characteristics.

Figure 66.- Concluded.

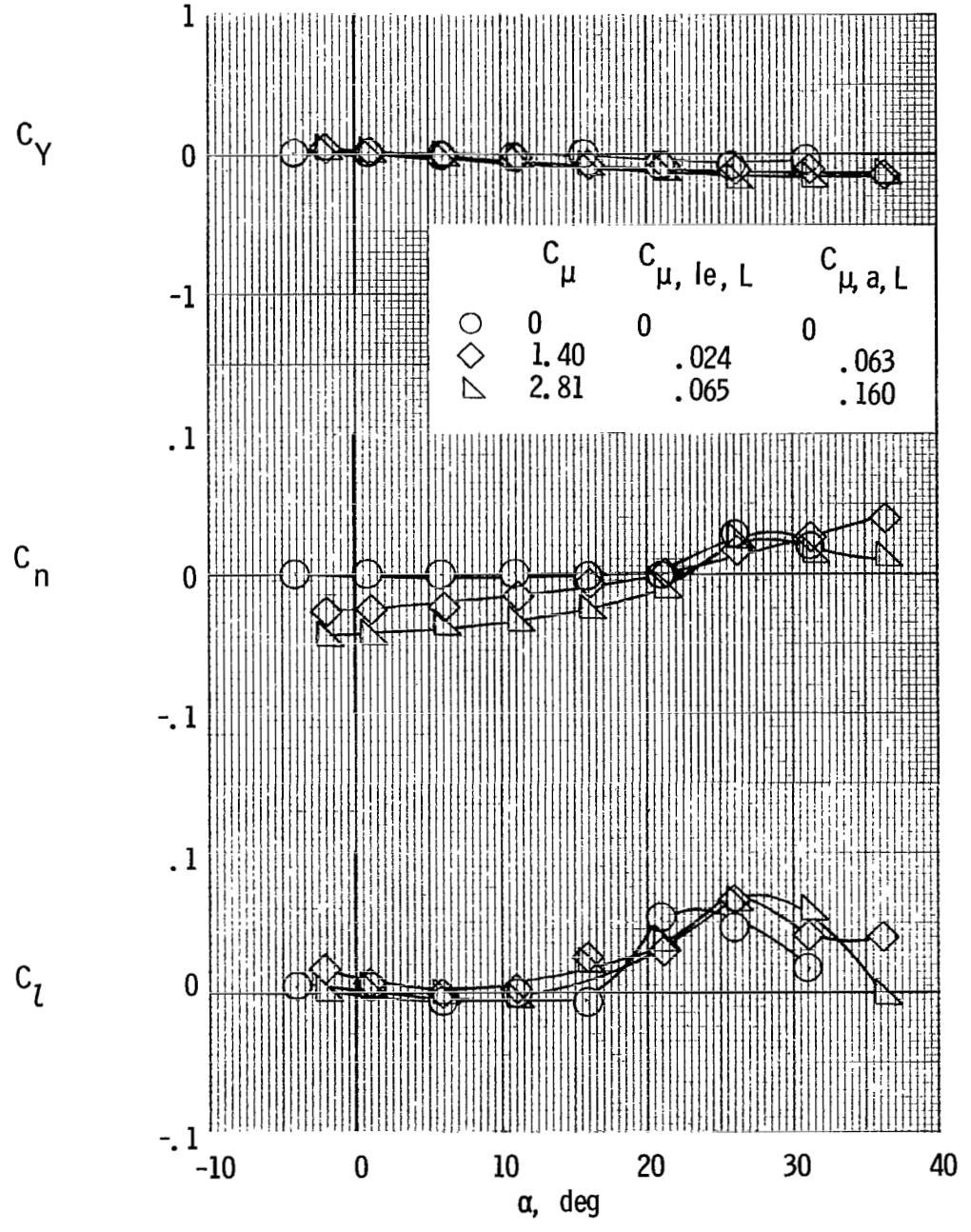

(a) Lateral characteristics. Left outboard engine not operating.

Figure 67.- Lateral and longitudinal characteristics of model with tail off and clustered engines. One left engine not operating; leading-edge and aileron blowing; $\delta_f = 35^0$.

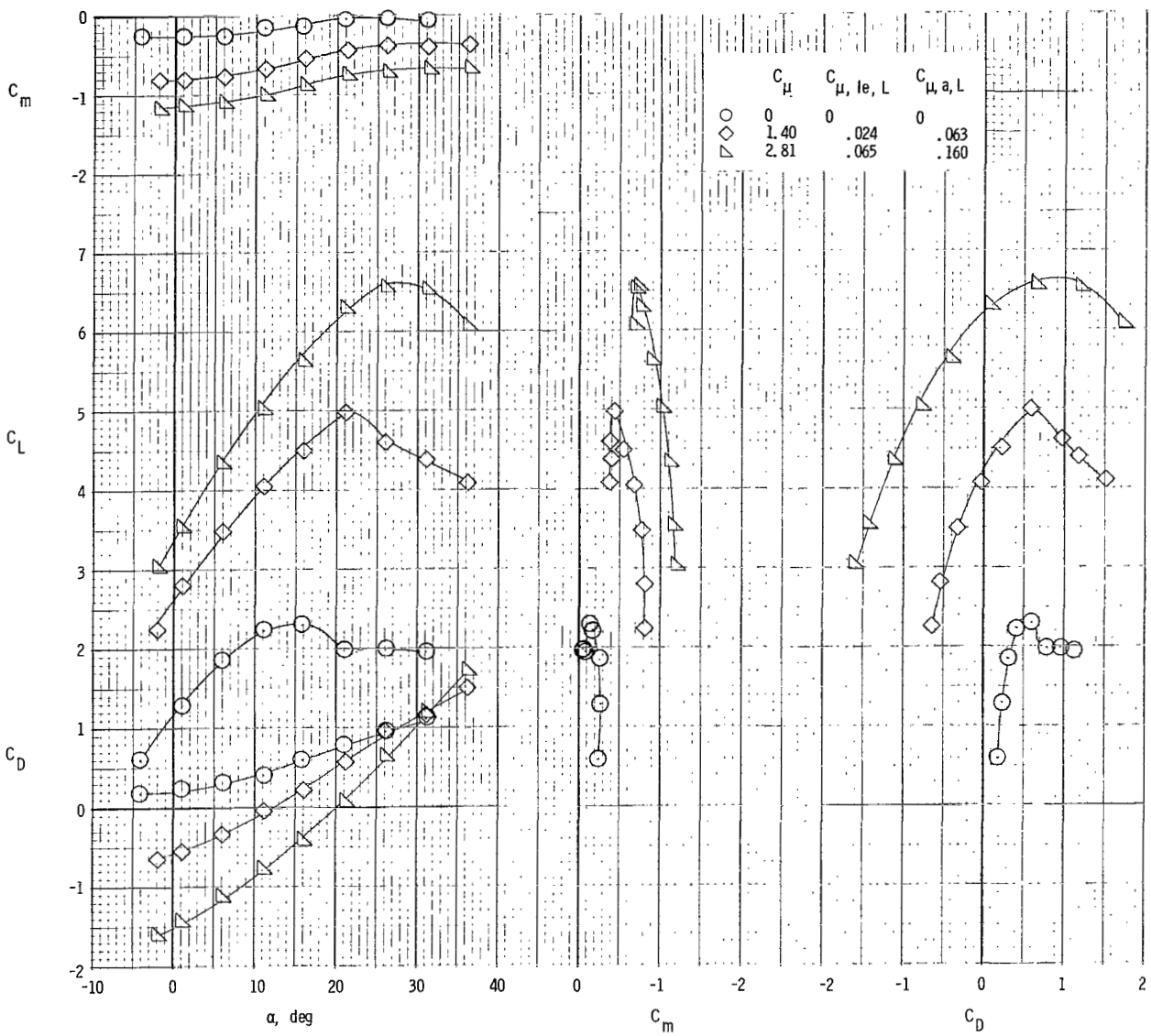

(b) Longitudinal characteristics. Left outboard engine not operating.

Figure 67.- Continued.

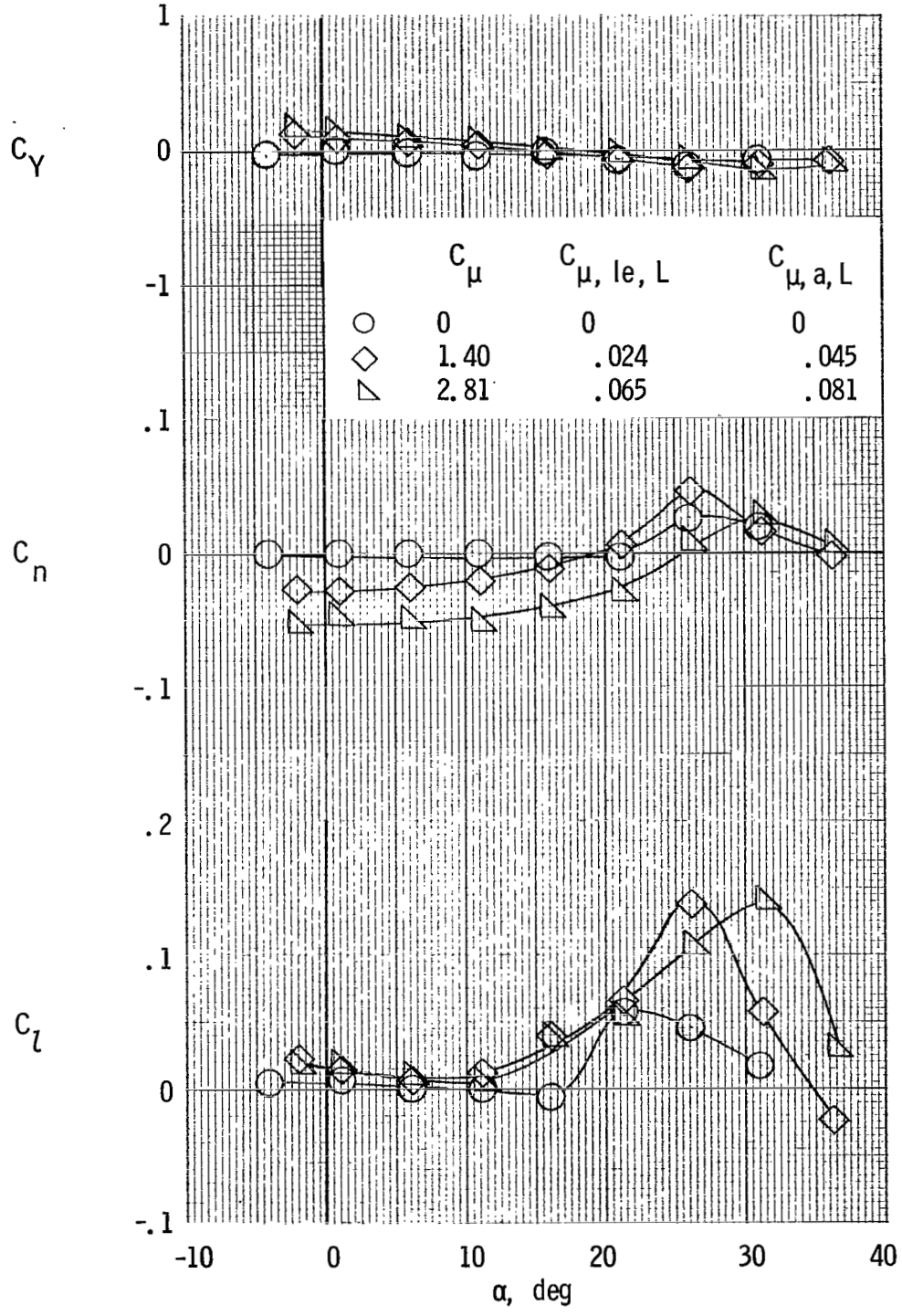

(c) Lateral characteristics. Left inboard engine not operating.

Figure 67.- Continued.

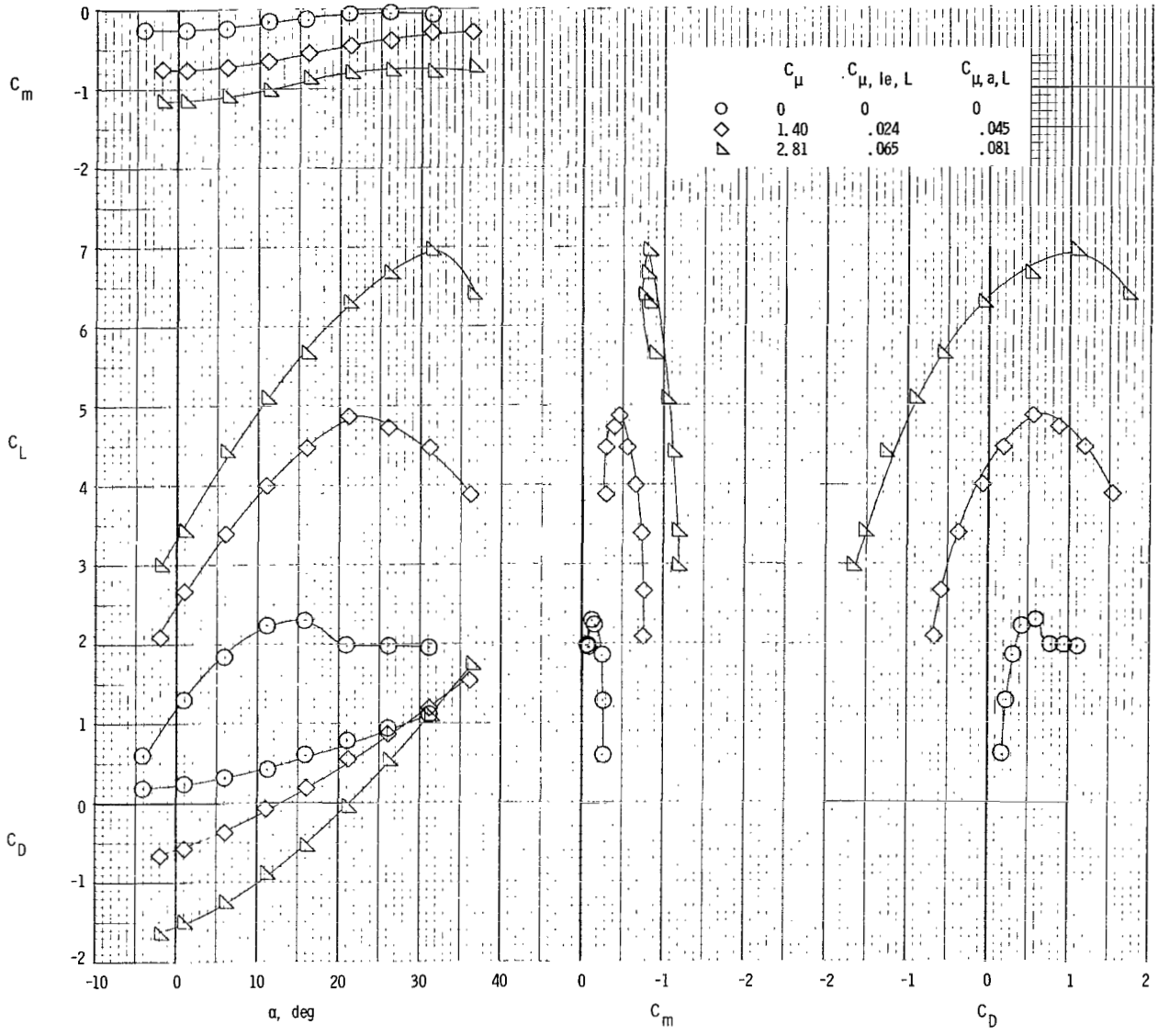

(d) Longitudinal characteristics. Left inboard engine not operating.

Figure 67.- Concluded.

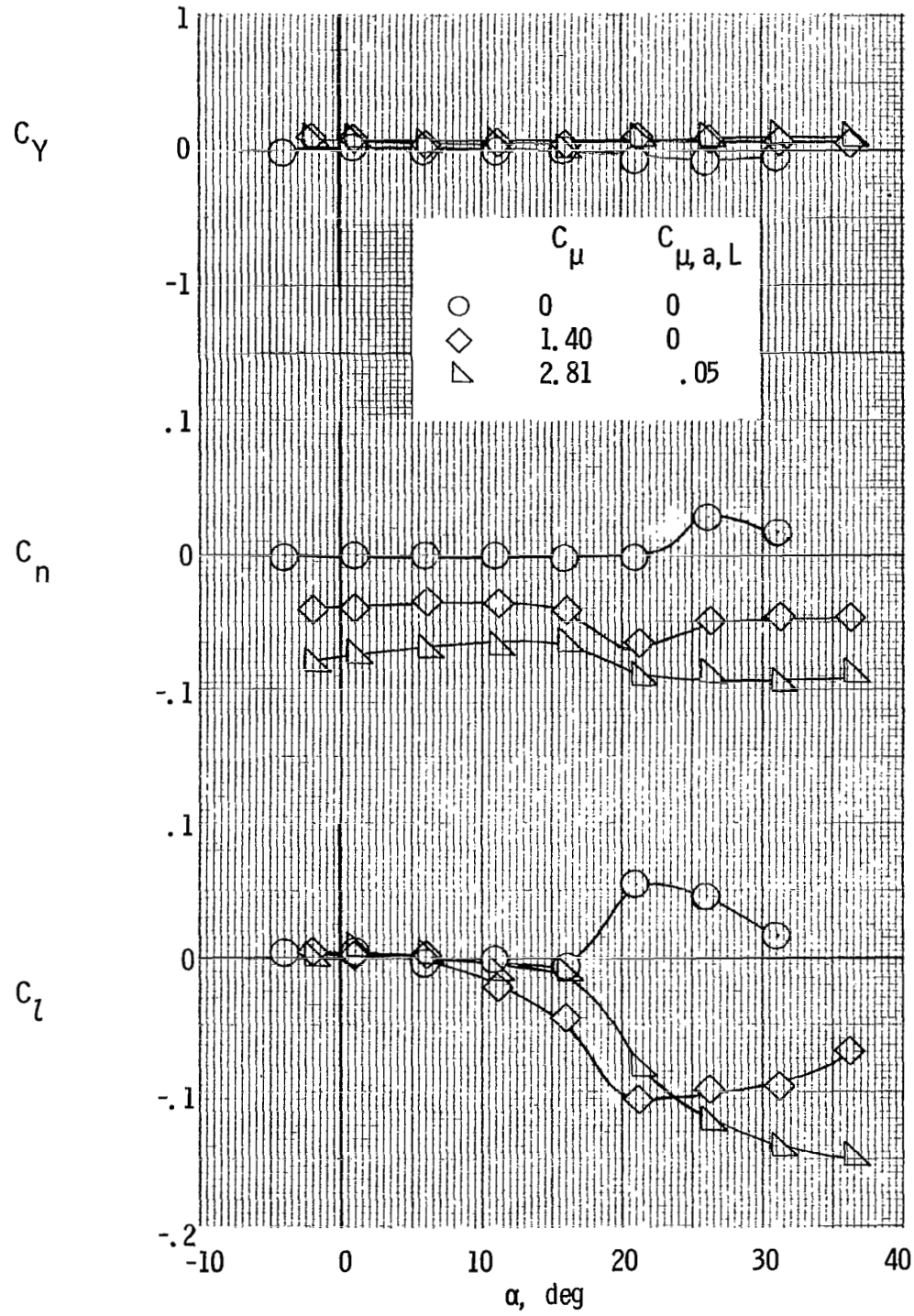

(a) Lateral characteristics.

Figure 68.- Lateral and longitudinal characteristics of model with tail off and clustered engines. Left outboard engine not operating; aileron blowing; $\delta_f = 35^0$; $\delta_s = 40^0$, right wing tip; $C_{\mu,le} = 0$.

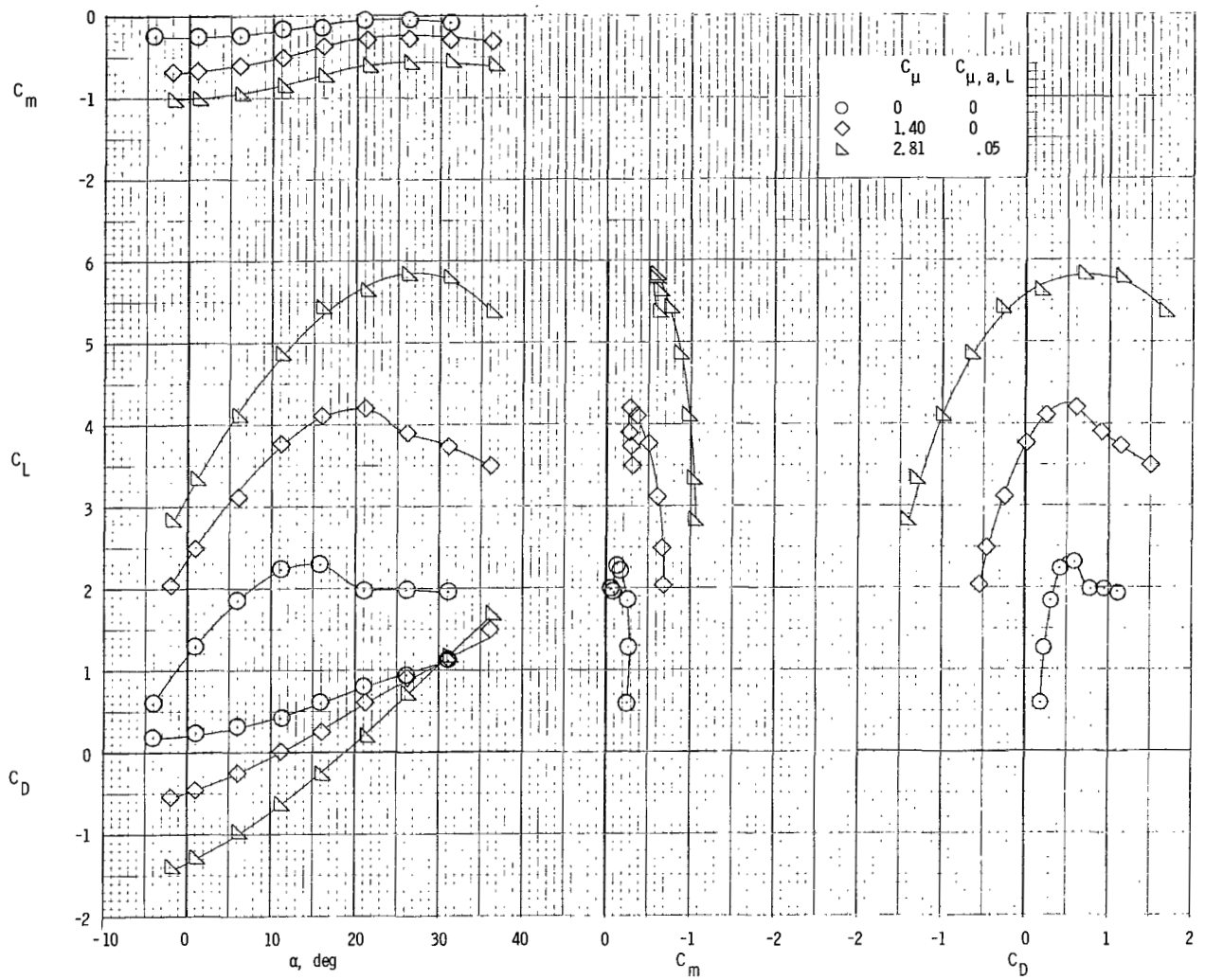

(b) Longitudinal characteristics.

Figure 68.- Concluded.

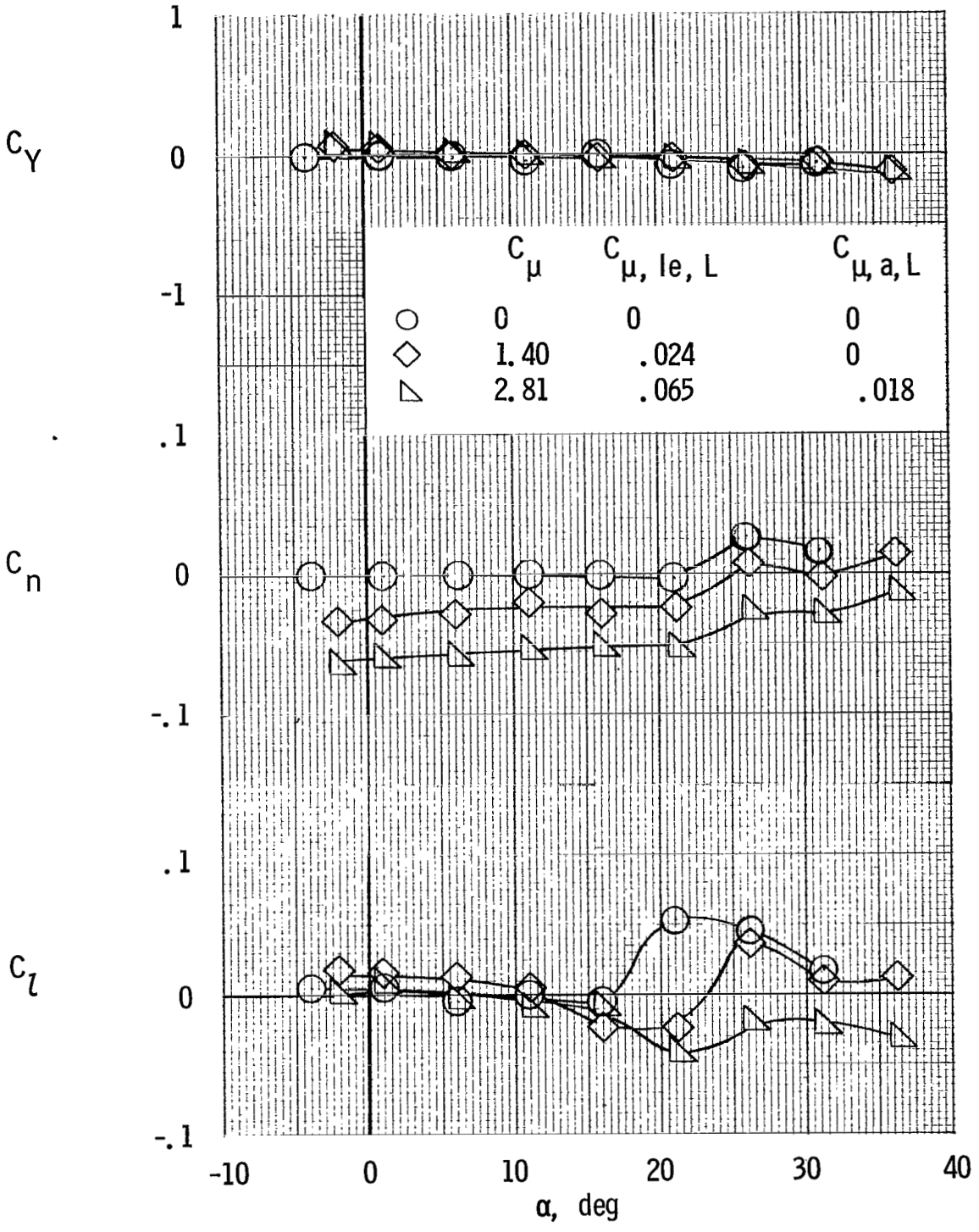

(a) Lateral characteristics. Left outboard engine not operating.

Figure 69.- Lateral and longitudinal characteristics of model with tail off and clustered engines. One left engine not operating; leading-edge and aileron blowing; $\delta_f = 35^o$; $\delta_s = 40^o$, right wing tip.

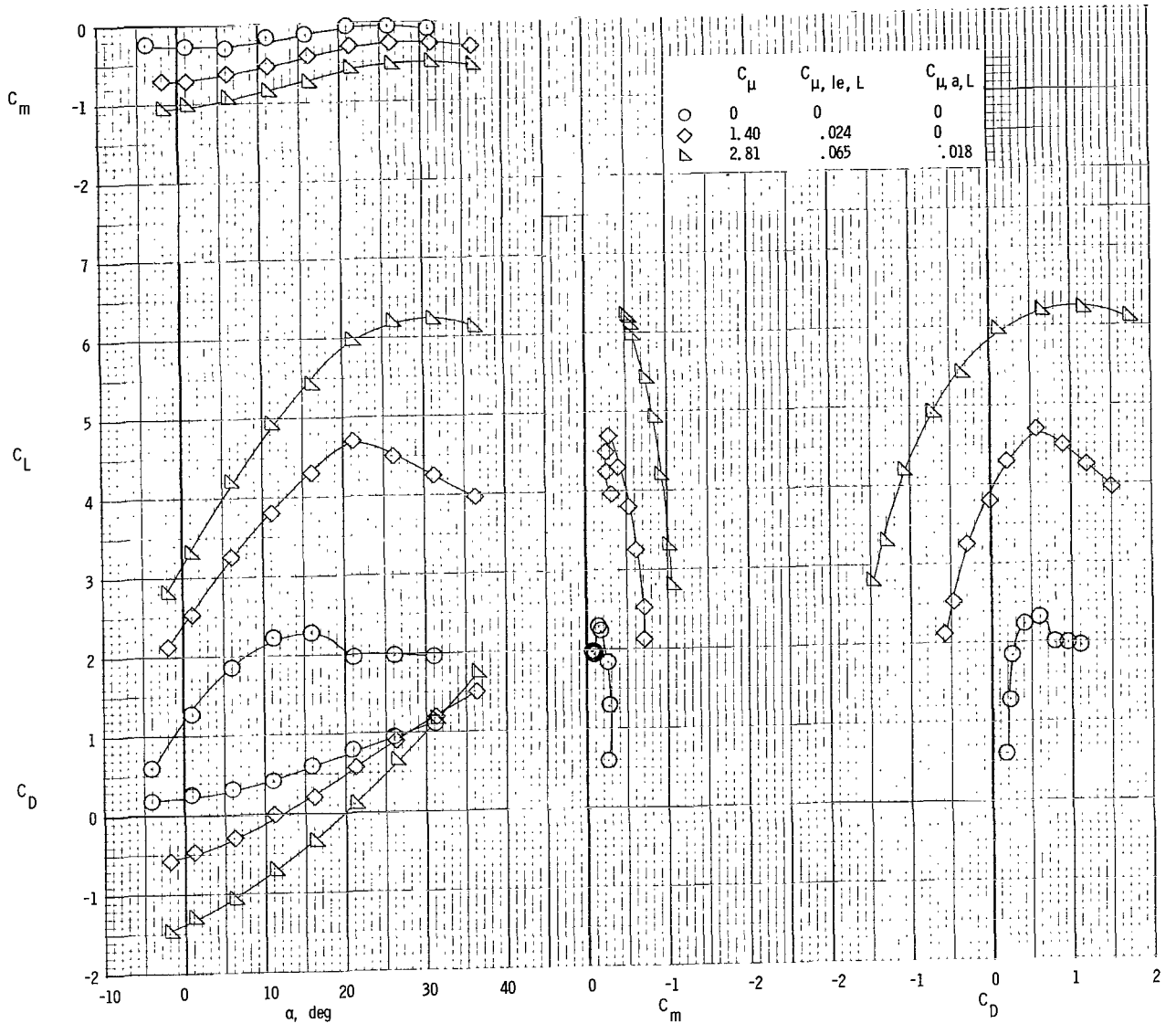

(b) Longitudinal characteristics. Left outboard engine not operating.

Figure 69.- Continued.

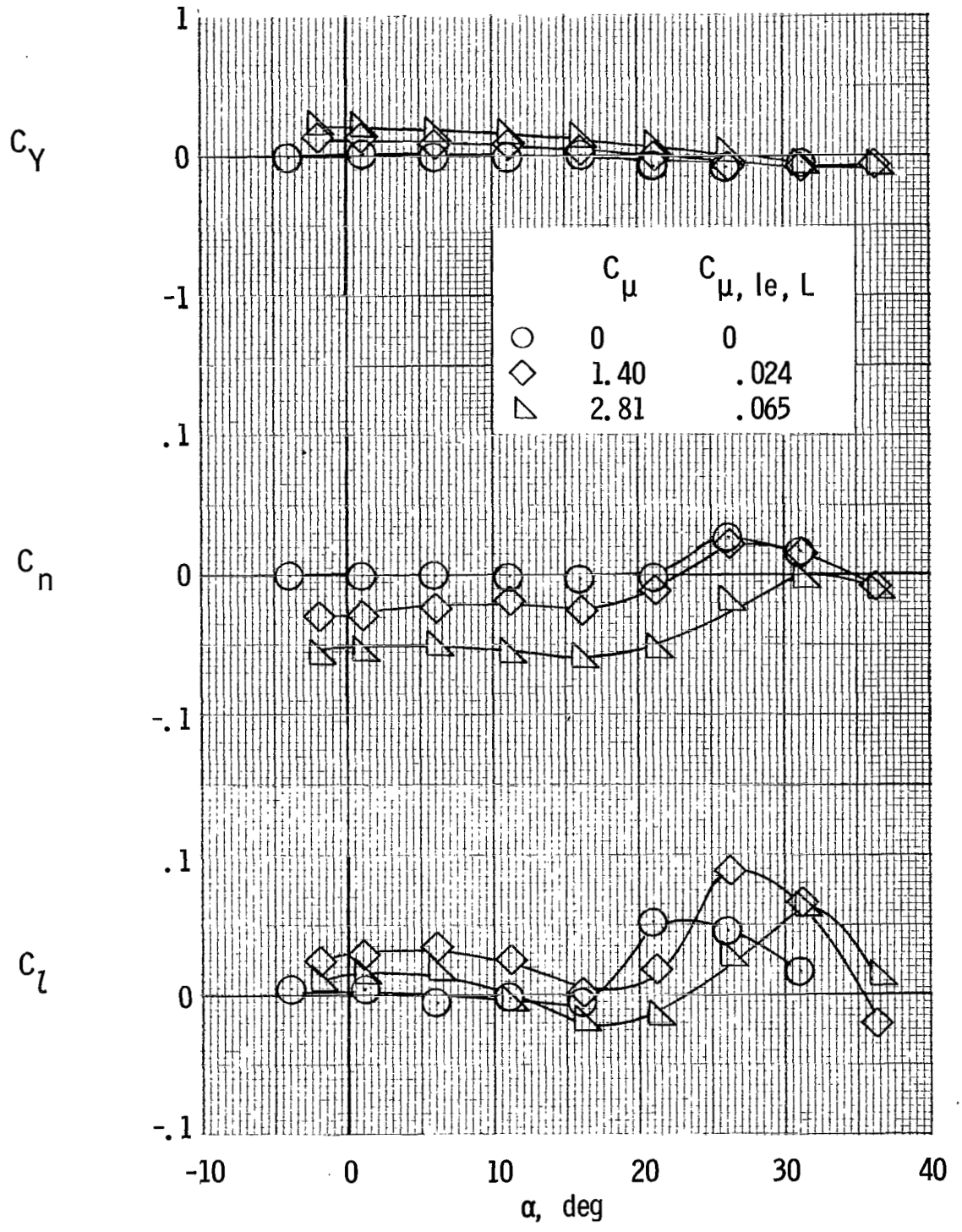

(c) Lateral characteristics. Left inboard engine not operating; $C_{\mu,a} = 0$.

Figure 69.- Continued.

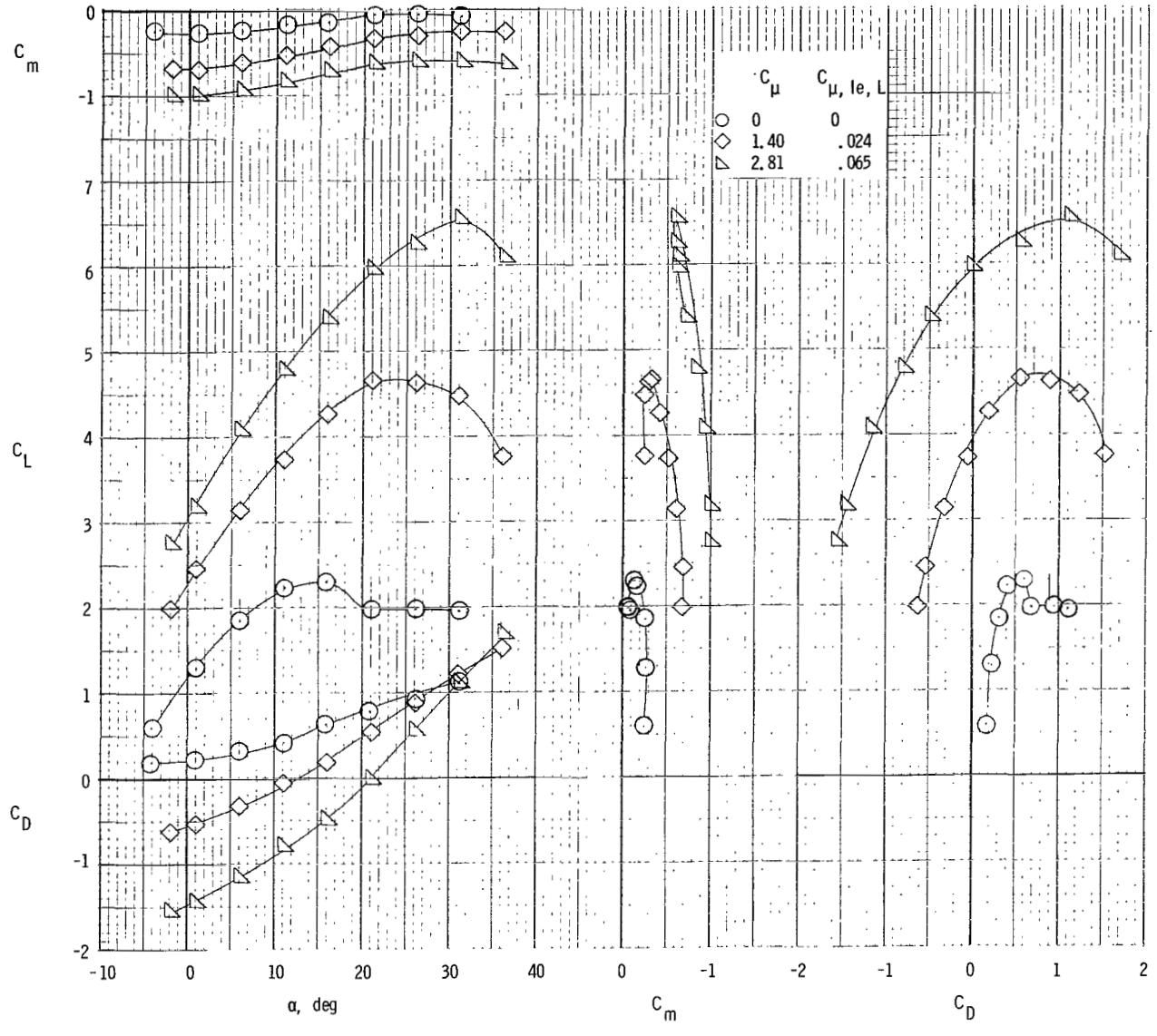

(d) Longitudinal characteristics. Left inboard engine not operating; $C_{\mu,a} = 0$.

Figure 69.- Concluded.

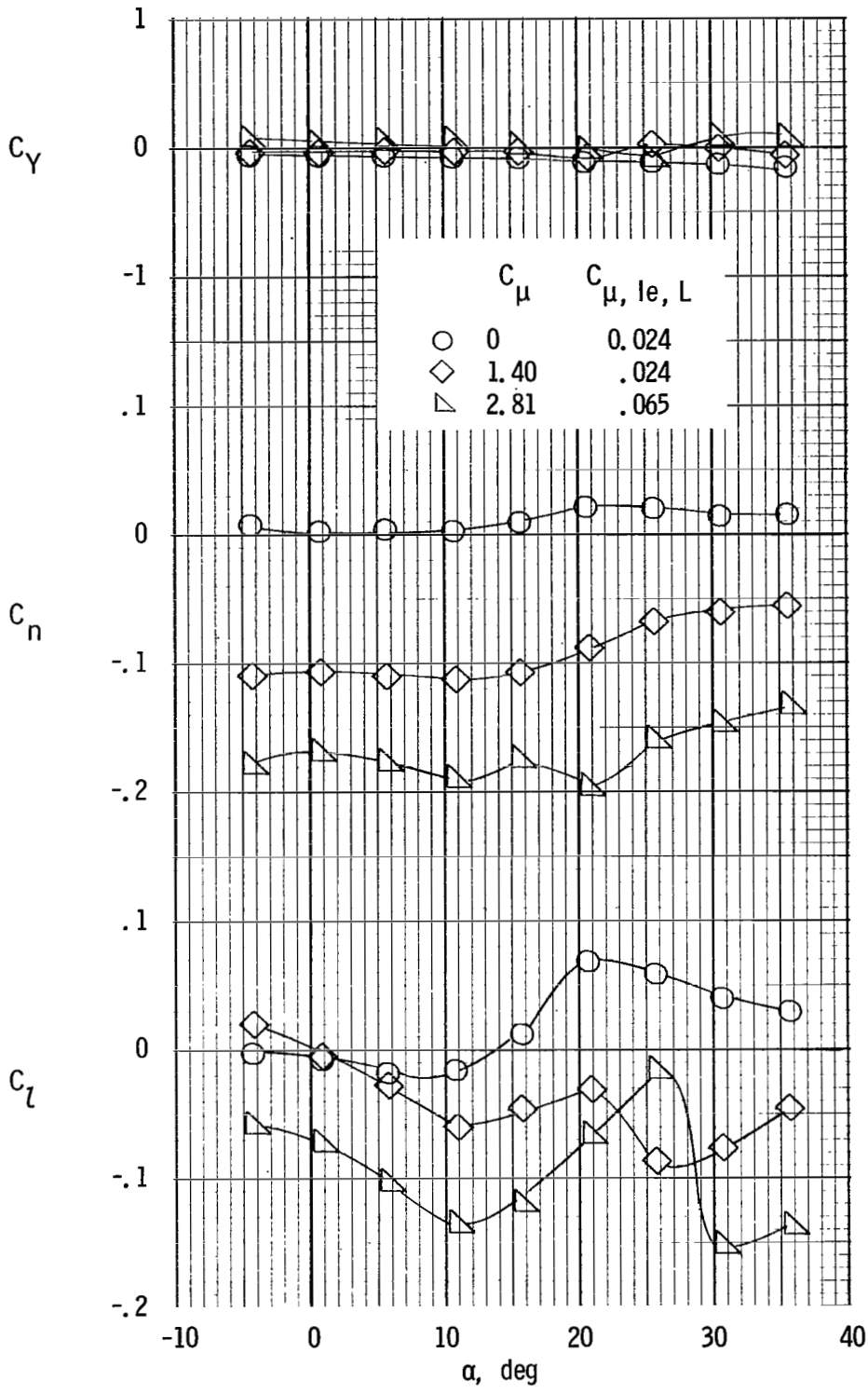

(a) Lateral characteristics. Left outboard engine not operating.

Figure 70.- Lateral and longitudinal characteristics of model with tail on and spread engines. One left engine not operating; leading-edge blowing; differential flap deflection; $\delta_{f,L} = 80^0$; $\delta_{f,R} = 40^0$.

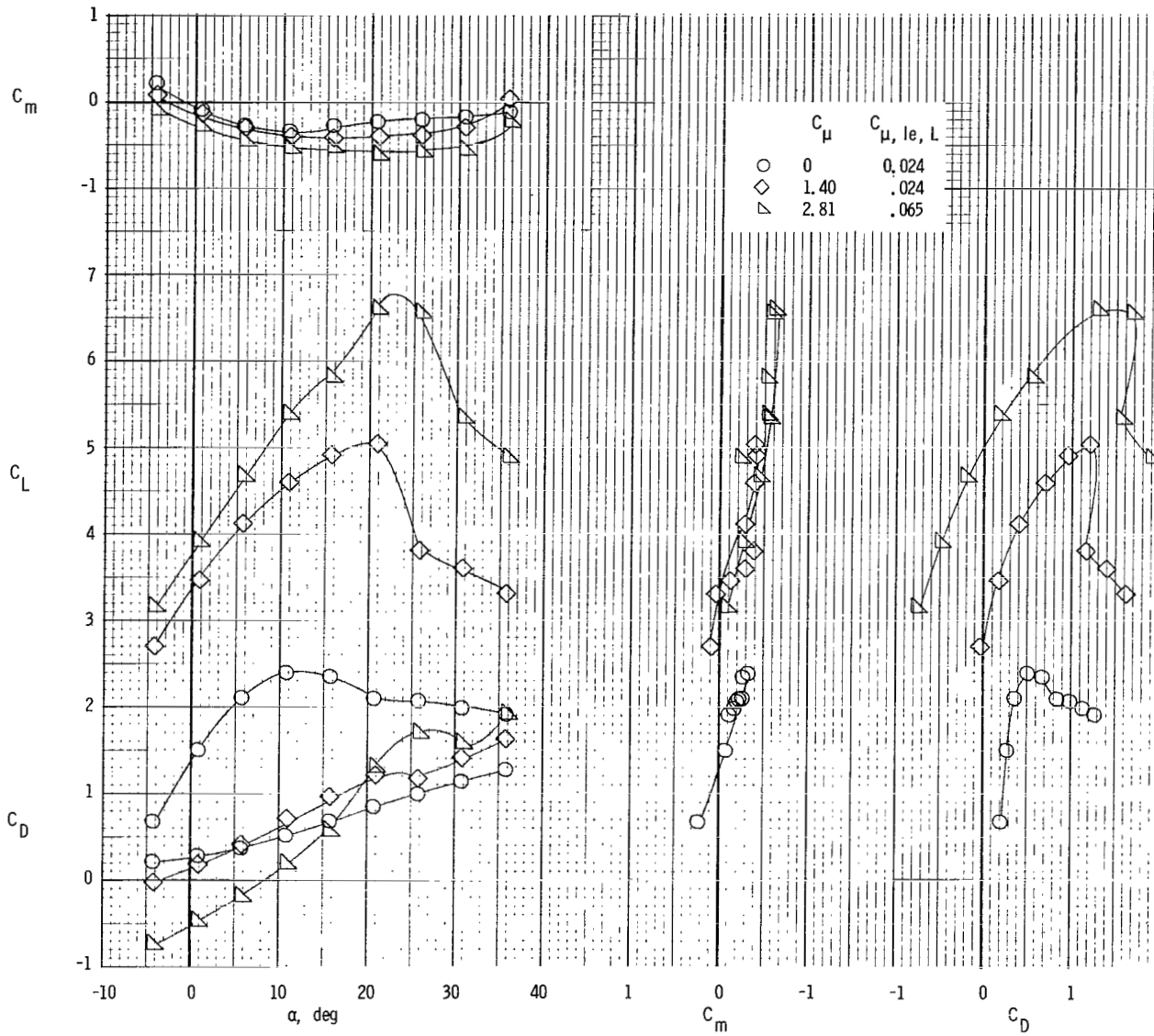

(b) Longitudinal characteristics. Left outboard engine not operating.

Figure 70.- Continued.

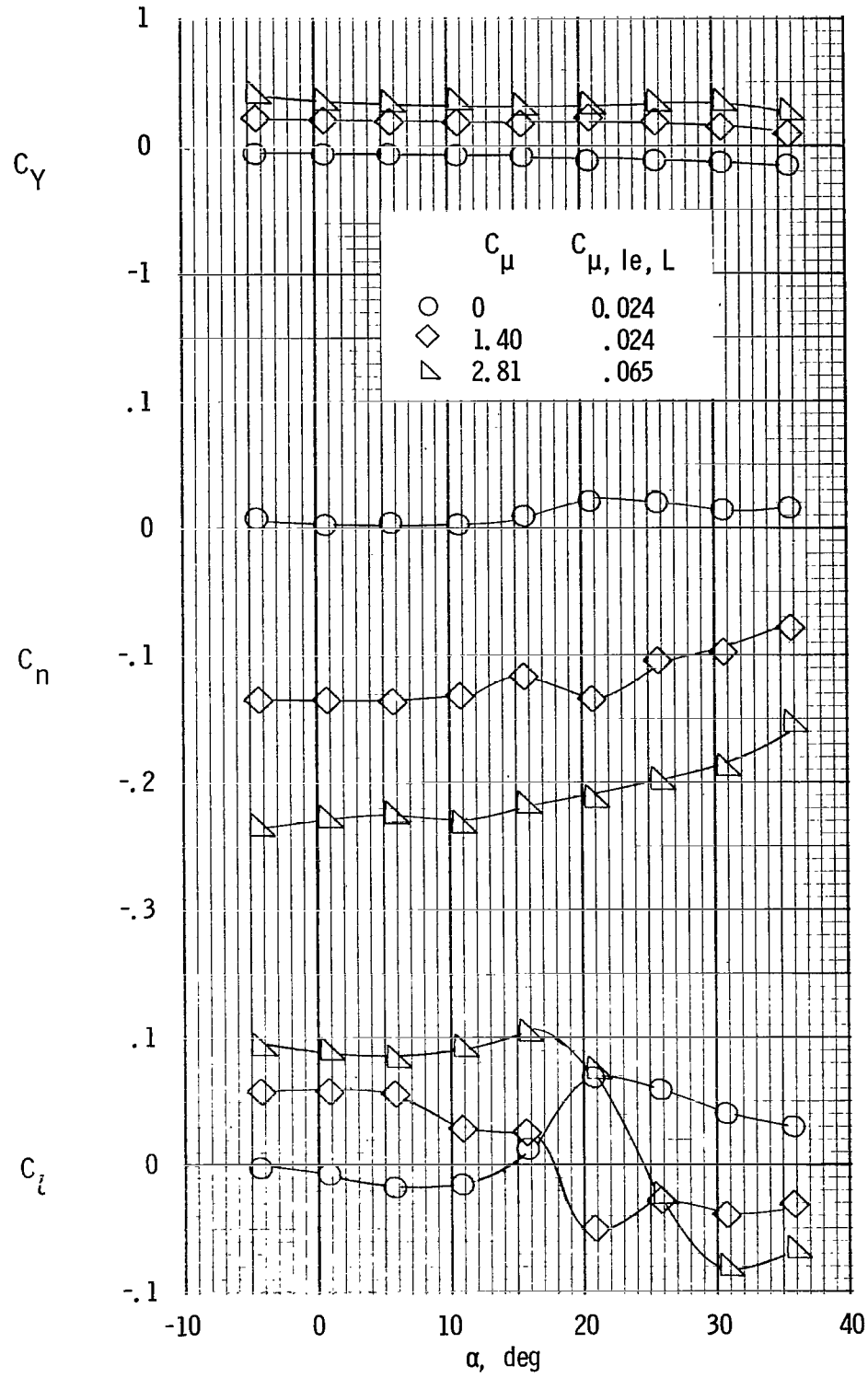

(c) Lateral characteristics. Left inboard engine not operating.

Figure 70.- Continued.

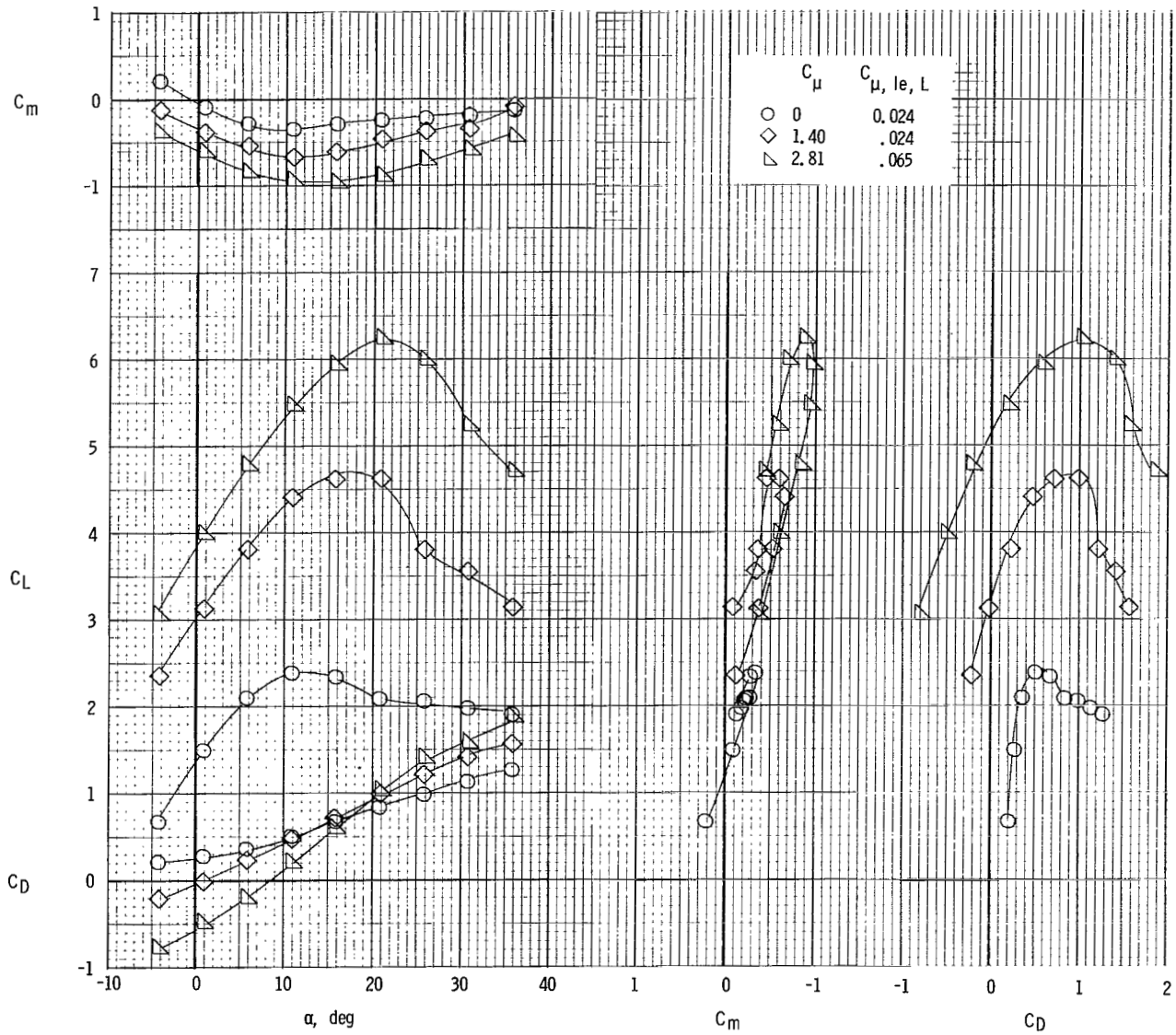

(d) Longitudinal characteristics. Left inboard engine not operating.

Figure 70.- Concluded.

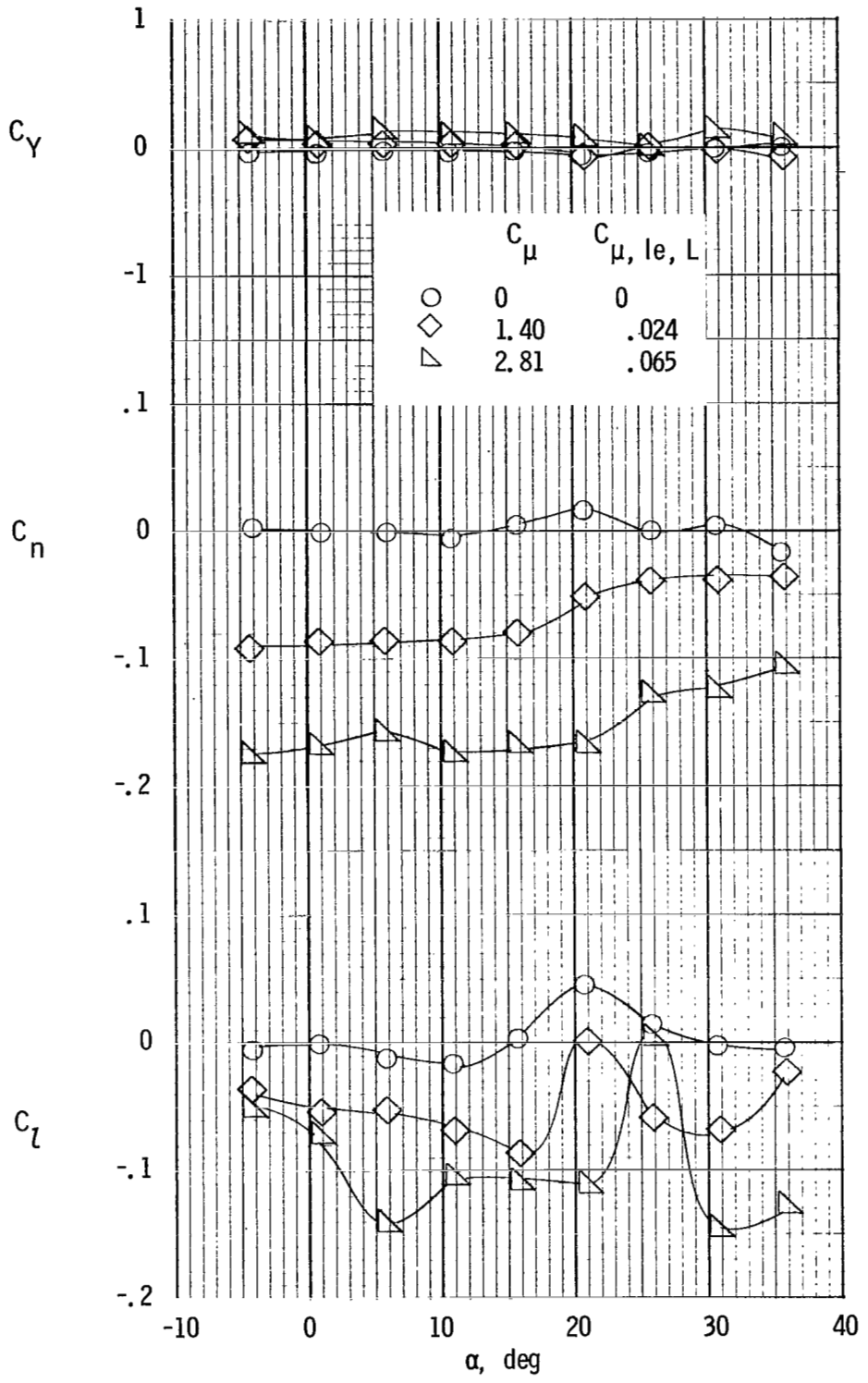

(a) Lateral characteristics. Left outboard engine not operating.

Figure 71.- Lateral and longitudinal characteristics of model with tail on and spread engines. One left engine not operating; leading-edge blowing; $\delta_f = 80^0$, left inboard; $\delta_f = 40^0$, right inboard; $\delta_f = 60^0$, left and right center and outboard.

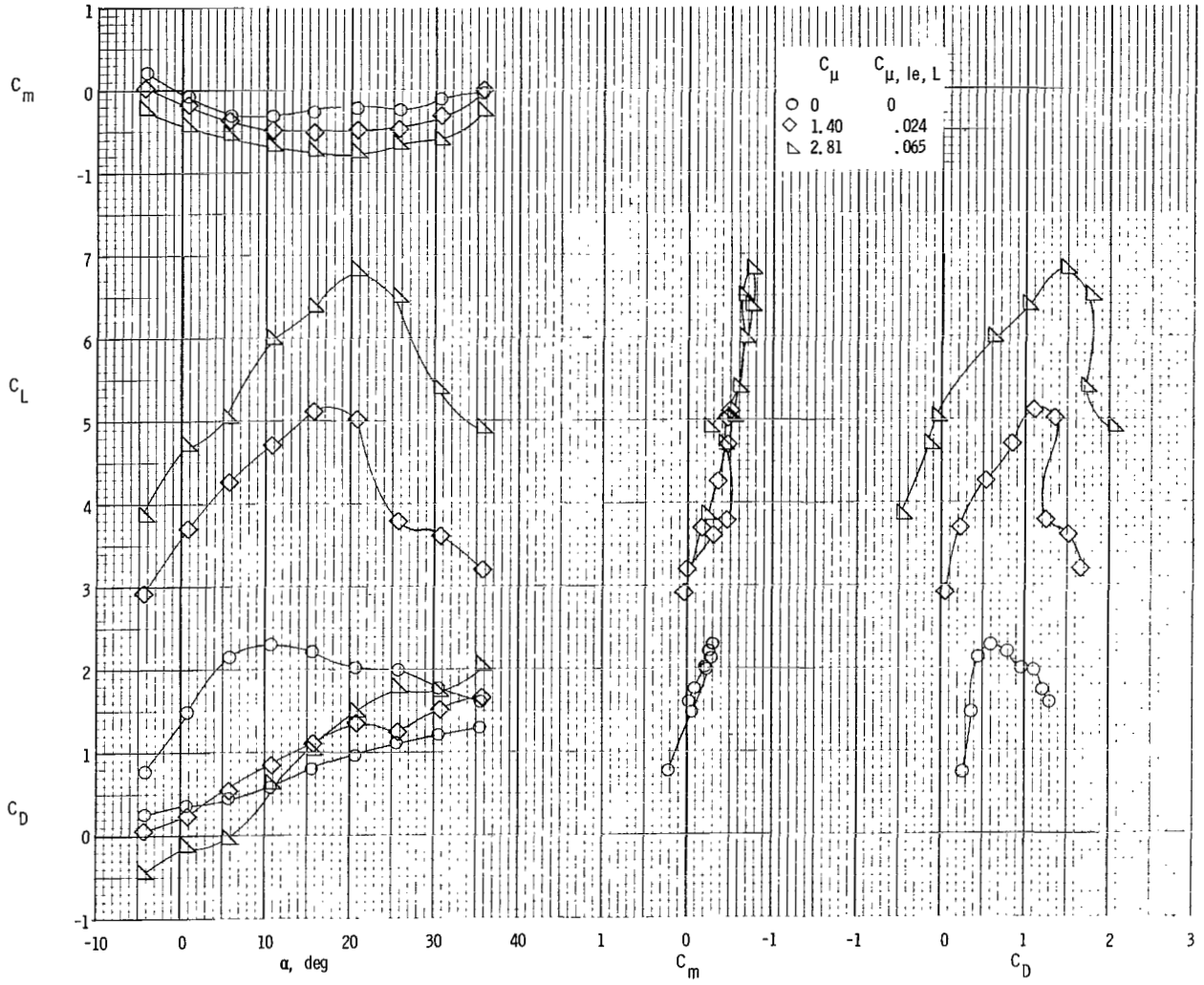

(b) Longitudinal characteristics. Left outboard engine not operating.

Figure 71.- Continued.

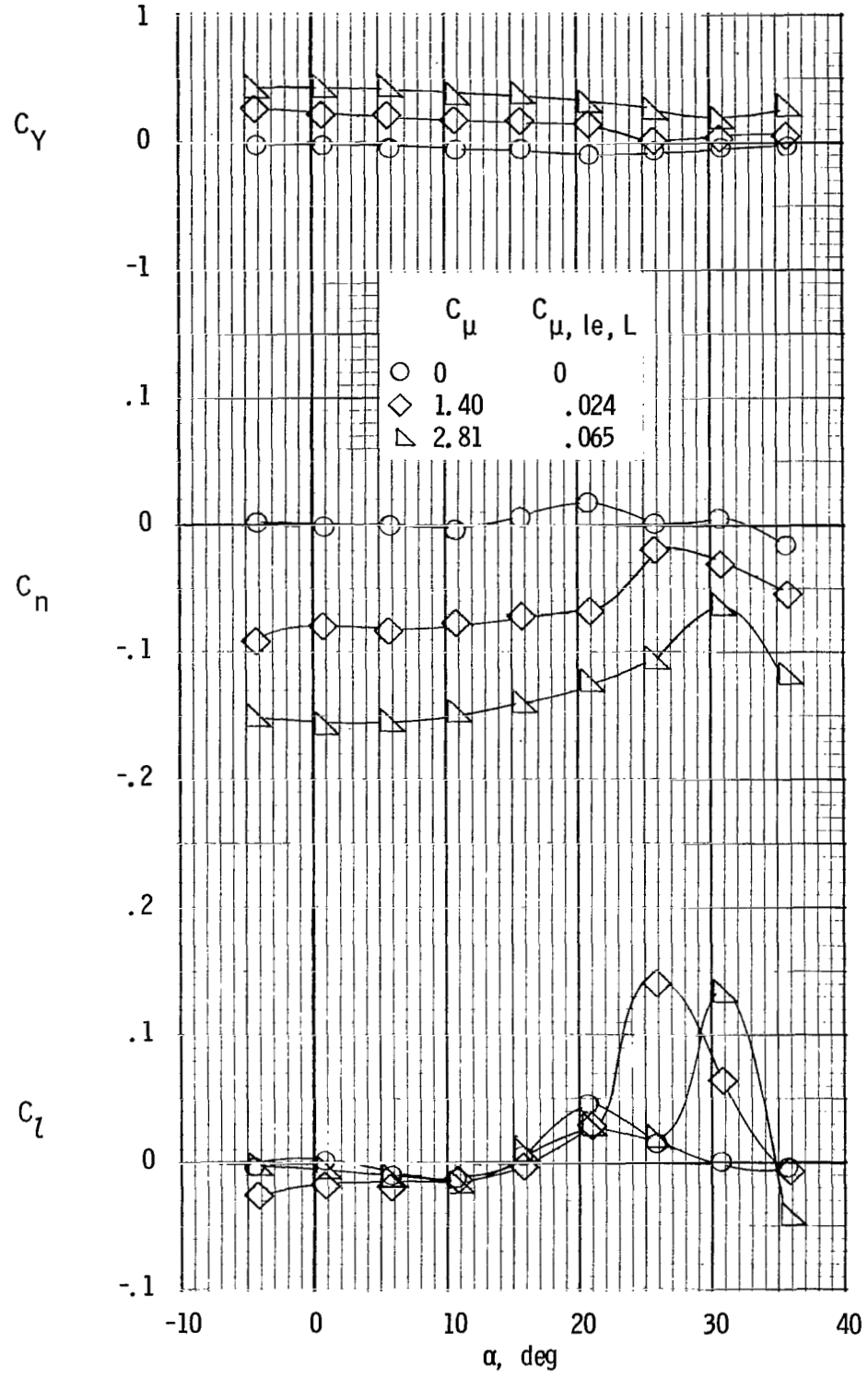

(c) Lateral characteristics. Left inboard engine not operating.

Figure 71.- Continued.

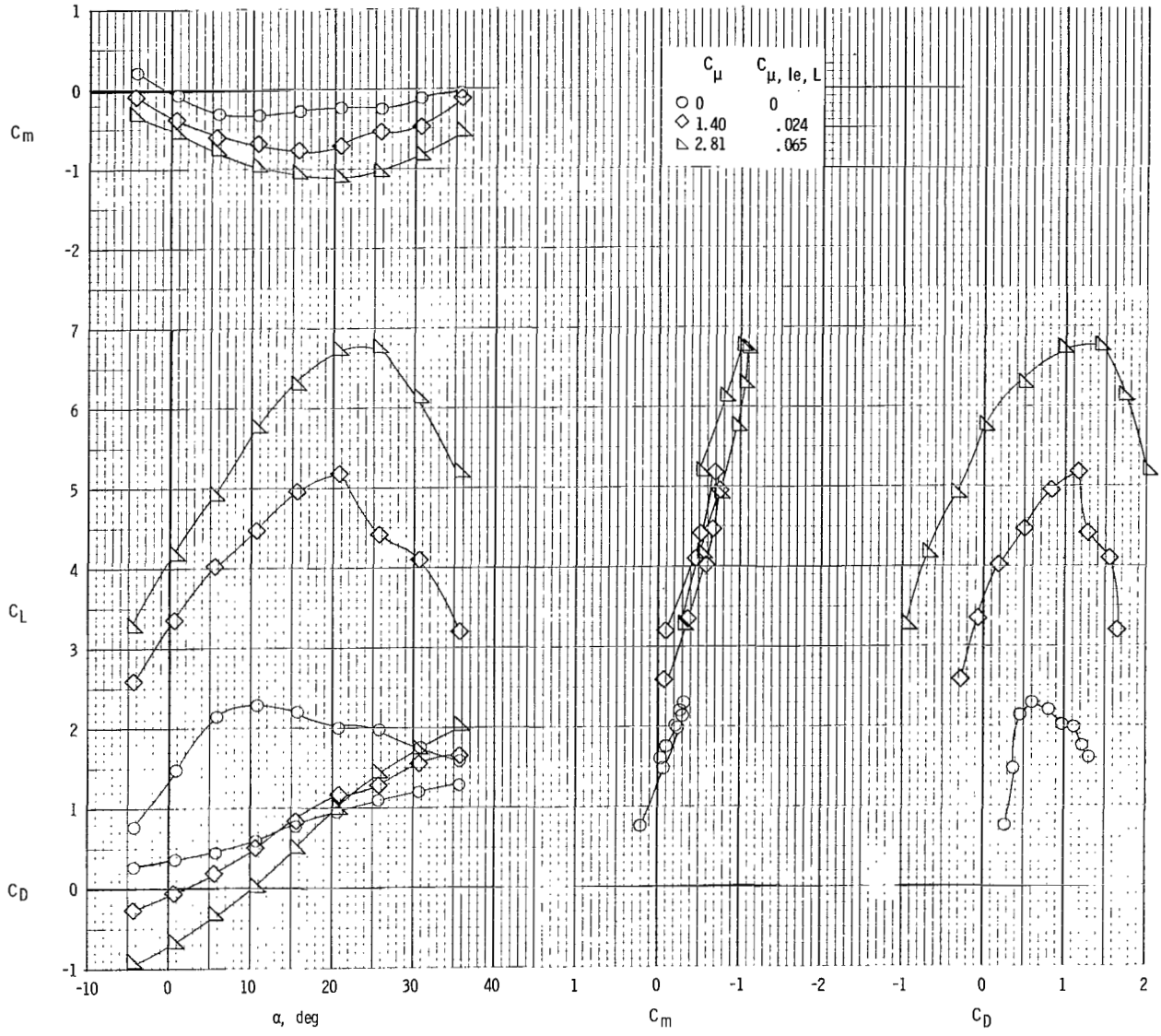

(d) Longitudinal characteristics. Left inboard engine not operating.

Figure 71.- Concluded.

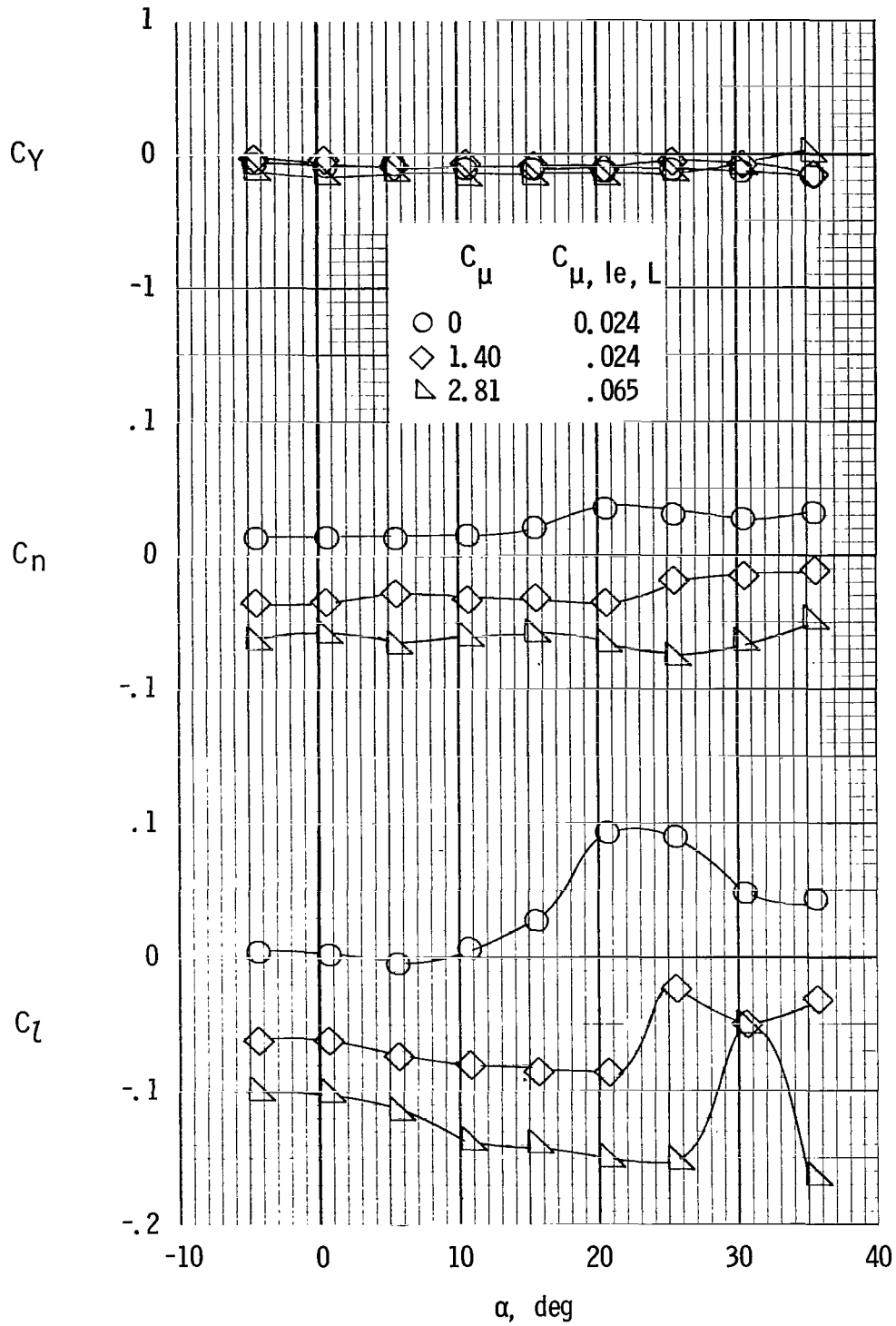

(a) Lateral characteristics. Left outboard engine not operating.

Figure 72.- Lateral and longitudinal characteristics of model with tail on and spread engines. One left engine not operating; leading-edge blowing; $\delta_f = 80^0$, left center; $\delta_f = 40^0$, right center; $\delta_f = 60^0$, left and right inboard and outboard.

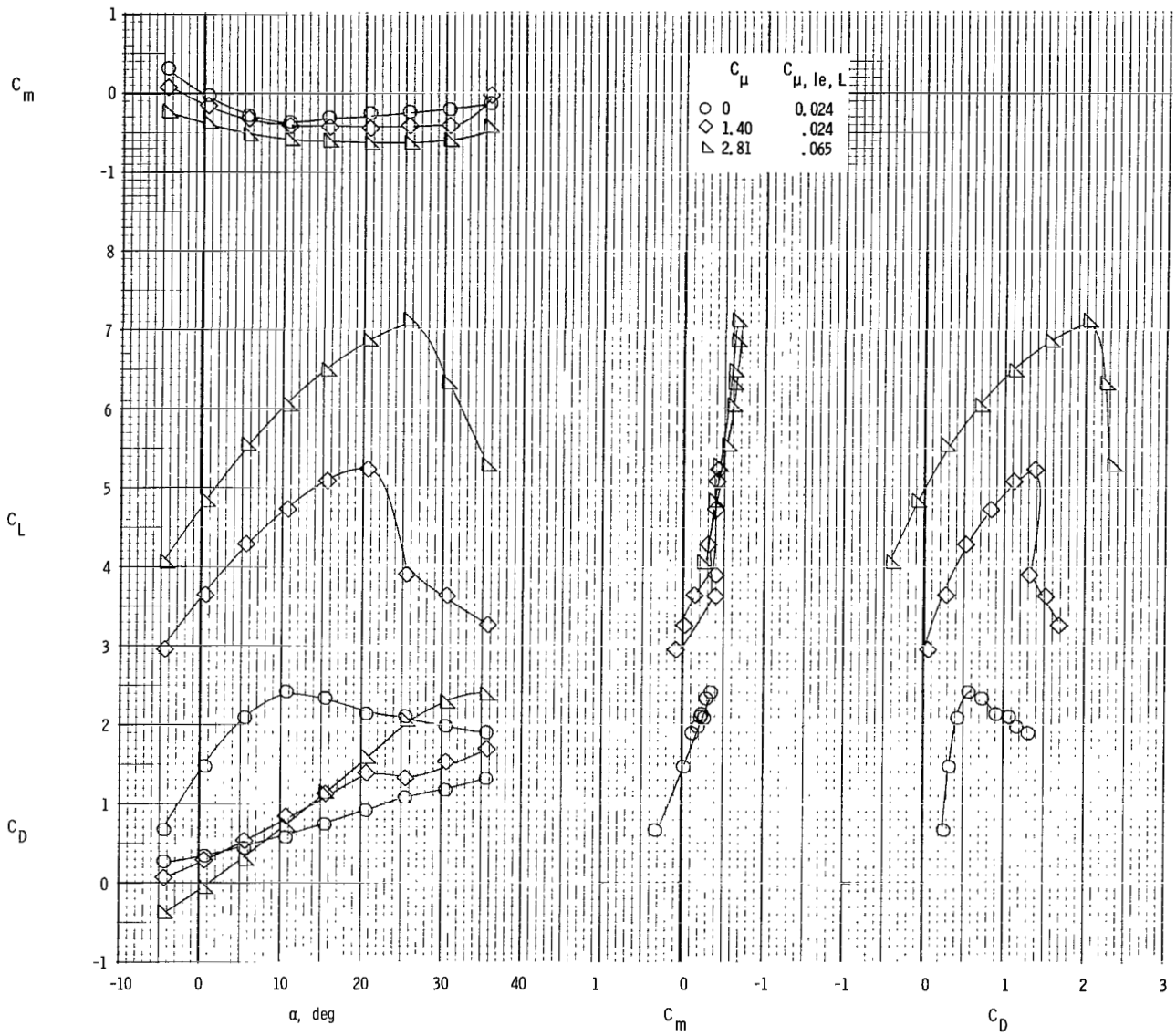

(b) Longitudinal characteristics. Left outboard engine not operating.

Figure 72.- Continued.

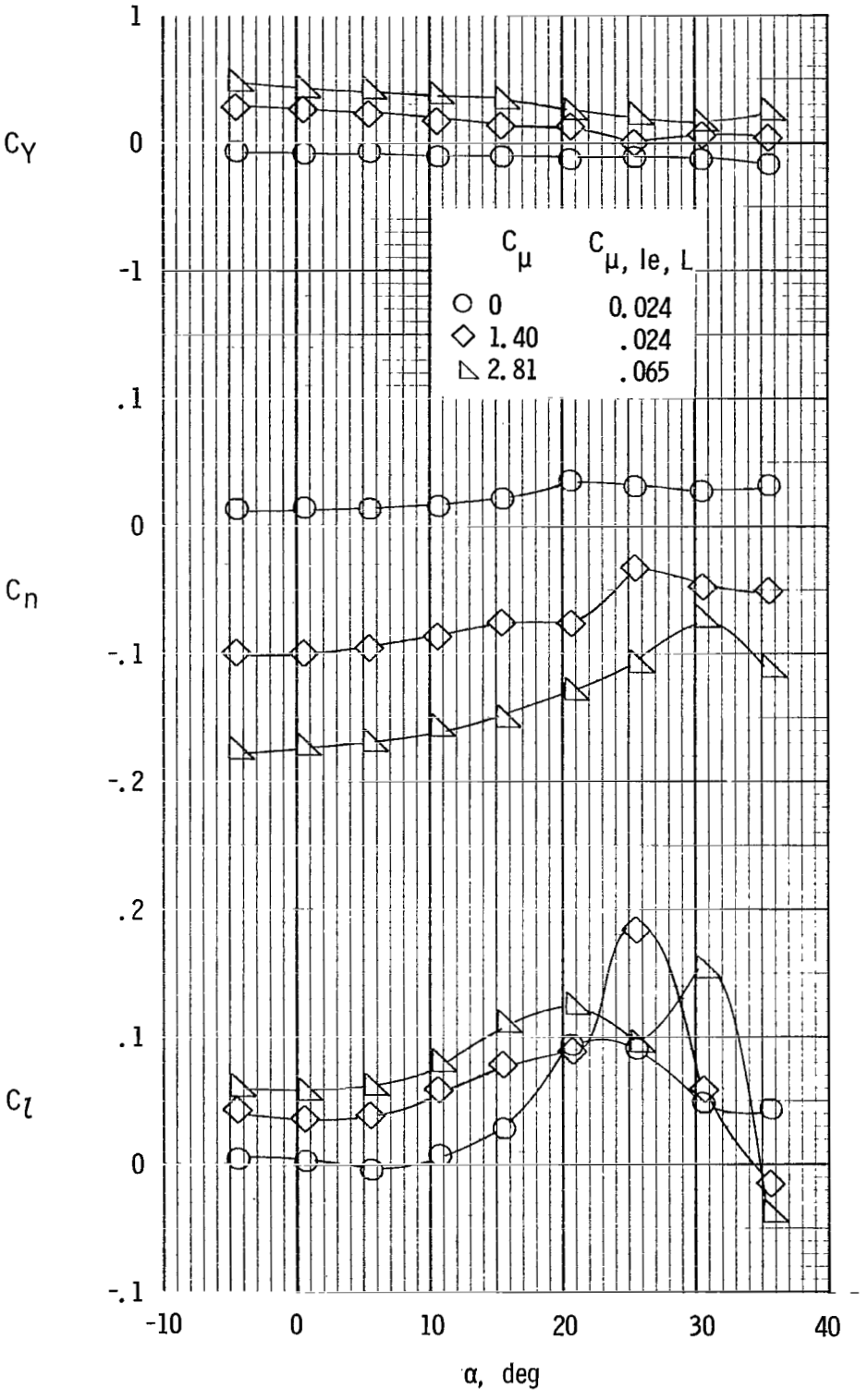

(c) Lateral characteristics. Left inboard engine not operating.

Figure 72.- Continued.

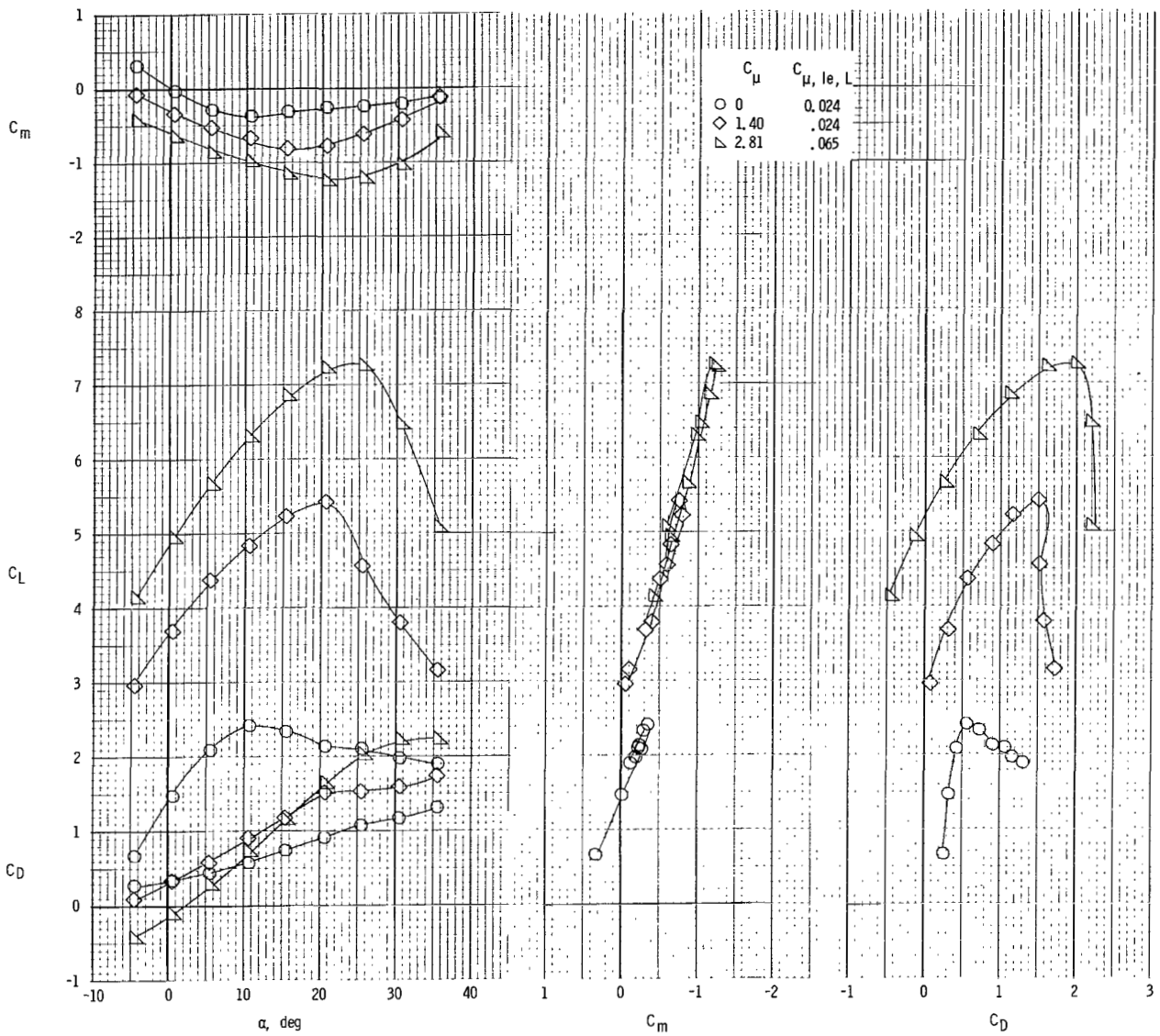

(d) Longitudinal characteristics. Left inboard engine not operating.

Figure 72.- Concluded.

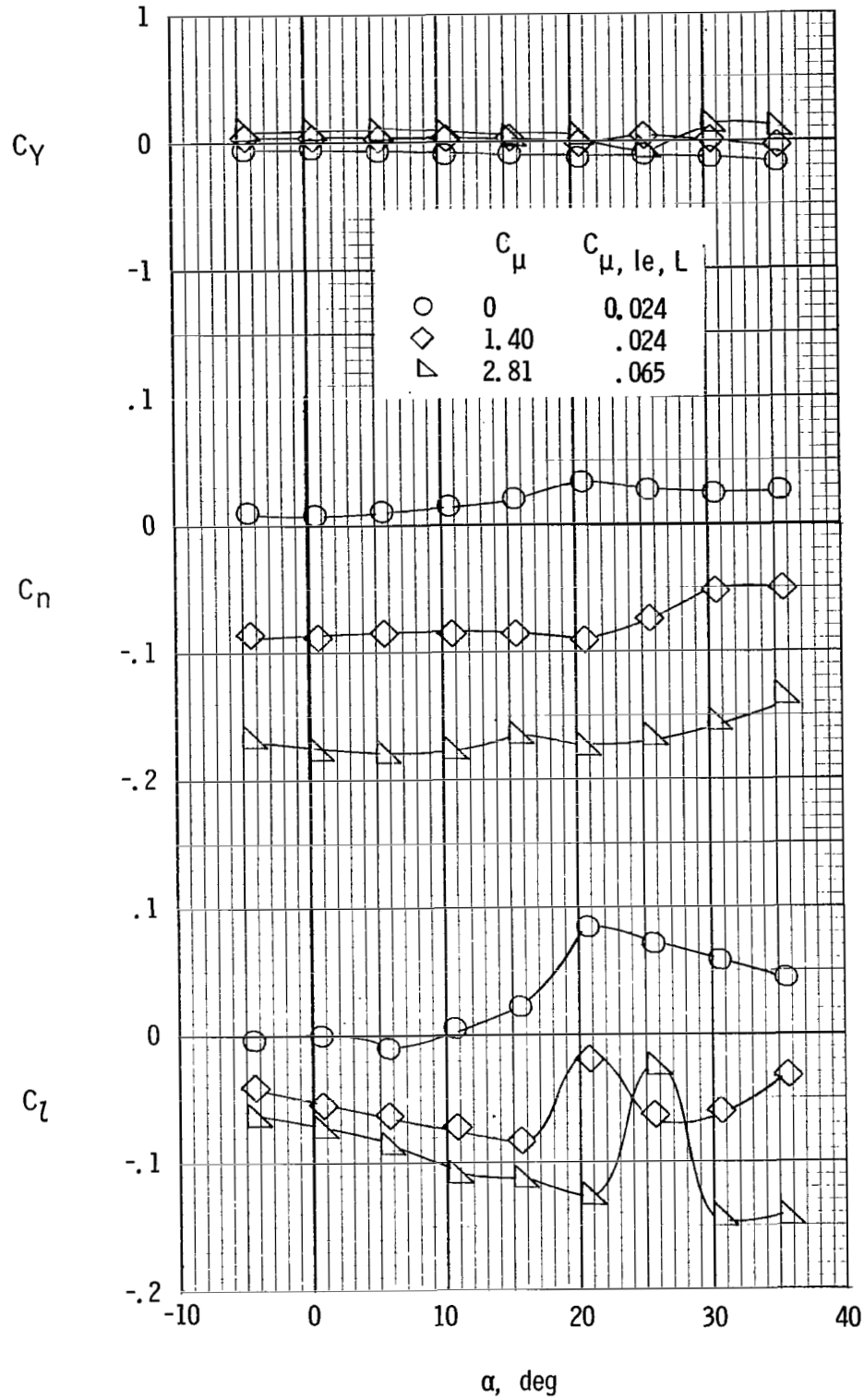

(a) Lateral characteristics. Left outboard engine not operating.

Figure 73.- Lateral and longitudinal characteristics of model with tail on and spread engines. One left engine not operating; leading-edge blowing; $\delta_f = 80^0$, left inboard and center; $\delta_f = 40^0$, right inboard and center; $\delta_f = 60^0$, left and right outboard.

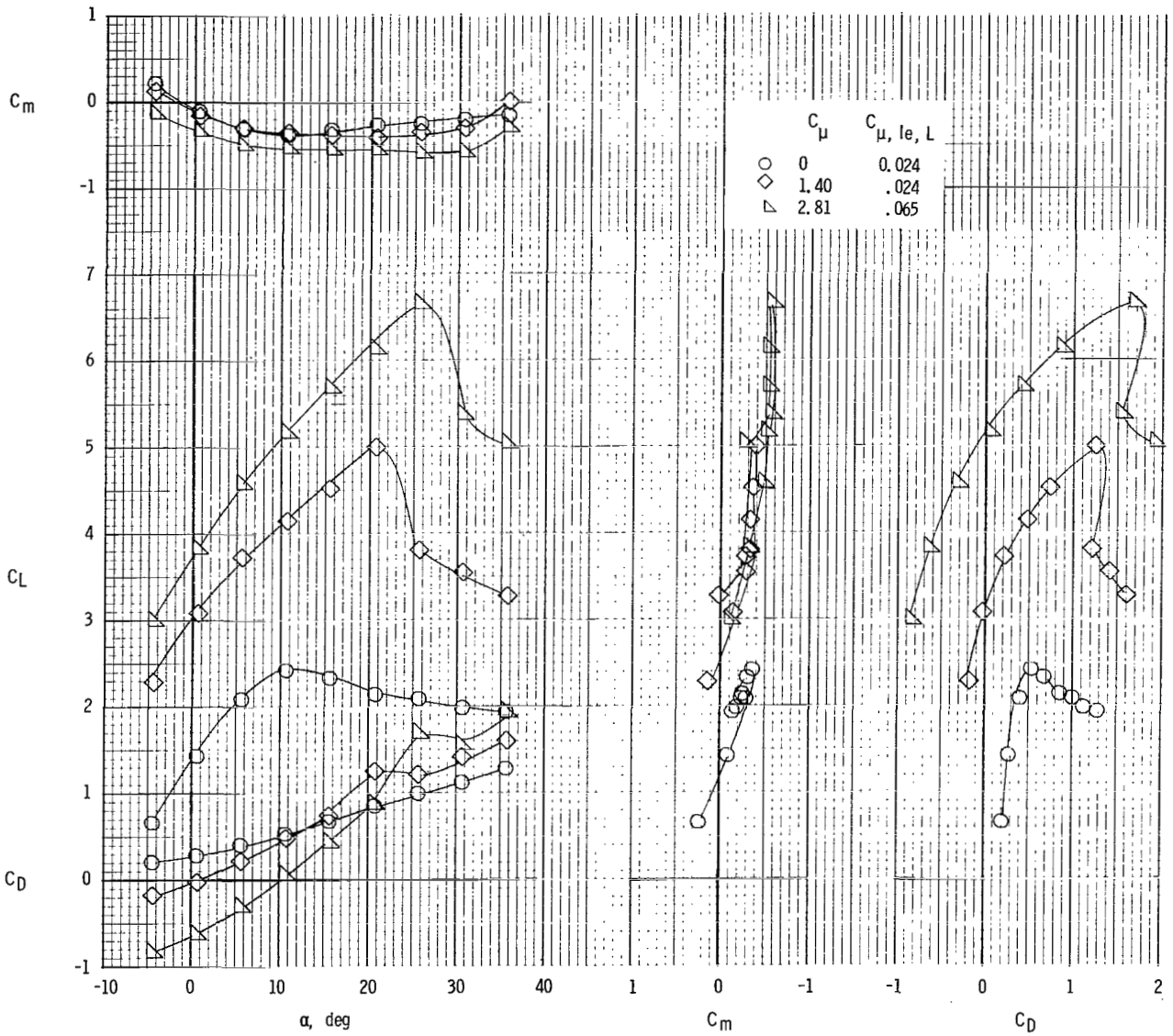

(b) Longitudinal characteristics. Left outboard engine not operating.

Figure 73.- Continued.

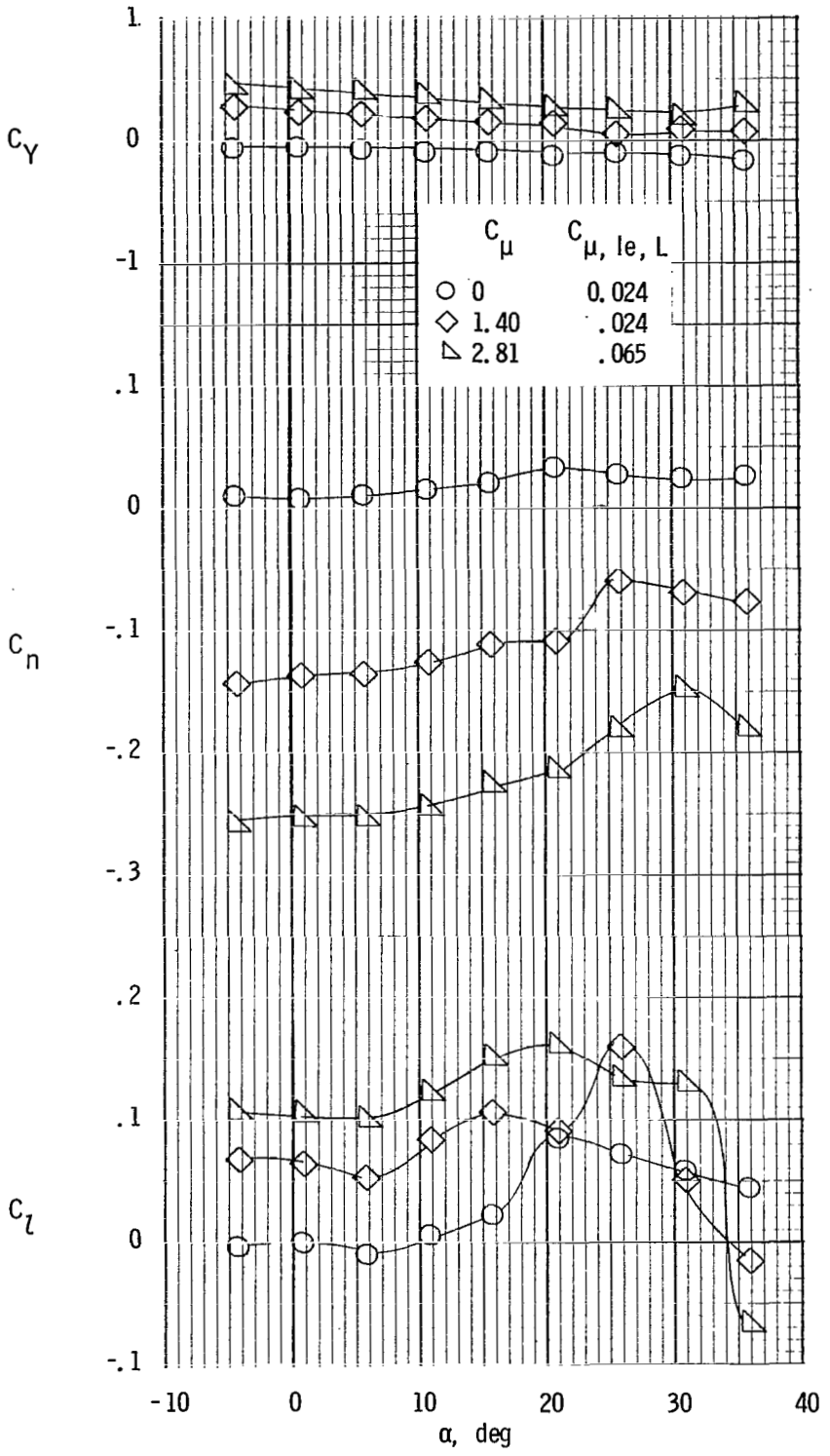

(c) Lateral characteristics. Left inboard engine not operating.

Figure 73.- Continued.

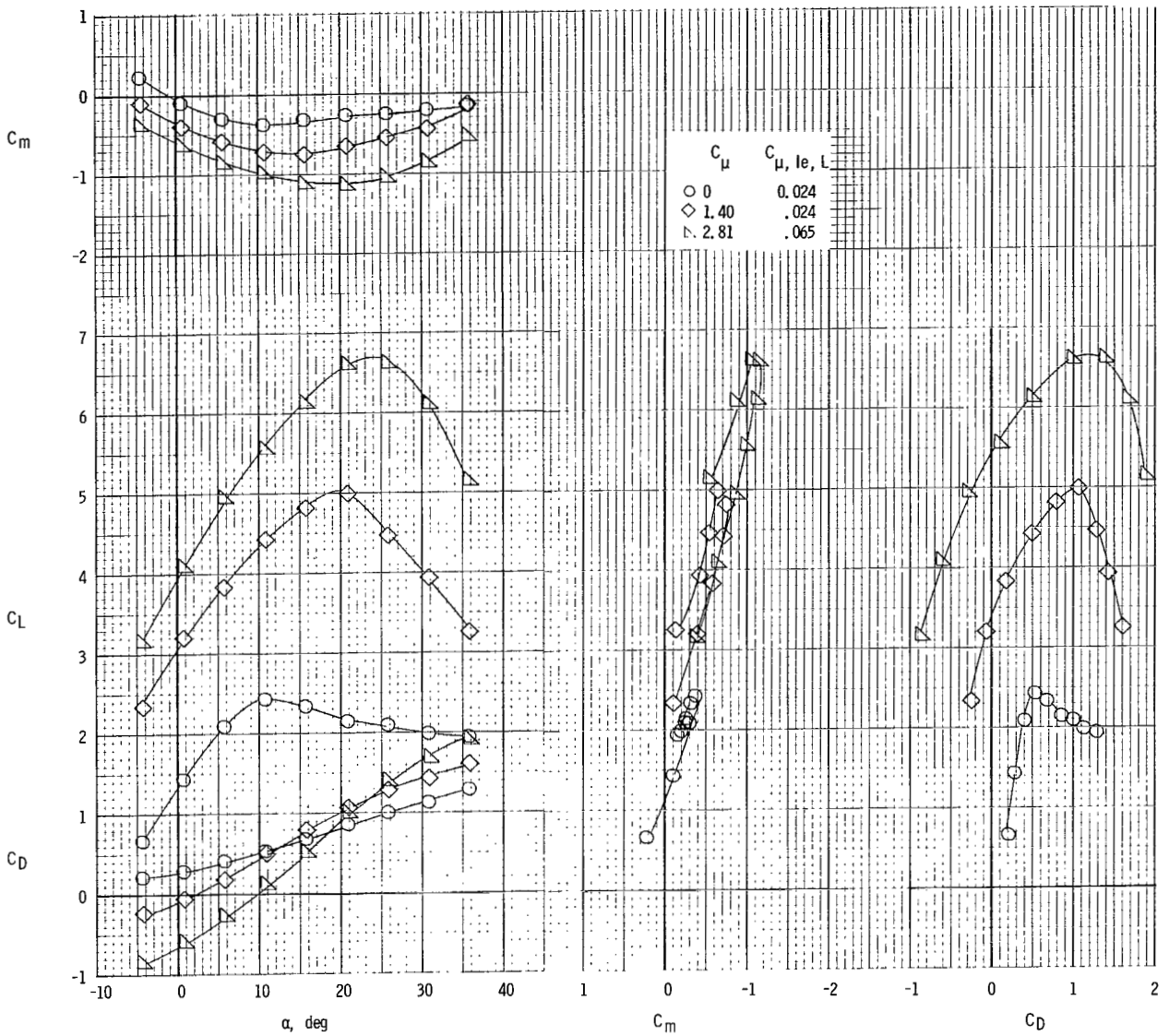

(d) Longitudinal characteristics. Left inboard engine not operating.

Figure 73.- Concluded.

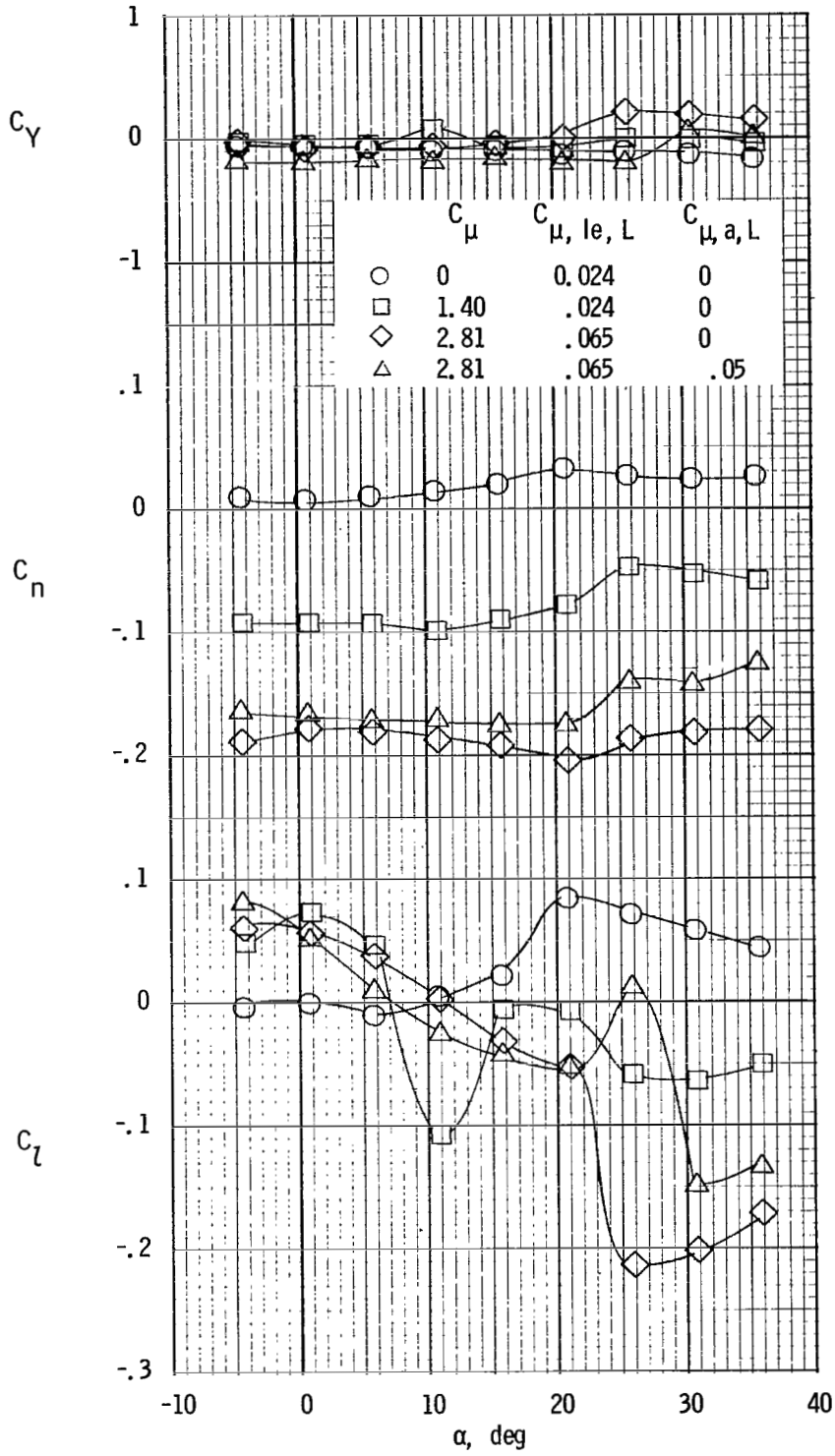

(a) Lateral characteristics.

Figure 74.- Lateral and longitudinal characteristics of model with tail on and spread engines. Left outboard engine not operating; leading-edge and aileron blowing; $\delta_f = 80^o$, left inboard and center; $\delta_f = 40^o$, right inboard and center; $\delta_f = 60^o$, left and right outboard; $\delta_s = 40^o$, right wing tip.

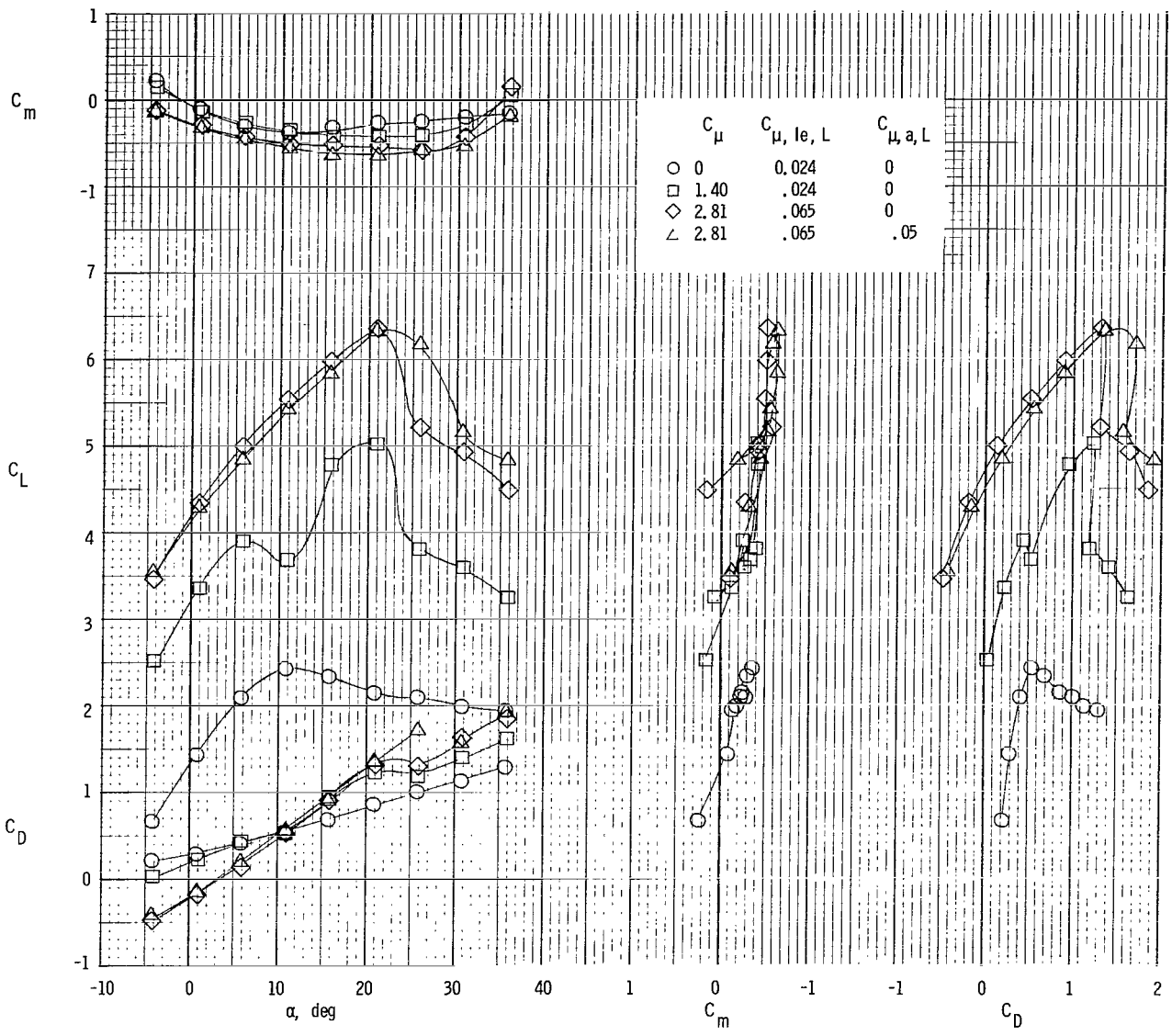

(b) Longitudinal characteristics.

Figure 74.- Concluded.

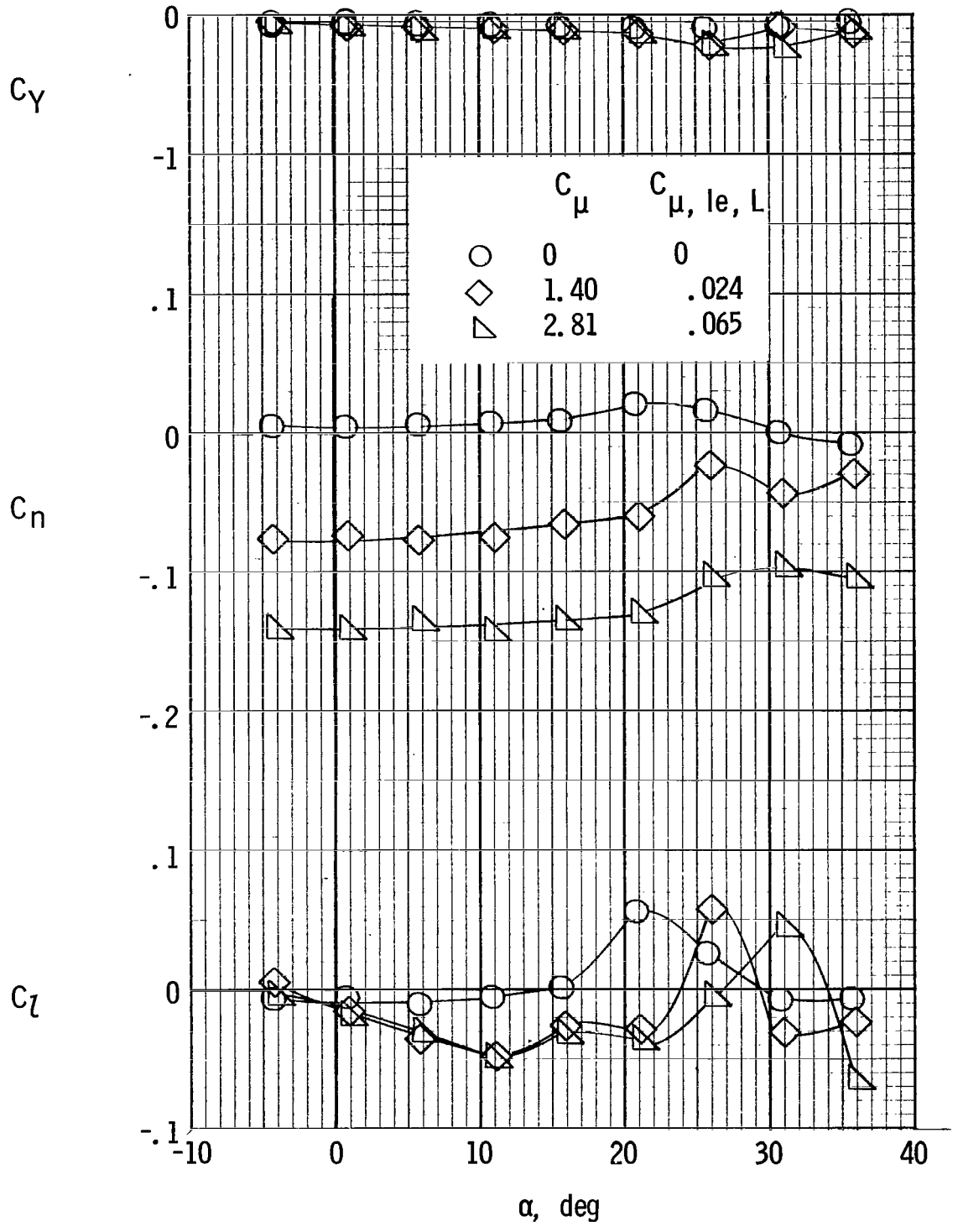

(a) Lateral characteristics, no spoiler deflection.

Figure 75.- Lateral and longitudinal characteristics of model with tail on and spread engines. Left outboard engine not operating; leading-edge blowing; differential flap deflection; $\delta_{f,L} = 50^0$; $\delta_{f,R} = 30^0$.

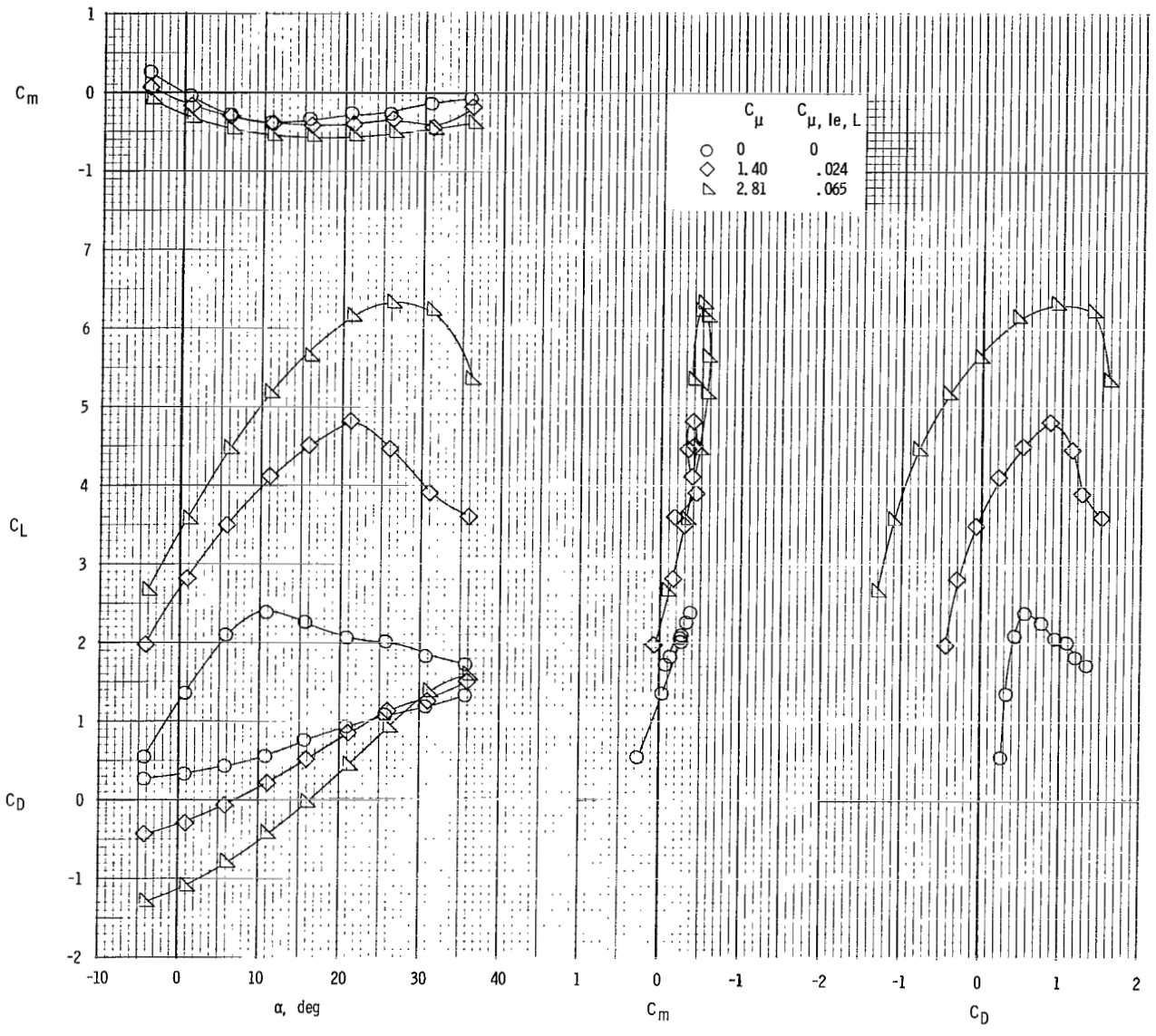

(b) Longitudinal characteristics. No spoiler deflection.

Figure 75.- Continued.

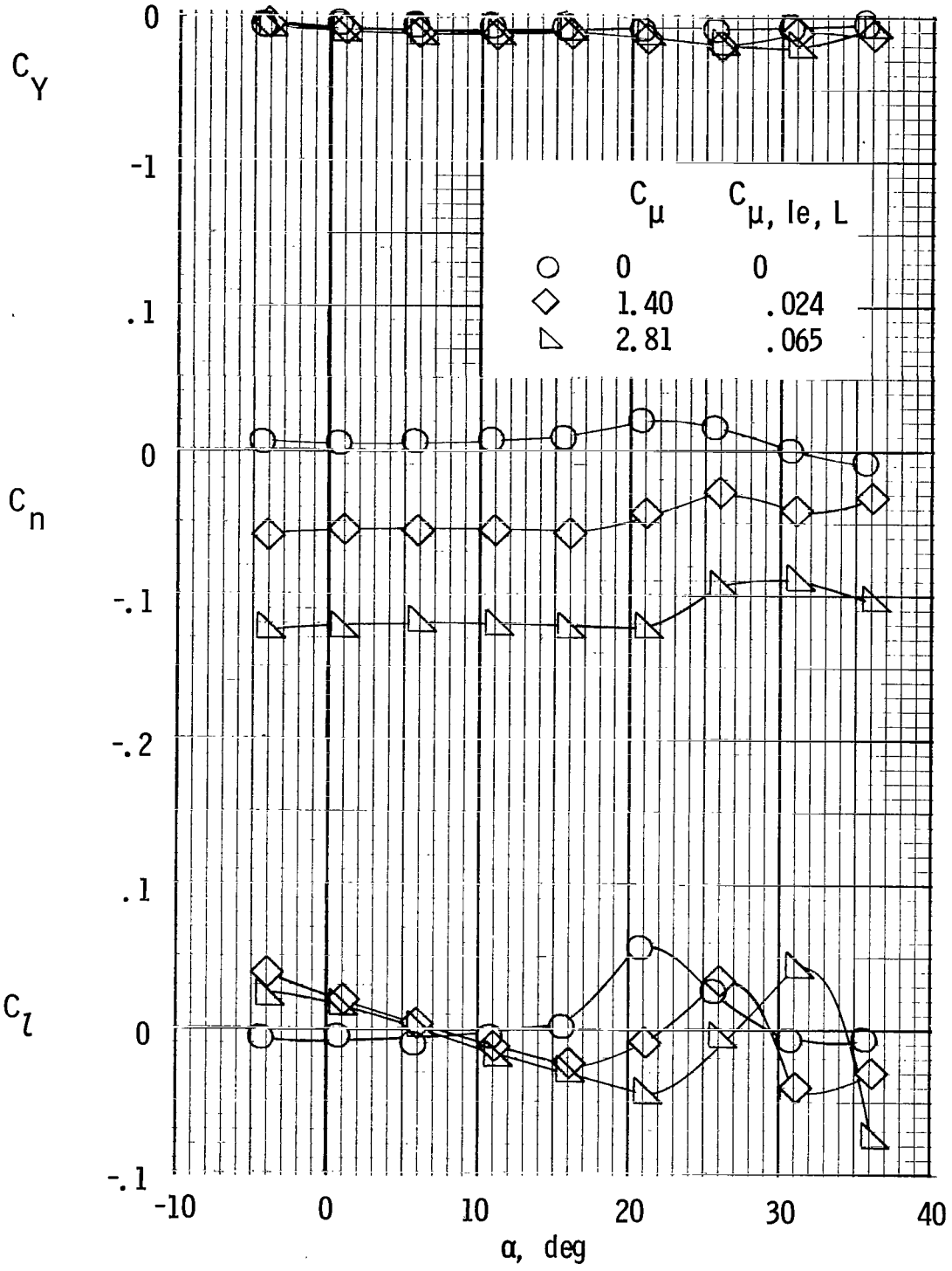

(c) Lateral characteristics. $\delta_s = 40^0$, right wing tip.

Figure 75.- Continued.

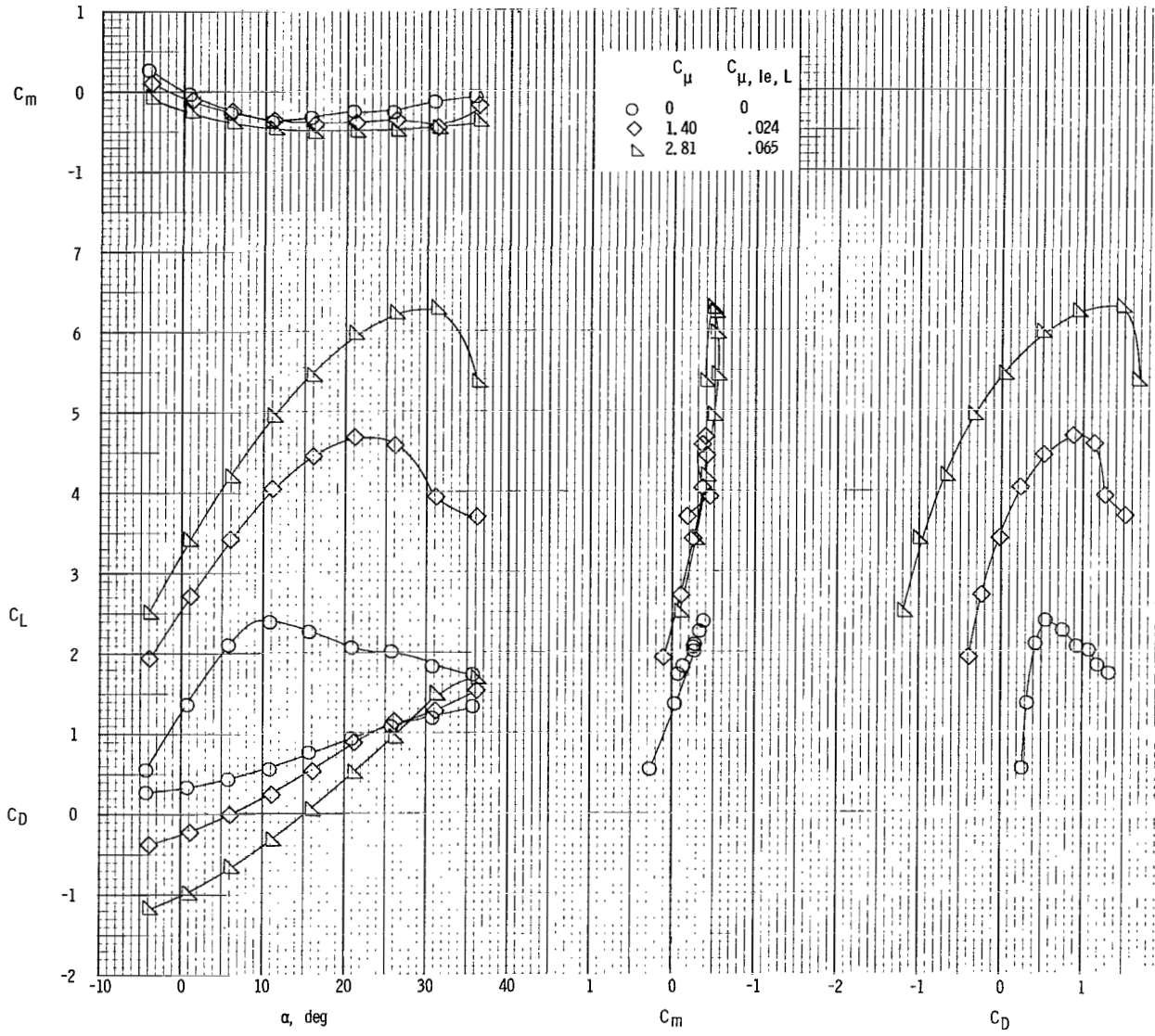

(d) Longitudinal characteristics. $\delta_s = 40^0$, right wing tip.

Figure 75.- Concluded.

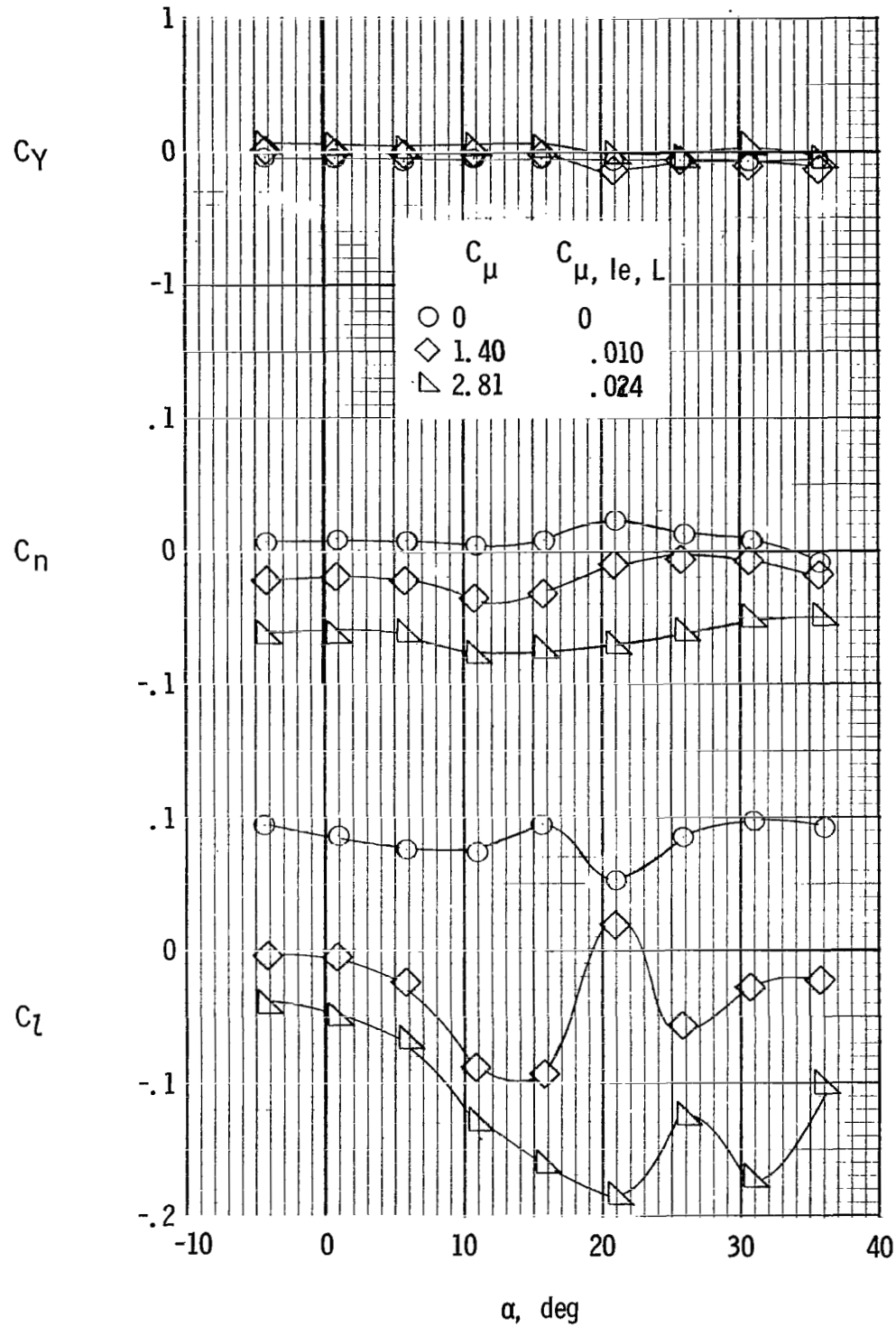

(a) Lateral characteristics. Left outboard engine not operating.

Figure 76.- Lateral and longitudinal characteristics of model with tail on and spread engines. One left engine not operating; leading-edge blowing; $\delta_f = 60^0$; $\delta_s = 40^0$, right wing tip; $C_{\mu,a,L} = 0.13$.

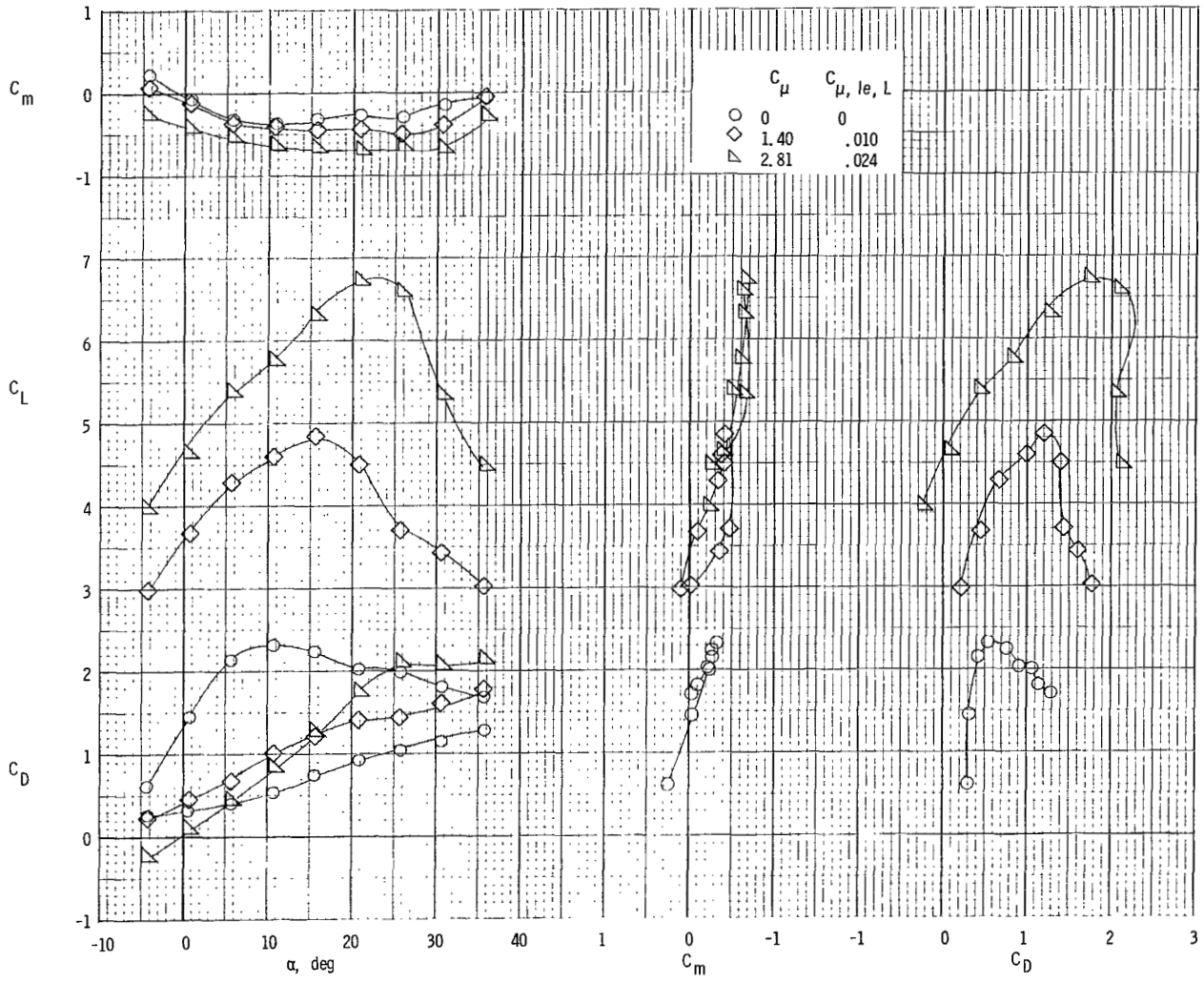

(b) Longitudinal characteristics. Left outboard engine not operating.

Figure 76.- Continued.

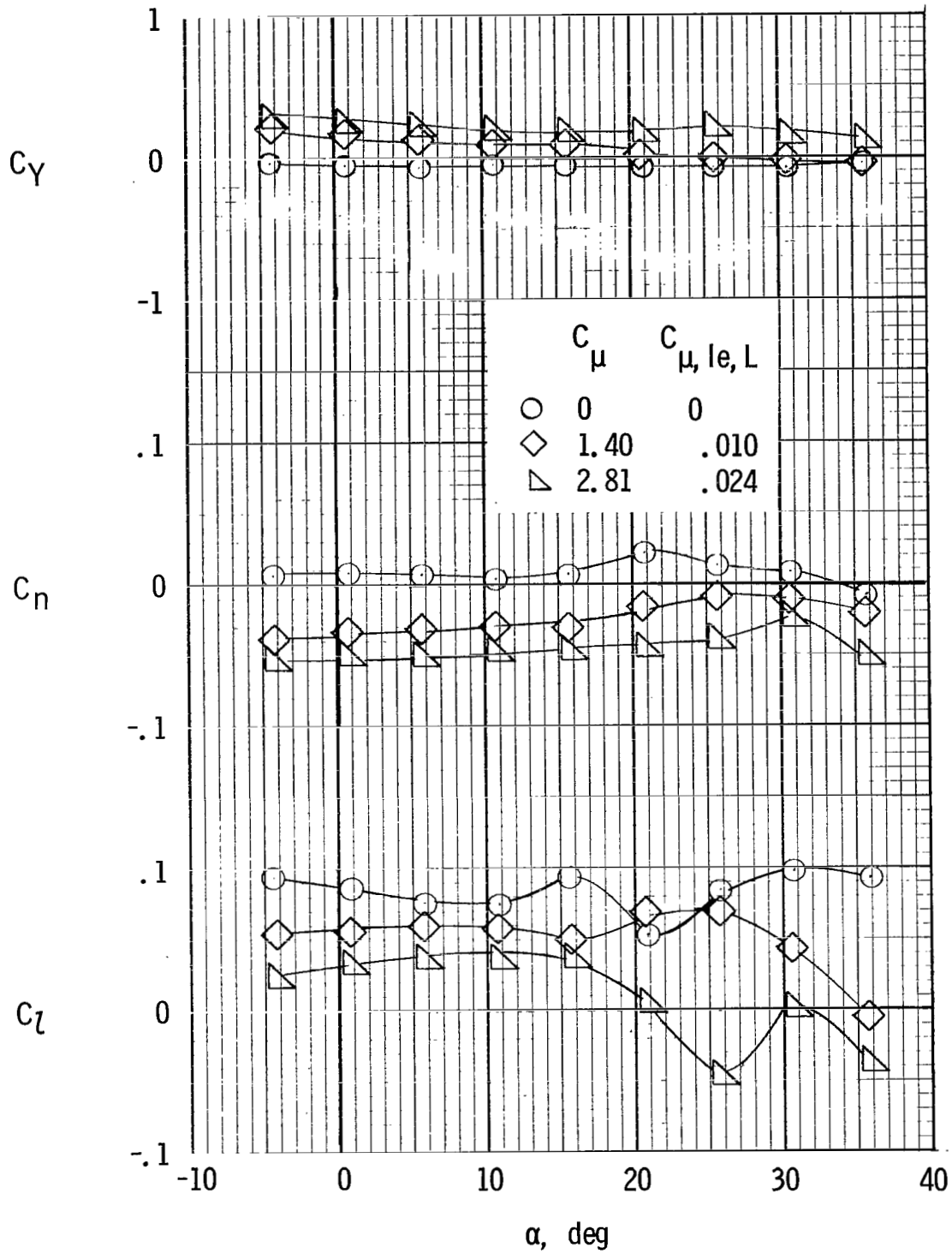

(c) Lateral characteristics. Left inboard engine not operating.

Figure 76.- Continued.

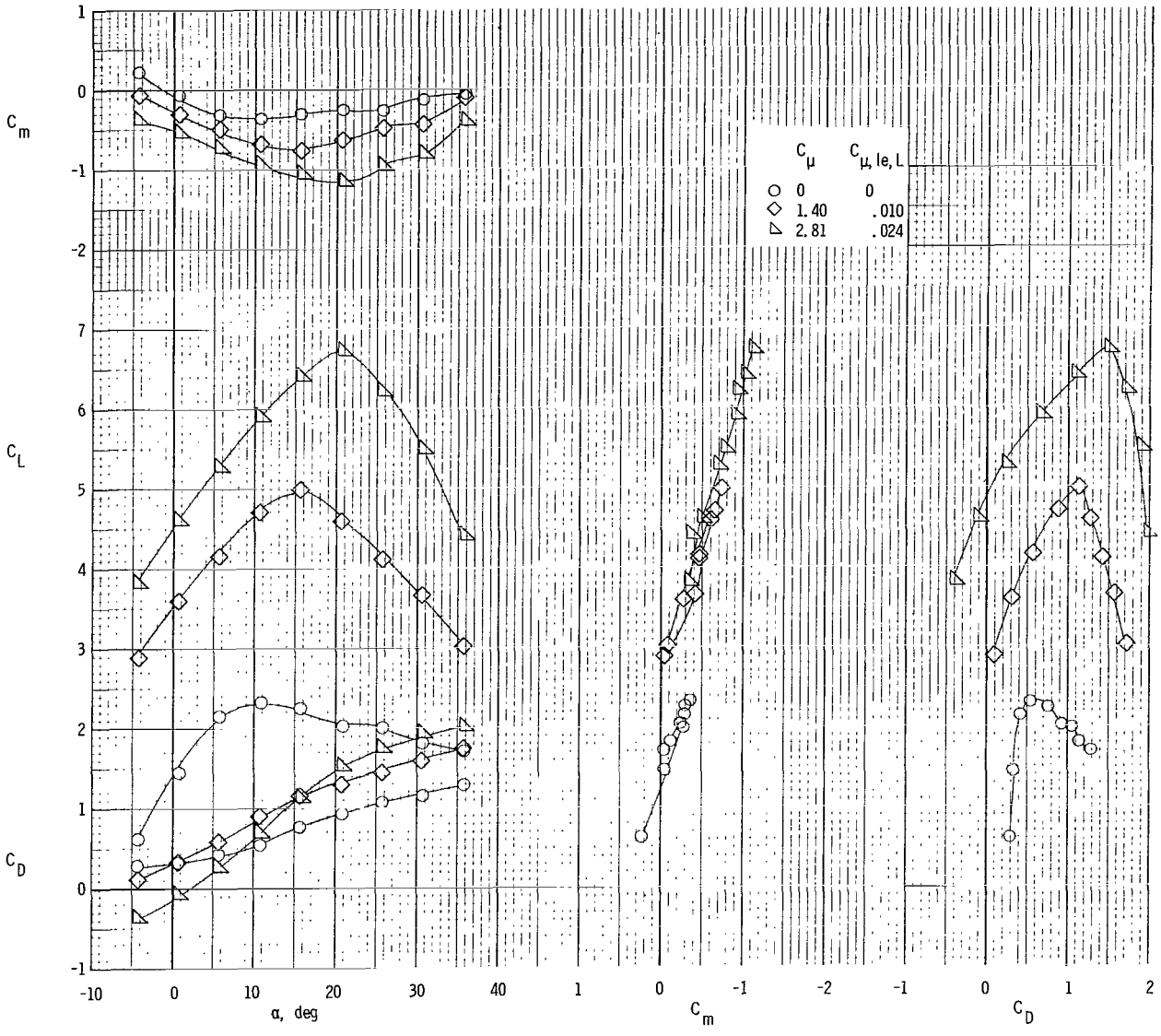

(d) Longitudinal characteristics. Left inboard engine not operating.

Figure 76.- Concluded.

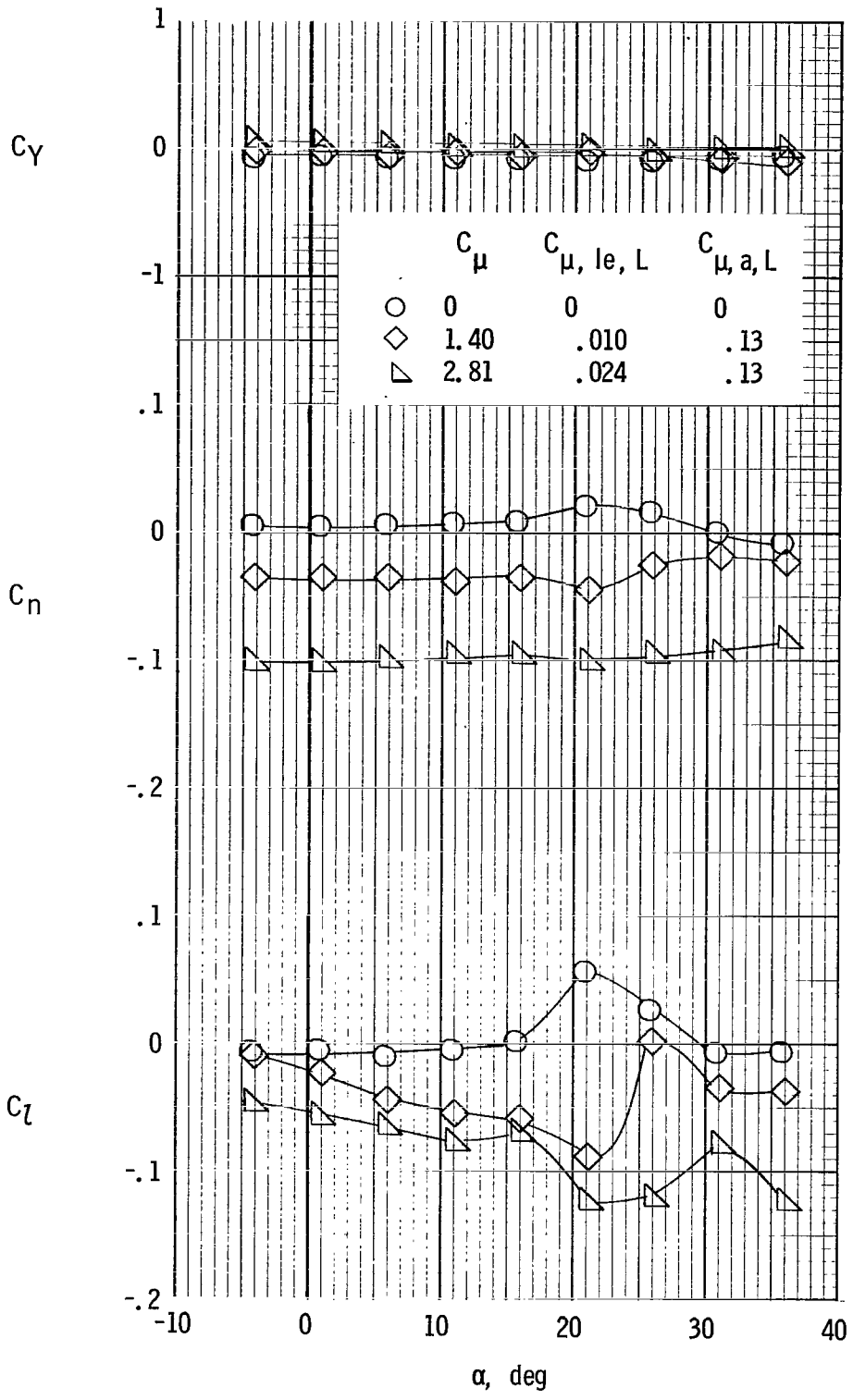

(a) Lateral characteristics. Left outboard engine not operating.

Figure 77.- Lateral and longitudinal characteristics of model with tail on and spread engines. One left engine not operating; leading-edge and aileron blowing; $\delta_f = 40^0$.

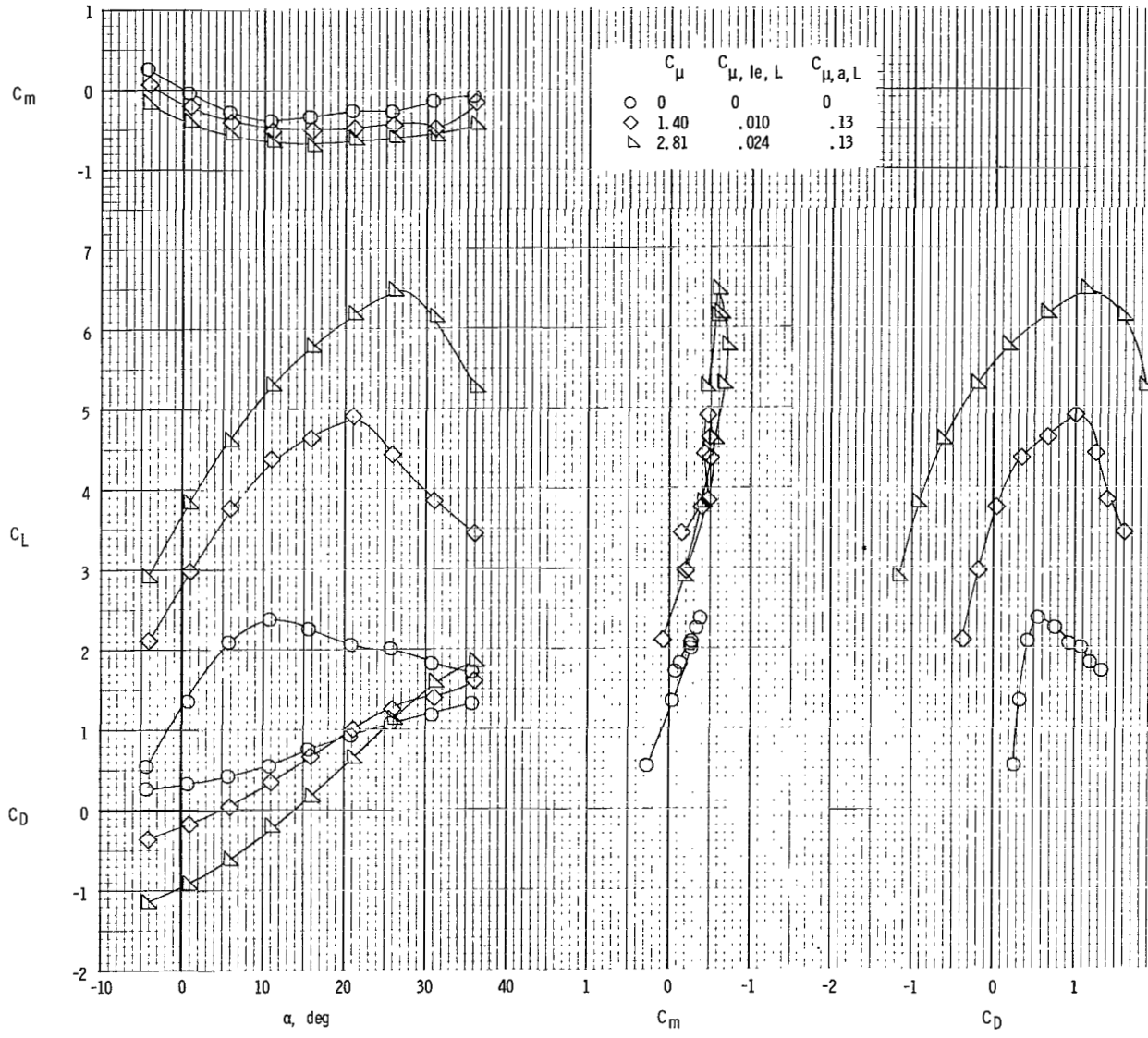

(b) Longitudinal characteristics. Left outboard engine not operating.

Figure 77.- Continued.

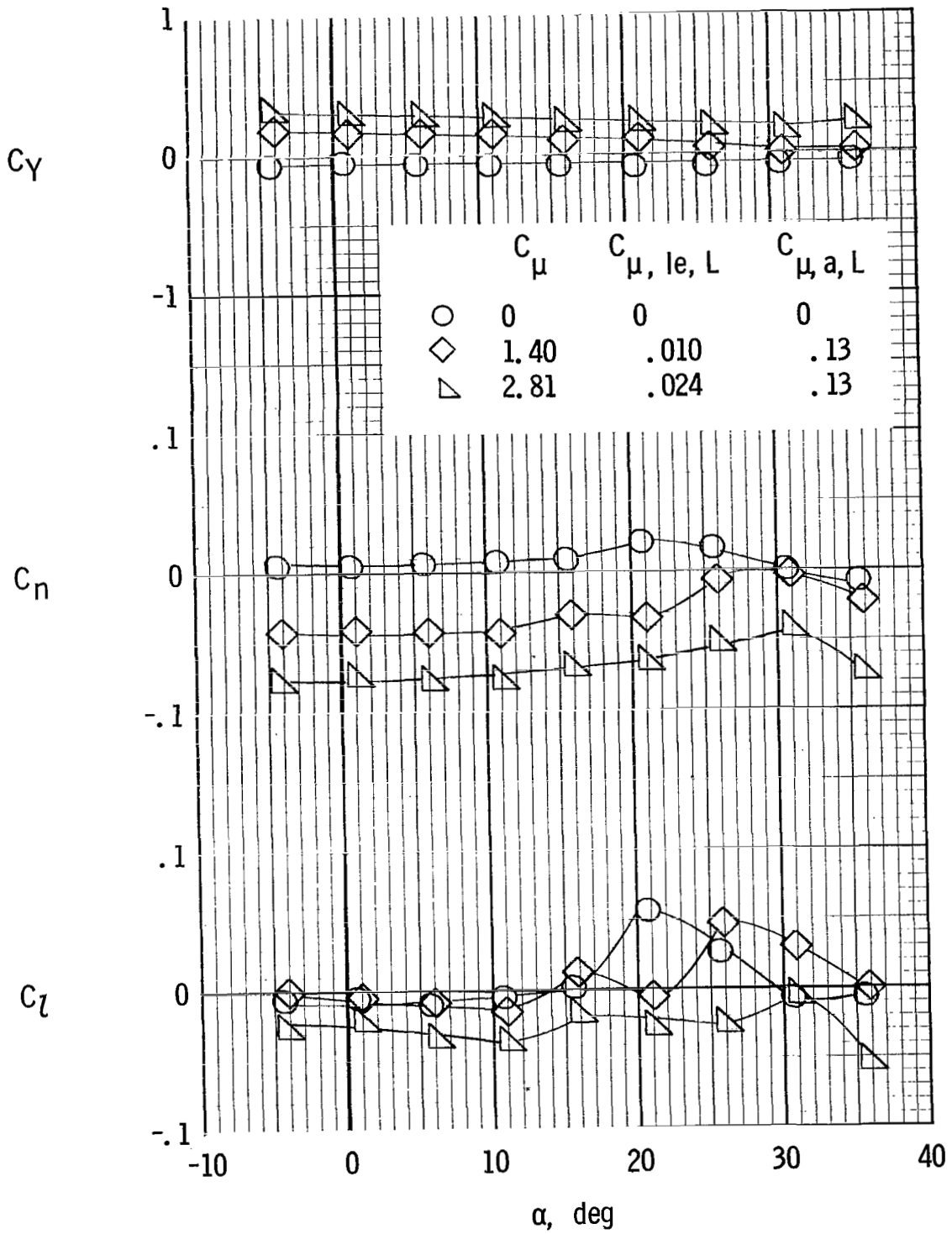

(c) Lateral characteristics. Left inboard engine not operating.

Figure 77.- Continued.

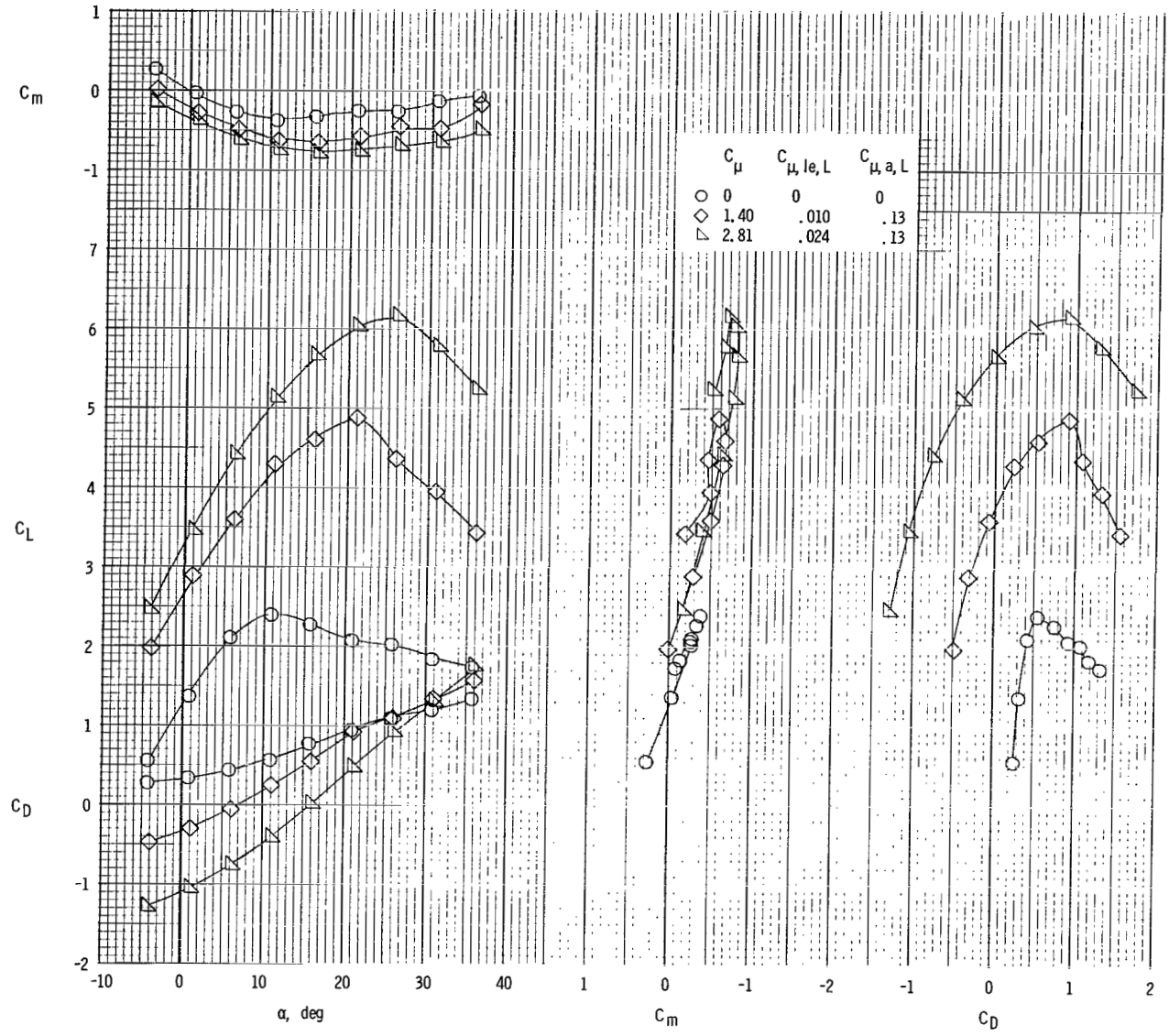

(d) Longitudinal characteristics. Left inboard engine not operating.

Figure 77.- Concluded.

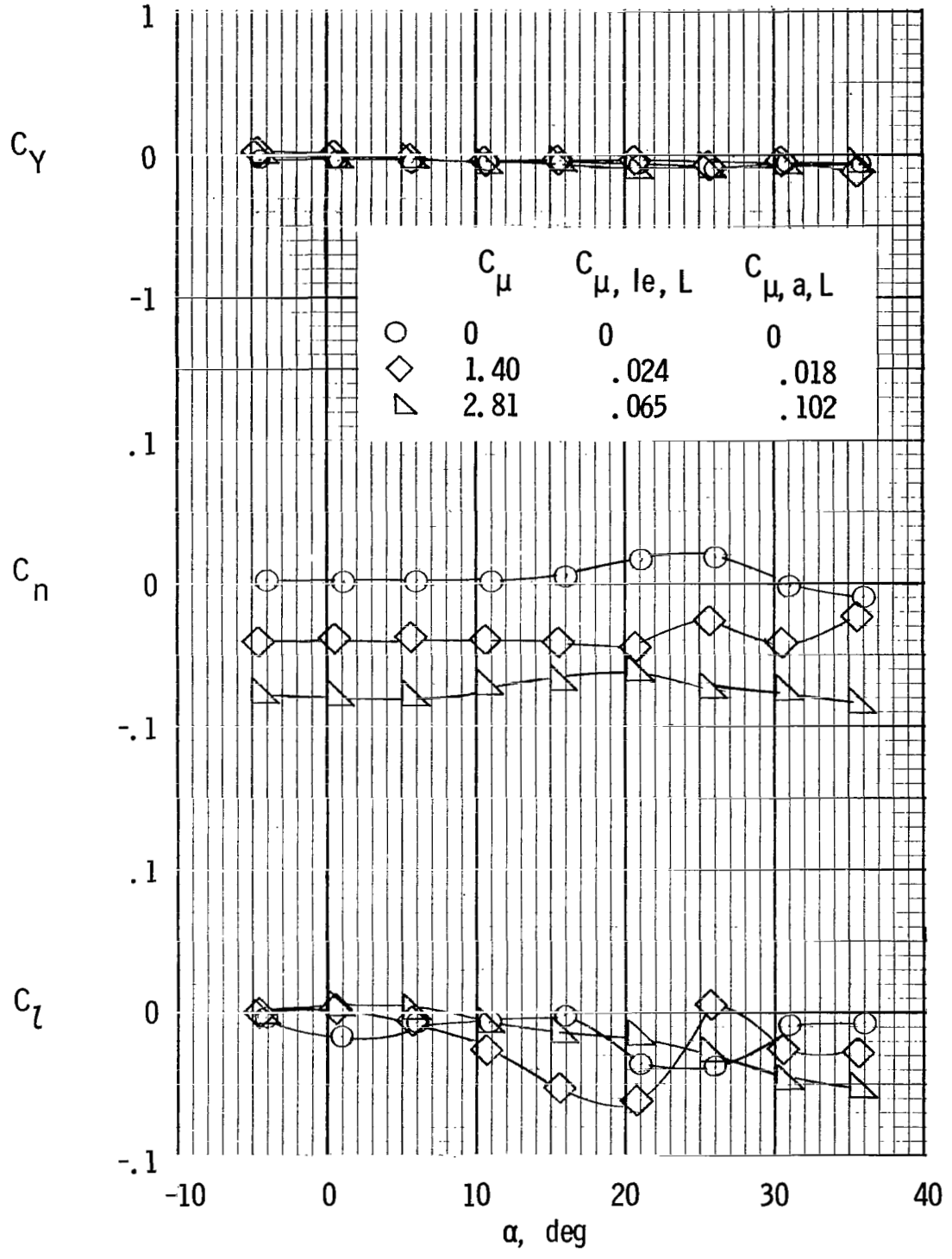

(a) Lateral characteristics.

Figure 78.- Lateral and longitudinal characteristics of model with tail on and spread engines. Left outboard engine not operating; leading-edge and aileron blowing; $\delta_f = 35^o$; $\delta_s = 40^o$, right wing tip.

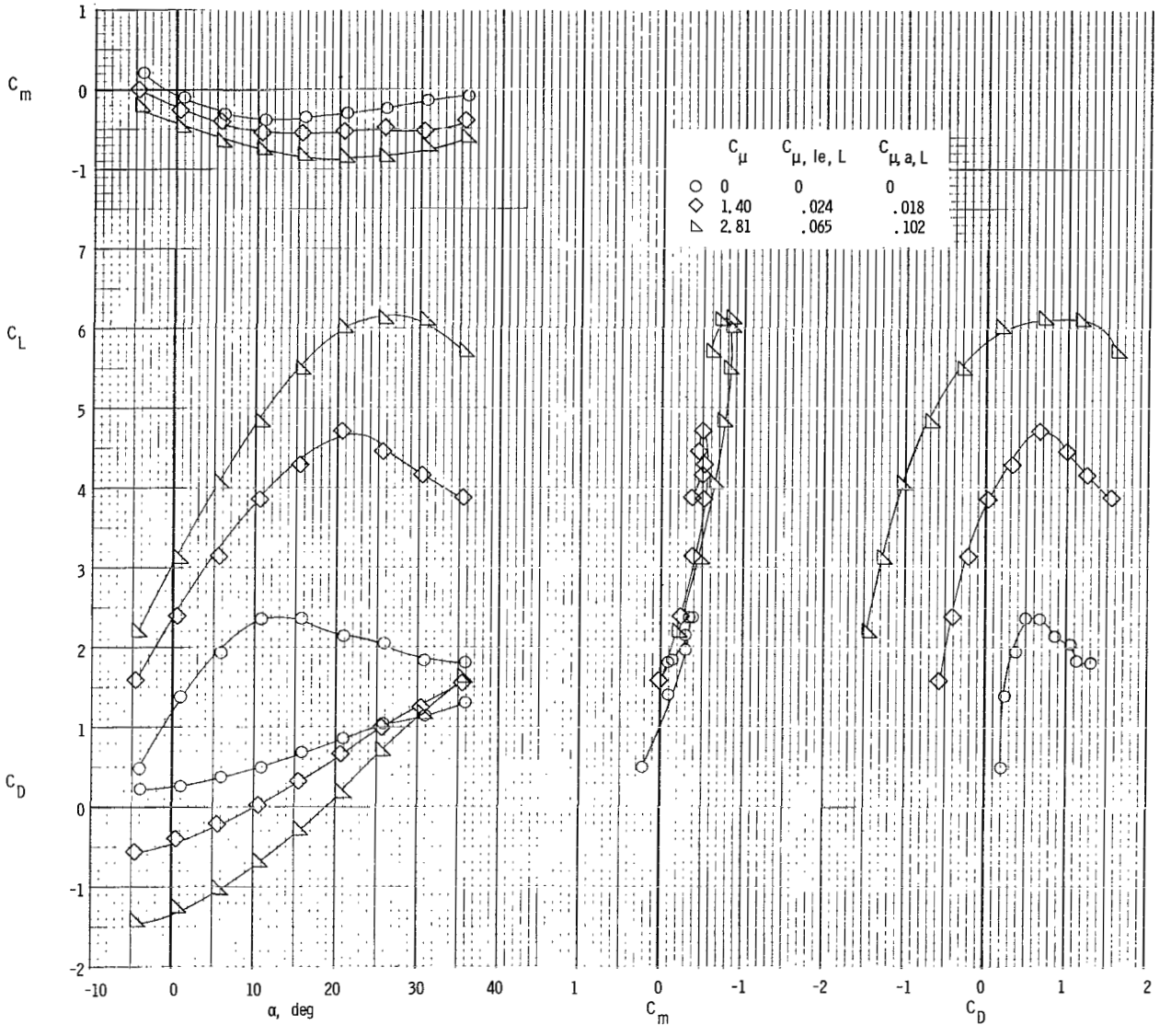

(b) Longitudinal characteristics.

Figure 78.- Concluded.

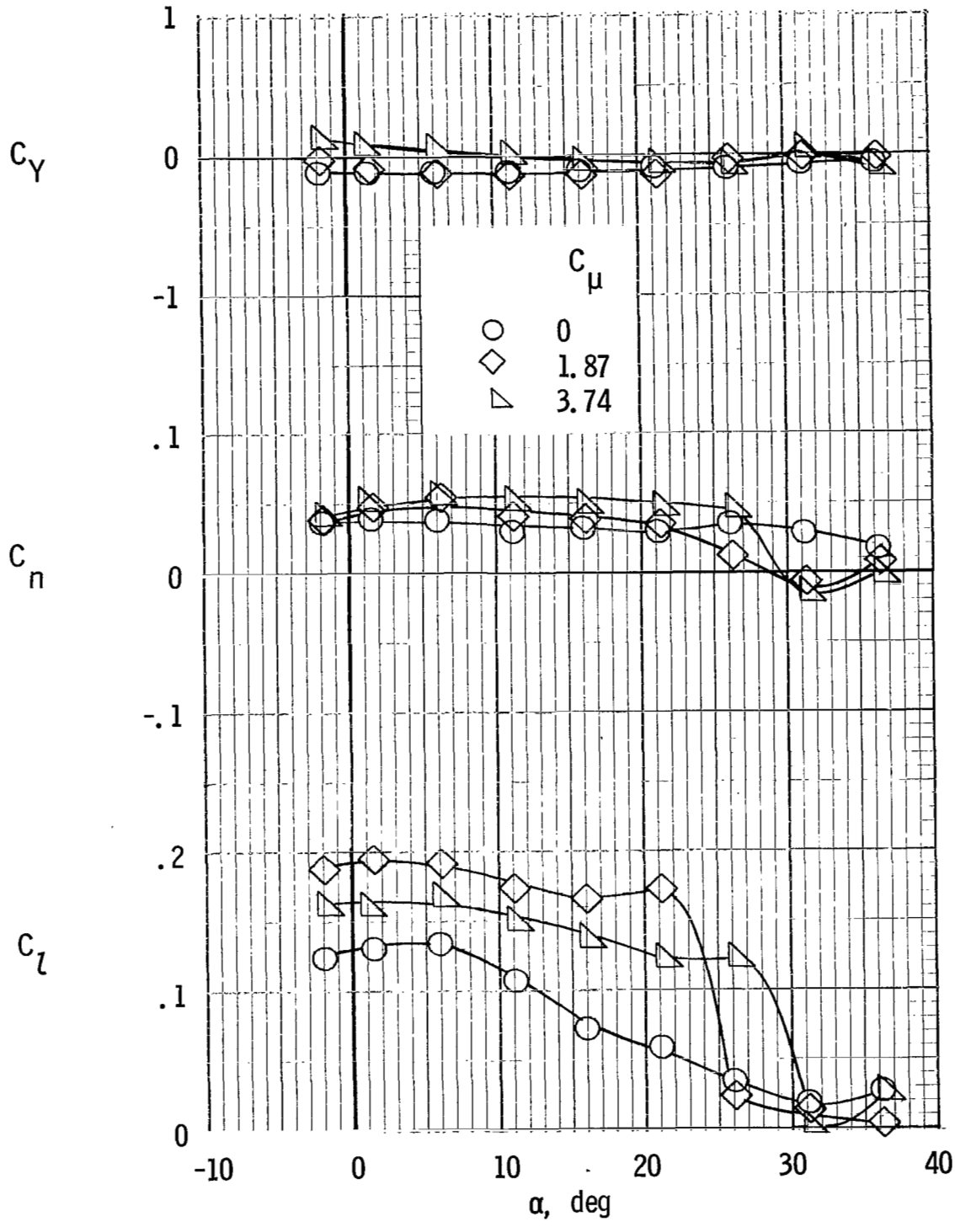

(a) Lateral characteristics. $C_{\mu,le} = 0$.

Figure 79.- Spoiler effectiveness for model with tail on and clustered engines. $\delta_f = 60^0$; $\delta_s = 60^0$, full right semispan.

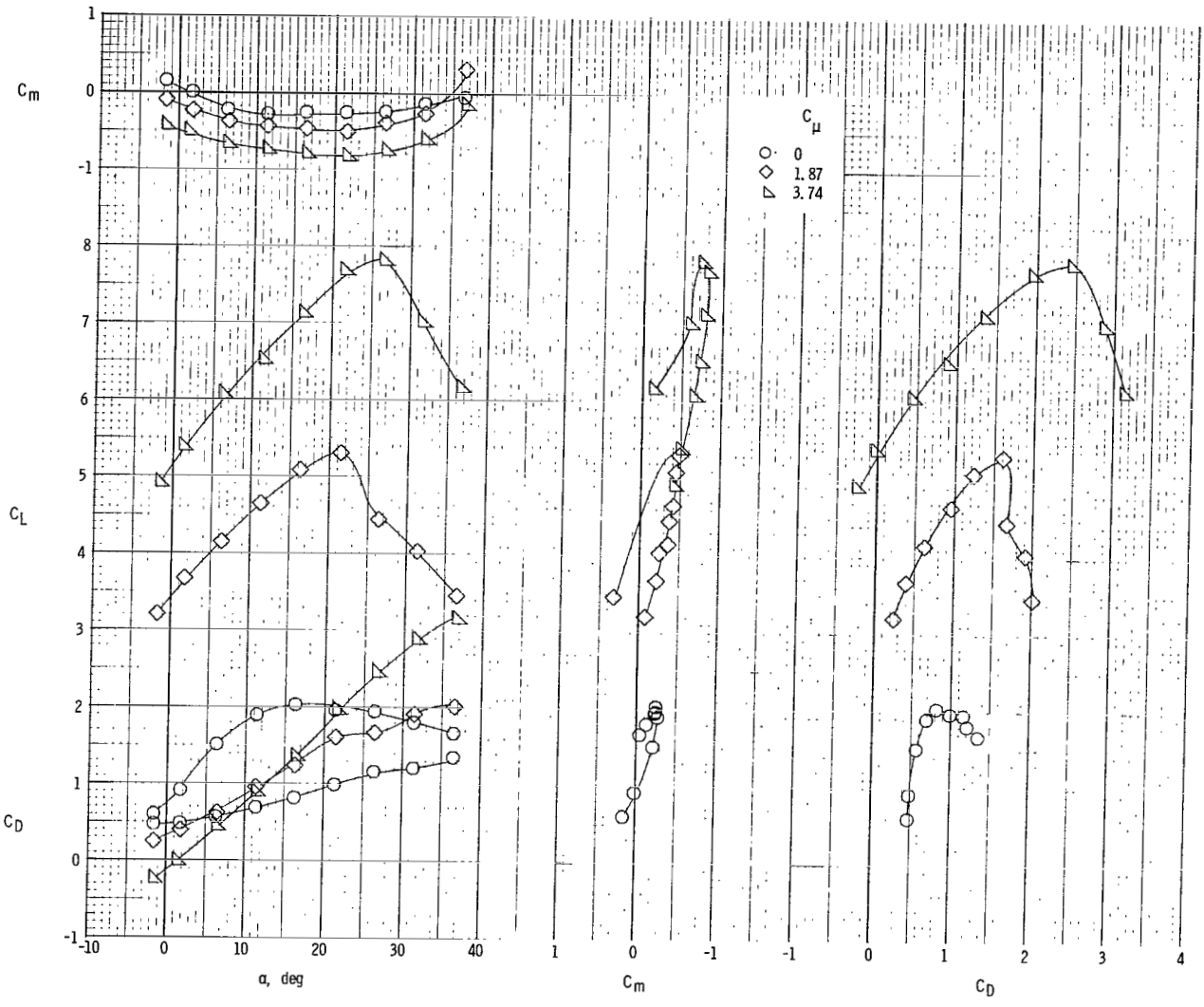

(b) Longitudinal characteristics. $C_{\mu,le} = 0$.

Figure 79.- Continued.

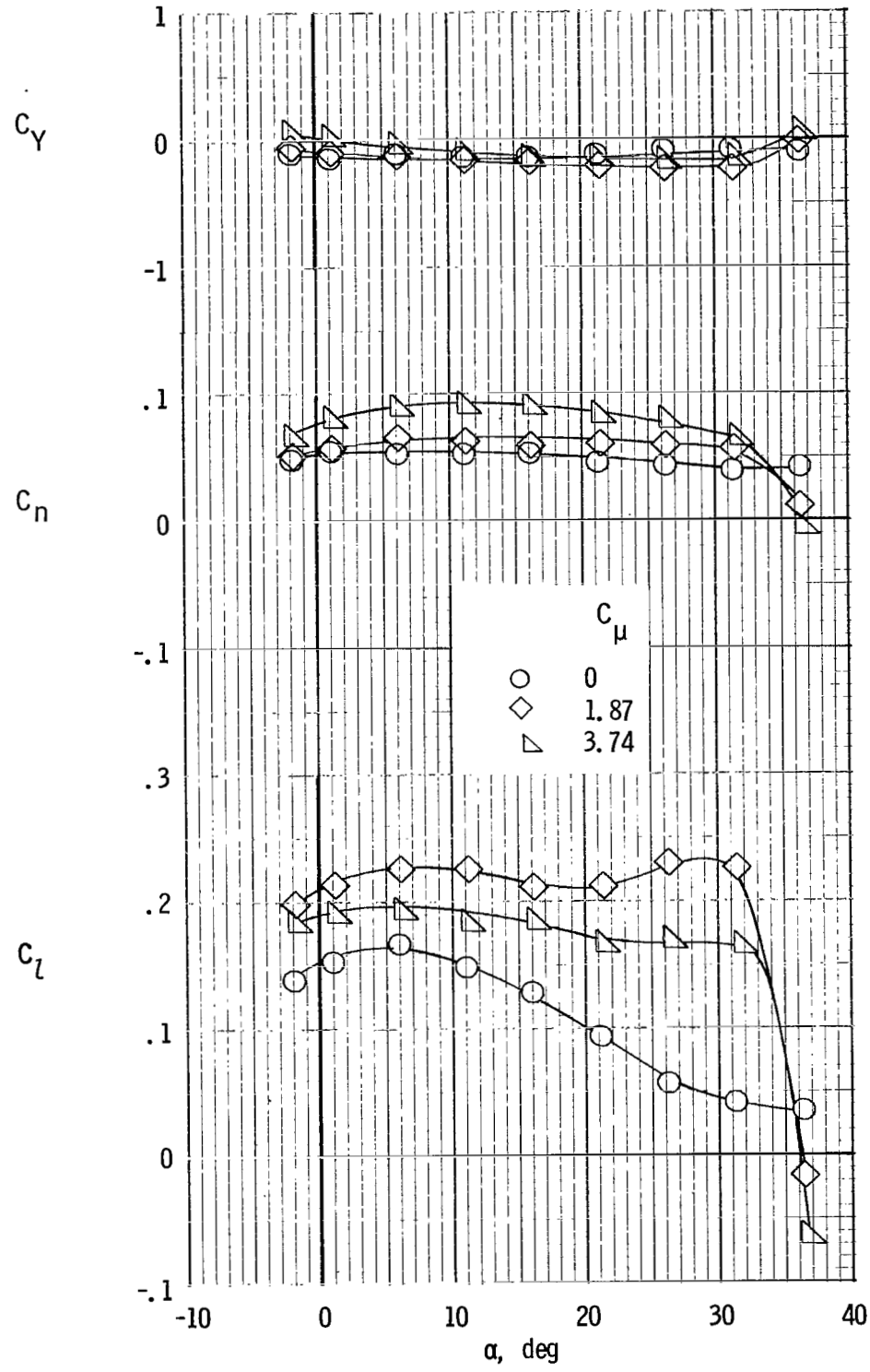

(c) Lateral characteristics. $C_{\mu,le} = 0.024$.

Figure 79.- Continued.

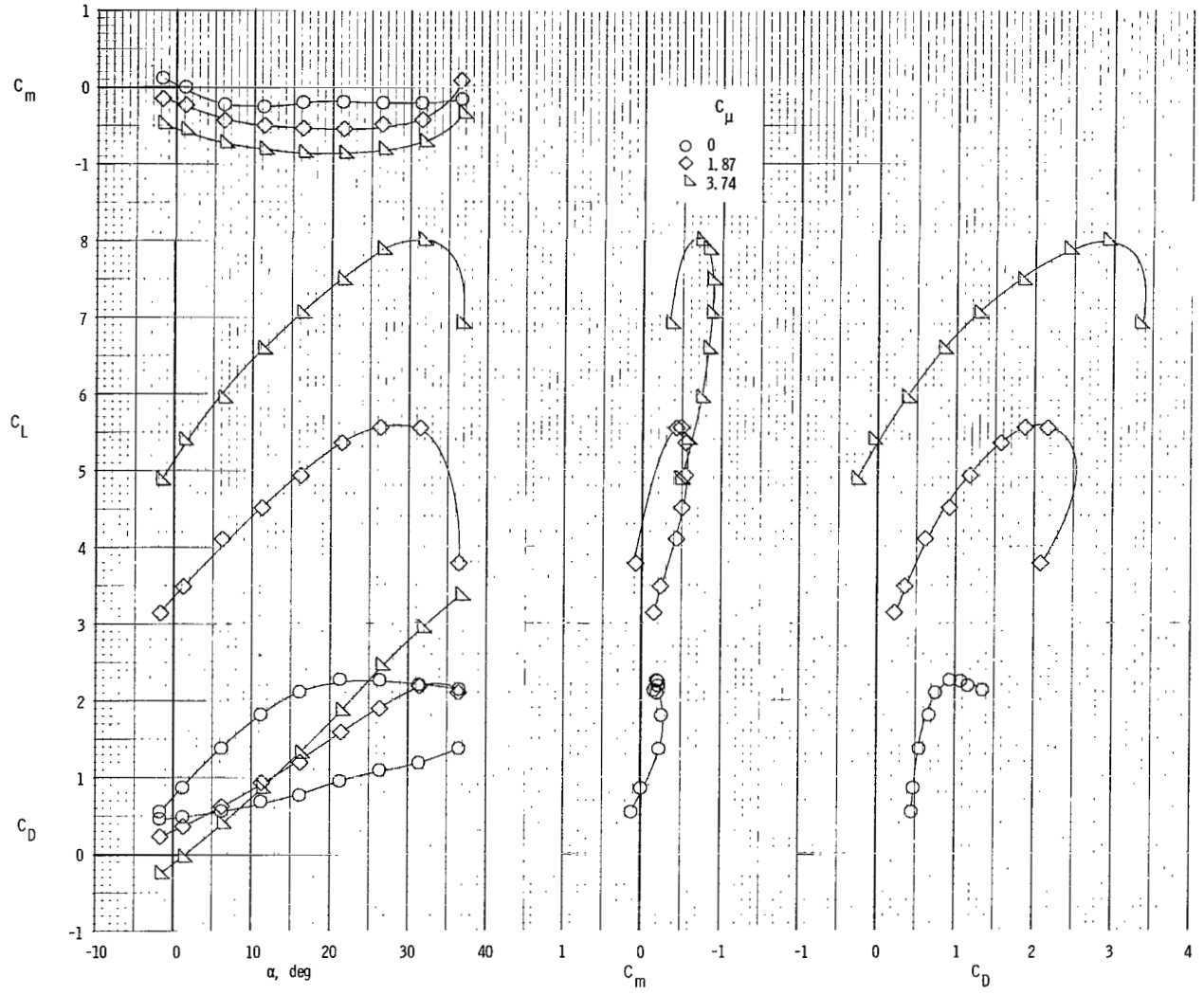

(d) Longitudinal characteristics. $C_{\mu,le} = 0.024$.

Figure 79.- Concluded.

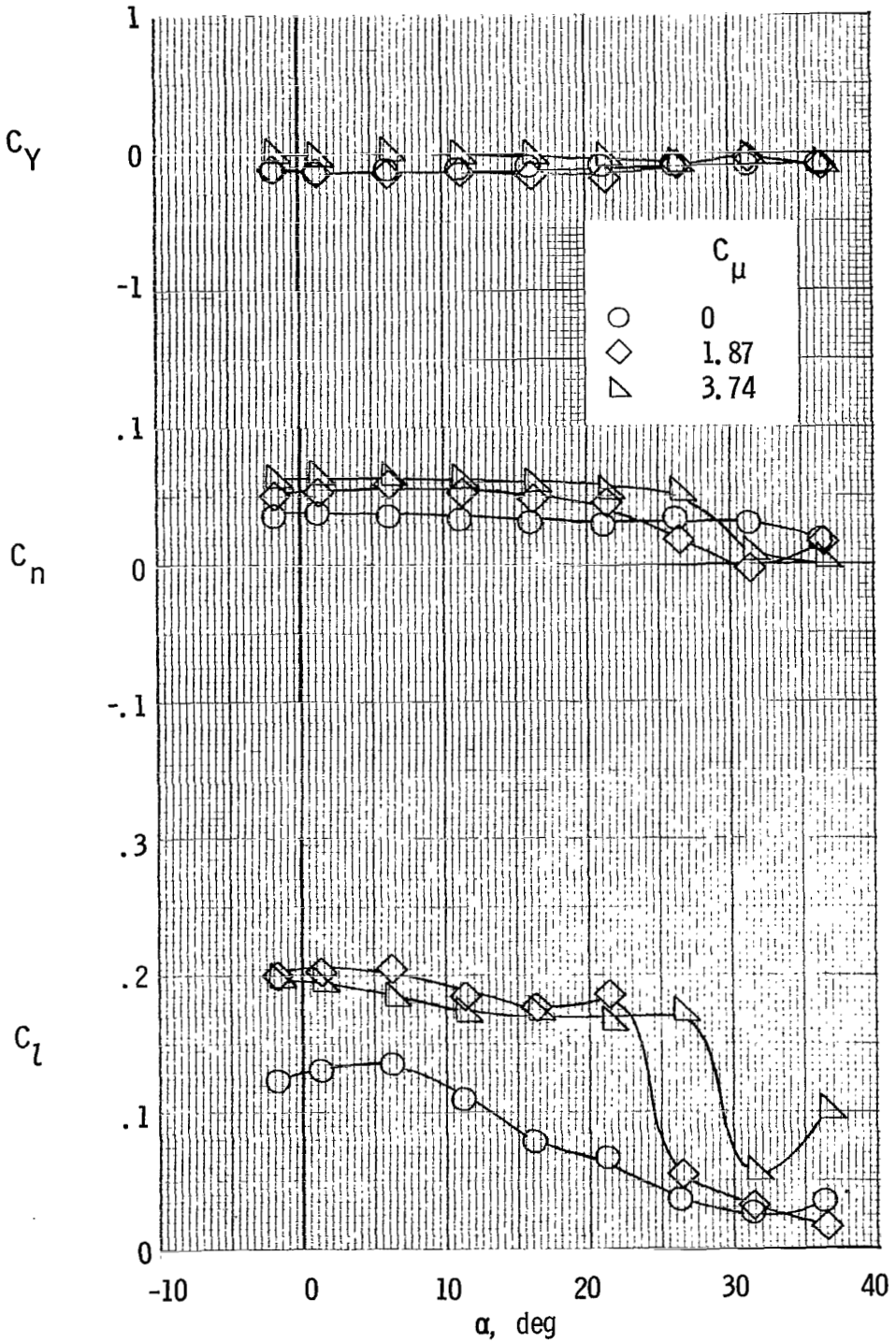

(a) Lateral characteristics.

Figure 80.- Spoiler effectiveness for model with tail on and clustered engines. $\delta_f = 60^0$; $\delta_s = 60^0$, full right semispan; spoilers on flap and wing; $C_{\mu,le} = 0$.

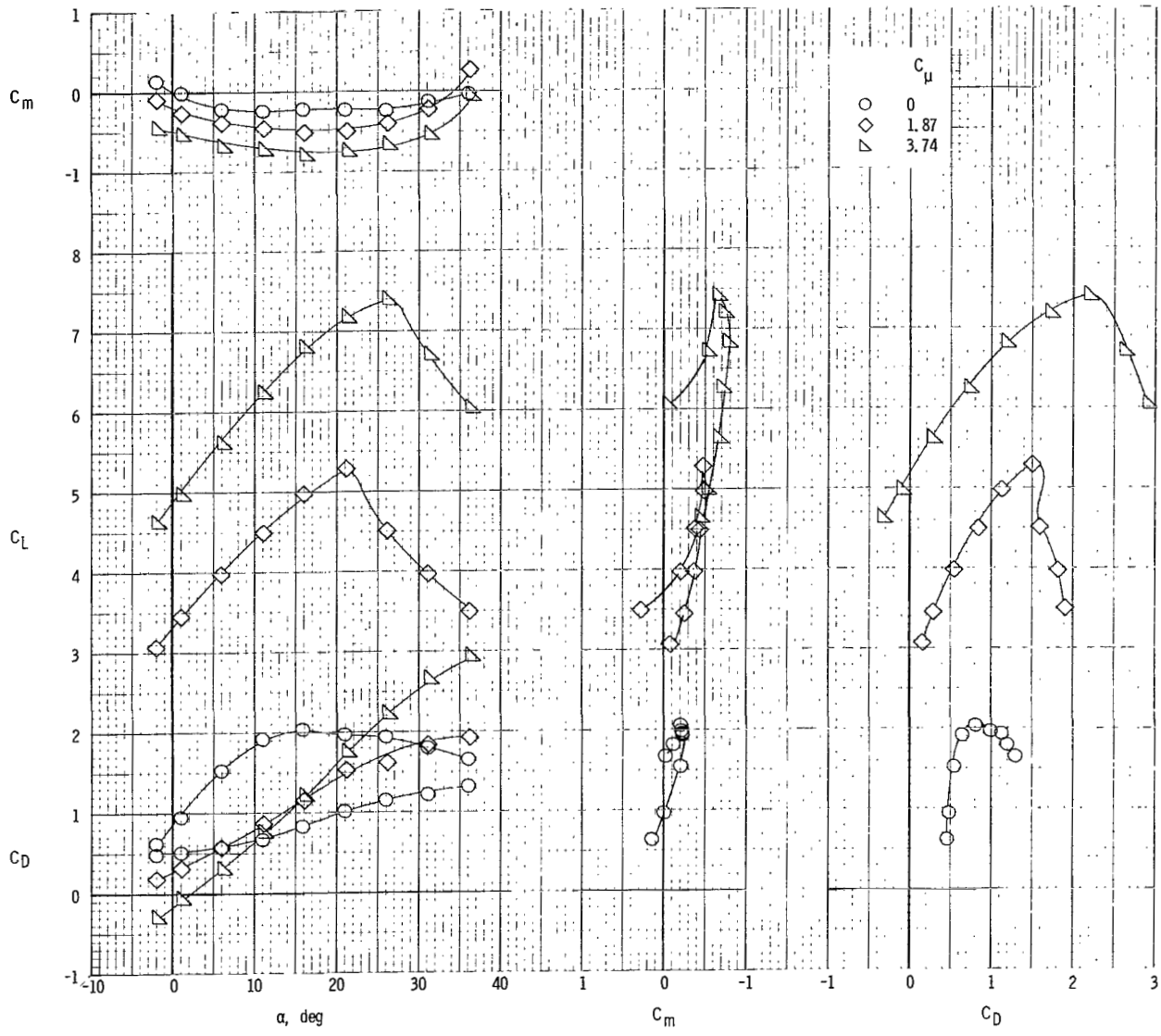

(b) Longitudinal characteristics.

Figure 80.- Concluded.

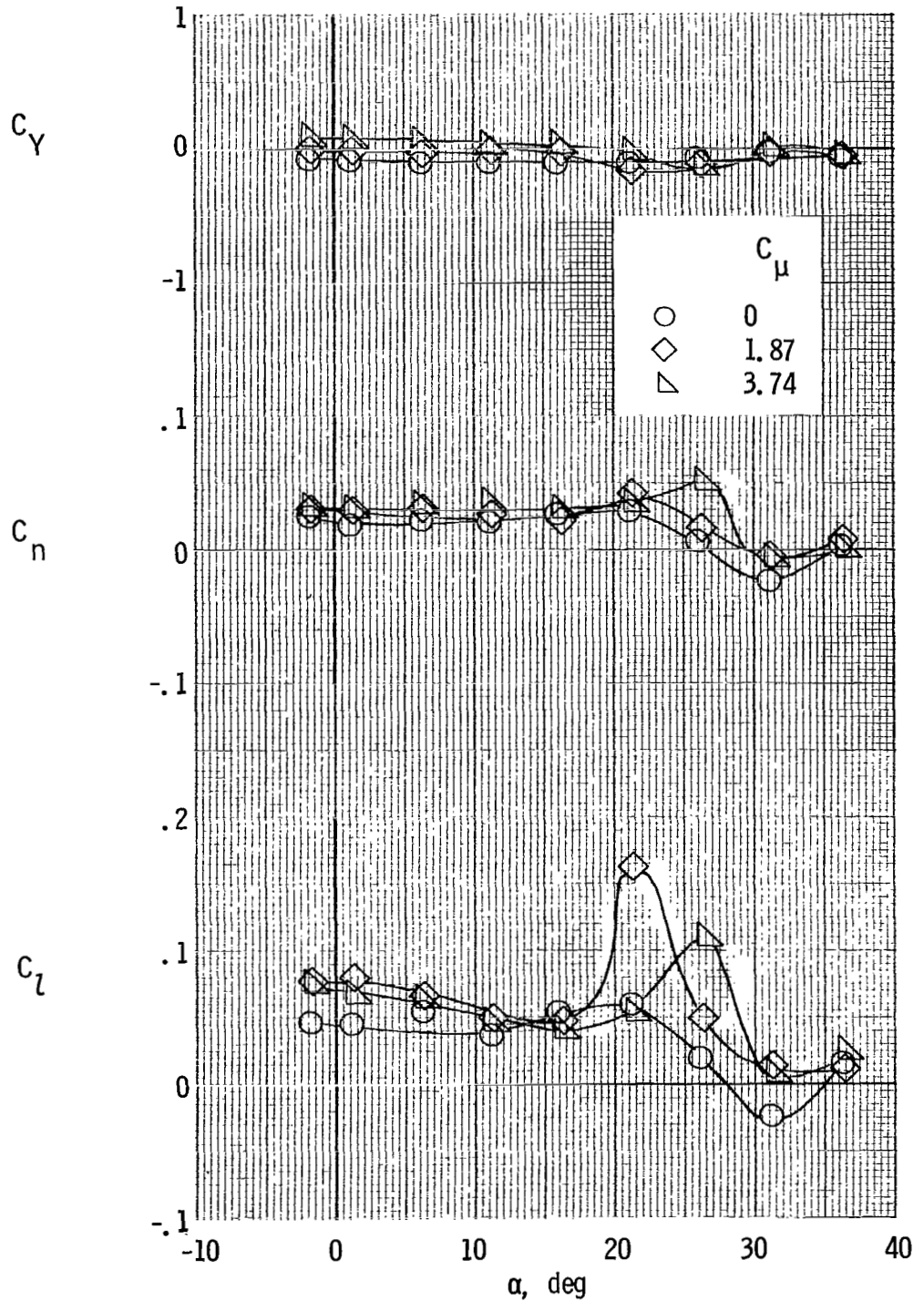

(a) Lateral characteristics.

Figure 81.- Spoiler effectiveness for model with tail on and clustered engines. $\delta_f = 60^o$; $\delta_s = 60^o$, right wing tip; flap spoiler, right tip; $C_{\mu,le} = 0$.

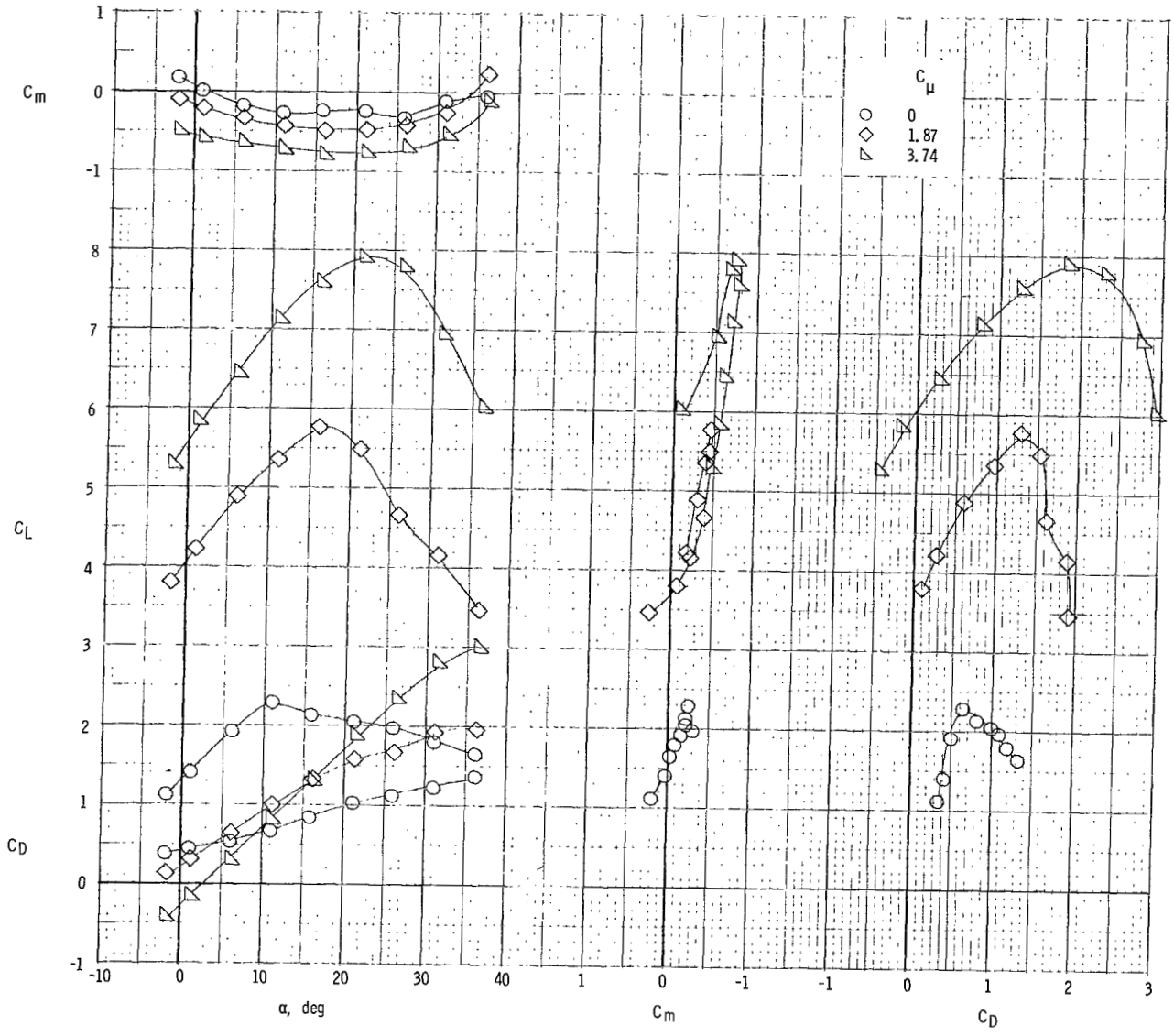

(b) Longitudinal characteristics.

Figure 81.- Concluded.

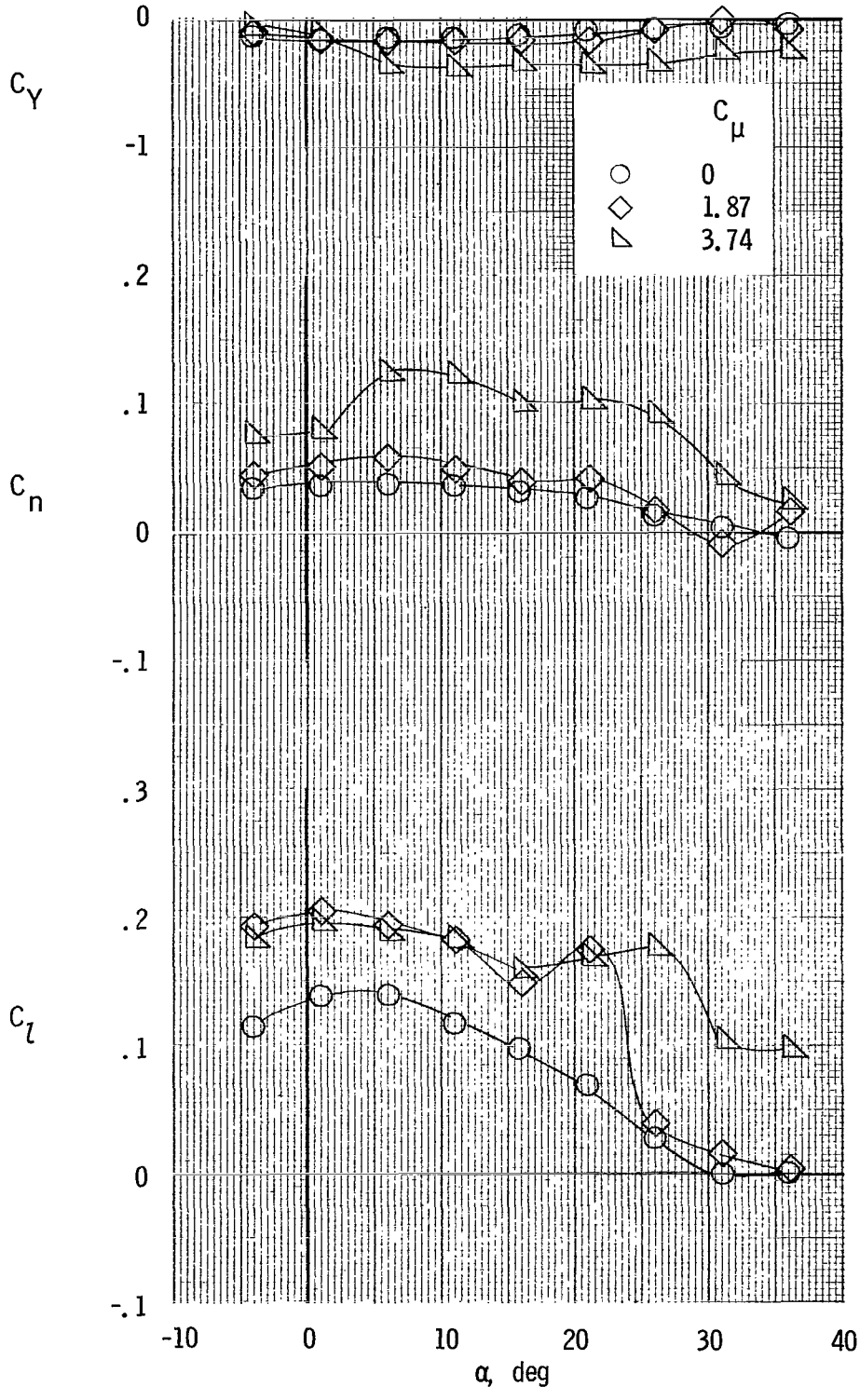

(a) Lateral characteristics. Without flap spoiler.

Figure 82.- Spoiler effectiveness for model with tail on and clustered engines. $\delta_f = 60^0$; $\delta_s = 60^0$, full right semispan (slot behind spoiler enlarged); $C_{\mu,le} = 0$.

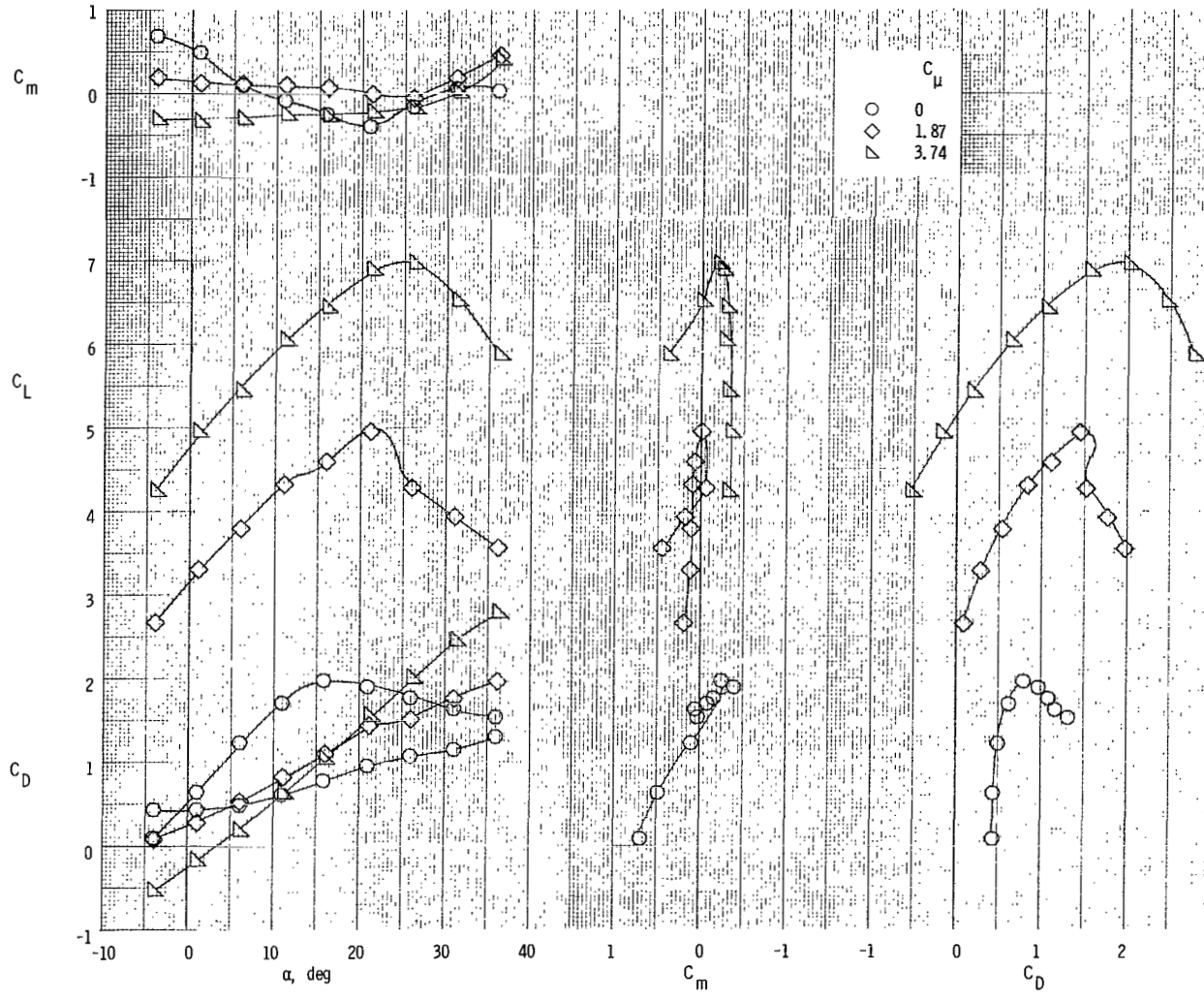

(b) Longitudinal characteristics. Without flap spoiler.

Figure 82.- Continued.

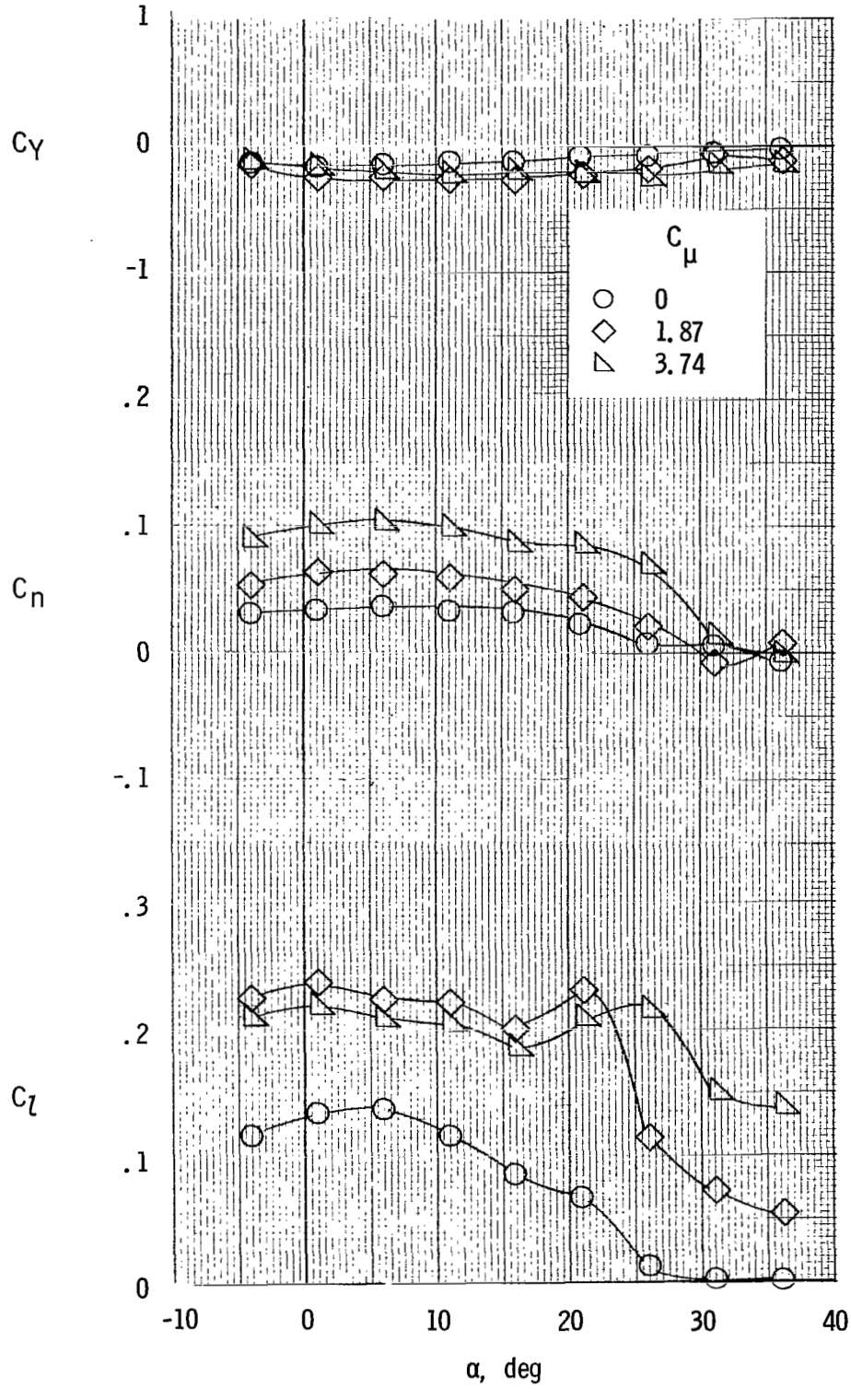

(c) Lateral characteristics. With flap spoiler.

Figure 82.- Continued.

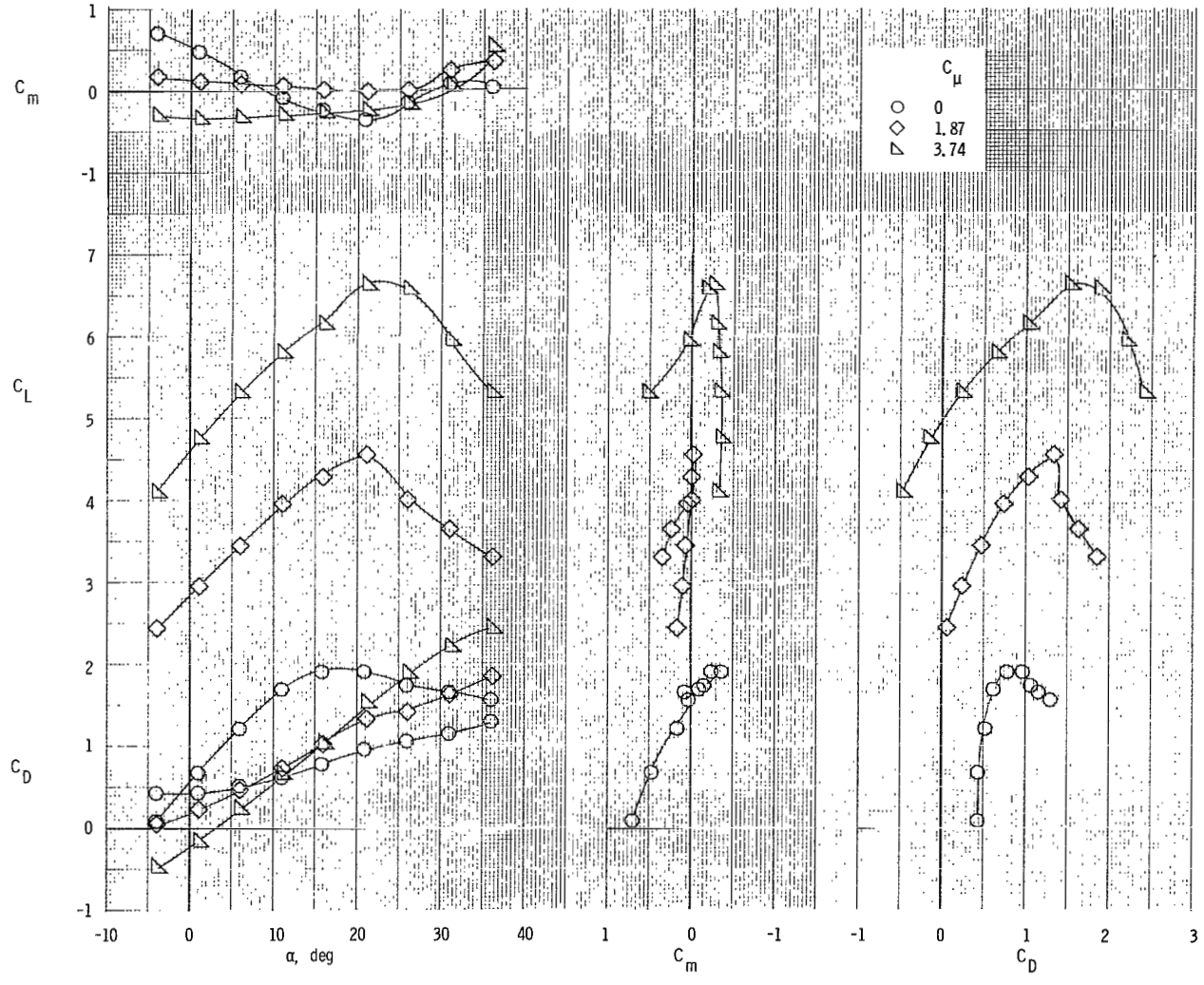

(d) Longitudinal characteristics. With flap spoiler.

Figure 82.- Concluded.

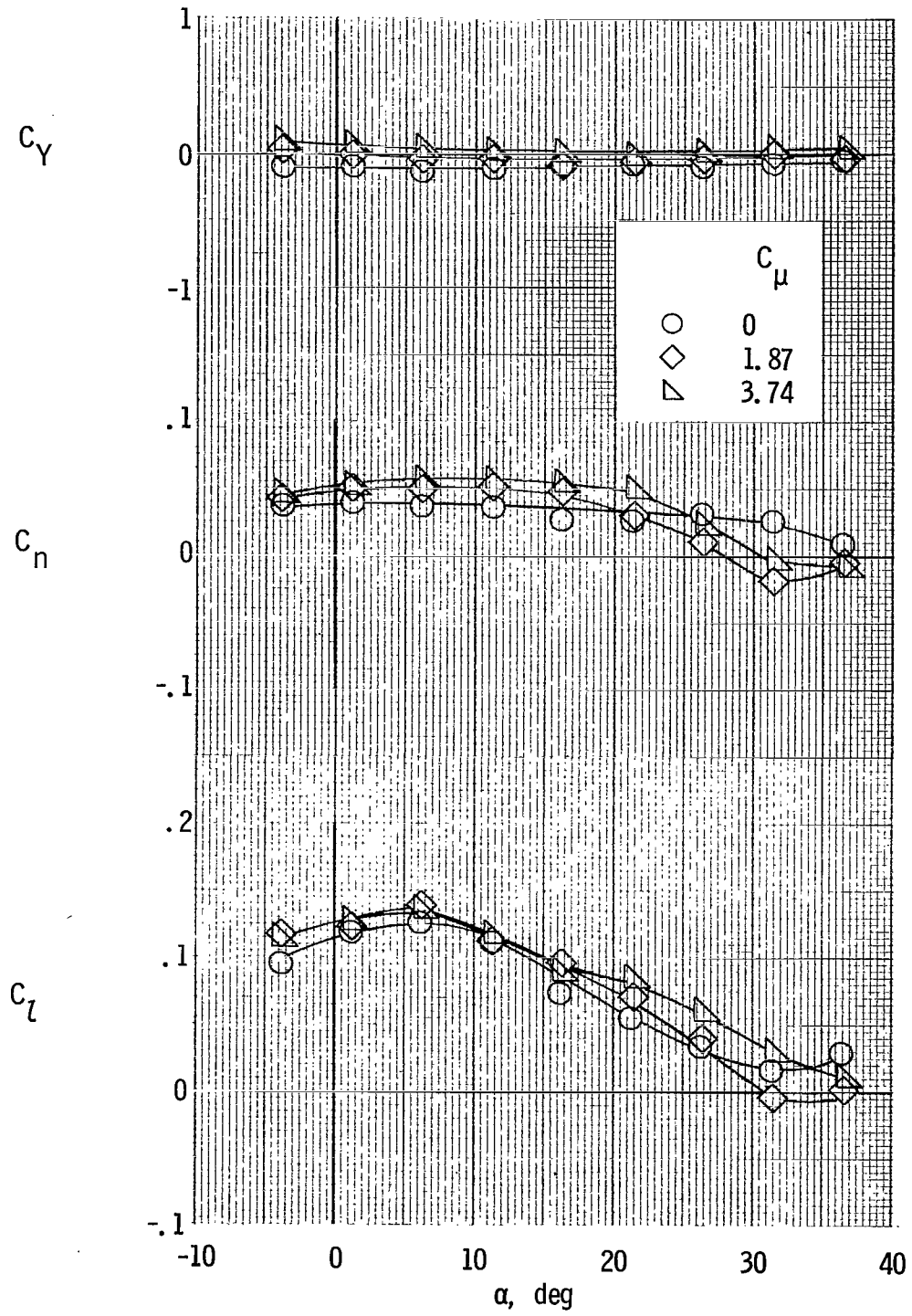

(a) Lateral characteristics. $C_{\mu,le} = 0$.

Figure 83.- Spoiler effectiveness for model with tail on and clustered engines. $\delta_f = 35^0$; $\delta_s = 60^0$, full right semispan.

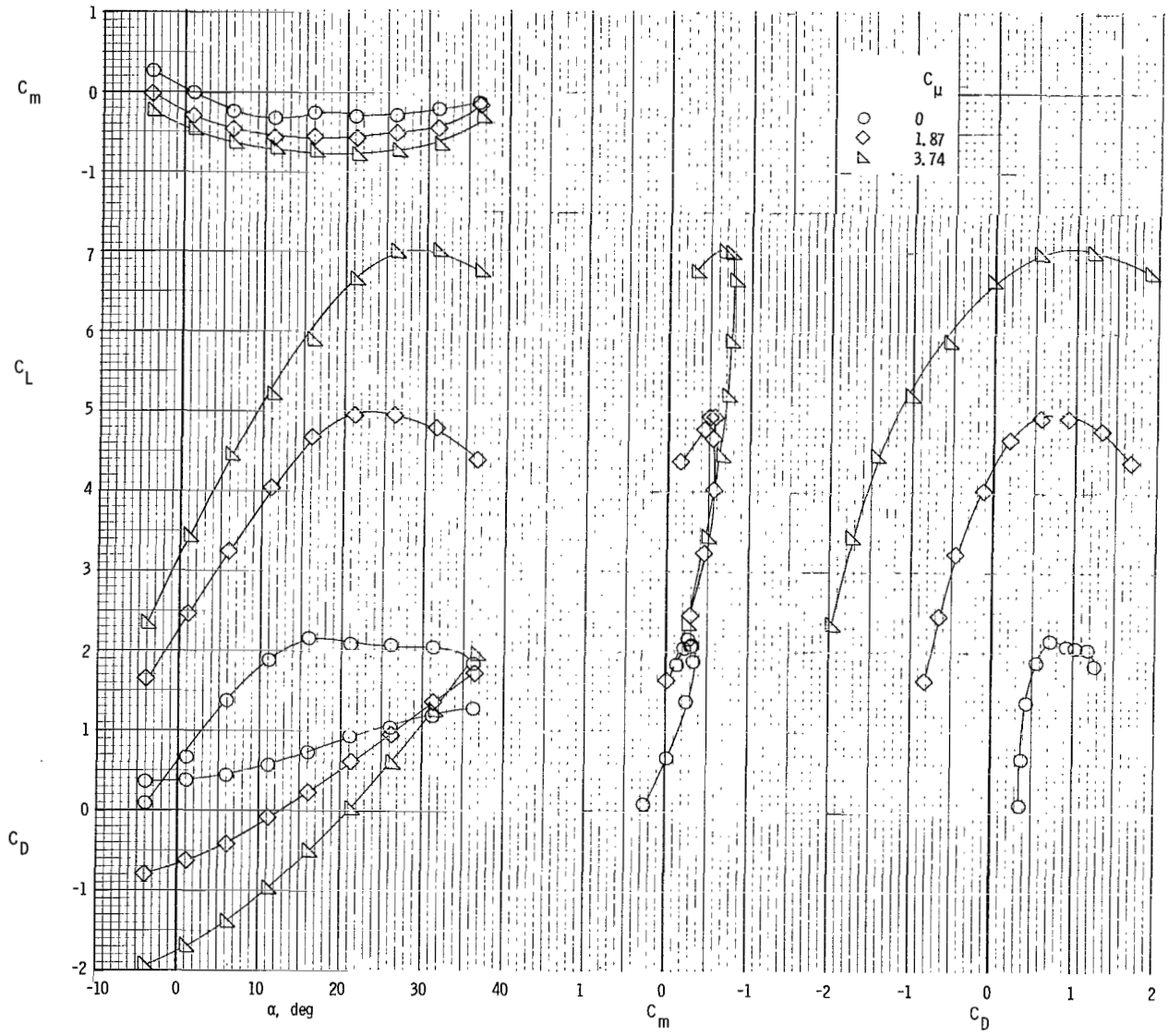

(b) Longitudinal characteristics. $C_{\mu,le} = 0$.

Figure 83.- Continued.

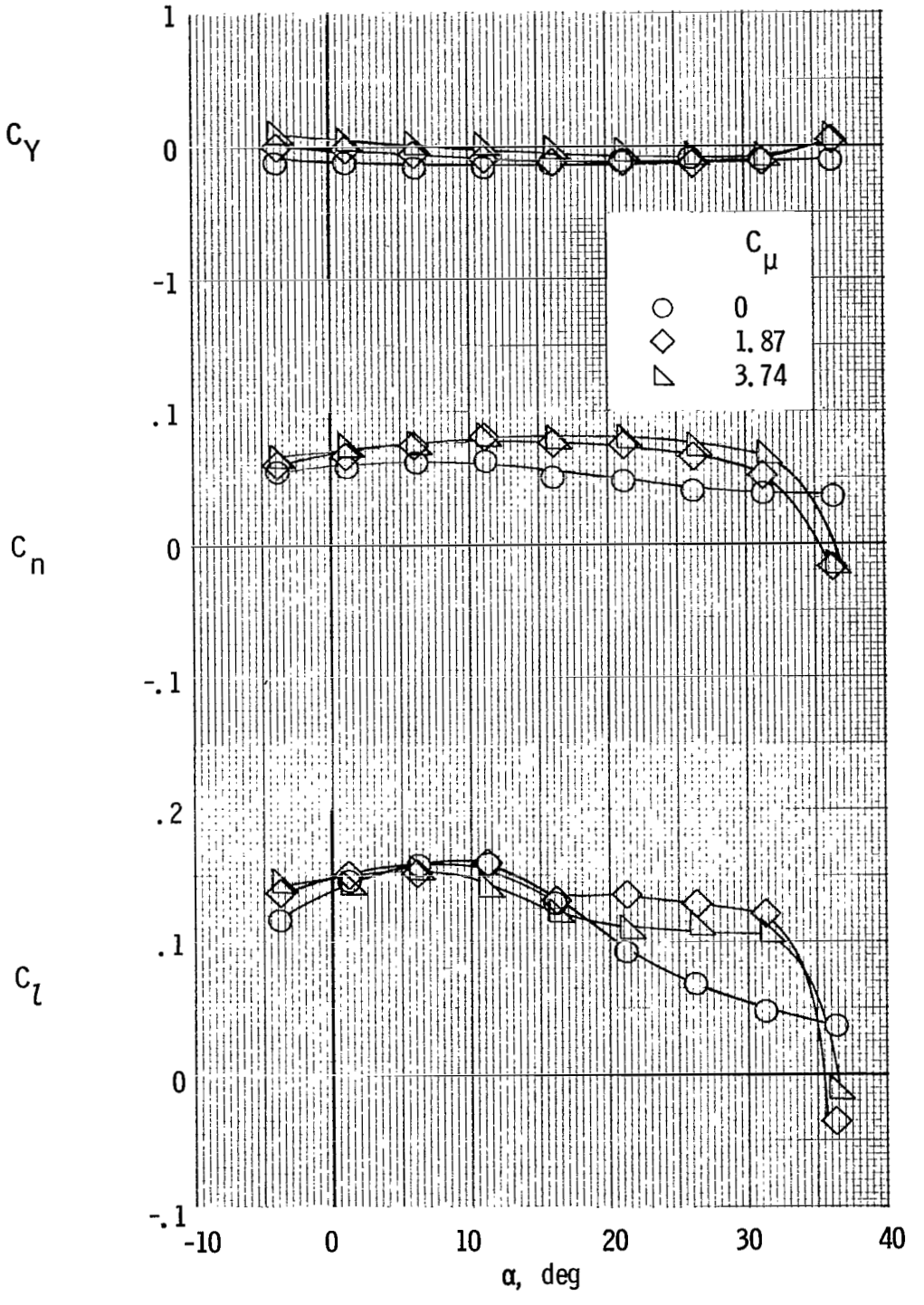

(c) Lateral characteristics. $C_{\mu,le} = 0.024$.

Figure 83.- Continued.

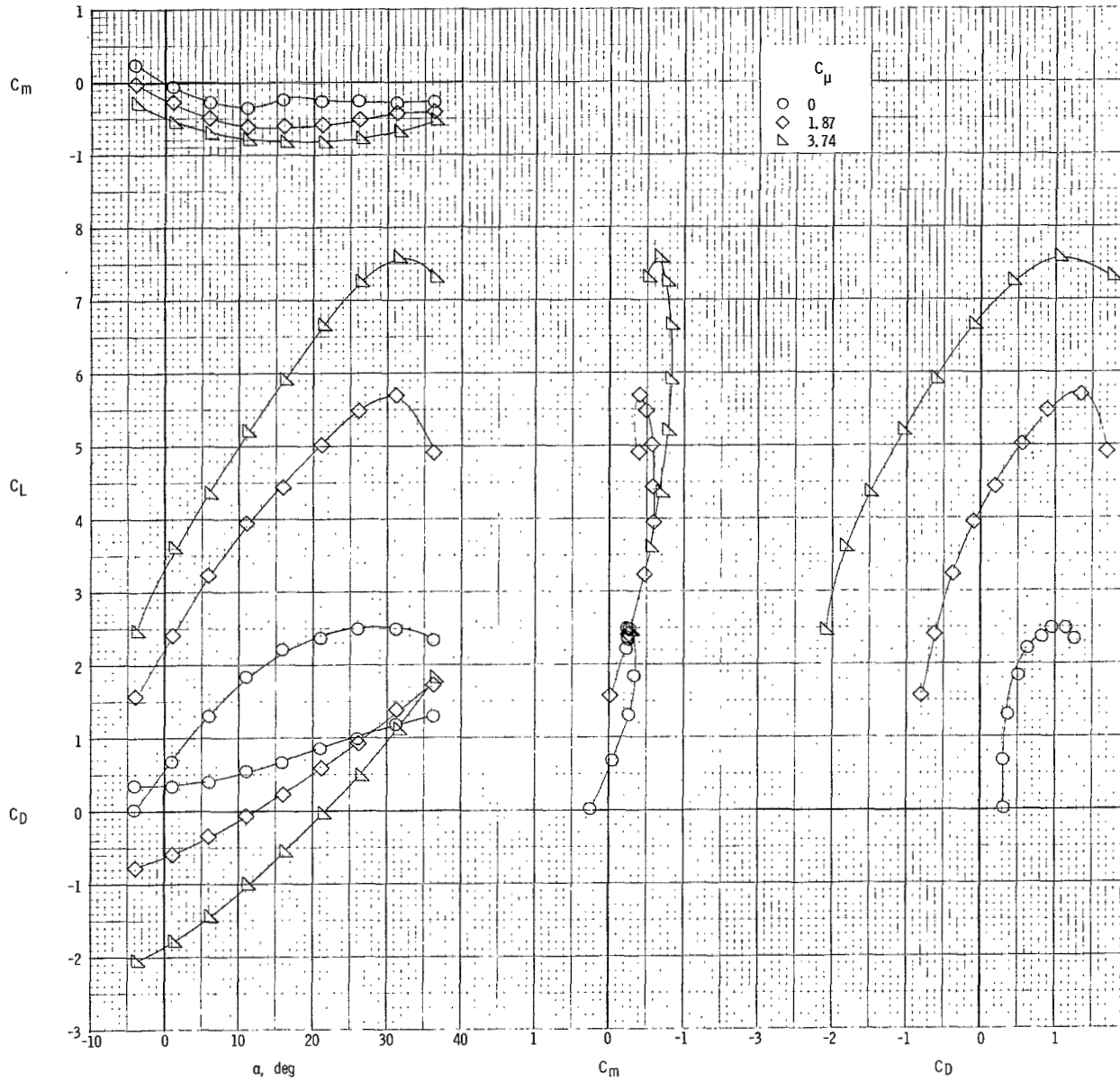

(d) Longitudinal characteristics. $C_{\mu,le} = 0.024$.

Figure 83.- Concluded.

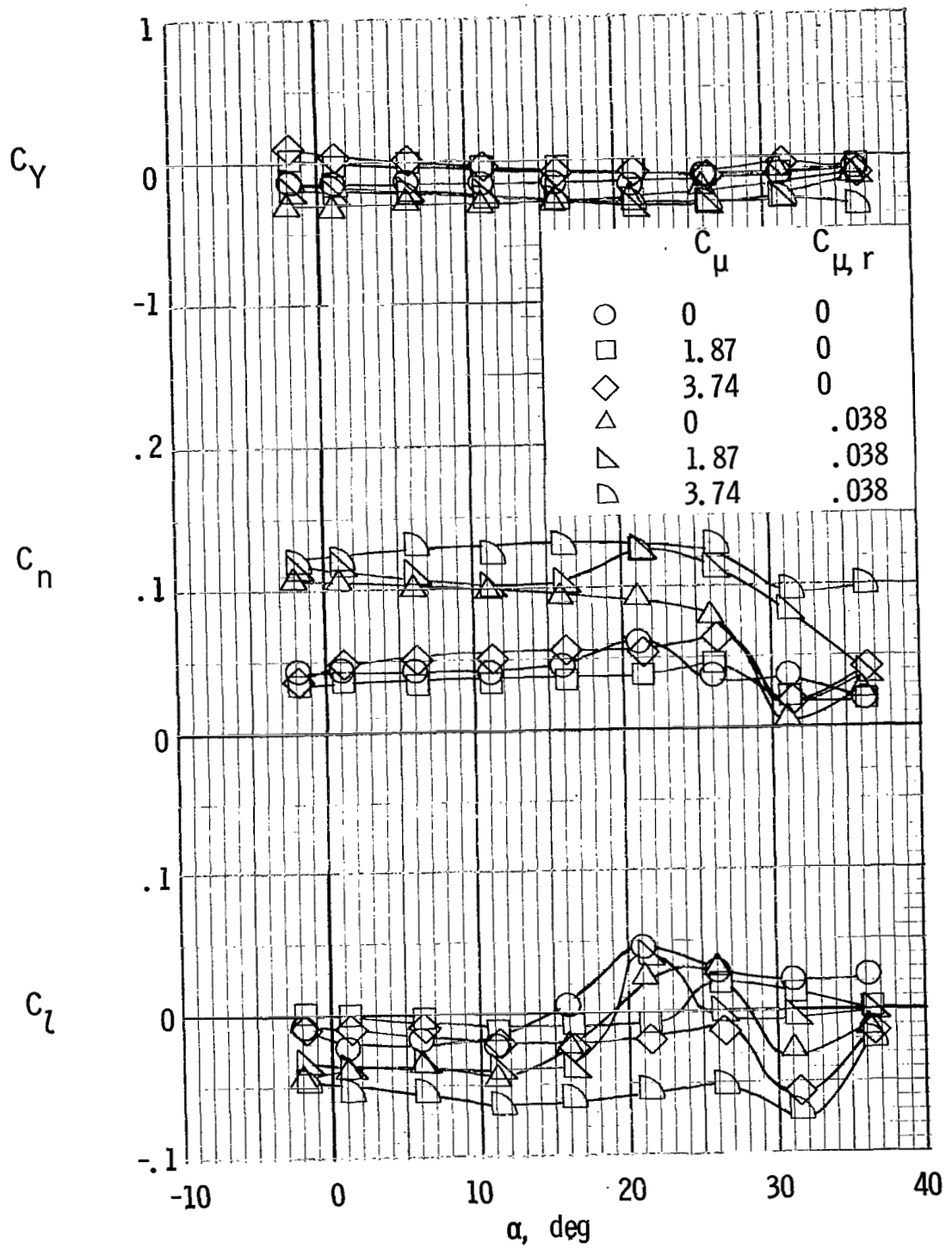

(a) $\delta_r = -20^o$.

Figure 84.- Rudder effectiveness for model with tail on and clustered engines. $\delta_f = 60^o$; $C_{\mu,le} = 0$.

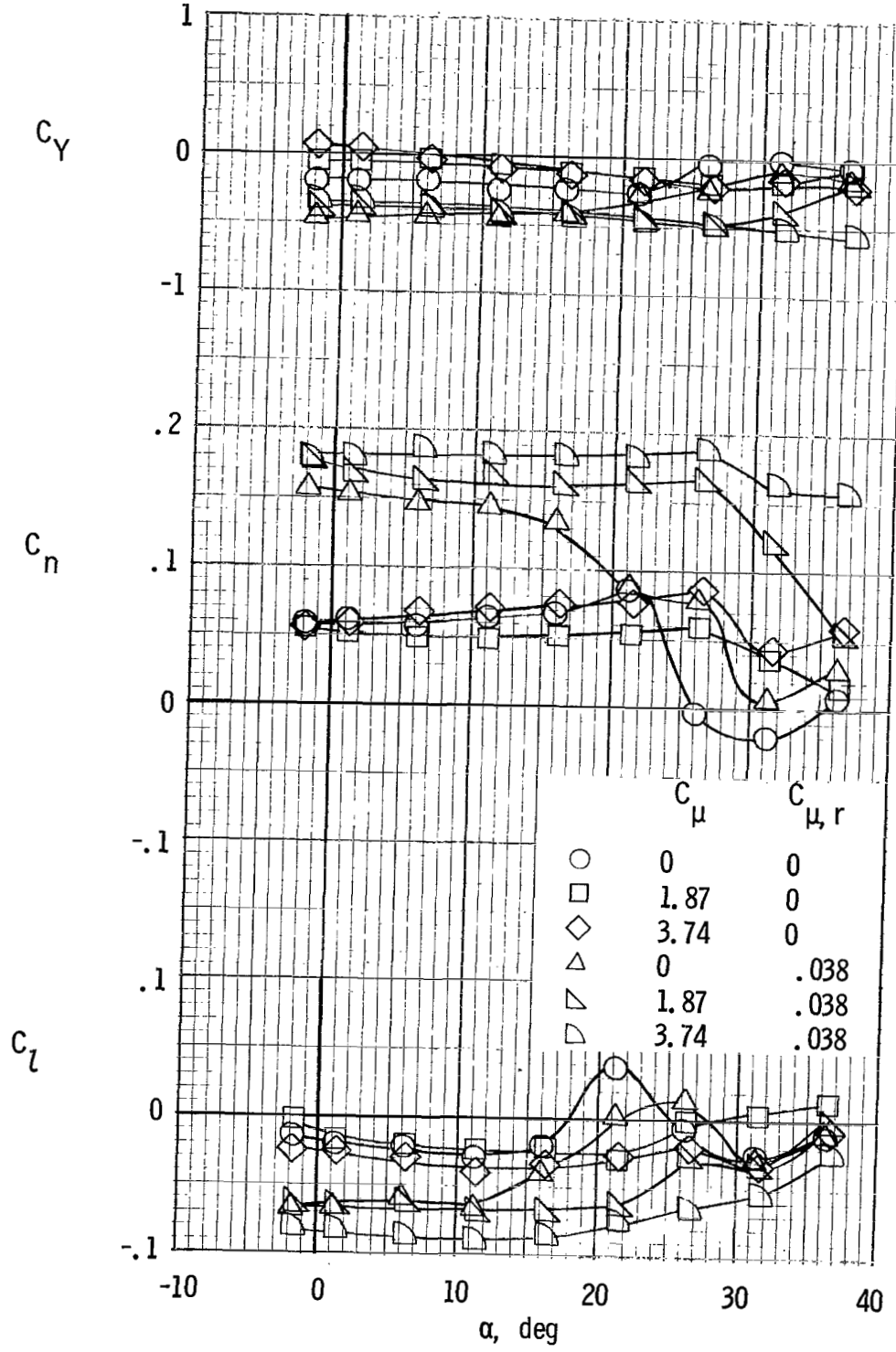

(b) $\delta_r = -40^0$.

Figure 84.- Concluded.

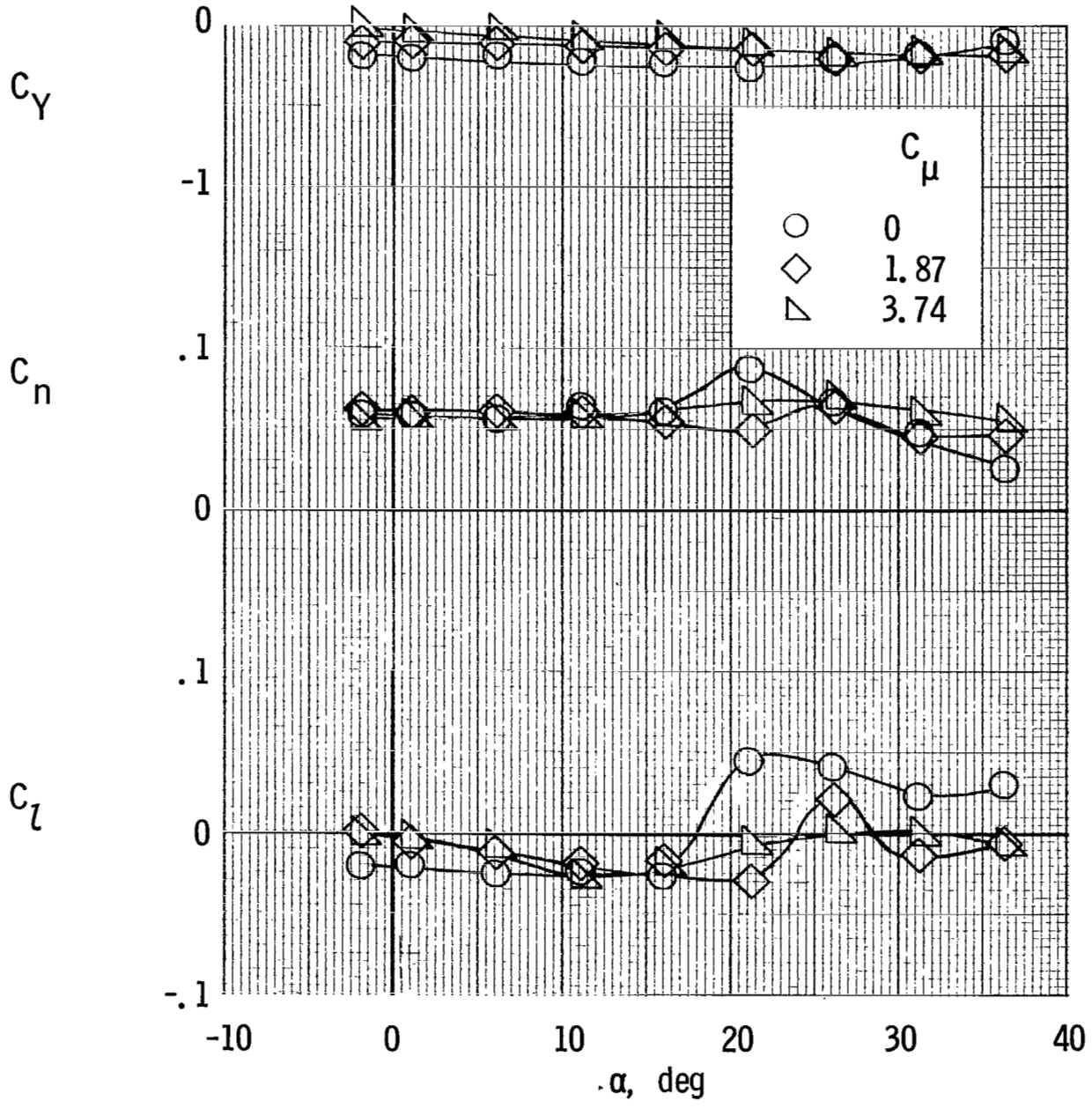

(a) $\delta_r = -40^0$; $C_{\mu,r} = 0$.

Figure 85.- Rudder effectiveness for model with tail on and clustered engines. $\delta_f = 35^0$; $C_{\mu,le} = 0$.

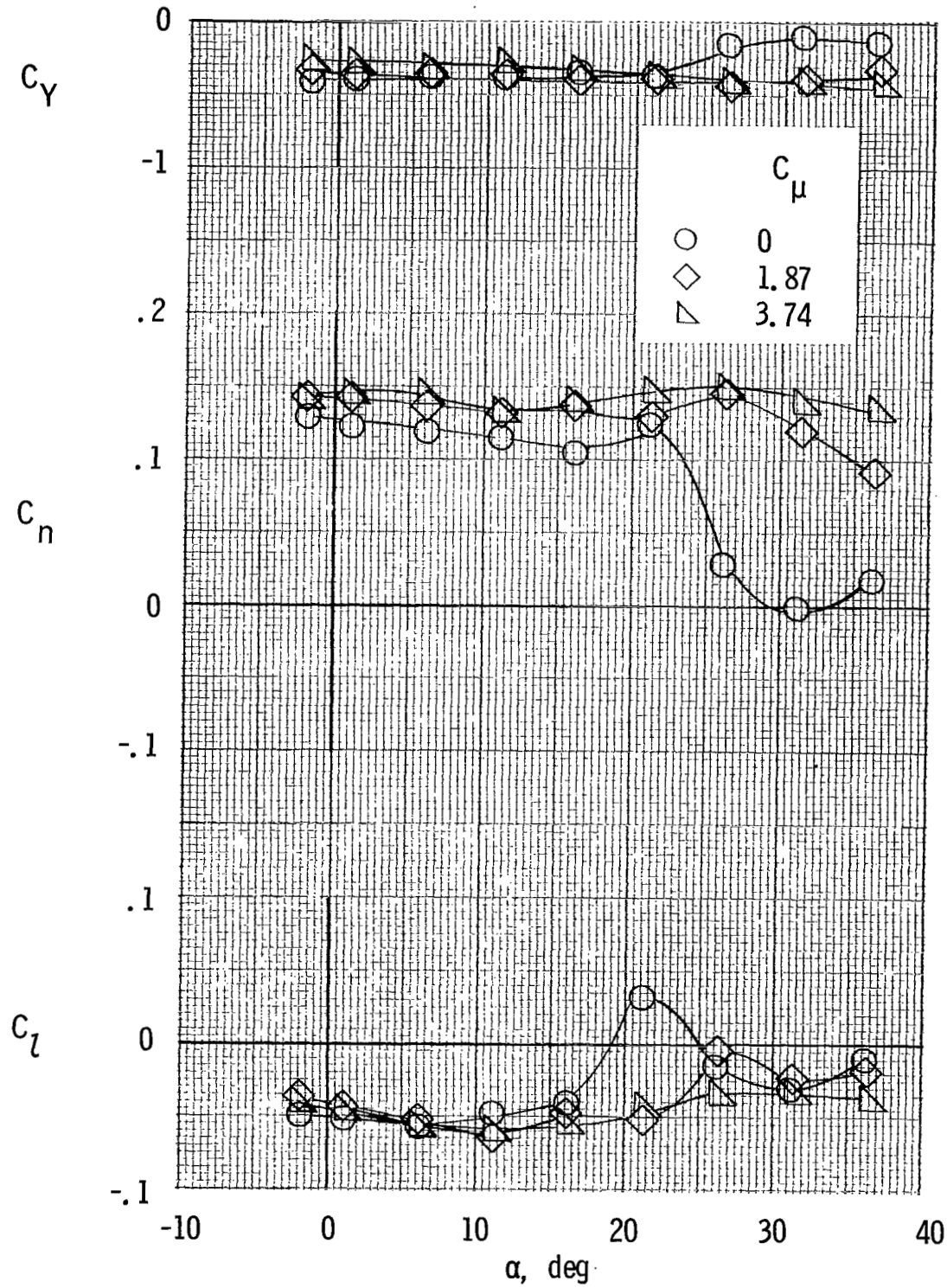

(b) $\delta_r = -40^0$; $C_{\mu,r} = 0.038$.

Figure 85.- Continued.

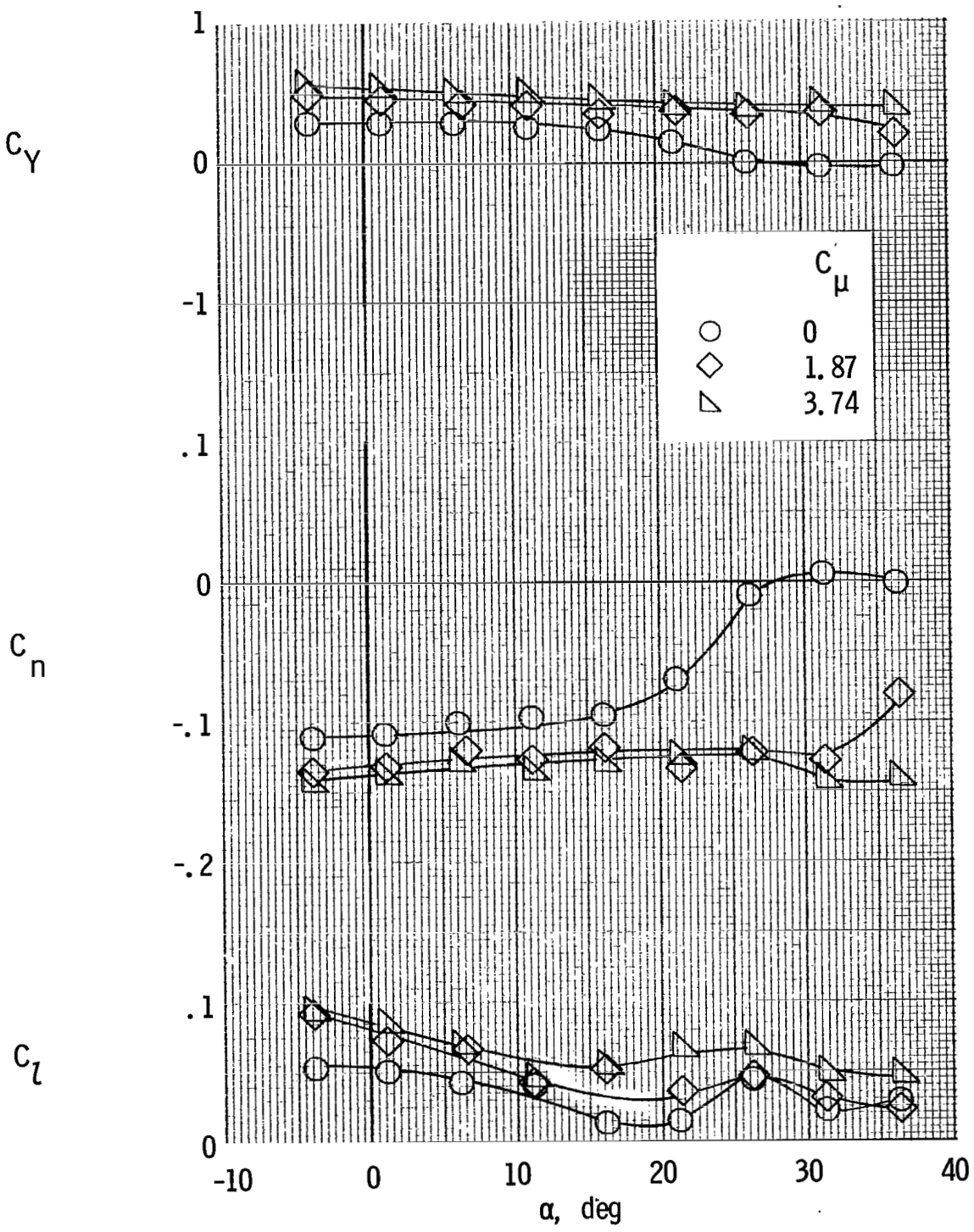

(c) $\delta_r = 40^0$; $C_{\mu,r} = 0.038$.

Figure 85.- Concluded.

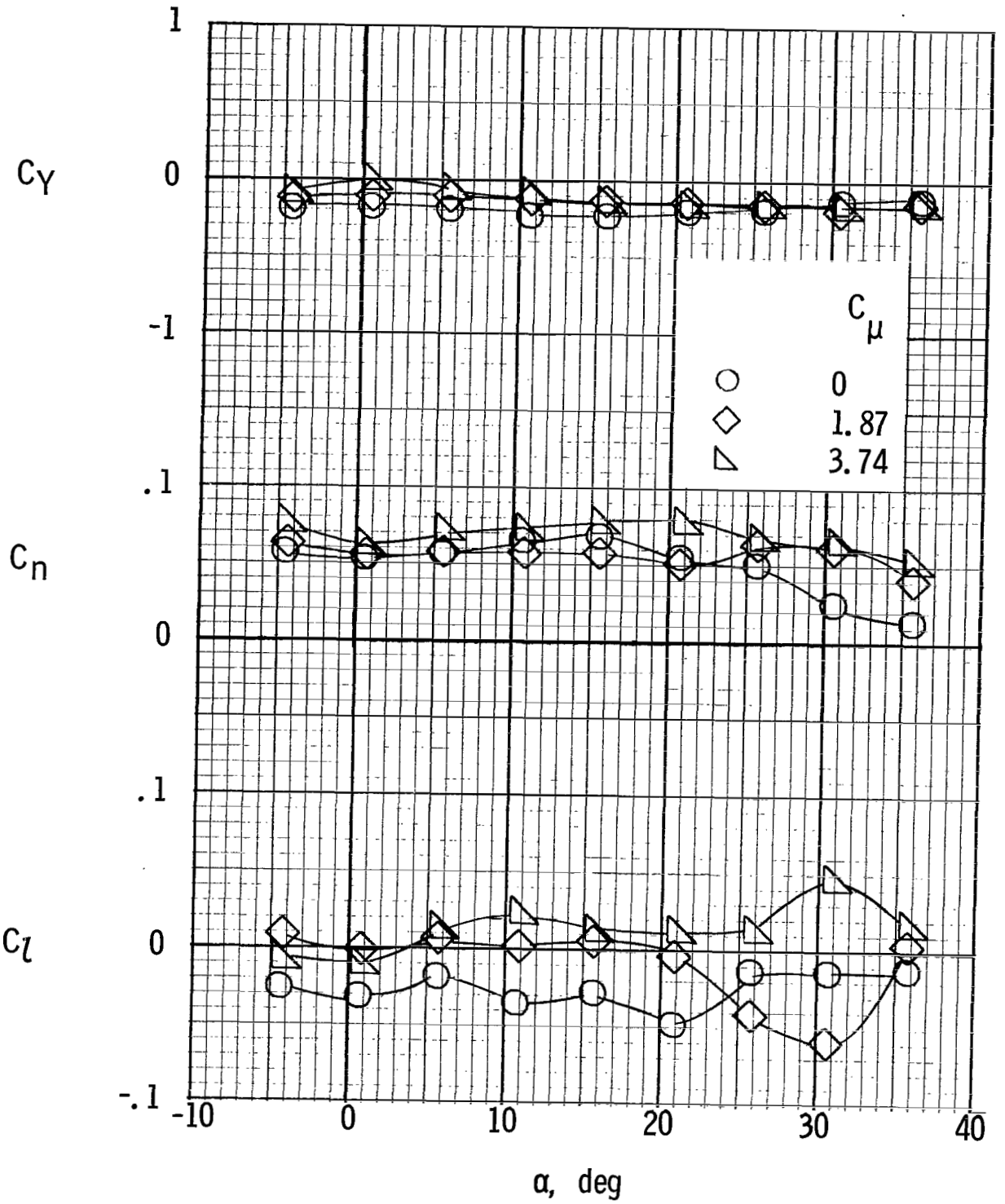

(a) $C_{\mu,r} = 0$.

Figure 86.- Rudder effectiveness for model with tail on and and spread engines. $\delta_f = 60^0$; $\delta_r = -40^0$; $C_{\mu,le} = 0.024$.

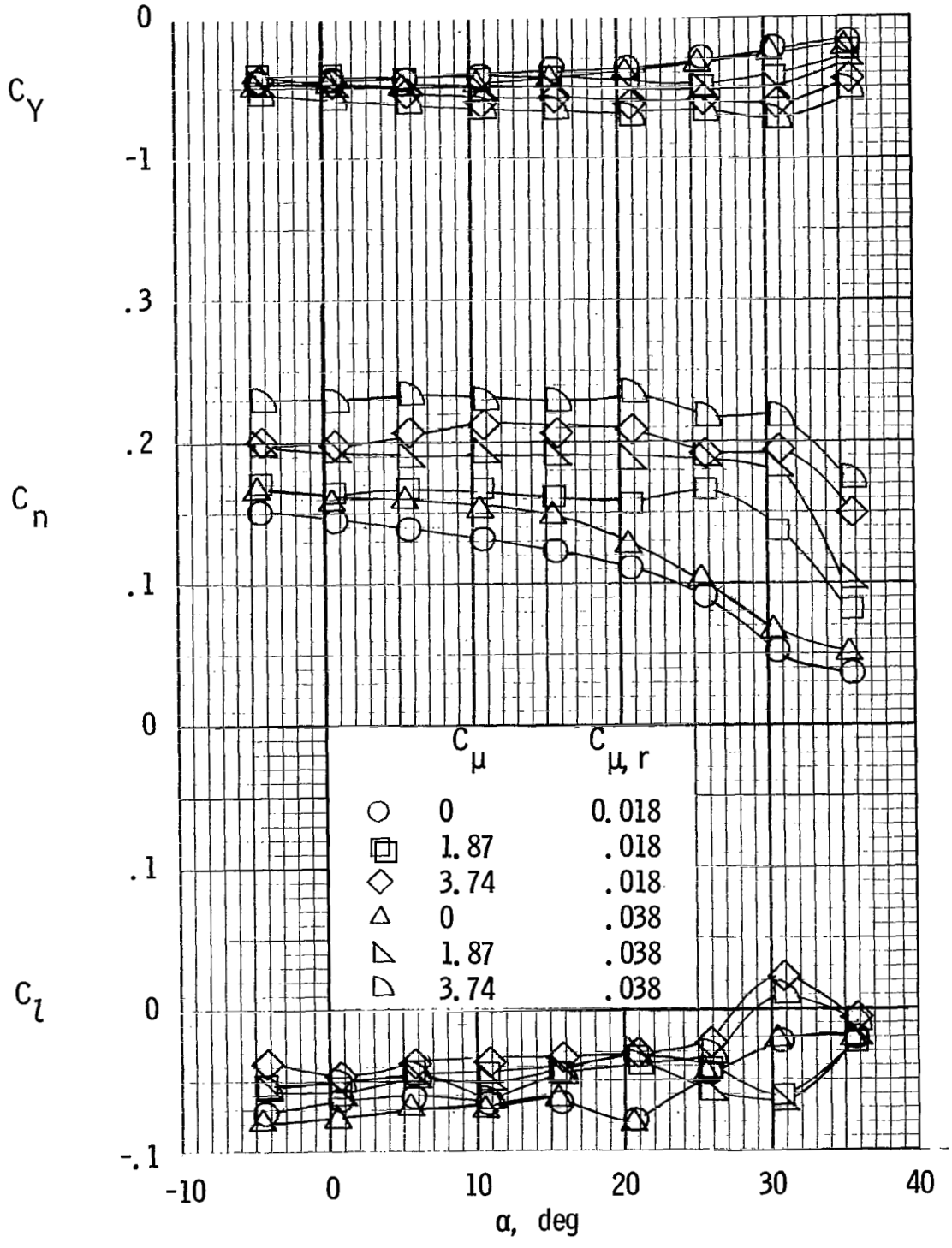

(b) Blowing on rudder.

Figure 86.- Concluded.

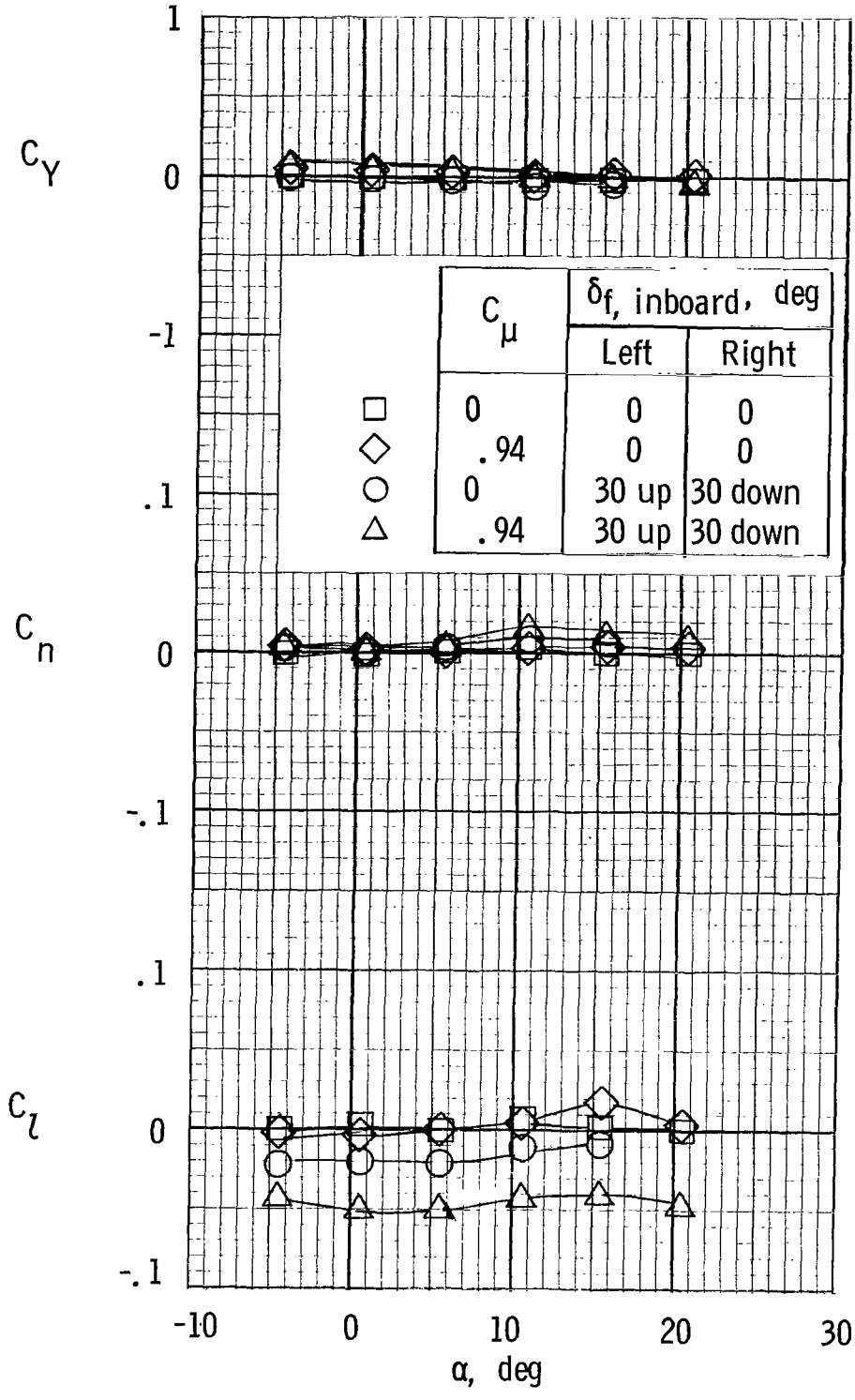

Figure 87.- Control effectiveness of inboard trailing-edge flap segments for model with tail off and spread engines. $\delta_f = 0^o$, left and right center and outboard segments.

NASA-Langley, 1971 — 2 L-7730

"The aeronautical and space activities of the United States shall be conducted so as to contribute . . . to the expansion of human knowledge of phenomena in the atmosphere and space. The Administration shall provide for the widest practicable and appropriate dissemination of information concerning its activities and the results thereof."

— NATIONAL AERONAUTICS AND SPACE ACT OF 1958

NASA SCIENTIFIC AND TECHNICAL PUBLICATIONS

TECHNICAL REPORTS: Scientific and technical information considered important, complete, and a lasting contribution to existing knowledge.

TECHNICAL NOTES: Information less broad in scope but nevertheless of importance as a contribution to existing knowledge.

TECHNICAL MEMORANDUMS: Information receiving limited distribution because of preliminary data, security classification, or other reasons.

CONTRACTOR REPORTS: Scientific and technical information generated under a NASA contract or grant and considered an important contribution to existing knowledge.

TECHNICAL TRANSLATIONS: Information published in a foreign language considered to merit NASA distribution in English.

SPECIAL PUBLICATIONS: Information derived from or of value to NASA activities. Publications include conference proceedings, monographs, data compilations, handbooks, sourcebooks, and special bibliographies.

TECHNOLOGY UTILIZATION PUBLICATIONS: Information on technology used by NASA that may be of particular interest in commercial and other non-aerospace applications. Publications include Tech Briefs, Technology Utilization Reports and Technology Surveys.

Details on the availability of these publications may be obtained from:

SCIENTIFIC AND TECHNICAL INFORMATION OFFICE

NATIONAL AERONAUTICS AND SPACE ADMINISTRATION

Washington, D.C. 20546